

**PREDICTION METHODS
FOR
JET V/STOL PROPULSION
AERODYNAMICS**

ITEM # 0374

JULY 1975

VOLUME I



**NAVAL AIR SYSTEMS COMMAND
RESEARCH & TECHNOLOGY GROUP**

NAVAL AIR SYSTEMS COMMAND
RESEARCH AND TECHNOLOGY GROUP

PREDICTION METHODS
for
JET V/STOL PROPULSION AERODYNAMICS
VOLUME I

Proceedings of a Workshop
held at the
Institute for Defense Analyses
Arlington, VA

on

July 28-31, 1975

Editor and Chairman: M. F. Platzner
Naval Postgraduate School
Monterey, CA

This Workshop was organized by the Research Administrator
of the Naval Air Systems Command, AIR-310.

Distribution of the proceedings is unlimited.

TABLE OF CONTENTS

	Page
FOREWORD	ix
ACKNOWLEDGMENTS	xi
LIST OF PARTICIPANTS	xii

MAIN PRESENTATIONS

VOLUME I

A. Introductory Session

Chairman: L. V. Schmidt, Naval Air Systems Command

Donald F. Sattler, LTV Aerospace Corporation "V/STOL Concept Sensitivity Study"	1
S. M. Hudson, Detroit Diesel Allison "V/STOL Propulsion System Requirements"	36
M. Sajben, McDonnell Douglas Corporation "Problems of Internal Fluid Mechanics"	46
D. H. Hickey and J. V. Kirk, NASA Ames "Studies of Forces Induced on V/STOL Aircraft by Propulsion Flows"	56

B. Duct Flow Studies

Chairman: B. Anderson, NASA Lewis Research Center

P. R. Eiseman and H. McDonald, United Technologies Research Center "A Method for Computing Three-Dimensional Flows in Ducts"	83
G. H. Hoffman, McDonnell Douglas Corporation "Calculation of Separated Flows in Internal Passages"	114
R. R. Allran, J. R. Fagan, P. J. Haley, Detroit Diesel Allison "Elements of Three-Dimensional Duct Flow"	125
G. K. Serovy and P. Kavanagh, Iowa State University "Duct Flow Analysis Methods for V/STOL Propulsion System Applications"	147

	Page
C. Ground Effects and Induced Loads	
Chairman: D. Migdal, Grumman Aerospace Corporation	
F. Wohlleben, Grumman Aerospace Corporation "Design and Development of a Hover Rig for Model Tests"	179
D. J. Renselaer and R. J. Oberto, Rockwell International . . . "Jet Effects in Hover of a VTOL Aircraft Model Using Water as a Test Medium"	194
M. M. Winston, L. F. Albang, G. L. Gentry, Jr. NASA Langley . . "A Simplified Approach for Preliminary Estimation of VTOL Induced Effects in Hover"	214
A. Karemaa, General Dynamics Corporation and E. M. Lynch, Naval Air Systems Command "Model Tests of Jet Lift VTOL Aircraft Configuration in the Proximity of a Raised Porous Deck"	229
J. Louisse and F. L. Marshall, Boeing Aerospace Co. "Prediction of Ground Effects for VTOL Aircraft with Twin Lifting Jets" x)	
R. A. Cea and R. E. Krepski, Grumman Aerospace Corporation. . . "Experimental Evaluations of Aero/Propulsion Effects for Lift Plus Lift/Cruise V/STOL Aircraft"	265
D. R. Kotansky and W. W. Bower, McDonnell Douglas Corporation . "Forces and Moments Produced on a Two-Dimensional Body in a Strong Lift-Jet/Airframe/Ground Interaction"	288

x) This paper is available as AIAA-paper No. 74-1167, AIAA/SAE 10th Propulsion Conference, San Diego, California, October 21-23, 1974 and will be published shortly in the AIAA Journal of Aircraft

D. Flow and Thermal Effects

Chairman: R. E. Kuhn, NASA Langley Research Center

J. V. Kirk and J. P. Barrack, NASA Ames	304
"Exhaust Gas Reingestion Studies on Lift-Engine VTOL Fighter Configurations"	
W. Barron and H. Frauenberger, Grumman Aerospace Corp.	334
"Ground Footprint Theoretical and Experimental Studies"	
H. A. Weber and A. Gay, General Dynamics Corporation	358
"VTOL Reingestion Model Testing of Fountain Control and Wind Effects"	
W. G. Hill, Jr., T. Luzzi, R. C. Jenkins, Grumman Aerospace	381
Corporation "Experimental Studies of Multi-jets in Ground Effect"	
D. H. Hickey, W. L. Cook, NASA Ames	396
"Correlations of Low-Speed Wind Tunnel and Flight Test Data for a VTOL and STOL Aircraft"	
A. L. Rosenblatt, Grumman Aerospace Corporation	417
"Ground Platform Thermal Footprints for VTOL Aircraft"	

E. Flow Vectoring Devices

Chairman: J. Curry, Naval Air Propulsion Test Center

E. H. Miller, Grumman Aerospace Corporation	433
"Development of Vectoring Devices for Jet V/STOL Aircraft"	
B. K. Hodder and J. V. Kirk, NASA Ames	458
"Large-Scale Studies of Propulsion-Flow Turning Devices for Fan-Powered V/STOL Aircraft"	
J. L. Palcza, Naval Air Propulsion Test Center	479
"Nozzle Deflectors for Navy V/STOL Fighters"	
T. A. Wynosky, Pratt & Whitney Aircraft Co.	496
"V/STOL Deflector Studies"	

VOLUME II

F. Thrust Augmenting Ejector Studies

Chairman: B. Quinn, Air Force Office of Scientific Research

K. S. Nagaraja, Air Force Flight Dynamics Lab "Wind Tunnel Studies of an Ejector-Wing Model Applicable to an Ejector Thrust Augmented V/STOL Aircraft" ^{x)}	
D. B. Garland, De Havilland Aircraft of Canada "Static Testing of Large-Scale Augmenter Wing Models"	518
W. J. Maegley, J. M. Lefferdo, Martin-Marietta "Critical Wall Jet Parameters for Suppressing Diffuser Stall in a Thrust Augmenting Ejector"	530
D. D. Papailiou, Jet Propulsion Laboratory "The Structure of Two-Dimensional Wall-Jets in the Presence of Adverse Pressure Gradients"	554
W. G. Hill, Jr. and R. C. Jenkins, Grumman Aerospace Corp. "Effects of Initial Conditions on Mixing Rates of Turbulent Jets"	624
E. F. Schum, Rockwell International Corporation "Techniques for Increasing Jet Spreading Rates for Ejector Type Augmentors"	639
V. R. Stewart, E. R. White, W. E. Palmer, Rockwell International. "Aerodynamic Analysis of an Integrated V/STOL Thrust Augmenter Lift System Concept"	664
T. C. Tai, Naval Ship Research & Development Center "Analysis and Design of Thrust Augmenting Ejectors"	702

^{x)} This paper was not submitted for publication

G. Lift Fan Studies

Chairman: D. H. Hickey, NASA Ames Research Center

N. O. Stockman, NASA Lewis Research Center	722
"Potential and Viscous Flow Prediction in V/STOL Propulsion System Inlets"	
K. S. Nagaraja, Air Force Flight Dynamics Lab	
"A Two-Dimensional Potential Flow Theory for a Fan-in-Wing Type V/STOL Aerodynamic Problem" x)	
R. A. Rozendaal, J. D. Schmitt, N. A. Durando,	743
McDonnell Douglas Corporation "Lift Induced on a Wing by an Adjacent Lift/Cruise Fan"	
U. W. Schaub, National Research Council of Canada	777
"Analytical Prediction of the Aerodynamic Performance of an Axially Short Lifting Fan in a Cross Flow"	
D. R. Hoad, NASA Langley	833
"Techniques and Problems Associated with Wind Tunnel Testing of Multi-Fan VTOL Aircraft Models"	
R. L. Kosson and R. L. Grossman, Grumman Aerospace Corporation . .	853
"Theoretical and Experimental Studies of a Rotary Augmentor"	
J. H. Diedrich, NASA Lewis	874
"Summary of Model VTOL Lift Fan Tests Conducted at NASA Lewis Research Center"	
D. J. Renselaer, Rockwell International Corporation	897
"Effects of Jet Exhausts on Aerodynamic Characteristics of a Twin-Lift-Fan Aircraft in the STOL Mode"	

x) This paper was not submitted for publication

	Page
H. Transition Aerodynamics	
Chairman: P. T. Wooler, Northrop Corporation	
R. P. Weston, NASA Langley	918
"A Description of the Vortex Pair Associated with a Jet in a Cross Flow"	
H. Snel, National Aerospace Laboratory, Amsterdam	951
"The Interaction between a Jet and a Non-Uniform Mainflow and Jet-Airframe Interaction"	
M. M. Winston, NASA Langley	978
"Propulsion Induced Aerodynamic Interference Effects on Jet-Lift VTOL Aircraft"	
M. Siclari, D. Migdal, Grumman Aerospace Corporation	998
J. L. Palcza, Naval Air Propulsion Test Center "Development of Theoretical Models for Jet Induced Effects on V/STOL Aircraft"	
R. E. Mineck, NASA Langley	1016
"Comparison of Theoretical and Experimental Interference Effects on a Jet VTOL Airplane Model"	
J. R. Chambers, NASA Langley	1035
"Free-Flight Model Investigation of Vertical-Attitude VTOL Fighters"	

FOREWORD

High-speed V/STOL aircraft operating from widely dispersed platforms have become of increasing interest to the U.S. Navy. Implementation of this dispersed force concept requires a well developed high-performance V/STOL aircraft technology base so that the production of such aircraft can proceed with a minimum of technical and financial risk.

There are a number of phenomena and problems unique to high-speed V/STOL aircraft which do not occur on conventional aircraft or on low-speed V/STOL aircraft and therefore require special attention and understanding. Jet-incuded phenomena (jet-induced lift and control effects, hot-gas footprint and reingestion characteristics etc.) can have a decisive influence on the performance of lift-plus-lift/cruise engine powered aircraft. Equally important are the flow phenomena that occur on aircraft using the lift fan or ejector concept. The proper design of these aircraft must account for the interdependence of the aerodynamic and propulsion phenomena. Unfortunately, the flows involved are so complex as to preclude their purely theoretical prediction at this time. Realistic flow simulation in model tests, on the other hand, is hampered by the present uncertainty about the proper scaling laws and by the strong dependence on a variety of parameters requiring testing of many different configurations in order to find an optimal design. Therefore, better predictive techniques are clearly needed in order to reduce these testing requirements and to guide the planning of experimental programs.

In recognition of the need to review the current state-of-the-art in this field and to stimulate research on prediction methods for propulsive flows and propulsion/aerodynamic interference effects on Jet-V/STOL aircraft

the Naval Air Systems Command conducted a "Workshop on Prediction Methods for Jet-V/STOL Propulsion Aerodynamics". It was quite gratifying to see the excellent response to the call-for-contributions and the participation during the meeting which was much greater than anticipated. The following pages contain the formal papers presented during the Workshop which are made available to serve as a source of reference and stimulus for further work in this field.

H. J. MUELLER
Research Administrator
Naval Air Systems Command

ACKNOWLEDGEMENTS

A number of people contributed to the success of this Workshop and their contributions are gratefully acknowledged.

Dr. H. J. Mueller of the Naval Air Systems Command initiated and supported this meeting. Mr. R. Margason of NASA Langley and Mr. D. Hickey of NASA Ames provided much helpful advice and assistance.

CAPT von Gerichten, the Director of the Advanced Systems Directorate at the Naval Air Systems Command, gave the welcome address which was very much appreciated.

Dr. L. V. Schmidt, Mr. J. Curry, Mr. D. H. Hickey, Mr. R. J. Margason, Dr. D. Migdal, Dr. B. Quinn, Prof. G. K. Serovy and Dr. P. T. Wooler contributed greatly to the panel discussion at the end of the meeting.

Mrs. Bette Harvey and Miss Janet Perkins assisted in numerous ways with careful attention to detail.

Finally, and most importantly, special thanks go to the session chairmen and participants for their many contributions and excellent cooperation.

MAX F. PLATZER
Workshop Chairman
and Proceedings Editor

List of Participants

WORKSHOP ON PREDICTION METHODS FOR JET V/STOL PROPULSION AERODYNAMICS

28-31 July 1975

Anderson, Bernhard
NASA Lewis

Barron, Walter A.
Grumman Aerospace Corp.

Bellar, Dr. F. J.
Rockwell International
Columbus

Beverage, Allan D.
General Electric Co.
Cincinnati, Ohio

Brennan, Thomas J.
NADC

Brown, Milfred W.
NAVAIR

Castells, Onofre
General Electric
Evendale, Ohio

Cavage, Robert L.
Rockwell International
Los Angeles

Cea, Robert A.
Grumman Aerospace

Chandra, Subrato
West Virginia University

Clark, John W.
NADC

Crosse, George W.
British Embassy

Davenport, Franklyn J.
Boeing Commercial Airplane Co.

Davies, Eric R.
Rolls Royce Aero Engines, Inc.

De Los Santos, S.
DT NSRDC

Driggers, Herbert H.
LTV Vought Systems Division

Durando, Norbert A.
McDonnell Douglas

Englar, Robert J.
Naval Ship R&D Center

Fagan, John R.
Detroit Diesel Allison Div. GMC

Ford, John C.
Rockwell International
Los Angeles

Fortenbaugh, Robert L.
NADC

Frank, Lawrence A.
Naval Ship R&D Center

Frauenberger, Howard C.
Grumman Aerospace Corp.

Garland, D. B.
DeHavilland Aircraft of Canada

Gibbs, Edward H.
West Virginia University

Girard, Peter F.
Teledyne Ryan Aeronautical

Gustafson, W. A.
Purdue University

Hakkinen, Raimo J.
McDonnell Douglas

Halkett, Alexander M.
Dept. of Industry, Can. Gov't.

Harris, Julius E.
NASA Langley

Heimberger, Howard C.
McDonnell Aircraft

Hawkins, W. Kent LTV Aerospace	McDonald H. United Tech. Res. Center
Hockman, Marion T. NAVAIR	Migdal, David Grumman Aerospace Corp.
Hoffman, Gilbert H. McDonnell Douglas	Mikolajczak, A. A. Pratt & Whitney Aircraft
Hudson, S. Michael Detroit Diesel Allison GMC	Miller, Eugene Grumman Aerospace Corp.
Jenkins, Richard C. Grumman Aerospace Corp.	Miller, Richard H. NAVAIR
Johnston, Roy S. Teledyne Ryan Aeronautical	Mueller, Dr. H. J. NAVAIR
Kaminski, Joseph L. NADC	Murphy, Richard D. David W. Taylor Naval Ship R&D Center
Kemper, Robert G. LTV Aerospace	Murray, James J. U.S. Army Research Office
Kirk, Jerry V. NASA Ames	Nagaraja, K. S. AFFDL, WPAFB
Kotansky, Donald R. McDonnell Douglas Research Lab.	Nichols, Donald L. LTV Aerospace Corp.
Kuhn, R. E. NASA Langley	O'Donnell, Robert M. Advanced Technology Ctr.
Lynch, Elizabeth M. NAVAIR	Palcza, John L. NAPTC
Luzzi, Theodore E. Grumman Aerospace Corp.	Palmer, William E. Rockwell International Columbus
Maegley, Wendel J. Martin-Marietta	Papailiou, Demos D. JPL/CIT
Margason, Richard J. NASA Langley	Patterson, Ashton M. Canadian Embassy
Markow, Edward G. Grumman Aerospace Corp.	Patton, James R. Jr. ONR
Marshall, Frank Boeing	Platzer, Prof. Max F. Naval Postgraduate School
McCormick, Barnes W. Penn State University	

Quinn, Brian
AFAPL

Renselaer, Dirk J.
Rockwell International
Los Angeles

Roberts, Alan F.
AFR Co.

Rosenblatt, Arnold L.
Grumman Aerospace Corp.

Rosenstein, Harold
Boeing Vertol Co.

Sajben, Miklos
McDonnell Douglas Res. Lab.

Sanders, Karl L.
NWC

Sattler, Donald F.
LTV Aerospace Corp.

Schaub, Uwe W.
National Research Council of Canada

Schmidt, Prof. Louis V.
NAVAIR

Schindel, Leon H.
NSWC

Schum, Gene
Rockwell International
Columbus

Schweiger, M.
Rockwell International
Columbus

Sears, William B.
LTV

Serovy, George
Iowa State University

Sherrieb, Harold E.
LTV

Skifstad, James G.
Purdue University

Smith, Robert E. Jr.
Lockheed-Calif. Co.

Snel, Herman
Nat. Aerospace Lab NLR

Standahar, Ray M.
ODDR&E

Stark, Will W.
Northrop Corp.

Stewart, Vearl R.
Rockwell International
Columbus

Stockman, Norbert O.
NASA Lewis

Straub, William L. Jr.
LTV Aerospace

Tai, Tsze C.
David Taylor Naval Ship R&D Center

Tankursley, John C.
USN

Thames, Frank C.
LTV Aerospace Corp.

Walker, Sylvanus C.
LTV Aerospace Corp.

Wang, Timothy
The Boeing Co.

Ward, John F.
NASA

Weber, Henry A.
General Dynamics Convair

Weston, Robert P.
NASA Langley

Wilson, Thomas L.
ONR

Winston, Matthew M.
NASA Langley

Wohllebe, Fred A.
Grumman Aerospace Corp.

Wolfe, George W.
LTV Aerospace Corp.

Woolard, Henry W.
USAF Flight Dynamics Lab.
WPAFB

Wooler, Peter T.
Northrop Corporation

Wynosky, Thomas A.
Pratt & Whitney Aircraft

Viets, Hermann
Aeropropulsion Lab/RJT
WPAFB

"V/STOL CONCEPT SENSITIVITY STUDY"

D. F. Sattler

LTV AEROSPACE CORPORATION

ABSTRACT

The study objective was to provide a definitive basis for long range V/STOL related R&D planning within the Navy. Six varied VTOL aircraft concepts served as the basis for conducting sensitivity studies of twenty-three aero-propulsion interface technology topics. The end item of the study was a ranking of the technology topic sensitivity results in terms of incremental takeoff gross weight, which permits selecting and justifying future R&D tasks.

V/STOL CONCEPT SENSITIVITY STUDY

I. INTRODUCTION

Prior to considering the various facets of Jet V/STOL Propulsion Aerodynamics Prediction Methodology, it is of interest to examine the impact of these phenomena on aircraft design. Vought Systems Division of LTV Aerospace Corporation has conducted a "V/STOL Concept Sensitivity Study" under contract to the Naval Air Development Center to investigate the impact of technology uncertainties on aircraft takeoff gross weight (TOGW). The objective of the study was to provide a definitive basis for long-range V/STOL related R&D planning within the Navy by identifying high impact technology topics.

To fulfill the study objective, four tasks were completed. First, six V/STOL design concepts were sized to common mission rules. Next, each of twenty-three technology topics was translated into a physical variable and estimates of these variables were determined. Thirdly, the sensitivity of the topics in terms of incremental takeoff gross weight was evaluated. The results were then ranked as a basis for establishing R&D priorities. The purpose of this paper is to describe the aircraft and propulsion concepts, discuss the technology topics, show the impact of technology uncertainties, and summarize the conclusions of the study.

II. MISSION DEFINITION AND PROPULSION CONCEPTS

Highlights of the ground rules used to size the baseline aircraft are presented in Figure 1. The propulsion system, weight, and aerodynamic technology levels reflect an IOC of 1983.

The design missions are shown in Figure 2. The Deck Launched Intercept (DLI) and Subsonic Surface Surveillance (SSS) missions are treated with equal importance. The DLI mission calls for a vertical takeoff (VTO), supersonic dash to target, combat at the target, and a best cruise altitude and velocity (BCAV) return to base. The SSS mission defines BCAV outbound and return segments with a loiter and combat period while on station. External fuel and a short takeoff (STO) capability are permitted for the SSS mission. Specific levels of the following performance constraints are also demanded:

- o Specific Excess Power (SEP)
- o Maximum Mach Number
- o Acceleration Time
- o Load Factor
- o Ceiling
- o Vertical T/W Ratio
- o STO Distance

PROPULSION SYSTEMS

Six diverse propulsion systems provide generality and assure that study results are broadly applicable. The propulsion systems (Figure 3) range from a low disk loading (X-wing) concept to a Multi Bypass Ratio (MBPR) propulsion system powered aircraft. Other designs are a lift plus lift/cruise, deflected thrust, vectored thrust (AV-8A type) and thrust augmented wing (XFV-12A type). Six aircraft were configured to incorporate these propulsion systems as follows:

Lift Plus Lift/Cruise (Figure 4)

The lift plus lift/cruise aircraft is a modified delta canard arrangement utilizing two lift jets and a vectored lift/cruise engine equipped with a ventral nozzle for VTOL operation. Lift engine bleed air is used for control in hover.

X-Wing (Figure 5)

The X-wing design is a high risk approach utilizing an "X" wing planform as a rotor for VTOL and stopped for conventional flight. Cyclic pitch is used for pitch and roll control in hover with yaw provided by a thrust vectoring device. Residual engine thrust is used in hover to counter the "rotor" torque.

Deflected Thrust (Figure 6)

This concept incorporates a separate flow engine with a remote turbine. Thrust vectoring is achieved by turning the secondary fan air by a flap system while primary air is turned by the Coanda effect. Burning of the secondary air in hover is required to minimize aircraft size. A JP-LOX system is used for hover control.

Vectored Thrust (Figure 7)

The vectored thrust aircraft is a modified delta canard arrangement equipped with a Pegasus type engine with vectorable nozzles and burning in hover. Control in hover is achieved by engine bleed air.

TAW (Figure 8)

The thrust augmented wing (TAW) design utilizes the hypermizing nozzle principle developed at ARL. Experimental data shows that ejector augmentation ratios of 2.0 can be achieved. Considering installation effects, a propulsion system augmentation ratio of 1.71 is projected for the concept. Differential thrust is used for control in hover.

CFF (Figure 9)

The cross flow fan (CFF) aircraft features a multi bypass ratio propulsion system. The cross flow fan serves as a thrust augmentor in hover and provides an efficient bypass ratio for subsonic cruise. For supersonic flight the cross flow fans are shut down and the turbojets are utilized.

III. TECHNOLOGY TOPICS

The second task was to quantify twenty-three aero-propulsion interface technology topics. The topics are divided into seven major groupings dealing with:

Inlet Performance

Flying Qualities

Design Thrust to Weight

Propulsion Induced Effects

Temperature

Noise

Aerodynamic Effects

For each of the six aircraft concepts nominal, optimistic, and pessimistic levels of the twenty-three technology topics were identified. The nominal level was used in sizing the baseline aircraft. The optimistic and pessimistic levels identify the technology uncertainty limits which reflect confidence in the estimation process and suggest the need for R&D. An example of the quantification procedure is illustrated in Figure 10. The nominal value of pressure recovery is 0.96, whereas the optimistic level is 0.99 and the pessimistic level is 0.93. For several of the topics the optimistic level, which potentially results in a TOGW reduction, was taken at the approximate physical limit. An example of a physical limit is considering the skin friction drag associated with laminar flow instead of turbulent flow. The pessimistic level potentially results in a TOGW penalty and is representative of the risk involved if a technology topic level does not materialize. In the following paragraphs the twenty-three technology topics are briefly reviewed to:

- o Identify the associated aircraft design problem
- o Quantify the optimistic, nominal and pessimistic technology levels
- o Show the factor affecting TOGW

The lift plus lift/cruise aircraft, where possible, is used to illustrate the quantification process.

INLET PERFORMANCE

Four topics addressing inlet performance effects, as shown in Figure 11, are:

- o Inlet Pressure Recovery - Hover
- o Hot Gas Ingestion
- o Inlet Temperature Distortion
- o Inlet Pressure Distortion

All four topics impact on TOGW by affecting installed thrust.

Inlet pressure recovery-hover, which is the ratio of total pressure at the engine face (P_{T_2}) to the ambient total pressure (P_{T_0}), has lift engine quantification levels of 1.00, 0.99, 0.96 for the optimistic, nominal, and pessimistic levels respectively. Recovery level is a critical item considering that a 1% change in pressure recovery affects lift engine thrust by about 2.5%.

Hot gas ingestion, which is treated as a uniform inlet temperature rise, considers both near field and far field recirculation. For the lift plus lift/cruise aircraft the near field effects are the more critical consideration. The optimistic, nominal, and pessimistic levels of hot gas ingestion are 0°, 12°, and 20°F respectively. Temperature rise affects installed thrust by approximately 1% per 3°F temperature change.

Inlet temperature and pressure distortion are non-uniform variations that may ultimately result in surge and/or compressor stall. Temperature and pressure distortion levels of 10% deviation from the nominal, result in 2.5% and 1.6% change in thrust levels respectively.

FLYING QUALITIES

The three topics addressing flying qualities effects, presented in Figure 12, are:

- o Control Power Level
- o Buoyant Pitching Moment
- o Induced Trim Change

The optimistic, nominal, and pessimistic control power levels were determined by examining the capability of successful VTOL aircraft and using MIL-83300 as a guide. The levels also agree well with AGARD 577. Aircraft size is affected by engine bleed and/or differential thrust levels for propulsion systems which are integrated into the attitude control system.

Buoyant pitching moment deals with the induced flow field in ground effect hover and the resultant moments on the aircraft. The effect diminishes at higher levels of h/b , see Figure 12, from reference 1.

Induced trim change due to power considers the transition problem and the influence of thrust balance and the induced flow field over the control surfaces. The influence on the control power requirements is the driving consideration.

DESIGN THRUST TO WEIGHT

Installed thrust to weight ratio topics (Figure 13) are:

- o T/W Margin-Installed
- o T/W Margin - STO/VL
- o Engine-Out Thrust Asymmetry

Thrust to weight margin - installed is varied between 1.0 and 1.3 in ground effect (IGE). This variation in the topic is used to assess the impact of installed T/W on TOGW. A high value of installed T/W may be required for growth potential, operation in more severe atmospheric conditions than design, or to account for more severe values of other technology topics such as suckdown or hot gas ingestion.

Thrust to weight margin-STO/VL addresses the impact of eliminating the VTOL requirement and replacing it with a STO requirement. Thrust to weight ratio is varied between 0.75 and 1.00. It is interesting to note that for vertical landing, a 0.75 T/W corresponds to a rate of sink of 25 fps from 40 feet with no forward speed.

Engine-out thrust asymmetry examines the effect of designing for an engine failure. The three multiple engine concepts are evaluated by varying engine size to achieve a $T/W = 1.0$ with the critical engine failed.

PROPULSION INDUCED EFFECTS

Topics addressing the propulsion induced effects as presented in Figure 14 are:

- o Suckdown
- o Lift Augmentation

- o Downwash Velocity

Suckdown is the force associated with the entrainment of air by a jet causing reduced pressure on the lower fuselage and/or wing surfaces resulting in a net downward force or suckdown. Suckdown forces can be reduced or cancelled by a strong fountain which is formed by the meeting of two or more wall jets. As shown in the Figure 14, from reference 2, at a height to span ratio (h/b) of 0.2, the suckdown force can vary by 10% depending on configuration and fountain strength. A note of caution for a concept utilizing a hot jet - the stronger the fountain, the more attention hot gas ingestion has to be given.

Lift augmentation, or augmentation ratio, is critical to the TAW and CFF aircraft because of installed thrust requirements. The TAW aircraft utilizes an ejector augmentation ratio of 2.0, which ARL test data, reference 3, shows can be achieved. Due to installation effects, e.g. duct losses and three-dimensional effects, the nominal propulsion system augmentation ratio is 1.71 with the optimistic and pessimistic levels being 1.85 and 1.50 respectively.

Downwash velocity is affected to a small extent by varying bypass ratio, but a variation between the six baseline aircraft yields the best overall sensitivity. If low downwash is a driving consideration, the X-wing aircraft offers this potential.

THERMAL ENVIRONMENT

Thermal environment investigates the structural heating problems associated with VTOL aircraft. Figure 15 shows the structural heating problem in the area of the lift engines as well as the heating due to the fountain between the lift and lift/cruise engines. Aircraft TOGW sensitivity is achieved by varying structural temperature by $\pm 200^\circ\text{F}$ from the nominal of 900°F and assessing the structural weight impact.

NOISE EFFECTS

The topics addressing the impact of noise, shown in Figure 16, are:

- o Acoustic (Structural) Environment
- o Audible Sound

Audible sound may be a critical item based on detection, cockpit, or ground crew noise consideration. Bypass ratio yields a small variation, whereas a comparison between concepts gives the best overall sensitivity. The X-wing designs offers the potential of the lowest noise level of the six concepts. Acoustic (structural) environment examines the influence of noise on aircraft TOGW. Noise level is varied by $\pm 6\text{dB}$ from the nominal of 186 dB to assess the impact of noise on structural weight.

AERODYNAMIC EFFECTS

The topics affecting the aerodynamics of the aircraft, Figure 17, are:

- o Equivalent Skin Friction Drag Coefficient - C_{f_e}
- o Drag Rise Coefficient Based on Frontal Area - ΔC_{D_π}
- o Drag Divergence Mach Number - M_{DD}
- o Oswald Efficiency Factor - e
- o Buffet Onset Lift Coefficient - $C_{L_{B_0}}$
- o Vectored Thrust Lift Augmentation - $\Delta C_{L_{B_0}}$
- o Buffet-Free Descent Corridor

The first five parameters are applicable to CTOL aircraft as well as VTOL. The optimistic level of the topics was established by determining the approximate physical limit. For C_{f_e} , this level corresponds to laminar flow over the wing, tails, and 50% of the fuselage yielding a C_{f_e} level of approximately .0010. The physical limit of ΔC_{D_π} (≈ 0.10) is achievable based on tests of Adams low drag bodies. Drag divergence Mach number physical limit is assessed at 1.0 considering shockless flows. The physical limit of Oswald efficiency factor "e" is projected to be 2.0, which is considered achievable by developing an efficient means of cancelling the tip vortex or possibly by an out-of-plane arrangement. The optimistic level of buffet onset at the maneuver condition is based on attaining a pressure distribution approaching an absolute vacuum.

Vectored thrust augmentation and buffet-free descent corridor are unique to VTOL. Thrust vectoring is used to enhance maneuverability by yielding additional load factor capability. Buffet-free descent corridor capability is a primary consideration for aircraft that rely on power for induced lift and drag while maintaining acceptable angle of attack and descent capability such as for a tiltwing turboprop aircraft, but of limited value for the aircraft considered in the study.

IV. TECHNOLOGY IMPACT

Incremental TOGW is used as the criteria to measure the payoff of a technology. TOGW, while not being all inclusive, is used as the "yardstick" because of its readily identifiable nature and its overall appeal.

Figure 18 shows a typical sensitivity comparison for all six designs. The optimistic, nominal, and pessimistic levels of inlet pressure recovery - hover are noted by O, N, and P respectively. The deflected thrust and TAW aircraft show the highest overall sensitivity. Notice that the vectored thrust and CFF aircraft have certain critical performance constraints precluding additional TOGW reductions at high levels of recovery.

For the lift plus lift/cruise aircraft pitch control is achieved by bleed from the lift engines. Figure 19 shows that if the high (pessimistic) levels of pitch control power are demanded, a 2200 lb TOGW penalty results. However, reducing the control power level to the lower (optimistic) level results in only a 900 lb TOGW reduction due to the $T/W = 1.10$ constraint becoming a critical sizing consideration.

Figure 20 indicates that increasing suckdown from the 3% nominal value to 10% results in a 400 lb TOGW penalty for the lift plus lift/cruise aircraft. Reducing suckdown to 0% reduces TOGW about 150 lb.

The impact of reducing C_{f_e} to the physical limit is presented in Figure 21. The lift plus lift/cruise aircraft shows a significant 3750 lb weight reduction if these levels of drag can be achieved.

V. RANKING OF TECHNOLOGY TOPICS

The following approaches are utilized to assure the proper selection of high impact technology topics for establishing R&D priorities:

- o Potential Improvement Assessment
- o Potential Risk Assessment
- o Combined Improvement and Risk Assessment by Concept
- o Combined Ranking Matrix

Figure 22 presents the "Potential Improvement Assessment", which is the total of TOGW increments for the six aircraft concepts at the optimistic uncertainty level. The study indicates that three aerodynamic parameters when taken to the physical limit offer the highest potential TOGW reduction. The highest ranking VTOL oriented topic is "T/W margin-installed."

The "Potential Risk Assessment", Figure 23, is the total of TOGW increments for the six aircraft concepts at the pessimistic uncertainty level. The figure shows that the potential TOGW increase is most significant for the VTOL oriented topics. Six VTOL oriented topics show sensitivity rankings higher than the aerodynamic parameter. Thus the potential risk of a topic failing to achieve nominal technology levels is highest for the VTOL oriented technology topics.

The "Combined Improvement and Risk Assessment" is shown for the lift plus lift/cruise concept in Figure 24. This is the TOGW variation between the optimistic and pessimistic levels and may be thought of as the "state of the art" band. For the lift plus lift/cruise aircraft " C_{f_e} " is the most sensitive topic with "control power level" second. Accomplishing a similar technology topic ranking for each concept leads to a ranking matrix in Figure 25. A ranking of "1" denotes that the topic has the highest sensitivity. Summing the rankings of the six concepts and dividing by the

number of concepts effected yields an average ranking. Again " C_{fe} " is the most sensitive topic overall with "T/W margin-installed" second.

VI. CONCLUSIONS

Based on the preceding ranking approaches, the following technology topics have the largest potential TOGW impact and are recommended for R&D planning:

VTOL Oriented Topics

- o T/W Margin-Installed
- o Inlet Pressure Recovery-Hover
- o Control Power Level
- o Lift Augmentation
- o Suckdown
- o Hot Gas Ingestion

Topics Applicable to both VTOL and CTOL

- o Equivalent Skin Friction Drag Coefficient - C_{fe}
- o Drag Rise Coefficient Based on Frontal Area - $\Delta C_{D\pi}$
- o Oswald Efficiency Factor - e

REFERENCES

1. Krenz, G. and Barche, J., "Jet Influence on V/STOL-Aircraft in the Transitional and High Speed Flight Regime", AGARD-CP-27, Paper 2, September 1967.
2. Barche, J., "Jet Lift Problems of V/STOL Aircraft", AGARD-CP-143, Paper 16, April 1974.
3. Quinn, B., "Recent Developments in Large Area Ratio Thrust Augmentor", AIAA Paper No. 72-1174, AIAA/SAE 8th Joint Propulsion Specialist Conference, November-December 1972.

- SCS VFA STUDY GUIDELINES – 25 APRIL 1973
- IOC OF 1983
- RUBBERIZED PROPULSION SYSTEMS
- DESIGN MISSIONS
 - DLI
 - SSS
- ADVANCED MATERIALS
- FBW – RSS (LONGITUDINAL)

EQUAL IMPORTANCE

FIG. 1 HIGHLIGHTS OF STUDY GROUND RULES

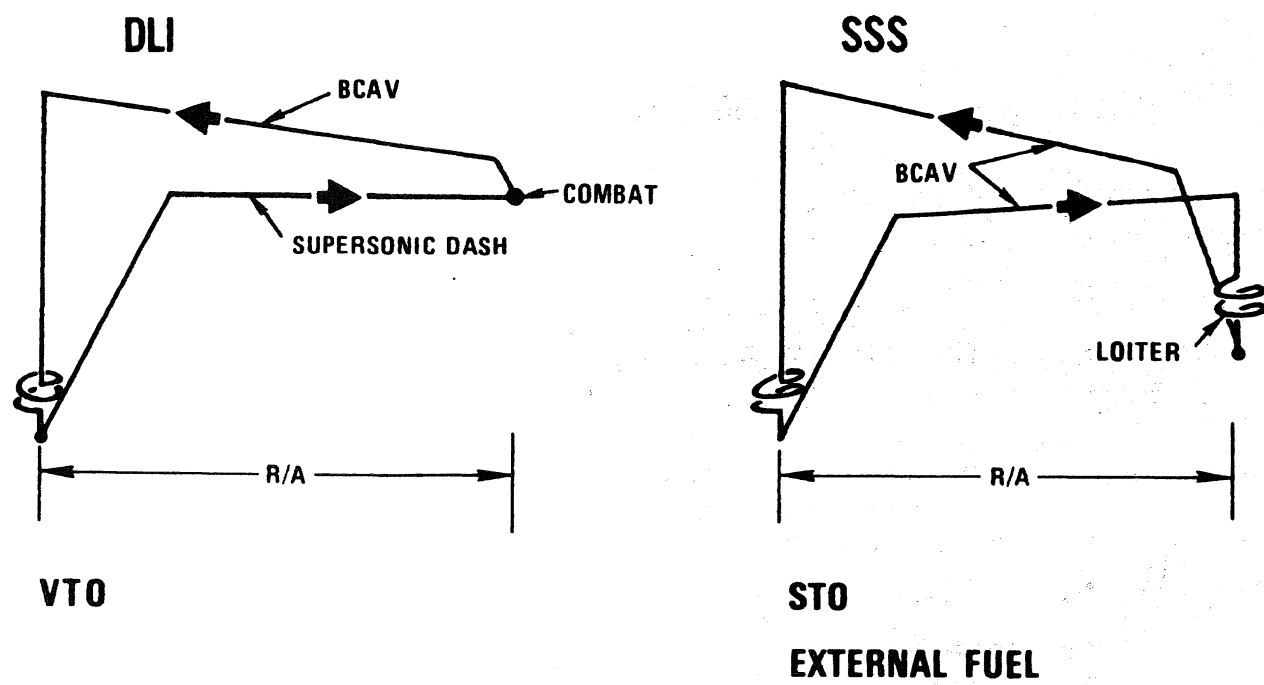
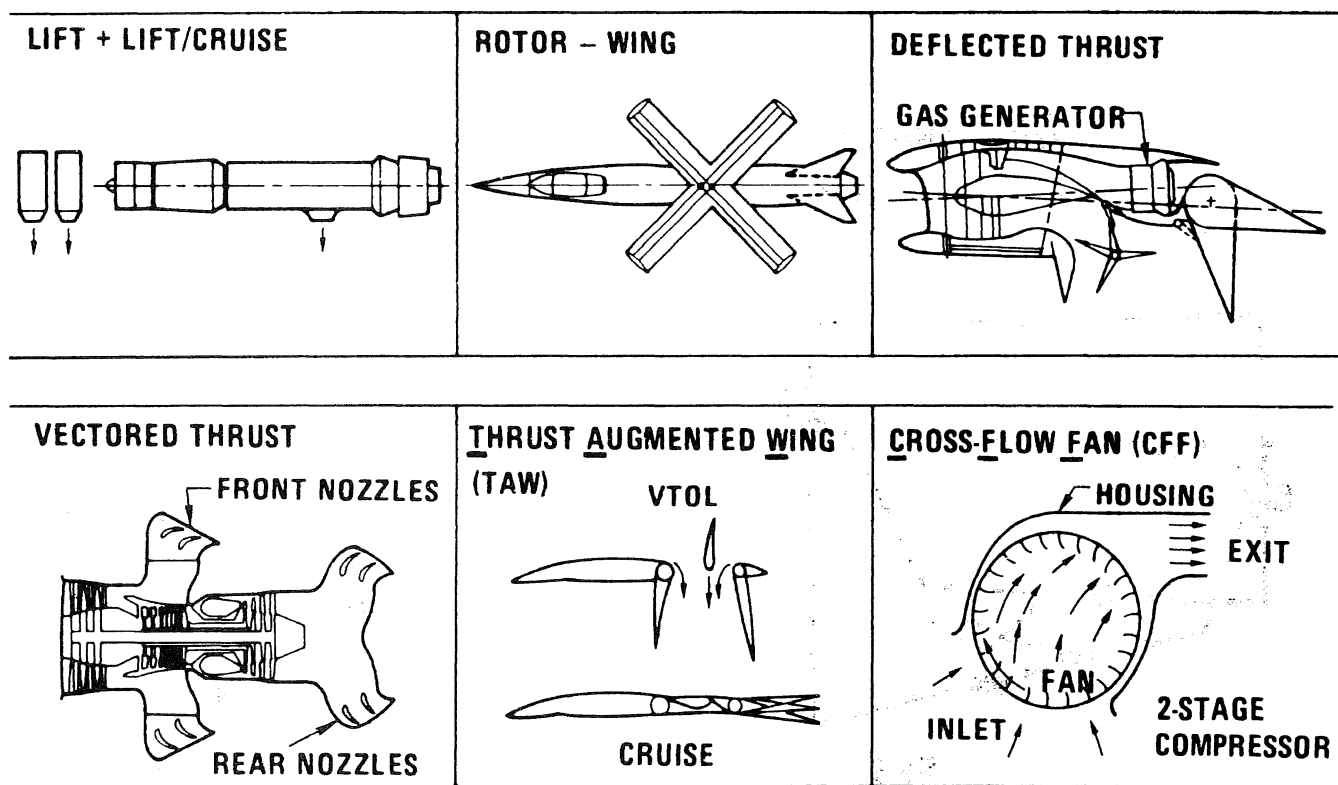


FIG. 2 MISSION DEFINITION



• SIX VTOL CONCEPTS PROVIDE GENERALITY AND ASSURES R&D IS BROADLY APPLICABLE

FIG. 3 BASELINE PROPULSION SYSTEMS

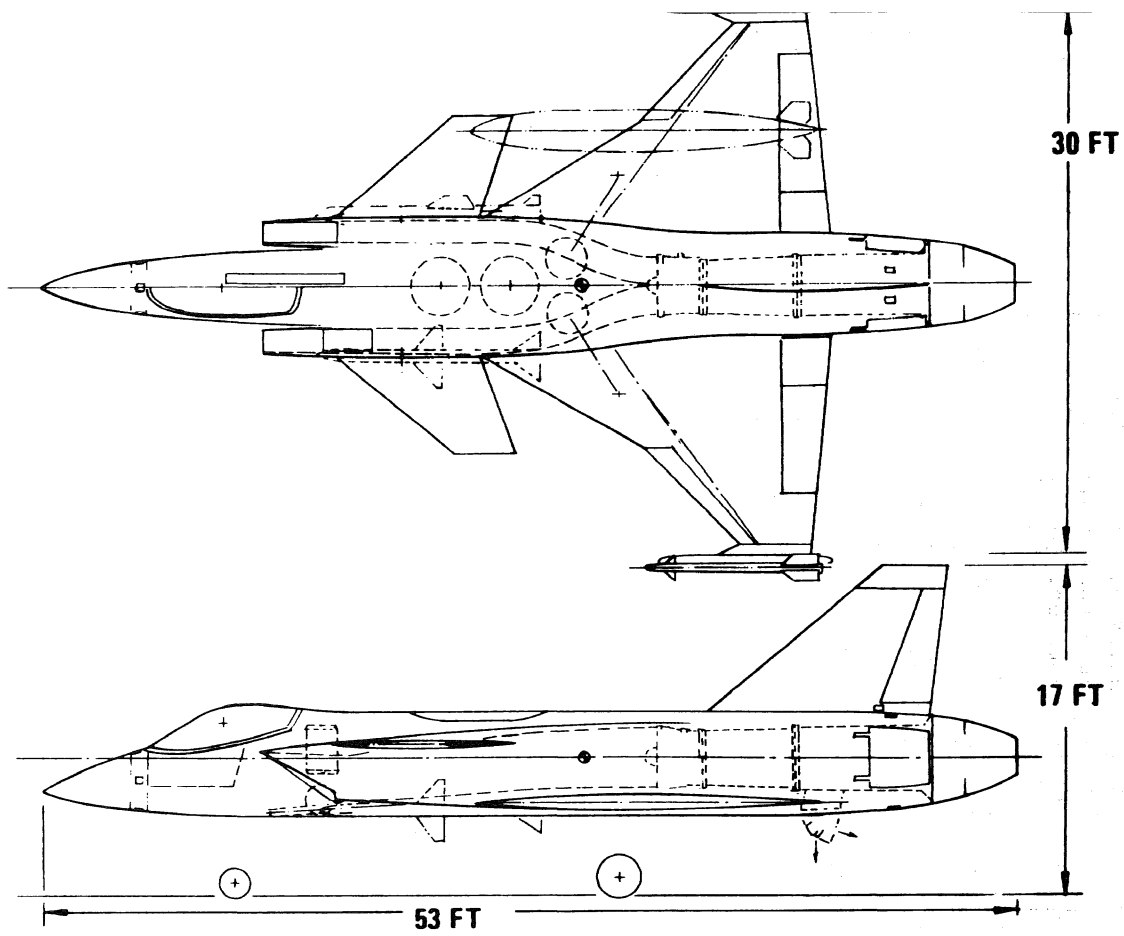


FIG. 4 LIFT PLUS LIFT/CRUISE AIRCRAFT

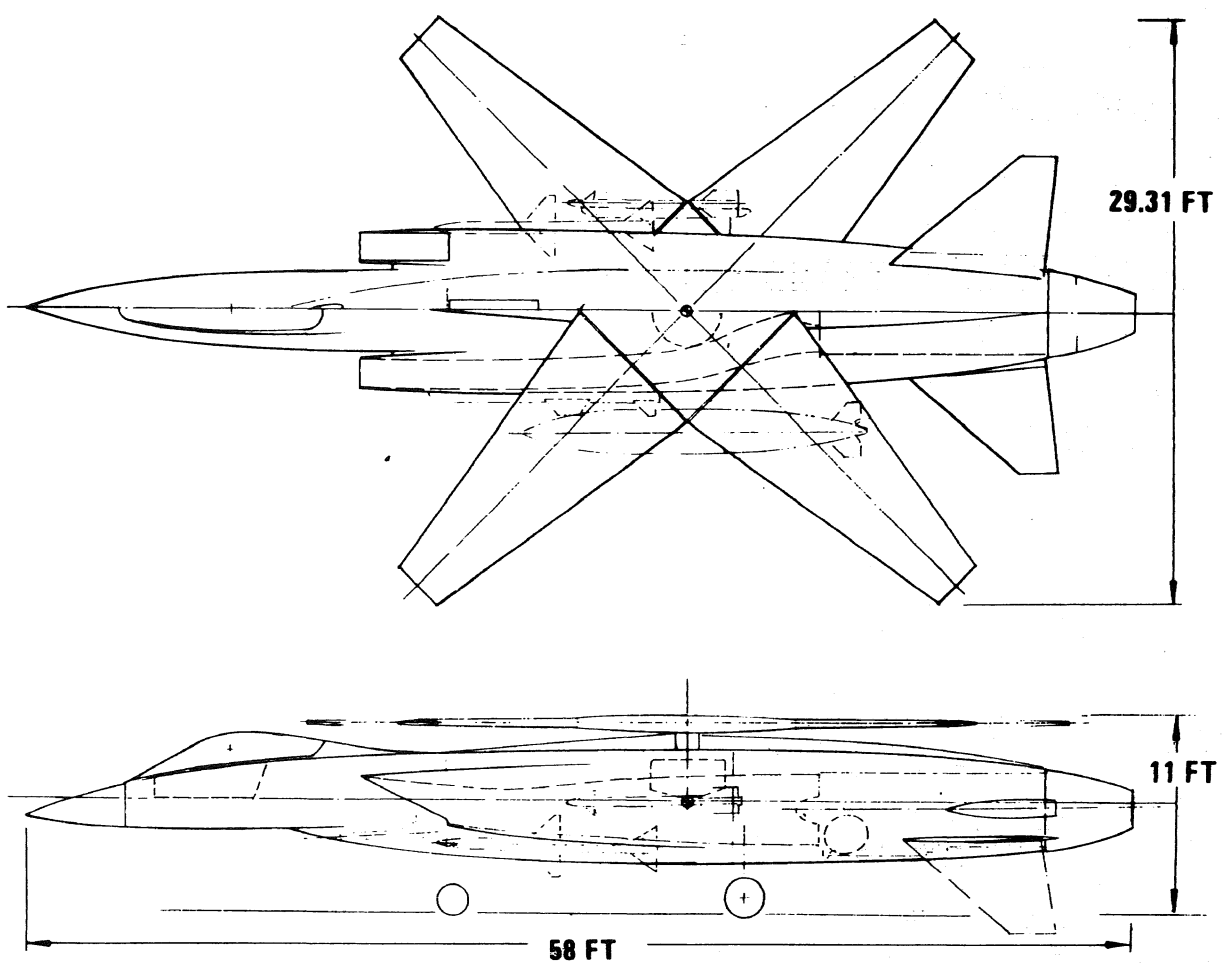


FIG. 5 X-WING AIRCRAFT

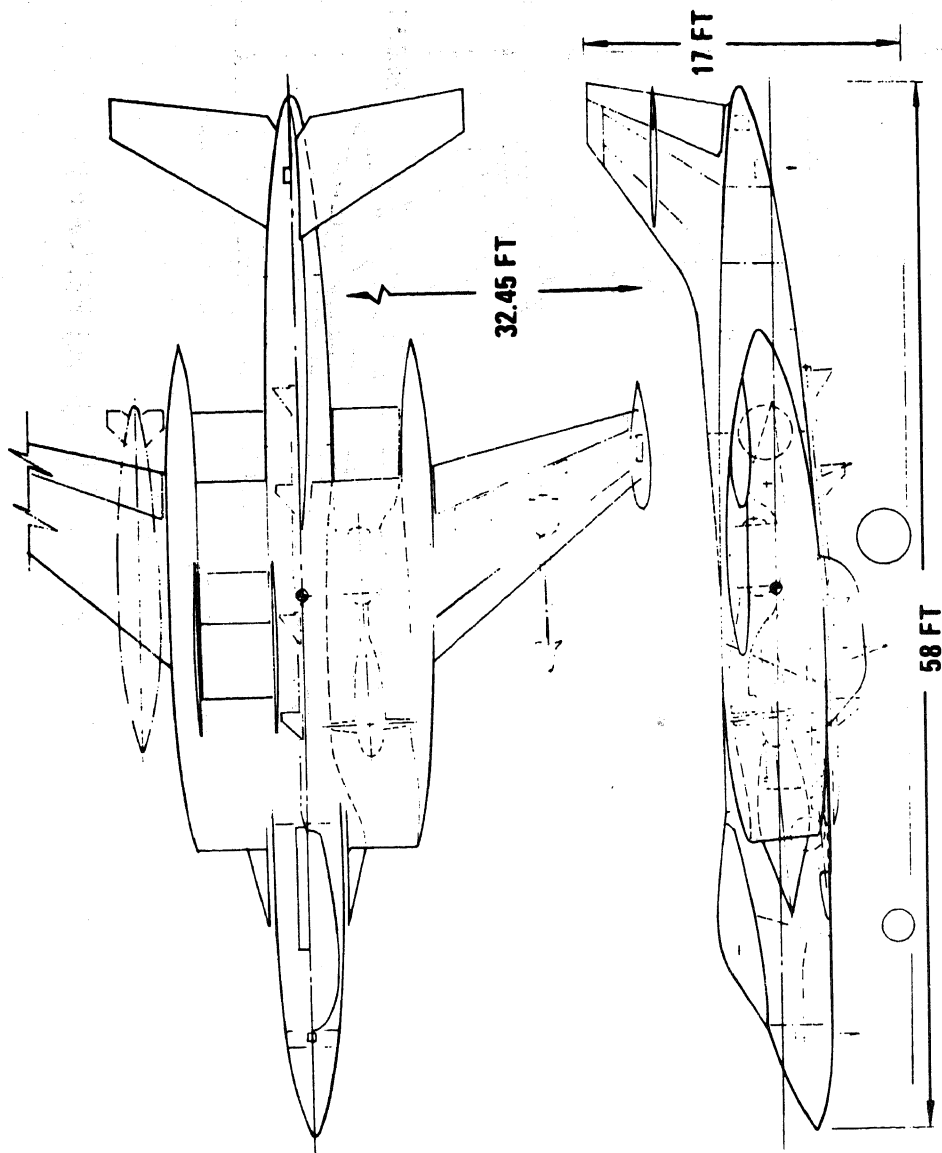


FIG. 6 DEFLECTED THRUST AIRCRAFT

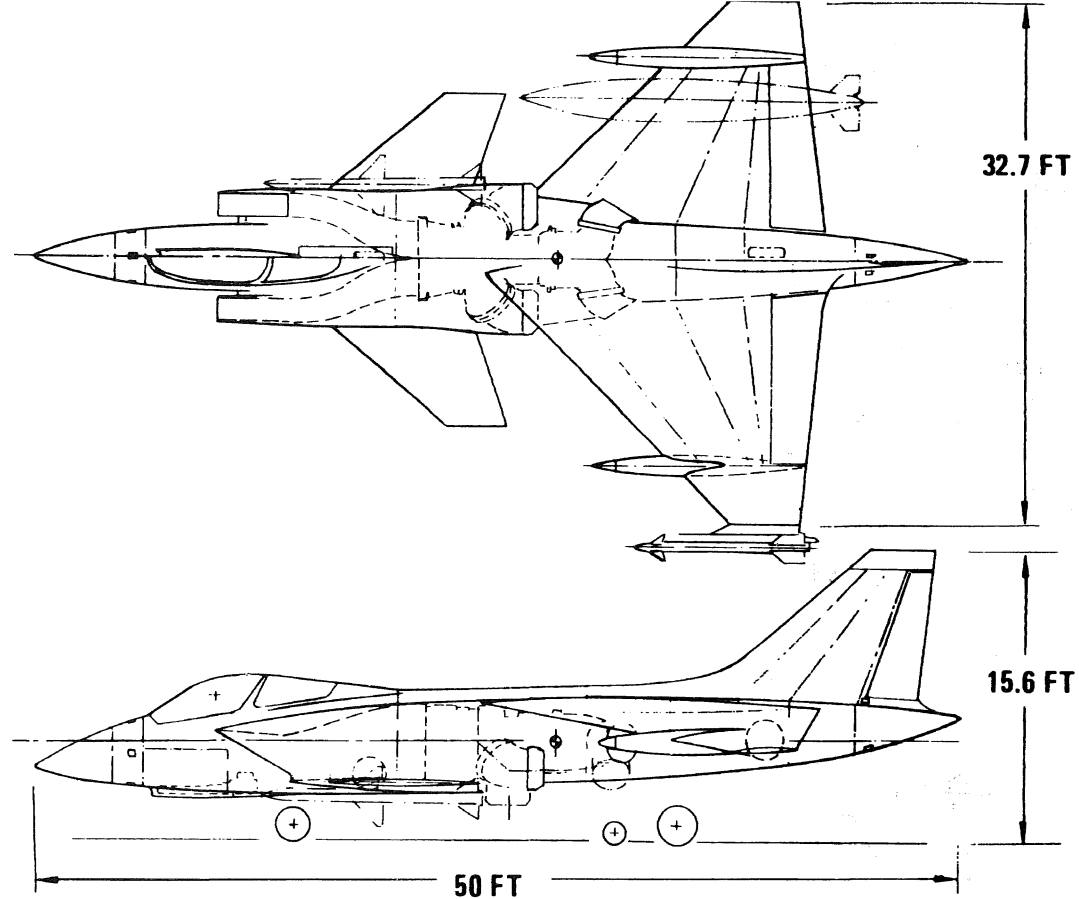


FIG. 7 VECTORED THRUST AIRCRAFT

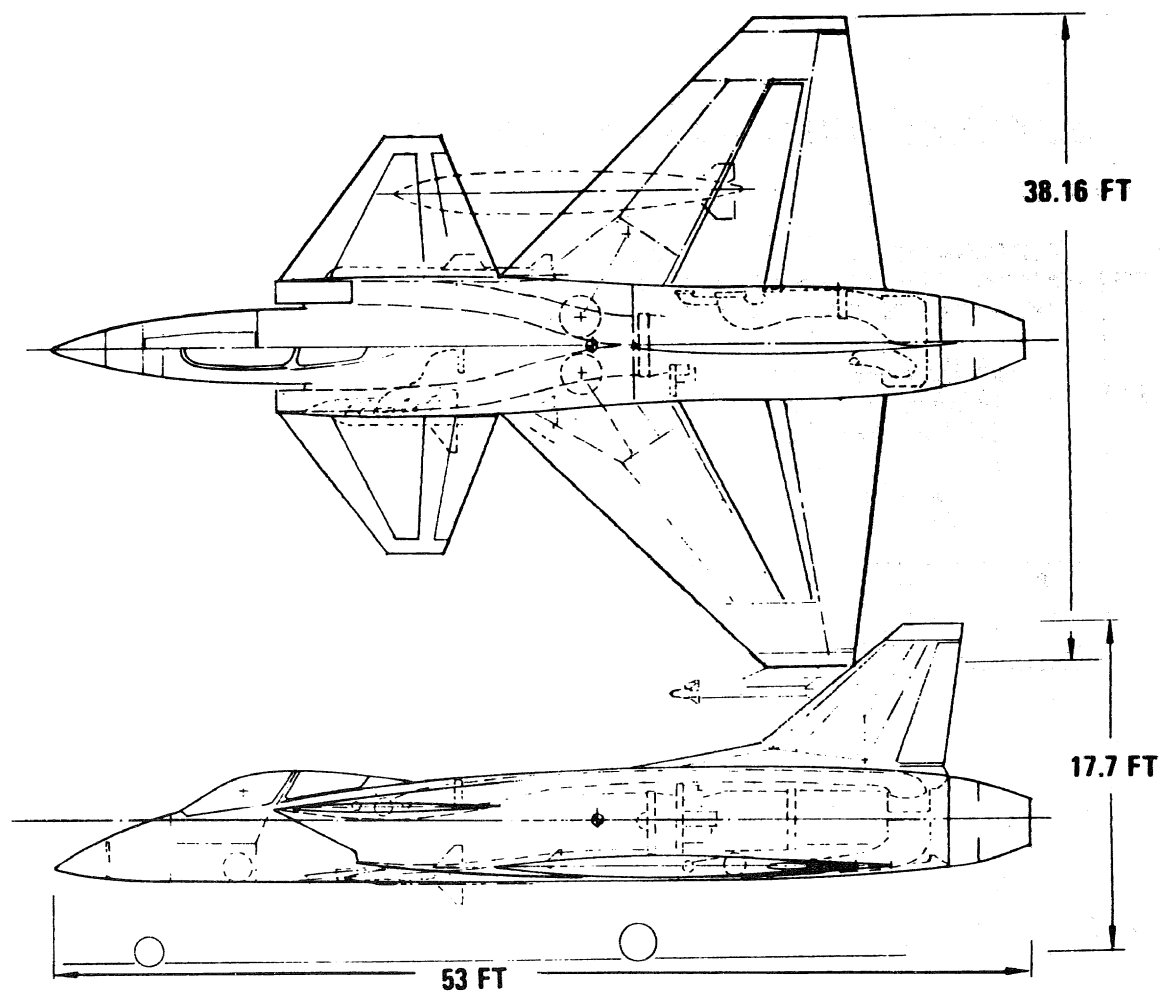


FIG. 8 THRUST AUGMENTED WING AIRCRAFT

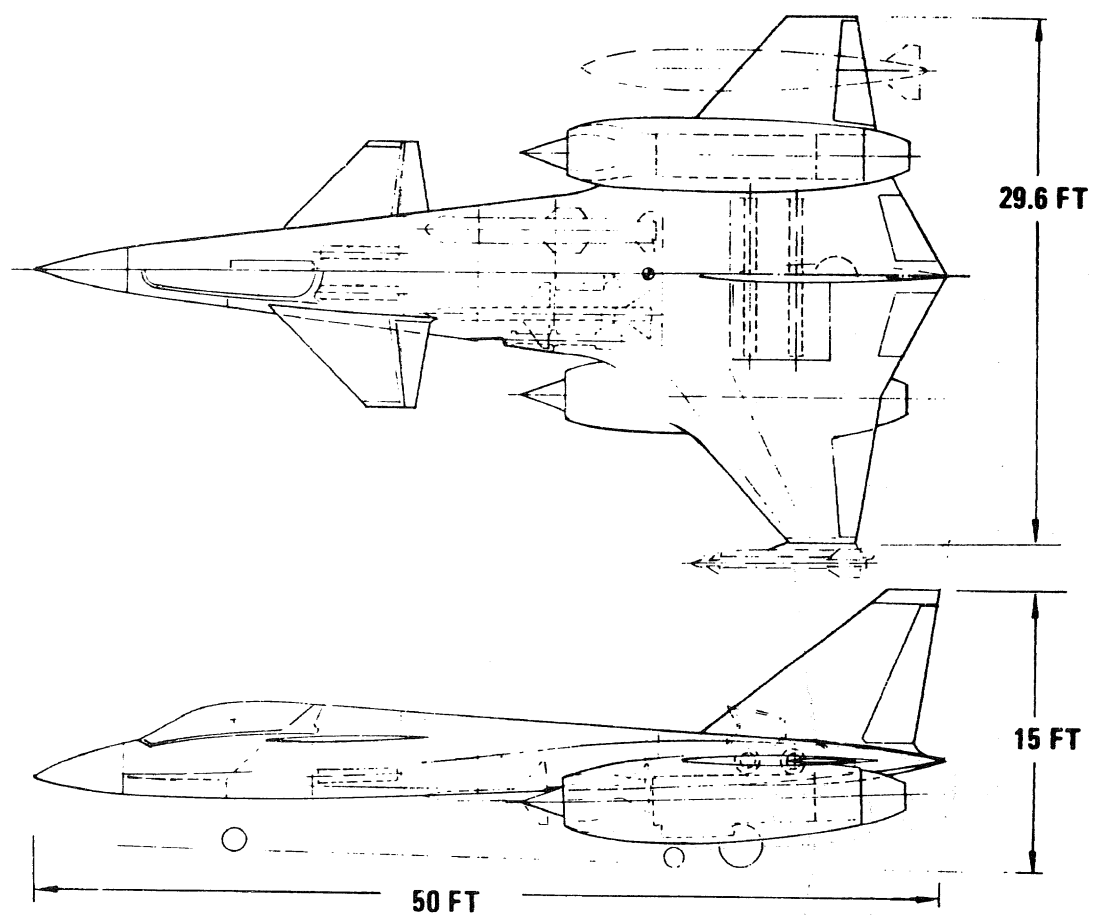


FIG. 9 CROSS FLOW FAN AIRCRAFT

FOR EACH OF THE 6 DESIGNS QUANTIFY

- NOMINAL VALUE OF TECHNOLOGY TOPIC
 - USED IN BASELINE ANALYSIS
 - OPTIMISTIC UNCERTAINTY LIMIT
 - POTENTIAL TOGW REDUCTION
 - PESSIMISTIC UNCERTAINTY LIMIT
 - POTENTIAL TOGW INCREASE
- TO REFLECT CONFIDENCE IN ESTIMATION PROCESS

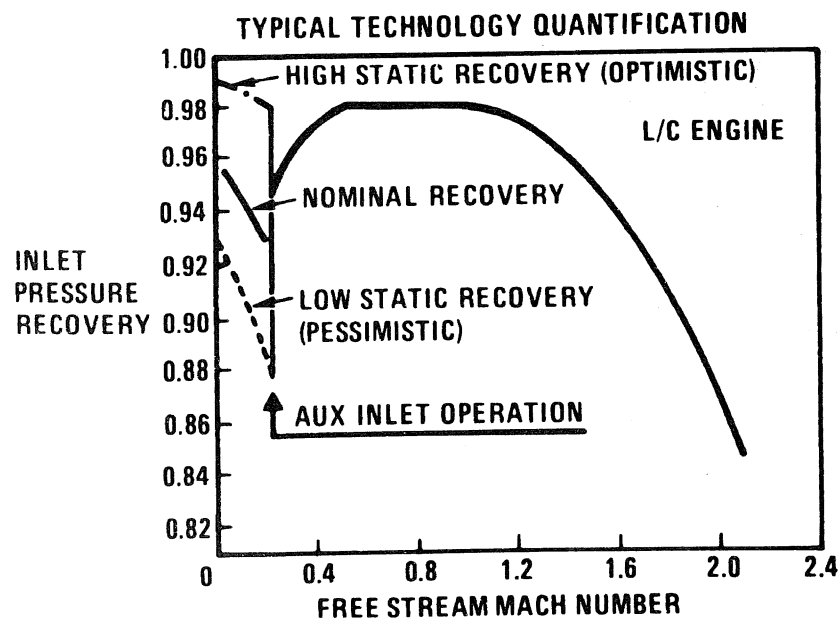


FIG. 10 TYPICAL TECHNOLOGY QUANTIFICATION

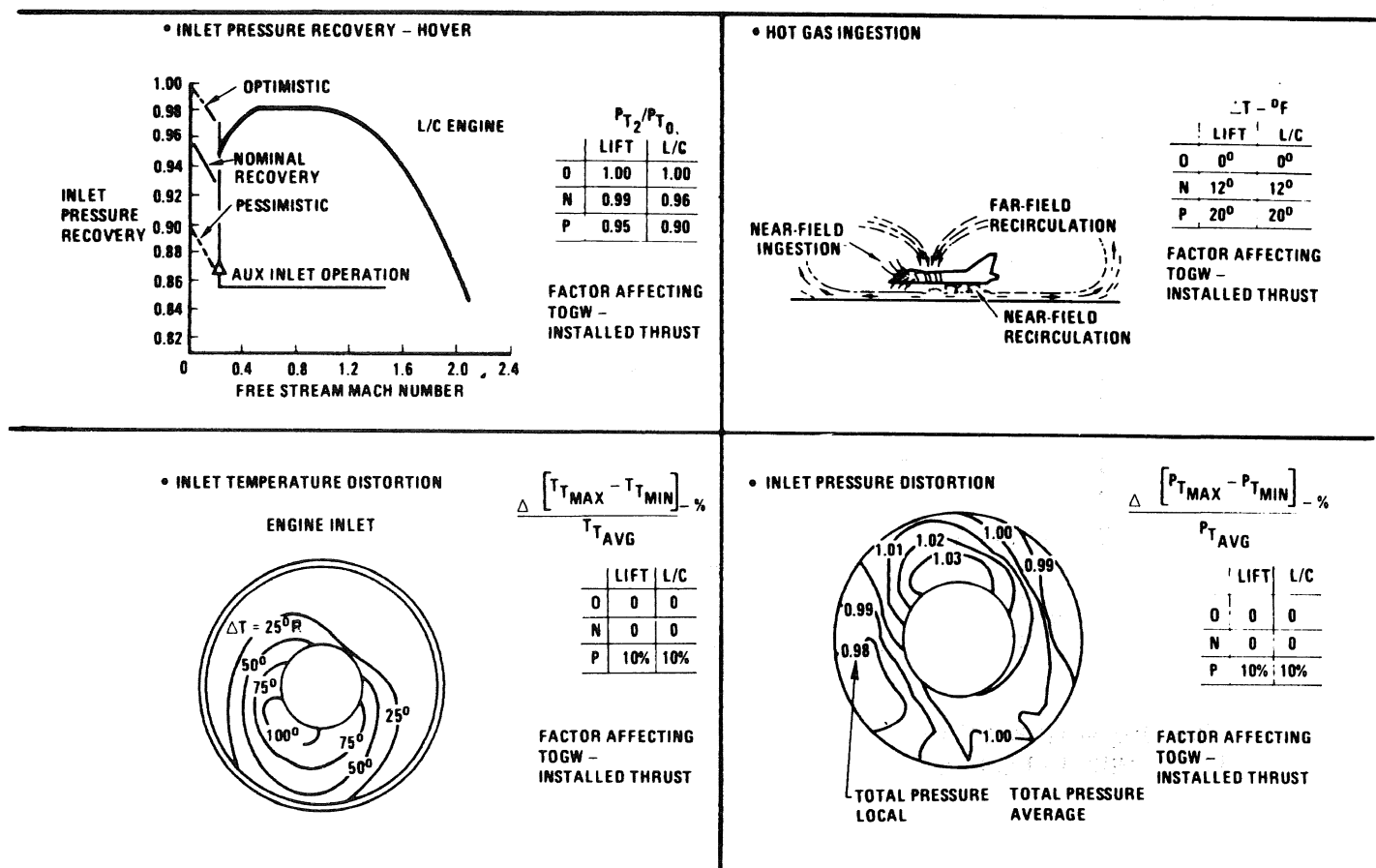


FIG. 11 INLET PERFORMANCE TOPIC QUANTIFICATION

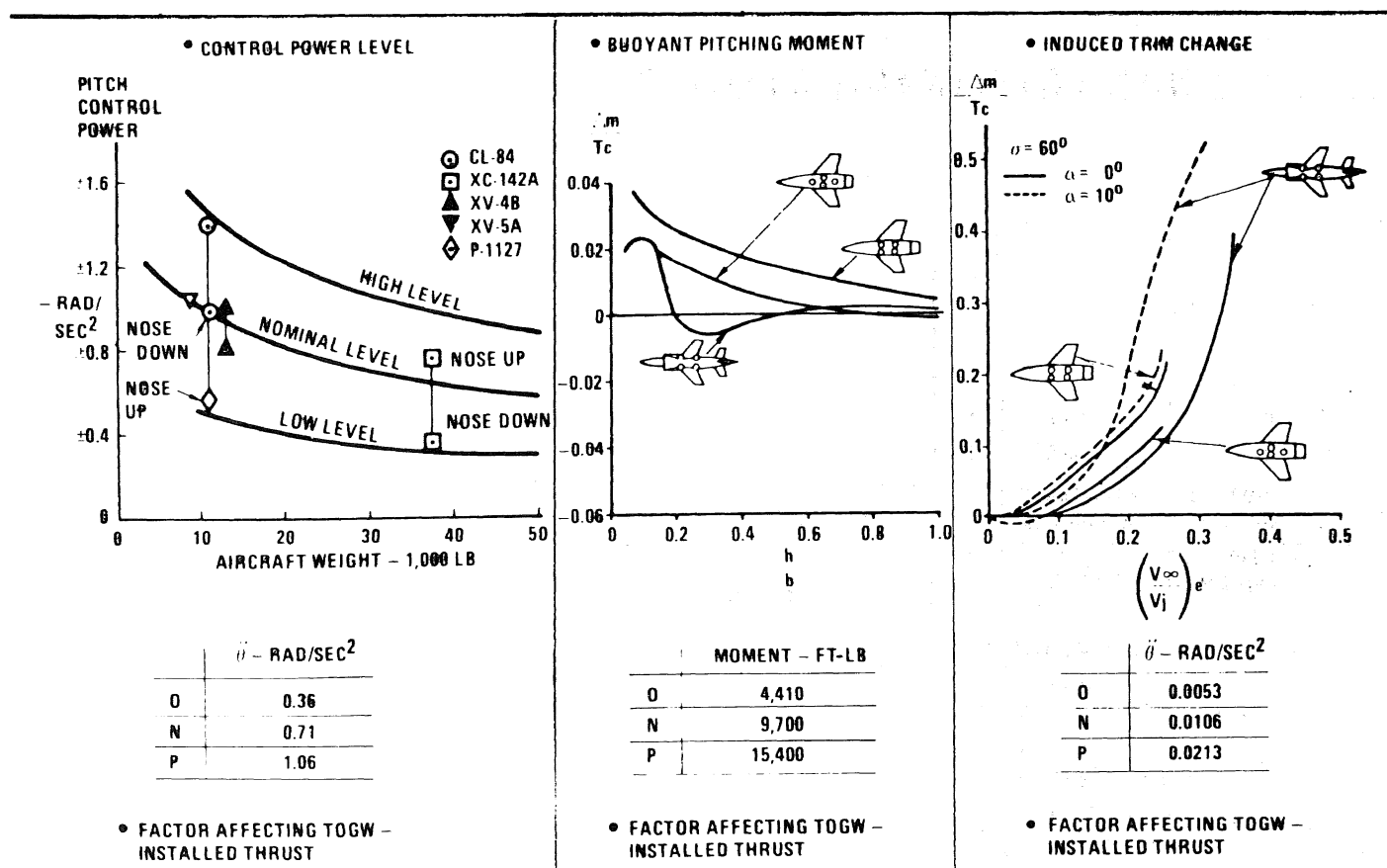


FIG. 12 FLYING QUALITIES TOPIC QUANTIFICATION

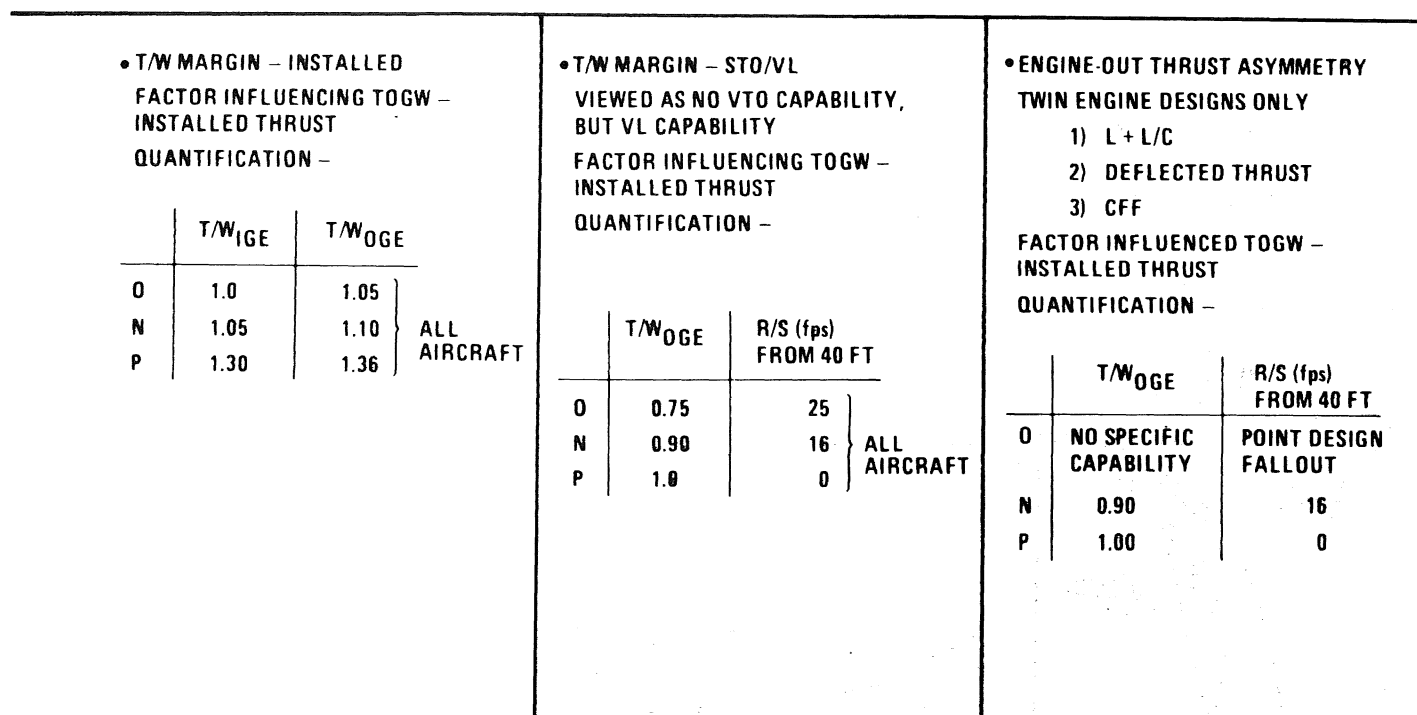


FIG. 13 DESIGN T/W TOPIC QUANTIFICATION

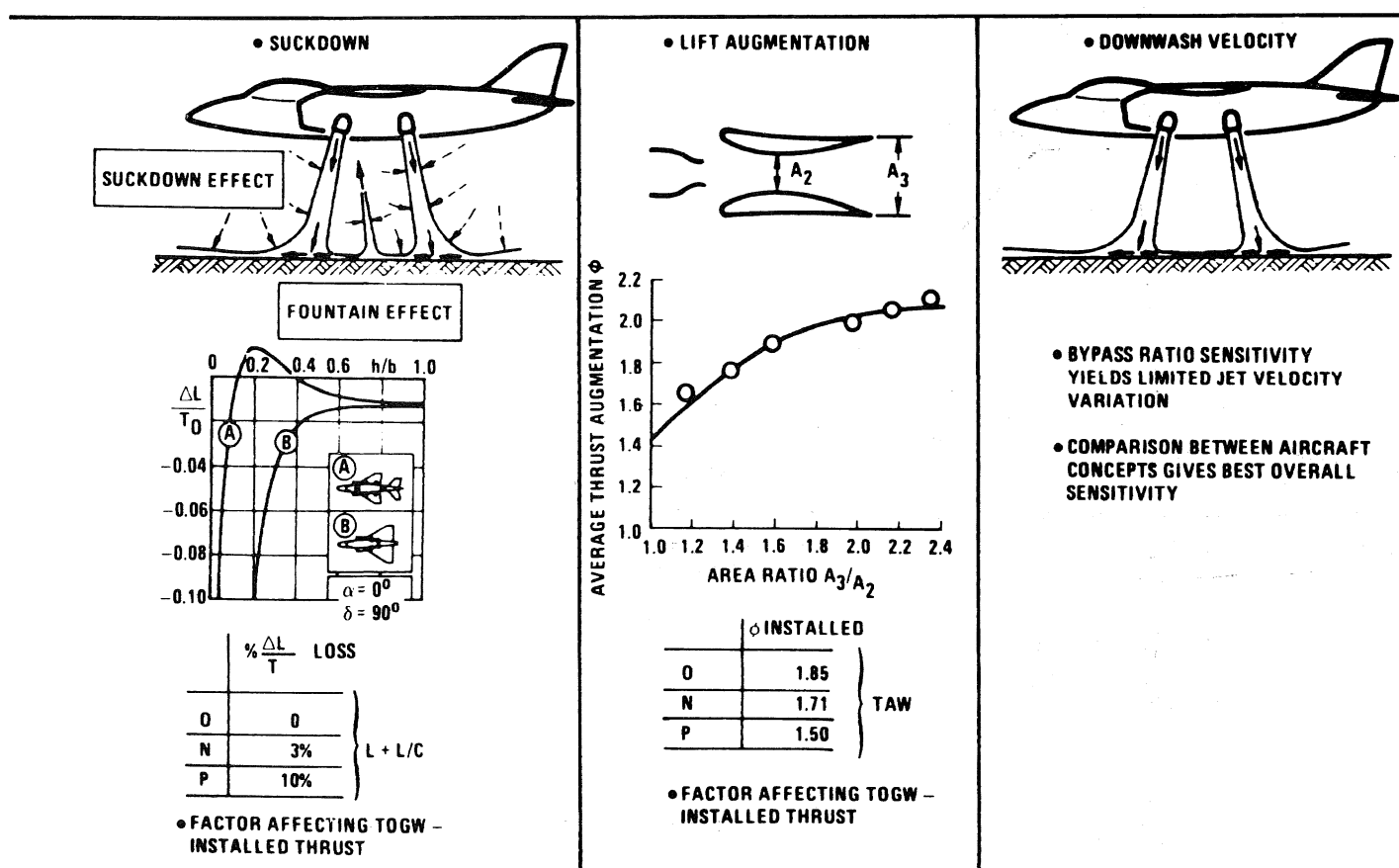


FIG. 14 PROPULSION-INDUCED EFFECTS TOPIC QUANTIFICATION

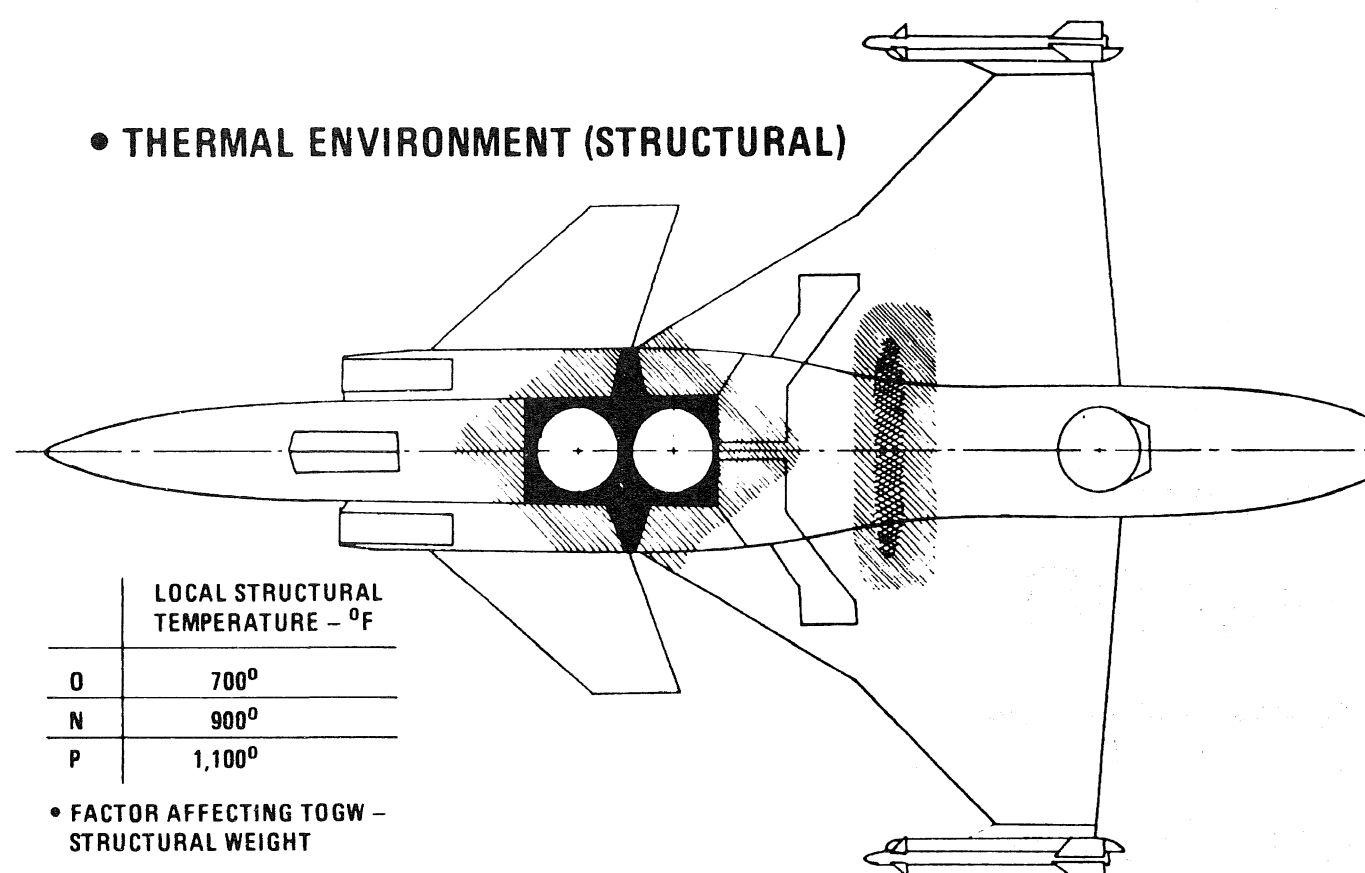
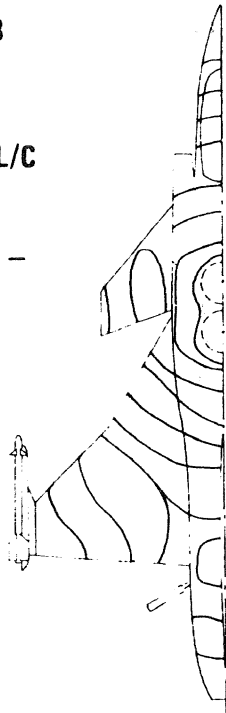


FIG. 15 TEMPERATURE EFFECTS TOPIC QUANTIFICATION

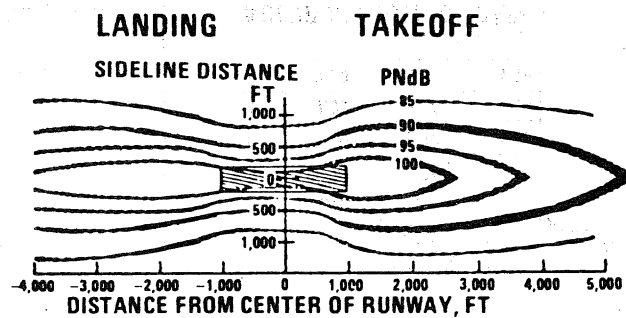
• ACOUSTIC (STRUCTURAL)
ENVIRONMENT

	NOISE LEVEL - dB	
O	180	} L + L/C
N	186	
P	192	

• FACTOR AFFECTING TOGW -
STRUCTURAL WEIGHT



• AUDIBLE SOUND

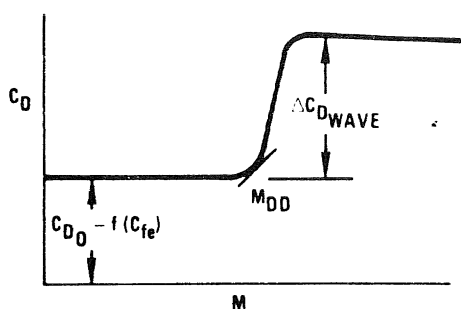


• BYPASS RATIO SENSITIVITY YIELDS LIMITED
NOISE LEVEL VARIATION

• COMPARISON BETWEEN AIRCRAFT CONCEPTS
GIVES BEST OVERALL SENSITIVITY

FIG. 16 NOISE EFFECTS TOPIC QUANTIFICATION

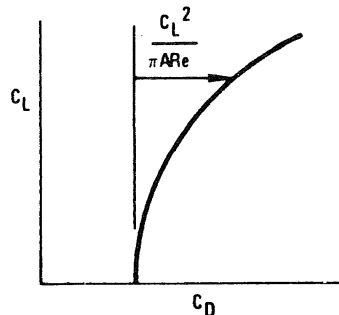
EQUIV SKIN FRICTION DRAG COEFFICIENT - C_{fe}
DRAG RISE COEFFICIENT - $\Delta C_{D\pi}$ ($\Delta C_{D\text{WAVE}}$)
DRAG DIVERGENCE MACH NO. - M_{DD}



	C_{fe}	$\Delta C_{D\pi}$	M_{DD}
O	0.0011	0.109	1.00
N	0.0032	0.20	0.93
P	0.0038	0.24	0.88

FACTORS AFFECTING TOGW -
MISSION FUEL AND CONSTRAINT
PERFORMANCE

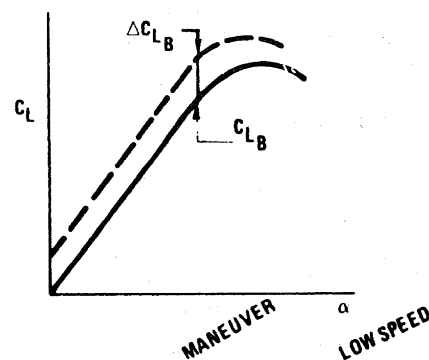
WING EFFICIENCY FACTOR - e



	e
O	2.00
N	0.94
P	0.80

FACTORS AFFECTING TOGW -
MISSION FUEL AND CONSTRAINT
PERFORMANCE

BUFFET LIFT COEFFICIENT - C_{LB}
VECTORED THRUST LIFT AUGMENTATION - ΔC_{LB}
BUFFET FREE DESCENT CORRIDOR - C_{LB} (LOW SPEED)



	C_{LB}	ΔC_{LB}	C_{LB}
O	1.80	0.20	1.80
N	1.00	0.10	1.60
P	0.80	0	1.40

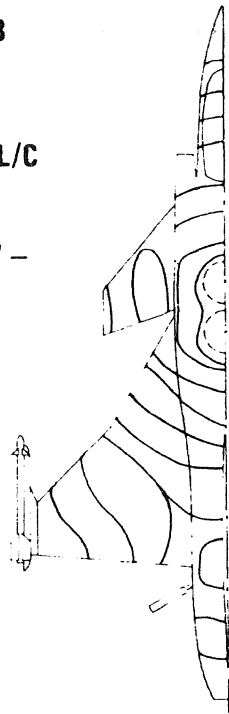
FACTOR AFFECTING TOGW -
CONSTRAINT PERFORMANCE

FIG. 17 AERODYNAMIC EFFECTS TOPIC QUANTIFICATION

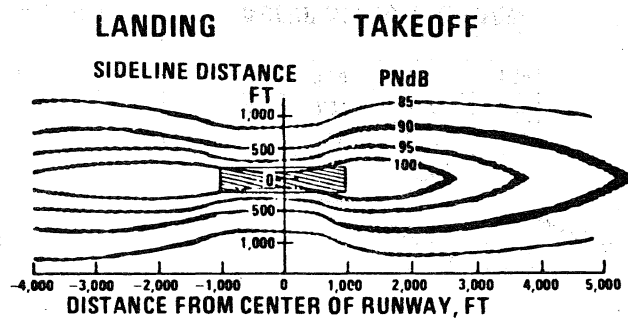
• ACOUSTIC (STRUCTURAL)
ENVIRONMENT

	NOISE LEVEL - dB
O	180
N	186
P	192

• FACTOR AFFECTING TOGW -
STRUCTURAL WEIGHT



• AUDIBLE SOUND

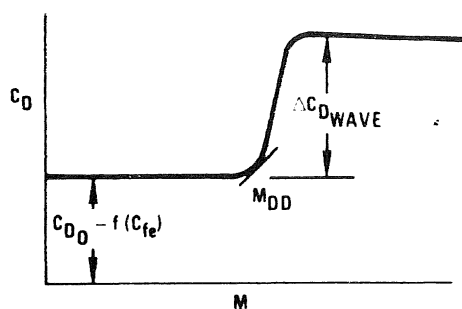


• BYPASS RATIO SENSITIVITY YIELDS LIMITED
NOISE LEVEL VARIATION

• COMPARISON BETWEEN AIRCRAFT CONCEPTS
GIVES BEST OVERALL SENSITIVITY

FIG. 16 NOISE EFFECTS TOPIC QUANTIFICATION

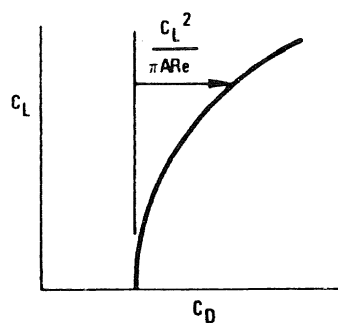
EQUIV SKIN FRICTION DRAG COEFFICIENT - C_{fe}
DRAG RISE COEFFICIENT - $\Delta C_{D\pi}$ ($\Delta C_{D\text{WAVE}}$)
DRAG DIVERGENCE MACH NO. - M_{DD}



	C_{fe}	$\Delta C_{D\pi}$	M_{DD}
O	0.0011	0.109	1.00
N	0.0032	0.20	0.93
P	0.0038	0.24	0.88

FACTORS AFFECTING TOGW -
MISSION FUEL AND CONSTRAINT
PERFORMANCE

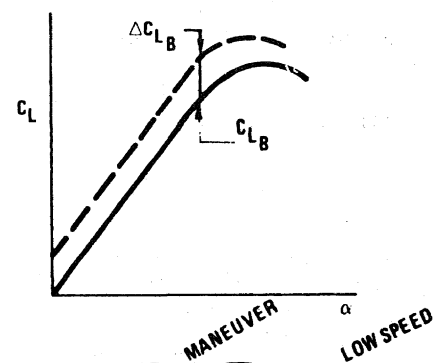
WING EFFICIENCY FACTOR - e



	e
O	2.00
N	0.94
P	0.80

FACTORS AFFECTING TOGW -
MISSION FUEL AND CONSTRAINT
PERFORMANCE

BUFFET LIFT COEFFICIENT - C_{LB}
VECTORED THRUST LIFT AUGMENTATION - ΔC_{LB}
BUFFET FREE DESCENT CORRIDOR - C_{LB} (LOW SPEED)



	C_{LB}	ΔC_{LB}	C_{LB}
O	1.80	0.20	1.80
N	1.00	0.10	1.60
P	0.80	0	1.40

FACTOR AFFECTING TOGW -
CONSTRAINT PERFORMANCE

FIG. 17 AERODYNAMIC EFFECTS TOPIC QUANTIFICATION

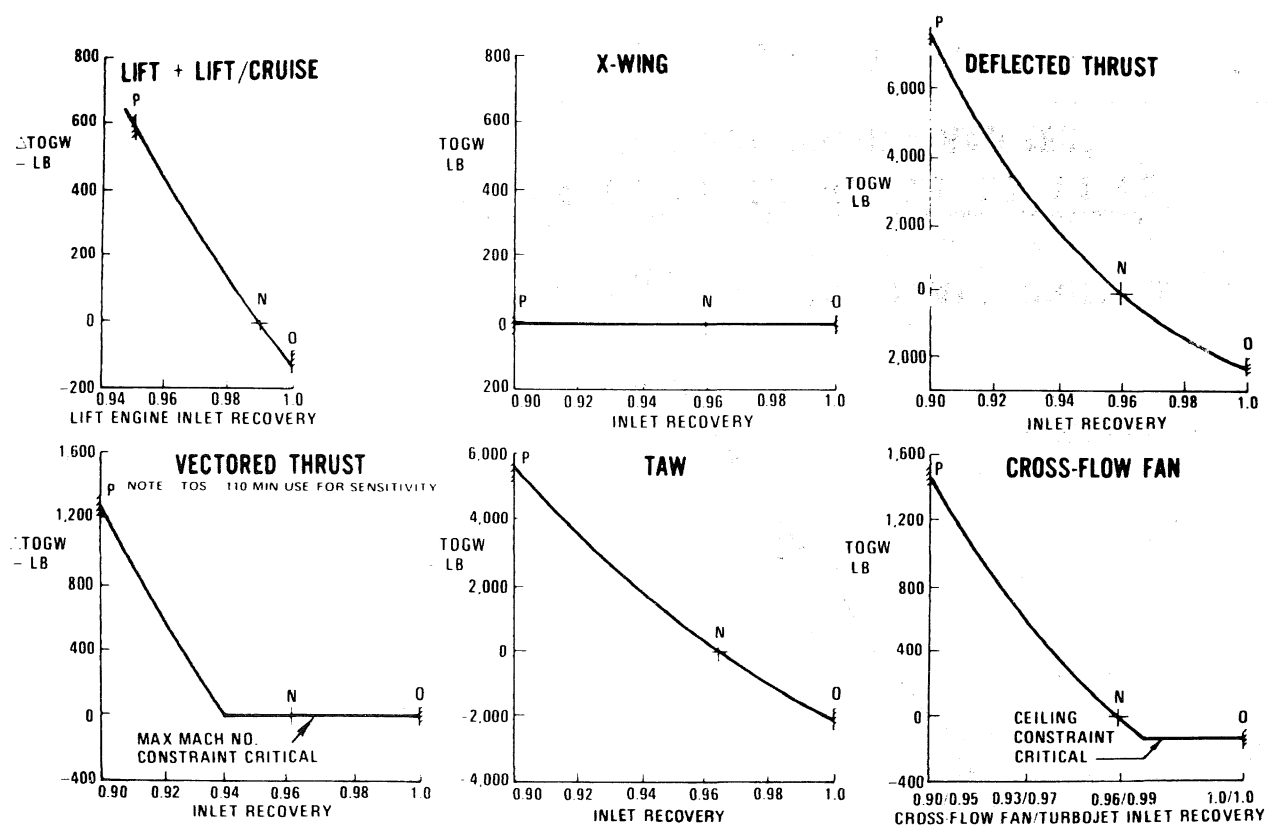


FIG. 18 TYPICAL DESIGN COMPARISON

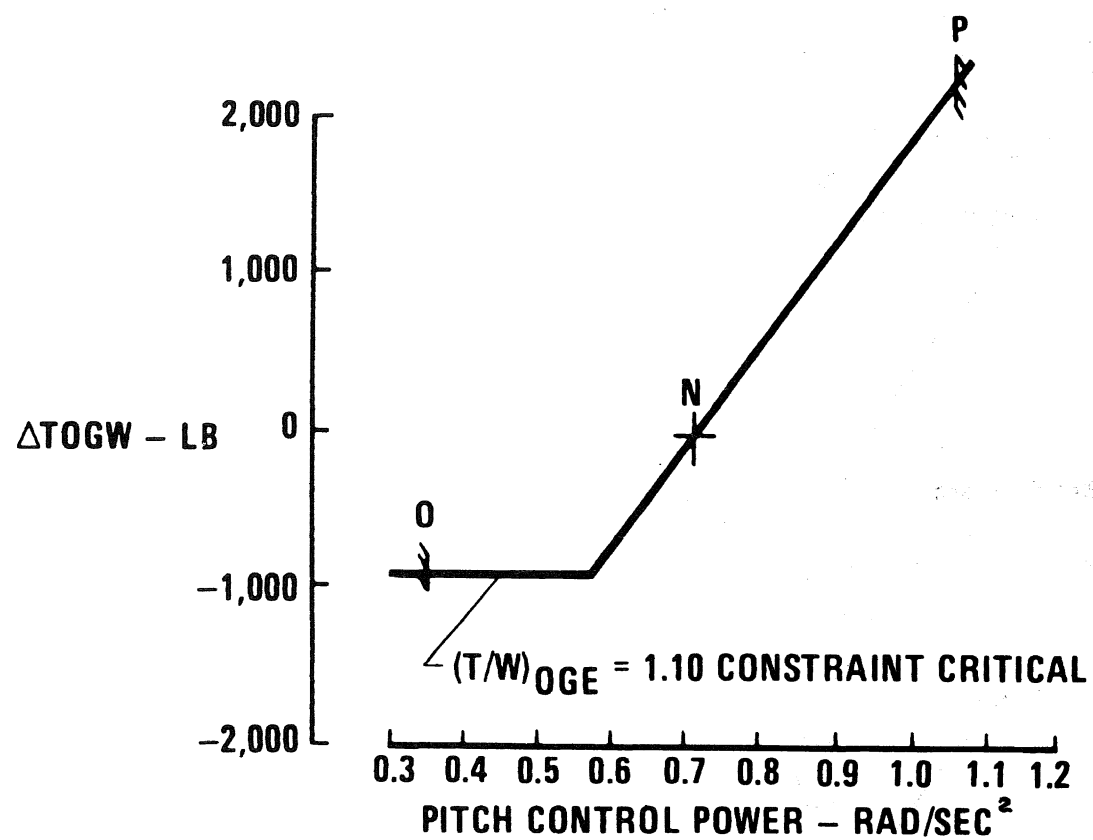


FIG. 19 INCREMENTAL TOGW SENSITIVITY TO PITCH CONTROL POWER LEVEL

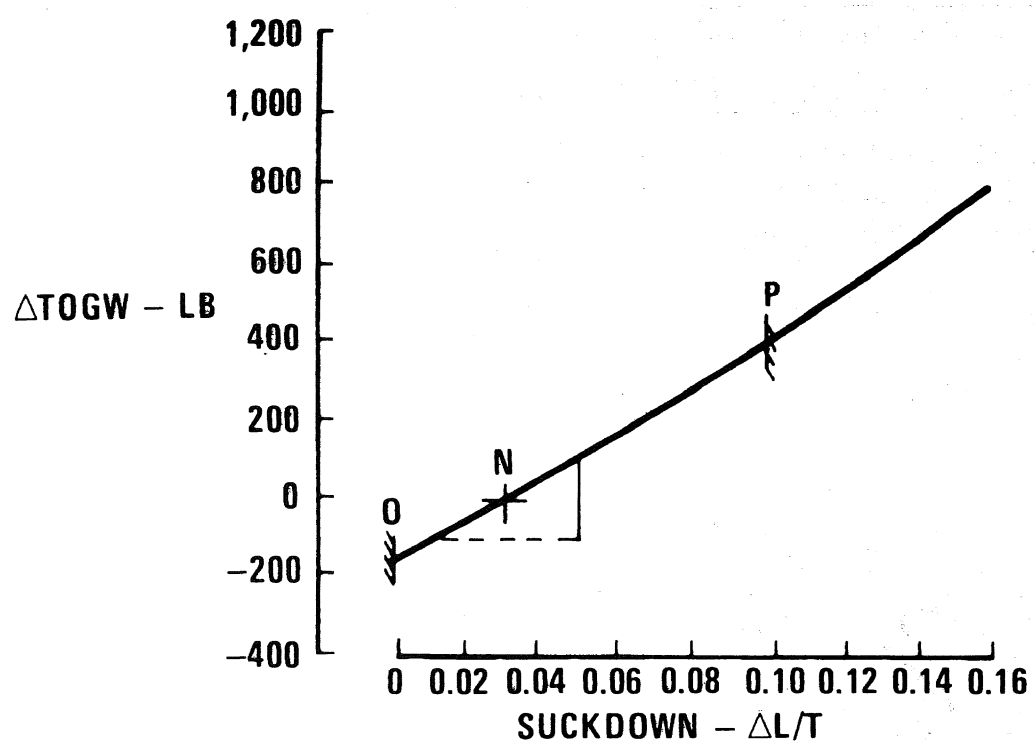


FIG. 20 INCREMENTAL TOGW SENSITIVITY TO SUCKDOWN

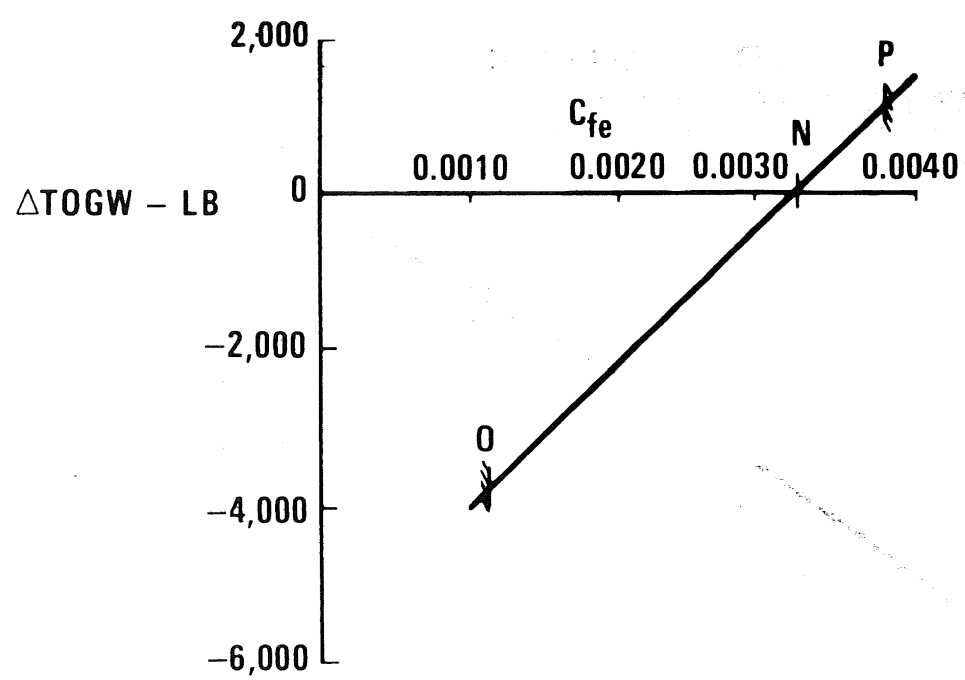


FIG. 21 INCREMENTAL TOGW SENSITIVITY TO SKIN FRICTION DRAG COEFFICIENT

OVERALL RANKING	TECHNOLOGY TOPIC	ΣTOGW INCREMENTS AT OPTIMISTIC LIMITS OF UNCERTAINTY – LB
1*	EQUIVALENT SKIN FRICTION DRAG COEFFICIENT, C_{fe}	–25,565
2	WING EFFICIENCY FACTOR, e	–16,285
3	DRAG RISE BASED ON FRONTAL AREA, $\Delta C_{D\pi}$	– 9,630
4	T/W MARGIN – INSTALLED	– 7,140
5	CONTROL POWER LEVEL	– 5,740
6	INLET PRESSURE RECOVERY – HOVER	– 4,565
7	LIFT AUGMENTATION	– 3,090
8	SUCKDOWN	– 2,130
9	THERMAL ENVIRONMENT	– 1,360
10	T/W MARGIN – ENGINE OUT	– 1,340
11	BOUYANT PITCHING MOMENT	– 960
12	DRAG DIVERGENCE MACH NO., M_{DD}	– 565
13	ACOUSTIC (STRUCTURAL) ENVIRONMENT	– 411
14	INDUCED TRIM CHANGE	– 121

*HIGHEST SENSITIVITY

FIG. 22 POTENTIAL IMPROVEMENT ASSESSMENT - ALL CONCEPTS

OVERALL RANKING	TECHNOLOGY TOPIC	ΣTOGW INCREMENTS AT PESSIMISTIC LIMITS OF UNCERTAINTY – LB
1*	T/W MARGIN – INSTALLED	23,180
2	INLET PRESSURE RECOVERY – HOVER	16,540
3	ENGINE-OUT THRUST ASYMMETRY	14,300
4	CONTROL POWER LEVEL	10,100
5	LIFT AUGMENTATION	8,770
6	SUCKDOWN	7,030
7	EQUIVALENT SKIN FRICTION DRAG COEFFICIENT, C_{fe}	5,830
8	DRAG RISE BASED ON FRONTAL AREA, $\Delta C_{D\pi}$	5,500
9	WING EFFICIENCY FACTOR, e	5,050
10	HOT GAS INGESTION	2,640
11	INLET PRESSURE DISTORTION	1,630
12	T/W MARGIN – ENGINE OUT	1,600
13	THERMAL ENVIRONMENT	1,540
14	INLET TEMPERATURE DISTORTION	1,250
15	BOUYANT PITCHING MOMENT	1,115
16	BUFFET FREE DESCENT CORRIDOR	740
17	ACOUSTIC (STRUCTURAL) ENVIRONMENT	514
18	DRAG DIVERGENCE MACH NO., M_{DD}	463
19	BUFFET ONSET LIFT COEFFICIENT	330
20	INDUCED TRIM CHANGE	241

*HIGHEST SENSITIVITY

FIG. 23 POTENTIAL RISK ASSESSMENT - ALL CONCEPTS

LIFT + LIFT/CRUISE

OVERALL RANKING	TECHNOLOGY TOPIC	Σ TOGW INCREMENTS AT UNCERTAINTY LIMITS – LB
1*	EQUIVALENT SKIN FRICTION DRAG COEFFICIENT, C_{fe}	4,850
2	CONTROL POWER LEVEL	3,130
3	ENGINE-OUT THRUST ASYMMETRY	2,700
4	WING EFFICIENCY FACTOR, e	2,415
5	DRAG RISE BASED ON FRONTAL AREA, $\Delta C_{D_{\pi}}$	2,350
6	T/W MARGIN – INSTALLED	1,230
7	T/W MARGIN – ENGINE OUT	1,040
8	BUOYANT PITCHING MOMENT	900
9	INLET PRESSURE RECOVERY – HOVER	715
10	SUCKDOWN	590
11	THERMAL ENVIRONMENT	400
		Σ = 20,320

*HIGHEST SENSITIVITY

FIG. 24 COMBINED IMPROVEMENT AND RISK ASSESSMENT BY CONCEPT

TECHNOLOGY TOPIC	CONCEPT						CONCEPTS AFFECTED	AVERAGE RANKING
	LIFT + LIFT/CRUISE	X-WING	DEFLECTED THRUST	VECTORED THRUST	TAW	CROSS-FLOW FAN		
EQUIVALENT SKIN FRICTION DRAG COEFFICIENT	1	1	4	1	5	1	6	2.2*
T/W MARGIN – INSTALLED	6	–	1	2	1	3	5	2.6
ENGINE-OUT THRUST ASYMMETRY	3	–	3	–	–	4	3	3.3
WING EFFICIENCY FACTOR	4	3	8	3	6	2	6	4.3
CONTROL POWER LEVEL	2	–	5	8	4	5	5	4.8
INLET PRESSURE RECOVERY – HOVER	9	–	2	4	3	7	5	5.0
LIFT AUGMENTATION	–	–	–	–	2	8	2	5.0
DRAG RISE BASED ON FRONTAL AREA	5	2	11	5	8	6	6	6.2
SUCKDOWN	10	–	6	6	7	9	5	7.6
HOT GAS INGESTION	–	–	7	9	–	–	2	8.0
T/W MARGIN – ENGINE OUT	7	–	9	–	–	–	2	8.0
BUOYANT PITCHING MOMENT	8	–	–	–	10	10	3	9.33
THERMAL ENVIRONMENT	11	–	10	7	11	–	4	9.75
INLET PRESSURE DISTORTION	–	–	12	–	9	–	2	10.5
INLET TEMPERATURE DISTORTION	–	–	14	–	–	–	1	14.0

*HIGHEST SENSITIVITY

FIG. 25 RANKING MATRIX

V/STOL PROPULSION SYSTEM REQUIREMENTS
AN ENGINE PROJECT ENGINEER'S PERSPECTIVE

S. M. Hudson

Detroit Diesel Allison
Division of General Motors Corporation
Indianapolis, Indiana

The V/STOL aircraft problem statement presents the propulsion system designer unique requirements in addition to those found in conventional aircraft. The basic requirements of maximizing powered lift, providing "flyable" control and achieving efficient cruise in the conventional mode are examined and translated into specific propulsion system objectives. Analytical and experimental tools for defining these requirements are discussed.

V/STOL PROPULSION SYSTEM REQUIREMENTS

An Engine Project Engineer's Perspective

INTRODUCTION

The history of V/STOL airplanes in the U.S. is characterized by a host of highly innovative aircraft but still we have only one operational system. The recurring question which we face is whether we in the aircraft community have generated adequate technology to drive the "cost" of the system below the "price" the market place can bear and in turn produce a "profit" in terms of total weapon system capability. The burden of generating the required technology falls largely on the disciplines of engine design and engine-airframe integration since contemporary V/STOL flight is predicated on powered lift. The engine project engineer therefore enjoys an interesting position in the pursuit for a viable V/STOL weapon system since he forms the interfaces between the propulsion technology specialist and both the military customer establishing the requirements and the aircraft designer who is "wrapping an airframe around the engine". It is from this perspective as an interpreter of requirement and a negotiator of differences between the various technical disciplines that this paper is written.

BASIC REQUIREMENTS

The basic requirements of the V/STOL propulsion system seem trivial in respect to the amount of effort that has been expended on detailed design and development addressing the specifics. However, it might be well to start with three of the more basic requirements and expand these into requirements within the specific disciplines. These three requirements are:

- o The maximization of low speed or static lift for a given size of propulsion system
- o The provision of "flyable control through inherent stability or active thrust management
- o The minimization of cruise fuel consumption.

A fourth basic requirement which applied to all the other requirements may be expressed in a single word - quantify. We must strive to reduce each requirement to a specific set of numbers. For it is only through numbers that we can communicate

for example from the military requirements specialist to the aircraft aerodynamicist - to the inlet designer - to the wind tunnel researcher - to the fan aerodynamicist - to the mechanical blade designer - to the production engineer and finally back to the military.

BASICS TO SPECIFICS

V/STOL lift maximization - the basic requirement to maximize low speed lift for a given size of propulsion system impacts the propulsion areas of turbomachinery, inlets and nozzles and thrust augmentors. Turbomachinery systems to date may be categorized as being lift-cruise engines, lift engines and remote fans. The lift-cruise engines and the lift engines benefit from the tremendous and continuing investment the U.S. has in both military and commercial cruise engines. This lumping together of lift-cruise and lift engines is not meant to belittle the difficulty of the lift engine designer's task for there are significant detailed design differences which require lift engine development investments. However, as an example the Allison XJ99 lift engine, shown in Figure 1, with its 20:1 thrust-to-weight utilizes a relatively conventional compressor and turbine systems.

The remote fans have found their source of technology support solely in the V/STOL applications in the past. The remote variable pitch fan being used in current Navy/NASA V/STOL system studies may be an exception to this since it is a direct adaptation of the fan configurations identified as optimum for quiet commercial STOL transports⁽¹⁾ and being developed for this purpose thru NASA support on QCSEE and related programs by two U.S. companies. ^(2&3) These very high bypass ratio fans have also been found attractive for missions having low fuel consumption requirements such as land based ASW.

Turbomachinery requirements for V/STOL look very similar to those of cruise engines. V/STOL applications place extra emphasis on the minimization of weight and volume. Turbine temperatures need to be high to maximize specific thrust. The ever present problem of system losses must be minimized in V/STOL propulsion in order to maximize thrust. Ducts, transitions and inherently inefficient components must be designed out of the system or justified on a total system basis.

V/STOL nozzles have been the subject of extensive design and development effort. ⁽⁴⁾ The thrust deflecting hoods, swiveling elbows and three bearing pipes have recently been joined by the two dimensional vectoring nozzle. The Allison vectoring trap door shown in Figure 2 is typical of the "2D" approach. A more

(¹) Numbers in parenthesis refer to references at the end of the paper.

direct approach to thrust vectoring is the swiveling engine used on the German VJ 101. ⁽⁵⁾ The swiveling engine eliminates nozzle complexity and in several applications can be shown to be the optimum configuration. Vertical to horizontal engines are not new since as early as 1955 Allison was building turbine engines to operate both vertically and horizontally for use in the "tailsitter" class of aircraft.

The criterion for nozzle selection reduces largely to a trade between maximization of take-off-thrust and a minimization of cruise drag per unit nozzle weight. It is important that nozzle selections be based on system capability considering the mission profile and the selected engine cycle. It is interesting to note that at the low fan pressure ratios of some of the remote fans one percent in exhaust system loss is equivalent to an eight percent loss in thrust.

Thrust augmentors means different things to different people. Here it applies to engine exhaust gas reheat. The augmentor/ejector is a system unto itself and not included here. With this definition the first question relating to augmentors is whether we will be allowed to afterburn in the vertical mode or not. The answer to this question impacts engine sizing, nozzle selection and aircraft configuration. Sufficient work has been done on augmented engines to demonstrate the feasibility of burning-and-turning. These systems benefit from the technology work being conducted on cruise engines however the lift-cruise engine with vectoring nozzles is unique enough and will be installation peculiar enough to warrant additional development effort. Another potential configuration is one in which the engine is non-augmented in the lift mode and augmented in the horizontal flight mode. The combination trap door-star nozzle system shown in Figure 2 is ideally suited to this type of configuration.

Engine-airframe integration is usually thought of as applying to the maximization of thrust minus thrust-related-drag for the propulsion system at the critical mission points. V/STOL application broadens this definition since lift is also related to thrust. Thrust distribution in the V/STOL mode becomes a major consideration since it effects the balance of the aircraft. The evaluation of the total system thrust-to-weight must recognize this requirement to balance forces. A high thrust-to-weight lift-cruise engine with a vectoring nozzle located at the extreme rear of the aircraft loses much of its effectiveness if it can be operated only to part power due to balance restrictions. Of equal concern is the solution which offers an oversized lift engine in the nose to balance the rear lift cruise vectors. This requirement to distribute thrust around the air-

craft may be the justification for the complexity associated with the variable cycle engine. Also associated with balance and maximizing powered lift is the technique of thrust spoiling for control. If thrust is continually spoiled in anticipation of a thrust requirement the propulsion system is being oversized. Engine placement to maximize lift has been the subject of considerable research and discussion. Both good and bad effects on lift have been demonstrated for different engine placements. (6)

Control and stability - the requirements for "flyable" stability in V/STOL aircraft is fundamental to the success of V-mode operational capability. These reduce to the generation of roll, pitch and yaw forces, thrust redistribution in response to power interruption, and stable and easily selectable thrust levels. The generation of normal control forces usually takes the form of high pressure reaction jets, rapid trim vectoring of the lift nozzles, spoiling of the lift thrust or flow modulation through fan pitch variations. Flow and thrust modulation for fixed pitch fans without spoiling is too slow to meet flight control rate requirements. The reaction jet approach requires the propulsion system compressor to be sized to allow large quantities of bleed flow. Trim vectoring takes the form of articulating louvers or moving nozzles which are linked to the flight controls. Spoiling of thrust provides rapid and positive control forces. Provisions for roll and pitch control at a constant altitude with this system implies an excess of thrust on the aircraft disposed in vectors about the aircraft center of gravity. Thrust spoiling is applied to maintain the desired altitude and is increased at one point and decreased at another to produce the required control moment while maintaining constant total vertical thrust. The level of thrust that must be spoiled in anticipation of a requirement for rapid thrust increase defines the extent of oversizing required for the propulsion system. This can be directly converted into aircraft gross weight and SFC increase.

The variable pitch fan introduces another variable component to the flight control system. In return the system produces a direct method of thrust vector transfer when all of the fans are coupled by shafting. This configuration allows the propulsion system to be sized to meet the vertical lift requirement while providing control thrust modulation through air flow variations produced by blade setting angle changes.

Stable thrust control implies a propulsion system which can maintain the requested thrust levels under the desired operating conditions. This requires an engine control system which can "communicate" with the aircraft flight control system, be that the pilot directly or an automatic flight control computer to

select and produce engine operating parameters to generate the desired thrust. The current engine electronic fuel controls are natural for integration into this type of fly-by-wire system.

Another implication of the requirements for stable thrust is a stable compression system. The propulsion system fans and compressors must operate surge free and any engine thrust deterioration must be accounted for in the thrust sizing. The engine inlets and the compressions systems should be designed together to produce the best (lightest, most inexpensive, stable) propulsion system.

Fuel consumption minimization - The minimization of cruise fuel consumption dictates requirements for system frontal area and volume, clean, low drag exhaust systems, efficient turbomachinery and properly sized engines to produce efficient cycle conditions. The volume and frontal area of the V/STOL aircraft is highly propulsion system sensitive. The propulsion systems with inherently high volumes must therefore be justified through offsetting advantages in other areas. As noted previously the system turbomachinery benefits from cruise engine research. The V/STOL propulsion system designer should apply this technology while minimizing internal losses such as duct pressure drops and selecting optimum pressure ratio and tip speeds. The desire to resize the engine for cruise and minimize nozzle boattail drag again suggest that V/STOL aircraft may be candidates for variable cycle engines.

The basic V/STOL requirements can be converted into more specific requirements relating to turbomachinery design, cycle and configuration selection and engine/airframe interface integration. The techniques required to specifically define elements of these general requirements are discussed below from a project engineers point of view.

WHAT DO WE NEED?

Both inlet and back pressure distortion are of concern to both aerodynamist and mechanical designer. Inlet distortion may be separated into pressure and temperature gradients. Analytical techniques exist which predict the sensitivity of compressor systems to distortion patterns. To complete the analytical "picture", techniques to predict pressure and temperature pattern are required. These techniques exist in various forms ⁽⁴⁾⁽⁶⁾ but are not sufficiently verified and operational to be used on a routine basis. A similar deficiency also exists in the area of flow visualization and experimental techniques. The French chalk, smoke wand, steam, injection and gas and bubble tracer all have significant deficiencies. With adequate tools in hand we can define the conditions which are causing the

problems and began to provide the best solution on a total system basis. These solutions may well take the form of active boundary layer control inlets and fans designed for distortion.

The area of nozzle design is another in which we have analytical tools for internal performance prediction but are deficient in the area of engine/airframe interface related performance. In this area we have developed sound experimental techniques to investigate configuration performance in wind tunnel tests. Therefore in this case we need an increased analytical capabilities to investigate configuration performance prior to committing it to model test. Additional analytical techniques to predict the details of secondary flow patterns are also in order. These tools would allow better definition of temperature and pressure patterns in vectoring nozzle and better establish the loads and conditions for the mechanical designers. With better tools one would hope to see more innovations in nozzle design as we obtain a better understanding of the flow turning phenomenon.

Thrust augmentation through reheat is attractive on a specific thrust basis. We in the U.S. have largely tried to apply cruise type afterburners to the V/STOL mode. We need to couple our understanding of external flow field patterns and V/STOL control and sizing requirements to define some new and innovative forms of augmentation.

The area of engine cycles and configuration was discussed above. We have built a sound analytical capability in cycle analysis which extend from simple building block program to full variable cycle parametric performance decks. We now need to rigorously exercise their capabilities in system studies to define optimum techniques for selecting and tailoring the engine configuration and cycle to the required mission. We need to answer the question of whether the variable cycle engine with its increased complexity can be justified in terms of increased mission capability. These studies need to address the advantages of new technology such as is represented by the variable pitch fan with its rapid thrust response and "movable" efficiency islands.

It is appropriate to close with the "other" basic requirement. We need to continue in our efforts to define common avenues of communication. The ARP 681B definitions for performance card decks is representative of what is needed. Further the work on definition of inlet distortion communication tools by the SAE S16 committee provides specific guidance in a field of direct interest to the V/STOL designer. We must be able to

communicate rapidly and effectively between government agency, engine contractors and airframe contractors if we are to make rapid advancements in V/STOL development.

References:

- ¹ Influence of Noise Requirements on STOL Propulsion Systems Designs, Raymond S. Rulis April 1973 SAE 730358.
- ² Quiet Clean Short-Haul Experimental Engine (QSCEE) Design Rationale, A. P. Adamson SAE 750605 May 1975.
- ³ Q-Fan Demonstrator Engine Testing - Robert Levintan AIAA 73-1215 Sept. 1973.
- ⁴ J. E. Petit, M. B. Scholey - A Study of V/STOL Thrust Vectoring and Thrust Reversing Nozzles, AFAPL-TR-72-109.
- ⁵ Propulsion System of the VJ 101C VTOL Aircraft Philosophy and Practical Experiences, Werner Biehl, AGARD Conference Proceedings No. 135, Sept. 1973.
- ⁶ Baron, W. A. and Palcza, J. L. - Jet-Induced Thermal Effects for VTOL Aircraft, ASME Paper 75-GT-96, March 1975.

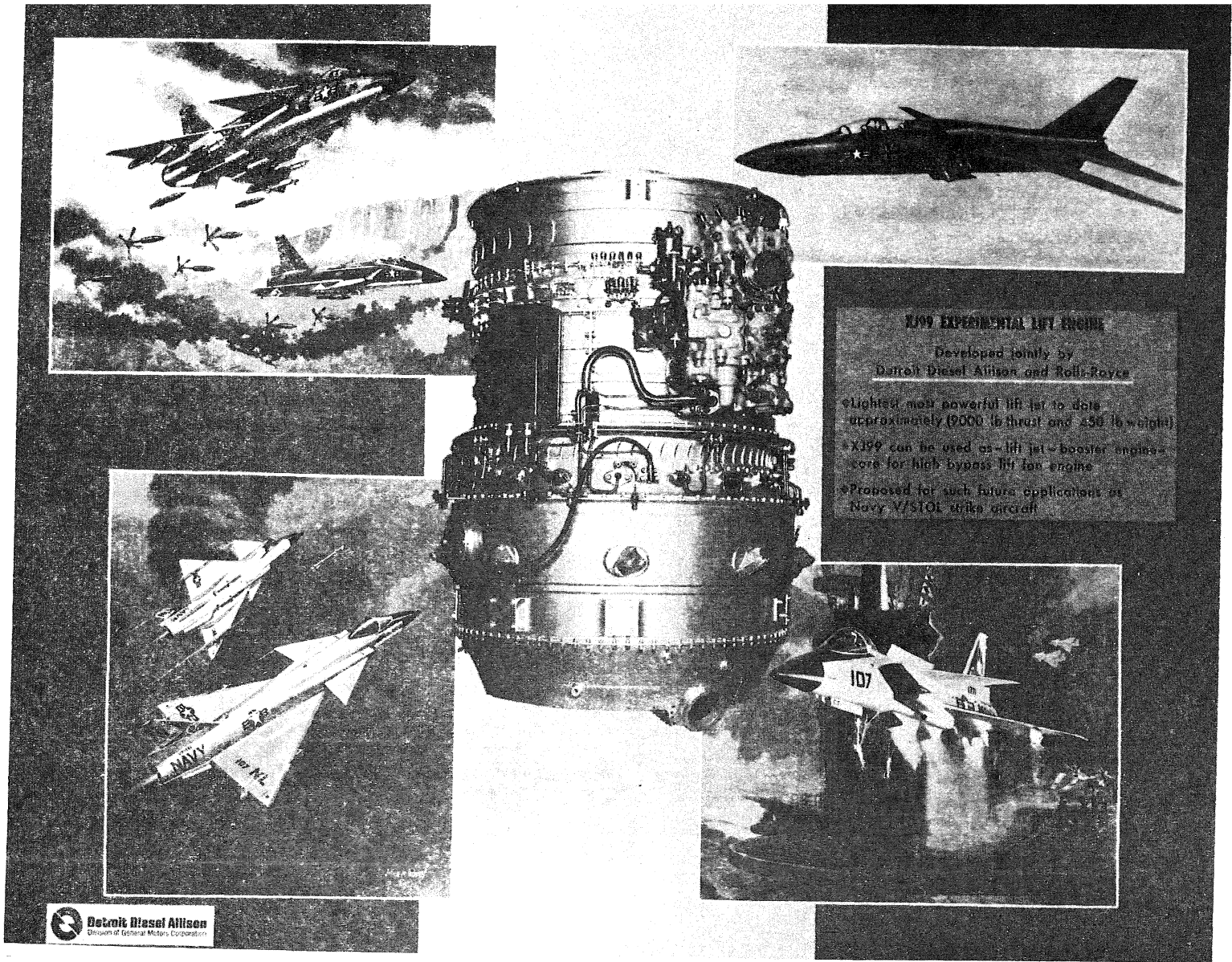
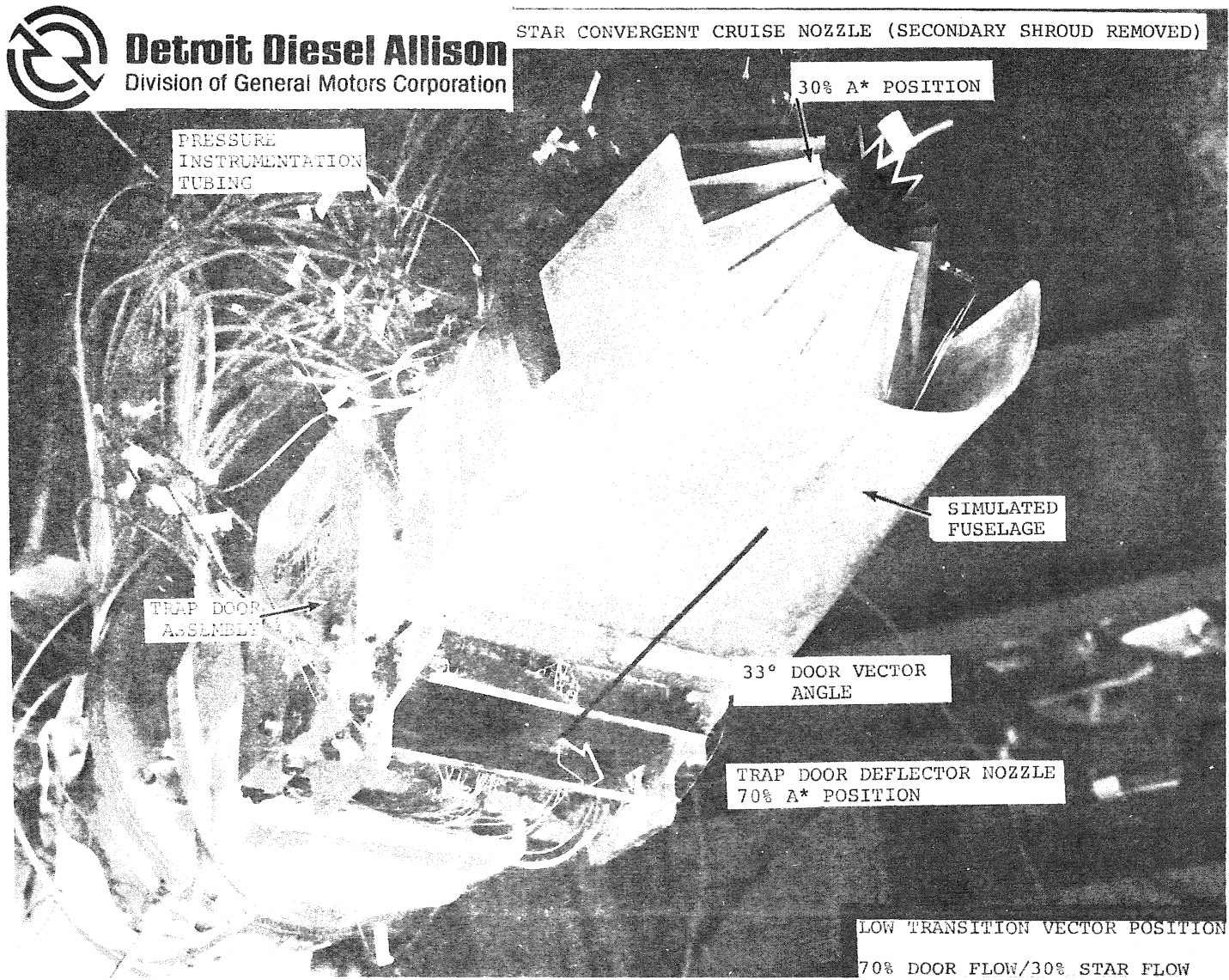


Figure 1 J99 Lift Engine



PROBLEMS OF INTERNAL FLUID MECHANICS*

by

Miklos Sajben

*McDonnell Douglas Research Laboratories
McDonnell Douglas Corporation
St. Louis, Missouri 63166*

Abstract

Many fluid dynamic problems in various types of propulsion systems for V/STOL and conventional jet aircraft can be generalized as flows in relatively short, irregularly shaped ducts. Flows in inlets, flow vectoring devices, nozzles and ejectors have many similar features that are infrequent or unimportant in external aerodynamics. Research efforts in support of V/STOL propulsion system design can be made more efficient by choosing topics of high commonality. This paper discusses several often-neglected problem areas qualifying under this criterion. Among others, the following problems are discussed: interactions between duct elements in series, inlet boundary conditions in test and in installation, simulation of inlet conditions in testing, effects of gross nonuniformities of mean flow, and high levels of turbulence.

**This research was conducted under the McDonnell Douglas Independent Research and Development Program.*

Introduction

The aerodynamic design and development of air breathing propulsion systems are complex processes involving theoretical and experimental work, the latter being usually dominant in terms of cost. This disproportionality is traceable to our inadequate understanding of the complex flow processes present in propulsion systems. More insight into fundamental processes would lead to more reliable theories and computation procedures, reduce the amount of testing required, and thereby reduce cost. Progress in this direction requires fundamental investigations that should not be expected to contribute directly to the development of any specific configuration. There should be, however, some indirect benefits, and it is desirable to minimize the time span required to realize them. The imposition of such time constraints makes the definition of a research topic a very critical problem requiring explicit and careful consideration.

This paper is an attempt to define some of the problem areas for such time-constrained research by considering aspects of the aircraft propulsion system development process and describing significant problems that are common to many cases. This process predictably leads to some well recognized and much investigated topics, but also points to some that have not to date achieved popularity.

After a short discussion of parallel and contrasting aspects of internal vs. external flow, a number of problems will be discussed that repeatedly arise in internal fluid mechanics and are, in this writer's view, legitimate candidates for future research. No claims are made for completeness; other problems could be identified and added to the list.

Scope

In the context of jet aircraft propulsion systems, the central problem of internal fluid mechanics is the measurement, understanding, and prediction of flows inside relatively short ducts of arbitrary shape ($L/D \lesssim 10$). The term duct is used here in a general sense to designate any channel with two or more identifiable inlet or exit openings (referred to here by the common name port) and includes subsonic and supersonic inlets, diffusers, nozzles, bends, and ducts for distributing air in various V/STOL schemes. It also includes all interior passages in jet engines, although the presence of moving boundaries, combustion, and the multiplicity of flow passages create special circumstances that set engine problems apart from those of the airframe maker.

The author's closer familiarity with the latter category introduces a strong bias into this paper, but much of the discussion should be of interest to engine designers as well. Subsonic flow is assumed inside the duct unless specifically stated otherwise.

Internal and External Flows

Internal fluid dynamics was introduced into aircraft design on a significant scale with the advent of jet aircraft in the early forties. Its relative importance has been steadily growing since then, roughly paralleling the increase of thrust-to-weight ratios. It plays a large role in the design of propulsion systems for jet aircraft of all types, faces an additional set of difficulties in the design of highly maneuverable fighters, and encounters its most complex problems in the design of jet VTOL planes.

Internal and external fluid mechanics clearly have a great deal in common in both their theoretical and experimental aspects. They also differ from important points of view. One of the immediately apparent differences is in maturity. The history of significant application of external fluid dynamics in the aircraft industry is nearly twice as long than is the history of internal aerodynamics in this field. External aerodynamics also benefited because extensive human and material resources could be focused on a few subjects of demonstrably critical importance such as airfoils, axisymmetric slender bodies, and some idealized equivalents such as flat plates, spheres, cones, and cylinders. It is, therefore, not surprising that the science of external fluid dynamics has attained a greater capability of solving problems theoretically. Internal fluid mechanics, in contrast, appears not to have reached a comparable level of sophistication and relies more heavily on empirical methods. It suffers from dealing with less clearly defined, less visible and not so obviously important subject material. Research on sophisticated design methods for airfoil contours is standard procedure in the aircraft industry, while the details of internal contours of inlets are usually assigned to loft engineering.

By far the biggest handicap, however, is the greater complexity of problems generally encountered in internal aerodynamics. This will be demonstrated by discussing problem areas that are specific to internal aerodynamics or are more critical than in external aerodynamics.

Interaction Between Adjacent Duct Elements

Boundary conditions in classical aerodynamics cause few headaches. In the overwhelming majority of the problems considered, the flow is postulated to be parallel, uniform, and known at infinity. This condition is fixed and not dependent on the near-field behavior. It is nearly valid for free flight and may be well realized in carefully designed wind tunnels.

Conditions are vastly different in internal flow problems (Fig. 1). For technological and commercial reasons, the system must be broken down into components whose performance must be considered individually. A typical breakdown of a supersonic propulsion system might be: supersonic inlet diffuser, subsonic diffuser, engine, afterburner, and nozzle (Fig. 2). Each component occupies a finite region and interfaces with two other adjacent components, or, in the case of inlets and nozzles, with a duct component at one port and with the freestream at the other. Consideration of the flow within each region as a well-posed problem requires that boundary conditions be given at the two port surfaces. This requirement causes a very basic and invariably present problem because the conditions at the ports are almost never known a priori. The duct element investigated interacts with the two adjacent components, and conditions at either port depend on the flow in both elements on the two sides of the port surface.

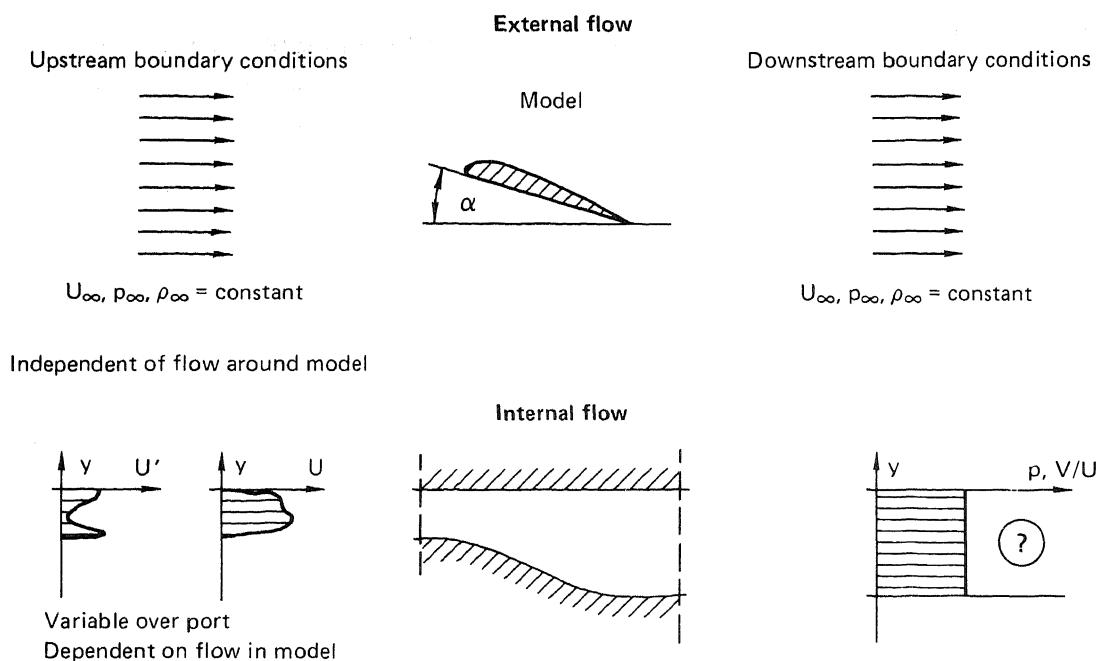


Fig. 1 Comparison of upstream/downstream boundary conditions

This situation is fundamentally different from the type of problem usually dealt with in external flows or in conventional duct flow computations. In internal flow problems, the processes outside the domain of interest do not enforce fixed distributions of any property at the ports (e.g., constant pressure, parallel flow, or any other condition customarily applied); they merely influence certain properties to varying degrees. The real problem is not so much to satisfy a given boundary condition but to match the solution to others describing the flow in adjacent domains.

The situation is further aggravated by the shortness of the ducts (usually ≤ 10 -15 diameters long), so that the boundary conditions at the port are often dominant factors determining the flow in any given section.

The problem of interaction is largely artificial, introduced by commercial realities, such as different manufacturers for the inlet and the engine. Nevertheless, the burden of overcoming this difficulty is real and must be faced routinely by aircraft and engine makers.

The situation is summed up by recognizing that (a) port boundary conditions are extremely important and (b) they are determined by an interaction with the flow outside the duct element of interest.

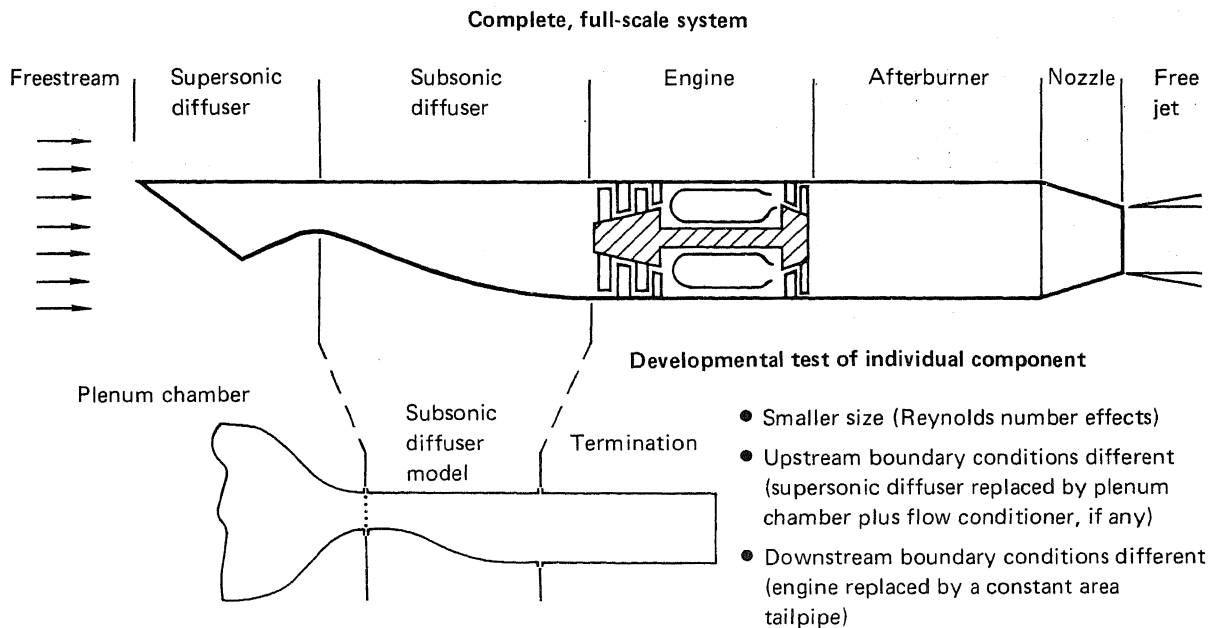


**Fig. 2 Problems of simulation in component testing
(Subsonic diffuser case)**

The ultimate solution to this interaction problem is to test the entire propulsion system as a unit. Such tests, however, are not only extremely costly, but are impossible until the development process is complete. Separate tests of components are mandatory in earlier stages, and each component test has a unique interaction problem: the effects of the missing neighbors of the component must be simulated.

A proposition perhaps next best to testing entire systems would be to include portions of the upstream and downstream neighboring elements. The streamwise extent of these elements could be increased in a trial-and-error fashion until further increases no longer change the flow within the duct element of interest.

This prescription applies, in principle, both to theoretical and experimental efforts. In practice, however, it does not work very well in either case. Present computational capabilities are seldom reliable enough to predict flows in single elements, let alone in entire strings of duct shapes. Experimental work encounters the same obstacles as the testing of entire systems - high cost and the frequent lack of final configurations for adjacent elements.

The conclusion is that under the presently existing constraints on development processes, the interaction problem must be solved by artificially simulating the effects of adjacent elements. The creation of certain desired flow conditions (flow conditioning or flow manipulation) is an experimental skill playing a far larger role in internal fluid dynamics than it does in the serene world of $U_\infty = \text{constant}$.

and how closely? The criteria would surely depend on the purpose of the simulations, e.g., divergent ducts clearly require tighter tolerances on the inlet flow than do contraction sections.

This aspect of simulation may be far more important in duct flow experiments than either Reynolds or Mach number similarity based on overall length and speed scales. In many circumstances, we have a fairly good appreciation of the effects of approximate duplication of Mach or Reynolds numbers. In contrast, we know far less about the nature of approximate equality of port boundary conditions.

Nonuniformity

Assuming that the appropriate boundary distributions are known, and can in fact be realized experimentally (or incorporated in calculation procedures theoretically), a common source of difficulty is that these distributions are grossly nonuniform.

This fact introduces a new dimension of variables that is required to specify the problem. Unlike in most external flow studies, where the geometry of approach conditions can be characterized by two constants (angle of attack and yaw), internal flow studies require definition of the entire distribution of one or more variables over both ports. Prescribing a parallel but nonuniform velocity profile at the inlet or constant pressure at the exit are common examples. The choice of distributions that can or should be prescribed at the ports in order to properly pose the problem is an intricate problem.²⁴ A duct segment performs differently if these distributions are changed, and its performance can never be considered "known" in the sense an airfoil behavior is known when its $C_l(\alpha)$ and $C_d(\alpha)$ characteristics are available. From the experimental viewpoint, the principal consequence is an inexhaustible supply of test variables which grossly increases the size of test matrices and thereby cost.

From the theoretical viewpoint, gross nonuniformities eliminate the distinction between freestream and boundary-layer, which places the validity of classical boundary layer theory in doubt. If the boundary layer is thick compared with the length scale of the cross section, changes in boundary layer displacement thickness will cause sizeable changes in the streamwise pressure distributions. The interaction between boundary layer and freestream is strong and must be taken into account.²⁵ Although boundary layer methods have yielded surprisingly good results in some duct flow situations,²⁶ the limits of applicability are not clear. There is a need for computation schemes that do not employ boundary layer approximations. Finite difference methods using the time-averaged Navier-Stokes equations and various turbulence models deserve (and are receiving) close attention. The combination of a rotational, inviscid freestream with a suitably matched boundary layer could perhaps be used as an economical approximation.

High Turbulence Levels

The turbulent intensities in propulsion system flows are usually much higher than those found in external flows. Several characteristics of internal flow account for this: thick boundary layers, the presence of unsteady zones of separated flow, shock wave oscillations, and, in the afterburner and nozzle regions, a high intensity of turbine exhaust turbulence. A number of difficulties are attributable to this situation.²⁷

High turbulence levels may invalidate many empirical inputs included in boundary layer theories or finite difference computations and used successfully in flows with low freestream turbulence. Transition and separation criteria are influenced. Turbulent modeling assumptions are likely to change if channel and eddy scales become comparable.

Experimental difficulties are also numerous. Total pressure measurements using pressure probes are known to be in error; they are generally too high, which may lead to optimistic conclusions concerning diffuser performance and pessimistic conclusions concerning nozzles. (Note that turbulence intensities are generally larger at the larger area end of a duct passage, regardless of whether it is a diffuser or contraction section.) The magnitude of error is not well known and estimates vary. Hot-wire signals are difficult to interpret in large-scale, three-dimensional turbulence. Laser Doppler anemometers offer promise, but they do not sense pressure and are difficult to use inside channels of irregular shape. Long test times may be required to obtain significant averages, causing drift problems and raising test cost.

Contributions to alleviating this complex problem might come from theoretical/numerical studies of hybrid methods in which the large eddies are computed in detail and the behavior of small (sub-grid) eddies is described by suitable modeling assumptions.²⁸ While this approach will be time consuming, it may represent the minimal level of complexity with the potential to describe phenomena of great practical importance such as dynamic inlet distortion.

One profitable area of related experimental work would involve measurements in intensely turbulent shear flows, specifically designed to determine turbulent quantities required for modeling various terms in finite difference schemes. The connection between quantities measured and the calculation procedure should be direct and demonstrable. Overall level of turbulence would be a prime variable.

Another area is the exploration of the response of various types of pressure probes to turbulence at various turbulent scales and mean shear. Despite the appearance of more sophisticated instrumentation (hot wires and the laser Doppler anemometer) such probes remain the mainstay of industrial practice because of their simplicity and low cost. The interpretation of their response is a large part of development programs. A considerable amount of related recent work has been published,^{29,30} but the interpretation of probe signals still leaves much to be desired.

Reference Quantities and Coefficient Definitions

In problems of classical, external aerodynamics, the conditions at infinity are used to define a natural coordinate system and to normalize the flow quantities of interest. These quantities include well-defined integral properties such as lift, drag, and moments. The related definitions of various coefficients are widely accepted and used (e.g., C_L , C_D , and C_p).

In duct flow research, no clearly superior system of reference quantities exists, except in simple cases involving straight, symmetric ducts with uniform approach flow conditions. The length, time, and mass (or pressure) scales required for normalization may be based on a variety of choices, none of which is clearly preferable. The dilemma is usually between an easily measurable local quantity (some specific wall pressure, peak velocity, or total pressure at some location) and more meaningful but hard-to-measure cross-sectional averages.

A closely related problem is the lack of broadly applicable definitions to describe overall performance of a duct element. Depending on the context, various aspects of performance are of interest and definitions must be formulated accordingly. Unfortunately, the number of definitions in use is greater than necessary, making comparison of data from various sources difficult and frequently impossible. Agreement may exist within a particular specialty, but it seldom transcends the limits of a particular line of application. Inlet designers use area averaged total pressures; ejector engineers talk about skewness factors based on mean exit velocity; nozzle experts are concerned with flow coefficients normalized by isentropic flow rates; and low-speed diffuser designers prefer static pressure recoveries based on mean inlet density and mean inlet velocity squared.

Lack of a common language retards the flow of information, leads to numerous duplications of effort, and reduces the effectiveness of internal flow research. It would be desirable to develop more formalized conventions with regard to reference quantities and performance coefficients. The pros and cons of various possibilities will not be debated here. Factors to be considered in arriving at a choice would include: a) clear relationship to basic principles, b) experimental convenience, and c) relation to traditional definitions.

Summary

Some recurrent problems in the fluid mechanic design and development of air breathing propulsion systems are examined to identify phenomena that are common to many applications. The motivation is to link industrial practice to applied research and to help define problem areas of maximum utility for the latter.

Many of the problems are essentially the practical consequences of the ellipticity of subsonic flows and the finiteness of the domain of interest. High turbulence level is also considered as a major factor aggravating both experimental and theoretical work.

References

1. J.R. Henry, C.C. Wood, and S.W. Wilbur, *Summary of Subsonic Diffuser Data*, NACA RM L56F05, 1956.
2. G. Sovran and E. D. Klomp, *Experimentally Determined Optimum Geometries for Rectilinear Diffusers with Rectangular, Conical or Annular Cross Sections*, Fluid Mechanics of Internal Flow, (Elsevier Pub. Co., 1957), pp. 270-319.
3. M. Sajben, J. C. Kroutil, A. V. Sedrick and G. H. Hoffman, *Experiments on Conical Diffusers with Distorted Inflow*, AIAA Paper No. 74-529, AIAA 7th Fluids and Plasma Dynamics Conference, Palo Alto, California, 17-19 June 1974.
4. R.W. Fox and S.J. Kline, *Flow Regimes in Curved Subsonic Diffusers*, *J. Basic Engrg.* 84, 303 (1962).
5. G. J. Williams and S. J. Stevens, *The Influence of Initial Turbulence on the Performance of Annular Diffusers*, Loughborough Univ. of Technology, Dept. of Transportation Technology, Rept. TT-7101, 1971.
6. V. K. Sharan, *Improving Diffuser Performance by Artificial Means*, *AIAA J.* 10, 1105 (1972).
7. S. Wehofer and R. J. Matz, *Turbine Engine Exhaust Nozzle Performance*, AIAA Paper No. 73-1302, AIAA/SAE 9th Propulsion Conference, Las Vegas, Nevada, 5-7 Nov 1973.
8. M. Sajben, J. C. Kroutil and A. V. Sedrick, *Forces Acting on Conical Diffusers and Their Relation to Integral Performance Parameters*, AIAA Paper No. 73-686, AIAA 6th Fluid and Plasma Dynamics Conference, Palm Springs, California, 16-18 July 1973.
9. Anon., *Performance of Conical Diffusers in Incompressible Flow*, Engineering Sciences Data Unit, London, England, Rept. No. ESDU-73024, 1973.
10. A. L. Braslow and E. C. Knox, *Simplified Method for Determination of Critical Height of Distributed Roughness Particles for Boundary-Layer Transition at Mach Numbers from 0 to 5*, NACA TN 4363, 1958.
11. P. S. Klebanoff and K. D. Tidstrom, *Mechanism by which a Two-Dimensional Roughness Element Induces Boundary Layer Transition*, *Physics of Fluids* 15, 1173 (1972).
12. I. Tani, *Boundary Layer Transition*, Annual Review of Fluid Mechanics, (Annual Reviews, Inc., 1969) Vol. 1, p. 169.
13. H. M. Nagib, M. V. Morkovin, J. T. Yung, and J. Tan-Atichat, *On Modeling of Atmospheric Surface Layers by the Counter-Jet Technique*, AIAA Paper No. 74-638, AIAA 8th Aerodynamic Testing Conference, Bethesda, Maryland, 8-10 July 1974.
14. P. Bradshaw and R. C. Pankhurst, *The Design of Low Speed Wind Tunnels*, *Progress in Aeronautical Sciences* 5, 1 (1964).
15. J.O. Hinze, *Turbulence* (McGraw-Hill, 1959).
16. F.H. Champagne, V.G. Harris and S. Corrsin, *Experiments on Nearly Homogeneous Turbulent Shear Flow*, *J. Fluid Mech.* 41, 81 (1970).
17. H.M. Nagib, *Experiments on Management of Freestream Turbulence*, AGARD-R-598, 1972.
18. J. H. McCarthy, *Steady Flow Past Nonuniform Wire Grids*, *J. of Fluid Mech.* 19, 491 (1964).
19. M. Sajben, J. C. Kroutil, G. H. Hoffman, and A. V. Sedrick, *Generation of Velocity Profiles Using Screens of Nonuniform Solidity*, *AIAA J.* 13, 417 (1975).
20. J. W. Elder, *Steady Flow Through Nonuniform Gauzes of Arbitrary Shape*, *J. Fluid Mech.* 5, 355 (1959).
21. D. R. Kotansky, *The Use of Honeycomb for Shear Flow Generation*, *AIAA J.* 4, 1490 (1966).

References

22. R. J. Baumbick, *Device for Producing Dynamic Distortion Patterns at Inlets of Air Breathing Engines*, NASA TM X-2026, 1970.
23. P.H. Kutschenreuter, Jr., T.P. Collins and W.F. Vier III, *The P³ G – A New Dynamic Distortion Generator*, AIAA Paper No. 73-1317.
24. A. A. Gans and R. A. Serra, *Boundary Conditions and Uniqueness in Internal Gas Dynamic Flows*, AIAA J. 12, 263 (1974).
25. W. W. Bower, *An Analytical Procedure for the Calculation of Attached and Separated Subsonic Diffuser Flows*, AIAA Paper No. 74-1173, AIAA/SAE 10th Propulsion Conference, San Diego, California, 21-23 Oct 1974.
26. P. Bradshaw, R. B. Dean and D. M. McEligot, *Calculation of Interacting Turbulent Shear Layers: Duct Flow*, Imperial Coll. of Sci. and Tech. Rept. No. IC-Aero-71-14, 1971.
27. P. Bradshaw, *Effect of Free Stream Turbulence on Turbulent Shear Layers*, Imperial College Rept. IC-Aero-74-10, 1974.
28. J. W. Deardorff, *A Numerical Study of Three-Dimensional Turbulent Channel Flow at Large Reynolds Numbers*, J. Fluid Mech. 41, 453 (1971).
29. A.E. Fuhs, Ed., *Instrumentation for Airbreathing Propulsion*, (MIT Press, 1974).
30. H. A. Becker and A. P. G. Brown, *Response of Pitot Probes in Turbulent Streams, Part I*, J. Fluid Mech. 62, 85 (1974).

STUDIES OF FORCES INDUCED ON V/STOL AIRCRAFT BY PROPULSION FLOWS

David H. Hickey* and Jerry V. Kirk†
Ames Research Center, NASA
Moffett Field, California 94035

ABSTRACT

Operation of VTOL powerplants induces forces and moments on an aircraft over and above those from the direct-thrust vector. Because these induced effects are not necessarily small, they should be considered in the design of an airplane, both to avoid adverse effects and to enhance performance. The results from several investigations at various fan arrangements are presented, and trends discussed. A survey of induced-lift prediction methods indicates that potential flow methods are available, but, since their accuracy is questionable, they should be improved, possibly with better models of the wake and some allowance for viscous effects.

*Assistant Chief, Large-Scale Aerodynamics Branch.

†Operations Manager, Large-Scale Aerodynamics Branch.

NOMENCLATURE

A_f	fan area, m^2 (ft^2)
A_j	jet area, m^2 (ft^2)
A_L	lifting element area, m^2 (ft^2)
A_T	tunnel cross-section area
a	distance from fan axis to center of pressure, m (ft)
b	half-span of wing, m (ft)
C	local wing chord, m (ft)
CL_{δ_1}	the variation of lift coefficient with flap deflection for unity flap-wing-chord ratio, per radian
C_p	pressure coefficient, $\Delta P/q$
c	two-dimensional wing chord, m (ft)
c_ℓ	two-dimensional lift coefficient
$\frac{C_\ell}{\delta_j}$	the variation of two-dimensional lift coefficient with jet momentum coefficient, per radian, $3.0\sqrt{C_\mu}$
D	fan diameter, m (ft)
D_e	effective fan diameter, $\left(\frac{4A_f}{\pi}\right)^{1/2}$, m (ft)
L_i	lift induced by fan operation
q	dynamic pressure, N/m^2 (lb/ft^2)
R	fan radius, m (ft)
r	radial distance from fan axis, m (ft)
S	wing area, m^2 (ft^2)
T	fan or engine gross thrust in the vertical direction, N (lb)
V	airspeed, m/s (knots)

V_j	airspeed of fan exhaust, m/s (knots)
x	distance from leading edge of wing to fan radius, m (ft)
α	angle of attack, deg
β	angle of exit louvers from the vertical, deg
δ_f	flap deflection, deg
δ_j	two-dimensional jet flap angle, $\frac{90 - \beta}{57.3}$, radians
δ_n	angle of lift-cruise engine nozzles from the vertical, deg
η	fraction of semispan

Subscripts

s	$V = 0$
1, 2, 3	pertaining to the areas in figure 14
2d	two-dimensional

INTRODUCTION

Research has shown that the lifting powerplants incorporated in V/STOL aircraft, with their high power and large exhaust deflections, induce additional forces and moments on the airframe over and above the direct contribution of the powerplants. These additional forces and moments, called "induced" herein, may be either favorable or unfavorable, depending on powerplant location on the airframe.

Ames Research Center has conducted a comprehensive experimental program to define favorable lift-fan placements (refs. 1-12). Table I summarizes the geometry of 11 models that were studied. Fan-in-wing, fans-in-pods, and independent fan arrangements have been studied. At the present time, fan-in-wing arrangements are not in favor because of wing loading limitations, thus most of the paper will consider the induced aerodynamics of fan-powered aircraft with fans at other locations.

This paper shows the induced aerodynamic trends of various fan arrangements and discusses prediction schemes for induced aerodynamics.

EXPERIMENTAL INDUCED-LIFT MEASUREMENTS

Since fan-in-wing arrangements are not of current interest, the results discussed here are for podded or remote installations. Figure 1 shows several large-scale podded-fan installations in the Ames 40- by 80-Foot Wind Tunnel. These models used 1.1 pressure ratio, 0.91 m (3 ft) diameter, GE X376 fans driven by a T-58 gas generator.

The results presented here are uncorrected for wind-tunnel wall effects. For the comparisons presented in this paper, both experimental and theoretical, the lack of corrections to the experimental data does not effect the conclusions.

Podded Configurations

Figure 2 shows the ratio of induced lift to static (fan) thrust where induced lift is defined as total force minus fan thrust and power-off lift for forward-mounted fans as a function of the ratio of forward speed to jet velocity. For these configurations, induced lift becomes negative as forward speed is increased. The configurations with fans located at the 50% semispan location have less negative induced lift than fans mounted at the forward wing root or forward fuselage, thus more outboard fan locations minimize the adverse effect on lift.

Figure 3 shows similar results for aft-mounted fans. The configurations with fans mounted at the wing-root trailing edge had a larger positive induced lift than the configurations with the fan mounted at 50% semispan at the wing trailing edge or at the aft fuselage. However, all aft-mounted fans produced positive induced lift in contrast to the forward-mounted fans, which produced zero or negative induced lift.

The arrangements in figures 2 and 3 do not represent practical VTOL configurations, because the lift at hover produces large moments. A practical VTOL configuration requires fans both fore and aft. Figure 4 presents induced effects of such arrangements. The podded configuration with forward fans at 50% semispan and aft fans at the trailing-edge root provided the highest induced lift for podded configurations; this lift was comparable to an all fan-in-wing configuration. The amount of induced lift varied with configuration; the poorest being the configuration with fans mounted fore and aft in the fuselage.

The effect of trimming drag with exit louvers on induced lift can be derived from the data on figure 5 (from ref. 13). Here the variation of total lift to static thrust ratio is shown as a function of flight velocity ratio for the condition that thrust equals drag. Data are shown for flaps up and down. The induced lift is greatly reduced from the value untrimmed; however, at 40 m/s (80 knots), the total lift is still 15% greater than the installed static thrust. This can represent as much as an 80% increase in payload for STOL operation, thus aerodynamic lift is well worth designing for.

The induced-lift forces can also produce pitching moments which can cause trimming problems. Figure 6 shows pitching moment normalized by lift and effective fan diameter as a function of flight velocity ratio. As can be seen, the fan-in-wing configuration has a large variation of moment with airspeed, whereas, with the podded configuration, the variation is relatively small. Since some of the podded arrangements have nearly as much induced lift as the fan-in-wing arrangement, the podded configurations would seem to be superior on an overall basis.

Up to this point, we have been discussing induced forces on similar installations, with 1.1 pressure ratio tip-turbine-driven fans. As a matter of interest, some tests were conducted at Ames to confirm that fan pressure ratio would have little effect on induced aerodynamics when compared on a velocity ratio basis. Accordingly, both a 1.3- and a 1.1-pressure-ratio fan were installed in the same wing panel with a semispan mounting. Everything, including rotation, internal flow paths, etc., were matched as closely as the different fan designs would allow. The results, for induced lift, are shown in figure 7. We see that, once again, induced lift is significant. Since the fan area to tunnel cross-section area is only 0.0025, the wall effects should be insignificant and the induced-lift values should be accurate. However, the variation of induced lift with velocity ratio is quite different. The cause is unknown, but the results point out that small installation differences or fan-design differences can alter induced aerodynamics significantly. It then follows that, when modeling fan-powered aircraft, every effort should be made to accurately reproduce the full-scale installation.

A further indication of the importance of installation effects is shown in figure 8. Here the ratio of thrust at forward speed to static thrust is presented as a function of velocity ratio. The folding fans of model 7 had a relatively generous inlet radius and showed a substantial increase in fan thrust before the trend was reversed and thrust decreased. The thrust variation with model 3 was more representative of fan-in-wing configurations, and is the value measured for the XV-5A. This was a shallow inlet but had several fixed guide vanes to improve fan inflow. The other curves on figure 8 are from fans in various locations on fan-in-wing model 4, where inlet radius available was a function of local wing thickness. As fan radius grew smaller, the reduction in thrust with forward speed became greater.

To summarize, in this section of the paper, we have shown that to maximize positive induced lift, forward fans should be located as far outboard as feasible and aft fans should be located near the wing-root juncture. It was also shown that induced forces are dependent on small changes in configuration around the fans (or possible fan-flow profile, stream tube shape, etc.).

Remote Lifting Powerplants

Remote lifting powerplants are defined as those not in pods and not connected directly to the wing. One such arrangement is the nose fan on the XV-5A (model 3). Figure 9 shows measured fan thrust and overall lift of the model with only the nose fan operating. With this relatively thick installation, fan thrust always increased with forward speed, however, the total lift of the model decreased as speed increased until, at a velocity ratio of 0.4, the lift was about 1/2 the static thrust. This, of course, is a case of "suck down," as studied on jets exhausting from plates. The negative pressure at the sides and downstream from the jet cause the lift reduction.

Another case of adverse induced lift from a forward-mounted fan is shown in figure 10. For the cases shown, the smallest adverse effect is with the fan mounted well below the wing chord plane. In this case, the adverse effect is caused by the downwash from the flow going through the fan. This downwash unloads the wing substantially. An example of the wing unloading is shown later in this paper, along with a theoretical prediction of the unloading.

Figure 11 shows similar results for an engine exhausting upstream of a wing. In this case, since the engine exhaust was hot, it was necessary to use momentum ratio rather than velocity ratio. The parameter chosen is qS/T . Here again, the downwash induced by the jet flow unloaded the wing. However, in this case the maximum lift loss was about 10%.

The results in figures 9–11 clearly show that, when possible, powerplants in the nose of the aircraft or ahead of the wing should be avoided to provide the most favorable induced lift.

THEORETICAL CALCULATION OF INDUCED FORCES

The flow mechanisms that produce induced forces are varied, as the discussion of experimental results indicate. In the case of the fan-in-wing and podded arrangements we have a thick jet flap which may exhaust at any location from a surface. As early as 1967 (ref. 14), fan-in-wing configurations were represented using finite element techniques. At the present time, Ames has just developed a similar capability to represent a complete configuration with multi-energy flow sources such as lifting elements. However, because none of these methods account for the separation behind the jet efflux, they may give erroneous lift and moment results. The problem is illustrated in figure 12. The flow through the fan emerges as a thick jet sheet and immediately behind the fan is an area that has a pressure coefficient as low as -2 . The main problem is how to represent that area in prediction methods. A simplified equation for the predictions of induced lift, derived in reference 15, uses a combination of two-dimensional jet flap theory and three-dimensional flap-loading theory.

$$\frac{L_i}{T_s} = \frac{V^2}{V_{js}^2} \frac{C_L \delta_1}{4\pi A_f/S} \left[\frac{C_\ell}{\delta_j} \cdot \delta_j \frac{S_1}{S_{2d}} - \left(\frac{V_j}{V} \right)^{3/2} \frac{S_3}{S_{2d}} \right] \quad (1)$$

The right-hand term within the bracket of Eq. (1) was derived empirically to account for the separated area behind the fan. This simplistic approach gave reasonable agreement for lift (fig. 13). The calculated lift can be used with appropriate moment arms to calculate the variation of moment with airspeed.

$$\frac{a}{R} = \frac{\left(\frac{L_{i1}}{T_s} \right) \left(\frac{x}{R} + 2 \right) - \frac{L_{i3}}{T_s} \left(\frac{c}{R} - \frac{x}{R} \right)}{2 \left(\frac{T}{T_s} + \frac{L_{i2}}{T_s} + \frac{L_{i3}}{T_s} \right)} \quad (2)$$

The results calculated from Eq. (2) also showed reasonable agreement with experiment (fig. 14). However, when the area behind the jet became large, the agreement in lift and moment deteriorated markedly, indicating the inability of the simple function to account for the lift loss in that area. The author is aware of one theoretical effort (ref. 16) to properly account for this flow anomaly. In this two-dimensional approach, the airfoil and jet are represented by source or sink distributions. As shown in figure 15, the static pressure in the separated area, the jet shape, and the free stream-line shape are assumed. The solution is then developed through an iteration procedure that changes the shape of the jet sheet to balance pressure and centrifugal forces. It is suggested that this method should be expanded to include finite thickness jets and jets in tandem.

Reference 17 used finite-element techniques to calculate the unloading of a wing by a forward-mounted fan. The theory (fig. 16) represents the fan with an actuator disk and the wake, using the model developed by Wooler.

Figure 17 compares theory with experimental results. The theory generally overpredicted the unloading of the wing. However, since the model inlet was vertically oriented and far from the wing, it may not be the same as the theoretical model. The effect of a fan in front of the wing of model 7 on wing loading is shown in figure 18. At a V/V_j of 0.13, the theoretical jet path intersects the tunnel floor, so, for comparison with experiment, the path was modified to stay within the tunnel walls. This modification changed C_L about 0.17. Even with the modification, the theory underpredicted the adverse lift effect by 0.09 C_L (about 17%). For the present state of the art of prediction methods, this is good agreement.

CONCLUDING REMARKS

Extensive experimental work has given broad guidelines for the placement of lifting powerplants to provide favorable induced lift with small variation of pitching moment with airspeed. However, the ability to predict induced effects accurately for complex configurations is lacking. Potential flow models are available and can probably yield accurate results for some configurations. However, for many configurations, it will be necessary to develop methods that allow for the separated area behind the jet issuing out of a pod or a fuselage.

REFERENCES

1. Aoyagi, Kiyoshi; Hickey, David H.; and deSavigny, Richard A.: Aerodynamic Characteristics of a Large-Scale Model with a High Disk-Loading Fan Mounted in the Fuselage. NASA TN D-775, 1961.
2. deSavigny, Richard A.; and Hickey, David H.: Aerodynamic Characteristics in Ground Effect of a Large-Scale Model with a High Disk-Loading Lifting Fan Mounted in the Fuselage. NASA TN D-1557, 1963.
3. Hickey, David H.; and Hall, Leo P.: Aerodynamic Characteristics of a Large-Scale Model with Two High Disk-Loading Fans Mounted in the Wing. NASA TN D-1650, 1963.
4. Kirk, Jerry V.; Hickey, David H.; and Hall, Leo P.: Aerodynamic Characteristics of a Full-Scale Fan-In-Wing Model Including Results in Ground Effects with Nose-Fan Pitch Control. NASA TN D-2368, 1964.
5. Kirk, Jerry V.; Hodder, Brent K.; and Hall, Leo P.: Large-Scale Wind-Tunnel Investigation of a V/STOL Transport Model with Wing-Mounted Lift Fans and Fuselage-Mounted Lift-Cruise Engines for Propulsion. NASA TN D-4233, Nov. 1967.
6. Hodder, B.; Kirk, J.; and Hall, L.: Aerodynamic Characteristics of a Large-Scale Model with a Lift Fan Mounted in a 5-percent-Thick Triangular Wing, Including the Effects of BLC on the Lift-Fan Inlet. NASA TN D-7031, Dec. 1970.
7. Hall, Leo P.; Hickey, David H.; and Kirk, Jerry V.: Aerodynamic Characteristics of a Large-Scale V/STOL Transport Model with Lift and Lift-Cruise Fans. NASA TN D-4092, 1967.

8. Hickey, David H.; Kirk, Jerry V.; and Hall, Leo P.: Aerodynamic Characteristics of a V/STOL Transport Model with Lift and Lift-Cruise Fan Power Plants. NASA SP-116, Paper No. 7, April 4-5, 1966.
9. Dickinson, Stanley O.; Hall, Leo P.; and Hodder, Brent K.: Aerodynamic Characteristics of a Large-Scale V/STOL Transport Model with Tandem Lift Fans Mounted at Mid-Semispan of the Wing. NASA TN D-6234, 1971.
10. Kirk, Jerry V.; Dickinson, Stanley O.; Hall, Leo P.; and Coffman, Mary G.: Aerodynamic Characteristics of a Large-Scale Lift Fan Transport Model with Podded Fans Forward and Lift-Cruise Fans Mounted Above the Wing. NASA TM X-62,151, April 1972.
11. Hall, Leo P.; and Kirk, Jerry V.: Large-Scale Wind-Tunnel Investigation of a V/STOL Transport Model with Podded Lift Fans Forward and Aft of a Low Mounted Wing. NASA TM X-62,102, Feb. 1971.
12. Atencio, Adolph, Jr.; Hall, Leo P.; and Kirk, Jerry V.: Low-Speed Wind-Tunnel Investigation of a Large-Scale Lift Fan STOL Transport Model. NASA TM X-62,231, Feb. 1973.
13. Hickey, David H.: V/STOL Aerodynamics: A Review of the Technology. AGARD CP-143, Oct. 1974.
14. Rubbert, P.; Saaris, G.; Schoeley, M.; Standen, N.; and Wallace, R.: A General Method for Determining the Aerodynamic Characteristics of Fan-In-Wing Configurations. USAAVLABS Tech. Report 67-61A and 67-61B, The Boeing Company, Dec. 1967. See also NASA SP-218, Sept. 1969.
15. Hickey, D.; Cook, W.: Aerodynamics of V/STOL Aircraft Powered by Lift Fans. Paper presented at a Specialists Meeting of the Fluid Dynamics Panel of AGARD, Goettingen, Sept. 1967 (N68-22498).
16. Hu, Galen; Lotz-Flugge, I.; and Karamcheti, K.: An Analysis of a Two-Dimensional Propulsion Wing. Ph.D. Thesis, Stanford Univ., March 1971.
17. Mendenhall, M. R.; Dillenius, M. F. E.; and Spangler, S. B.: Theoretical Investigation of the Aerodynamic Interference Induced by Cruise and Lift Fans on Transport Type Aircraft. NASA CR-1730, Aug. 1971.

Table I Geometry of large-scale lift-fan-powered model tested in the 40- by 80-Foot Wind Tunnel.







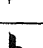




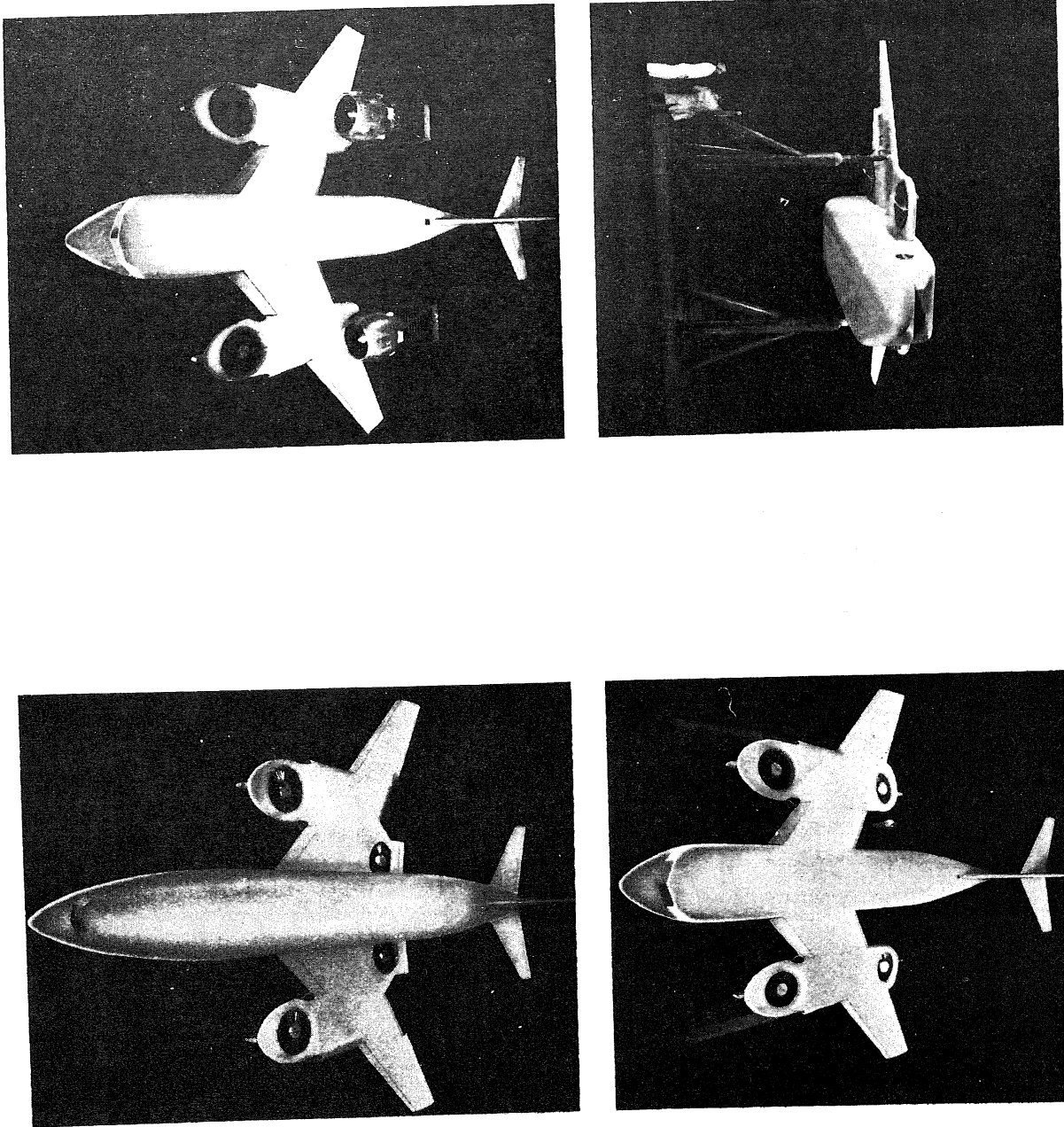
MODEL	TYPE		WING ASPECT RATIO	SWEEP OF QUARTER CHORD LINE	TAPER	$\frac{A_f}{S}$	$\frac{D}{C}$	$\frac{D}{b}$	$\frac{X}{C}$	REFERENCE
1	FAN-IN-FUSELAGE		5	0°	.5	.084	.552	.147	.25	1,2
2	FAN-IN-WING		3.5	16°	.5	.099	.428	.269	.392	3
3	FAN-IN-WING		3.11	16°/25°	.32	.147	.48	.349	.43	4
4	FAN-IN-WING, 6 FANS AFT FAN-IN-WING, 4 FANS AFT FAN-IN-WING, 2 FANS AFT FAN-IN-WING, 6 FANS FORWARD		3.43	20°	.47	.115 .076 .038 .115	.292 .268 .245 .292	.505 .336 .168 .505	.42 .43 .44 .322	5
5	FAN-IN-WING		2.2	52.4°	0	.12	.335	.363	.63	6
6	TANDEM LIFT FAN FAN-IN-WING, 2 FANS AFT FAN-IN-WING, 2 FANS FORWARD		5.8 (BASIC) 3.44(GROSS)	35°	.3	.073 .036 .036	.796 .398 .398	.164 .164 .164	.286 1.24 -.657	7,8
7	FOLDING LIFT FAN ROTATING CRUISE FAN		5.8	35°	.3	.123	—	—	—	7,8
8	TANDEM PODDED LIFT FAN 2 FANS FORWARD 2 FANS AFT		5.8 (BASIC) 4.04(GROSS)	35°	.3	.086 .043 .043	.946 .473 .473	.164 .164 .164	— -.80 1.16	9
9	LIFT-CRUISE FAN 2 FANS FORWARD (PODDED) 2 CRUISE FANS AFT		5.8 (BASIC) 4.4 (GROSS)	35°	.3	.094 .047 .047	— .473 —	.164 .164 .164	— -.80 —	10
10	LOW WING TANDEM LIFT FAN 2 FANS FORWARD (PODDED) FAN-IN-WING, 2 FANS AFT		5.6 (BASIC) 3.7 (GROSS)	35°	.3	.080 .040 .040	— .473 .370	.165 .165 .165	— -.80 1.19	11
11	LOW WING, 2 LIFT FANS FORWARD 2 LIFT/CRUISE FANS AFT		8.14	23.5°	.23	.115 .057 .057	— .48 .48	.134 .134 .134	— -2.56 2.61	12

Figure 1.— Typical lift fan models installed in the 40- by 80-Foot Wind Tunnel.



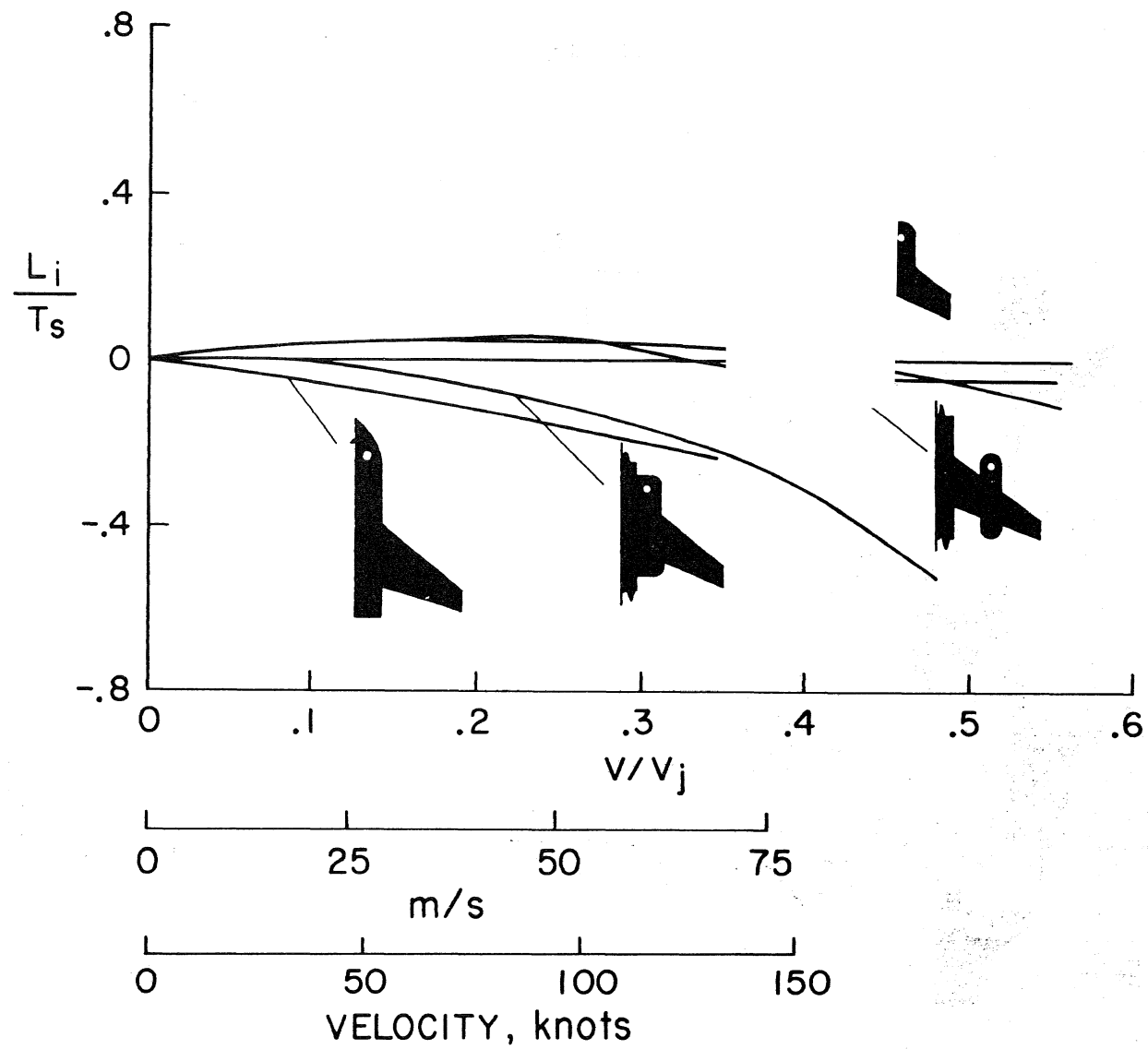


Figure 2.— Variation of induced lift with airspeed for front-mounted lift fans.

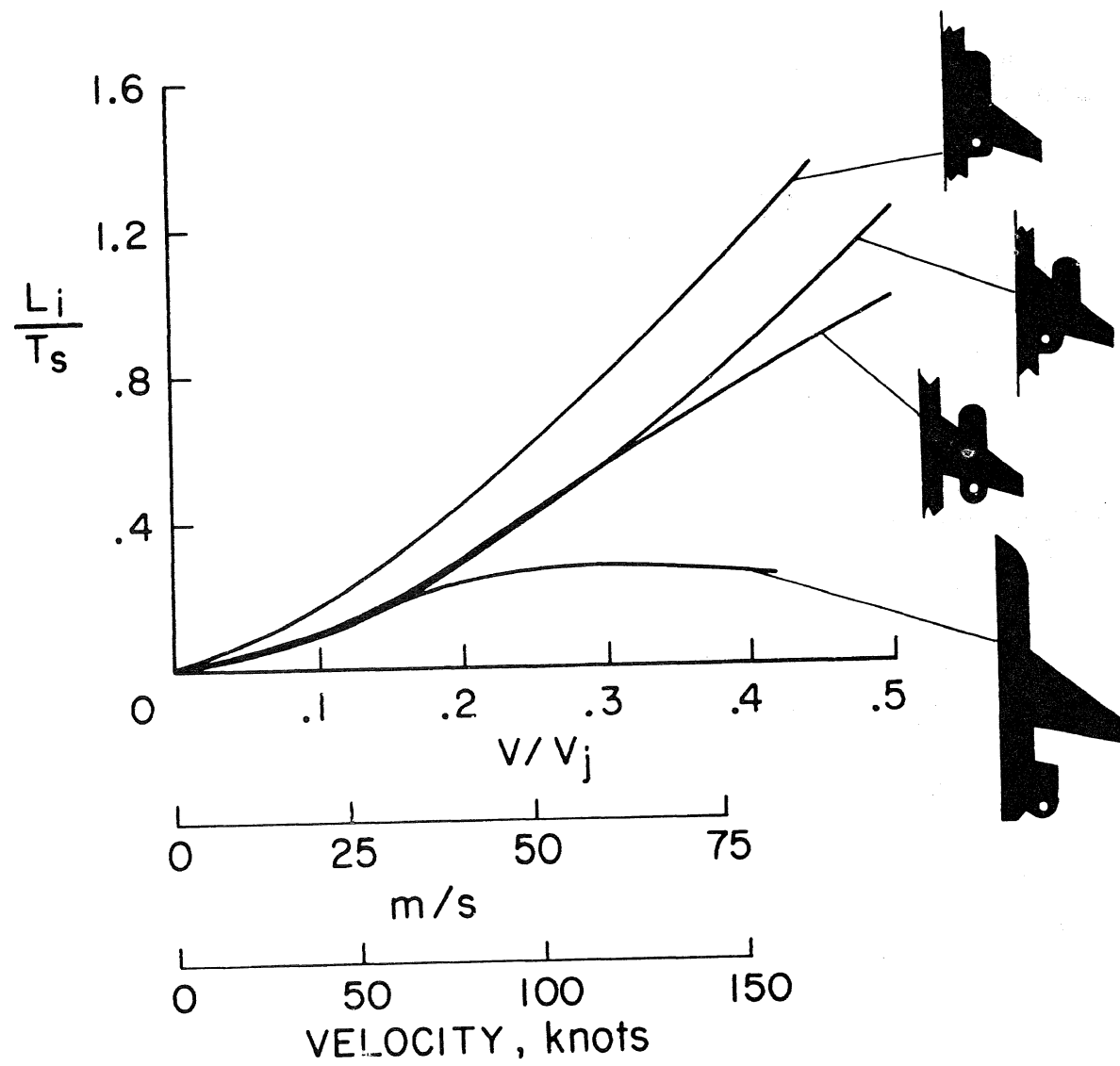


Figure 3.— Variation of induced lift with velocity ratio for aft-mounted lift fans.

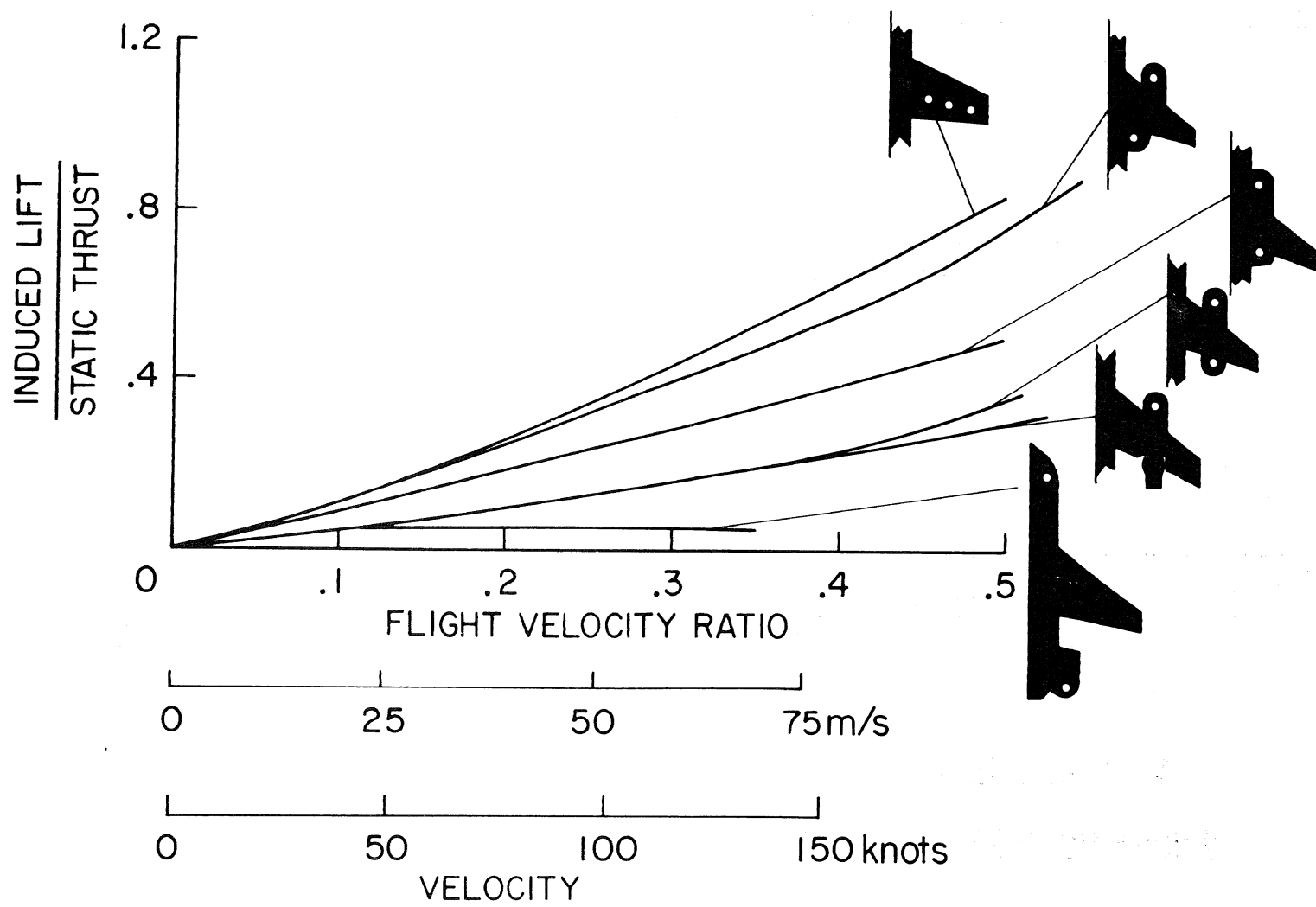


Figure 4.— Variation of induced lift with velocity for complete lift-fan models.

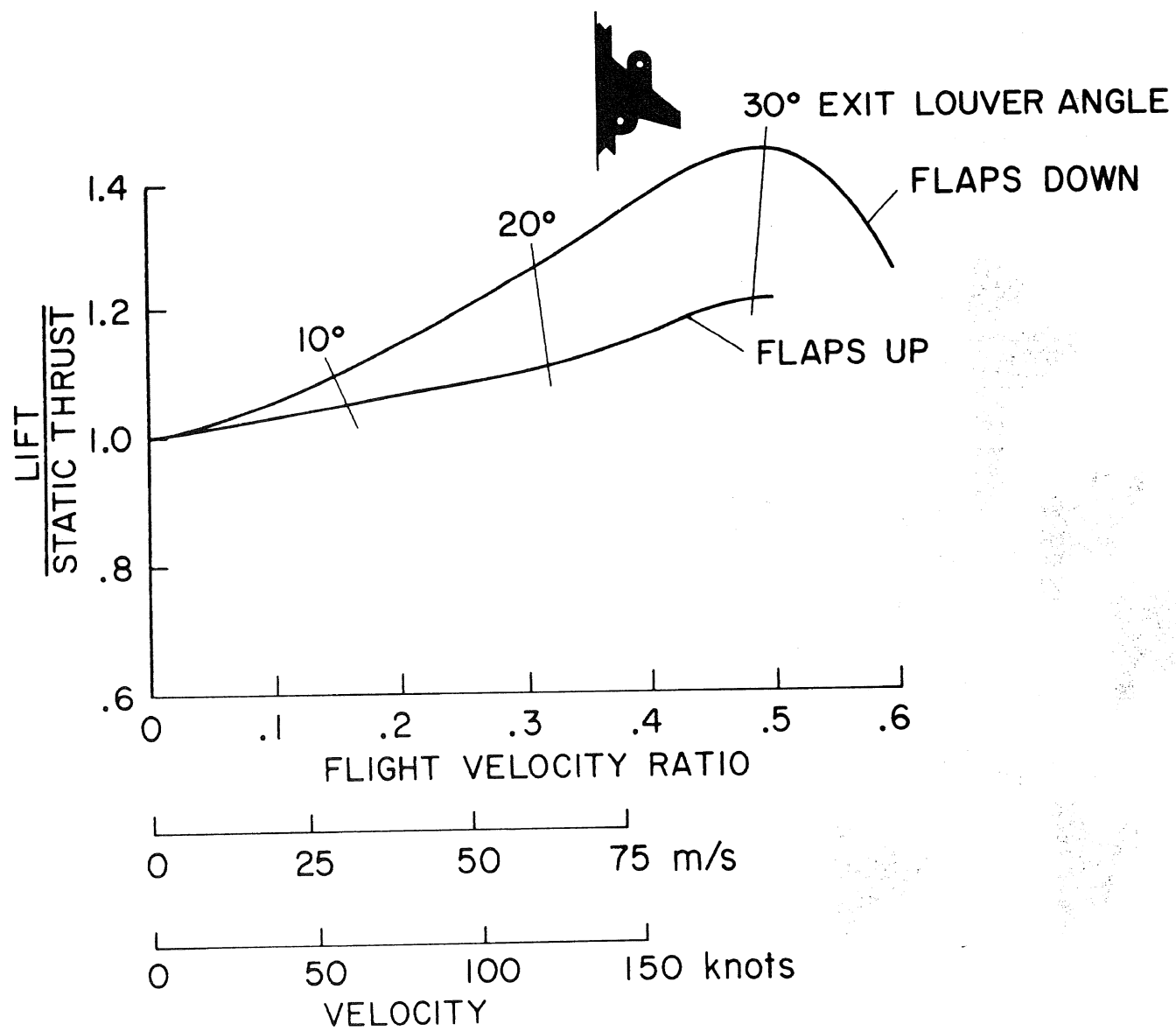


Figure 5.— Variation of trimmed lift with airspeed for unaccelerated flight.

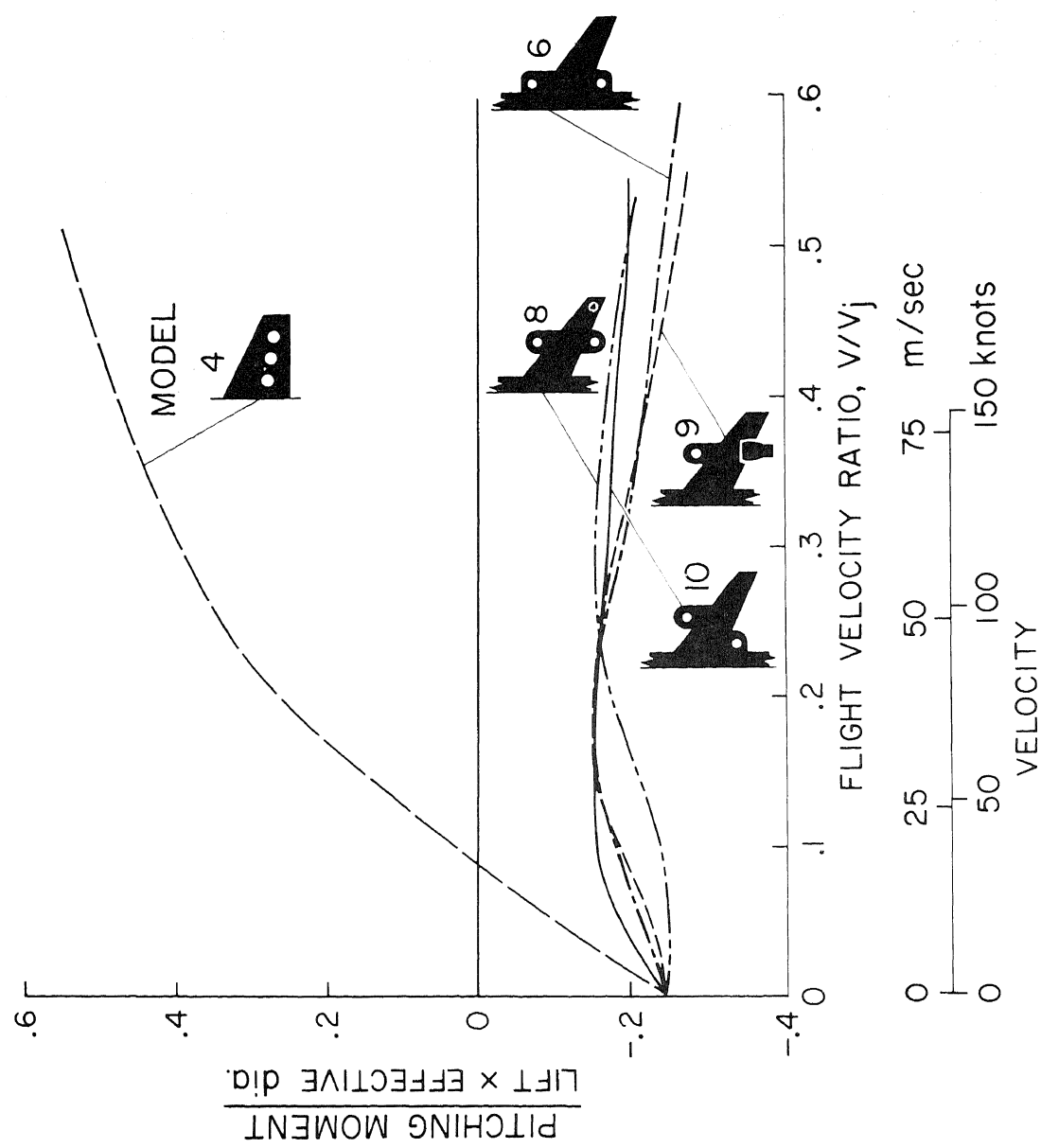


Figure 6.— Variation of pitching moment with airspeed for several lift-fan configurations.

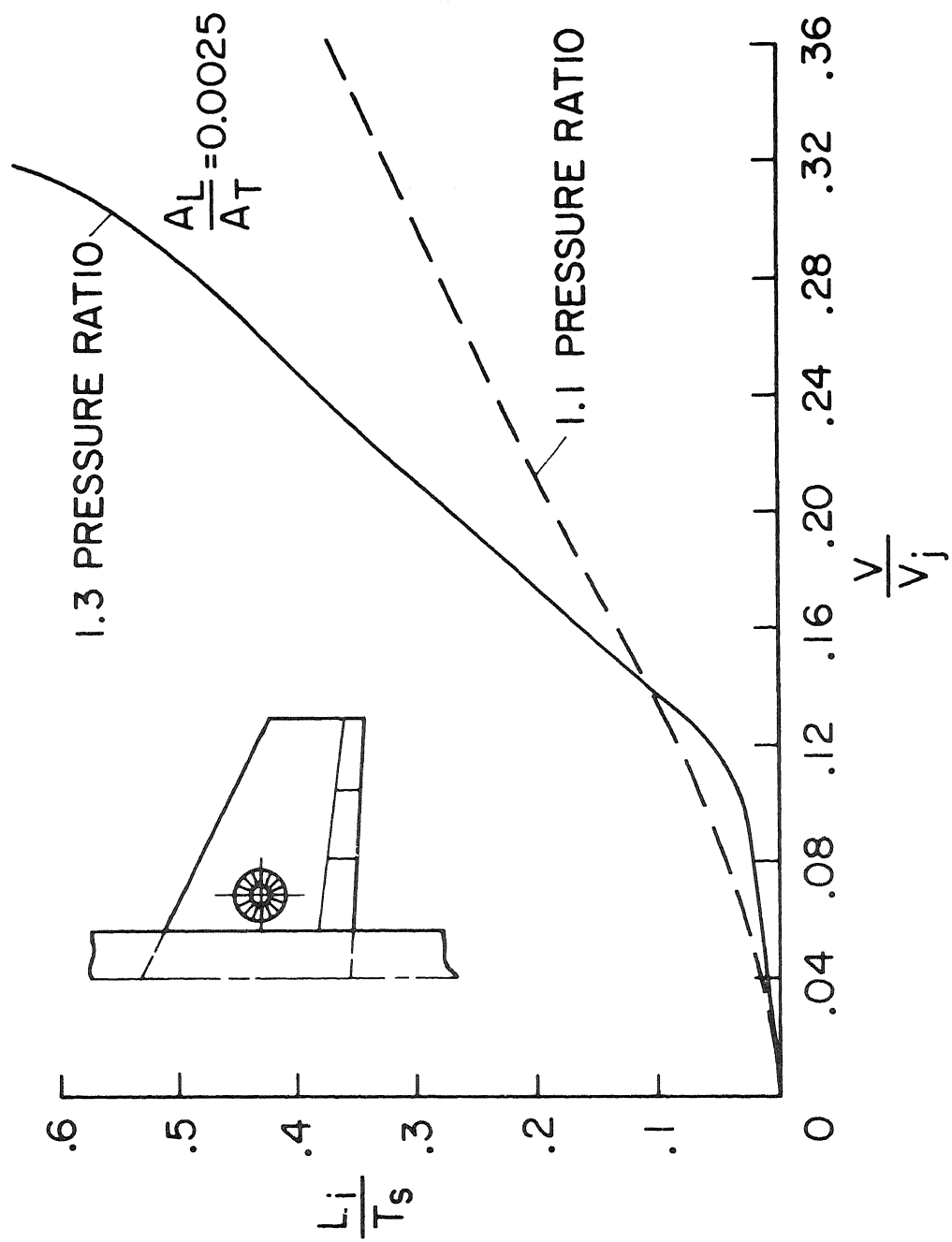


Figure 7.— Effect of fan pressure ratio and internal design on induced lift, with $\frac{A_L}{A_T} = 0.0025$.

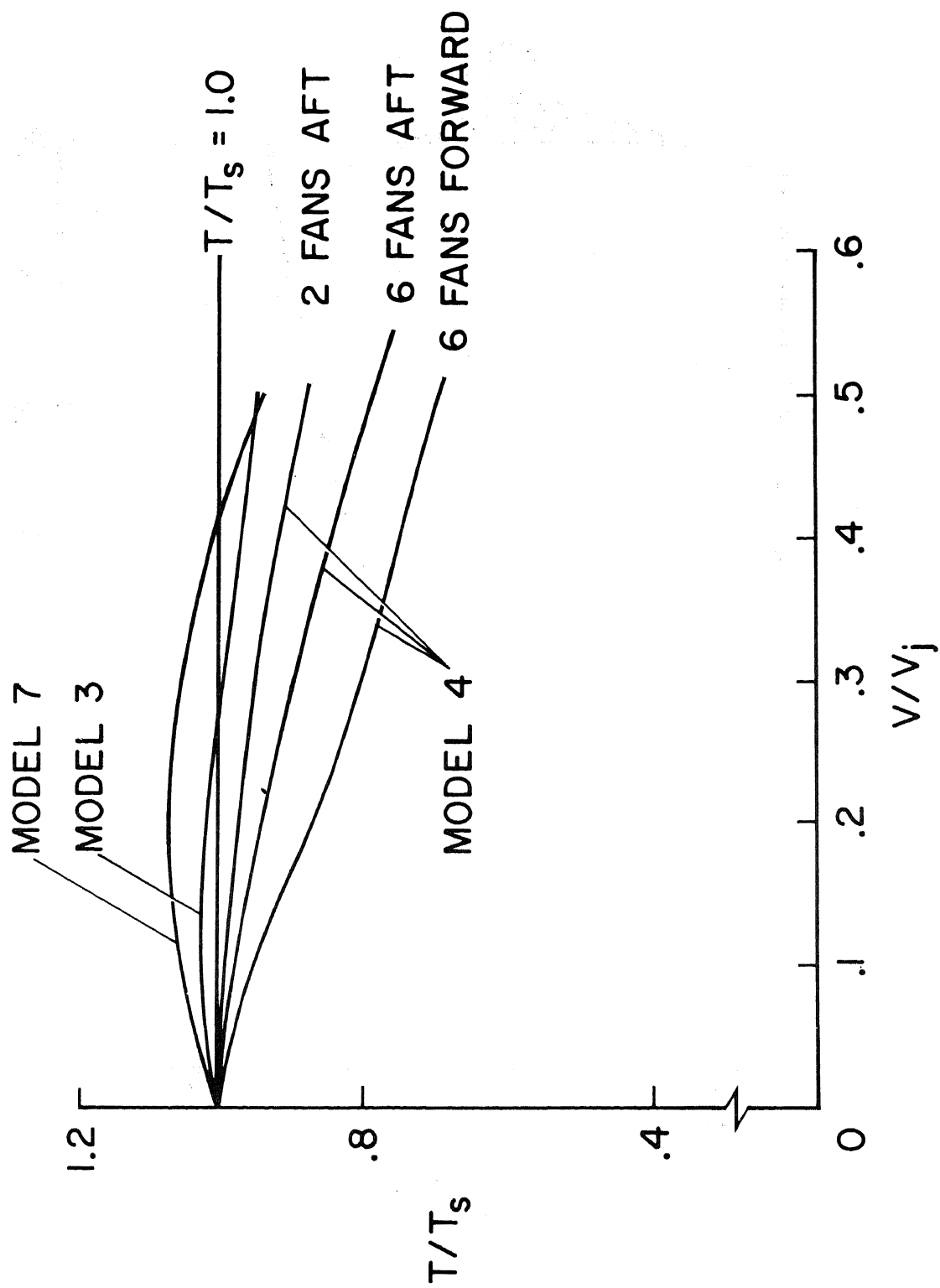


Figure 8. — Effect of installation on the variations of fan thrust with forward speed, $\beta = 0$.

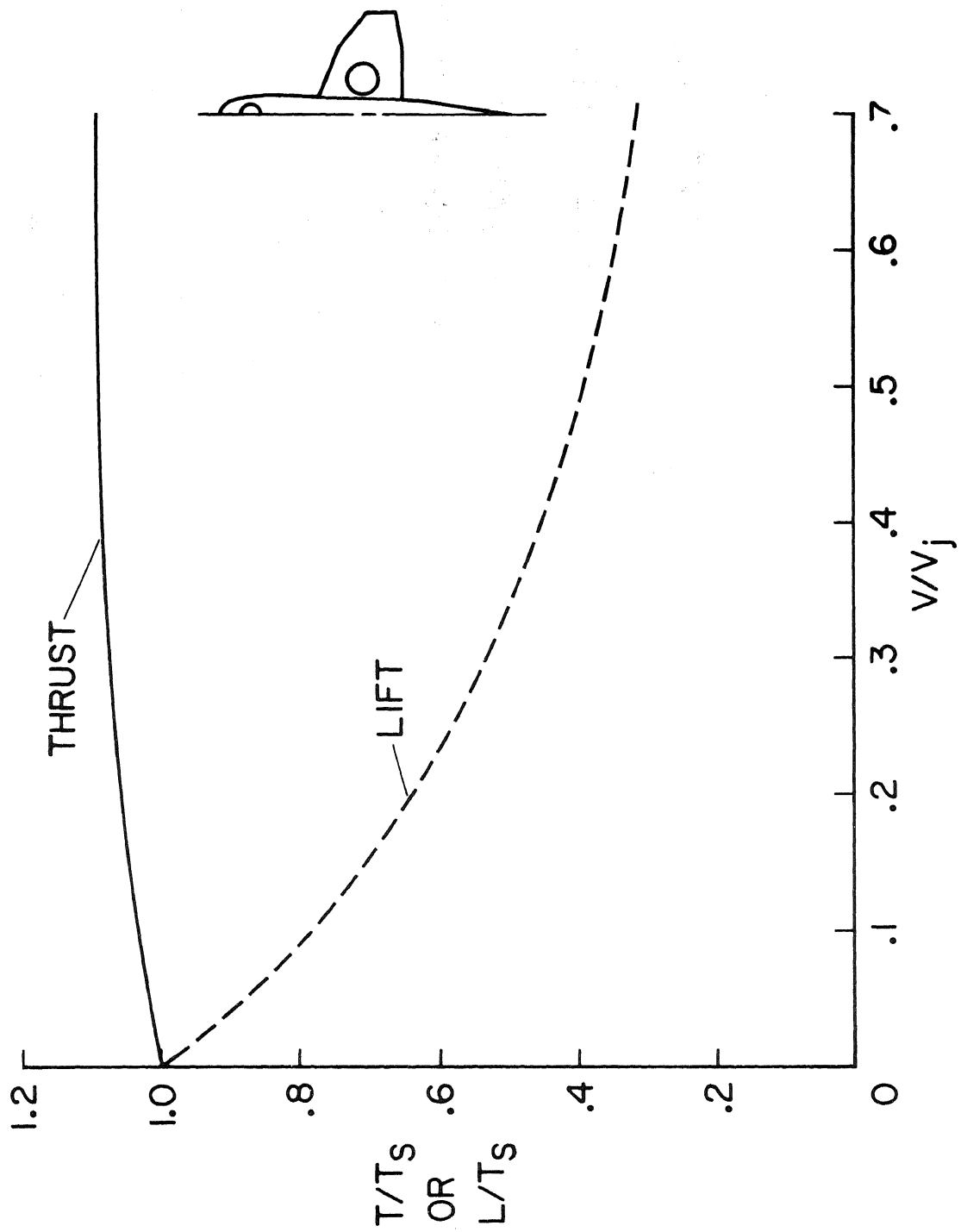


Figure 9.— Lift contribution of a nose fan.

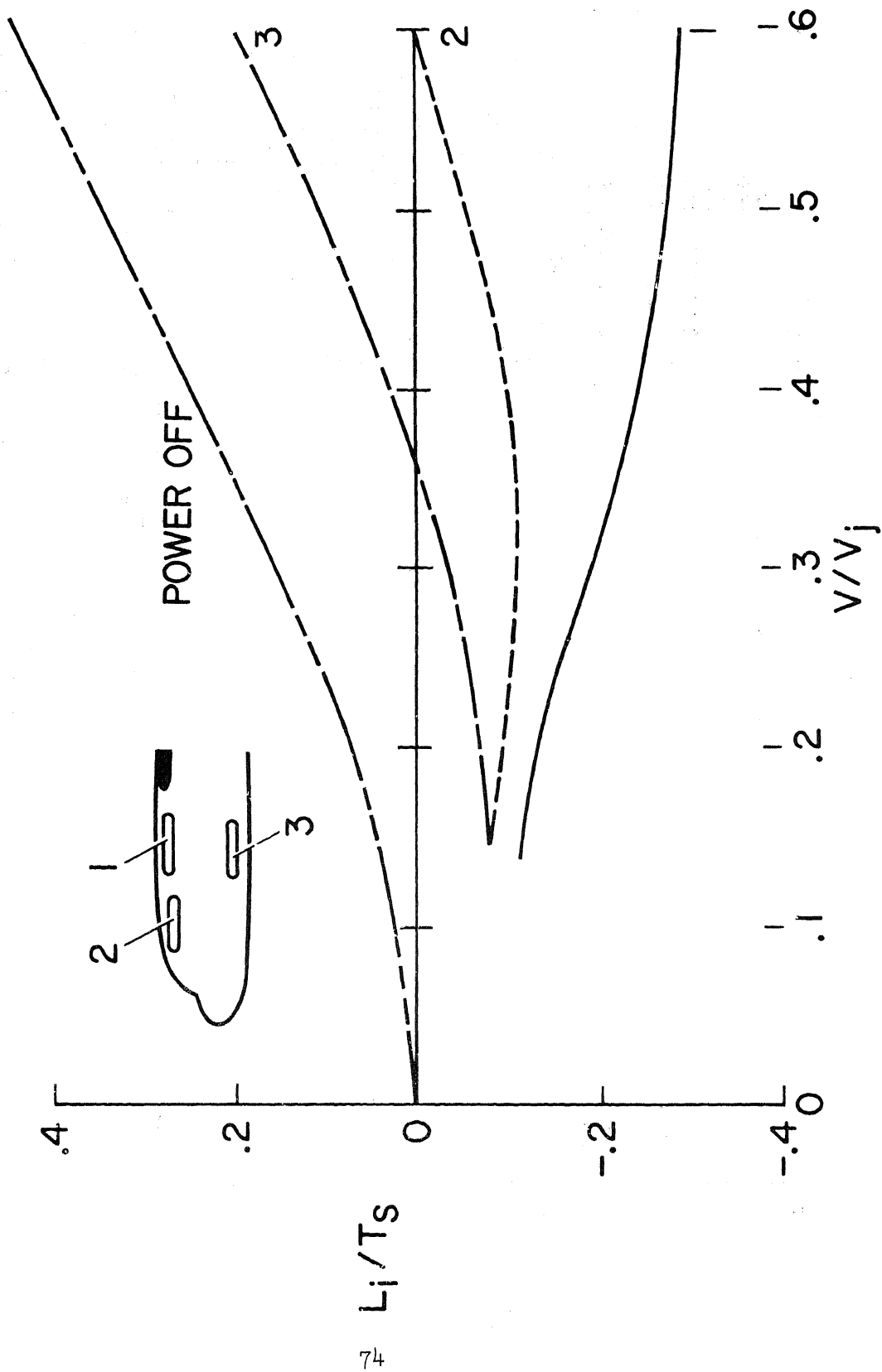


Figure 10.— Variation of lift induced by fans mounted forward of a wing, for $\alpha = 0^\circ$, $\delta_f = 0^\circ$, $\beta = 0^\circ$.

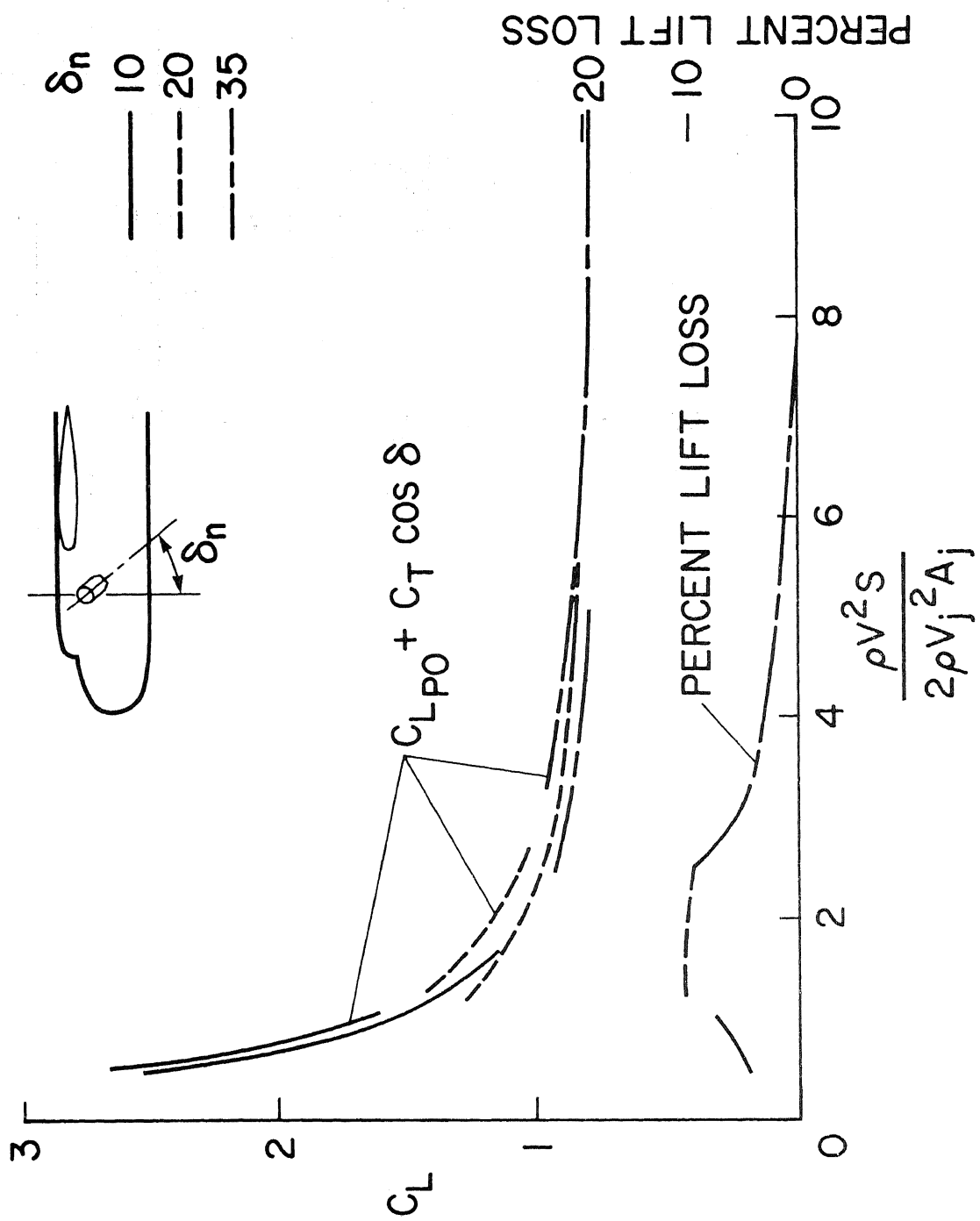


Figure 11.— Lift loss from operation of vectored lift-cruise engines operating ahead of the wing, for model 4 at $\delta_f = 40^\circ$ and $\alpha = 0^\circ$.

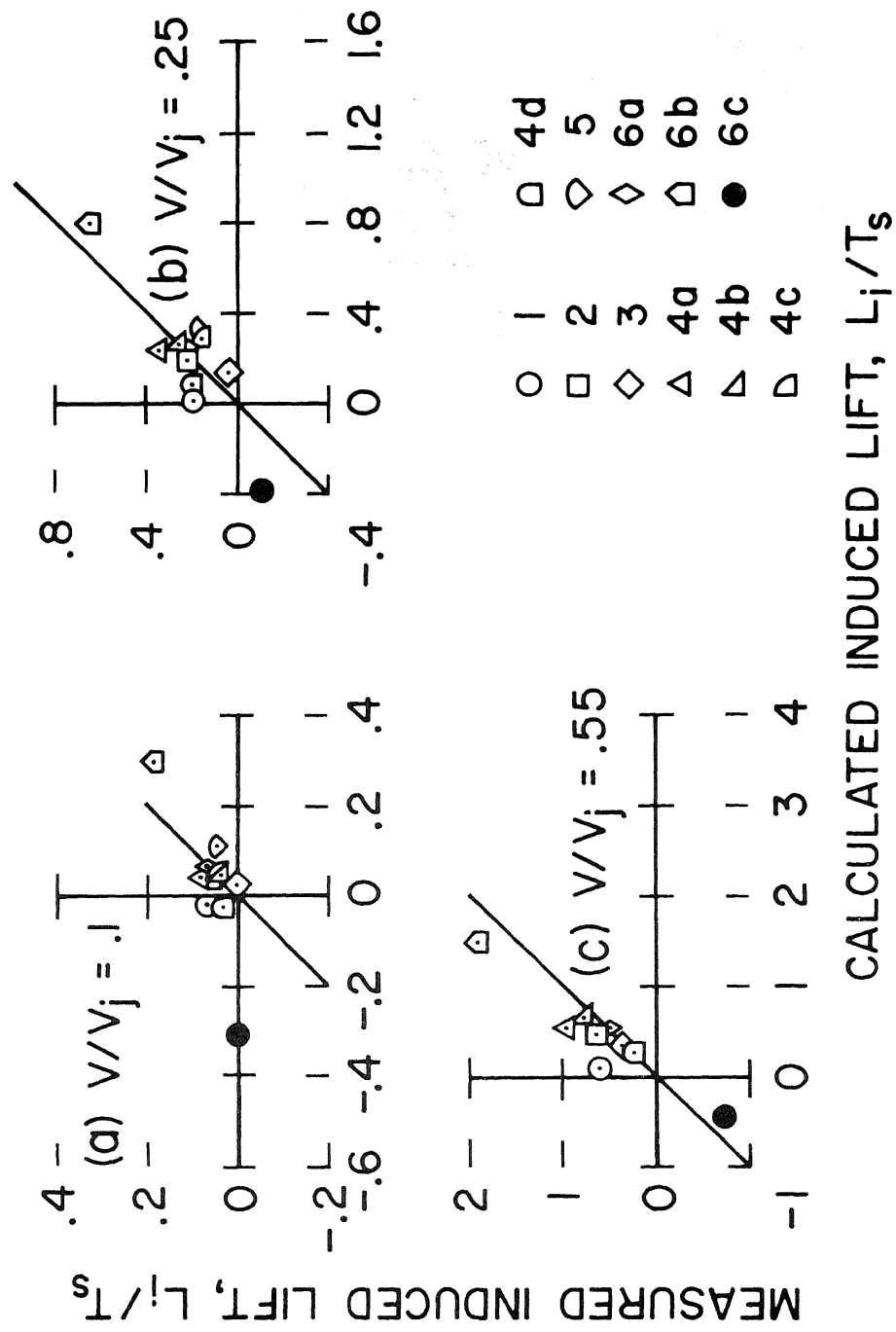
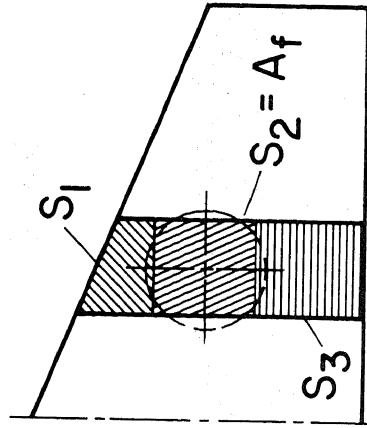
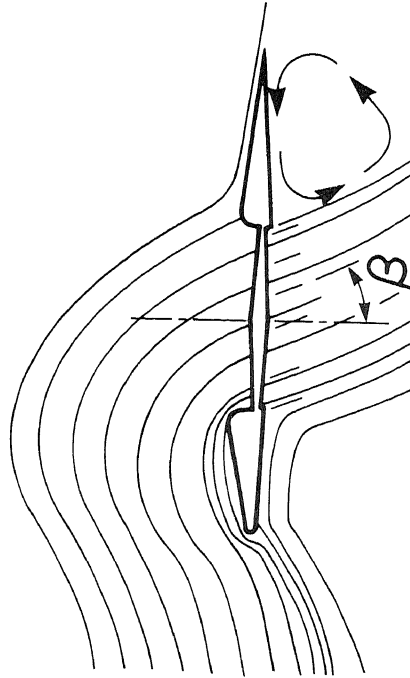


Figure 13.— Comparison of measured and calculated induced lift for several velocity ratios with flaps up at $\beta = 0^\circ$.

THE FLOW FIELD WITH FAN OPERATING

$$\delta_j = 90 - \beta$$

$$\frac{L_i}{T_s} = \frac{V^2}{V_{js}^2} \frac{C_L \delta_1}{4 \pi A_f / S} \left[\frac{C_L}{\delta_j} \cdot \delta_j \frac{S_1}{S_{2d}} - \left(\frac{V_j}{V} \right)^{3/2} \frac{S_3}{S_{2d}} \right]$$



AREAS FOR INDUCED LIFT CALCULATION

Figure 12. – Flow field diagram and calculation model. (a) Flow field with fan operating, for $\delta_j = 90 - \beta$. (b) Areas for induced lift calculation.

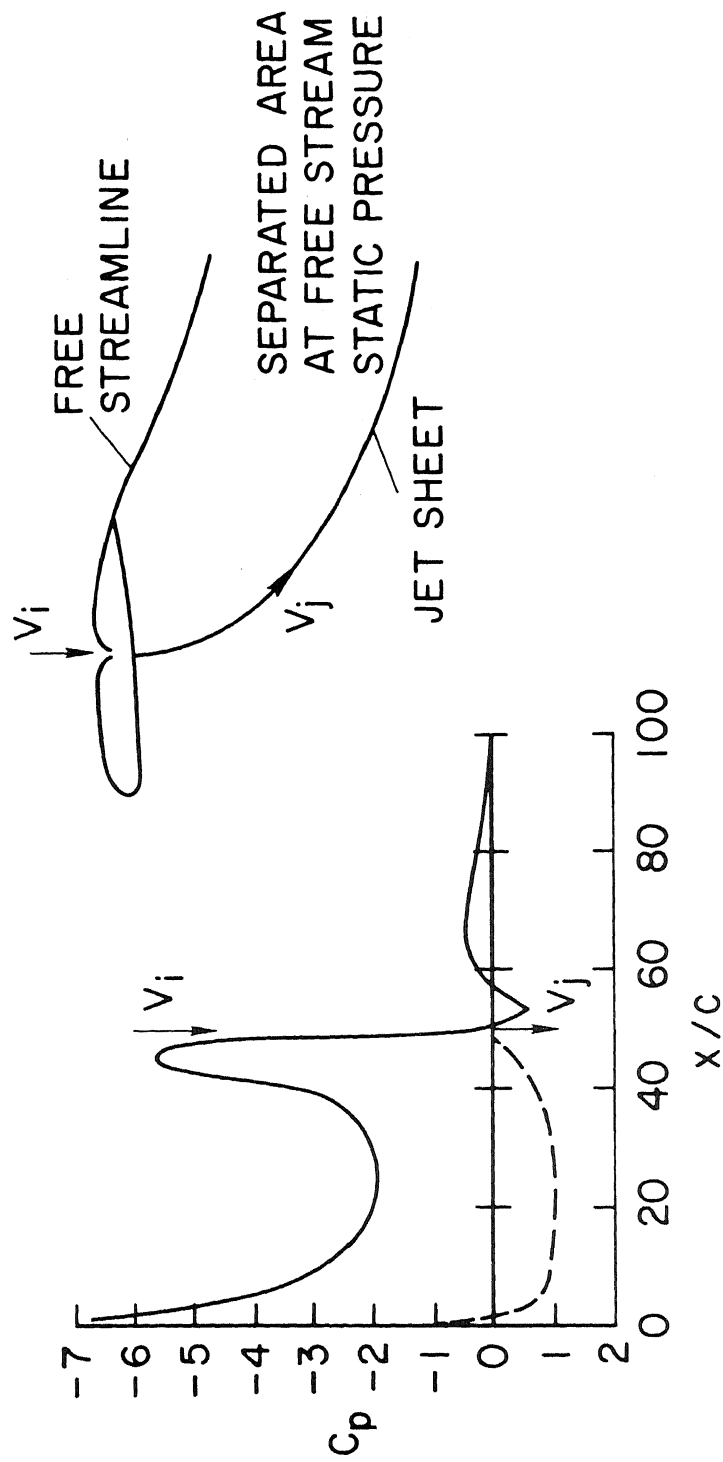


Figure 15.— Calculation of two-dimensional fan-in-wing aerodynamics.

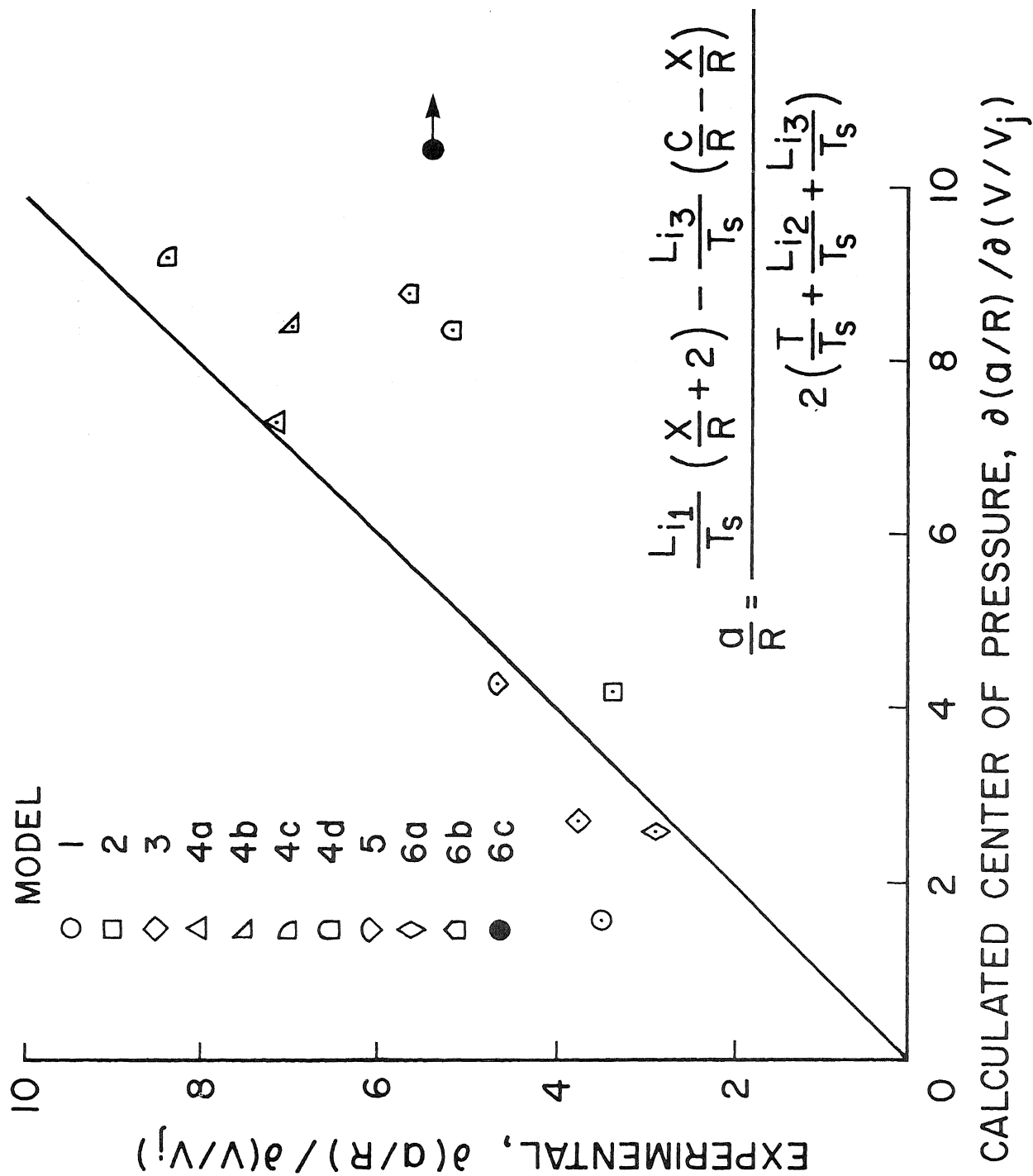


Figure 14.— Correlation of center-of-pressure variations.

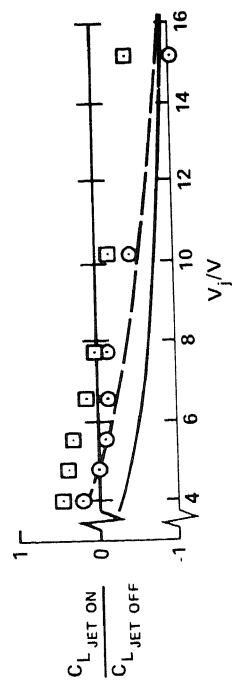
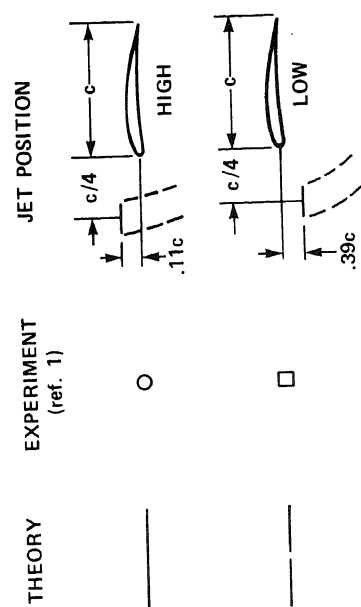


Figure 17.— Comparison of predicted and measured interference on lift for a rectangular wing of aspect ratio.

$$\frac{x}{D} = \sqrt{7} \left(\frac{V}{V_j} \frac{z}{d} \right)^{5/2}$$

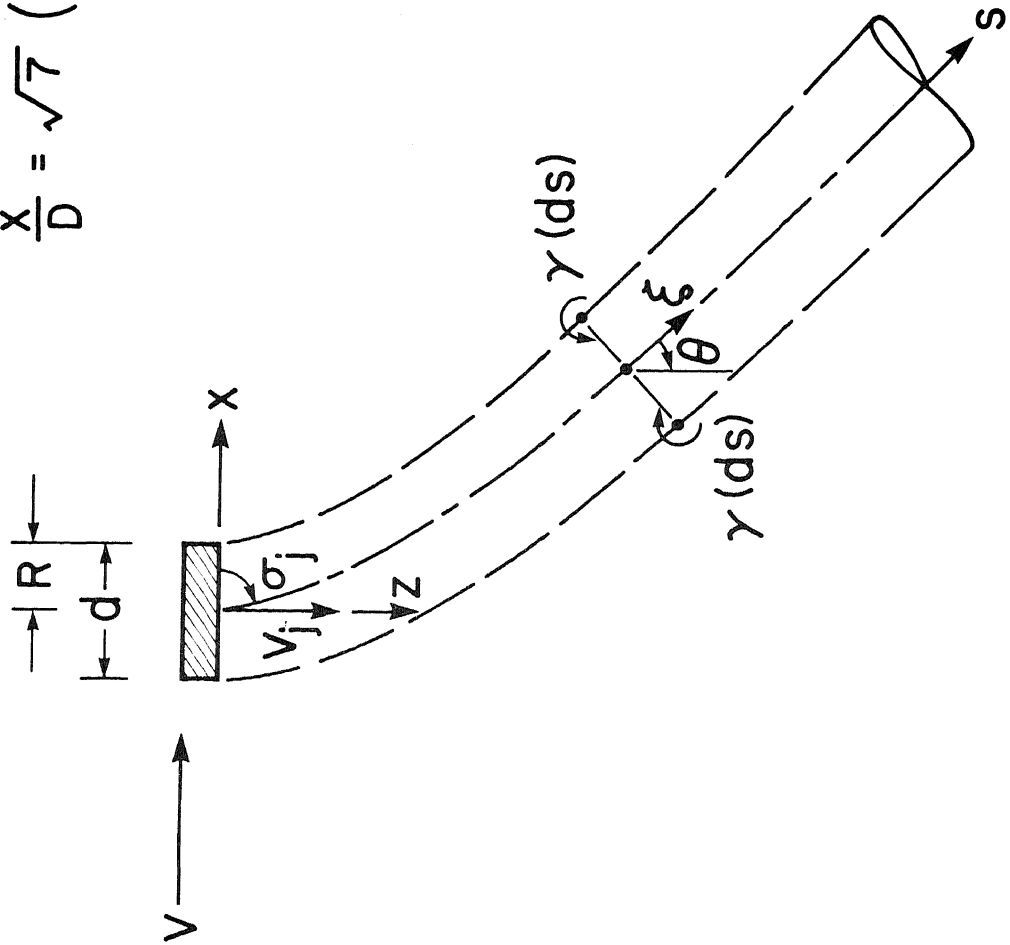


Figure 16.— Mathematical model of lifting jet in crossflow.

Session B

DUCT FLOW STUDIES

Chairman: B. Anderson, NASA Lewis Research Center

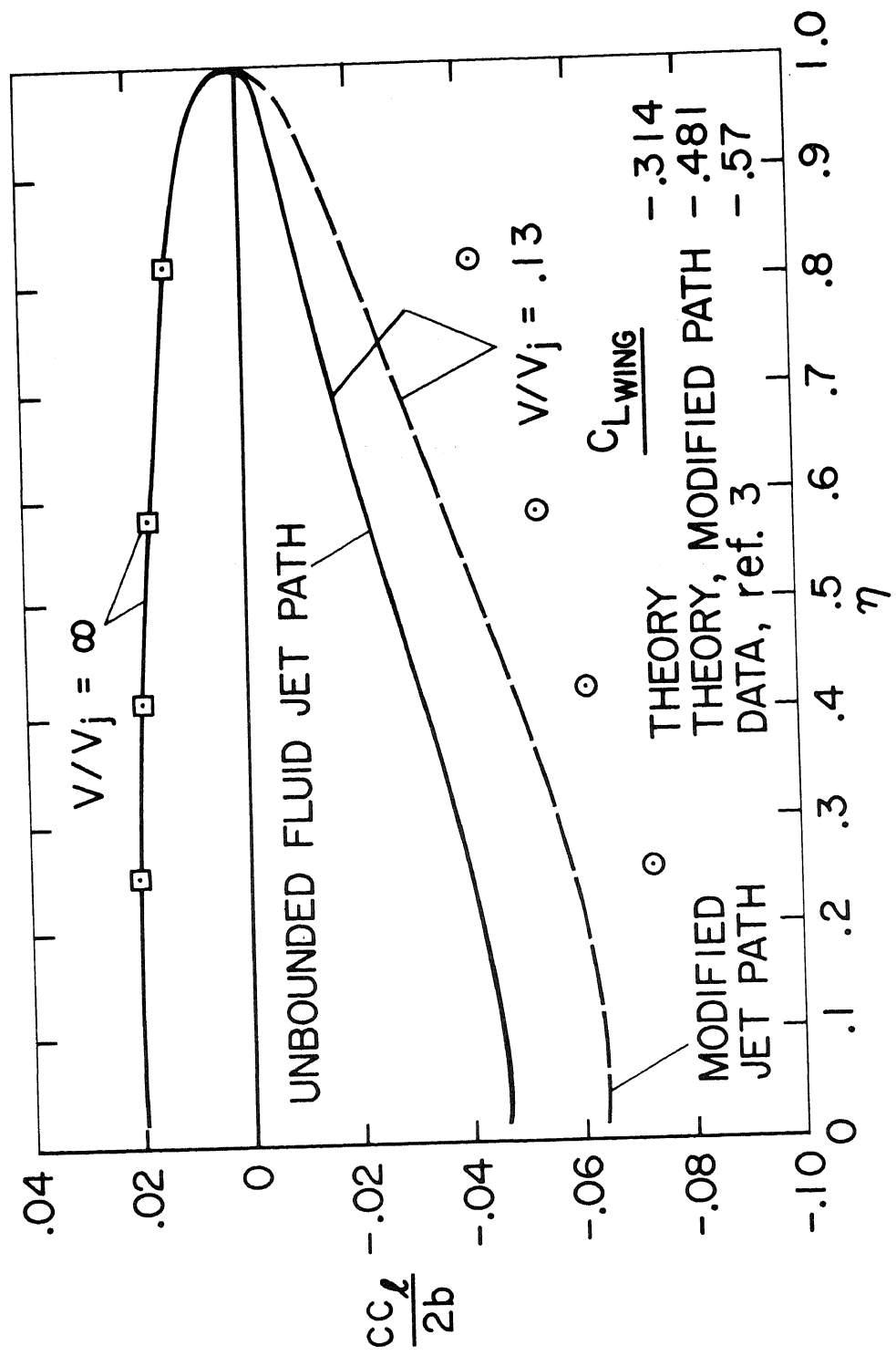


Figure 18.— Comparison of predicted and measured wingspan load characteristics.

A Method for Computing Three-Dimensional
Flow in Ducts

by

Peter R. Eiseman

and

Henry McDonald

UNITED TECHNOLOGIES RESEARCH CENTER

A Method for Computing Three-Dimensional Flow in Ducts

INTRODUCTION

A continuing problem in the development of the intakes for airbreathing propulsion systems is the design of efficient subsonic diffusers. Not only is the engineer faced with building an efficient diffuser, but frequently he must tailor the diffuser geometry to conform to certain physical constraints imposed by the propulsion engine and airframe. Lacking accurate generalized analytical design methods, the engine must rely almost exclusively on empirical design methods based on correlations of experimental data. In the case of three-dimensional inlet diffusers, the cross-sectional shape of the ducting must vary in the axial direction, and it is frequently necessary to introduce offset bends (curved duct centerlines). The diffuser geometry is, therefore, complicated, but perhaps more important, the offset bends induce strong secondary flows which have important effects on diffuser performance. Because of the vast number of geometric and flow parameters, comprehensive experimental programs necessary to develop generalized correlations become very costly. Clearly, the availability of better analytical design tools can significantly reduce the time and cost required to arrive at an efficient diffuser design. A generalized subsonic diffuser analysis capable of being used as a design tool must account for several physical phenomena which frequently occur in practical diffusers. First, the analysis must be capable of treating the case when the wall boundary layers are turbulent and possibly of a thickness comparable to the dimensions of the diffuser flow passage. Secondly, the analysis must account for pressure gradients transverse to the direction of flow which can arise because of curvature of the duct centerline. Finally, the analysis should be capable of treating strong interaction problems; i.e., problems in which the viscous flow interacts with the inviscid flow.

Because of their complexity, and particularly the interaction which occurs between primary and secondary flows and viscous and inviscid regions, three-dimensional flows in curved ducts have been extremely difficult to analyze. Rotational inviscid flow theory has provided insight into the behavior of some secondary flows (Hawthorne, Ref. 1), and has now been developed to the point where solutions to the full incompressible, rotational inviscid equations of motion can be computed (Stuart & Hetherington, Ref. 2). Techniques for computing three-dimensional laminar and turbulent boundary layers have also been developed. Some of these are surveyed by Nash & Patel (Ref. 3). However, there are considerable difficulties associated with the synthesis of secondary flow analysis and boundary layer theory into a cohesive method of duct flow analysis. Not the least of these difficulties is the lack of applicability of three-dimensional boundary layer theory in corner regions, a means for patching or interfacing boundary layer and rotational inviscid flow regions, and the treatment of interaction between viscous and inviscid flow regions.

TABLE OF CONTENTS

	<u>Page</u>
.....	1
COORDINATES	3
.....	5
.....	6
.....	12
tes	12
.....	15
.....	20
REFERENCES	23
FIGURES	

In efforts to circumvent these difficulties, Patankar & Spalding (Ref. 4), Caretto, Curr, & Spalding (Ref. 5), and Briley (Ref. 6) devised numerical methods for solving approximate governing equations which are a more or less natural generalization of three-dimensional boundary layer theory. In these studies, solutions were computed for laminar incompressible flow in straight ducts with rectangular cross sections. The governing equations were solved by integrating in a primary flow coordinate direction while retaining viscous stresses in both transverse coordinate directions as opposed to only one direction for three-dimensional boundary layer theory. In addition, certain assumptions were made about the behavior of pressure gradient terms for incompressible flow to permit solution by forward marching integration. Subsequently, this general approach has been used to compute laminar incompressible flow in helical tubes by Patankar, Pratap, & Spalding (Ref. 7).

Recently in companion studies, Briley & McDonald (Ref. 8) and McDonald & Briley (Ref. 9) have developed stable and efficient noniterative implicit numerical techniques for application to systems of coupled nonlinear multidimensional parabolic and/or hyperbolic equations. These general techniques were applied by McDonald & Briley (Ref. 9) to the computation by forward marching integration of laminar supersonic flow in rectangular jets. Subsequently, the laminar incompressible straight-duct analysis of Briley (Ref. 6) and the improved numerical techniques of McDonald & Briley (Ref. 9) for compressible flows were extended and synthesized by Briley & McDonald (Ref. 10) and Eiseman, McDonald, and Briley (Ref. 11) into a method for computing subsonic turbulent flow in curved ducts. The present study represents a further generalization of the latter method, to encompass general coordinates and highly complex geometries.

Of particular interest in the present study is the treatment of complex diffuser geometries. Here an approximate set of governing equations is derived for flow passages whose bounding walls lie in coordinate surfaces of a general coordinate system. A coordinate system analysis is then performed for the special case of a diffuser having a curved centerline and superelliptic cross sections which can vary continuously between a circle and a mean rectangle. Examples of this class of diffuser geometry are shown in Fig. 1 with the aid of some computer graphics provided by B. Anderson of NASA Lewis Research Center. The boundary of the flow passage is a tube-like coordinate surface which can be thought of as a generalization of a cylindrical surface.

GOVERNING EQUATIONS IN CURVILINEAR COORDINATES

Central to the present analysis is the formulation of approximate governing equations which can be solved by forward marching integration in the direction of a "primary flow". The entire flow field can thereby be obtained by a sequence of essentially two-dimensional calculations, and this feature of the method results in a substantial saving of computer time and storage compared to that which would be required for solution of the full (elliptic) Navier-Stokes equations. The equations are derived in a coordinate independent manner. A vector field that reasonably approximates the primary flow direction is chosen and then used as the basis for an approximation of the stress tensor. The time-averaged equations are written in general conservation law form, and then the approximate stress tensor is inserted to obtain the approximate equations. Note that this process depends only on the choice of a primary vector field, and not on the particular coordinate system used for the numerical solution. The primary vector field used here consists of the tangent vectors to a certain family of coordinate curves that are roughly aligned with the flow geometry.

The governing equations are derived from the Navier-Stokes equations for compressible flow of a viscous, perfect gas. In conservation law form (Ref. 12), and, in general, curvilinear coordinates (y^1, y^2, y^3) , these equations are given by

$$\frac{\partial \rho}{\partial t} + \frac{\partial}{\partial y^i} (\rho v^i \sqrt{g}) = 0 \quad (1a)$$

for continuity and

$$\frac{\partial}{\partial t} \left[\rho v^i \frac{\partial x^s}{\partial y^i} \sqrt{g} \right] + \frac{\partial}{\partial y^j} \left[(\rho v^i v^j + \tau^{ij}) \frac{\partial x^s}{\partial y^i} \sqrt{g} \right] = 0 \quad (1b)$$

for momentum. Constant total temperature is assumed, and thus an energy equation is not required. We have used (x^1, x^2, x^3) for fixed cartesian coordinates, ρ , for density, (v^1, v^2, v^3) for curvilinear velocity components, and τ^{ij} for the components of stress including the pressure. From the ideal gas law and the constant total temperature assumption, the perfect gas relation has the form

$$p = A\rho + B\rho g_{ij}v^i v^j$$

where A and B are constants and g_{ij} is the metric tensor, which is defined by the fundamental element of arc length, $(ds)^2 = g_{ij}dy^i dy^j$. In all of the above, the Einstein summation convention is assumed. That is, matching upper and lower indices are to be summed from 1 to 3 unless otherwise stated.

It is assumed that, for high Reynolds number, viscous effects are negligible except in thin layers near the walls, and thus boundary layer concepts can be employed to examine the relative importance of viscous terms in the governing equations. Consequently, viscous terms which are considered important for boundary layer flow on walls are retained; other viscous terms are neglected. In this sense, the present approach can be regarded as a natural extension of three-dimensional boundary layer theory. Unlike conventional

boundary layer theory, however, the approximate equations are to be applicable in the inviscid flow region as well as the viscous region and, thus, no approximations are made for inviscid terms other than those to be discussed for the pressure field in subsonic flow.

To account for turbulent transport processes, the governing equations are time-averaged in the usual manner for turbulent flows (e.g., Hinze, Ref. 13). This process of averaging produces turbulent correlations which are conventionally termed Reynolds stresses. Certain components of viscous stress are removed from the time-averaged equations. The removal process is based upon the assumption that a primary flow direction exists.

Our approximation to the Navier-Stokes equations can be written explicitly in the conservation law form given previously. The time-averaging for turbulent fluctuations, however, requires some additional notation. Specifically, the dependent variables are represented as the sum of a time-averaged quantity denoted by a straight overbar (-) and an instantaneous fluctuating quantity denoted by a curved overbar (~). After time-averaging, the equations become

$$\frac{\partial}{\partial y^i} \left[(\bar{\rho} \bar{v}^i + \bar{\rho} \tilde{v}^i) \sqrt{g} \right] = 0 \quad (2a)$$

for continuity, and

$$\begin{aligned} \frac{\partial}{\partial y^i} \left[(\bar{\rho} \bar{v}^i \bar{v}^j + \bar{\rho} \overline{\tilde{v}^i \tilde{v}^j} + \bar{\rho} \tilde{v}^i \bar{v}^j + \bar{\rho} \tilde{v}^j \bar{v}^i \right. \\ \left. + g^{ij} (\bar{p} + \bar{v}^{ij}) \frac{\partial x^k}{\partial y^i} \sqrt{g} \right] = 0 \end{aligned} \quad (2b)$$

for momentum where the \bar{v}^{ij} are the time averaged components of the approximate viscous stress. The triple cross correlation terms have been neglected. Since the remaining components of Reynolds stress are coefficients in the tensor product basis $\frac{\partial}{\partial y^i} \otimes \frac{\partial}{\partial y^j}$ they can be expressed in any needed form via a change of tensor product basis.

For entirely supersonic flows, the approximate equations together with boundary and initial conditions can be solved by forward marching integration in the x direction without any assumptions about the pressure field, as was demonstrated by McDonald & Briley (Ref. 9) for laminar flow in rectangular jets. For subsonic flow, however, the inviscid flow region is known to be governed by equations which are elliptic; that is, by equations which require downstream boundary conditions for solution. In this circumstance, solution by forward marching integration is not appropriate, at least not without some sort of iterative procedure to satisfy the downstream boundary conditions. To circumvent this problem for subsonic flows, it is therefore assumed that the pressure field appropriate for irrotational inviscid flow through the passage represents a given, reasonable first approximation to the

actual pressure field. Thus, inviscid axial pressure gradients computed with appropriate downstream boundary conditions are "imposed" upon the flow, much as in conventional boundary layer theory, so as to permit solution by forward marching integration for subsonic flows. For internal flows, the inviscid pressure gradients are corrected for internal flow losses associated with the well known viscous pressure drop and blockage effects by a process which is consistent with forward marching integration. The imposition of inviscid pressure gradients incorporates a priori the elliptic effects associated with a subsonic pressure field without the necessity of solving elliptic equations other than for an inviscid flow. The inviscid pressure field can be generated from any convenient source and does not necessarily require the solution of compressible or even three-dimensional inviscid flow equations.

METHOD OF SOLUTION

The governing equations can be solved (after modeling the Reynolds stresses) following the general approach developed by McDonald & Briley (Ref. 9) for laminar supersonic flow in rectangular jets. A detailed discussion of the calculation procedure is not included here, as such a discussion would be lengthy, and discussions of the general approach are available elsewhere (Briley & McDonald, Ref. 8; McDonald & Briley, Ref. 9). The method used is based on an implicit scheme which is potentially stable for large step sizes. Thus, as a practical matter, stability restrictions which limit the axial step size relative to the transverse mesh spacing and which become prohibitive for even locally refined meshes (e.g., in laminar sublayers) are not a factor in making the calculations. The general approach is to employ an implicit difference formulation and to linearize the implicit equations by expansion about the solution at the most recent axial location. Terms in the difference equations are then grouped by coordinate direction and one of the available alternating-direction implicit (ADI) or splitting techniques is used to reduce the multidimensional difference equations to a sequence of one-dimensional equations. These linear one-dimensional difference equations can be written in block-tridiagonal or a closely related matrix form and solved efficiently and without iteration by standard block elimination techniques. The general solution procedure is quite flexible in matters of detail such as the type and order accuracy of the difference approximations and the particular scheme for splitting multidimensional difference approximations. Based on previous experience of the authors, however, it is believed that the consistent use of a formal linearization procedure, which incidentally requires the solution of coupled difference equations in most instances, is a major factor in realizing the potential favorable stability properties generally attributed to implicit difference schemes.

THE ROLE OF GENERALIZED COORDINATES

The governing equations for a viscous fluid were purposely expressed and approximated in generalized coordinates. Like any physical process, the dynamics of a fluid is independent of coordinates; and is, therefore, describable in terms of arbitrary coordinates. The practical implication of this coordinate independence is that the analyst has the freedom to select coordinate systems which are easy to construct and which simplify the solution process.

In the numerical solution of fluid dynamic problems there are many advantages to be gained by judicious choice of coordinates. The most obvious advantage is that the physical boundaries of a flow region can be represented by coordinate surfaces. This removes the need for fractional cells in general and hence removes the complications and loss of accuracy associated with an interpolation algorithm for the boundaries. This does not exclude, however, the possibility of a hybrid technique where, for example, internal boundaries are to be interpolated by some algorithm and external boundaries are to be coordinate surfaces. The need for such a hybrid technique would arise when the construction of a coordinate system suitable for all boundaries would become absurdly difficult to construct. For example, consider a duct with several simple internal objects. Here it seems most suitable to first generate duct coordinates and then to interpolate the internal boundaries relative to the coordinates generated from the duct. If, in addition, the simple internal objects should move relative to the duct walls then the hybrid method would effectively remove the need for moving coordinates. Another advantage in the use of generalized coordinates is that a uniform numerical method can be used. The solution can then be performed with a fixed number of cells in any given direction and with a uniform mesh spacing. The result is a simplification of the computer logic; and hence, a savings in time for both the computer and the programmer. Unless a hybrid technique is used, there is no need to construct an elaborate interpolation routine. For the ADI method of solution that we use, the one-dimensional rows and columns each have fixed lengths; and hence, we are not faced with the combinatorial problem of monitoring the lengths of rows and columns which would otherwise be caused by geometric changes in the boundaries. In addition to the above there is the advantage of an implicit mesh distribution. The uniform mesh of computational space is simply mapped into an appropriately distributed mesh in physical space. Thus, the coordinate transformation can be chosen to contain the distributional information as well as the boundary specifications. The resolution of a rapidly changing solution is the major objective in selection of a coordinate mesh distribution. A classical example is the resolution of attached boundary layers where the solution is known to have large velocity gradients. Another more subtle example is the resolution of large gradients in computational coordinates due to regions of high curvature on the bounding surfaces. When the transformation contains the distributional information there is no need to construct the apparatus for the

discrete approximation of derivatives on a nonuniform mesh. This is a savings in both computer logic and storage. With a different motivation, however, it may be desired to automate the difference molecule so that the numerical technique can be changed with a few parameters. Changes, in practice, usually amount to a selection between forward, backward or central differences. For any given direction we need three parameters for first derivatives and four parameters for second derivatives. Thus, even with such an automation of the numerical method we save on computer logic and storage. Specifically, for an ADI direction of length N we need only 11 parameters as opposed to $7N$ parameters for nonuniform meshes. The extra 4 parameters are for the boundary molecules. A further advantage is that for a given problem we can select coordinates from a large class of coordinate systems. In the process of sorting through the various possible coordinate systems we are guided by two criteria. First, the new coordinates must lead to a real simplification; and secondly, the coordinates must be easily generated. Since bounding surfaces usually become coordinate surfaces the first criterion is almost always met. The remaining complexity in the first criterion is directly measured by consideration of the metric tensor (g_{ij}) which is obtained from the expression for the fundamental element of arc length

$$(ds)^2 = g_{ij} dy^i dy^j \quad (3)$$

Specifically, an increase in the number of nontrivial elements in the expression of the metric tensor is accompanied by a corresponding increase in the number of terms in the equations of motion. The result is an increase in the computational work that is needed after the coordinates have been generated along with the necessary metric data. The second criterion, unlike the first, is most often neglected. The unfortunate result is that there is often more work involved in making the coordinates than in solving the original problem with a less efficient satisfaction of the first criterion. In fact, both of the criteria above usually are at opposite polarities in complexity. The prudent selection of coordinates is then a balance between these criteria.

Our criteria for selecting a suitable system of coordinates can be used to compare the various classes of coordinate systems and to evaluate the relative utility of each. We will start with conformal transformations and continually enlarge the class until we obtain the most general time-dependent coordinates.

For conformal transformations the metric tensor is simply given by a scalar multiple of the identity. That is, $g_{ij} = h(\vec{y}) \delta_{ij}$ where the kronecker symbol δ_{ij} vanishes unless $i = j$ in which case it is unity. From this expression it is easy to show that $h = (J^2)^{1/n}$ where J is the Jacobian of the n -dimensional conformal transformation. The simplicity of the metric leads to very simple equations of motion at the expense of greatly restricting the class of easily obtained transformations.

These transformations are generally obtained by the solution of partial differential equations which may in itself be costly. In addition, the control over the mesh distributions is indirect at best. In two dimensions, however, conformal transformations have been successfully used on many occasions. Here the metric is given by $g_{ij} = |J| \delta_{ij}$, and the theory of functions of one complex variable is a powerful tool that is at our disposal. When the boundaries of the flow region can be matched with well-known conformal transformations there is nothing that can effectively compete with this way of generating coordinates. We have simply optimized on the generation of the equations of motion and on their solution process for any given method of solution. In a number of cases boundaries can be matched through a sequence of well-known transformations. However, in most cases of practical importance the boundaries are too complicated; and consequently, cannot be simply defined as desired. Thus, we are lead to approximate methods. For the general airfoil shapes there is the method of Theodorsen (Ref. 14) and along similar lines there is the more recent work of Ives (Ref. 15) which employs the Fast Fourier Transform. Both techniques map airfoils to near circles through a sequence of well-known maps; and then use a Fourier type of approximation. The method of Anderson (Ref. 16) uses the Schwartz - Christoffel transformation to approximate arbitrary shapes with piecewise linear curves. This technique works best for simply connected regions where no branch cuts are needed. A basic limitation in this method is the poor representation of wall curvature. This can be partially resolved by using the Schwartz - Christoffel transformation with rounded corners as in Henrici (Ref. 17). But then there is little control over the rounding process, and the arc length matching that was so critical to the success of the techniques in Anderson (Ref. 16) becomes much more difficult. This level of difficulty is comparable with methods that rely on the numerical solution of differential equations to obtain analytic functions. At this point we are probably going to spend too much time on just the generation of the coordinate system. However, if the potential flow information is desired then it may still be fruitful to incur the extra expense to get it. Once the conformal transformation is obtained the potential flow is an immediate result. But for viscous flows the potential flow information may be of limited utility. This is especially obvious since viscous displacement effects and/or boundary layer separation and reattachment can and usually does cause a significant deviation from potential flow. For even dimensional spaces of dimension greater than two, the theory of several complex variables can be used. Here, the same comments as with one complex variable apply. The theory however, is much more difficult. The basic tools come from sheaf theory, algebraic geometry, and complex manifolds (Gunning and Rossi, Ref. 18). These methods would most likely find applications for flows in phase space which mathematically would be considered as flows in a tangent bundle. Such flows occur in plasma physics where, for example, the Fokker-Planck equations often occur.

When conformal mappings become overly difficult to construct, it is best to consider the slightly larger class of orthogonal transformations. For orthogonal transformations the metric tensor is given by the diagonal form $g_{ij} = [h_i(\vec{y})]^2 \delta_{ij}$.

Note that, unlike the conformal transformations, the diagonal entries of the metric can be different. The deviation from conformality can now easily be measured by an examination of the ratios of the functions h_i . To see why this is so we need an explicit geometric interpretation of the metric. For a position vector field \vec{x} , the vector field $\vec{e}_i = \frac{\partial \vec{x}}{\partial y^i}$ is the natural tangent vector field along coordinate curves generated by holding the remaining coordinates $y^1, \dots, y^{i-1}, y^{i+1}, \dots, y^n$ constant. It is often common practice to use the operator notation where the position vector field is omitted. By an application of the chain rule, the fundamental element of arc length can be expanded as

$$(ds)^2 = d\vec{x} \cdot d\vec{x} = \left(\frac{\partial \vec{x}}{\partial y^i} dy^i \right) \cdot \left(\frac{\partial \vec{x}}{\partial y^j} dy^j \right) = \frac{\partial \vec{x}}{\partial y^i} \cdot \frac{\partial \vec{x}}{\partial y^j} dy^i dy^j = (\vec{e}_i \cdot \vec{e}_j) dy^i dy^j \quad (4)$$

and hence, by linear independence $g_{ij} = \vec{e}_i \cdot \vec{e}_j$. Now note that we have an orthogonal metric if and only if the \vec{e}_i and \vec{e}_j are perpendicular when $i \neq j$. But perpendicularity of \vec{e}_i and \vec{e}_j at a point is equivalent to the perpendicular crossing of the associated coordinate curves at the point in question. Consequently our intuitive notion of orthogonality in terms of coordinate curves is equivalent to the metric expression above. In addition the functions h_i are easily seen to be equal to the lengths of the corresponding natural tangent vectors \vec{e}_i . In a small neighborhood of a point the functions h_i are nearly equal to their values at the point and thus, the measurement of distance along coordinate curves is very nearly given by distance measurements along the respective vectors \vec{e}_i in the tangent plane at the point in question. When the functions h_i are all equal, the distance measurement in the tangent plane is merely a uniform dilation or contraction of the original cartesian system. Thus, length ratios and, hence, angles are preserved between the cartesian system and the tangent plane. But the projection of tangent vectors onto the curvilinear system preserves angles. Hence, with equal diagonal entries the transformation preserves angles and is, therefore, called conformal. Consequently, as the ratios of the h_i deviate from unity, the transformation smoothly deviates from conformality. With fewer constraints on the metric the selection of coordinates from the class of orthogonal transformations is slightly less restrictive than a selection from the class of conformal transformations. The process of coordinate generation is usually accomplished by geometric methods. The desire is to create families of mutually orthogonal coordinate surfaces. As a starting point, one usually begins the process with a given family of surfaces that are generated in some way from the boundary of the flow region. Families of orthogonal surfaces are then to be constructed to complete the specification of coordinates. The first family of surfaces defines a unique normal vector field. This vector field is then extended to a smooth field of orthogonal frames which must be integrated to generate the other coordinate surfaces. The condition is that the Lie derivative of frame vectors vanish. That is, that the hypotheses of the Frobenius Theorem on integrability is satisfied (Bishop and Crittenden, Ref. 19). The process however, leads to

the solution of a system of differential equations which may turn out to be a somewhat difficult exercise just to obtain orthogonal coordinates. In fact, it may not even be desirable to use orthogonal coordinate systems. For example, consider the family of superellipses of degree 5 and the orthogonal family of superhyperbolas of degree -3. This orthogonal superelliptic coordinate system is illustrated in Fig. 2 by the computer plots of Larsen (Ref. 20). This coordinate system tends to unnaturally concentrate mesh points along or near the superelliptic diagonals at the expense of the off diagonal regions. Thus, a numerical procedure would over resolve the diagonal regions and under resolve off diagonal regions. In addition, artificially large geometric gradients would be produced between these regions and as a result, the solution in computational coordinates would react as if it were trying to solve a boundary layer problem without resolving the boundary layer region. In such a case instability would probably result. Consequently, the use of orthogonal coordinates may be undesirable because of potentially poor mesh distributions.

General nonorthogonal coordinates are often to be preferred since the mesh distributions can be controlled and since the coordinates are considerably easier to generate. The construction process is entirely geometric and generally does not rely on the solution of differential equations. Furthermore, points can be essentially distributed at will. For example, a replacement of the superhyperbolic curves by polar lines would lead to a considerable improvement over the superelliptic coordinates depicted in Fig. 2. Mesh distribution functions can often be directly inserted into the transformation in a manner which directly distributes the points. The considerable improvement in flexibility associated with the class of general spacial coordinates does come with a small price. Specifically, the metric tensor has generally nontrivial off diagonal elements. As with the difference between orthogonal and conformal coordinates, the deviation of the general nonorthogonal coordinates from orthogonality can be measured directly from the metric. That is, the cosine of the angle between distinct coordinate curves is given by the dot product of the associated unit tangent vectors. The cosine of the angle between curves i and j can be written as:

$$\left(\frac{\vec{e}_i}{|\vec{e}_i|} \right) \cdot \left(\frac{\vec{e}_j}{|\vec{e}_j|} \right) = \frac{\vec{e}_i \cdot \vec{e}_j}{\sqrt{(\vec{e}_i \cdot \vec{e}_i)(\vec{e}_j \cdot \vec{e}_j)}} = \frac{g_{ij}}{\sqrt{g_{ii} g_{jj}}} \quad (5)$$

Thus when g_{ij} vanishes for distinct i and j we have orthogonality, and when g_{ij} increases from 0 the coordinates smoothly deviate from orthogonality with deviation given by the arc cosine of the above. This deviation can be used to advantage by creating almost orthogonal coordinates in certain regions of importance. For example, one may wish to treat boundary layers with nearly orthogonal coordinates and let regions of greater nonorthogonality fall into largely inviscid regions.

When time-dependent problems are considered the general nonorthogonal spacial coordinates can be used provided that the boundaries of the flow region are rigidly fixed relative to the region. However, if the region changes shape as a function of time, then the purely spacial coordinate analysis above is no longer valid unless special precautions are taken. In terms of the metric we now have the pseudoriemannian metric from special relativity. The classical equations of motion are simply obtained from the vanishing divergence of the stress-energy tensor. Terms of order $\frac{1}{c^2}$ relative to unity are neglected when the approximation of motion much slower than the velocity of light c is applied. This is discussed at more length by McVittie (Ref. 21). Possible applications for such coordinate systems include ducts with moving walls such as blood flow problems as well as flutter problems where airfoils may be oscillating relative to each other. As special cases we obtain the classical Eulerian and Lagrangian coordinates as well as everything in between.

THE COORDINATE SYSTEM

The Construction of Tube-like Coordinates

Tube-like coordinates will be constructed in general to provide a natural setting for the study of flows within, between, or outside of a set of prescribed tubes. The prescribed boundary tubes then become coordinate surfaces, and, as a result, the specification of fluid dynamic boundary conditions is greatly simplified. Although the equations of motion contain more terms than for a cartesian system, this does not add excessively to the run time of a program. In addition, there must be some control over the resolution of regions near bounding tubes so that the effects of wall curvature and the growth of attached boundary layers can be adequately treated. Such controls are obtained from the specification of coordinate distribution functions which shall appear only as parameters in the basic geometric construction of the coordinates. The basic geometry of the bounding tubes then provides the intrinsic constraints upon the coordinate construction. Since the primary goal is the computation of fluid flows within nontrivial geometries and not the development of coordinate systems per se, the coordinates will be kept as simple as possible, given the desired generality.

Considering various past successes of two-dimensional conformal mappings to obtain coordinates, one might naturally wish to obtain similar transformations for three-dimensions. Unfortunately, there is no three-dimensional theory of conformal transformations analogous to complex variables, and consequently, in three dimensions one is left with a complicated system of partial differential equations which generally would require numerical solution. To circumvent the considerable computational labor required for solution of such equations, a constructive process is used for the development of tube-like coordinates.

The first step in the construction of tube-like coordinates is to create a suitable family of two-dimensional surfaces which, in some sense, are transverse to a given centerline. If orthogonal coordinates are desired, then these surfaces would have to bend and flex as the tube would undergo changes in cross section at different centerline positions. In addition to the problem of constructing transverse surfaces which bend and flex, there is also the problem of constructing an orthogonal grid on a surface which has variations in Gaussian curvature, and hence, is not flat. This second problem, in fact, requires a more complicated construction than the first which in itself is not easy. Thus, the sheer magnitude of the work involved in the construction of orthogonal coordinates certainly would remove the desire for their use in fluid dynamic problems which undoubtedly would require less computation in non-orthogonal coordinates than in the construction of an orthogonal system alone. By contrast, if the transverse surfaces are selected to be two-dimensional planes, then the construction of coordinates is greatly simplified while the fluid dynamic computation is only marginally different due to coordinate nonorthogonality. Consequently the coordinate system that we shall construct will have planar transverse surfaces.

Since each planar transverse surface is a linear subspace of the real three-dimensional Euclidian vector space R^3 , any such plane can be completely specified by any two spanning linearly independent vectors in R^3 . The specification of the planar family of transverse surfaces is then a result of a construction of two vector fields along a given centerline curve in R^3 . The origin of each plane is chosen to coincide with the associated centerline point. (See Fig. 3) To assure that the planes are always indeed transverse, it will be assumed that they are orthogonal to the centerline at their origins. Ultimately, tube-like surfaces will be generated by loops about the planar origins which deform in some way as we move along the centerline curve; in general, these tube-like surfaces will not intersect the transverse planes orthogonally. Thus, only the centerline direction determines the transverse nature of the cross sectional planes. Specifically, the centerline tangent vectors form a vector field which at each point is orthogonal to the plane of the two transverse vectors, and thus each centerline point carries a triple of linearly independent vectors. By the Gram-Schmidt orthogonalization procedure, each such triple of vectors can be made into an orthogonal set, and hence, an orthonormal set which is simply called a frame. Thus, tube-like coordinate systems are constructed from a specified centerline curve and an associated frame field. Now the basic question is whether there is a canonical construction of tube-like coordinate systems from either a given centerline or a given frame field. From the theory of space curves (Ref. 22), it is well known that for positive curvature and specified torsion there is a local one-to-one correspondence between frame fields and space curves which pass through a given point. Thus, for nonzero curvature the centerline space curve has a canonical frame field which is known as the Frenet frame. Consequently, the coordinates will be derived from the Frenet frame when it exists. At centerline points of zero curvature, the Frenet frame is degenerate and must be treated specially.

Once the Frenet frame of the space curve $\bar{\gamma}$ has been established, the unit normal and binormal vectors \bar{V}_2 and \bar{V}_3 at each point of $\bar{\gamma}$ determine a transverse plane orthogonal to the unit tangent vector \bar{V}_1 . (See Fig. 4) Relative to any such transverse plane, these vectors are also the standard orthonormal basis. Consequently, we can examine the plane separately from the curve, $\bar{\gamma}$, which will only appear as the point at the origin. In two dimensional functional terminology, the unit normal direction can be considered as the abscissa and the unit binormal as the ordinate; or more simply, as x and y axes, respectively. Since the tube-like coordinates are to be generated from some family of tubes encasing the space curve, $\bar{\gamma}$, a cross-sectional cut by a transverse plane produces within the plane a family of loops about the origin. We shall assume that each loop is representable by a strictly monotone radial function of angle. In this regard, a polar type of description is the most suitable. But, of course, the loops are usually more complicated than circles, and thus, we must replace the radius by a function L of both radial and angular variables r and θ . Furthermore, when noncircular loops bound a cross section of fluid, there are regions of varying wall curvature. In a numerical solution, it is desirable to put proportionately more mesh points in regions of higher curvature than in regions of less curvature. Consequently, an angular distribution function, Θ , is a good replacement for the simple angular specification, θ , of simple polar coordinates. The net result is a generalization where polar coordinates are replaced by a pseudo-radius, r and

pseudo-angle, θ . Since the loops generally vary from transverse plane to transverse plane, the pseudo-radii and angles must also be functions of axial location, t , on the centerline space curve, $\vec{Y}(t)$. Since the normal and binormal directions are usually functions only of the centerline curve, $\vec{Y}(t)$, our loops may have symmetries that do not reflect about either of these Frenet directions. Since the use of known symmetries is a great simplification in most problems, we need an option which allows one to define axes that can be aligned in an optimal way. This option is easily established from the specification of a function, $\Omega(t)$, which is a rigid rotation relative to the normal-binormal directions. To bring this development of tube-like coordinates within the framework of the preceding tensor derivations, we shall use the notation, $y^1=\theta$, $y^2=r$ and $y^3=t$ for pseudo-angular, pseudo-radial, and axial variables. In this notation, we have thus far developed (1) a length factor, $L=L(y^1, y^2, y^3)$, which is a generalization of radius, (2) an angular distribution function, $\Theta=\Theta(y^1, y^3)$ which is a generalization of angle, (3) a rotation function, $\Omega=\Omega(y^3)$, and (4) the Frenet frame, $(\vec{V}_1, \vec{V}_2, \vec{V}_3)=(\vec{V}_1(y^3), \vec{V}_2(y^3), \vec{V}_3(y^3))$ upon which the coordinates are built. That the length factor, L , and the angular distribution function, Θ , give us a generalization of polar coordinates is obvious since polar coordinates are easily retrieved by taking $L(y^1, y^2, y^3)=y^2$ and $\Theta(y^1, y^3)=y^1$. It is also worth noting that the angular distribution function, Θ , was chosen to be independent of pseudo-radius, y^2 . Although it is not immediately evident, we have removed a considerable amount of potential computational complexity in the process of obtaining metric information, by limiting the number of derivatives which must be computed. Furthermore, there is no real loss of flexibility in the construction of angular distribution functions. Since most commonly used analytic descriptions of loops are, in fact, controlled by a collection of parameters which depend only on axial location, y^3 , a knowledge of only these parameters is often sufficient for the construction of the angular distribution function. For example, if the loops were to consist of a family of concentric homogeneous ellipses, then the major and minor axes of the outermost ellipse would form a collection of two such parameters.

With the above functions and the Frenet frame, the class of tube-like coordinates comes directly out of the transformation

$$\vec{x} = \vec{Y} + L\{\vec{V}_2 \cos \varphi + \vec{V}_3 \sin \varphi\} \quad (6)$$

which transforms curvilinear coordinates, $\vec{y} = (y^1, y^2, y^3)$ into cartesian coordinates $\vec{x} = (x^1, x^2, x^3)$ where

$$\varphi(y^1, y^3) = \Theta(y^1, y^3) + \Omega(y^3). \quad (7)$$

At each transverse location, y^3 , the space curve vector, \vec{Y} , translates the origin to the space curve. At a given pseudo-angle, y^1 , a unit vector, $\vec{V}_2 \cos \varphi + \vec{V}_3 \sin \varphi$, is determined by the sum, $\varphi = \Theta + \Omega$ of the radial distribution function, Θ , and the transverse rotation, Ω . This unit vector sweeps out a full 360 degs in the transverse plane as y^1 passes through all of its values. Hence, we could call this a direction pointer for the transverse plane. When this direction pointer is scaled by the

which takes, $\gamma_2(\theta) = H(\theta, 0)$ uniformly and smoothly into $\gamma_1(\theta) = H(\theta, 1)$ as r goes from 0 to 1. (For a general definition of homotopy see Reference 23). This is illustrated in Fig. 7. If the loop γ_2 is degenerate then the coefficient $F_2(\theta)$ vanishes and the length factor reduces to $L(\theta, r) = rF_1(\theta)$, we thus have the cross section of a duct generated by one loop. By the continuity of L as a function of γ_2 , the duct generated by one loop γ_1 can be considered as a limit of annular type regions between loops γ_2 and γ_1 as γ_2 closes tightly upon the origin. This concept is often quite useful since the origin in coordinates generated from one loop suffer from the same singularity problem that occurs with simple polar coordinates. This singularity can be circumvented, however, by using an auxiliary loop γ_2 which is near enough to the origin to create a good approximation to the original region. To preserve overall accuracy in a numerical computation, $\|\gamma_2\| = \max_{\theta} F_2(\theta)$ must be less than the numerical truncation error. In fact, the well-defined limiting process would lead one to believe that there would be no problem at all in taking $\|\gamma_2\|$ arbitrarily small. But if $\|\gamma_2\|$ is taken within the region of machine roundoff error, then the singularity problem may reappear by default. Consequently, it is best to choose $\|\gamma_2\|$ to be much less than truncation errors but greater than roundoff errors.

The final stage of length factor construction is accomplished by a replacement of the polar coordinates r and θ by radial and angular distribution functions $R(r, t)$ and $\Theta(\theta, t)$ for axial location t . Now since R and Θ are to be the actual polar locations of a loop we must reinterpret r and θ as pseudo-radial and pseudo-angular locations on the same loop. Within this context the two-tube length factor becomes

$$L(\theta, r, t) = R(r, t) F_1(\Theta(\theta, t)) + [1 - R(r, t)] F_2(\Theta(\theta, t)) \quad (9)$$

and the associated unit vector becomes

$$(\cos(\Theta(\theta, t) + \Omega(t)), \sin(\Theta(\theta, t) + \Omega(t))) \quad (10)$$

where the rotation $\Omega(t)$ of the Frenet frame has been included for completeness.

We shall now proceed with a detailed examination of the geometric content of the length factor, which for our purposes will be assumed to be linear in r . The geometric content is most readily displayed when an arbitrary coordinate loop is excised from a cross sectional coordinate system composed of loops and radial lines. For simplicity we will consider only one bounding loop. Since there is a one-to-one correspondence between coordinate loops and fixed values of r , the radii of a fixed r -loop are given by a unique function $L_r(\theta) = L(\theta, r)$ which will be useful in our examination of some examples.

The specific examples of length factors to be examined are chosen for their utility in the design of subsonic diffusers having cross sections which vary from circles or ellipses to rectangles or near rectangles. The examples are given in the order of increasing generality. In particular, we shall examine the circle, the ellipse, and the superellipse. Since cross sections generated from superellipses can vary from pure ellipses to near rectangles, the superelliptic parameters can be replaced by

smooth functions of location along the duct centerline, and consequently, tubes having continuously varying cross sections can be generated. In developing the analysis, however, it was found that such tubes are not smooth enough for practical flow calculations. Consequently, a technique based on interpolation between an ellipse and a sufficiently smooth superellipse with large exponent was devised. The interpolation is accomplished by a double mini-max procedure which yields an interpolating function for superellipses with exponents between 2 and the chosen large exponent.

We begin with the simplest geometric loop, namely, the circle. In this case, the function L_r is the constant function $L_r = r$, and the result is the polar coordinate loop.

The ellipse is slightly more complicated than the circle. When the ellipse crosses the x-axis at $\theta = 0, \pi$ the radial function L_r attains equal local maxima and similarly when the y-axis is crossed at $\theta = \pi/2, 3\pi/2$ equal positive local minima are obtained. Since the function L_r is smooth and monotonically decreasing from its local maximum at $\theta = 0$ to its local minimum at $\theta = \pi/2$, the graph of L_r from 0 to $\pi/2$ looks like a lifted cosine curve. By symmetry about the axes, the lifted cosine-like graph is continued over the entire interval $[0, 2\pi]$. The same result may be observed analytically. The equation for the ellipse is given in cartesian coordinates by

$$\left(\frac{x}{Mr}\right)^2 + \left(\frac{y}{mr}\right)^2 = 1 \quad (11)$$

or

$$b^2 x^2 + y^2 = M^2 r^2 \quad (12)$$

where $b = \frac{m}{M}$ controls the shape of the ellipse and M controls the size of the ellipse. The parameter M is known as the major axis of the ellipse, and the parameter b can reasonably be called the shape factor of the ellipse. In polar coordinates (L_r, θ) we have

$$\begin{aligned} L_r &= \frac{Mr}{[b^2 \cos^2 \theta + \sin^2 \theta]^{1/2}} \\ &= \frac{Mr}{[1 + (b^2 - 1) \cos^2 \theta]^{1/2}} \end{aligned} \quad (13)$$

from which the local extrema can be identified. If for example, $b < 1$, then local maxima correspond to values of θ for which $\cos^2 \theta = 1$. The local maxima are then $L_r(0) = L_r(\pi) = Mr$. Similarly the local minima are $L_r(\pi/2) = L_r(3\pi/2) = mr$. By differentiation, we have

$$L_r(\theta) = \frac{\frac{1}{2}Mr(b^2 - 1)}{[1 + (b^2 - 1)\cos^2 \theta]^{3/2}} \sin 2\theta \quad (14)$$

from which the monotonically decreasing behavior from 0 to $\pi/2$ can be observed.

If the exponent of 2 in the ellipse is replaced by a real number and if x and y are replaced by $|x|$ and $|y|$, then the ellipse is generalized to a superellipse (Ref. 20). The equation for the superellipse (Fig. 8a) in cartesian coordinates becomes

$$\left(\frac{|x|}{Mr}\right)^a + \left(\frac{|y|}{mr}\right)^a = 1 \quad (15)$$

or

$$b^a |x|^a + |y|^a = m^a r^a \quad (16)$$

where the exponent a is any real number. The absolute values insure that the superellipse is symmetric about the axes. The most significant change is the parameterization of the exponent a . When $a = 1$ a diamond shaped loop is obtained. The loop is continuous but not differentiable at the axes. As a is varied from 1 to 2 the diamond shaped loop is continuously deformed into the ellipse. The loops corresponding to exponents a between 1 and 2 do not have second derivatives on the axes. However, the ellipse ($a = 2$) has infinitely many continuous derivatives. Now suppose that $|y| < m$. Then as a increases from 2 to infinity,

$$|x| = Mr \{1 - (\frac{|y|}{m})^a\}^{1/a} \quad (17)$$

monotonically increases to Mr . Similarly, if $|x| < M$, then $|y|$ monotonically increases to mr as a approaches infinity. Thus the superellipse is an approximation to a rectangle for sufficiently large exponent a .

The convergence of superellipses to rectangles (Fig. 8c) is a fairly rapid function of the exponent. The convergence rate is most easily demonstrated in polar coordinates (L_r, θ). The polar radius for the superellipse is given by

$$L_r(\theta) = \frac{mr}{\{b^a |\cos \theta|^a + |\sin \theta|^a\}^{1/a}} \quad (18)$$

Note that, unlike the pure ellipse, there are no readily available trigonometric simplifications. By examination of the rectangle (Fig. 8c) that the family of superellipses (Fig. 8a) are to approximate with increasing exponent, we further note that radial convergence will be slowest along radial lines into the corners of the rectangle. From symmetry, it is sufficient to restrict our examination to the first quadrant corner P of the rectangle (Fig. 9a) which has length $r\sqrt{m^2+M^2}$ which bounds the length of the superelliptic radius along the same angle to Q. But then the sine and cosine of the angle are easily obtained from the rectangle itself as

$$\frac{m}{\sqrt{m^2 + M^2}} \quad \text{and} \quad \frac{M}{\sqrt{m^2 + M^2}} \quad (19)$$

respectively. A direct substitution then yields the superelliptic polar radius

$$L_r = 2^{-1/a} r \sqrt{m^2 + M^2} \quad (20)$$

and hence the maximum absolute error in the superelliptic approximation of rectangles is given by the expression

$$r \sqrt{m^2 + M^2} [1 - 2^{-1/a}] \quad (21)$$

The degree of rectangular approximation is evident from the table of relative error $1 - 2^{-1/a}$ in (Fig. 9b). Since the superelliptic exponent controls the degree of rectangular approximation, it is a measure of squareness near the superelliptic corner. For this reason it would be reasonable to call the exponent a squareness factor.

The radial function L_r for a superellipse (Fig. 8a) with exponent greater than 2 is depicted in Fig. 8b. When the superellipse crosses the x-axis at $\theta = 0, \pi$ the function L_r attains local maxima equal to M_r , and similarly when the y-axis is crossed at $\theta = \pi/2, 3\pi/2$ local minima equal to m_r are obtained. Observe that these extrema are identical with those of the pure ellipse. The main difference in the L_r curves, however, is a loss of monotonicity on quadrants. Unlike the ellipse, the radial function L_r of the superellipse increases with θ as a corner is approached and then decreases until the next extremum. In Fig. 8a as corner A is approached the graph of L_r in Fig. 8b approaches a maximum at A'. Since there is symmetry about the y-axis, the second quadrant of the superellipse can be obtained by a reflection of the first quadrant about the y-axis. Under the reflection corner A goes into corner B and the graph of L_r from 0 to $\pi/2$ is reflected about $\pi/2$ extending the graph to π . The reflected maximum B' is the same distance from $\pi/2$ as is the first quadrant maximum. Continuing in the same manner, symmetry is applied about the x-axis. The upper half plane is reflected sending corners A and B into corners D and C, respectively. Then the graph of L_r is completed by a reflection about π sending maxima at A' and B' into maxima and D' and C', respectively corresponding to corners D and C, respectively.

The radial function L_r for the rectangle is very similar in shape to the corresponding superelliptic function. The distinguishing difference is that the maxima A', B', C', D' of Fig. 8d corresponding to corners A, B, C, D of Fig. 8c are cusped; and therefore, not differentiable. Otherwise the local extrema are almost identical with those of the superelliptic function of Fig. 8b.

COMPUTATIONAL RESULTS

The main aim of the present study was to develop a general method for the computation of three dimensional viscous diffuser flows. To test the feasibility of our method, geometrically simple test cases were run. Unless otherwise stated, for the cases presented herein a square jet was considered, although rectangular jets of varying aspect ratio have also been run without difficulty. The free stream Mach number was fixed at 1.66 and a gas stagnation temperature of 3750 deg R adopted. The ratio of jet exit centerline velocity to free stream velocity was 1.25 in all cases. A constant velocity core was ascribed to the jet and this core was smoothly faired into the free stream velocity over a distance of about one-quarter of a jet width using a hyperbolic tangent. A number of cases have been run successfully but only two broad categories are discussed here: first, where the density was specified such that the pressure at the initial plane was constant everywhere; and, second, where the jet pressure was 1.38 times the free stream pressure.

Considering the case of matched initial pressure, calculations were first performed at infinite Reynolds numbers. A Courant-Friedrichs-Lewy (CFL) number, Courant, et al., (Ref. 24) is defined as

$$\frac{\Delta X \tan \alpha \sin M^{-1}}{(\Delta y \text{ or } \Delta z)} \quad (22)$$

where Δx is the streamwise step and Δy or Δz the cross-sectional step size and M the streamwise local Mach number. Typically, many conditionally stable methods are evaluated on the basis of what fraction of the unit CFL number they can take for a streamwise step, given some transverse mesh. Indeed, as defined above, a unit CFL number would correspond to the axial step taken by a straightforward method of characteristics procedure integrating from every alternate transverse grid point. Calculations with the present method were performed using 45×45 grid points in the cross section for three streamwise meshes corresponding to CFL numbers of 12, 24, and 48. No significant difference between the results at various CFL numbers was observed and, in addition, the exact result that, for a pressure matched situation the inlet profile is convected downstream without alteration, was obtained correct to a minimum of five figures out of the eight carried by the machine (single precision was used throughout). Some error buildup was noted, however, near the upper boundaries, contaminating the fourth significant figure after twelve jet half height downstream but this error was quite localized. Calculations were performed by changing from a consistent three level second order linearization to a first order two level linearization simply by equating the n and $n-1$ levels in the linearized streamwise derivative of u^2 . For the meshes examined, the differences were quite insignificant. Since a quadrant of a square jet was being computed, symmetry of the solution about the diagonal was also checked and at about twelve jet half heights downstream was

held to a minimum of five significant figures on axial velocity except close to the outer boundaries. Computer run times were CFL independent and averaged three minutes of UNIVAC 1110 CPU time to march about eleven streamwise stations with 2025 grid points in the cross section.

Considering now the case of low Reynolds numbers, a viscous diffusion number is defined by analogy to simple heat flow equation (Richtmyer and Morton, Ref. 25) as

$$\frac{\Delta x}{R\rho u(\Delta y \text{ or } \Delta z)^2} \quad (22)$$

and for comparative purposes it is observed that in the diffusion dominated case of negligible convection the explicit method derived from a forward difference for the marching direction and a centered space difference at the explicit level would be stable for a time step corresponding to a diffusion number less than or equal to one-half. Several calculations were performed at low Reynolds numbers with a 45 x 45 cross-sectional mesh. Very little difference in the solutions can be observed and no difficulties were experienced in performing the calculations. The CFL numbers for these calculations were 48 and 12. The very interesting fluid mechanical observation was made in that although the pressure was constant everywhere at the inlet plane, quite rapidly as the flow developed, pressure gradients formed in the flow. After about thirteen jet heights downstream, symmetry was checked and at worst slight discrepancies in the fifth significant figure in axial velocity were observed. Since diffusion did cause changes at the outer boundaries, it was not clear whether or not significant error buildup at the boundary was occurring.

Also, at a Reynolds number of 11 and a 45 x 45 cross-sectional grid, calculations were performed but in this instance the spatial mesh was locally refined in the jet keeping the axial step the same. This transverse mesh refinement resulted in a doubling of the diffusion number. In this case the two calculations do not differ significantly. Again, symmetry was checked and at worst slight discrepancies in the fifth figure on axial velocity were observed.

Finally, the inlet density profile was adjusted to provide a jet static pressure of 1.38 times the free stream static and calculations performed for two Reynolds numbers for a 45 x 45 cross-sectional mesh. Apart from the inlet density profile the inlet conditions were identical to the pressure matched case and the inlet axial velocity profile. Immediately downstream of the inlet plane wiggles develop at the jet free stream interface but these wiggles are substantially gone by four or five jet heights downstream. Near the jet center the jet initially over expands then subsequently compresses. Once again a symmetry check some ten jet heights downstream indicated at worst slight discrepancies in the fifth place on axial velocities. An identical calculation at a Reynolds number of 5×10^3 and CFL number of 50 became unstable after the initial characteristic exited from the domain when over-constrained boundary conditions were applied. The calculation was rerun with the equivalency

condition applied and a stable solution obtained. From the results it was evident that although stable the axial step was larger than desired in view of the rapid changes in flow properties in the axial direction, particularly near the center of the jet.

Two additional high Reynolds number cases were run for demonstration purposes. The first of these is for the same over pressured conditions as before and with a jet exit Reynolds number of 5×10^4 . However, in this instance a rectangular jet of 2:1 aspect ratio was considered. For this particular case a relatively small axial step corresponding to a CFL number of about 1.4 was used with a 40×80 cross-sectional mesh. The velocity profiles at various axial locations downstream of the jet are shown in Fig. 10. The plots were constructed by B. Anderson of NASA Lewis. The last case presented was again for an over pressured jet and here an attempt was made to better define the flow within the jet itself by refining the mesh in this region. As in the earlier cases, a quadrant of square jet with a 45×45 cross-sectional mesh was used. With the refined mesh and an axial step sufficient to resolve the axial changes, the CFL number corresponding to the axial step was about 50. The severity of the outgoing pressure disturbance required the calculation be performed using the coupled four equation system and that the equivalency boundary conditions be imposed. When this was done little difficulty was experienced with the calculation.

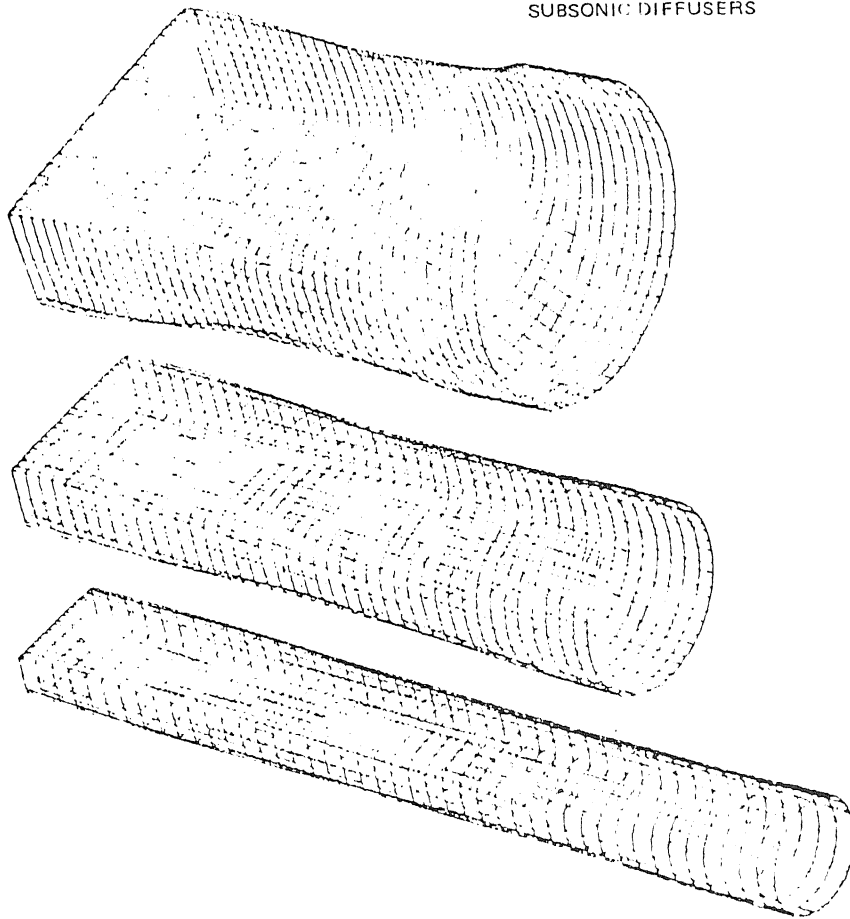
Using the same basic computational scheme a more complex calculation is presented in Ref. 10. There the scheme was used to compute the subsonic flow in a turbine vane passage. A conformal transformation was used to obtain the computational coordinates. The transformation was generated in a slab symmetric fashion directly from the Schwartz-Christoffel transformation obtained by the method of O. Anderson (Ref. 16). The duct, therefore, consisted of two-curved sides corresponding to Schwartz-Christoffel boundaries and two orthogonal planar end caps. At the present time a number of additional computations are being made for flows of varying degrees of complexity. Specifically, subsonic flows are being computed in various tube-like coordinate systems. These results will be reported upon at a later date.

REFERENCES

1. Hawthorne, W.R.: The Applicability of Secondary Flow Analyses to the Solution of Internal Flow Problems. Fluid Mechanics of Internal Flow, Gino Sovran, Ed.; Elsevier Publishing Co., New York, New York, 1967.
2. Stuart, A.R. and R. Hetherington: The Solution of the Three Variable Duct Flow Equations. In Fluid Mechanics, Acoustics and Design of Turbomachinery, NASA SP-304, 1974, pp. 135-154.
3. Nash, J.F. and V.C. Patel: Three-Dimensional Turbulent Boundary Layers, SBC Technical Books, Atlanta, 1972.
4. Patankar, S.V. and D.B. Spalding: A Calculation Procedure for Heat, Mass, and Momentum Transfer in Three-Dimensional Parabolic Flows. Int. J. Heat and Mass Transfer, Vol. 15, 1972, p. 1787.
5. Caretto, L.S., R.M. Curr, and D.B. Spalding: Computational Methods in Applied Mechanics and Engineering, Vol. 1, 1973, p. 39.
6. Briley, W.R.: Numerical Method for Predicting Three-Dimensional Steady Viscous Flow in Ducts. Journal of Computational Physics, Vol. 14, 1974, p. 8.
7. Patankar, S.V., V.S. Prataap, and D.B. Spalding: Prediction of Laminar Flow and Heat Transfer in Helically Coiled Pipes. Journal of Fluid Mechanics Vol. 62, 1974, p. 539.
8. Briley, W.R. and H. McDonald: An Implicit Numerical Method for the Multi-dimensional Compressible Navier-Stokes Equations. United Aircraft Research Laboratories Report M911363-6, November 1973.
9. McDonald, H. and W.R. Briley: Three-Dimensional Supersonic Flow of a Viscous or Inviscid Gas. United Aircraft Research Laboratories Report N111078-1, November 1974.
10. Briley, W.R. and H. McDonald: Computation of Three-Dimensional Turbulent Subsonic Flow in Curved Passages. United Aircraft Research Laboratories Report R75-911596-8, March 1975.
11. Eiseman, P.R., H. McDonald, and W.R. Briley: A Method for Computing Three-Dimensional Viscous Diffuser Flows. United Technologies Research Center Report R75-911737-1, July 1975.
12. Eiseman, P.R.: The Numerical Solution of the Fluid Dynamic Equations in Curvilinear Coordinates. Air Force Weapons Laboratory Technical Report AFWL-TR-73-172, August 1973.

13. Hinze, J.O.: Turbulence, McGraw-Hill Book Company, Inc., New York, 1959.
14. Theodorsen, T., and I.E. Garrick: General Potential Theory of Arbitrary Wing Sections, NACA TR No. 452 (1933).
15. Ives, D.C.: A Modern Look at Conformal Mapping, Including Doubly Connected Regions, AIAA paper, to appear.
16. Anderson, O.L.: User's Manual for a Finite-Difference Calculation of Turbulent Swirling Compressible Flow in Axisymmetric Ducts with Struts and Slot Cooled Walls, USAAMRDL-TR-74-50, Vol. 1, 1974.
17. Henrici, P.: Applied and Computational Complex Analysis Vol. 1., John Wiley and Sons, New York 1974.
18. Gunning, R.C., and H. Rossi: Several Complex Variables Prentice Hall, Inc., Englewood Cliffs, New Jersey, 1965.
19. Bishop, R.L. and R.J. Crittenden: Geometry of Manifolds. Academic Press, Inc. New York 1964.
20. Larson, T.: Superelliptic and Related Coordinate Systems. Laboratory of Electromagnetic Theory, The Technical University of Denmark, Lyngby, August 1969.
21. McVittie, G.C.: General Relativity and Cosmology. The University of Illinois Press, Urbana, Ill., 1965.
22. Laugwitz, D.: Differential and Riemannian Geometry. Academic Press, Inc., New York, 1965.
23. Hu, S.T.: Homotopy Theory. Academic Press, Inc., New York, 1959.
24. Courant, R., K. Friedrichs, and H. Lewy: On the Partial Differential Equations of Mathematical Physics. IBM Journal, March 1967, pp 215-234. Also, Mathematische Annalen, Vol. 100, 1928, pp 32-74.
25. Richtmyer, R.D. and K.W. Morton: Difference Methods for Initial-Value Problems. Interscience Tracts in Pure and Applied Mathematics, No. 4, Second Edition, 1967.

SUBSONIC DIFFUSERS



DIFFUSION RATE MODEL NO. 5 CASE C

DIFFUSION RATE MODEL NO. 3, CASE B

DIFFUSION RATE MODEL NO. 1 CASE A

Figure 1. Computer graphics by B. Anderson.

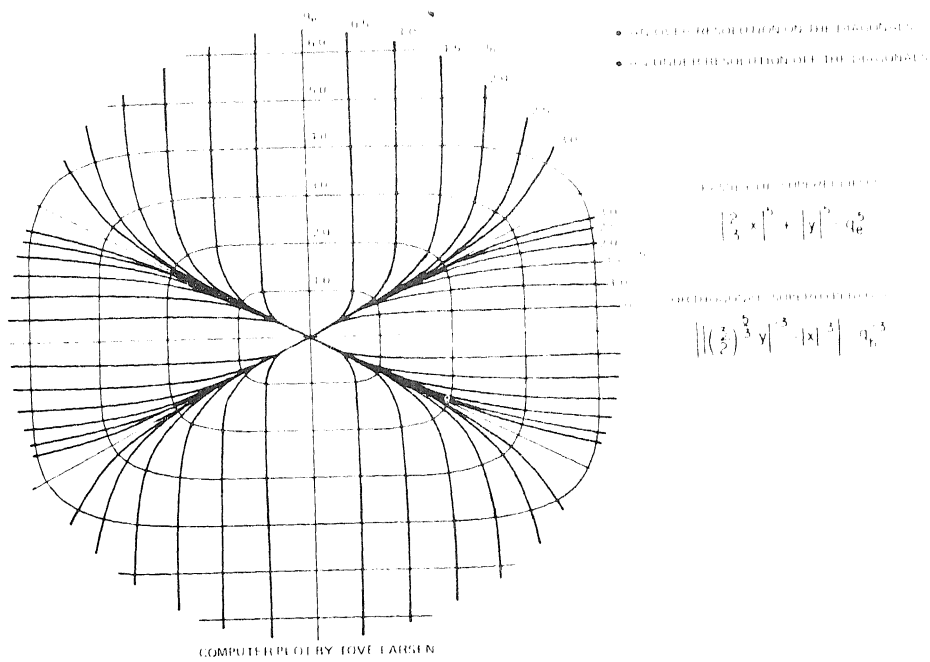


Figure 2. Orthogonal coordinates may lead to a poor mesh distribution.

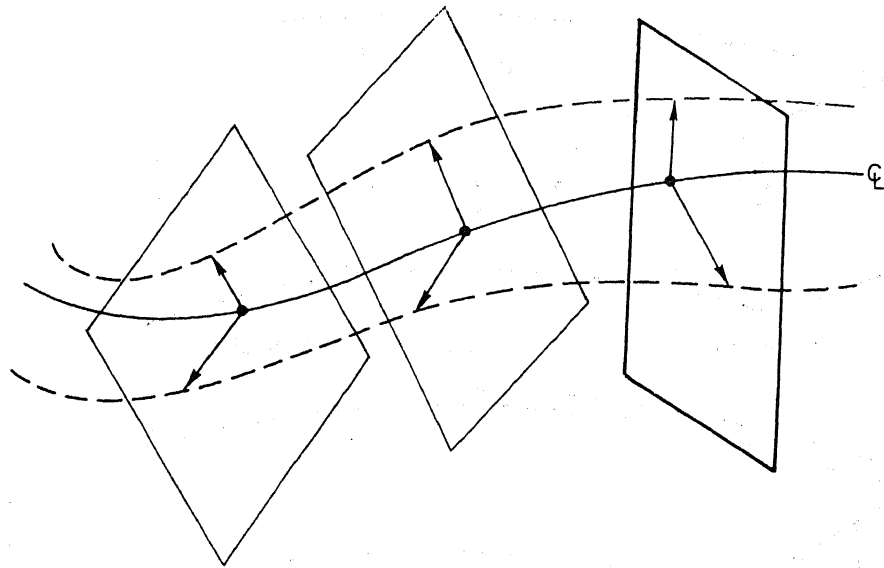


Figure 3. Generation of transverse planes from two vector fields.

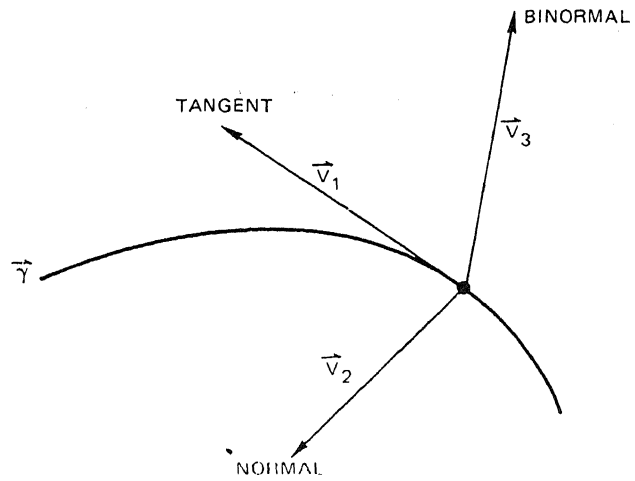


Figure 4. The Frenet frame.

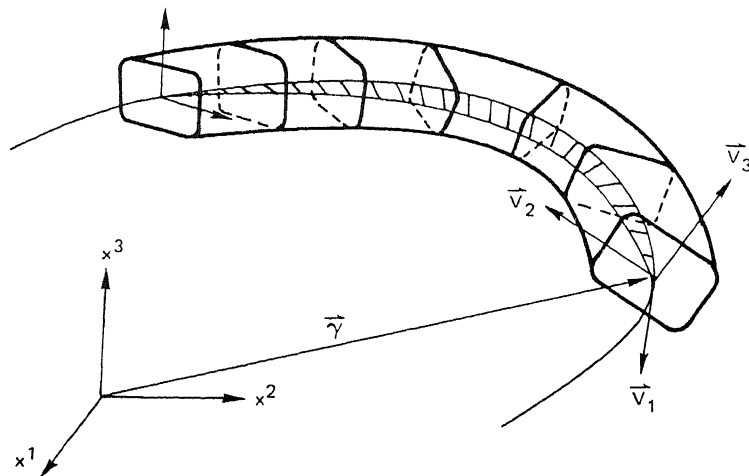


Figure 5. Transformation as an embedding into three dimensional Euclidian space.

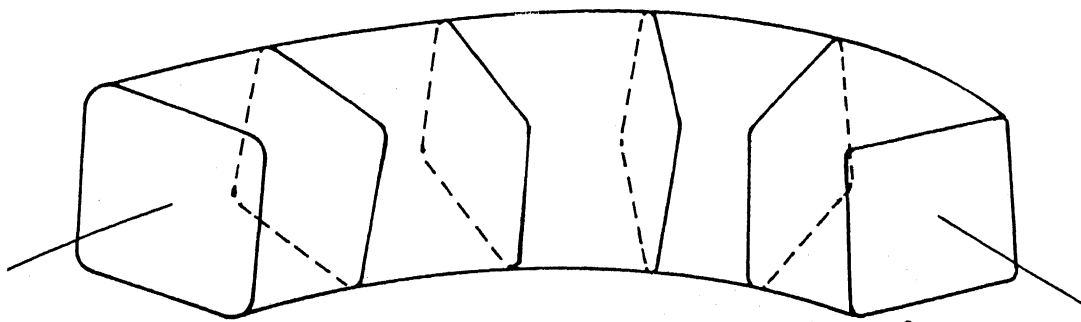


Figure 6a. Transverse planar cuts of constant axial location y^3 .

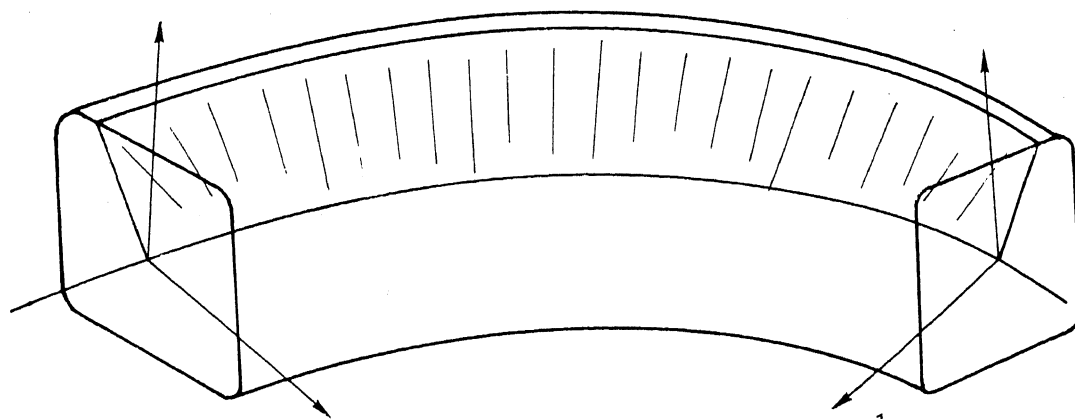


Figure 6b. Ruled surface of constant pseudo-angle y^1 .

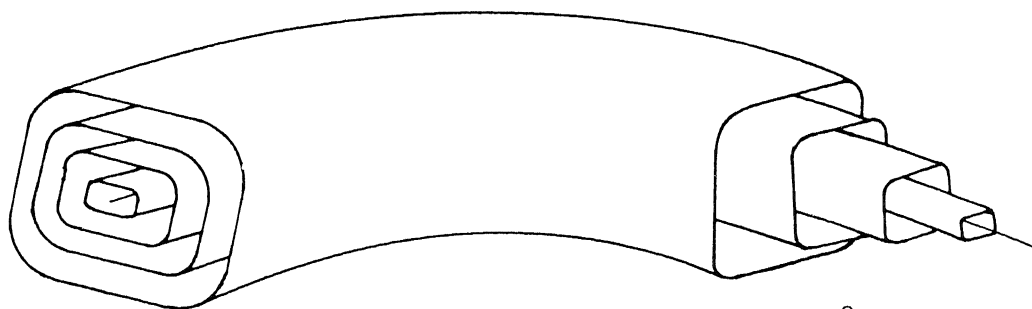


Figure 6c. Tube-like surfaces of constant pseudo-radius y^2 .

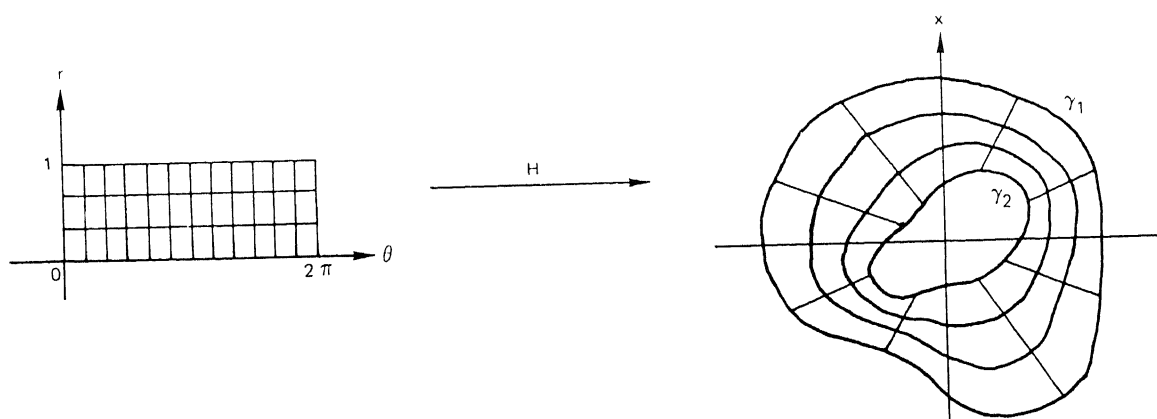


Figure 7. Linear homotopy between two loops.

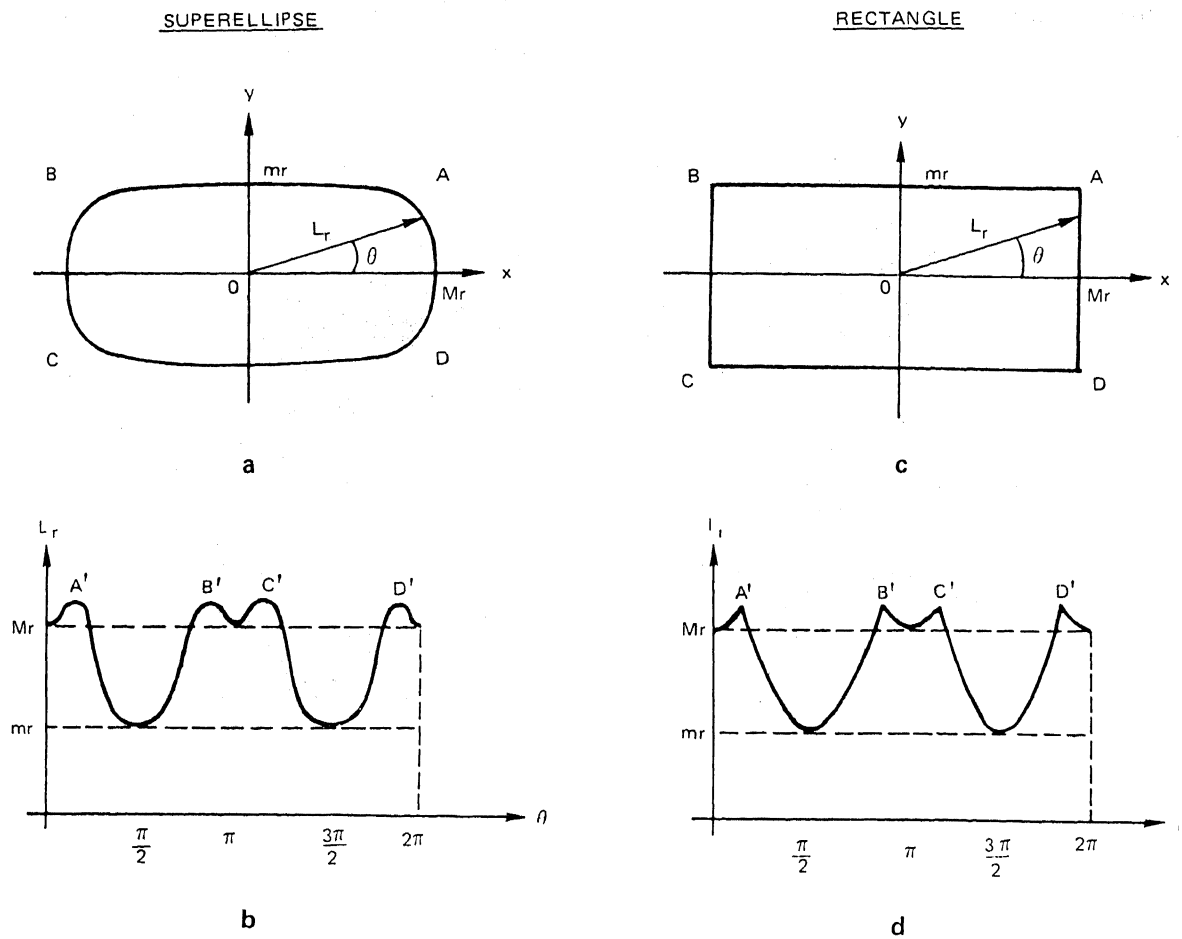


Figure 8. Polar representations of the superellipse and the rectangle.

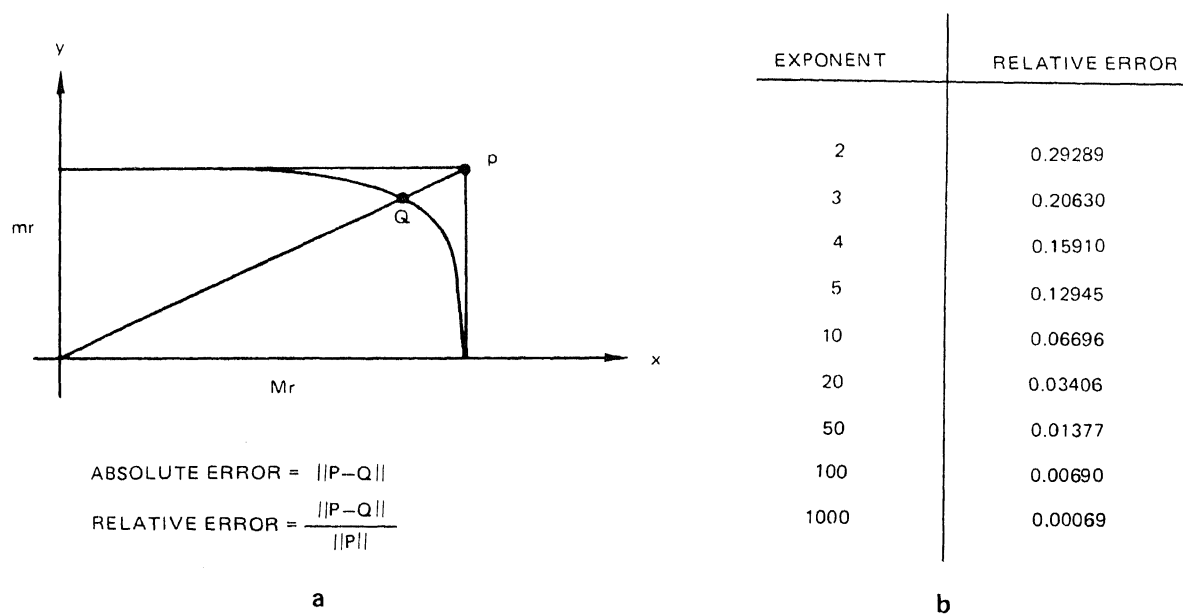


Figure 9. Superelliptic approximation of rectangles.

PRESSURE RATIO 1.33

CFL NO. = 1.4

JET MACH NO. 2.5
JET ASPECT RATIO 2:1

JET/FREE STREAM VEL. RATIO 1.33

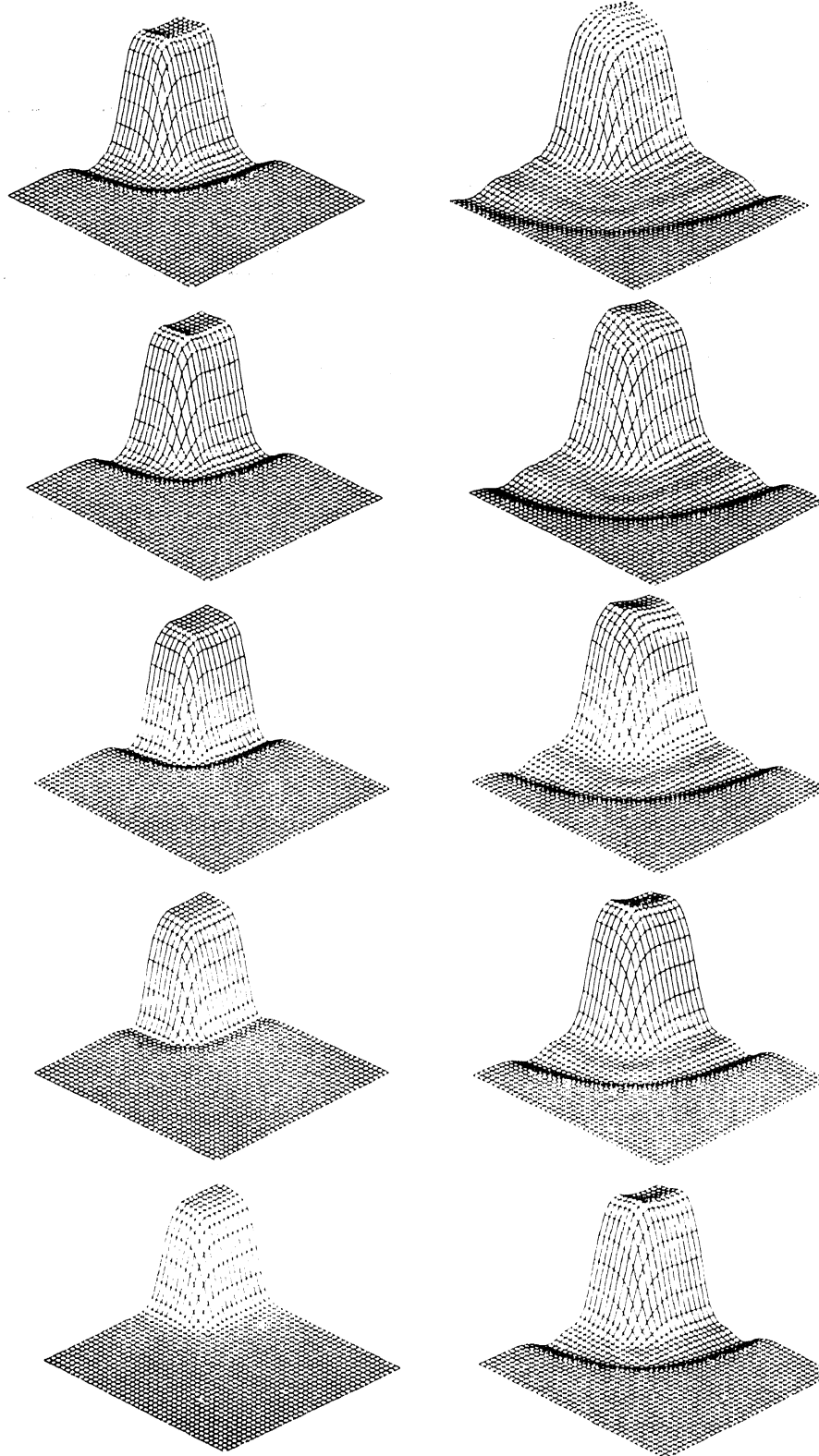


Figure 10. Under expanded rectangular jet velocity profiles.

CALCULATION OF SEPARATED FLOWS IN INTERNAL PASSAGES*

by

G.H. Hoffman

*McDonnell Douglas Research Laboratories
McDonnell Douglas Corporation
St. Louis, Missouri 63166*

Abstract

Research on the computation of turbulent, separated, internal flows at MDRL is reviewed. Some of the numerical aspects of the problem are discussed. A new algorithm applicable to quasilinear convection-diffusion equations is presented, and sample calculations for laminar flow in a driven square cavity are shown. Future research is outlined.

**This research was conducted under the McDonnell Douglas Independent Research and Development Program*

Introduction

Flows through certain types of internal passages, such as strongly divergent diffusers, are notorious for producing large separated regions and for being highly turbulent. The calculation of such flows necessarily requires the numerical solution of the full Navier-Stokes equations. At the present time, the most practical approach to the proper presentation of turbulence, from the standpoint of cost per solution, appears to be through turbulence modeling.

The field of numerical calculation of turbulent recirculating flows is still in its infancy. During the past seven years, however, successful computer codes for solving the full Navier-Stokes equations with transport-type turbulence models included have been written at Imperial College¹ and at Los Alamos². These codes are restricted to simple geometric boundaries formed by perpendicular lines. In the calculation of turbulent recirculating flows, much remains to be done in the development of fast, reliable computing methods, in improving the accuracy of the finite difference schemes, in exploring the range of applicability of turbulence models (and if need be in producing better models), and in developing methods to handle boundary shapes of practical interest.

Turbulent Flow Calculations at MDRL

For over two years, work has been underway at McDonnell Douglas Research Laboratories (MDRL) with the objective of creating a computer code to calculate two-dimensional turbulent flows in ducts with smooth arbitrary wall contours. This involves the numerical solution of the steady, time-averaged Navier-Stokes equations with a two-equation turbulence model. Viscous effects are also included so that the calculation will predict the laminar sublayer structure as well as a natural transition from laminar to turbulent flow in the streamwise direction.

The computer code is designed to calculate separation and reattachment points without the restrictive parallel flow assumptions that are commonly made in the sublayer¹. The extreme thinness of the sublayer requires that grid points be packed in that region for adequate definition. This naturally results in increased computation time over the usual practice of ignoring the detailed structure of the sublayer. In the present treatment, adequate grid definition in the sublayer is achieved by using stretching functions of the coordinate normal to a solid boundary.

Considerable work has been done in the detailed study of existing two-equation turbulence models. Extensive calculations with the turbulence models of Jones and Launder³ and Saffman⁴ in fully developed flows have been made to gain an understanding of their behavior in simple situations. As a consequence of this work, several improvements were made to the Jones and Launder model⁵. Based on this experience, the Saffman model is the current choice because it is numerically better behaved near a wall and does not require fitting functions in the sublayer. In addition, the so-called universal constants in this model are all chosen by the elegant means of applying it to simple limiting cases.

Paralleling the work with turbulence models has been an investigation of a number of finite difference techniques in connection with various types of iterative (relaxation) procedures for solving the Navier-Stokes equations. Most of this work has concentrated on laminar flows to understand the convergence behavior of the methods without the added complication of the turbulence equations. This work has resulted in the derivation of a new finite difference algorithm for convection-diffusion equations that possesses second-order accuracy and unconditional diagonal dominance.

In order to treat duct elements of arbitrary smooth contour, conformal mapping is being used to generate a computational grid. An orthogonal grid is desirable for use with the Navier-Stokes equations for convergence reasons. The inverse approach of Thom and Apelt⁶ is used to establish the network of grid points. Starting with a uniform grid in the computation plane, stretching functions are used to distribute grid points where needed. The solution of Laplace's equation for the physical coordinates enables the mapping modulus to be determined without interpolation. A computer code to perform inverse conformal mapping, without the stretching functions, has been written and is operational.

At the present time, the turbulence model of Saffman is being applied to entry flow in a channel. This requires only a simple Cartesian grid. The aim here is to gain experience with the highly nonlinear set of governing equations in a simple geometry before adding conformal mapping to treat more general boundary shapes.

Problem Formulation

The equations to be solved are the two-dimensional, steady, time-averaged Navier-Stokes equations incorporating the two-equation turbulence model of Saffman⁴. For simplicity, the flow is taken to be incompressible.

The set of nonlinear algebraic equations resulting from a suitable finite difference approximation of the steady equations is solved by relaxation. The solution by relaxation, if performed properly, can be accomplished in fewer cycles than the steady-state solution obtained as the asymptotic limit of the time-dependent approach. Savings in computer time of as much as 40% have been reported⁷.

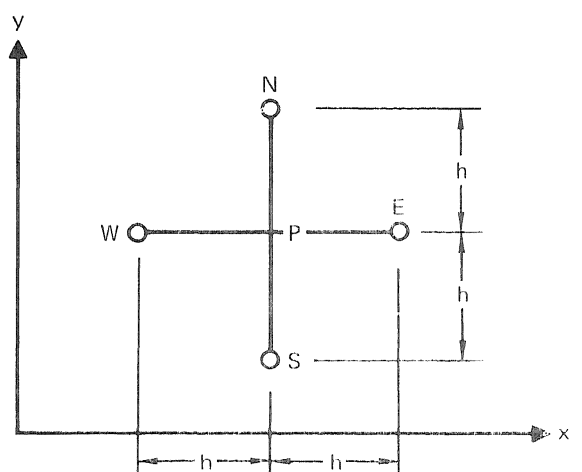
Since the flow is two-dimensional, stream-function vorticity formulation is used. With the addition of the two-equation turbulence model, the number of dependent variables is four. Vorticity and the two turbulence quantities (turbulent kinetic energy and turbulent pseudo-vorticity) all obey a quasilinear convection-diffusion equation of the form,

$$f_{xx} + R\alpha f_x + f_{yy} + R\beta f_y = S, \quad (1)$$

where α and β are convection coefficients depending on other dependent variables, S is a source-like term also depending on other dependent variables, and R is a parameter, such as Reynolds number, that can be large. The major source of difficulty in solving Eq. (1) arises from the nonlinear convective terms and, to a lesser extent, from the source-like term S .

Finite Difference Approximations

In the present work, only finite difference operators involving three or fewer grid points in a given direction have been considered. This means that the truncation error is at best second order. The grid pattern is the familiar five-point star shown in Fig. 1 where point-of-the-compass notation is used.



GP75 0573 1

Fig. 1. Five-point finite difference star

For purposes of illustration, the step size h is taken as uniform.

The five-point finite difference approximation of Eq. (1) can be written,

$$C_E f_E + C_W f_W + C_N f_N + C_S f_S - C_P f_P = S h^2. \quad (2)$$

The exact form of the coefficients C_j will depend upon the particular finite difference approximation. Also, the C_j are usually functions of the other dependent variables. Equation (2) applied over the entire field of grid points together with boundary conditions constitutes the approximating system of nonlinear algebraic equations to be solved.

In the simplest iterative scheme (point or line relaxation), the coefficients C_j and source term S are evaluated from the previous iterate, thereby decoupling the equations. The system for the new iterate therefore becomes linear. To ensure convergence of this type of iterative process, diagonal dominance of the coefficient matrix is required, as expressed by

$$|C_E| + |C_W| + |C_N| + |C_S| \leq |C_P|. \quad (3)$$

Strictly speaking, the satisfaction of Eq. (3) over the entire field assures convergence only for truly linear systems. For nonlinear equations, diagonal dominance does not necessarily assure convergence, as present experience has shown. Without diagonal dominance, the iterative process can be expected to diverge⁷.

Questions concerning diagonal dominance and truncation error led the author to spend considerable time exploring the characteristics of upwind differencing, central differencing, and the exponential differencing scheme of Allen and Southwell⁸ on simple laminar flows. This investigation led to the development of a new finite difference algorithm for Eq. (1) that has second-order accuracy and is always diagonally dominant.

Augmented Central Differences

The central difference (CD) approximation applied to Eq. (1) has a truncation error of $O(Rh^2)$ but is only conditionally diagonally dominant depending on the magnitude of $R\alpha$ and $R\beta$, the convective coefficients. As these coefficients become larger, diagonal dominance is lost. The author has extended the CD approximation so that diagonal dominance is always maintained while the truncation error remains $O(Rh^2)$. This new algorithm for Eq. (1) is called "augmented central differences" (ACD).

The CD approximation loses diagonal dominance because point P at the center of the finite difference star is not included in the expressions for the convective derivatives f_x and f_y . The CD approximation for f_x , e.g., is

$$(f_x)_P = \frac{f_E - f_W}{2h} - \frac{h^2}{6} (f_{xxx})_P. \quad (4)$$

The ACD idea is to evaluate $(f_{xxx})_P$ from Eq. (1) by differentiation and retain only leading terms containing R . The derivative $(f_{xx})_P$ in $(f_{xxx})_P$ arising from differentiation of the convective term is evaluated by the usual CD expression. After some algebra, the ACD expression for $(f_x)_P$ is

$$(f_x)_P = \frac{f_E - f_W}{2h} + \frac{1}{3} R\alpha_P (f_E - 2f_P + f_W) + \frac{1}{3} RS_1 h^2 + O(h^2, Rh^4), \quad (5)$$

where

$$S_1 = (\alpha_x f_x + \beta f_{xy} + \beta_x f_y)_P. \quad (6)$$

The leading term on the right-hand side of Eq. (5) is the CD contribution, the next term is a stabilizing term that assures diagonal dominance, and the final term maintains the truncation error at the same order as the CD approximation. The quantity S_1 is treated like a source term and evaluated from the previous iterate.

The ACD algorithm retains the form given by Eq. (2) except that the right-hand side is replaced by

$$\left[S_P - \frac{2}{3} R_g^2 (\alpha_P S_1 + \beta_P S_3) \right] h^2,$$

where R_g is the grid parameter defined as Rh and S_3 is a term occurring in the ACD expression for $(f_y)_P$ analogous to S_1 . The ACD coefficients C_j are given by

$$\begin{aligned} C_E &= 1 + R_g \alpha_P + \frac{2}{3} R_g^2 \alpha_P^2, \\ C_W &= 1 - R_g \alpha_P + \frac{2}{3} R_g^2 \alpha_P^2, \\ C_N &= 1 + R_g \beta_P + \frac{2}{3} R_g^2 \beta_P^2, \\ C_S &= 1 - R_g \beta_P + \frac{2}{3} R_g^2 \beta_P^2, \\ C_P &= 4 + \frac{4}{3} R_g^2 (\alpha_P^2 + \beta_P^2). \end{aligned} \quad (7)$$

Diagonal dominance will always be maintained by this system irrespective of the magnitudes of $R_g \alpha_P$ and $R_g \beta_P$. The ACD algorithm, because of the numerous arithmetic operations involved, requires almost twice as much computation time per grid point as the central or upwind difference algorithms.

Results

To date the ACD algorithm has been applied only to laminar flows with simple geometries. The aim has been to study its convergence properties. The problems solved were flow in a square cavity with a driven wall and a jet impinging perpendicularly on a planar wall. For both of these cases, published numerical results exist for comparison.

Figure 2 shows the cavity streamlines obtained with the ACD algorithm at a Reynolds number of 400 based on cavity depth and wall speed. The grid is 41×41 . A recirculating eddy is present in each of the lower corners. Figure 3 compares the distribution of horizontal velocity component u along the vertical centerline of the cavity at $R = 400$ computed using ACD, CD and upwind differencing. Also shown are the results of Burggraf⁹ obtained using a CD approximation. The agreement between ACD and CD solutions is excellent. The shifting of the upwind difference solution is caused by numerical viscosity (first-order truncation error). Even at this Reynolds number, boundary layers on the walls as well as an inviscid core can be seen developing.

Table 1 presents a comparison of the number of iterations required to reach convergence and computation time for the cavity at $R = 400$ as calculated by the three finite difference methods. A CDC 6500 computer was used. The convergence tolerances on stream function and vorticity were 10^{-6} and 10^{-4} respectively. The relaxation factors used are shown in the table. In all cases, point relaxation was used with no coupling of the equations.

Table 1 shows that ACD requires only a few more iterations to converge than UD but is the slowest of the three. As already mentioned, this is due to the added computations necessary at each grid point.

Initial runs on the cavity problem using line relaxation in conjunction with Newton's method¹⁰ indicate that the number of iterations required for convergence with the ACD method is reduced by 40% over the standard point relaxation scheme. With Newton's method, the coefficients in Eq. (2) are brought into the iteration with the result that all the finite difference equations become coupled. The labor required to invert this system adds

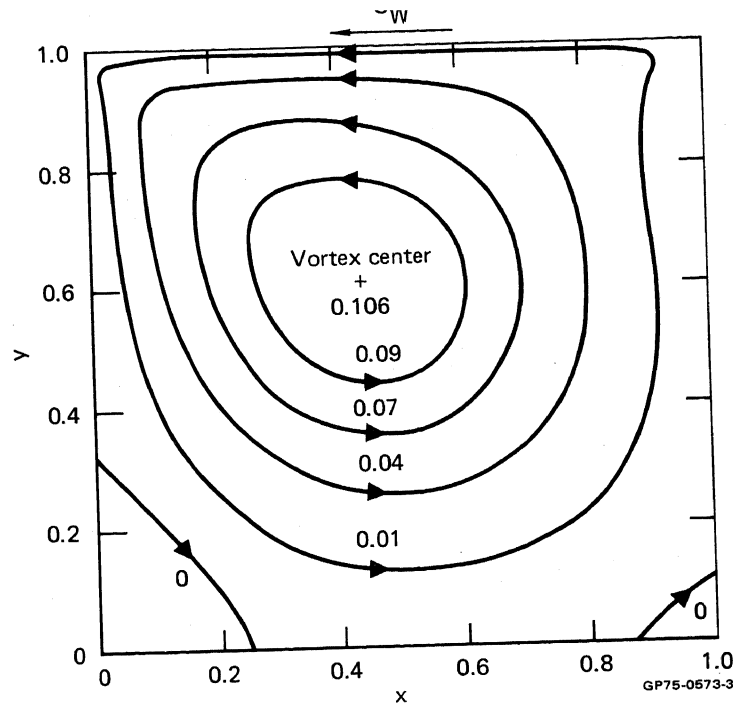


Fig. 2 Streamlines in a square cavity with a uniformly moving upper wall obtained with ACD algorithm
Reynolds no. = 400 41 x 41 uniform grid

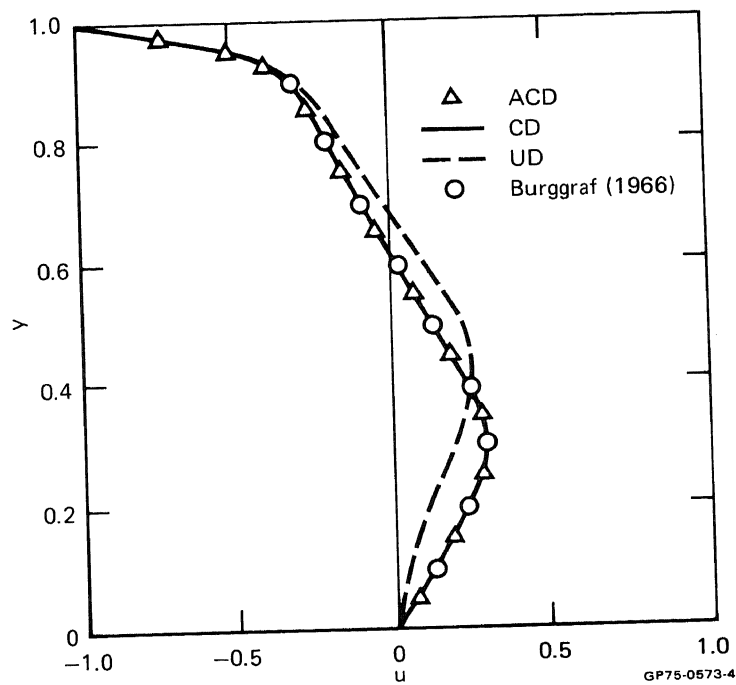


Fig. 3 Velocity profile on vertical centerline of square cavity
Reynolds no. = 400 41 x 41 uniform grid

Table 1 Solution parameters for cavity at R = 400

Method	No. iterations	CPU time (s)	Relaxation factors	
			Stream fn.	Vorticity
ACD	592	732	1.6	1.0
UD	541	359	1.6	1.0
CD	963	648	1.6	0.4

GP75-0573-2

computation time at each grid point. It is still too early to tell what the real advantages will be with this technique. Of course, coupling the equations during the iteration may turn out to be the only dependable way of ensuring convergence.

The turbulent entry flow program has only recently reached the checkout stage. At present, upwind differencing is used and the uncoupled form of the equations is solved by point relaxation. For this problem, the initial velocity profile at the entrance is taken to be uniform as are the turbulence profiles. Neumann conditions are used at the downstream boundary and symmetry conditions at the upper boundary. The lower boundary is the channel wall.

The program is still in the early stages of checkout. Preliminary runs indicate that decoupling the equations in the turbulent case is not warranted. In fact, divergence of an apparently stable scheme has been encountered.

Future Plans

The main task for the immediate future is to find a reliable, convergent iteration scheme for the turbulent entry flow problem. Once this is accomplished, the inverse conformal mapping will be added to enable flow calculations in duct elements with curved walls.

Present thinking is that coupling the turbulent finite difference equations using Newton's method will be necessary to ensure convergence. This will be done first using point relaxation, which is easiest to do, and then with line relaxation.

Direct inversion of the algebraic system, after applying Newton's method, may turn out to be the most reliable method to obtain a solution. This method requires large amounts of computer storage to accommodate the large matrices involved. Keller and his students at California Institute of Technology have used direct inversion successfully in solving laminar flow problems by the method of series truncations^{11, 12}. Morihara and Cheng¹³ have also used direct inversion on the laminar channel entry flow problem. They used higher order upwind differencing to ensure diagonal dominance in the block matrices. Only five iterations were required to achieve a convergence tolerance of 10^{-6} at $R = 2000$.

References

1. A.D. Gosman et al., Heat and Mass Transfer in Recirculating Flows, (Academic Press, London and New York, 1969).
2. A.A. Amsden and F.H. Harlow, "Transport of Turbulence in Numerical Fluid Dynamics," J. Comp. Phys. 3, 94 (1968).
3. W.P. Jones and B.E. Launder, "The Prediction of Laminarization with a Two-Equation Turbulence Model," Int. J. Heat Mass Transfer 15, 301 (1972).
4. P.G. Saffman, "Model Equations for Turbulent Shear Flow" Studies in Applied Math. 53, 17 (1974).
5. G.H. Hoffman, "Improved Form of the Low Reynolds Number k- ϵ Turbulence Model," Phys. Fluids 18, 309 (1975).
6. A. Thom and C.J. Apelt, Field Computations in Engineering and Physics (D. Van Nostrand, New York, 1961).
7. P.J. Roache, Computational Fluid Dynamics, (Hermosa Publishers, Albuquerque, 1972).
8. D.N. de G. Allen and R.V. Southwell, "Relaxation Methods Applied to Determine the Motion, in Two Dimensions, of a Viscous Fluid Past a Fixed Cylinder," Quart. J. Mech. Appl. Math 8, 129 (1955).
9. O.R. Burggraf, "Analytical and Numerical Studies of the Structure of Steady Separated Flows," J. Fluid Mech. 24, 113 (1966).
10. E. Isaacson and H.B. Keller, Analysis of Numerical Methods, (John Wiley and Sons, New York, 1966).
11. F. Nieuwstadt and H.B. Keller, "Viscous Flow Past Circular Cylinders," Computers and Fluids 1, 59 (1973).
12. D.C. Brabston, "Numerical Solutions of Steady Viscous Flow Past Spheres and Gas Bubbles," Ph. D. Thesis, Cal. Tech., 1974.
13. H. Morihara and R.T. Cheng, "Numerical Solution of the Viscous Flow in the Entrance Region of Parallel Plates," J. Comp. Phys. 11, 550 (1973).

ACD Finite Difference Algorithm

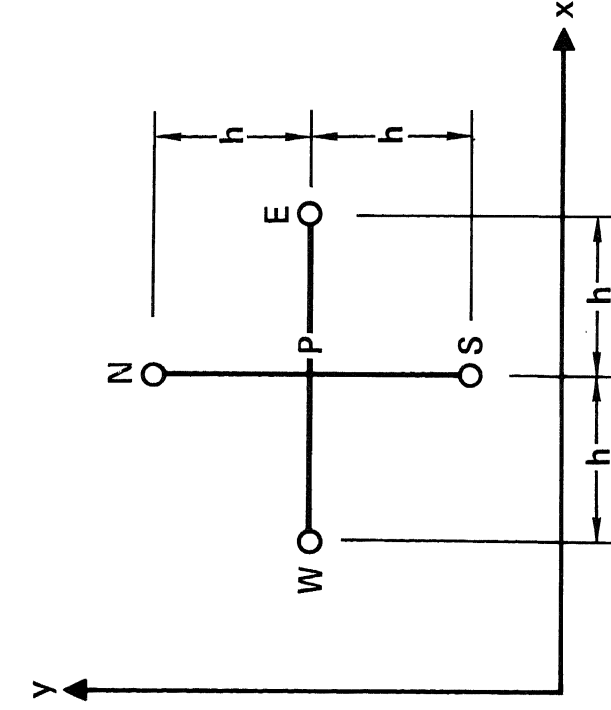
General form of Navier-Stokes and turbulent transport equations in 2-D

$$f_{xx} + 2R\alpha f_x + f_{yy} + 2R\beta f_y = S \quad (1)$$

where α , β and S in general are functions of f and other dependent variables.

ACD algorithm for linearized form of Eq. (1) is,

$$C_E f_E + C_W f_W + C_N f_N + C_S f_S - C_P f_P = \left[S_P - \frac{2}{3} R_g^2 (\alpha_P S_1 + \beta_P S_3) \right] h^2 + O(R_g h^3)$$



Finite difference "star"

h = step size

where:

$$C_E = 1 + R_g \alpha_P + \frac{2}{3} R_g^2 \alpha_P^2$$

$$C_W = 1 - R_g \alpha_P + \frac{2}{3} R_g^2 \alpha_P^2$$

$$C_N = 1 + R_g \beta_P + \frac{2}{3} R_g^2 \beta_P^2$$

$$C_S = 1 - R_g \beta_P + \frac{2}{3} R_g^2 \beta_P^2$$

$$C_P = 4 + \frac{4}{3} R_g^2 (\alpha_P^2 + \beta_P^2)$$

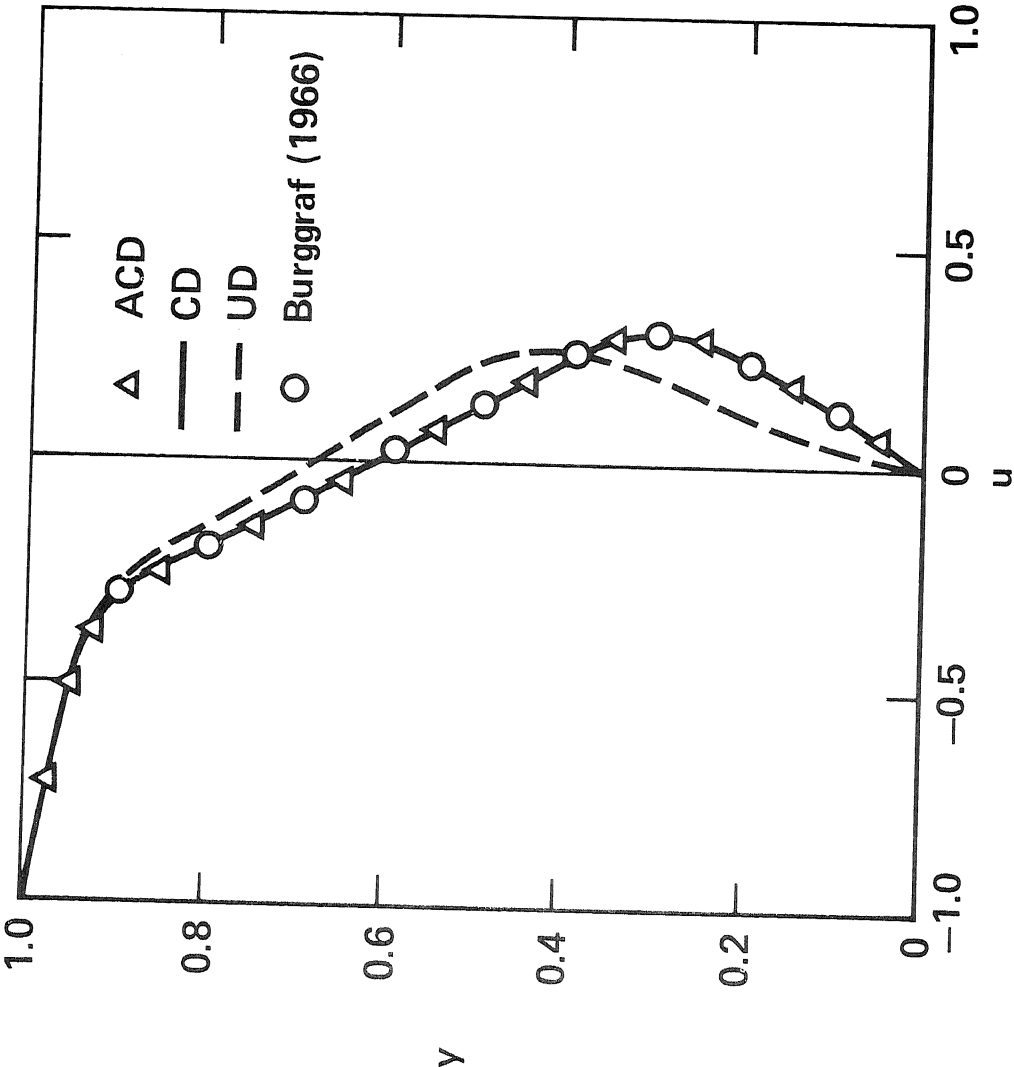
$$S_1 = (\alpha_x f_x + \beta f_{xy} + \beta f_{xy} + \alpha f_{xy}) P$$

$$S_3 = (\beta_y f_y + \alpha f_{xy} + \alpha f_{xy} + \alpha_y f_x) P$$

$$R_g = Rh$$

Velocity Profile on Vertical Centerline

Reynolds no. = 400 $h = 0.025$





Detroit Diesel Allison
Division of General Motors Corporation
Indianapolis, Indiana 46206

ELEMENTS OF THREE-DIMENSIONAL FLOW

by

R. R. Allran, J. R. Fagan and P. J. Haley

RESEARCH DEPARTMENT

July 25, 1975

ELEMENTS OF THREE-DIMENSIONAL FLOW

INTRODUCTION

Three-dimensional flow has long been recognized as playing an important role in the operation of aircraft engines. The use of the turbofan engine for V/STOL applications, particularly with respect to thrust vectoring nozzles, accentuates the importance of including rotational, 3-dimensional flow effects in the design system. This report describes a three-dimensional, rotational flow analysis program^{(1)*} developed by Detroit Diesel Allison under contract with the Naval Air Systems Command, Code: 310 and uses it to interpret the results observed in a number of rectangular, turning duct experiments. The principal conclusions obtained in this study are: (1) streamwise vorticity components of significant magnitude can be expected at the exit of turning ducts, and (2) the vortex structure makes major alterations in the static pressure and velocity components throughout the entire flow field.

* Superscripts denote listed references.

THEORETICAL MODEL

Steady, strictly adiabatic, inviscid flow of an ideal gas is frequently taken as the basis for fluid mechanics analysis of flow in turbomachines. Accepting this basis, the continuity equation, the three momentum equations, the energy equation, the equation of state, and the defining equation for total stagnation enthalpy form the governing equations. These seven equations, as shown in Figure 1, then form a closed system for the three velocity components, (v_x , v_y and v_z), the density (ρ), the entropy (S), the temperature (T) and the total stagnation enthalpy (H).

The primary mathematical difficulties in solving this set of equations arise from the simultaneous solution of the three complex momentum equations. This difficulty can be alleviated by forming the vector dot product of the velocity with the momentum equation and subtracting the energy equation. This equation, which states the entropy is constant along a streamline, can be used to replace one of the momentum equations. The modified set still requires the simultaneous solution of two momentum equations. As a matter of expediency, one of the momentum equations is usually eliminated at this point by assuming two-dimensional flow (i.e., one of the velocity components is zero). C. H. Wu⁽²⁾ pointed out that three-dimensional

flow fields can be built up from mathematically two-dimensional calculations by applying the analysis on a predetermined but arbitrary stream surface with variable stream tube thickness. In this procedure the equation of the stream surface replaces the second of the three momentum equations and the stream surface geometry is systematically updated as the calculation progresses from one two-dimensional problem to the next.

The application of the governing equations to a predetermined stream surface is illustrated in Figure 2 for the continuity equation. In this form the continuity equation is written entirely in terms of flow properties on the stream surface and a stream function, ψ , can be defined as shown in Figure 2. Substituting these special derivatives and the stream function into the one remaining momentum equation produces equation I of Figure 3. Introduction of the stream function, ψ , allows the energy equation and the entropy equation to be written quite simply as shown in equations II and III of Figure 3.

On the stream surface the total stagnation enthalpy, H , and the entropy, S , are functions of the stream function, ψ , alone. These functional relationships can be established from the inlet flow conditions. The remaining momentum equation is a second order, quasi-linear, partial differential equation. The solution is initiated by obtaining a first estimate of the stream function for incompressible, irrotational flow ($F=0$). This initial ψ

value is then used in the energy equation, the entropy equation, and the auxiliary relations for velocities and density to obtain an updated F distribution. This updated F distribution is then used in the momentum equation to improve the ψ estimate and this iterative procedure is continued until consistent sets of F and ψ values are obtained. It should be noted that the differential surface elements $(\partial x / \partial y)_{z=\text{constant}}$ of Figure 2 have been replaced by their equivalents in terms of unit normal surface vector components, n_y / n_x .

The full three dimensional flow field is produced by iteratively updating the stream surface geometry based upon the mathematically two-dimensional calculation described above. The calculation is initiated on a series of assumed stream furfaces ($\psi = \text{constant}$) as shown in Figure 4. On each of these stream surfaces a set of streamlines are calculated. A set of stream surfaces ($\phi = \text{constant}$) essentially orthogonal to the original surfaces are generated by connecting equal ϕ streamlines on the various ψ surfaces as shown in Figure 4. All of the information necessary to define the geometry of the new set of stream surfaces is available from the solutions on the initial set of stream surfaces. Thus, an iterative procedure is defined wherein the results of the calculations on one set of stream surfaces define a new set of stream surfaces. This iterative procedure continues until no further significant changes occur in the stream surface geometry.

CONTROLLING FLOW PHYSICS IN TURNING DUCTS

The first step faced in modeling any real flow situation is to establish the controlling flow physics elements. In the case of flow through turning ducts at moderate to high Reynolds numbers three important questions arise. These are: 1, whether the flow must be modeled including viscous forces; 2, whether an irrotational potential flow solution is adequate and 3, whether the three-dimensional effects are critical or a two-dimensional model will be sufficiently accurate. The following paragraphs compare results of the 3-D theoretical model described in the previous section to experimental data taken from a number of rectangular turning duct experiments. In order to compare data from various sources, it is useful to scale the experiment for known effects. The geometry of a rectangular turning duct can be fixed by three parameters: the turning angle, θ ; the duct width to radius ratio, $2a/R$; and the duct aspect ratio, b/a . These dimensions along with inlet profiles (i.e., inlet vorticity) are shown for a 90° bend in Figure 5. It is also informative for comparative purposes to consider the case of equilibrium, one-dimensional flow in a bend. As seen in Figure 6, both the r - and θ - momentum equations with $V_r=0$ and no inlet vorticity ($\frac{\partial H}{\partial r} = \frac{\partial H}{\partial \theta} = \frac{\partial S}{\partial r} = \frac{\partial S}{\partial \theta} = 0$) show the streamwise velocity component, V_θ , to be inversely proportional to the radius, r . Finally, normalizing the difference between the local static pressure and the inlet total pressure by the inlet dynamic head makes the

pressure differential insensitive to flow rate or inlet Mach No. Figure 7 compares the data of Young, Howard and Jerie⁽³⁾ with results of three-dimensional flow analysis and the one-dimensional equilibrium flow model. Generally good agreement is obtained between the pressure distribution along a radial line half way through the bend ($\theta = 45^\circ$) and along a constant radius ($r/R=.833$) near the ID of the duct along the length of the bend. Furthermore, the equilibrium flow model gave equivalent results to the full 3-D analysis. Inspection of the 3-D results show this should be the case since there was no inlet vorticity and the radial velocity was truly near zero throughout the bend. A key point is that the inlet boundary layer thickness was truly negligible with respect to the width (48") of the duct.

Figure 8 shows inner wall static pressure distributions for several smaller, rectangular, 90° bends. The data for $\frac{2a}{R} = 1$, $2/3$ and $1/2$ are from reference 4 and the data for $\frac{2a}{R} = 1/3$ are from reference 5. The reference 4 data were obtained on two inch square rectangular ducts with uniform inlets except for approximately $1/4$ inch thick boundary layers. The reference 5 data were obtained from a 5" wide and 10" high duct ($2a=5"$; $2b=10"$) with a strongly distorted inlet velocity profile. The static pressure levels of equilibrium flow are also shown on Figure 8 for each of the duct geometries tested. Unlike the results for the large duct shown in Figure 7, there is very poor agreement between the equilibrium results and these smaller duct data. The primary difference between these two data sets would appear

to be the inlet distortion parameters, $\frac{\delta a}{a}$ and $\frac{\delta b}{b}$. More specifically, the data which does not agree with equilibrium flow has significant inlet vorticity. Weske⁽⁶⁾ has studied the flow field development in turning ducts and has shown that the low energy inlet flow near the walls of the duct does not have sufficient streamwise momentum to resist the static pressure field developed by the turn. As shown in Figure 9, the low energy fluid is transported to the bend inner radius and can produce a separated eddying zone. These phenomena clearly differ from the assumptions of zero inlet vorticity and zero radial flow assumed in the equilibrium model.

Focusing more directly on the effects of inlet distortion or vorticity, the data of Joy⁽⁵⁾ was analyzed with the rotational, three-dimensional analysis. Figure 10 compares the theoretical and experimental total velocity profiles on planes at the inlet (0°) as well as 30° and 60° through the bend. Since the static pressure is nearly constant throughout the flow field these velocity profiles represent constant total pressure stream surfaces. These figures, which represent the lower half of the symmetrical duct, show the horizontal stream surfaces coming into the duct have rotated toward the inner radius of the bend by about 20° at the 30° station and over 90° at the 60° station. From these results it is clear that with strong vorticity throughout the inlet, the swirling motion reduces significantly the static pressure gradients that would otherwise be established to counteract the centrifugal forces in a two-dimensional, turning flow field.

CONCLUSIONS

The results of this study show that a potential flow model will not be representative of turning duct flow in cases where the inlet profile is distorted over a significant fraction of the inlet. The critical magnitude of the distortion and fraction of the inlet flow which must be distorted to cause appreciable deviations from potential flow are not known precisely at this time. Clearly, when the inlet distortion is sufficient to bring about these appreciable deviations it is as a result of rotational flow effects and a three-dimensional analysis is required. Insofar as viscous forces are necessary to develop the inlet flow profiles, they are critical in the analysis of flow through turning ducts. The data from the large duct of reference 3 show very acceptable agreement with the inviscid analysis as does the data of Joy, reference 5. The work of Weske^(6,7) on small bend radii, $\frac{2a}{R} = 4/3$, does not clearly separate the effects of viscosity in the inlet from that in the bend, but viscous forces clearly are important. These simple rectangular bend experiments provide the basis for interpretation of the controlling flow mechanisms. To assess the existence of rotational flow in more practical hardware configurations, an experiment was performed to measure the flow in the exit plane of a model turbine diffuser system. This particular system turns the flow 90° from the turbine exit to the exhaust of the collector. Figure 12 shows the measured total pressure losses and flow angles. The existence of two strong vortices is evident in this data.

REFERENCES

1. Fagan, J. R., "Three-Dimensional, Subsonic Duct Flow Analysis - Final Technical Summary Report", NAVAIR Contract N00019-71-C-0416, Detroit Diesel Allison Division EDR 7451 (1972).
2. Wu, C. H., "A General Theory of Three-Dimensional Flow in Subsonic and Supersonic Turbomachines of Axial -, Radial - and Mixed - Flow Types", NACA-TN-2604 (1954).
3. Young, J. W. S., Howard, J. H. G., and Jerie, J., "A Zero-Streamwise-Pressure Gradient, Three-Dimensional Turbulent Boundary Layer in a 90° Curved Rectangular Duct", Transactions Canadian Society of Mechanical Engineering, Volume 1, Number 2, P87-96 (1972).
4. Young, A. D., Green, G. L., and Owen, P. R., "Tests of High-speed Flow in Right-angled Pipe Bends of Rectangular Cross-Section, Royal Aeronautical Establishment R&M 2066 (1943).
5. Joy, W., "Experimental Investigation of Shear Flow in Rectangular Bends", M. S. Thesis, Massachusetts Institute of Technology (1950).
6. Weske, J. R., "Investigations of the Flow in Curved Ducts at Large Reynolds Numbers", Journal of Applied Mechanics, (December, 1948).
7. Weske, J. R., "Experimental Investigation of Velocity Distributions Downstream of Single Duct Bends", NACA-TN-1471 (1947).

(I)

$$\nabla \cdot \rho \vec{U} = 0$$

(II)

$$-\vec{U} \times (\nabla \times \vec{U}) = \nabla H - T \nabla S$$

(III)

$$(\vec{U} \cdot \nabla) H = 0$$

$$H = C_p T + \frac{1}{2} U^2$$

(continuity)

(Eqn. of State)

(momentum)

(energy)

Seven scalar equations in seven scalar unknowns:

$U_x, U_y, U_z, H, S, T, \rho$

with the added equation which can replace one of the momentum equations or the energy equation

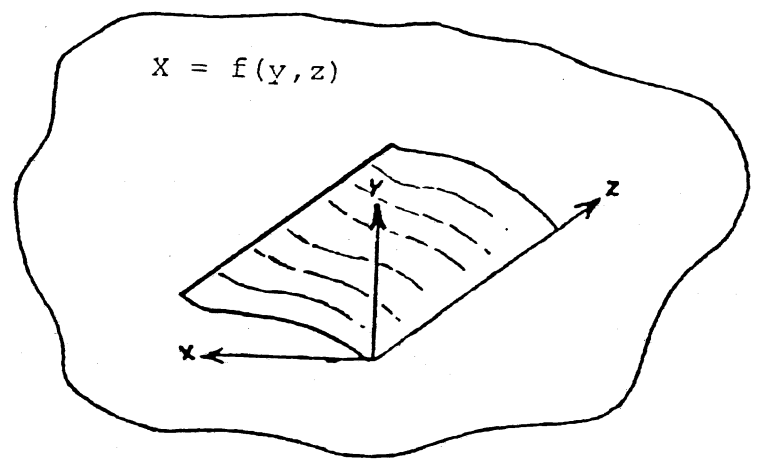
$$(\vec{U} \cdot \nabla) S = 0$$

FIGURE 1. Governing Equations for Steady, Inviscid, Strictly Adiabatic Flow

$$\frac{\partial \rho^V x}{\partial x} + \frac{\partial \rho^V y}{\partial y} + \frac{\partial \rho^V z}{\partial z} = 0$$

$$\frac{\partial}{\partial y} = \frac{\partial}{\partial y} + \frac{\partial}{\partial x} \frac{\partial x}{\partial y}$$

$$\frac{\partial}{\partial z} = \frac{\partial}{\partial z} + \frac{\partial}{\partial x} \frac{\partial x}{\partial z}$$



$$\frac{\partial \rho^V y}{\partial y} + \frac{\partial \rho^V y}{\partial z} = -\rho \left(\frac{\partial^V x}{\partial x} - \frac{\partial^V y}{\partial x} \frac{\partial x}{\partial y} - \frac{\partial^V z}{\partial x} - \frac{\partial^V z}{\partial x} \frac{\partial x}{\partial z} \right)$$

$$\frac{\partial (b \rho^V y)}{\partial y} + \frac{\partial (b \rho^V z)}{\partial z} = 0$$

$$\frac{\partial \psi}{\partial y} = b \rho^V z$$

$$\frac{\partial \psi}{\partial z} = -b \rho^V y$$

FIGURE 2. Continuity on a Stream Surface

$$(I) \quad \frac{\partial^2 \psi}{\partial y^2} + \frac{\partial^2 \psi}{\partial z^2} = F(H, S, \psi)$$

$$(II) \quad H = f_1(\psi)$$

$$(III) \quad S = f_2(\psi)$$

Three scalar equations in three unknowns:

$$H, S, \psi$$

supplemented by the auxiliary relations

$$F(H, S, \psi) = \frac{b\rho}{m v_z} \left[\frac{\partial H}{\partial y} - T \frac{\partial S}{\partial y} + \frac{\eta_y}{\eta_x} \frac{1}{\rho} \frac{\partial \rho}{\partial x} - v_x \frac{\partial^V x}{\partial y} \right] + \frac{\partial \psi}{\partial y} \frac{\partial \ln b\rho}{\partial} + \frac{\partial \psi}{\partial z} \frac{\partial \ln b\rho}{\partial}$$

$$\frac{\rho}{\rho_0} = \left(\frac{H - v^2/2}{\eta_0} \right)^{1/\gamma-1} e^{-\frac{S-S_0}{R}}$$

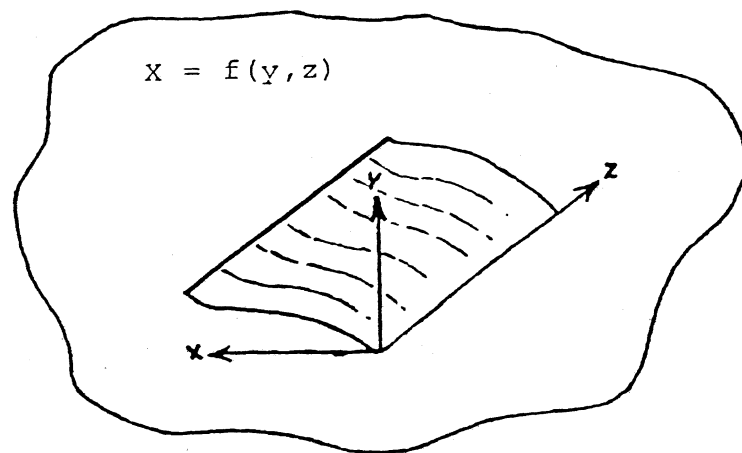
$$\frac{\partial \psi}{\partial y} = b \rho^V z \quad \frac{\partial \psi}{\partial z} = -b \rho^V y$$

FIGURE 3. Stream Surface Theory

$$\frac{\partial \rho^V x}{\partial x} + \frac{\partial \rho^V y}{\partial y} + \frac{\partial \rho^V z}{\partial z} = 0$$

$$\frac{\partial}{\partial y} = \frac{\partial}{\partial y} + \frac{\partial}{\partial x} \frac{\partial x}{\partial y}$$

$$\frac{\partial}{\partial z} = \frac{\partial}{\partial z} + \frac{\partial}{\partial x} \frac{\partial x}{\partial z}$$



$$\frac{\partial \rho^V y}{\partial y} + \frac{\partial \rho^V z}{\partial z} = -\rho \left(\frac{\partial^V x}{\partial x} - \frac{\partial^V y}{\partial x} \frac{\partial x}{\partial y} - \frac{\partial^V z}{\partial x} - \frac{\partial^V z}{\partial x} \frac{\partial x}{\partial z} \right)$$

$$\frac{\partial (b \rho^V y)}{\partial y} + \frac{\partial (b \rho^V z)}{\partial z} = 0$$

$$\frac{\partial \psi}{\partial y} = b \rho^V z \quad \frac{\partial \psi}{\partial z} = -b \rho^V y$$

FIGURE 2. Continuity on a Stream Surface

$$(I) \quad \frac{\partial^2 \psi}{\partial y^2} + \frac{\partial^2 \psi}{\partial z^2} = F(H, S, \psi)$$

$$(II) \quad H = f_1(\psi)$$

$$(III) \quad S = f_2(\psi)$$

Three scalar equations in three unknowns:

$$H, S, \psi$$

supplemented by the auxiliary relations

$$F(H, S, \psi) = \frac{b\rho}{m v_z} \left[\frac{\partial H}{\partial y} - T \frac{\partial S}{\partial y} + \frac{\eta_y}{\eta_x} \frac{1}{\rho} \frac{\partial \rho}{\partial x} - v_x \frac{\partial^V x}{\partial y} \right]$$

$$+ \frac{\partial \psi}{\partial y} \frac{\partial \ln b\rho}{\partial} + \frac{\partial \psi}{\partial z} \frac{\partial \ln b\rho}{\partial}$$

$$\frac{\rho}{\rho_0} = \left(\frac{H - v^2/2}{h_0} \right)^{1/\gamma-1} e^{-\frac{S-S_0}{R}}$$

$$\frac{\partial \psi}{\partial y} = b \rho^V z \quad \frac{\partial \psi}{\partial z} = -b \rho^V y$$

FIGURE 3. Stream Surface Theory

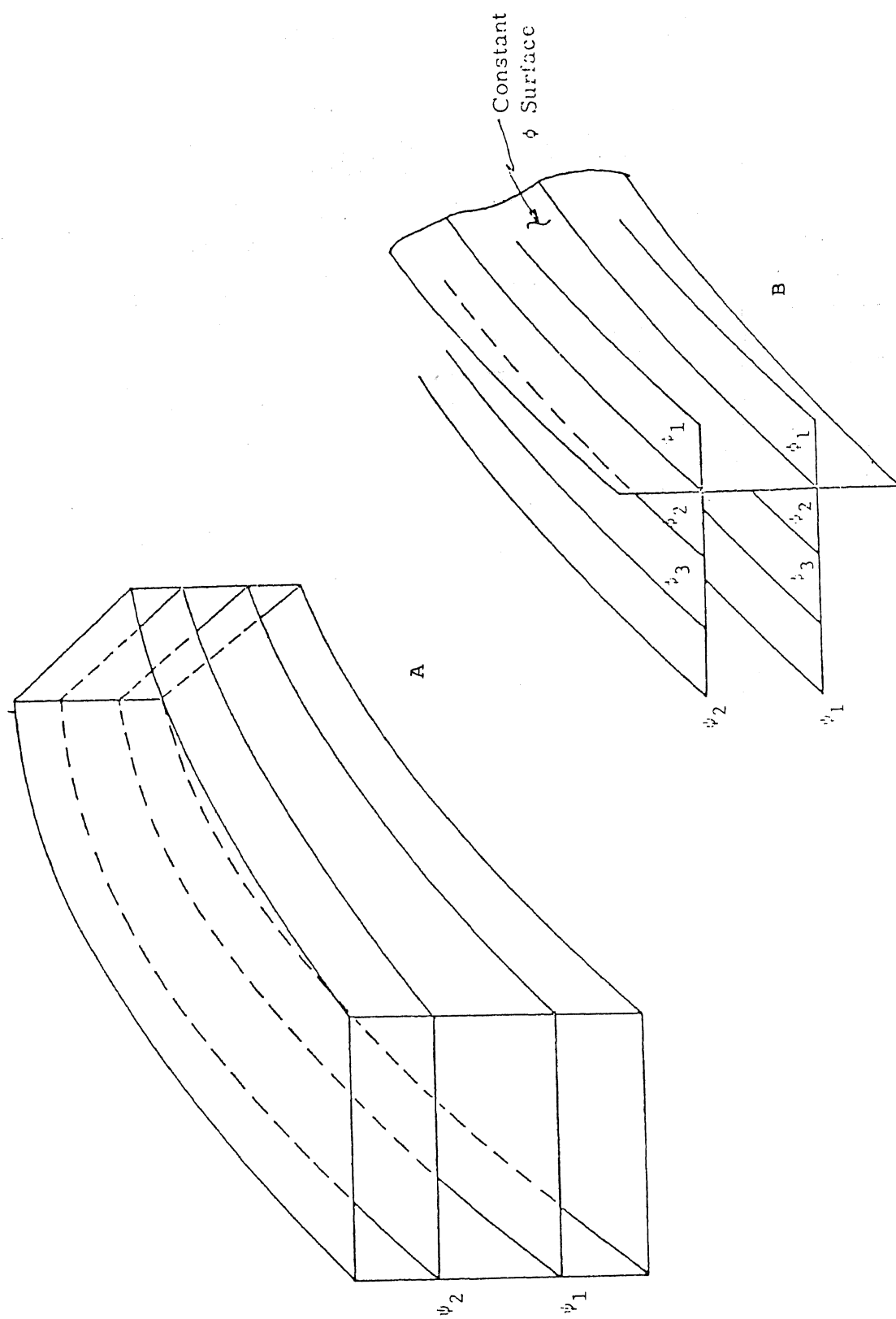
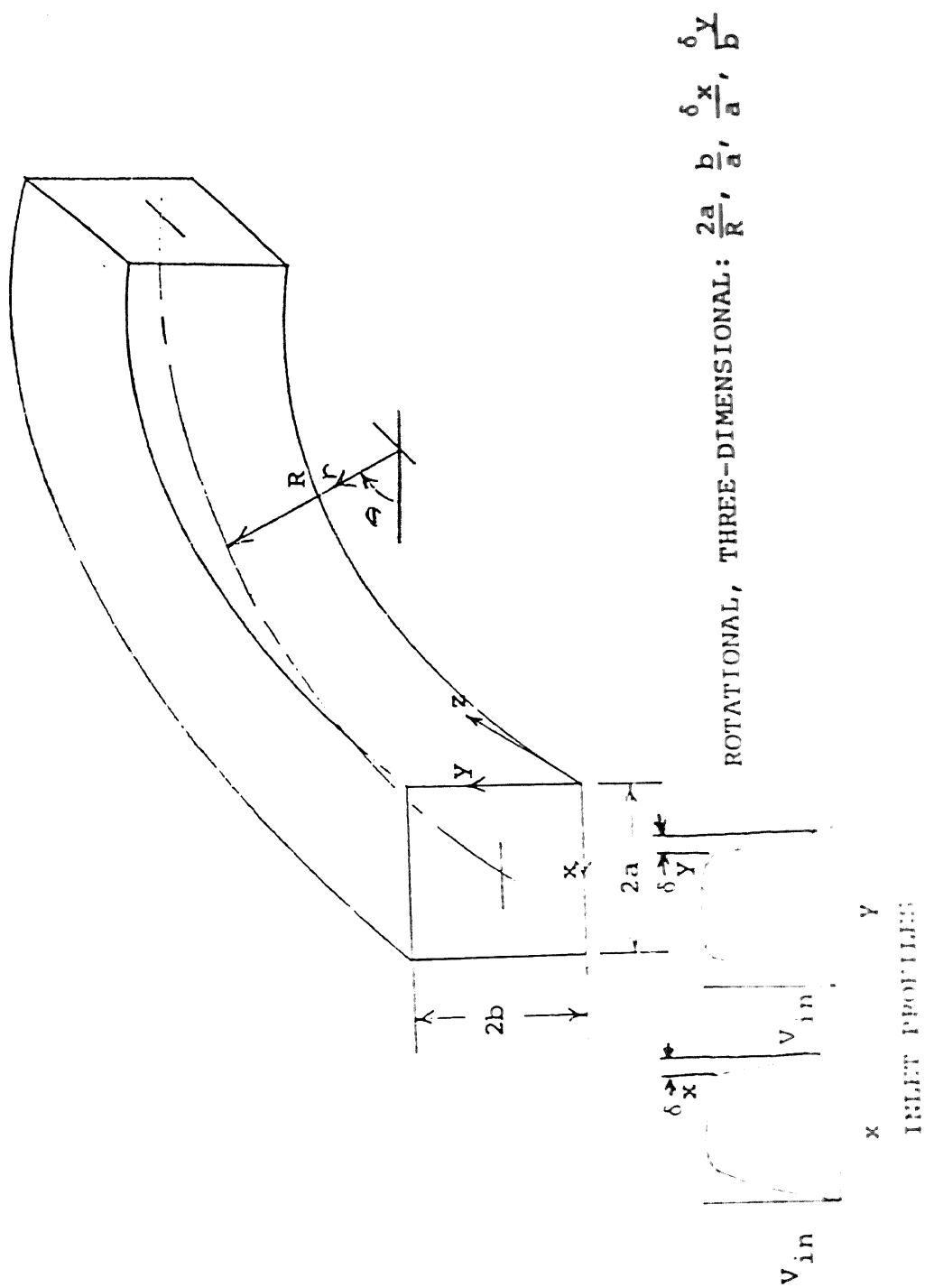


FIGURE 4. Schematic of Stream Surface Iteration



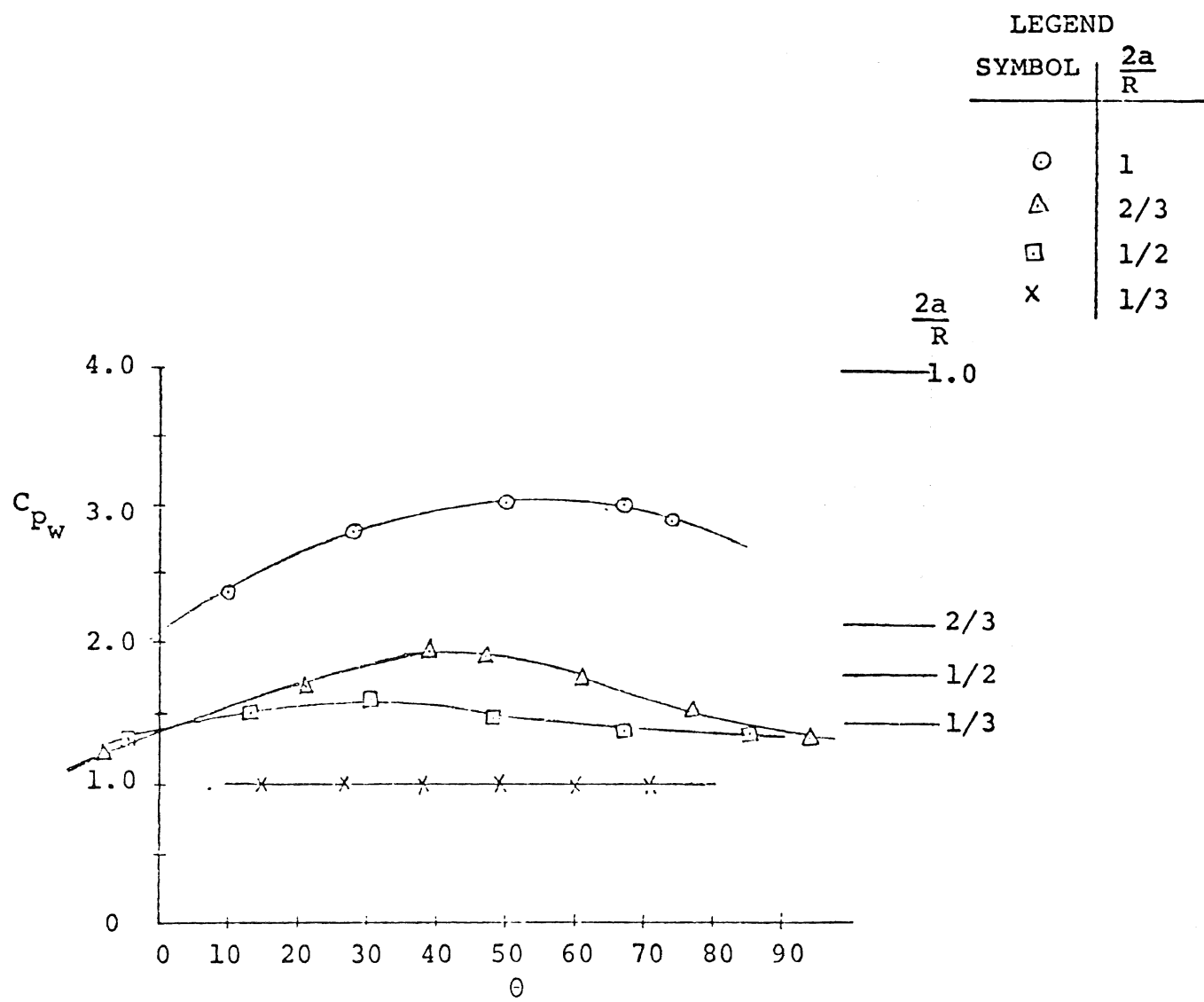


FIGURE 8. Static Pressure Distributions in Smaller Turning Ducts

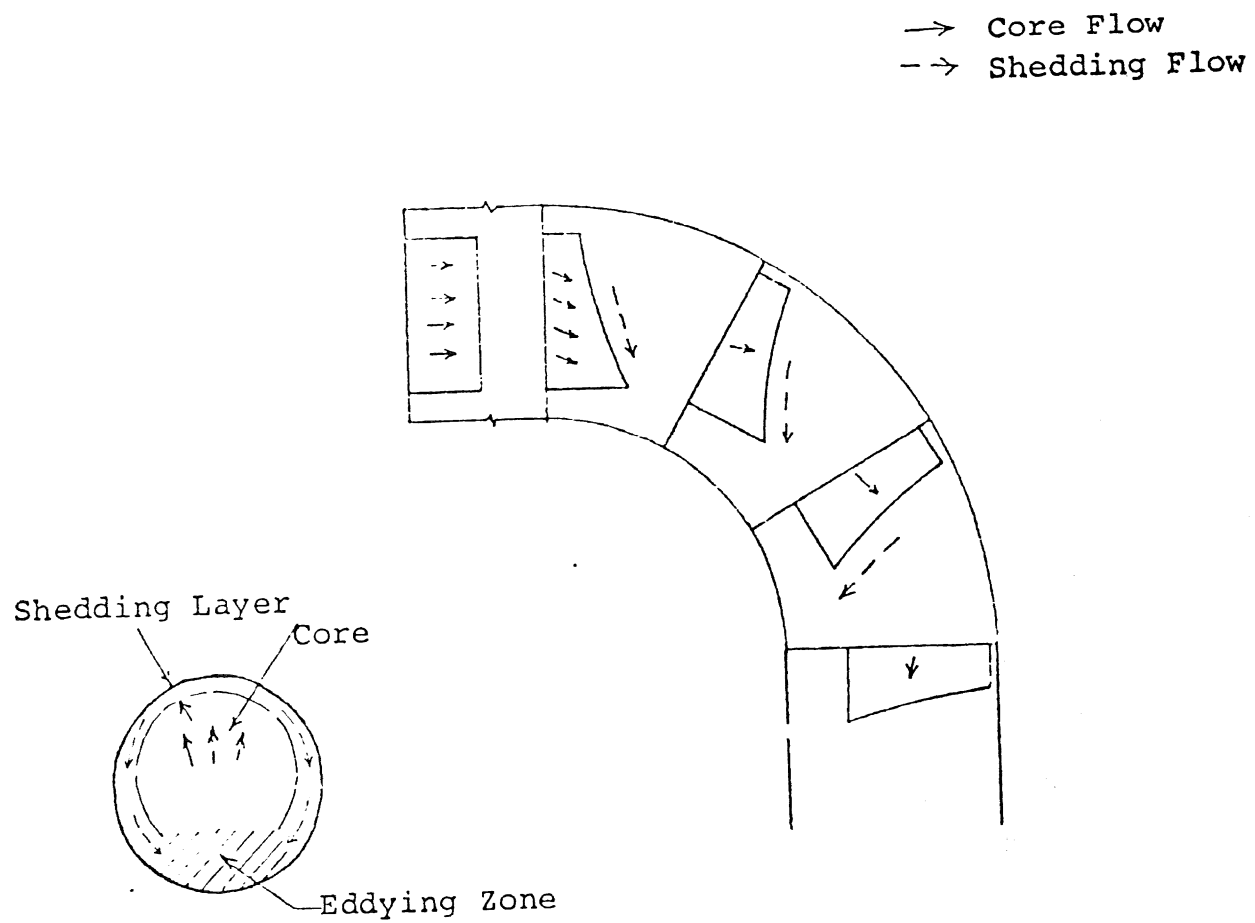


FIGURE 9. Basic Flow Patterns for High Reynolds Number Flow in Turning Ducts

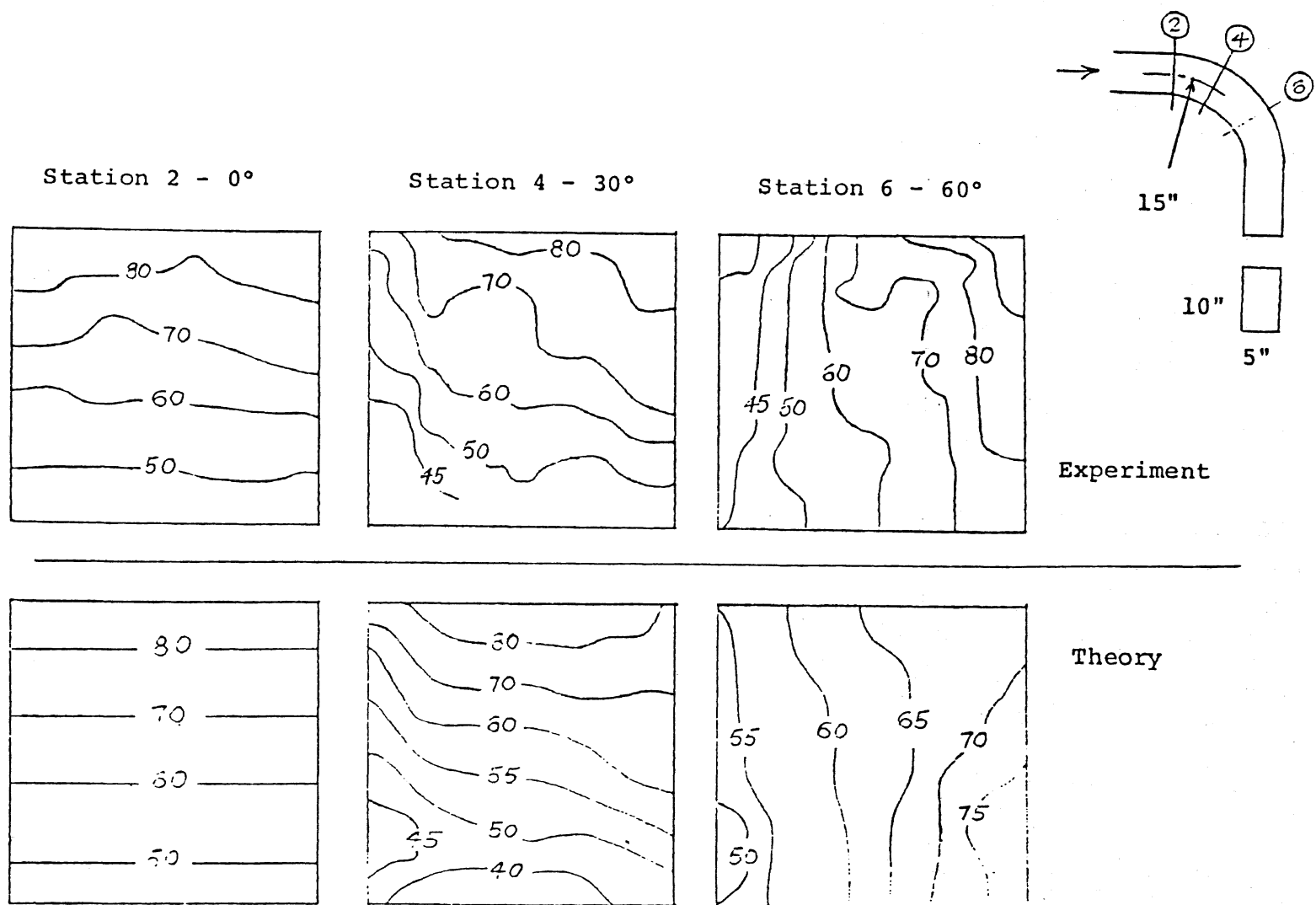


FIGURE 10. The Effects of Large Velocity Distortions in the Inlet of Turning Duct Flow

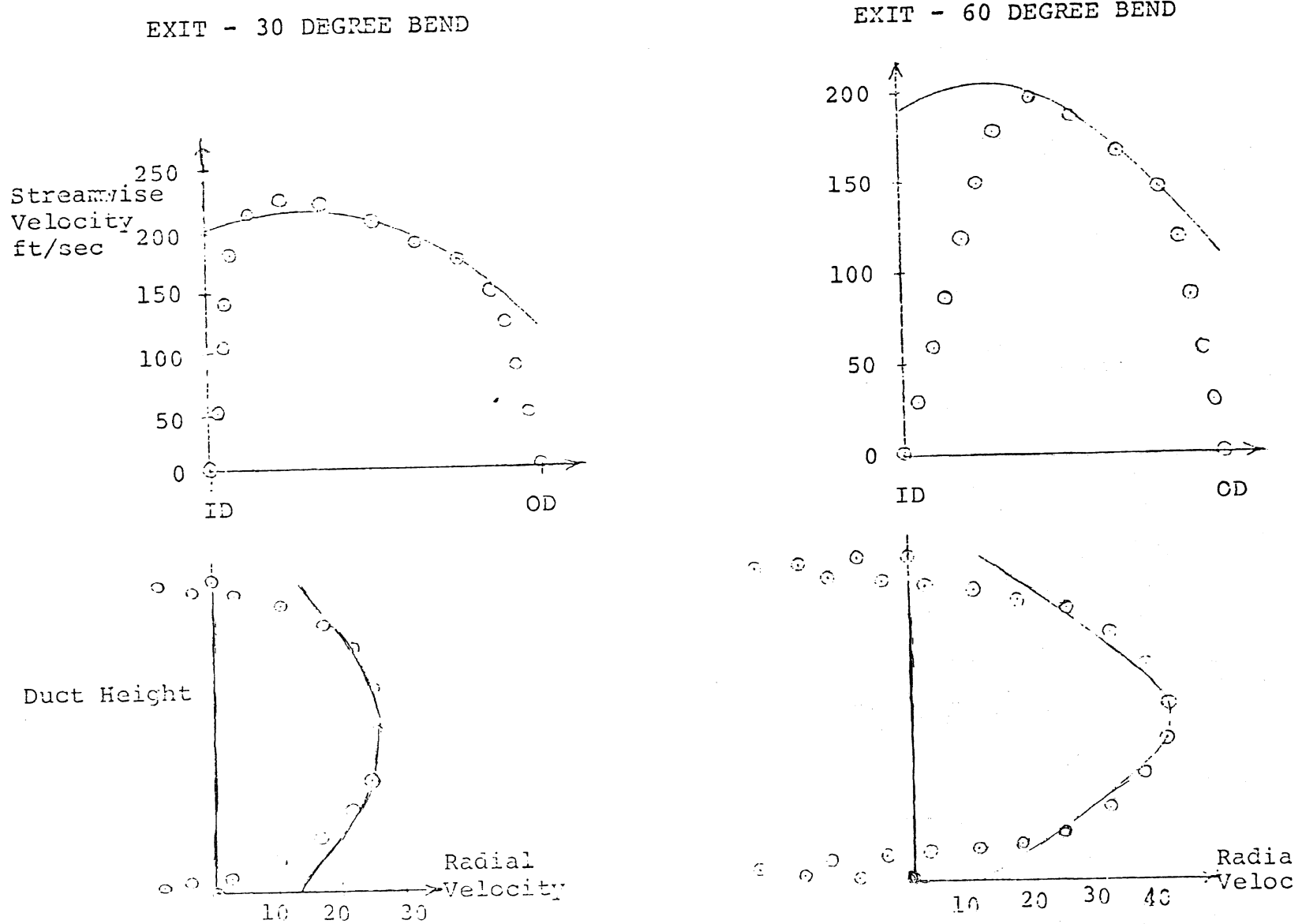


FIGURE 11. Velocity Field at the Exit of Rectangular Turning Ducts

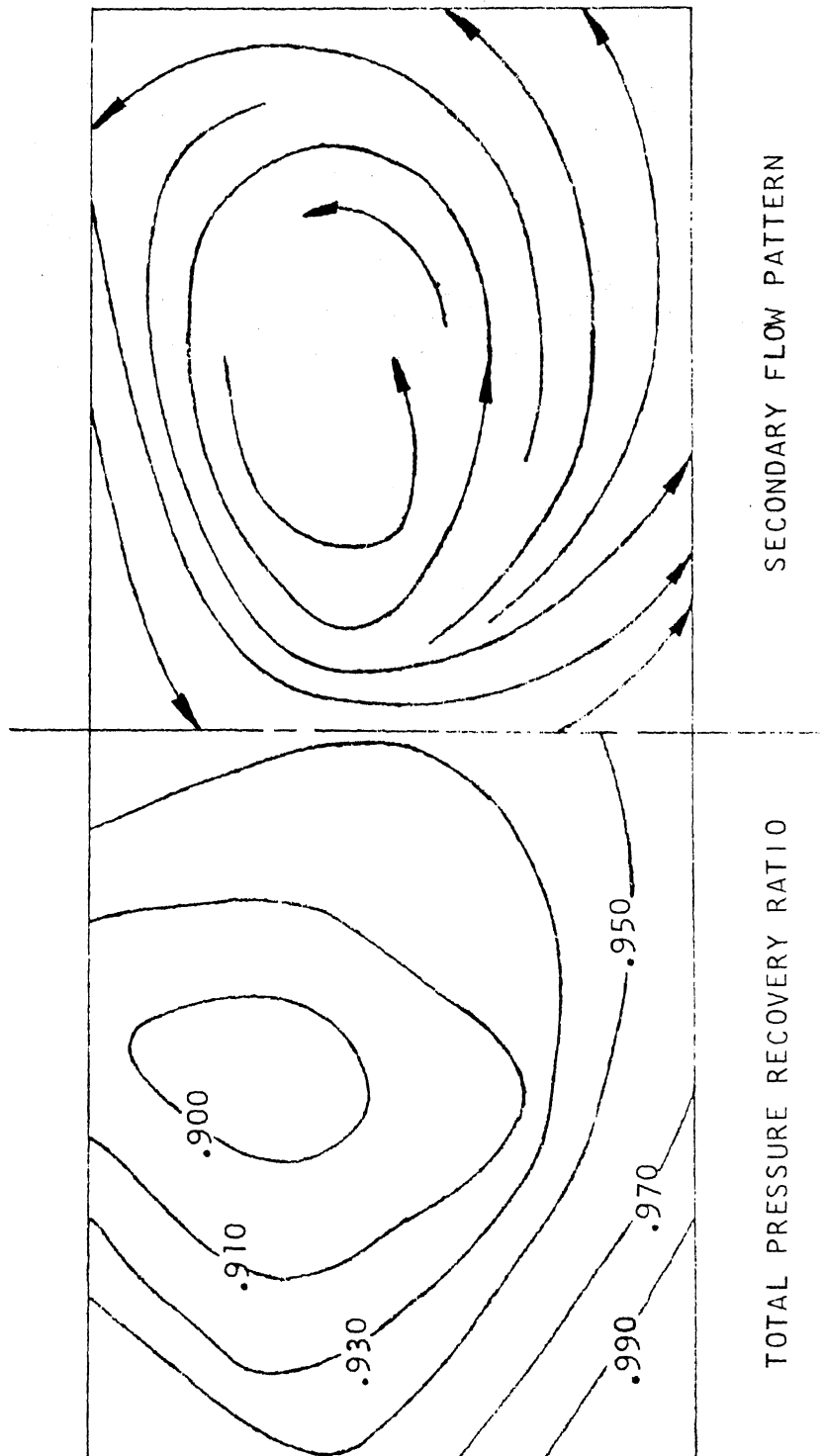


FIGURE 12. Exit Flow Field Measurements in a Turbine Exhaust Collector with 90 Degrees of Turning

ISU-ERI AMES-75085
TCRI-4

DUCT FLOW ANALYSIS METHODS FOR V/STOL PROPULSION SYSTEM APPLICATIONS

Final Report

George K. Serovy and Patrick Kavanagh
Engineering Research Institute
Iowa State University
Ames, Iowa 50010 USA

March 1975

Approved for public release: distribution unlimited

Prepared for
Department of the Navy
Naval Air Systems Command
Code 310
Washington, D.C. 20361 USA

TABLE OF CONTENTS

	<u>Page</u>
Introduction	1
V/STOL Propulsion Systems - Current Technology	3
Definition of the Internal and Mixed Internal/External Flow Problems Associated with V/STOL Propulsion	3
Flow in V/STOL Transfer, Augmentation, and Thrust- Vectoring Systems and Requirements for Design Analysis Methods	6
Present Availability of Design Analysis Methods	7
Propulsion System Component Flow Modeling - Trends and Expected Progress	8
Elements of the Flow Modeling Problem	9
Fluid Dynamic Considerations	9
Mathematical Considerations	10
Geometric Considerations	10
Status of Computational Fluid Dynamics as Related to Internal Flow Problems	11
Recommended Program Extension and Development	16
Requirements for Research in Computational Fluid Mechanics	17
Requirements for Application - Oriented Design Analysis Methods	18
Requirements for Supporting Experimental Data	19
References	20
Figures	26

INTRODUCTION

Attention was directed in this investigation to aerodynamic analysis methods for non-rotating elements of the flow path in air-breathing propulsion systems for V/STOL aircraft. A considerable volume of published information is available on V/STOL lift/thrust-vectoring/propulsion system requirements and on the relative merits of the numerous V/STOL aircraft configuration concepts. While these documents emphasize the critical importance of aircraft/propulsion system integration in development of high-performance V/STOL vehicles, there is limited discussion of the origin of assumed component performance characteristics. This might be acceptable if propulsion component operating environments or the engine configurations themselves were similar to those encountered in conventional aircraft for which long operating experience and a broad data base exists. However, V/STOL operating environments are unique and severe, and proposed propulsion system configuration arrangements invariably include geometric and aerodynamic features of a non-standard character.

Most currently attractive V/STOL lift/thrust-vectoring/propulsion systems include extensive and complex internal flow passages or transfer systems (in addition to those normally found in turbojet and turbofan engines). The nature of these passages or ducts is briefly reviewed in the following section, V/STOL PROPULSION SYSTEMS - CURRENT TECHNOLOGY. This discussion designates the fact and the reason that these passages are important to aircraft system performance. It also explains why analysis of the flow in these passages must often be considered as a combined internal/external flow problem. The section thus establishes

the requirement for effective analysis methods for the subject configurations and also indicates the present basis for development of these passages.

The subsequent section, PROPULSION SYSTEM COMPONENT FLOW MODELING-TRENDS AND EXPECTED PROGRESS, defines the fluid dynamic, mathematical, and geometric elements of the design analysis problem. It also suggests some decision guidelines for near-term use in determination of the feasibility of computational flow field analysis as contrasted with an experimentally-oriented approach.

The final section, RECOMMENDED PROGRAM EXTENSION AND DEVELOPMENT, includes conclusions and recommendations for research in three areas identified as important to the effective development and integration of current and future V/STOL aircraft propulsion systems. These areas cover a broad range of engineering and applied scientific research topics which should directly contribute to improvement of present methods for analysis of internal and mixed internal/external flow passage geometries.

This report was prepared by investigators with prior experience primarily in the field of turbojet and turbofan engine component research and development. The study itself was conducted with substantial and candid cooperation of numerous specialists in propulsion system application and integration as well as many individuals productive in computational fluid mechanics. The authors take responsibility for the accuracy of the content of this report, but at the same time must acknowledge the excellent guidance and data supplied by the government and industry personnel who were visited and consulted.

V/STOL PROPULSION SYSTEMS - CURRENT TECHNOLOGY

Vertical and short takeoff and landing aircraft concepts (with the exception of the helicopter) have been under intensive study for only about fifteen years. Earlier research and prototype development was not commercially or militarily conclusive. Even during the past ten years a substantial amount of the reported work has consisted of paper studies and feasibility analysis not supported by experimental demonstration. In the unclassified literature studied in this investigation, summary papers published by the National Aeronautics and Space Administration, for example, in 1971 [1] and 1972 [2], review activity in the United States, while additional programs have been described in AGARD papers [3] Münzberg [4], and Korbacher [5]. An overview of the VTOL situation by Pavlenko [6] gives a good comparative evaluation of western technology and at the same time gives some idea of Soviet internal programs. Because of the high degree of aircraft propulsion system integration associated with most V/STOL design concepts, it is not easy to produce a list of documents related primarily to V/STOL propulsion, but Pavlenko [6] and Sanders et al. [1] probably represent the best of the reviews available.

Definition of the Internal and Mixed Internal/External Flow Problems Associated with V/STOL Propulsion

The present study is intended to concentrate mainly on V/STOL lift/thrust-vectoring/propulsion systems and more specifically on aerodynamic features of those systems which are substantially different from those of conventional air-breathing propulsion systems. Some

the requirement for effective analysis methods for the subject configurations and also indicates the present basis for development of these passages.

The subsequent section, PROPULSION SYSTEM COMPONENT FLOW MODELING-TRENDS AND EXPECTED PROGRESS, defines the fluid dynamic, mathematical, and geometric elements of the design analysis problem. It also suggests some decision guidelines for near-term use in determination of the feasibility of computational flow field analysis as contrasted with an experimentally-oriented approach.

The final section, RECOMMENDED PROGRAM EXTENSION AND DEVELOPMENT, includes conclusions and recommendations for research in three areas identified as important to the effective development and integration of current and future V/STOL aircraft propulsion systems. These areas cover a broad range of engineering and applied scientific research topics which should directly contribute to improvement of present methods for analysis of internal and mixed internal/external flow passage geometries.

This report was prepared by investigators with prior experience primarily in the field of turbojet and turbofan engine component research and development. The study itself was conducted with substantial and candid cooperation of numerous specialists in propulsion system application and integration as well as many individuals productive in computational fluid mechanics. The authors take responsibility for the accuracy of the content of this report, but at the same time must acknowledge the excellent guidance and data supplied by the government and industry personnel who were visited and consulted.

V/STOL PROPULSION SYSTEMS - CURRENT TECHNOLOGY

Vertical and short takeoff and landing aircraft concepts (with the exception of the helicopter) have been under intensive study for only about fifteen years. Earlier research and prototype development was not commercially or militarily conclusive. Even during the past ten years a substantial amount of the reported work has consisted of paper studies and feasibility analysis not supported by experimental demonstration. In the unclassified literature studied in this investigation, summary papers published by the National Aeronautics and Space Administration, for example, in 1971 [1] and 1972 [2], review activity in the United States, while additional programs have been described in AGARD papers [3], Münzberg [4], and Korbacher [5]. An overview of the VTOL situation by Pavlenko [6] gives a good comparative evaluation of western technology and at the same time gives some idea of Soviet internal programs. Because of the high degree of aircraft propulsion system integration associated with most V/STOL design concepts, it is not easy to produce a list of documents related primarily to V/STOL propulsion, but Pavlenko [6] and Sanders et al. [1] probably represent the best of the reviews available.

Definition of the Internal and Mixed Internal/External Flow Problems Associated with V/STOL Propulsion

The present study is intended to concentrate mainly on V/STOL lift/thrust-vectoring/propulsion systems and more specifically on aerodynamic features of those systems which are substantially different from those of conventional air-breathing propulsion systems. Some

elements of the proposed V/STOL propulsion arrangements call for and have resulted in initiation of new research efforts. Other elements call for but do not appear to have resulted in new research.

The propulsion engines used in current V/STOL aircraft concepts almost invariably have at least two of the following three functions. They may be used to generate the conventional forward or reverse thrust component, to provide some or all of the vertical or lift force component, or develop a force component needed for aircraft control or stability. While nearly all installations have two of these functions, some involve all three. The aircraft concepts considered in this study to be V/STOL systems all fall in the class which some observers have called "powered lift" concepts, in which the fluid momentum developed by one or more of the engines is used as a means for producing the lift force needed for V/STOL performance. The dual- or triple-function character of V/STOL propulsion engines leads directly to added overall lift/thrust-vectoring/propulsion system complexity. This complexity is often evidenced by the presence of additions and extensions to the conventional engine flow path in the form of ducts or energy transfer systems. These additions and extensions carry a significant fraction of the total propulsion system gas flow, and their performance has an important influence on propulsion system and aircraft performance.

In this subsection a few arbitrarily selected examples are used to demonstrate or define what is meant by the terms internal and mixed internal/external flow problems as used in this study and to suggest some boundaries on the geometric and flow variables contained within these problems.

The AV-8A and AV-16 class attack aircraft use a single turbofan engine to develop powered lift VTOL capability, forward/reverse thrust and control/stabilization force vectors. In order to realize all of these functions the various engine models used in this aircraft family have involved a number of flow path variations as described by Küng [7]. In the present investigation the flows in these variations are classed as mixed internal/external flows because the passage flow boundary conditions are determined in part by the flow external to the aircraft.

In the augmentor-wing powered-lift research aircraft evaluated by NASA and de Havilland Aircraft of Canada [8,9,10], as well as the XFV-12A ejector thrust-augmenter fighter [11] now under development for the Naval Air Systems Command, the augmentation systems again represent mixed internal/external flow field problems, but in the NASA-de Havilland aircraft extensive crossover and bypass transfer systems may be considered as purely internal flow problems. Figures 1 and 2 show the general layout of the augmentor-wing engine and flow transfer system, as well as a schematic drawing of the wing and ejector for the NASA-de Havilland aircraft. Figures 3 and 4 give an excellent idea of the internal complexity of the transfer system of the XFV-12A aircraft and suggest the comprehensive quantitative estimates of losses which are needed in development of a flight prototype.

Remote lift fan V/STOL configurations, for example those studied by Eldridge et al. [12], Knight et al. [13], and Cavage et al. [14,15], generally have included extremely complicated internal flow transfer ducts as well as internal/external flow geometries associated with the

gas generator engines. Thrust-vectoring nozzles for the gas generators have been generally included as a major element of these aircraft concepts.

Flow in V/STOL Transfer, Augmentation, and Thrust-Vectoring
Systems and Requirements for Design Analysis Methods

The transfer duct, augmentation, and thrust-vectoring arrangements proposed for V/STOL propulsion systems will be critical to successful aircraft performance. They will be significant in terms of weight and occupied fuselage and wing volume. These facts have been recognized by most system designers and analysts who have reported on their work. Ducts, inlets, ejectors, and nozzles will also be important in terms of irreversibilities in the flow process and lost thrust. While neither problem appears in any sense to be insurmountable, it will be essential that careful and comprehensive preliminary optimization studies be made.

It is indicated that the internal flows will be compressible and turbulent, typically in the lower subsonic regime with Mach numbers under 0.5. The transfer system ducts will include asymmetric cross-section transitions, short-radius bends, offset bends, side holes, branches, and other interesting geometric variations. Initiation of transfer system flows is shown in proposed arrangements to occur in non-symmetric collectors located in the vicinity of fan, compressor, and turbine exit planes. Termination occurs in similarly non-standard flow distribution passages, including wide-angle diffusers, slots, vanes, and nozzles. In these seemingly unavoidable geometric variations,

there obviously appear the most difficult elements of the transfer system flow field analysis problem.

Where internally blown flaps, augmentor-wing or ejector-thrust augmentor systems are used, turbulent mixing occurs in a combined internal/external flow environment. Optimization of geometry for these components has been highly empirical up to the present.

Present Availability of Design Analysis Methods

For many years fluid system designers in aeronautical and aerospace applications have followed two parallel paths in internal flow passage design. With the exception of some axisymmetric and other geometrically two-dimensional inlet, diffuser, and nozzle flow paths and of the flow passages immediately adjacent to and internal to the components of turbomachinery (compressors, turbines, pumps), almost universal reliance has been placed on one-dimensional flow pattern analysis guided and supported by semi-empirical corrections and adjustments. These corrections and adjustments have been collected, correlated, organized, and systematized by numerous sources, for example Turner and Yoos [16], Kelnhofer and Smith [17], North American Rockwell [18], Miller [19], and Ward-Smith [20]. The enormous variety of geometries encountered in internal flow passages and the important influence of boundary conditions make general correlation impossible. As a result, justification exists for experimental evaluation as a concurrent feature of flow passage design. Experimental evaluation has taken many forms, including simulation using analog (water tables, conductive field platters) and scale models as well as full-scale prototype studies.

PROPULSION SYSTEM COMPONENT FLOW MODELING - TRENDS AND EXPECTED PROGRESS

The overall problem of propulsion system component aerodynamic performance estimation for aircraft has received a significant amount of attention during the past 25 to 30 years. Progress has been made, and major advances in component technology have resulted. The advances have frequently been associated with development of realistic computational flow models combined with increased capability in using the models rapidly and economically after they have been developed.

However, in computational flow field modeling, research is still a vital requirement. Much progress has been concentrated in computation of design point flow fields and in selection of a good geometric component configuration for design operating conditions, but numerous unresolved problems remain. This is very evident in compressor and turbine flow computation. Computational studies have failed to predict or identify numerous off-design aerodynamic performance problems. General computational flow modeling methods used for design and performance estimation have been singularly unsuccessful in this regard, and most of the useful analyses of special performance problems such as compressor surge, rotating stall, and inlet distortion effects have been based on restricted models. Very few of these have genuinely contributed to current design methods. Similar conclusions may be reached and justified in the case of non-rotating components (inlets, combustors, nozzles, ejectors).

Even without the imminent and general trend toward more complex aircraft propulsion cycles, compounded by the special requirements outlined above for V/STOL lift/thrust-vectoring systems, applied research

on component computational flow modeling, backed by more fundamental supporting work in applied mathematics and fluid mechanics would be called for. In view of the trends, an expanded effort is required.

Elements of the Flow Modeling Problem

In two Interim Reports submitted in connection with the current program [21,22], the internal or mixed internal/external flows in inlets, transfer systems, nozzles, and ejectors of V/STOL aircraft concepts were described, and bibliographic material was assembled to amplify these descriptions. In this Final Report similar consideration is divided into fluid dynamic, mathematical, and geometric aspects of the problem.

Fluid Dynamic Considerations

In examining the nature of the flow field problems under study, it might seem repetitious to again call attention to the fact that they are all partially internal flow problems. However, this is not trivial because the internal flow computational problem presents unique and demanding features rarely accommodated by and often completely outside the range of capability of external flow computation systems. The problem flows are compressible but do not often involve regions of transonic and supersonic flow. The flows are turbulent, and, although steady-flow operation is of interest and probably initially of overriding importance, it would be most useful to be able to evaluate the effects of flow disturbances on the flow field and system performance.

Zones of separated flow seem unavoidable in inlet, transfer system, nozzle, and ejector configurations. Because flow separation zones and their boundaries are basically unstable and unsteady in character, this characteristic of the expected flow field is of unusual concern.

Along with the phenomenological nature of the flow the aerodynamic requirements of the problem need to be understood. First in importance is the capability to predict total pressure loss and overall system irreversibility for the complete operating flow range required. To isolate the important sources of irreversibility a loss component breakdown of the overall performance should be available. Second, as an aid to optimization, internal flow field descriptions should be as complete as possible.

Mathematical Considerations

The overall internal flow field problem outlined above is mathematically overwhelming. The components and systems are physically large and interconnected. For these subsonic but compressible flows, flow field computation calls for boundary value specification. This is another non-trivial observation, made because of the numerous unsatisfactory and meaningless results generated in solution of problems where the boundary conditions were oversimplified in order to realize any results at all.

Geometric Considerations

Highly interactive with mathematical and fluid dynamic aspects of the transfer system problem are the geometric elements. The specific geometries which have to be considered in eventual solution of real

problems are complex to an almost unbelievable degree. As mentioned above, asymmetric cross sections, cross-section transitions, short-radius bends, offset bends, side holes, and branches are the rule, not the exception. Manifolds are common, and surface discontinuities appear in many proposed layouts.

It is in this area of geometry that a side-by-side comparison of existing flow computation work and proposed aircraft concept hardware shows the greatest divergence between capability and reality.

Status of Computational Fluid Dynamics as Related to Internal Flow Problems

In an Interim Report [21], emphasis was placed on a general review and comparison of the approach to design/analysis in turbomachinery as a field related to the problem at hand of duct flow analysis involving detailed computational fluid dynamical analysis. It was observed in that review that analysis systems for turbomachinery and the associated annulus flows have been partially empirical due to the complicated geometrical features of the problem and to the practicalities of incorporating necessary real fluid effects. Recent developments have brought the high-speed computer into the picture, particularly in the last ten years; however, empirical input to analysis and design systems for turbomachinery has remained an essential factor.

Turbomachinery flows involve configurations which are, for the most part, geometrically axisymmetric. Although flow models of past years have often assumed axisymmetric flow for computational convenience [23-28], the real flows are not axisymmetric [29], and approaches

to the resulting three-dimensional flow are in progress [30,31] although few results are available. The requirement for empirical input appears to remain in these advanced studies, and it continues to exist in the form of means for accounting for the effects of interacting blade and wall geometries on flow direction and the generation of losses.

Recently complex problems in a wider range of internal fluid dynamics have been studied using large, high-speed computers employing numerical techniques to solve the governing equations. As is the case with turbomachine flows, the solution of any of these flow problems must satisfy the continuity, momentum, and energy equations. Since these equations are highly nonlinear, there is no general method of solution for arbitrary initial and boundary conditions, and exact or so-called classical solutions exist only in special, simplified cases. In general, approximate methods of solution must be resorted to, and the computer is used to exercise the approximating difference equations in repetitive and iterative fashion to converged and, hopefully, accurate solutions. Although in a few specific cases the equations of fluid dynamics have been solved in closed or at least approximate form with results that are valuable in understanding flow phenomena, the vast majority of fluid dynamic problems must be approached in approximate fashion. Solutions must be obtained by alternate and adaptive means, employing high-speed computers for numerical solution of the fluid dynamic equations. The two factors, of course, which have fostered such development have been the development of computers themselves and the development of modeling and mathematical techniques that transform the basic differential equations into suitable form for nu-

merical analysis. The attendant and vital concerns of numerical stability and accuracy of solutions have grown along with the applications of computational fluid dynamics. That is, approximate equations run the danger of numerical instabilities that obscure the accuracy and may also fail to realistically exhibit instabilities inherent in the flow itself.

Two major differences between the more general computational fluid mechanics work and the restricted computation of turbomachinery flow stand out. The more general efforts reduce the empirical input required to a significant extent. The most interesting of these require little more than a "turbulence model," that is, a semi-empirical or empirical basis for computation of turbulent shear stresses. This is a distinct advantage. The second difference lies in the geometrical complexity of the test cases and of the apparent potential for handling complex geometries. The most attractive current programs deal with example geometries that, while challenging, are not in any degree as complex as a typical compressor or turbine. In this sense, the geometry of a V/STOL transfer system and/or augmentation configuration appears to be closer to a turbomachine in complexity than to the relatively simple curved ducts and flow passages used as computational examples in the general solutions. To utilize the presently competitive general computational flow models for more complicated passage shapes would add enormously to the computational costs as well as to the demands upon the flow model itself.

During the past several years a series of publications have appeared which do a genuinely good job of summarizing progress in compu-

tational fluid mechanics. These include a book by Roache [32] and papers or monographs by Harlow [33], Orszag and Israeli [34], Launder and Spalding [35], Smolderen [36], Butler [37], and Krause [38]. The approach to turbulence modeling has been discussed critically by Bradshaw [39], Launder and Spalding [40,41], and Huffman et al. [42].

The computational problem for turbulent internal flow has received more limited attention than might be expected. Some good examples from which conclusions may be reached about present capabilities are found in the reports of Anderson [43,44], Briley [45], McDonald and Briley [46,47], Launder and Ying [48], and Patankar et al. [49].

In the case of external flow computation, geometries of considerable complexity have been used as test cases for both inviscid and viscous flow fields. Generally, however, the boundary layer computation has been a special subelement of the field determination process. Some of the useful documentation in this area appears in work by Hess and Smith [50], Hess [51,52,53], and Beatty [54].

Turbulent boundary layer work is of interest because of the turbulence modeling approaches used. Blottner [55], Mellor and Herring [56,57], Albers and Gregg [58], McDonald and Kreskovsky [59], and Caretto et al. [60] have worked on important elements of this portion of the overall problem.

A possible set of conclusions from examination of the present status of computational activity in fluid flow is as follows:

1. The programs which determine inviscid flow fields for internal flow have been applied to a limited number of flow path geometries. Results may have value in establishing first

trial initial conditions for a complete flow field analysis.

For most internal flows of interest in V/STOL applications, iterative solutions involving separate boundary layer and core flow computations appear to have little or no potential.

2. Complete flow field models have produced inconclusive results up to the present, but the outlook for the future is encouraging in modeling turbulent flows in internal flow passages of relatively simple geometry.
3. Computational flow modeling of complex geometries, mixed internal/external flows and general unsteady flows is not likely to be achieved in a matter of a few years.

RECOMMENDED PROGRAM EXTENSION AND DEVELOPMENT

In review of the current status of V/STOL lift/thrust-vectoring/propulsion system technology, it is apparent that although a large number of the obvious internal and external aerodynamic problems have received preliminary study, an equally large number of problem areas have received little or no attention. In studies of V/STOL aircraft concepts, such problems are often unintentionally hidden within the complexities of the overall study. In the subject matter field of this report, duct flow analysis methods, there is clear evidence that the degree of success achieved by most V/STOL aircraft schemes, if not the question of success versus failure, will be strongly influenced by optimization of duct systems on the basis of both aerodynamic performance and weight. Yet in many design concept studies, the duct systems are shown only as lines on a schematic diagram, with little or no discussion of the engineering techniques used to account for these ducts in the overall aircraft system performance estimates.

On this basis recommendations for program extension and development in three areas are outlined in the following subsections. The three areas cover a broad range of engineering activity. As a result, it is an essential first requirement that communication be established and maintained between the individuals and organizations working on the most fundamental and most applied aspects of the problem as well as those who occupy the middle ground.

Requirements for Research in Computational Fluid Mechanics

Activity in the field of computational fluid mechanics has increased substantially throughout the world in recent years. Many programs identified as falling under this "umbrella" title are relatively new and show evidence that the investigators are not yet clear about their objectives. At the same time these programs frequently have considerable potential for contributing to mixed internal/external flow passage analysis in the intermediate- to long-term future. At present it is the conclusion of the authors that no research program in computational fluid mechanics should be viewed as an effort with the potential for application to general V/STOL system design during the next one- to five-year period.

A current research requirement exists for computational fluid mechanics studies which are clearly unrestricted in terms of possible future application to internal flow problems or to mixed internal/external flow problems. Flow models must be such that there is no characteristic introduced which would rule out internal flow cases. Although for external aerodynamics, inviscid flow analyses can be of some value, there are few instances in internal flow where a purely inviscid flow field model is useful. In fact, the current review demonstrates that the incorporation of effective accounting for viscous effects, emphasizing improved turbulence modeling should be considered as one of the more important problem areas.

Another subelement of the computational problem which requires careful evaluation is the development and utilization of numerical methods for flow field solutions. At present, serious questions may

be raised about the demonstrated capabilities in this area both as to quality of solution and cost of solution for meaningful problems.

Application of interactive computer graphic techniques in all phases of flow modeling should be carefully monitored.

Requirements for Application-Oriented Design Analysis Methods

There is an immediate requirement for improvements in design analysis methods for internal and mixed internal/external flows, with these improvements based on existing calculation systems and improved data correlations. There is a strong probability that V/STOL system concepts are not being comparatively evaluated on a consistent basis. Even in cases (and there are many such cases) where one-dimensional design analysis methods for duct flow and external flow are used, there seem to be differences of opinion and procedure.

As observed in the preceding subsection, genuinely general three-dimensional computational approaches to the problem of turbulent internal flow can at best be expected to lie somewhere in the intermediate (not immediate) future. However, some of the current research in computation of internal flows is genuine, if not general. Specifically, some of the research groups and individuals have a clear understanding of the problems which need to be solved. Some do not. An effort should be made to clarify the objectives of the application-oriented programs.

Requirements for Supporting Experimental Data

Experimentally oriented programs on thrust augmentation systems and related configurations have been reported from several sources [61-67]. Fundamental flow field measurements from similar projects will be needed to confirm computed performance estimates and to aid in optimization.

NASA integral and remote lift fan experimental work has been well coordinated with analysis [68-78]. The work should be continued.

Computational studies of internal flow should be coordinated with measurement of flow field characteristics in geometries that are systematically selected to challenge but not overwhelm the capabilities of the computation system. There is not a great deal of reliable data available for this purpose at present.

REFERENCES

1. Sanders, Newell D., et al. V/STOL Propulsion. In Aircraft Propulsion. NASA SP-259. 1971.
2. Denington, Robert J., et al. STOL Propulsion Systems. In STOL Technology. NASA SP-320. 1972. pp. 475-509.
3. Advisory Group for Aerospace Research and Development. V/STOL Propulsion Systems. AGARD Conference Proceedings 135. January 1974.
4. Münzberg, H. G. Flugantriebe. Berlin. Springer-Verlag. 1972.
5. Korbacher, G. K. Aerodynamics of Powered High-Lift Systems. Ann. Rev. Fluid Mech. 6: 319-358.
6. Pavlenko, V. F. The Power Plants of Vertical Takeoff and Landing Aircraft. Foreign Technology Division, Air Force Systems Command, WPAFB, Ohio. FTD-MT-24-715-73. 21 March 1974.
7. Küng, Paul. Rolls-Royce Pegasus. Entwicklung, Einsatzerfahrungen und Zukunftsaussichten. Flug Revue and Flugwelt International. No. 9, pp. 39-44. 1974.
8. Whittle, D. C. The Augmentor-Wing Research Program: Past, Present and Future. Can. Aeronaut. Space J. 45-56. 1968.
9. Whittle, D. C. Ejector-Powered Lift Systems for V/STOL Aircraft. Can. Aeronaut. Space J. 20:5:179-189. 1974.
10. Quigley, Herver C. and Vomaske, Richard F. Preliminary Results of Flight Tests of the Augmentor-Wing Jet STOL Research Aircraft. In STOL Technology. NASA SP-320. 1972. pp. 259-282.
11. Thronson, Lester W. Compound Ejector Thrust Augmenter Development. ASME Paper 73-GT-67. 1973.
12. Eldridge, W. M., Ferrell, J. A., McKee, J. W., Wayne, J. F., Jr. and Zabinsky, J. M. Conceptual Design Studies of Candidate V/STOL Lift Fan Commercial Short Haul Transport for 1980-85 V/STOL Lift Fan Study. NASA CR-2183. February 1973.
13. Knight, Ronald G., Powell, William V., Jr. and Prizlow, Jerome A. Conceptual Design Study of a V/STOL Lift Fan Commercial Short Haul Transport. NASA CR-2185. 1973.
14. Cavage, R. L. Lift-Fan Characteristics Selection for 1980-85 V/STOL Carrier Onboard Delivery Aircraft. ASME Paper 75-GT-98. 1975.

15. Cavage, Robert L., et al. Conceptual Design Study of Improved 1985 Remote Lift-Fan V/STOL Commercial Transports. NASA CR-2481. January 1975.
16. Turner, J. R. and Yoos, T. R. Pressure Loss Calculation Procedures for High Speed Gas Flow in Ducts. Report No. 261. Contract NObs-84282. June 20, 1961. Dynatech Corporation. Cambridge, Mass. (AD-707416).
17. Kelnhofer, William J., and Smith, Russell A. Testing of Gas Turbine High Velocity Duct Systems. Scientific Report (Final for period 1 September 1964 through 31 August 1966). Contract NObs 92176. The Catholic University of America. Washington, D. C. 31 August 1966. (AD640070).
18. North American Rockwell Corp., Columbus Div., Columbus, Ohio.
 Internal Aerodynamic Manual
 Volume I (AD723823) NR68H-434-Vol-1
 Volume II (AD723824) NR68H-434-Vol-2
 Appendix (AD723841) NR68H-434-App
 Contract NOW-66-0460. June 1970.
19. Miller, D. Internal Flow--A Guide to Losses in Pipe and Duct Systems. Cranfield. British Hydromechanics Research Association. Cranfield (Bedford), England. November 1971.
20. Ward-Smith, A. J. Pressure Losses in Ducted Flows. Butterworths Scientific Publication. London. 1971.
21. Serovy, George K., and Kavanagh, Patrick. Duct Flow Analysis Methods for V/STOL Propulsion System Applications, Interim Report for the period 1 April-30 June 1974. Engineering Research Institute, Iowa State University. ISU-ERI-Ames-74167, TCRL-2. August 1974.
22. Serovy, George K., and Kavanagh, Patrick. Duct Flow Analysis Methods for V/STOL Propulsion System Applications, Interim Report for the period 1 July-30 September 1974. Engineering Research Institute, Iowa State University. ISU-ERI-Ames-74253, TCRL-3. December 1974.
23. Novak, R. A. Streamline Curvature Computing Procedures for Fluid Flow Problems. Trans. ASME, Series A, 89:478-490. 1967.
24. Katsanis, T. Use of Arbitrary Quasi-Orthogonals for Calculating Flow Distribution in the Meridional Plane of a Turbomachine. NASA TN D-2546. 1964.
25. Frost, D. H. A Streamline Curvature Through-Flow Computer Program for Analyzing the Flow Through Axial-Flow Turbomachines. British Aero. Res. Council R & M No. 3687. 1970.

26. Wilkinson, D. H. Stability, Convergence and Accuracy of Two-Dimensional Streamline Curvature Methods Using Quasi-Orthogonals. Proc., Inst. Mech. Eng. 184 (Pt. 3G):108-119. 1970.
27. Marsh, H. A Digital Computer Program for the Through-Flow Fluid Mechanics in an Arbitrary Turbomachine Using a Matrix Method. British Aero. Res. Council R & M 3509. 1968.
28. Smith, L. H. The Radial Equilibrium Equation of Turbomachinery. ASME Paper 65-WA/GTP-1. 1965.
29. Wu, C. H. A General Through Flow Theory of Fluid Flow with Subsonic or Supersonic Velocity in Turbomachines of Arbitrary Hub and Casing Shapes. NACA TN 2302. 1951.
30. Smith, D. J. L. Computer Solutions of Wu's Equations for the Compressible Flow Through Turbomachines. International Symposium on the Fluid Mechanics and Design of Turbomachinery, Pennsylvania State University, University Park, Penn. 1970.
31. Katsanis, T. and W. D. McNally. Fortran Program for Calculating Velocities and Streamlines on the Hub-Shroud Mid-Channel Flow Surface of an Axial- or Mixed-Flow Turbomachine, I—User's Manual. NASA TN D-7343. 1973.
32. Roache, Patrick J. Computational Fluid Dynamics. Albuquerque, N. M. Hermosa Publishers. 1972.
33. Harlow, Francis H., ed. Computer Fluid Dynamics—Recent Advances. AIAA Selected Reprint Series. Volume XV. 1973.
34. Orszag, Steven A., and Israeli, Moshe. Numerical Simulation of Viscous Incompressible Flows. Ann. Rev. Fluid Mech. 6:281-318. 1974.
35. Launder, B. E., and Spalding, D. B. The Numerical Computation of Turbulent Flows. Comput. Methods Appl. Mech. Eng. 3:269-289. 1974.
36. Smolderen, J. J., editor. Numerical Methods in Fluid Dynamics. AGARD Lecture Series No. 48. May 1972.
37. Butler, T. D. Recent Advances in Computational Fluid Dynamics. LA-UR-73-1473. 1973.
38. Krause, Egon. Application of Numerical Techniques in Fluid Mechanics. Aeronaut. J. 78:337-354. 1974.
39. Bradshaw, P. The Understanding and Prediction of Turbulent Flow. Aeronaut. F. 76:403-418. 1972.

40. Launder, B. E., and Spalding, D. B. Turbulence Models and Their Application to the Prediction of Internal Flows. Heat and Fluid Flow. 2:43-54. 1972.
41. Launder, B. E., and Spalding, D. B. Lectures in Mathematical Models of Turbulence. London. Academic Press. 1972.
42. Huffman, G. D., Jones, C. D., and Brodkey, R. S. Optimization of Turbulence Models by Means of a Logical Search Algorithm. Appl. Sci. Res. 27:321-334. 1973.
43. Anderson, Olof L. A Comparison of Theory and Experiment for In-Compressible, Turbulent, Swirling Flows in Axisymmetric Ducts. AIAA Paper No. 72-43. 1972.
44. Anderson, O. L. Finite-Difference Solution for Turbulent Swirling Compressible Flow in Axisymmetric Ducts with Struts. NASA CR-2365. February 1974.
45. Briley, W. R. Numerical Method for Predicting Three-Dimensional Steady Viscous Flow in Ducts. J. Comput. Phys. 14:1. 1974.
46. McDonald, H., and Briley, W. R. Three-Dimensional Supersonic Flow of a Viscous or Inviscid Gas. UARL Report N111078-1. November 1974.
47. Briley, W. R., and McDonald, H. Computation of Three-Dimensional Turbulent Subsonic Flow in Curved Passages. United Aircraft Research Laboratories. Report R75-911596-8. March 1975.
48. Launder, B. E., and Ying, W. M. Prediction of Flow and Heat Transfer in Ducts of Square Cross-Section. Heat and Fluid Flow. 3:115-121. 1973.
49. Patankar, S. V., Prata, V. S. and Spalding, D. B. Prediction of Turbulent Flow in Curved Pipes. J. Fluid Mech. 67:583-595. 1975.
50. Hess, J. L., and Smith, A. M. O. Calculation of Potential Flow About Arbitrary Bodies. In Progress in Aeronautical Science, Volume 8. Oxford, Pergamon Press. 1967, pp. 1-138.
51. Hess, John L. The Problem of Three-Dimensional Lifting Potential Flow and Its Solution by Means of Surface Singularity Distribution. Comput. Methods Appl. Mech. Eng. 4:283-319. 1974.
52. Hess, John L. The Use of Higher-Order Surface Singularity Distributions to Obtain Improved Potential Flow Solutions for Two-Dimensional Lifting Airfoils. Comput. Methods Appl. Mech. Eng. 5:11-36. 1975.
53. Hess, John L. Review of Integral-Equation Techniques for Solving Potential-Flow Problems with Emphasis on the Surface-Source Method. Comput. Methods Appl. Mech. Eng. 5:145-196. 1975.

54. Beatty, T. D. A Theoretical Method for the Analysis and Design of Axisymmetric Bodies. NASA CR-2498. March 1975.
55. Blottner, F. G. Nonuniform Grid Method for Turbulent Boundary Layers. Sandia Laboratories. SAND-74-5023. 1974.
56. Mellor, George L. The Large Reynolds Number, Asymptotic Theory of Turbulent Boundary Layers. Int. J. Eng. Sci. 10:851-873. 1972.
57. Mellor, George L., and Herring, H. James. A Survey of the Mean Turbulent Field Closure Models. AIAA Journal. 11:590-599. 1973.
58. Albers, James A., and Gregg, John L. Computer Program for Calculating Laminar, Transitional, and Turbulent Boundary Layers for a Compressible Axisymmetric Flow. NASA TN D-7521. 1974.
59. McDonald, Henry, and Kreskovsky, John P. Effect of Free Stream Turbulence on the Turbulent Boundary Layer. Int. J. Heat Mass Transfer. 17:705-716. 1974.
60. Caretto, L. S., Curr, R. M., and Spalding, D. B. Two Numerical Methods for Three-Dimensional Boundary Layers. Comput. Methods Appl. Mech. Eng. 1:39-57. 1972.
61. Quinn, B. Compact Thrust Augmentors for V/STOL Aircraft. In V/STOL Propulsion Systems. AGARD Conference Proceedings 135. January 1974. pp. 19.1-19.11.
62. Quinn, Brian P. Compact Ejector Thrust Augmentation. Journal of Aircraft. 10:8:481-486. August 1973.
63. Bevilacqua, Paul M. Evaluation of Hypermixing for Thrust Augmenting Ejectors. J. Aircraft. 11:6:348-354. June 1974.
64. Gill, J. C. Advanced Technology Thrust Vectoring Exhaust Systems. J. Aircraft. 11:764-770. 1974.
65. Campbell, D. R., and Quinn, B. Test Results of a VTOL Propulsion Concept Utilizing a Turbofan Powered Augmentor. J. Aircraft. 11:467-471. 1974.
66. Hedges, K. R., and Hill, P. G. Compressible Flow Ejectors. Part I—Development of a Finite-Difference Flow Model. J. Fluids Eng. Trans. ASME, Series I., 96:272-281. 1974.
67. Hedges, K. R., and Hill, P. G. Compressible Flow Ejectors. Part II—Flow Field Measurements and Analysis. J. Fluids Eng. Trans. ASME, Series I., 96:282-288. 1974.
68. Stockman, N. O. Potential Flow Solutions for Inlets of VTOL Lift Fans and Engines. In Analytic Methods in Aircraft Aerodynamics. NASA SP-228. 1970. pp. 659-681.

69. Lieblein, S. Problem Areas for Lift Fan Propulsion for Civil VTOL Transports. NASA TM-52907. 1970.
70. Lieblein, S. A Review of Lift Fan Propulsion Systems for Civil VTOL Transports. AIAA Paper 70-670. June 1970. Also NASA TM X-52829. 1970.
71. Lieblein, S., Yuska, J. A., and Diedrich, J. H. Wind Tunnel Tests of a Wing-Installed Model VTOL Lift Fan with Coaxial Drive Turbine. NASA TM X-67854. 1971.
72. Haller, Henry C., Lieblein, Seymour, and Auer, Bruce M. Computer Program for Preliminary Design and Analysis of V/STOL Tip-Turbine Fans. NASA TN D-6161. February 1971.
73. Yuska, Joseph A., and Diedrich, James H. Fan and Wing Force Data from Wind-Tunnel Investigation of a 0.38-Meter (15-In.) Diameter VTOL Model Lift Fan Installed in a Two-Dimensional Wing. NASA TN D-6654. 1972.
74. Sagerser, David A., Lieblein, Seymour, and Krebs, Richard P. Empirical Expressions for Estimating Length and Weight of Axial-Flow Components of VTOL Powerplants. NASA TM X-2406. 1971.
75. Diedrich, J. H., Clough, N., and Lieblein, S. Installation Effects on Performance of Multiple Model V/STOL Lift Fans. J. Aircraft. 10:355-360. 1973.
76. Stockman, N. O., Loeffler, I. J., and Lieblein, S. Effect of Rotor Design Tip Speed on Aerodynamic Performance of a Model VTOL Fan Under Static and Crossflow Conditions. J. Eng. Power. Trans. ASME, Series A, 95:293-300. 1973 (October).
77. Albers, James A., and Felderman, E. John. Boundary-Layer Analysis of Subsonic Inlet Diffuser Geometries for Engine Nacelles. NASA TN D-7520. 1974.
78. Albers, J. A., and Stockman, N. O. Calculation Procedures for Potential and Viscous Flow Solutions for Engine Inlets. J. Eng. Power. Trans. ASME, Series A, 97:1-10. 1975.

ENGINE FOR AUGMENTOR WING AIRPLANE FROM SANDERS ET AL. (1971)

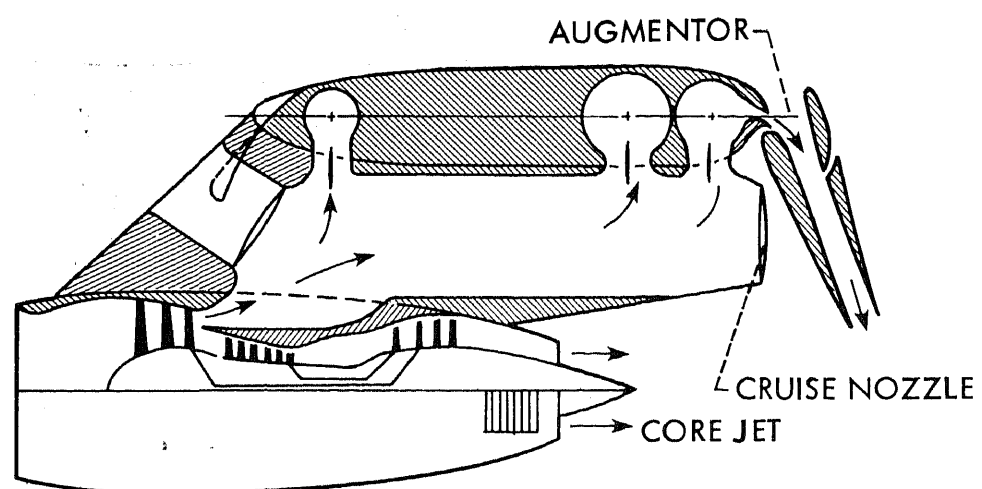


Figure 1(a). Typical augmentor wing aircraft turbopfan installation.

AUGMENTOR WING ENGINE INSTALLATION
FROM QUIGLEY AND VOMASKE (1972)

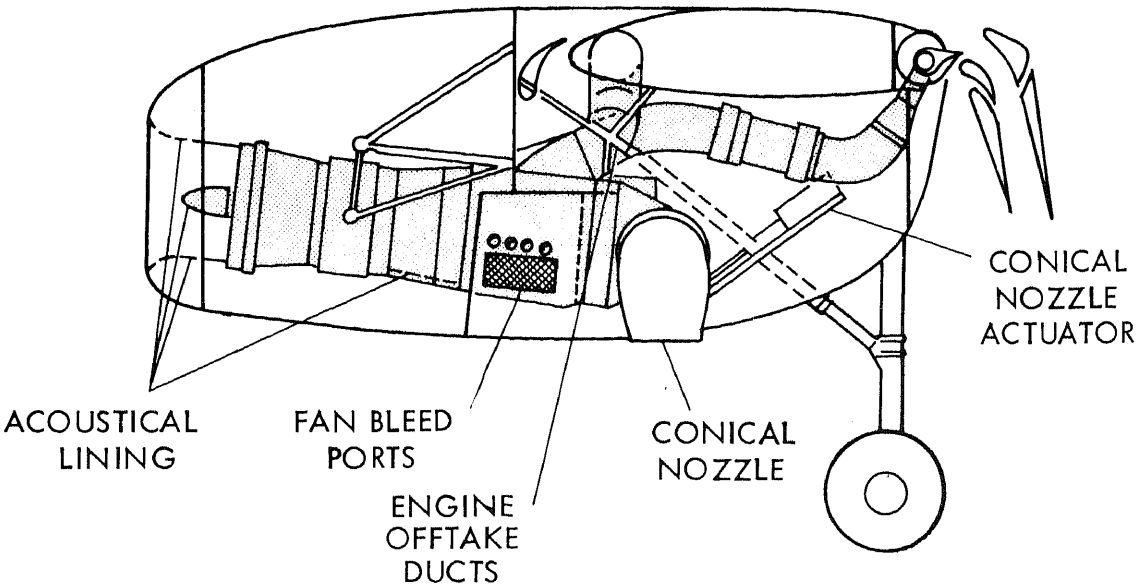


Figure 1(b). Typical augmentor wing aircraft turbofan installations.

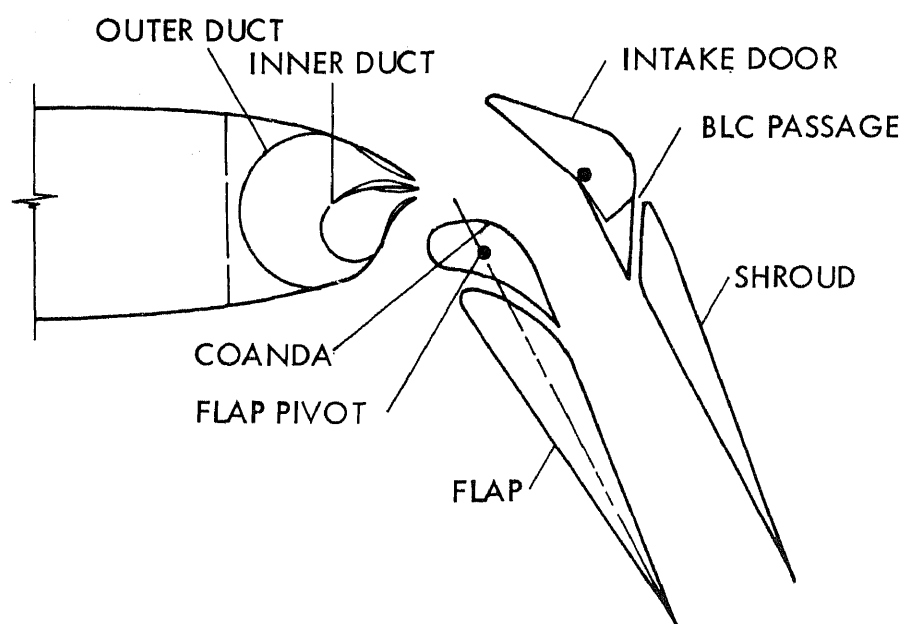


Figure 2. Details of an augmentor-wing flap geometry from Quigley and Vomaske (1972).

Engine Airflow

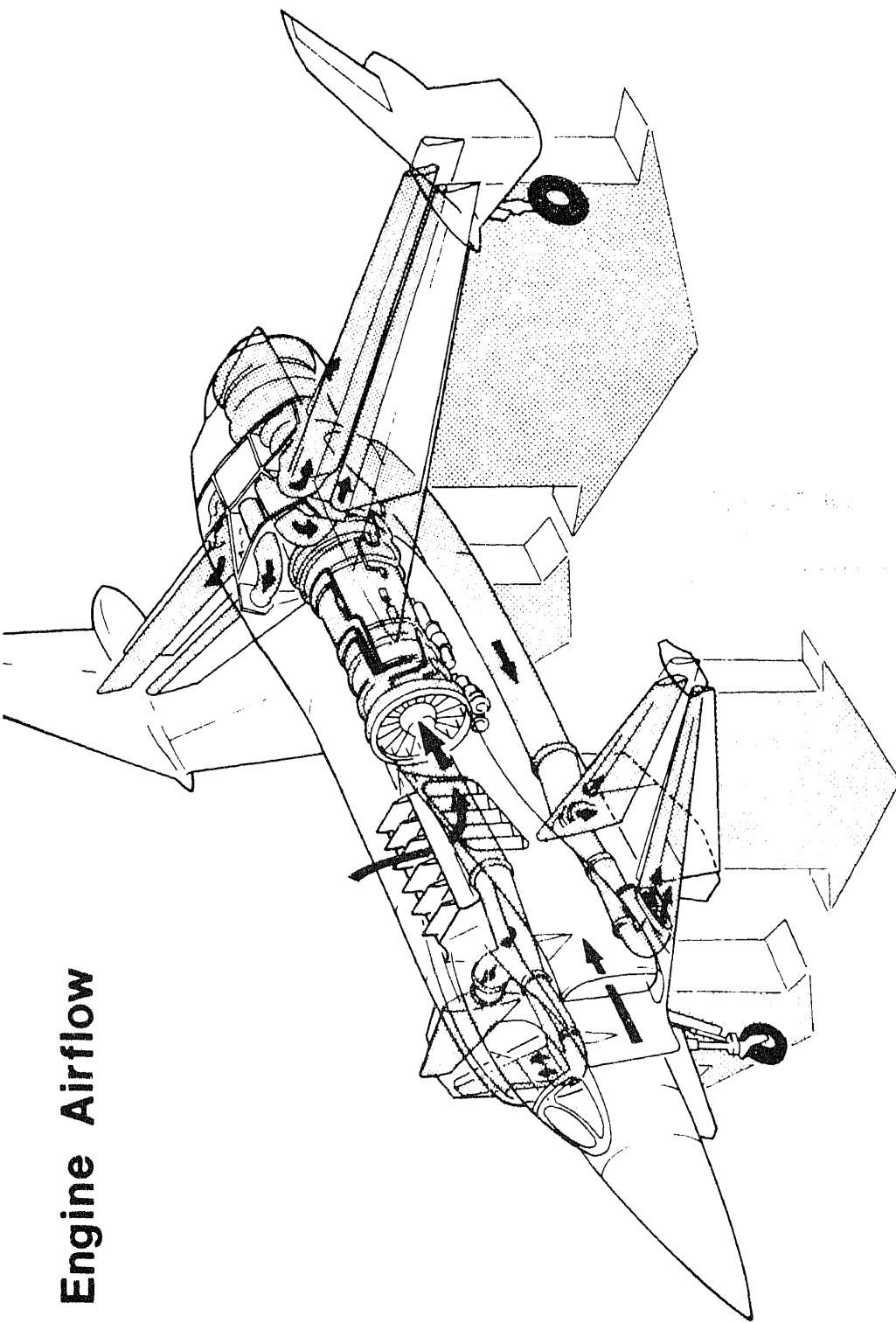


Figure 3. Schematic layout of engine installation, transfer system ducts and ejector thrust augmentation configuration for XFV-12A aircraft (courtesy of Columbus Aircraft Division, Rockwell International Corporation).

EFFICIENT DUCTING TO AUGMENTERS

BASED ON F-401 DATA

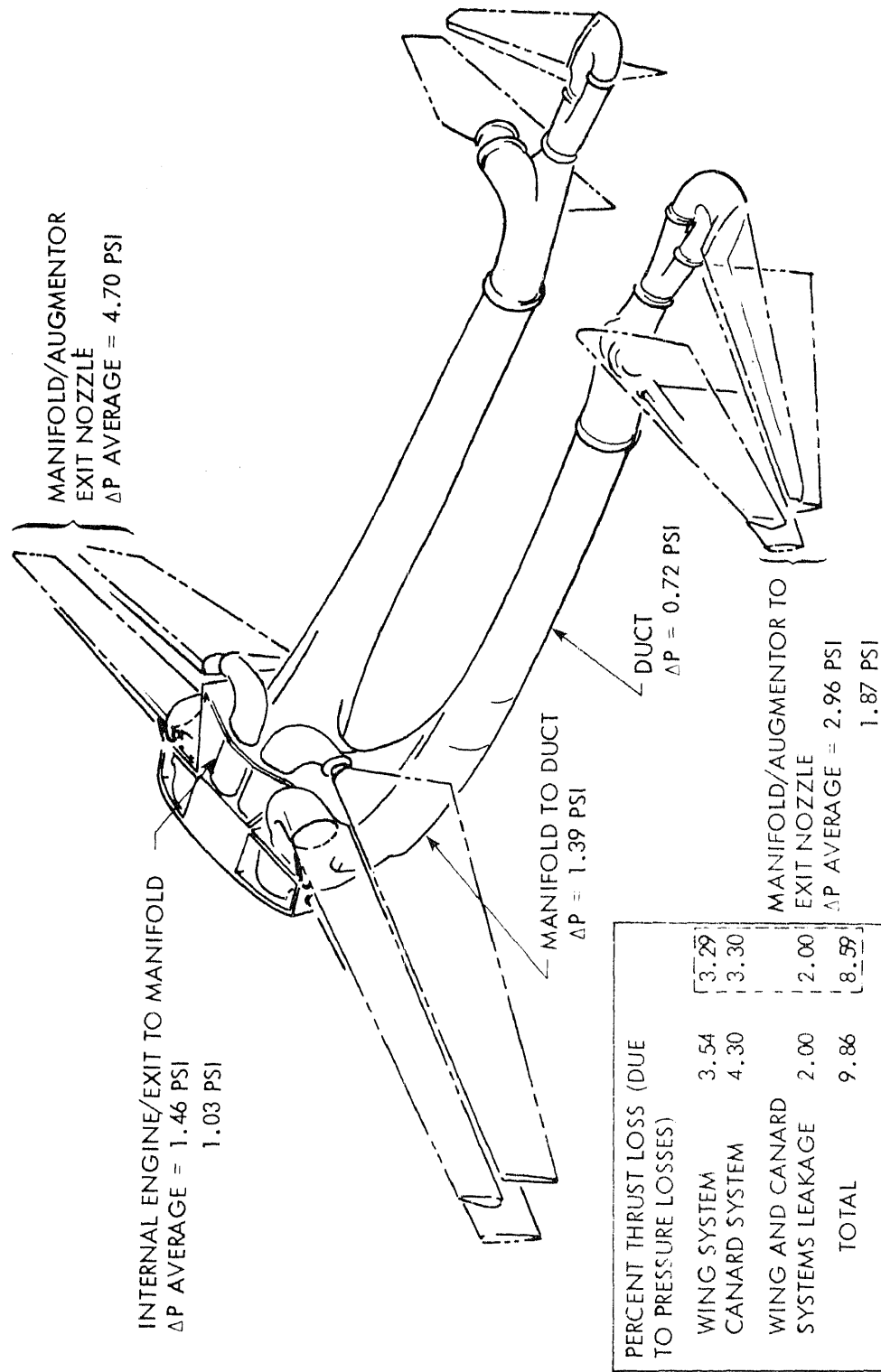


Figure 4. General arrangement of transfer system ducts showing estimated average losses (courtesy of Collumbus Aircraft Division, Rockwell International Corporation).

Session C

GROUND EFFECTS AND INDUCED LOADS

Chairman: D. Migdal, Grumman Aerospace Corporation

DESIGN & DEVELOPMENT OF A HOVER RIG FOR MODEL TESTS

Fred Wohllebe
Grumman Aerospace Corporation
Bethpage, New York 11714

ABSTRACT

A multi-jet hover test rig has been developed at Grumman to aid in evaluating new V/STOL configurations and to provide experimental support in developing theoretical prediction techniques. The rig is based on an air supply ordinarily used to power high-speed wind tunnels. Models of 1/8-scale V/STOL aircraft can be tested at nozzle pressure ratios in excess of 3.0. Results of tests using this facility have shown good agreement with large-test-section wind tunnel tests. The rig is easily adaptable to tests using hot gas with simulated inlet suction and forward speed.

INTRODUCTION

When a multi-jet V/STOL aircraft, such as that shown in Fig. 1, hovers close to the ground, significant aerodynamic forces are induced on the aircraft. These induced forces are caused by the entrainment of surrounding air by the free jets and spreading wall jet. The airflow caused by entrainment creates negative pressures on adjacent surfaces, which are usually the undersides of the aircraft.

Additionally, for multi-jet aircraft hovering close to the ground, a fountain can form between adjacent jets (Fig. 1). The fountain impinges on the underside of the aircraft and some of the fountain momentum is transferred to the aircraft. The combination of fountain force upward and entrainment induced force or "suckdown" determines the net force on the aircraft.

The aircraft designer must know during the design stage what the in-ground effect characteristics of his aircraft are going to be. He can be faced with a multitude of configuration variables yielding widely different results. Figure 2, for example, shows the variations of the induced-lift parameter ($\Delta L/T$) as a function of height above ground (h/b) obtained on different configurations.

Reliable theoretical prediction techniques are not yet available when more than two jets are involved and when configuration refinements such as strakes, nozzle aspect ratio, and nozzle toe-out angle are involved. For this reason and to better support internal methodology development efforts, Grumman undertook the development of a hover test rig. The test rig permits the experimental evaluation of advanced V/STOL configurations and provides important test results to assist in developing new analysis tools.

FACILITY DEVELOPMENT

Initially, consideration was given to using the Grumman 7 x 10 wind tunnel for hover testing. However, the model would have to be quite small to avoid interference from the tunnel walls. After a brief review, this approach was ruled out.

A 1/8-scale V/STOL model was tentatively selected and a required mass flow of 11.5 lb/sec was established to obtain critical nozzle flow in a typical V/STOL model having convergent nozzles. For economy and expediency, the development

tape before being printed and plotted. A real-time display allows the system operator to establish and monitor key parameters during a run.

Figure 8 is an overhead view of the test installation showing a test plenum and the 16- x 16-ft platform.

Figure 9 is a closeup view of the plenum showing the installation of a 16-tube total-pressure rake mounted on a front nozzle. This is part of a nozzle calibration procedure where an upstream pressure-drop plate is adjusted until desired exit total pressure conditions are obtained. Each nozzle is precalibrated in place on the plenum, and its thrust is related to a measured plenum total pressure. In this way known nozzle exit conditions can be re-established during a test run by setting the appropriate plenum conditions.

A final check on the distribution of flow between nozzles is made with a ground-plane oil-streak pattern. Such a pattern is shown in Fig. 10 for a cluster of four equal thrust nozzles. The symmetry of the pattern indicates proper operation of the nozzle group.

A complete V/STOL test model is shown in Fig. 11. This is Grumman Design 607A, a lift-lift/cruise configuration. This model features adjustable control surfaces, removable lifting surfaces, and nozzles that can be swiveled fore and aft and toed outward. The load points shown in the illustration are hard points on the model shell where weights are suspended to check the calibration of the strain-gage balance and to verify internal clearance between the model shell and plenum. Also shown in Fig. 11 is a total-pressure rake used to measure jet-decay properties.

TEST RESULTS

Typical jet-decay and jet-spreading characteristics of two adjacent free jets are shown in Fig. 12. Similarly, wall-jet total-pressure profiles were obtained (Fig. 13). These free-jet and wall-jet results have been used in Grumman's methodology programs to establish analytical models of the jet flow field.

Force and moment results from the hover test rig have shown good agreement with large-test-section wind tunnel tests. Figure 14 compares tests on two identical models of Design 607A. The wind tunnel tests were conducted for Grumman by the British Aircraft Corporation in their 5.5-meter wind tunnel.

Figure 15 illustrates the effect of pressure ratio on jet-induced lift. Here, the higher pressure ratio tests exhibit less suckdown than the low pressure ratio tests. A similar result has also been obtained by others.

An example of the effect of small configuration changes is shown in Fig. 16. Here, a mere 5-deg increase in nozzle toe-out angle produced a 2% reduction in suckdown close to the deck. This reflects itself as a 7% increase in mission fuel for a V/STOL aircraft having about 32,500 lb of takeoff thrust. The increase in suckdown of 1% at h/b greater than 0.4 is an acceptable penalty.

TEST RIG IMPROVEMENTS

Now under study is a plan to extend the capability of the test rig to include hot exhausts and cold inlet suction. Figure 3 shows the proximity of the pebble-bed

heater, which represents a controlled high-pressure hot-air source. Similarly, the nearby vacuum line could be tapped to provide inlet suction. The test site is nearly completely enclosed on three sides. For hot-gas reingestion tests, it would be necessary to complete the enclosure so that the disturbance-sensitive inlet temperature rise measurements could be made.

Also under study is the design of a low-velocity rectilinear airflow system using air from a nearby wind tunnel exhaust pipe. The proposed concepts are illustrated in Fig. 17. All the elements for a greatly improved test capability are available. It is now just a matter of putting them together.

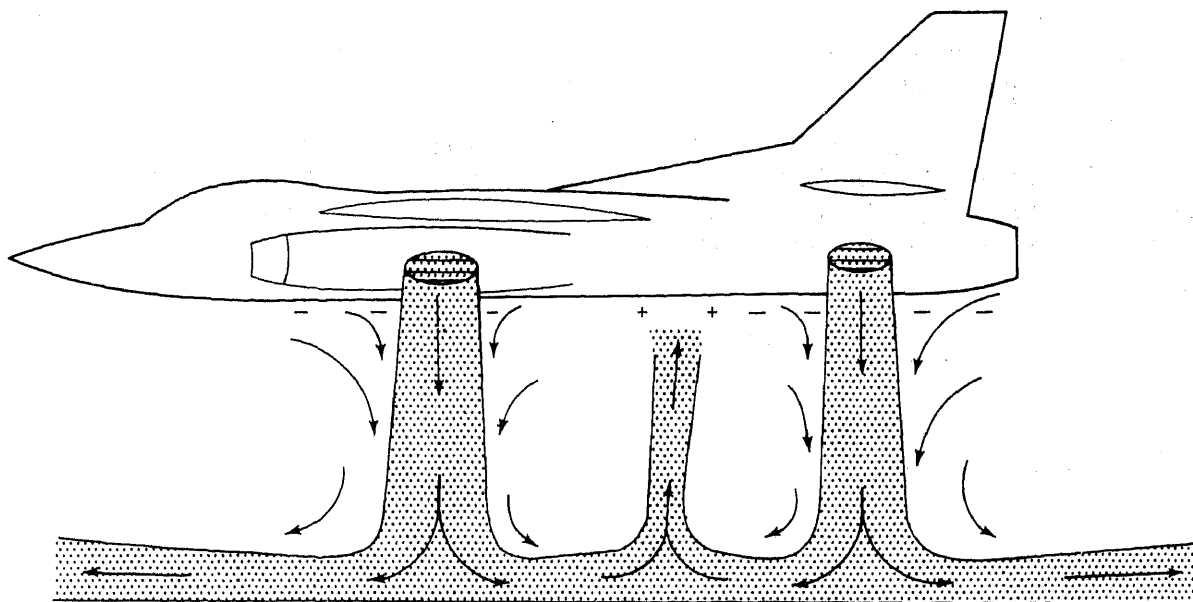


Fig. 1 Jet-Induced Effects

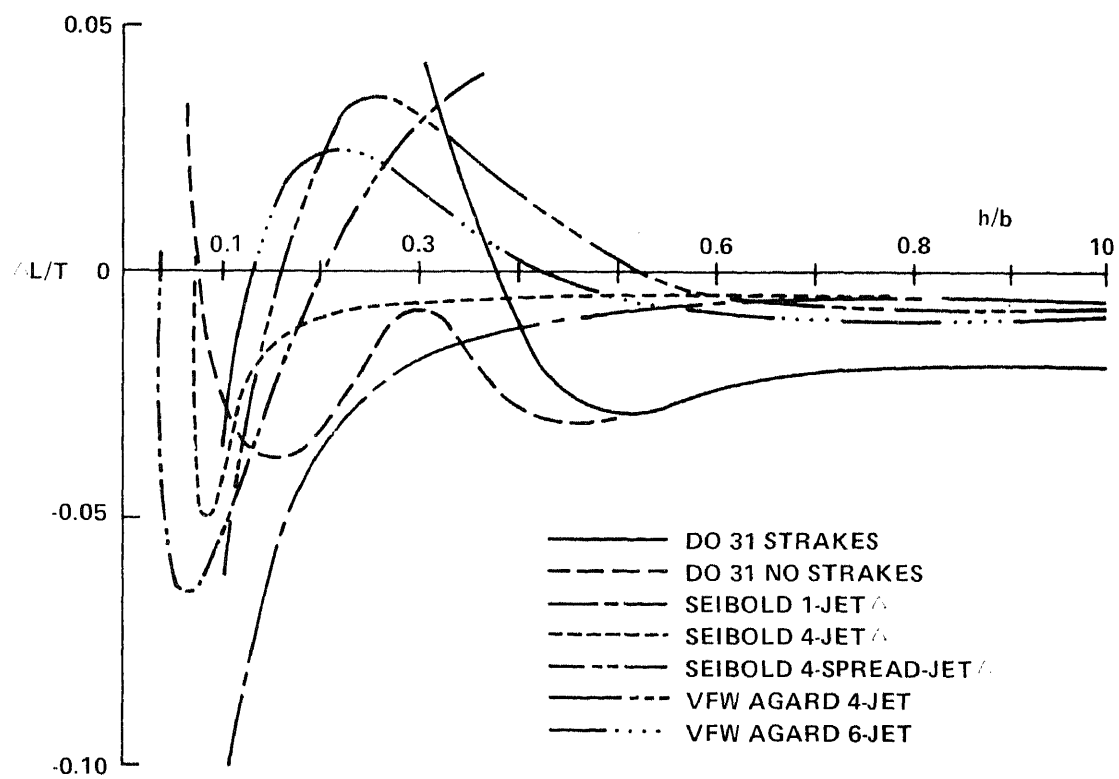


Fig. 2 Jet-Induced Lift In Ground Effect

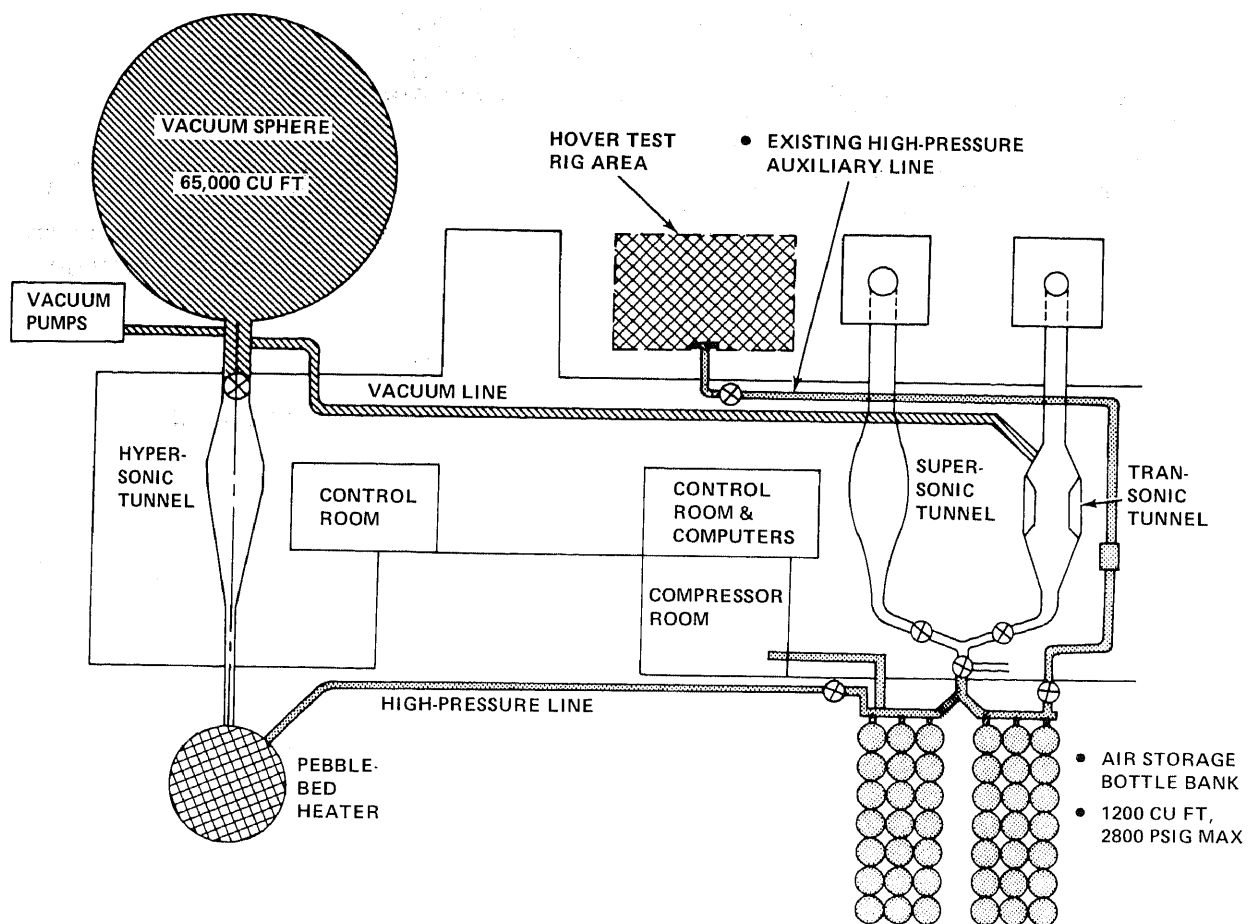


Fig. 3 Grumman High-Speed Wind Tunnels

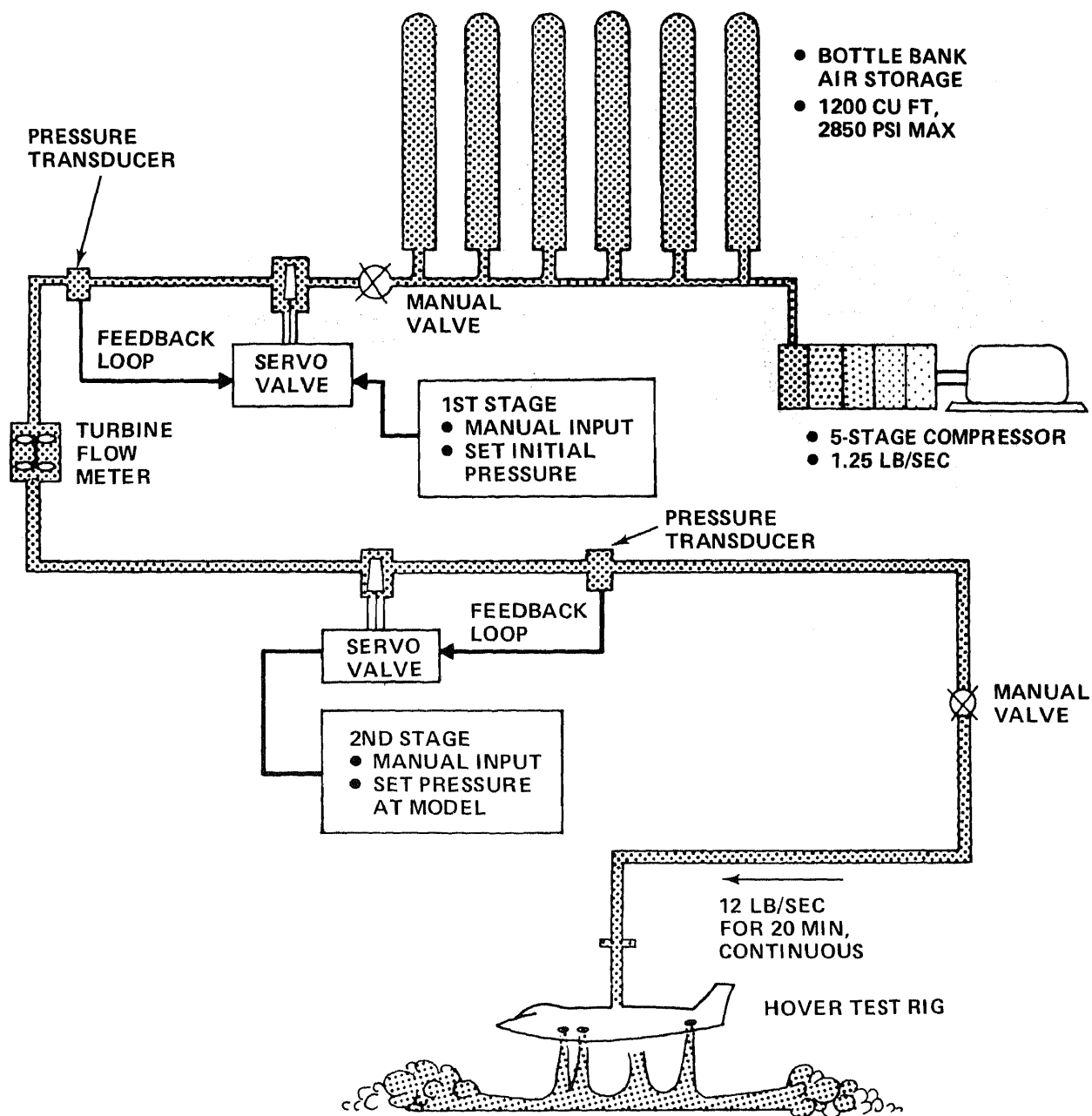


Fig. 4 Hover Test Rig Air System

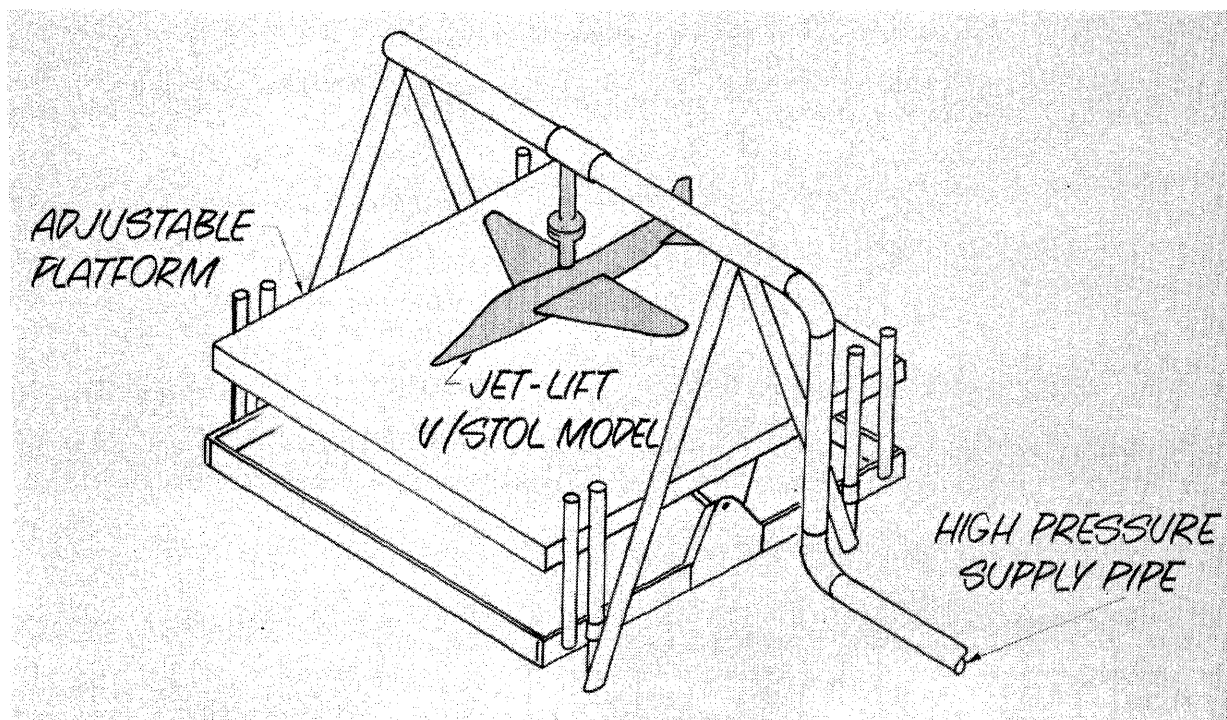


Fig. 5 Hover Test Rig

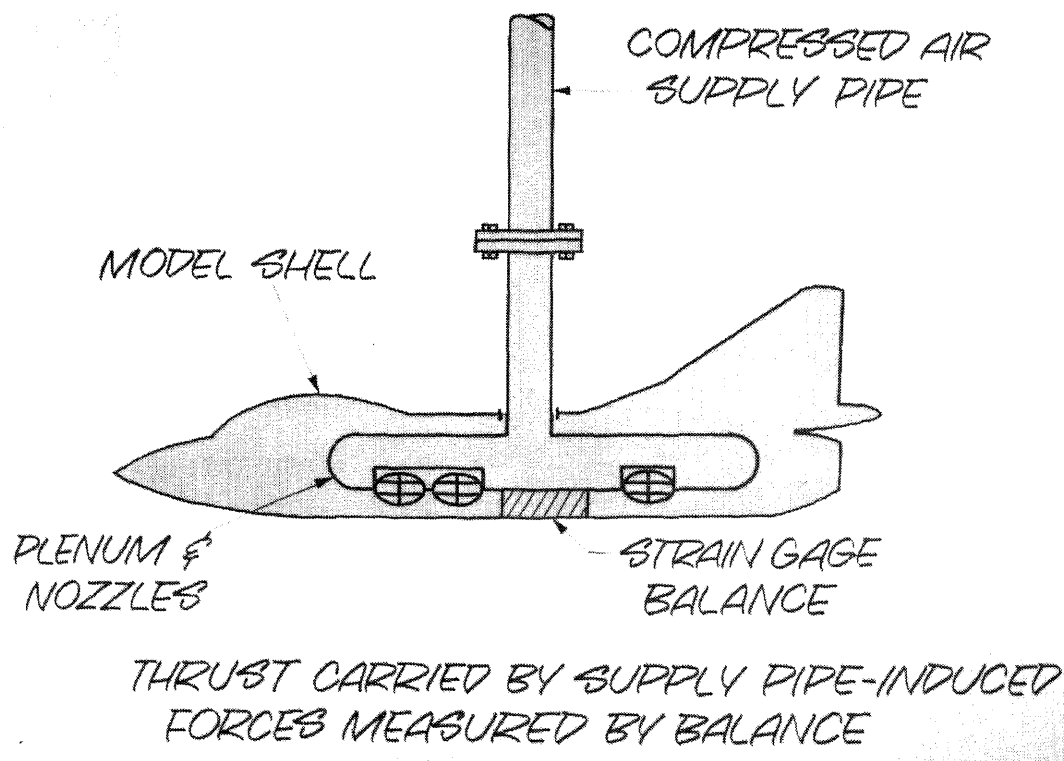


Fig. 6 Hover Test Model Internal Arrangement

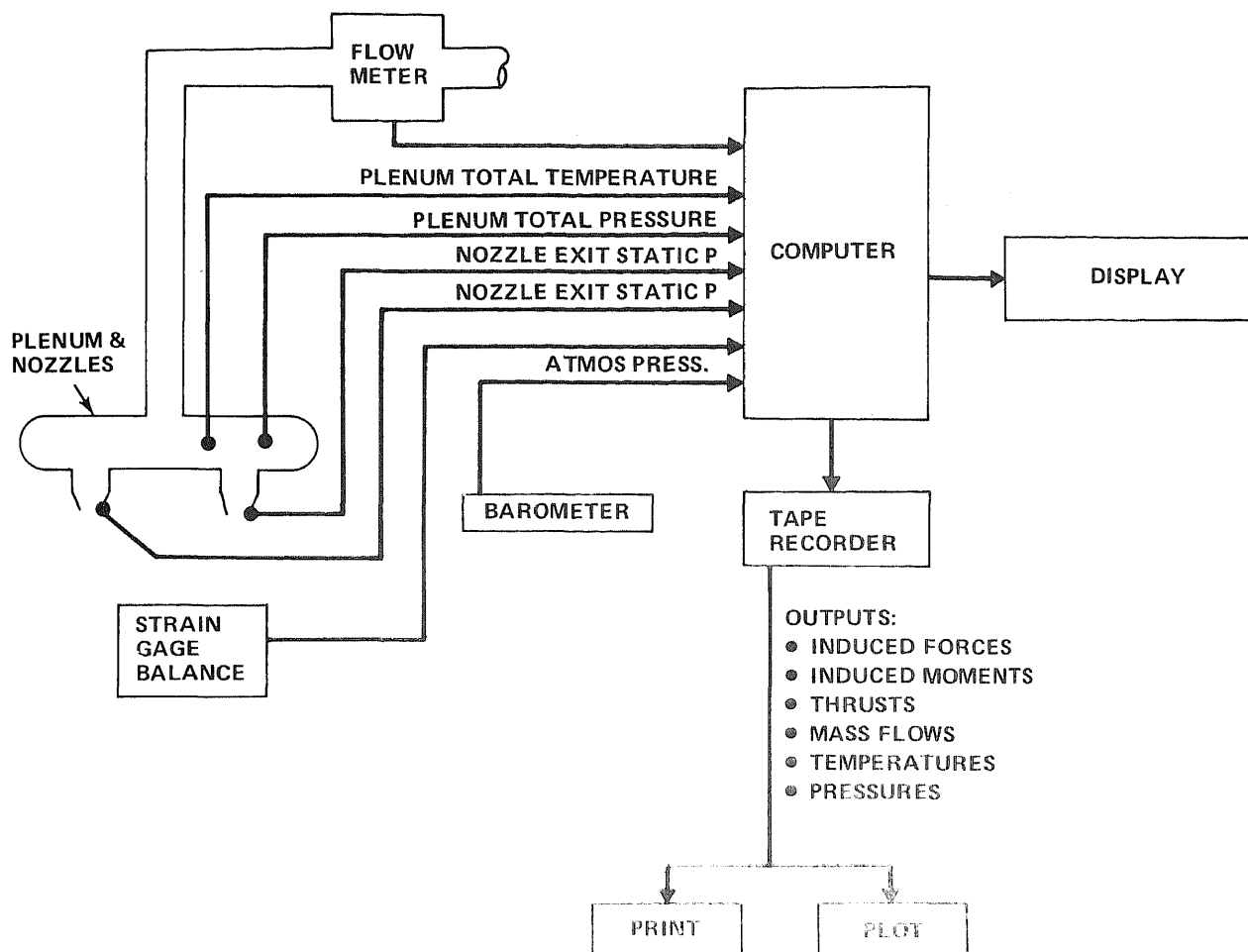


Fig. 7 Data Acquisition System

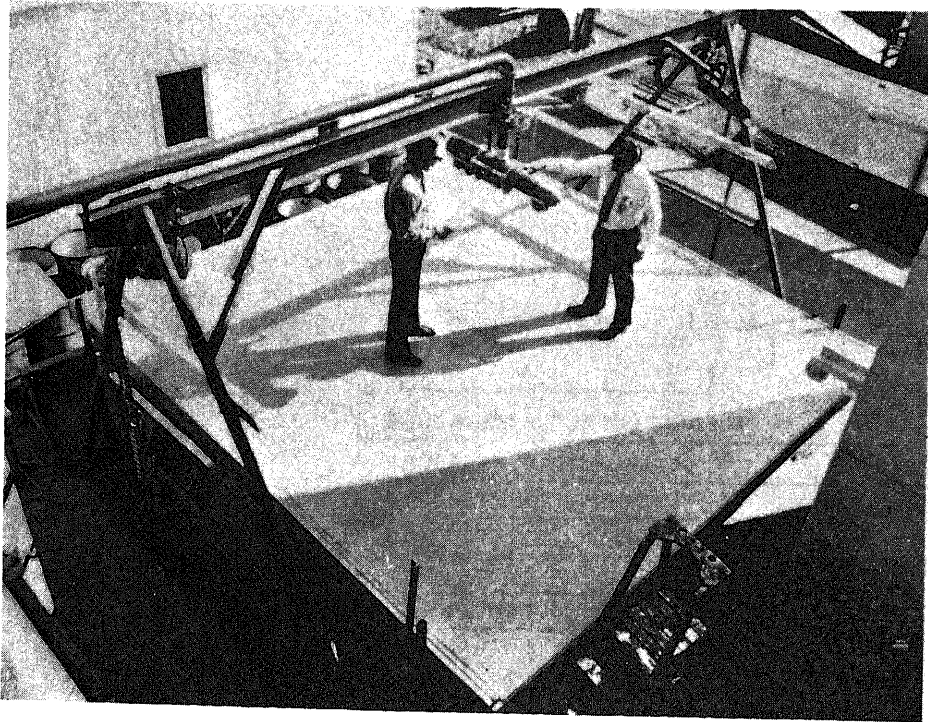


Fig. 8 Outdoor Test Rig

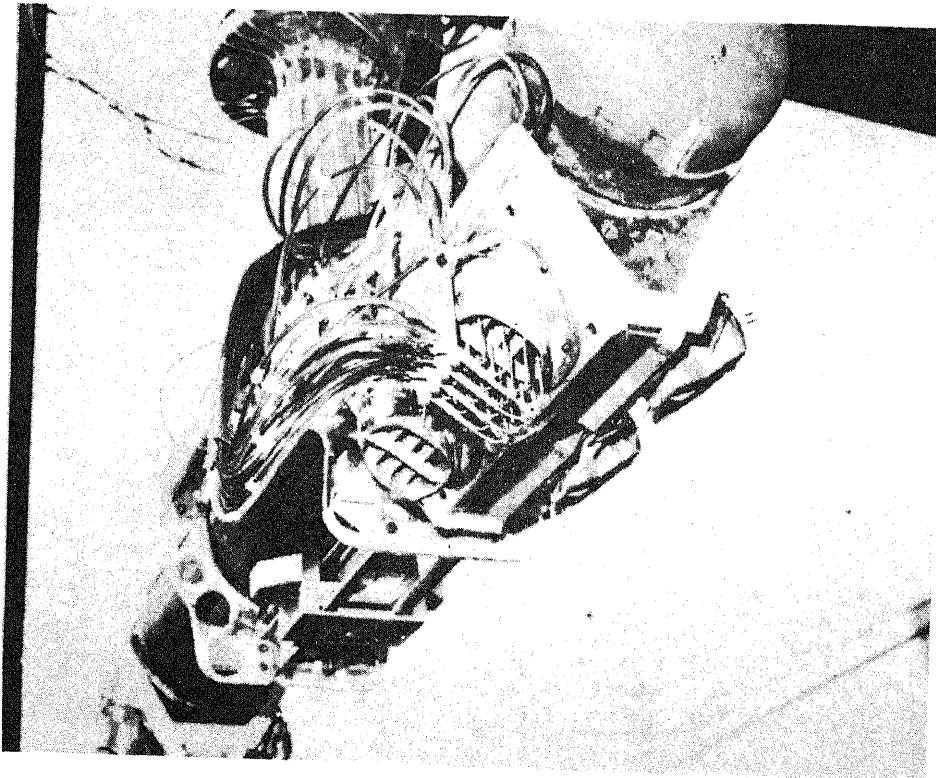


Fig. 9 Plenum & Nozzles

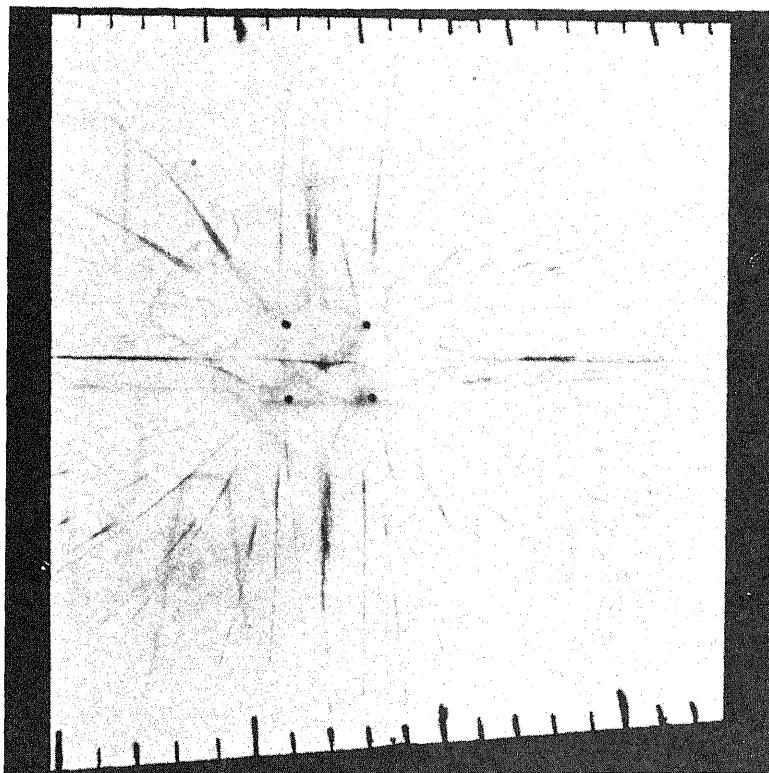


Fig. 10 Ground Plane Oil Streaks

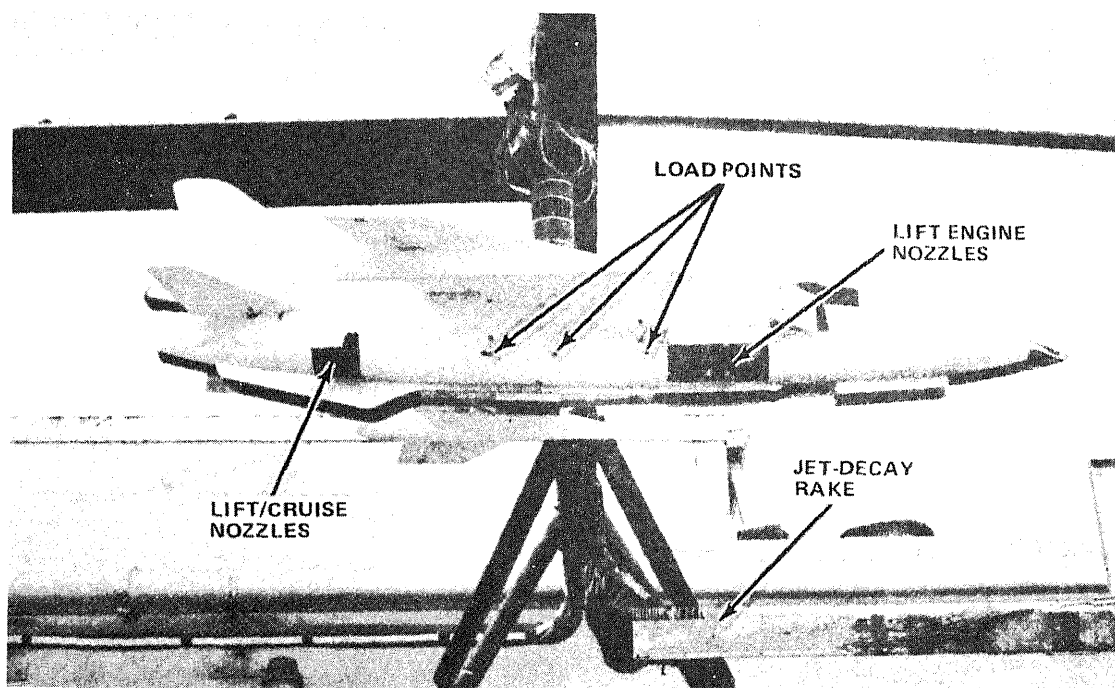


Fig. 11 Hover Test Model, Grumman Design 607A

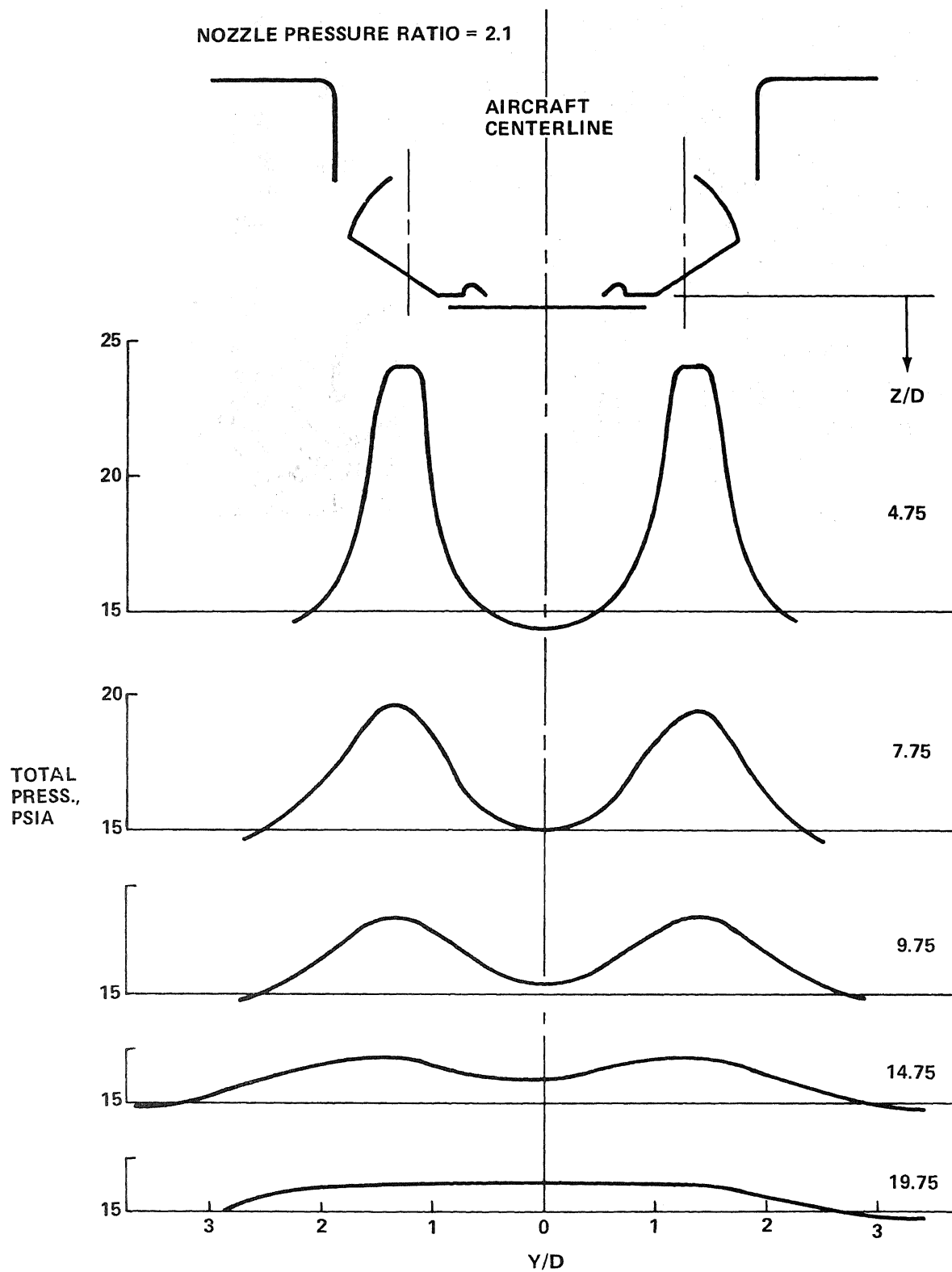


Fig. 12 Free-Jet Pressure Decay

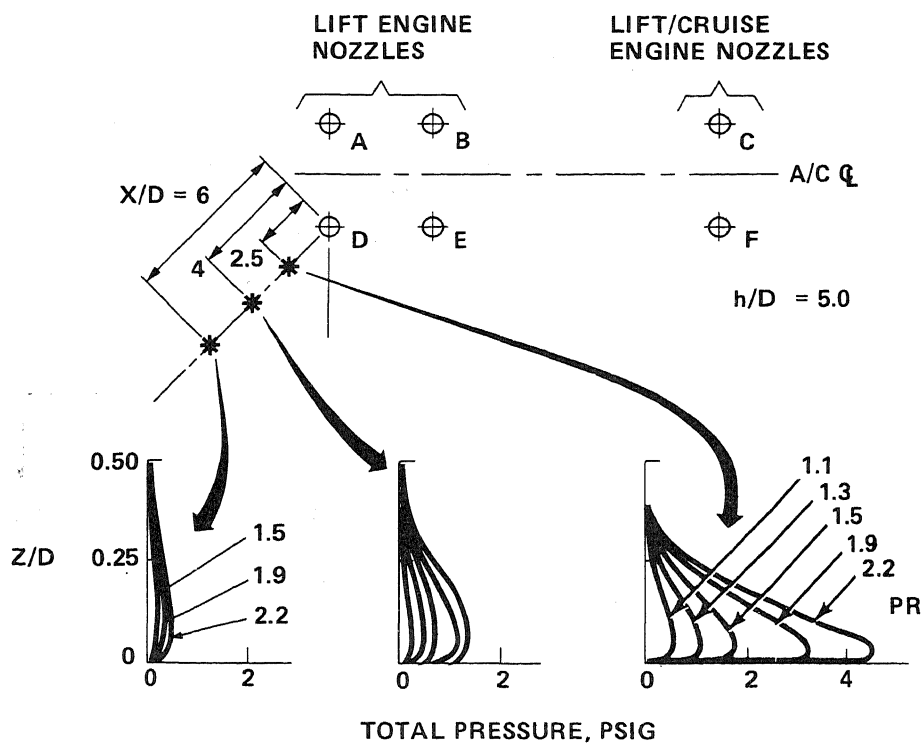


Fig. 13 Wall-Jet Total Pressure Profile

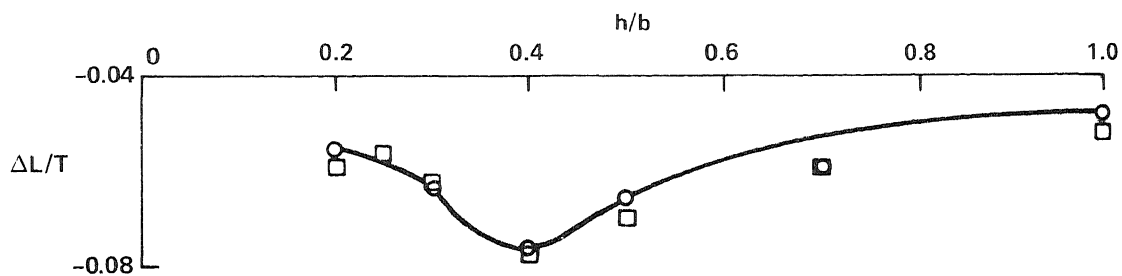
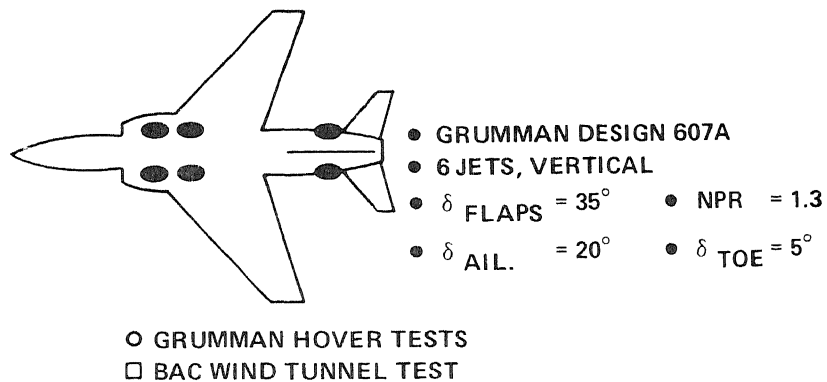


Fig. 14 Comparison of Hover Test Rig Results with BAC Wind Tunnel Tests

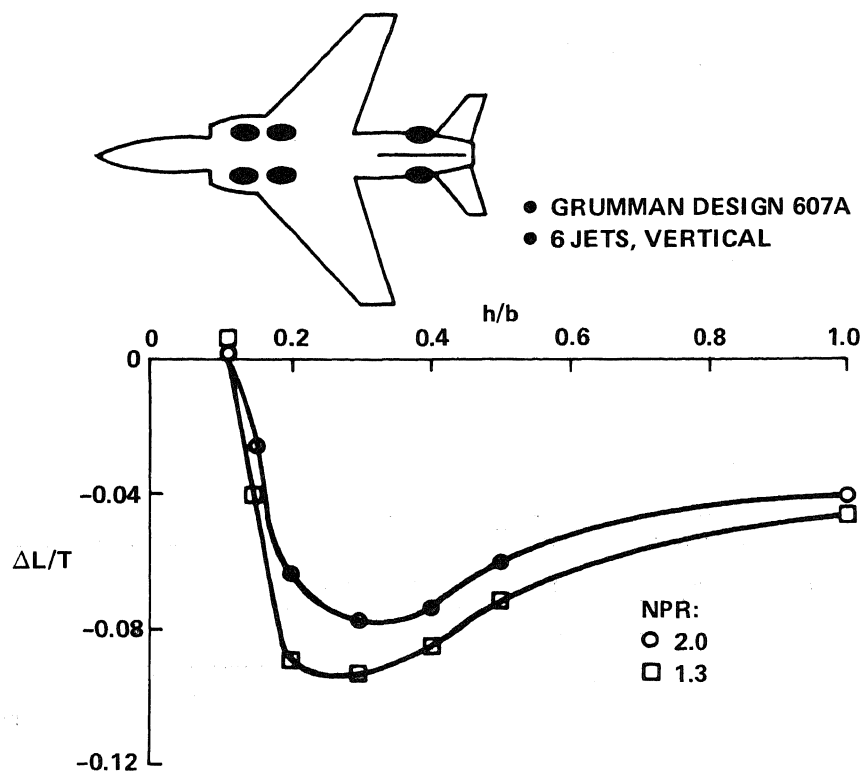


Fig. 15 Effect of Nozzle Pressure Ratio on Jet-Induced Lift

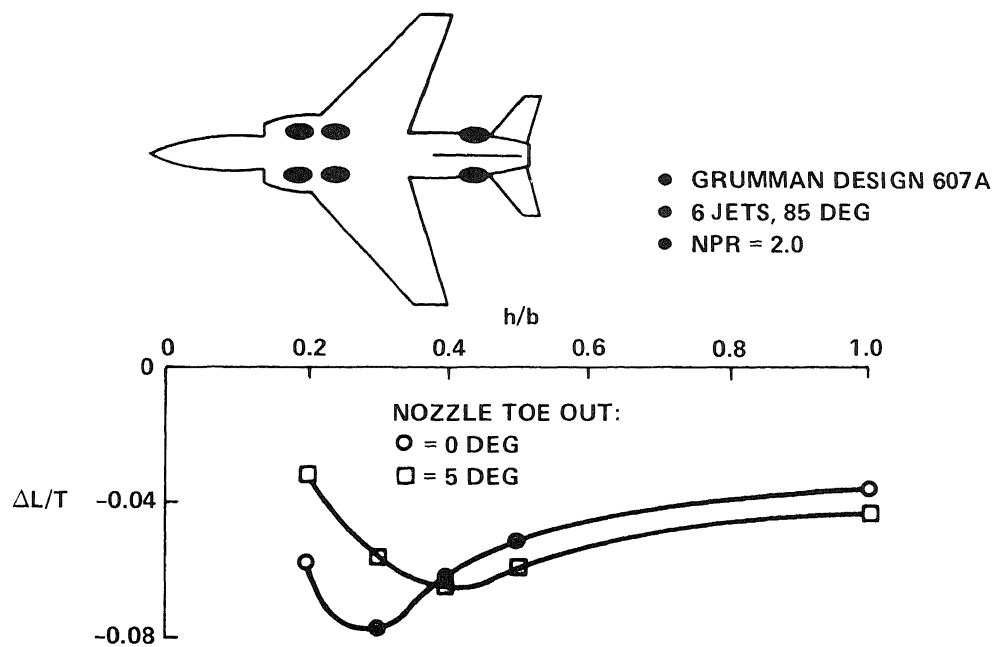


Fig. 16 Effect of Nozzle Toe-Out on Jet-Induced Lift

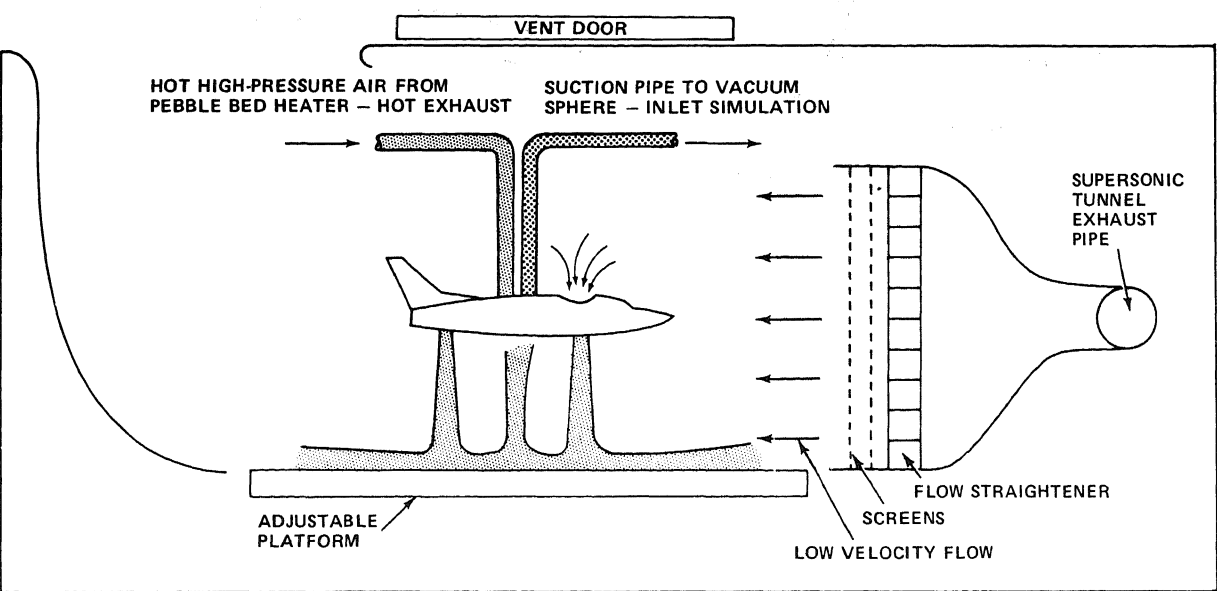


Fig. 17 Proposed Test Rig Improvements

JET EFFECTS IN HOVER
OF A VTOL AIRCRAFT MODEL
USING WATER AS A TEST MEDIUM

D. J. RENSELAER and R. J. OBERTO

Rockwell International
Los Angeles Aircraft Division

ABSTRACT

A water basin test facility was established capable of assessing VTOL aircraft ground effects in hover. Trend data can be generated with it quickly and inexpensively, suitable for preliminary design support. Data of lift and reingestion characteristics as derived in this facility are given for a twin lift fan VTOL transport design showing the benefits of strakes on the fuselage bottom and showing the adverse effect of bank angle and roll control on the lift characteristics.

INTRODUCTION

The purpose of this paper is to describe a small and inexpensive model test facility for the determination of first order ground effects in hover of VTOL aircraft, using water as a test medium, and to describe some of its test results regarding aerodynamic interference and reingestion characteristics of a recent twin fan VTOL aircraft design.

The test facility was generated specifically for preliminary design support because already during early design stages of VTOL aircraft, it is extremely important to have an assessment of ground proximity effects on the aircraft characteristics in hover.

Ground proximity reflects itself in four basic areas. Firstly, there is the change in aerodynamic lift due to power interference effects. Often this results in a lift loss near the ground, and a greater thrust-to-weight ratio may have to be designed into the aircraft to compensate for their loss. Secondly, exhaust gases from the power units are redirected or reflected by the ground, resulting in foreign object damage and hot gas reingestion with subsequent power loss. Thirdly, the back-pressure at the exhaust of the power unit is increased, resulting in a different thrust characteristic and perhaps in an increased possibility of blade stall. Also, ground proximity usually results in rolling moment disturbances when the aircraft is banked or when roll control is applied. Frequently, the roll control power decreases and the aircraft becomes unstable in roll.

In all four of these basic areas, adequate estimating procedures do not exist for preliminary design purposes, whereas wind tunnel tests are generally expensive on account of the required power units. Thus, such tests are likely limited to designs that are fairly well advanced, and the designer is faced with making assumptions in earlier design phases.

In order to prepare a basis to improve the quality of these assumptions, this test facility was established a few years ago suitable for trend data and using water as a test medium instead of air. This test facility can give qualitative answers inexpensively and quickly enough to be suitable for preliminary design support when major configuration changes are being considered in rapid succession.

Use of water is particularly suitable for inexpensive qualitative testing for the following reasons.

1 and no model motors are required because:

be replaced by pipes carrying pressur-

be used while the model forces and
number are still adequate.

be "engineered" for safety requirements
involved in the test medium are low and

s only to be small and the test instru-
rude because the models are small and
and moment levels need to be measured.

been used in the past to obtain interference ef-
aircraft lift and on rolling and pitching moments.

ax fan aircraft configurations were published in
References 1 through 3. References 2 and 3 also compare test results ob-
tained with water in this facility with test results obtained by NASA using
air for simpler models of identical shape. These tests indicated the val-
idity of water for trend analysis.

The present analysis shows data of a more recent test series; that of a twin
fan VTOL aircraft. In addition, for the first time in this test facility,
reingestion was measured, although crudely, and in line with the purpose of
obtaining trend data only. Force data obtained with this model are compar-
able to those given in Reference 5, but the present document adds a compre-
hensive investigation as to how to increase the lift near the ground.

However, the remaining major ground effects related to back pressure effects
and foreign object damage, are not discussed in the present document.

DESCRIPTION OF MODEL AND TEST FACILITY

A photograph of the general test facility is presented in Figure 1, showing
the water basin as a round container of approximately 5 feet diameter and
wall height of about 2 feet. Figure 2 gives a view into the container with
the model installed, but prior to adding water. The bottom of the container
has a plexiglass window to facilitate flow visualization. The model and all
associated plumbing for water jets and suction pipes, as well as all measuring
systems are attached to a framework above the water basin. The height of
the model in relation to the bottom of the basin can be varied by moving the
entire framework up or down by means of four jackscrews. The bottom of the
container is used as the ground plane for level aircraft attitudes. A false
bottom with inclination is used to simulate pitch or bank.

Engine exhausts are simulated by water jets. The exhaust thrust is measured
by scales as indicated in Figure 3a. The model forces can be measured inde-
pendently of the exhaust thrust, yielding the interference forces due to
power.

The plumbing schematic is presented in Figure 3b. The schematic shows a system for exhaust flow to generate thrust, and a suction system to measure reingestion characteristics. The container is indicated by letter A. The model is shown by letter B. Tap water (C) is used to fill the container to approximately 18 inches of water through the filler pipe D. A motor with centrifugal pump E is operated to pressurize plenums F and to feed the exhaust pipes J at the model. The exhaust pipes represent lift fans as well as pitch control pipes.

If reingestion characteristics are to be analyzed, a certain amount of pellets are deposited in the pellet filler cage H and subsequently transferred to the injection cage I. At desired time, a plunger in the injection cage is moved manually so that all pellets are injected into one main exhaust pipe and released at its nozzle opening J. Pellets are subsequently ingested into the suction system at the inlets K. These inlets represent fan flow inlets as well as gas generator inlets. The pellets are collected by screens in cages L. The cages are emptied by back flushing with tap water from C while the motor E is stopped. When the pellets emerge at K during the back flushing, a net is placed manually around the openings K which traps the pellets previously ingested and their number can then readily be counted. The remaining pellets still suspended in the water of container A are, at times, collected by the water vacuum cleaner M.

A photograph of the model, with 12 inch span and immersed in water, is presented in Figure 4. The model is suspended via force measuring scales at the fuselage nose and at the wing tips. The model is that of a twin lift fan aircraft with a fan located in each wing root and each are simulated by a water jet. The model has also a pitch pipe in the front and rear portion of the fuselage. All exhaust pipes are attached to a force measuring scale to set each exhaust at preselected thrust values. There are two inlets at the front of the fuselage, simulating gas generator inlets. In addition, two main inlets exist, one at each wing-body intersection, representing the main fan inlets. Each inlet has a cross shaped flow straightener to counteract the formation of an inlet vortex. Also, the main exhausts have a flow straightener, Figure 5. The latter are aimed at achieving a more symmetric exhaust flow field. Detail dimensions of the model are given in Figure 6.

DISCUSSION OF TEST RESULTS

In this section, a sample of data outputs from the test facility are given pertaining to the twin lift fan V/STOL aircraft of Figure 6. Lift and reingestion characteristics are given, but no rolling and pitching moments are presented here. However, moment characteristics can also be analyzed as shown in references 1, 2, and 3.

Aircraft In Level Attitude

Model lift characteristics are presented in Figure 7 as a function of height above the ground. The lift, L , is the total lifting force, being the sum of the exhaust thrust plus the interference forces on the model. The lift is non-dimensionalized by the sum of the thrusts of the exhaust. The model is

in its "basic" configuration, i.e., has no devices for a lift increase, and in this figure has no pitch nozzles operating.

The figure shows that a substantial negative interference lift exists. The lift loss is a result of flow being entrained into the exhaust flow, and while it is entrained, it generates a velocity on the lower wing surface and on the fuselage bottom. In turn, this velocity creates a negative pressure causing the lift loss or "suck down", see insert sketches of Figure 7. Additionally, a "fountain" effect exists, generated when the two exhaust flows are spread toward each other by the ground. Where they meet, the flow turns upward and generates a positive pressure on the fuselage. However, this positive lift increment is not strong enough to overcome the suckdown effects in this configuration. Various different thrust levels are used, showing identical results in the non-dimensional form and showing that no scale effects exist over the range of thrust levels tested.

Figure 8 shows an attempt to influence the flow field in such a way that less suckdown results. Strakes were placed sideways on the fuselage bottom in front and to rear of the exhausts. The idea was to stop some inflow on the fuselage bottom by using the strakes as a fence. Additionally, it was thought that the fences would generate a sideways flow from the fountain head that could stop some inflow from the lower wing surface. Results were only marginal, with net lift losses existing at fuselage heights less than $4.5D$ (measured from the fuselage to the bottom ground, where D is the inside diameter of one main nozzle).

Figure 9 shows the case where the strakes were placed longitudinally. The attempt was to operate only on the fuselage inflow by directing the flow from the fountain head fore and aft. This attempt resulted in more success, with net lift losses limited to a height less than $2.0D$ for a strake depth of $0.77D$. Figure 10 elaborates on this idea by trying various different strake heights. It appears that there is an optimum height of strakes, in the order of $0.6D$ (Note, that the strakes in this figure are curved, whereas in the previous figure they were straight, i.e., flat sided). However, the optimum height gives results only slightly different from that of $0.77D$.

Figure 11 shows the effect of wing fences in addition to the above longitudinal strakes. They gave an unfavorable result, probably because they increase the local inflow velocity under the wing. Further attempts to operate on the inflow on the wing were subsequently abandoned and, instead, flow phenomena on the fuselage bottom were concentrated upon.

The effect of adding sideways strakes in front and to rear of the longitudinal strakes is shown in Figure 12. In this fashion, the various strakes together form a box. Lift loss is completely eliminated for the "optimum" strake height, but still exists at a smaller strake height. The hypothesis is that the front and rear strakes act like a curtain behind which the positive pressures from the fountain head can advance further along a greater distance on the fuselage bottom. Straight versus curved strakes are compared in Figure 13, with the curved strakes showing an advantage with regard to the smoothness of the lift variation with ground height. Figures 14 and 15 present a variation of width and length of the strake box, showing best results for the widest box and showing an optimum length of about $5D$.

Effect of Pitch and Bank Angle

The effect of pitch attitude change on the aircraft lift characteristics is presented in Figure 16 for the basic configuration and for the case employing a strake box. The pitch attitude has relatively little effect except at larger ground distance for the case with strake box. It is surmised that the fountain head is moving gradually out of the box. Evidence of such a displacement of the fountain is presented in References 6 and 7. A design chart for the amount of displacement is given in Reference 8.

A similar plot is given in Figure 17 for the effect of a 10° bank angle change. Here the lift losses are more severe than during pitch attitude change. In particular for the case with the strake box installed, it seems that the fountain head may move completely out of the box. The minimum lift encountered during this bank angle is $L/T = 0.86$.

A combination of 7° pitch with 7° bank is shown in Figure 18, indicating a minimum lift of approximately $L/T = .90$.

Effect of Control Application

Pitch control application has only a minor effect in the case that a strake box is employed, Figure 19. A somewhat greater effect is obtained for the basic configuration (i.e., without strakes), where the pitch exhausts probably are instrumental in increasing the strength of the fountain and subsequently in increasing lift.

Application of roll control in the wings level condition can decrease the lift significantly as Figure 20 shows. It is expected that the fountain is moved sideways when the exhaust is unequal, as illustrated in the inserted sketch in the figure (See also Reference 8). This will decrease the effectiveness of the strake box significantly.

Reingestion

The percentages of reingestion of main fan exhaust into the fan inlets and gas generator inlets are presented in Figure 21 for the aircraft with zero pitch control thrusts. The percentages are the sum of left and right intakes. They are obtained from pellet counts over a time period of less than 1.5 seconds after ejection of a large amount of pellets from one of the main exhausts. The bulk of the reingestion occurs in a much lesser time. It is seen that a reingestion of 8% can be expected close to the ground in the basic configuration. However, with application of a strake box, the amount is significantly less. It is envisioned that the strake box forms a fence capable of retarding flow from the fountain head into the fan inlets. Figure 21 also shows that the gas generator inlets encounter less than 1% reingestion.

Reingestion characteristics with the pitch nozzle thrust in the full nose up control setting are given in Figure 22. Operation of this pitch up control increases the reingestion by 2% of the fan exhaust flow, but it has negligible effect in the gas generator inlet (not shown).

CONCLUSIONS

A test facility was established where force and moment trend data as well as reingestion characteristics could be assessed using water as a test medium. This facility is capable of acquiring these data inexpensively and quickly as desired for preliminary design support.

Lift data are presented for a twin lift-fan VTOL transport at various pitch and bank angles and at various pitch and roll control inputs. The basic, i.e., unmodified, aircraft has a significant lift loss due to ground proximity, but strakes were capable of yielding a positive lift increment in level attitude by capturing fountain flow. Pitch attitude and pitch control changes had a minor effect; however, bank angle changes on roll control inputs caused a lift loss presumably due to a loss in the fountain effect.

Reingestion was estimated, on the basis of pellet counts, to be less than one percent for the gas generator inlets, 2% to 4% for the main fan inlet for the airplane with a strake box, and approximately 6% to 8% for the basic aircraft without strakes, all in close proximity to the ground.

REFERENCES

1. "Lift Fan V/STOL Flight Control System Development. Flight Simulation Model", NASA CR-114586.
2. Renselaer, D. J., and Oberto, R. J., "Empirical Aerodynamic Ground Effect Data on a VTOL Model of a Gulfstream II Aircraft in Hover", NA-7-115, Rockwell International, Los Angeles Aircraft Division, February 1973.
3. Renselaer, D. J., "Description and Test Results of a Water Basin to Determine Ground Effect in Hover using Small Models", AIAA Paper 75-145, January 1975.
4. Renselaer, D. J., and Oberto, R. J., "The Rockwell International Water Basin Test Facility - Description, Test Capability, Results", NA-74-245, Rockwell International, Los Angeles Aircraft Division, April 1974.
5. Louisse, J., and Marshall, F. L., "Prediction of Ground Effects for VTOL Aircraft with Twin Lifting Jets", AIAA Paper 74-1167, October 1974.

6. Hall, G. R., and Rogers, K. H., "Recirculation Effects Produced by a Pair of Heated Jets Impinging on a Ground Plane", NASA CR-1307, 1969.
7. Margason, R. J., "Review of Propulsion-Induced Effects on Aerodynamics of Jet/STOL Aircraft", NASA TN D-5617, February 1970.
8. Barron, W. A., and Palcza, J. L., "Jet-Induced Thermal Effect for VTOL Aircraft", ASME 75-GT-96, March 1975.

FIGURE 1. PHOTOGRAPH OF GENERAL TEST FACILITY

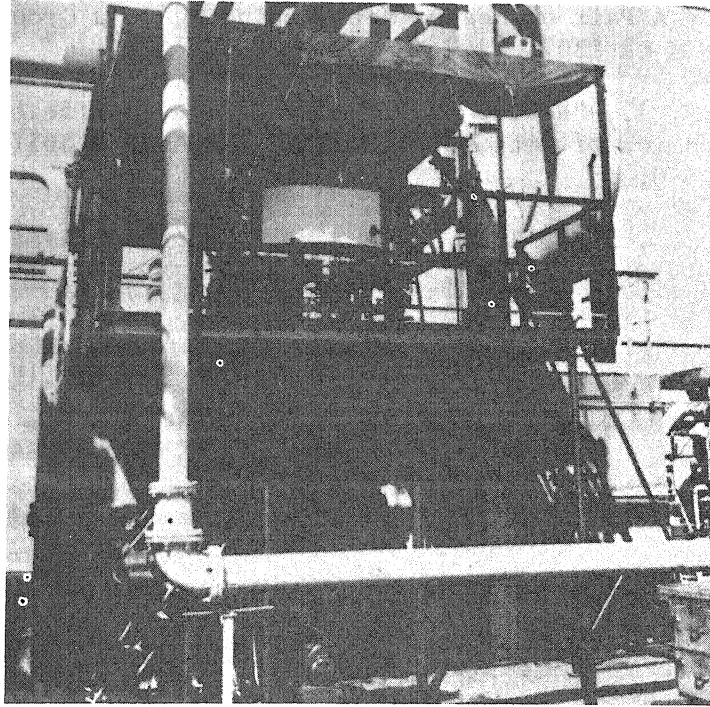


FIGURE 2. PHOTOGRAPH OF INSTALLATION - TOP VIEW

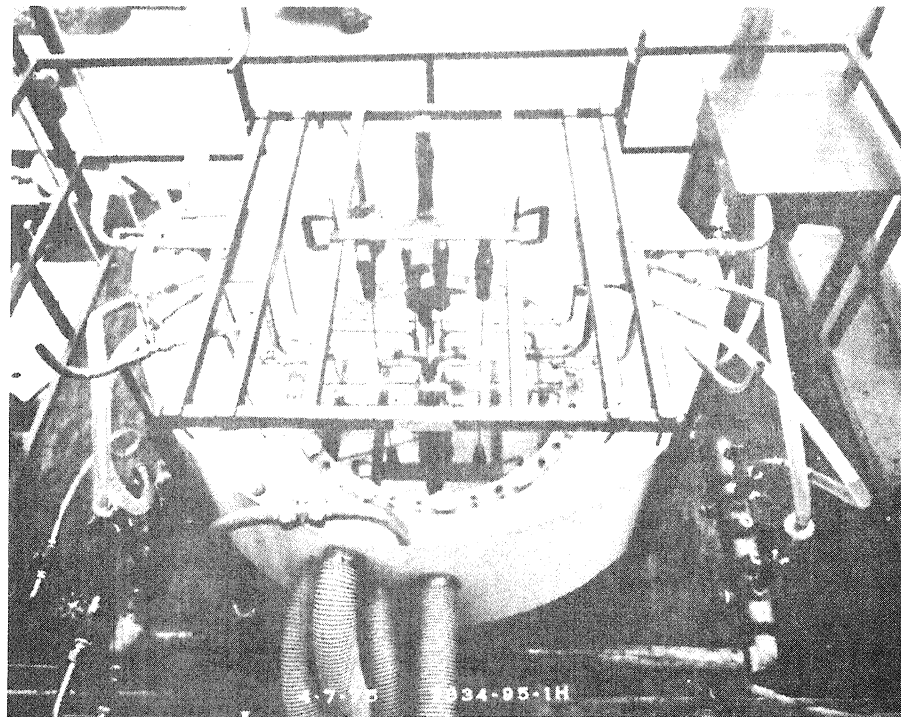


FIGURE 3A. SCHEMATIC OF FORCE MEASUREMENT

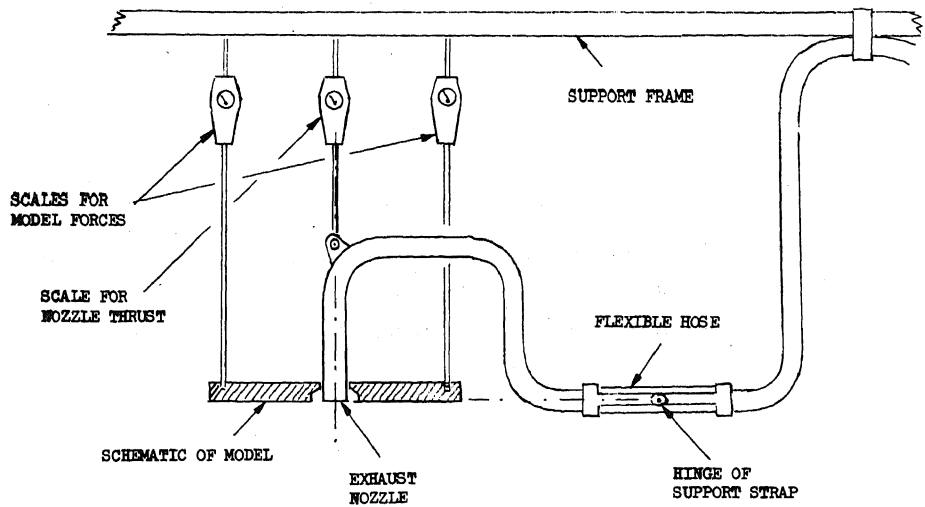


FIGURE 3B. PLUMBING SCHEMATIC

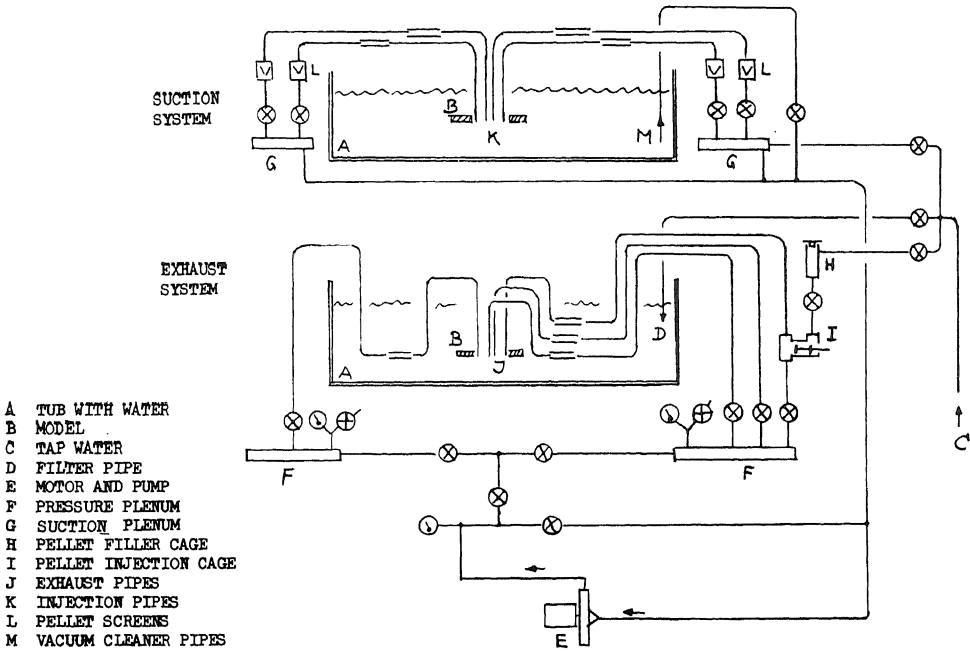


FIGURE 4. PHOTOGRAPH OF MODEL INSTALLATION DETAIL - TOP VIEW

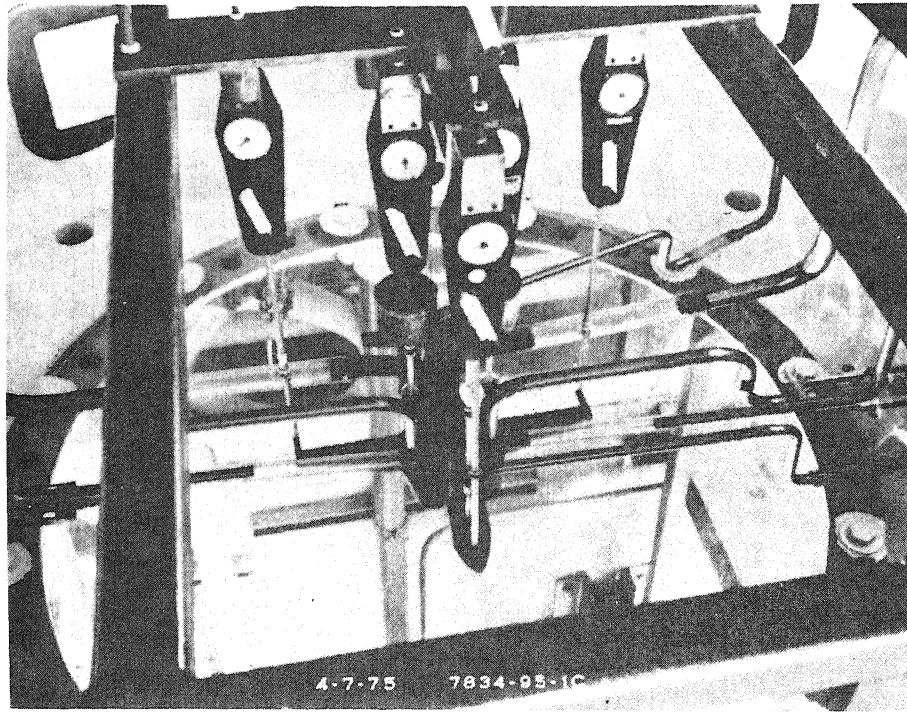


FIGURE 5. PHOTOGRAPH OF INSTALLATION - BOTTOM VIEW

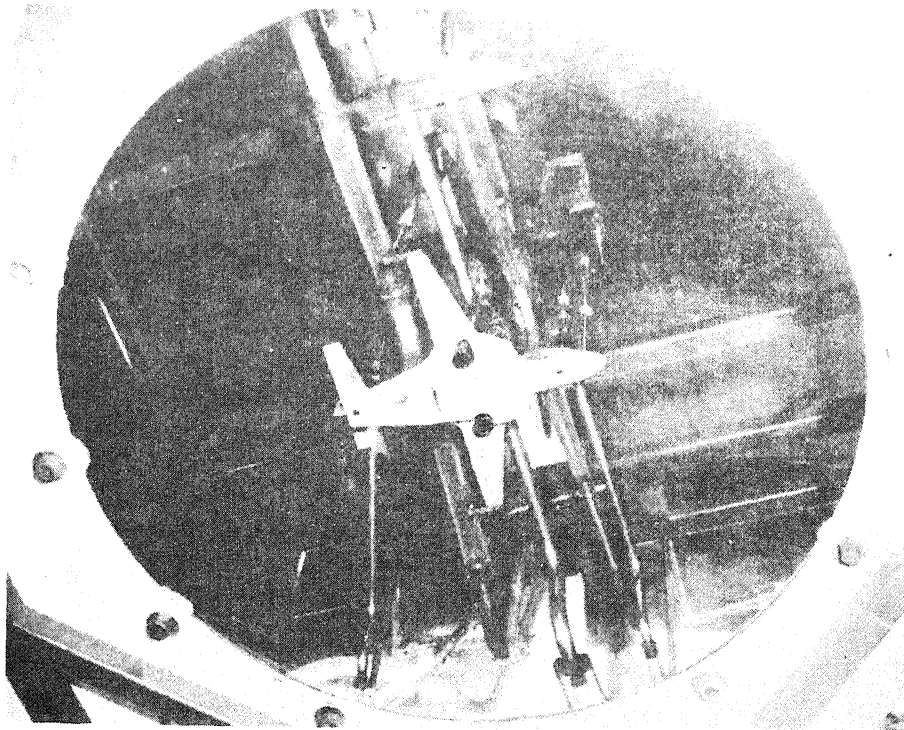


FIGURE 6. MODEL GEOMETRY

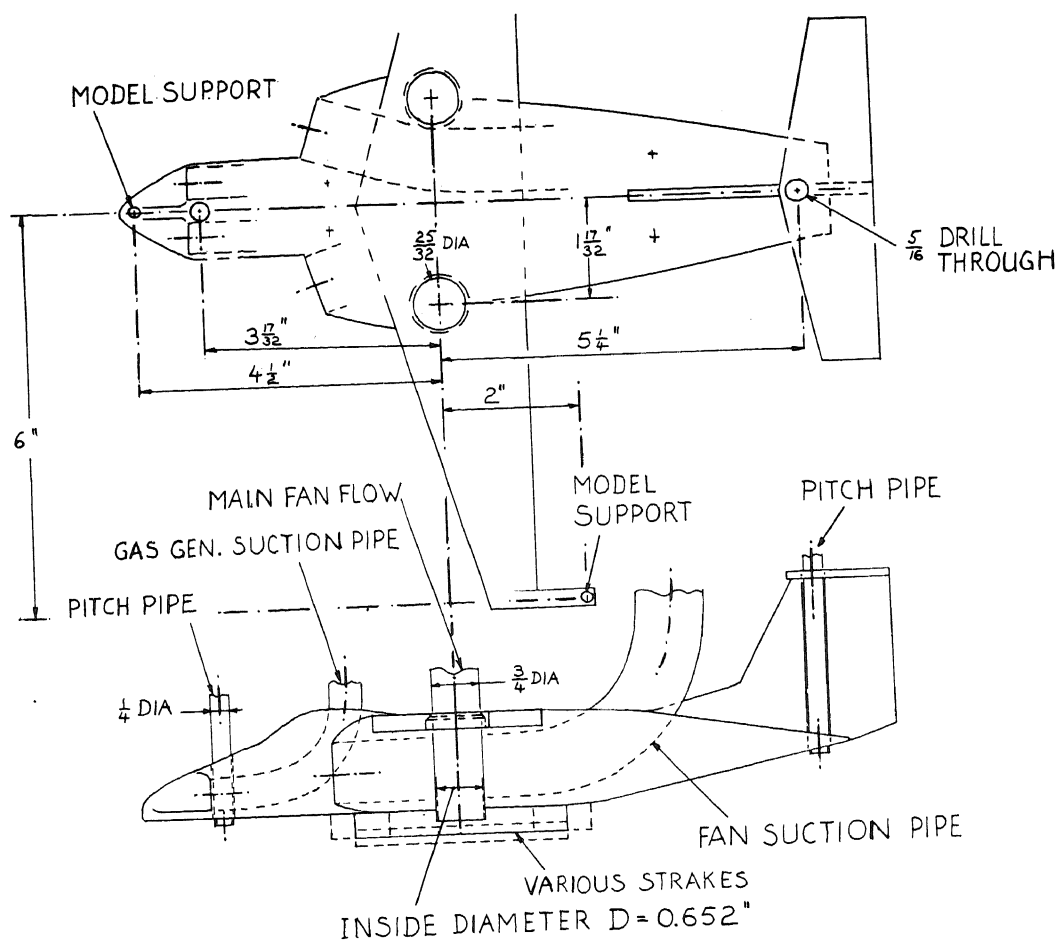


FIGURE 7. EFFECT OF THRUST LEVEL ON LIFT INTERFERENCE

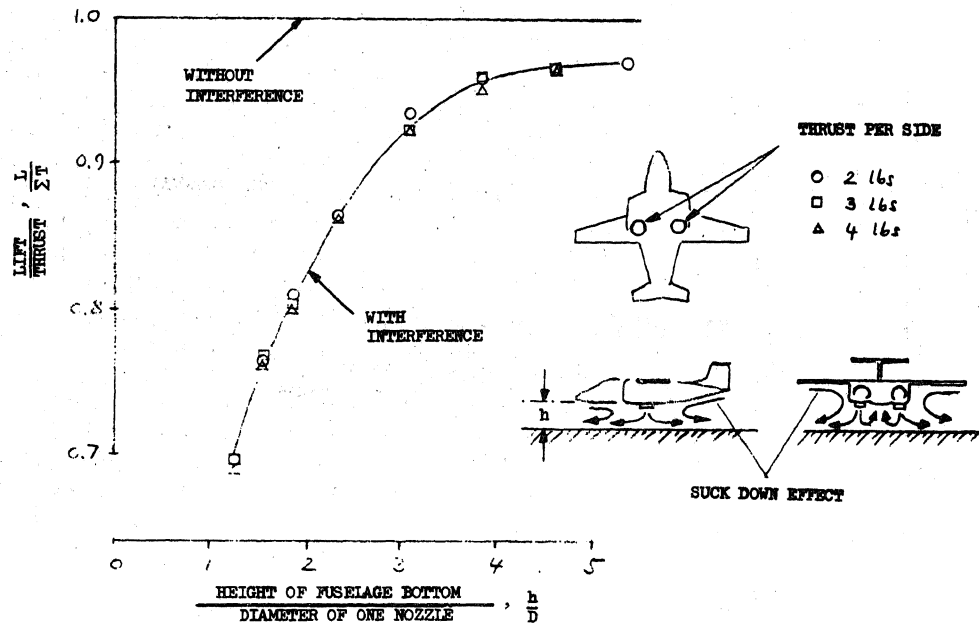


FIGURE 8. EFFECT OF LATERAL STRAKES

(STRAKES FLAT SIDED, DEPTH 0.77D)

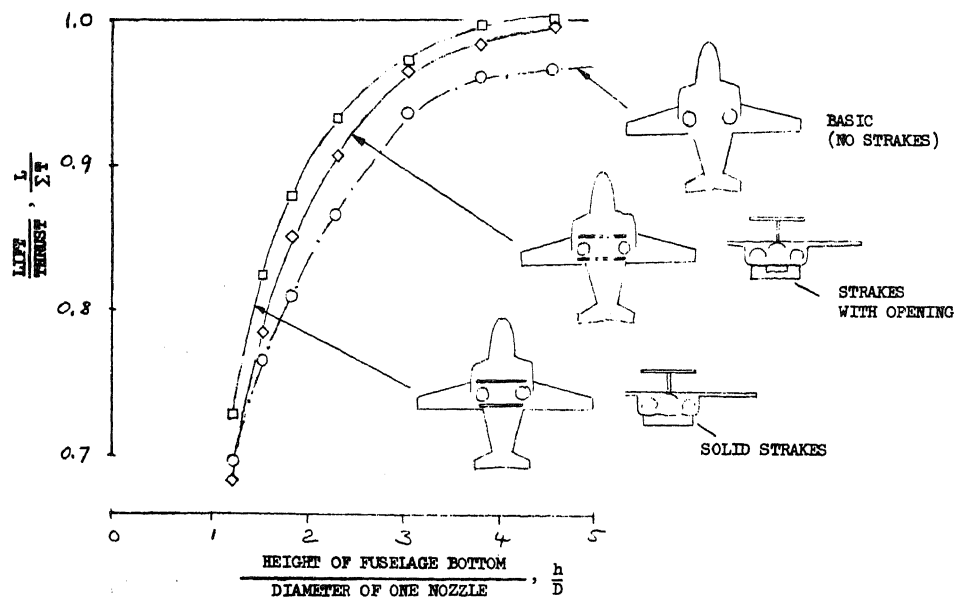


FIGURE 9. EFFECT OF LONGITUDINAL STRAKES
(STRAKES FLAT SIDED, DEPTH 0.77D)

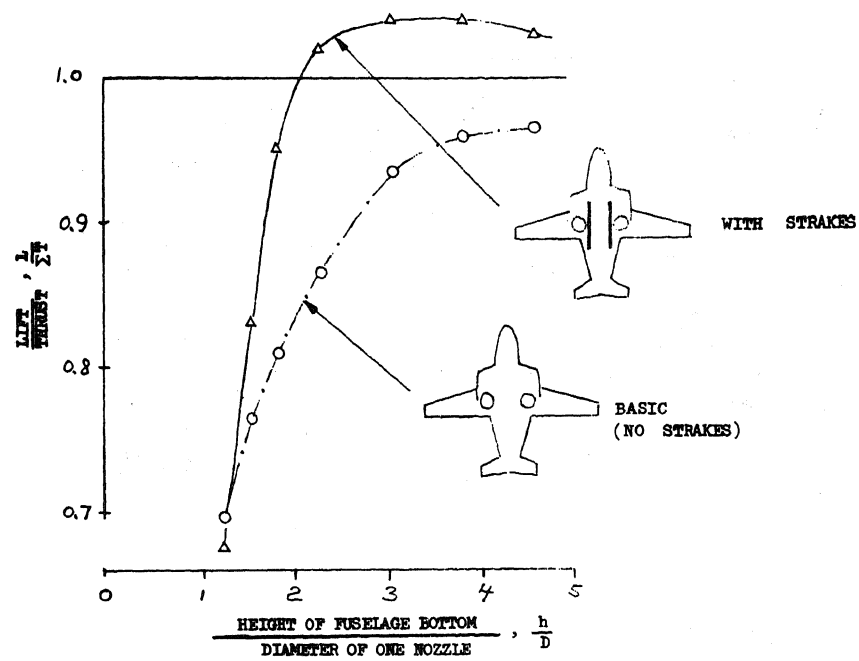


FIGURE 10. EFFECT OF DEPTH OF LONGITUDINAL STRAKES
(CURVED STRAKES)

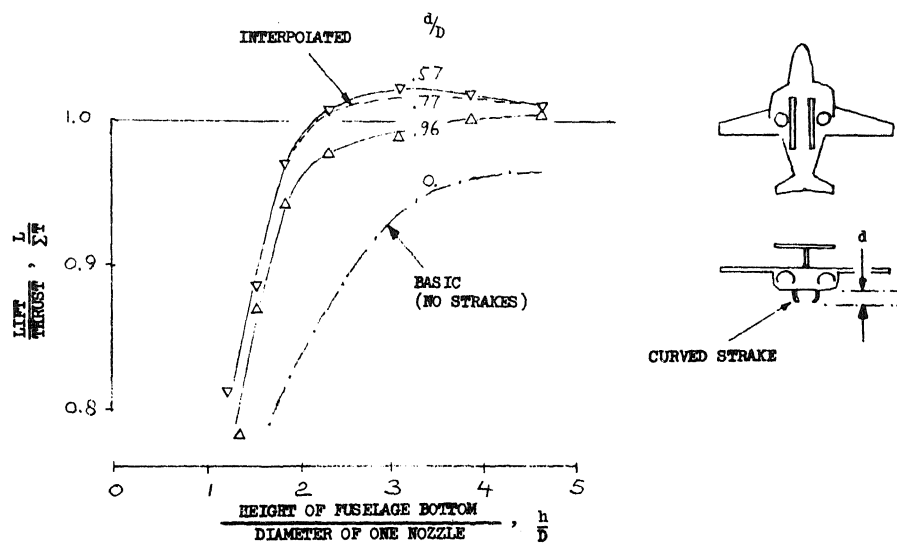


FIGURE 11. EFFECT OF WING FENCES

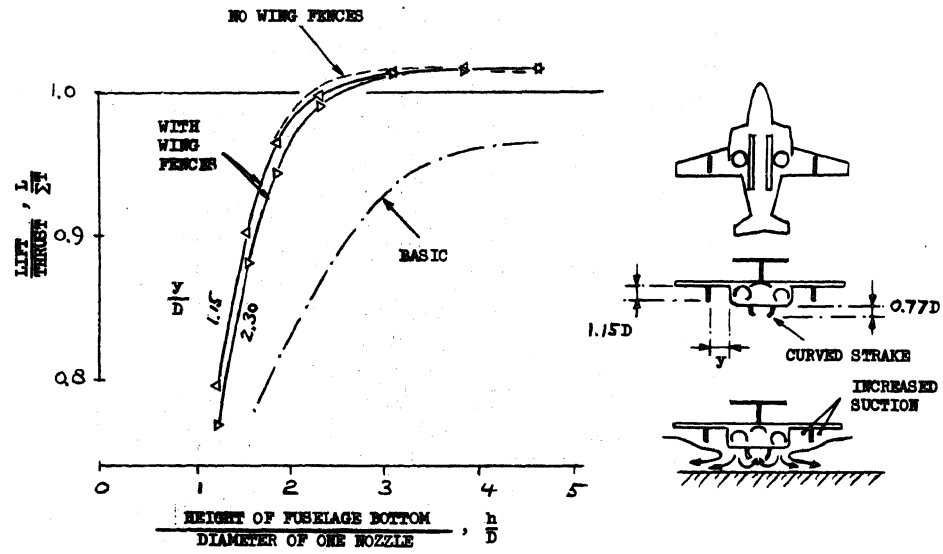
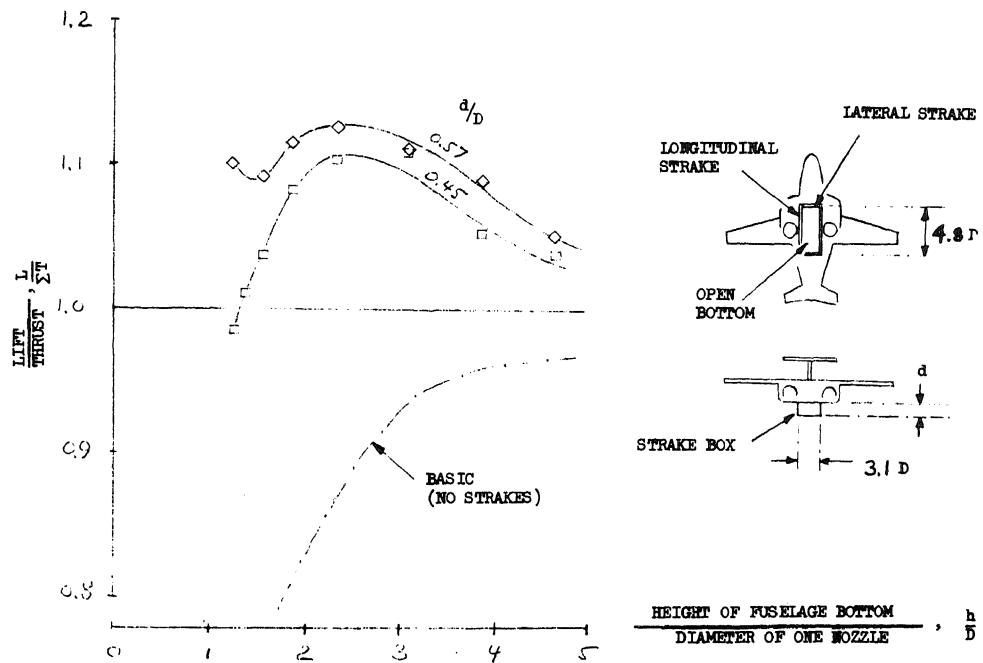


FIGURE 12. EFFECT OF STRAKE BOX (STRAKES FLAT SIDED)



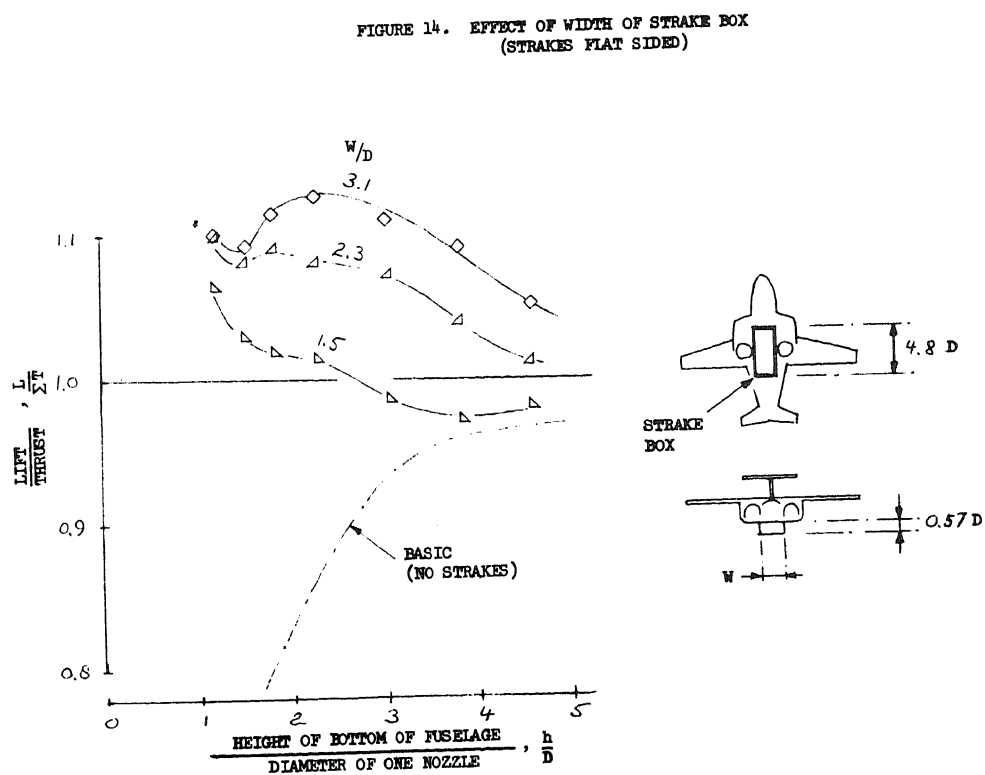
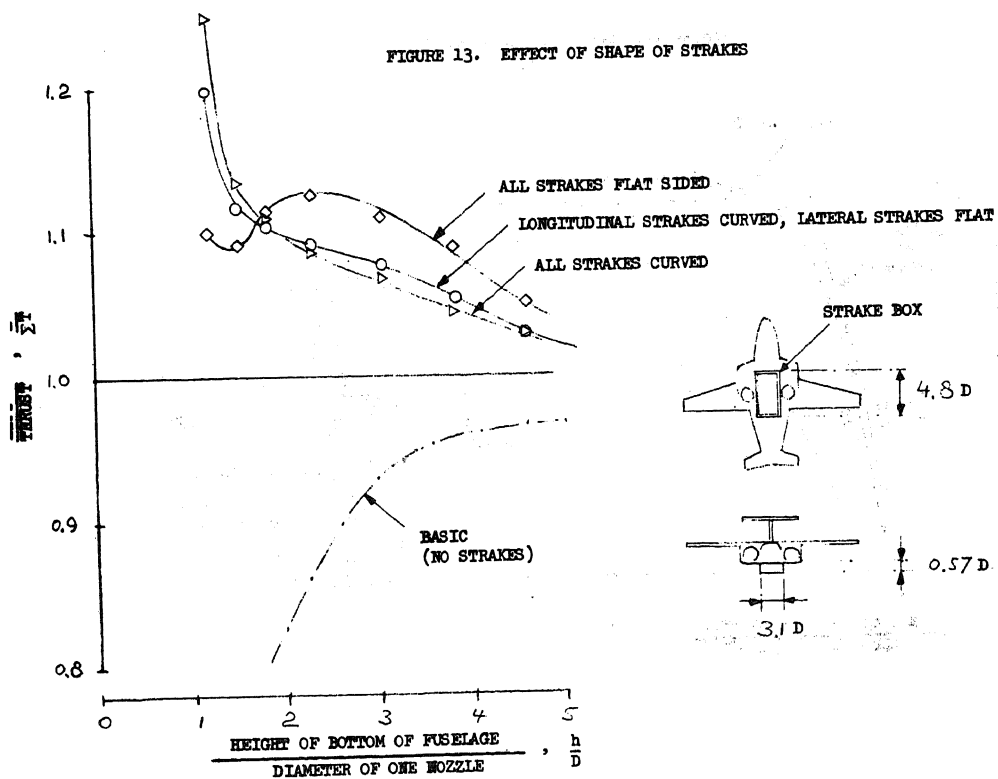


FIGURE 15. EFFECT OF LENGTH OF STRAKE BOX
(STRAKES FLAT SIDED)

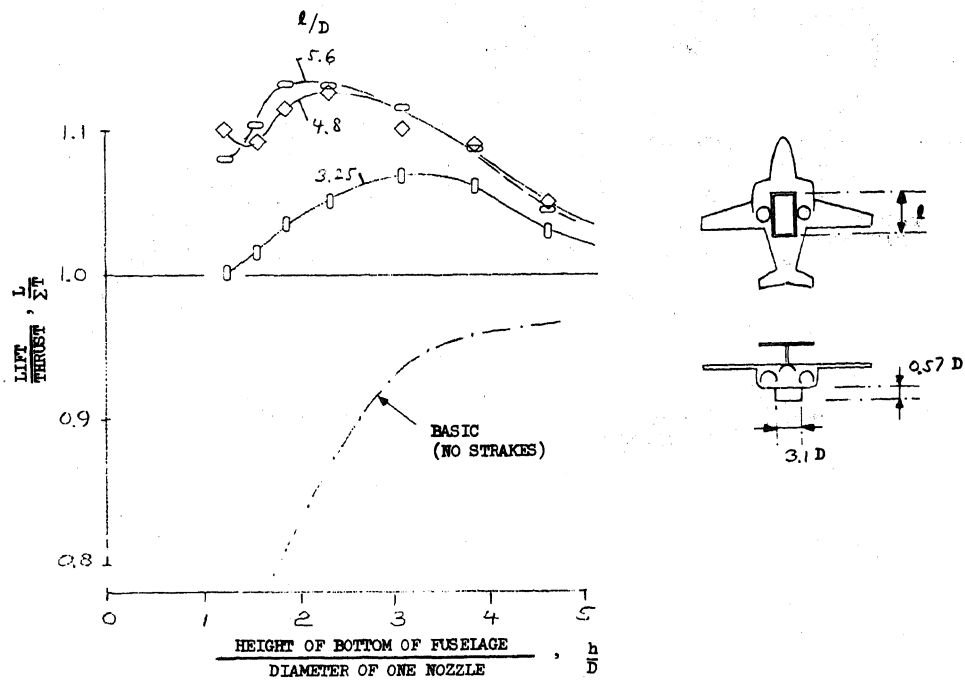


FIGURE 16. EFFECT OF PITCH ANGLE
(ZERO BANK ANGLE)

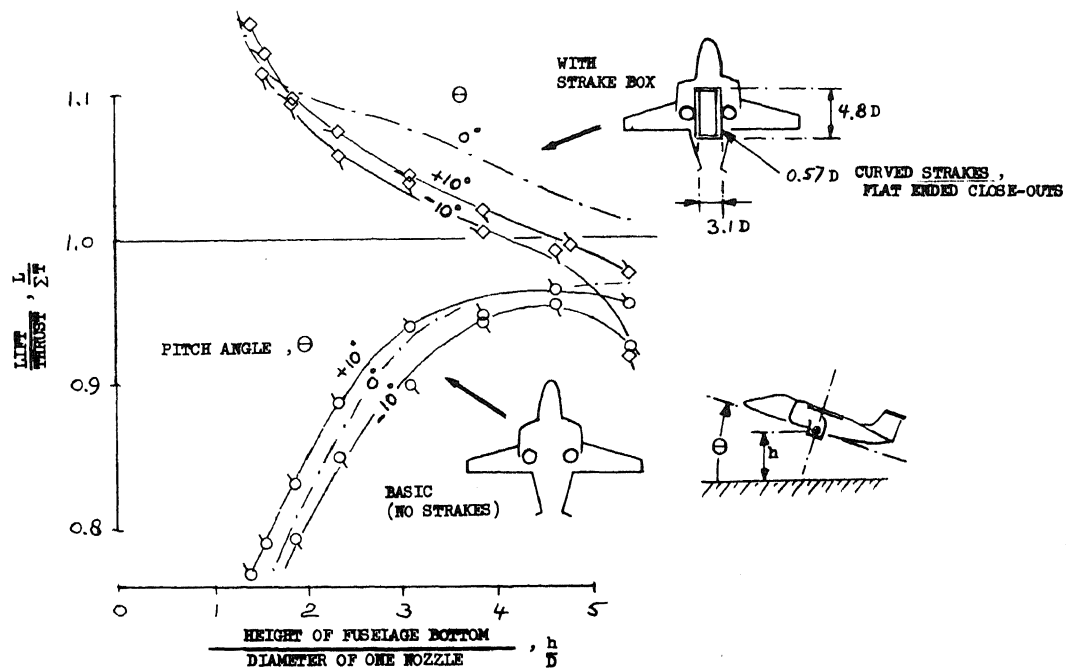


FIGURE 17. EFFECT OF BANK ANGLE
(ZERO PITCH ANGLE)

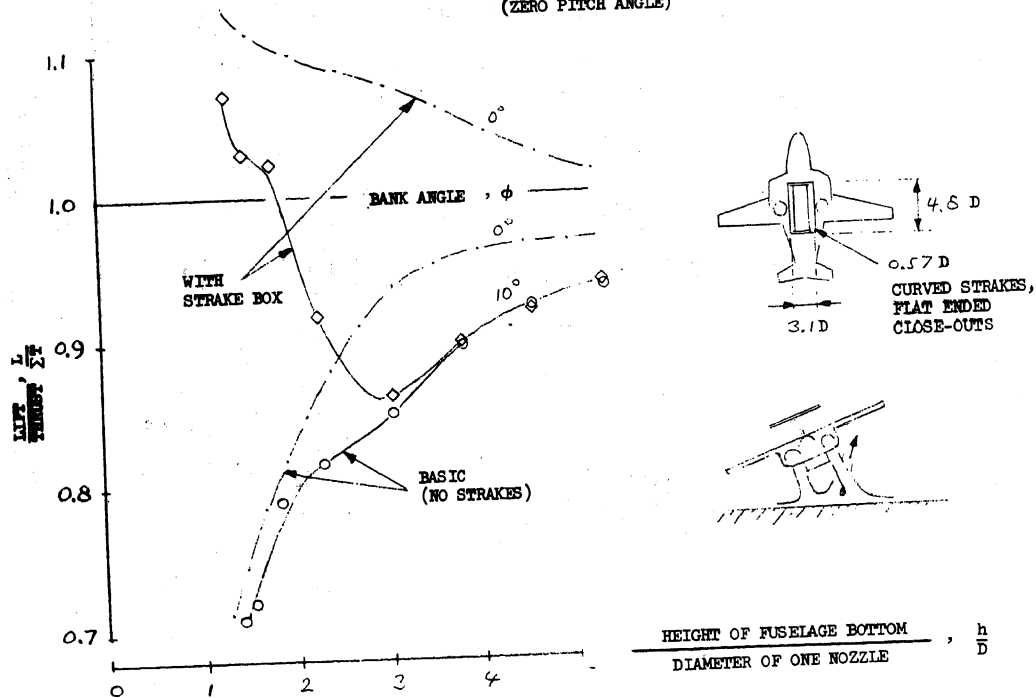


FIGURE 18. EFFECT OF SIMULTANEOUS PITCH AND BANK

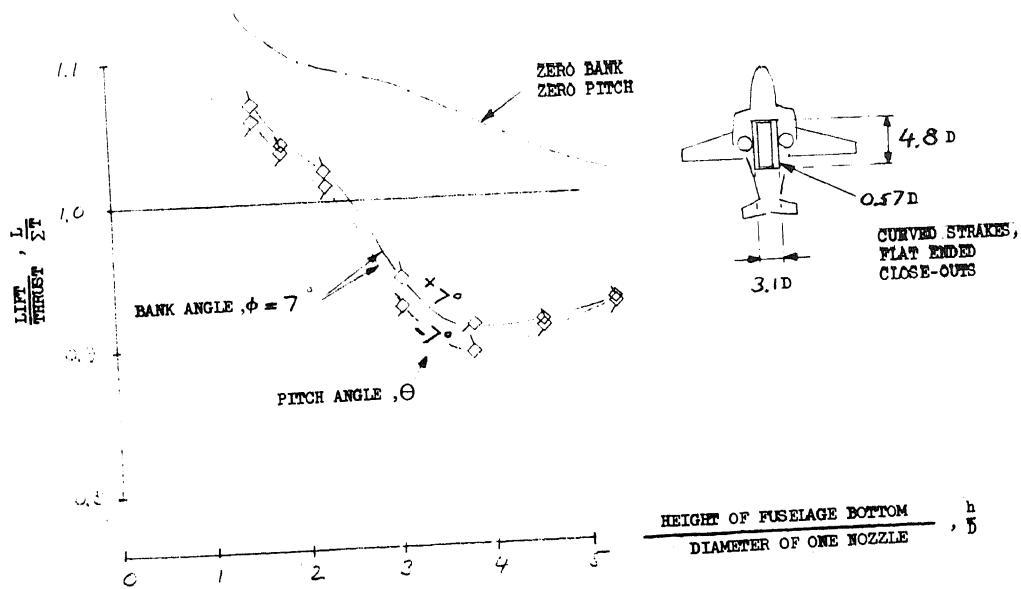


FIGURE 19. EFFECT OF PITCH NOZZLE THRUST

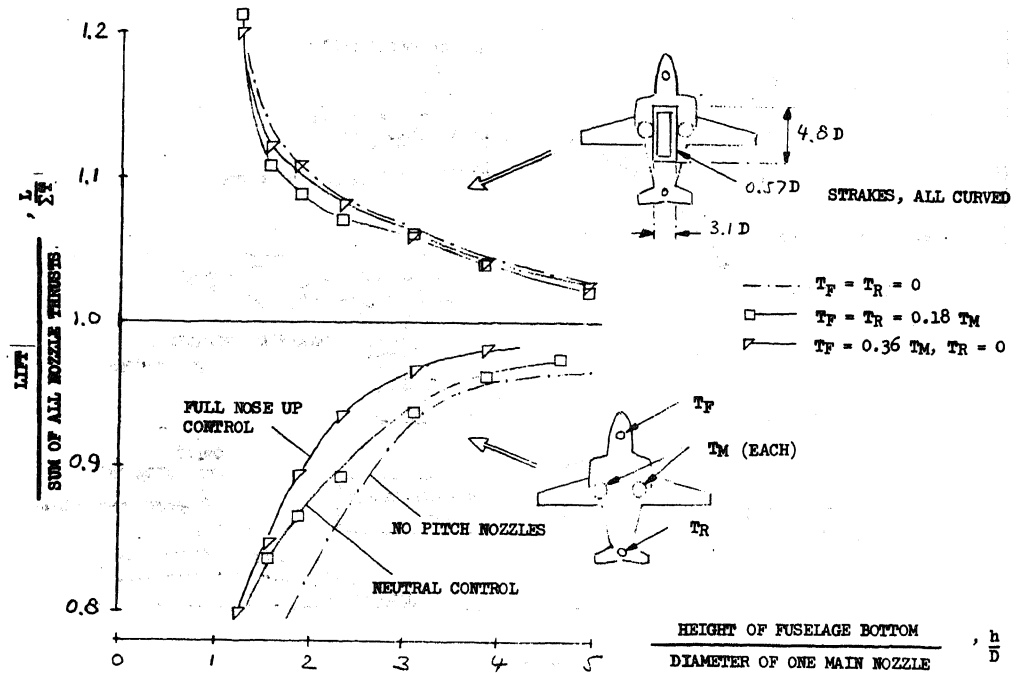


FIGURE 20. EFFECT OF ROLL CONTROL AT VARIOUS PITCH ANGLES
(CONTROL BY DIFFERENTIAL THRUST, $T \pm 20\%$)
(ZERO BANK)

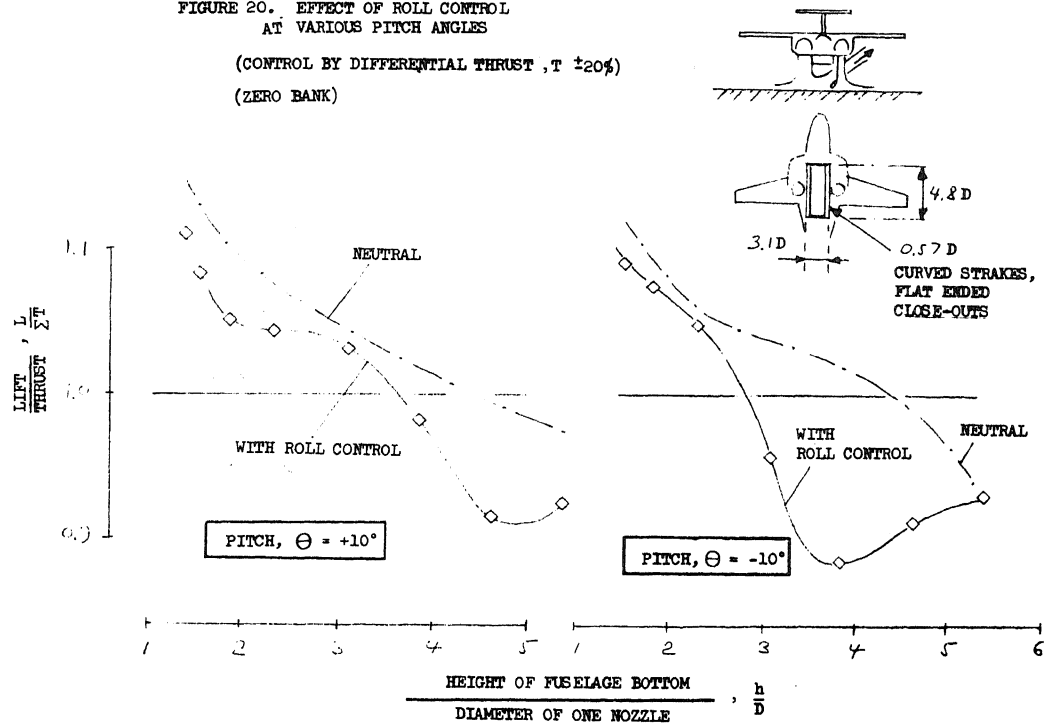


FIGURE 21. REINGESTION CHARACTERISTICS

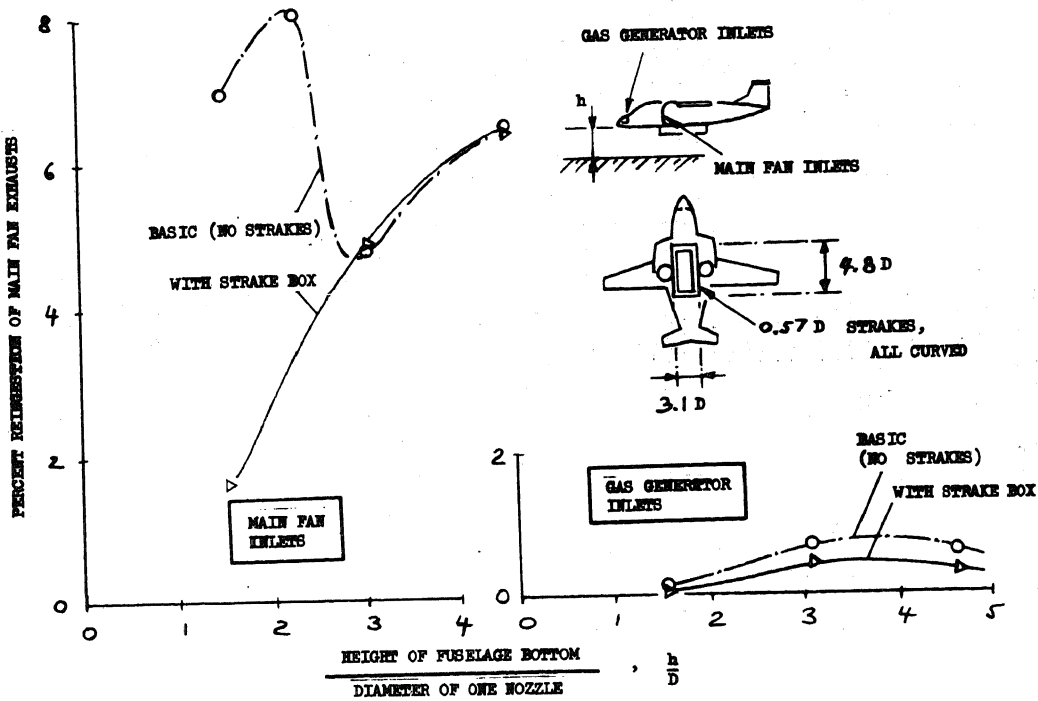
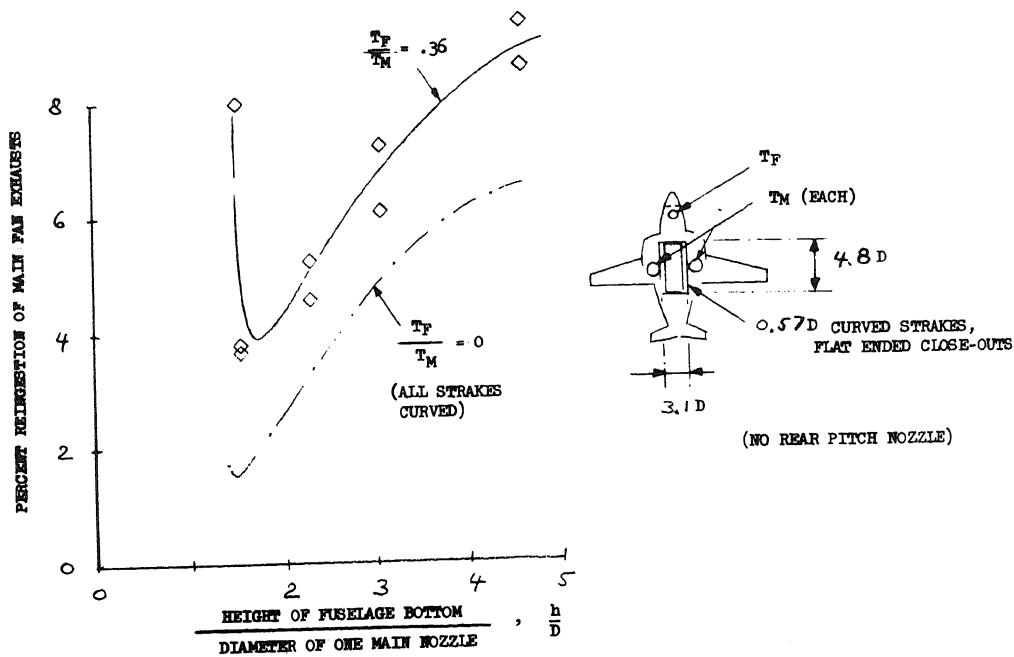


FIGURE 22. REINGESTION CHARACTERISTICS WITH PITCH NOZZLE OPERATING (MAIN FANS)



A SIMPLIFIED APPROACH FOR PRELIMINARY ESTIMATION OF
VTOL INDUCED EFFECTS IN HOVER

Matthew M. Winston,
Leroy F. Albang, and Garl L. Gentry, Jr.

NASA Langley Research Center
Hampton, Virginia 23665

Presented at the
Navy Workshop on Prediction Methods for
Jet V/STOL Propulsion Aerodynamics

July 28-31, 1975
Washington, D.C.

A SIMPLIFIED APPROACH FOR PRELIMINARY ESTIMATION OF VTOL INDUCED EFFECTS IN HOVER

Matthew M. Winston,
Leroy F. Albang, and Garl L. Gentry, Jr.

NASA Langley Research Center
Hampton, Virginia 23665

ABSTRACT

The experimental approach is outlined, the test apparatus in the Langley V/STOL tunnel static test area is described, and sample results are presented. The potential of the technique as an inexpensive tool for preliminary assessment of jet-induced effects in hover is indicated, and possible refinements are discussed.

INTRODUCTION

The design of jet or fan-lift VTOL aircraft requires a detailed knowledge of thrust losses due to engine installation effects. Typically such losses are due to duct-flow phenomena, thrust-vectoring and control-bleed requirements, hot-gas ingestion, and exhaust-flow induced effects. The internal flow losses can be reasonably well determined from isolated tests. Hot-gas ingestion, at this time, appears to be a problem which must be avoided by inlet protection schemes and operational procedures. However, thrust-vectoring and control-bleed requirements, and consequently total thrust requirements, can only be determined when the jet-induced aerodynamic effects are known. One type of induced loss is due to entrainment of ambient air by the jet-exhaust flow resulting in negative pressures on the aircraft undersurfaces as illustrated in figure 1. This condition is predominant for all types of jet arrangements hovering out of ground effect and also for single and multiple clustered jets hovering in ground effect. For multiple dispersed jets hovering in ground effect (as shown in fig. 2), there is an additional induced flow phenomena known as the "fountain effect" which results from the upflow caused by the merging of individual jets following ground impingement. The net induced loads due to entrainment and fountain effects have been shown to be sensitive to many variables, and since adequate prediction methods are not available, extensive testing is required of each new configuration. This paper describes an experimental modeling technique intended to reduce the complexity and expense of using complete powered models for preliminary hover performance studies and gives sample results obtained from two different model configurations. A more comprehensive treatment of this subject is given in reference 1.

SYMBOLS

D_e	equivalent diameter, diameter of a circle having an area equivalent to total jet exit area, m (ft)
h	distance from bottom of model to the ground plane, m (ft)
ΔL	induced lift, N (lb)
T	static thrust, N (lb)

MODEL DESIGN APPROACH AND TEST SETUP

Past experience has shown jet-induced effects in hover to be heavily dependent upon: (1) height above the ground; (2) the ratio of jet-exit area to surrounding aircraft surface area (usually expressed as jet area to total planform area); and (3) jet "quality", a term relating to such factors as turbulence, exit-velocity profiles, dynamic pressure decay rates, etc. It was hypothesized that, since these parameters can be investigated independent of fuselage and wing vertical surface contours, the model airframe can be simulated by a flat plate in the shape of the projected planforms as long as the jet efflux similarity is maintained. Also, since the induced effects are of primary interest, the simulated model should be mounted independently of (but in proper relation to) its propulsion system so that only the induced forces and moments are measured. The apparatus which was subsequently devised is shown schematically in figure 3. Air was fed to a large plenum chamber from a high pressure supply line. From this chamber, air was supplied to individual propulsion simulators. The supply pressure to each simulator was adjustable through manually operated valves. The flat-plate model was mounted on a sting-supported strain-gage balance above the air-supply system with cut-outs provided for the propulsion simulators. The cut-outs were sized to provide a 0.318-cm (0.125-in.) gap between the plate and each propulsion unit. The effect of the gap on the induced loads was subsequently analyzed and determined to be negligible. A 3.63 m² (12-ft²) plywood ground board was supported on adjustable jack screws above the test setup so that pitch and roll attitude variations as well as height variations could be obtained. A photograph of the entire apparatus in the Langley V/STOL tunnel static test area is given as figure 4.

TESTS

The test procedure was designed to provide comparisons of induced forces and moments between complete powered wind-tunnel models and their respective flat-plate representations. The wind-tunnel models had been previously investigated as part of other research programs, and considerable preliminary testing was necessary to ascertain similarity between the jet-efflux characteristics of the propulsion units used during the present study and those installed in the wind-tunnel models. Having achieved satisfactory jet-exit simulation, the models were tested at various heights above the ground at various thrust levels for various pitch and roll attitudes. Measurements of induced lift, pitching moment, and rolling moments were obtained at each test condition. The measured heights from the ground board to the plate surface were subsequently adjusted to account for vertical dimensionality of the wind-tunnel models.

RESULTS

Comparison of induced forces and moments from the flat-plate tests and wind-tunnel model tests are made for two different VTOL configurations. Since both configurations had horizontal tail surfaces mounted high on the vertical tail, tail-off and tail-on data from one of the wind-tunnel models were compared. The results indicated no measurable influence of the high horizontal tail on the induced loads. The flat-plate model of this configuration was fabricated in the tail-off configuration. The second flat-plate model included the horizontal tail in the projected planform area.

Model 1 Results

A three-view sketch of wind-tunnel model number 1 is shown in figure 5. It represented a lift-fan transport aircraft having two lift fans in pods on each wing at the mid-semispan stations and two lift/cruise fans in nacelles at the aft fuselage. Figure 6 shows a sketch of the corresponding flat-plate model. The podded fans were simulated with circular cold air ejectors equipped with circular centerbodies to represent fan hubs. The lift/cruise fans were also simulated with ejectors, but no centerbodies were required since the efflux at the ejector exits was found to be representative of the efflux from the aft fan ducts on the wind-tunnel model. A comparison of the induced lift for this configuration is given in figure 7. The results indicate similar trends over the height range, and the flat-plate model closely predicts the height where the maximum fountain-effect occurs. The difference in magnitude and direction of the induced lift is believed to be partially due to the outboard cant of the fan thrust vectors on the wind-tunnel model, a feature which was not simulated on the flat-plate model. Previous investigations have shown that slight amounts of outboard cant can significantly reduce the positive lift contribution from the fountain effect. The need to simulate nozzle cant angle (and possibly wing dihedral) points out that, while the flat-plate technique may be comparatively simple, attention to certain details is essential to its usefulness.

Model 2 Results

A three-view sketch of model 2 is shown in figure 8. This model represents a fighter configuration having a direct-lift engine in the forward fuselage and lift/cruise engines mounted on each wing. Figure 9 shows a sketch of the corresponding flat-plate model. The propulsion system consisted of cold-air ejectors identical to those used on the wind-tunnel model. The induced-lift comparison for this configuration is made in figure 10. For heights up to four effective diameters, the agreement is good. At greater heights, the induced-lift differences of 2 to 4 percent of the thrust cannot be accounted for by the anhedral of the wind-tunnel model wing. Also, the differences in induced lift do not appear to be attributable to the height differences of the horizontal tails since no fountain occurs in that region, and differences in entrainment effects due to proximity of the flat-plate tail to the rear jets would be expected to give the opposite results. It may be that the longitudinal channels between the fuselage and nacelles on the wind-tunnel model generate secondary effects which do not occur on the flat plate. The results of a limited study involving the attachment of wood contours to the flat plate to simulate the fuselage underside of another model did not show significant effects. However, those tests were not sufficiently comprehensive to rule out the need for this type of refinement to the basic flat-plate technique particularly for models having complex undersurface shapes, wheel wells, stores attachments, etc. For this reason and from considerations mentioned previously, further investigations are planned in order to assess the types and extent of refinements required to improve the usefulness of this technique without introducing undue complications.

SUMMARY

The use of flat-plate models for preliminary estimation of hover-induced effects appears promising based on results from a lift-fan transport configuration and a jet-lift fighter configuration. The experiences gained during the experiment together with the comparative results from the two-dimensional and three-dimensional models indicate the need for attention to certain details and suggest areas where the experimental technique may require refinements.

REFERENCE

1. Albang, Leroy F.: Analysis of Spread Multi-Jet VTOL Aircraft in Hover. Old Dominion University Tech. Rep. 74-T8, Dec. 1974

SINGLE-JET ENTRAINMENT

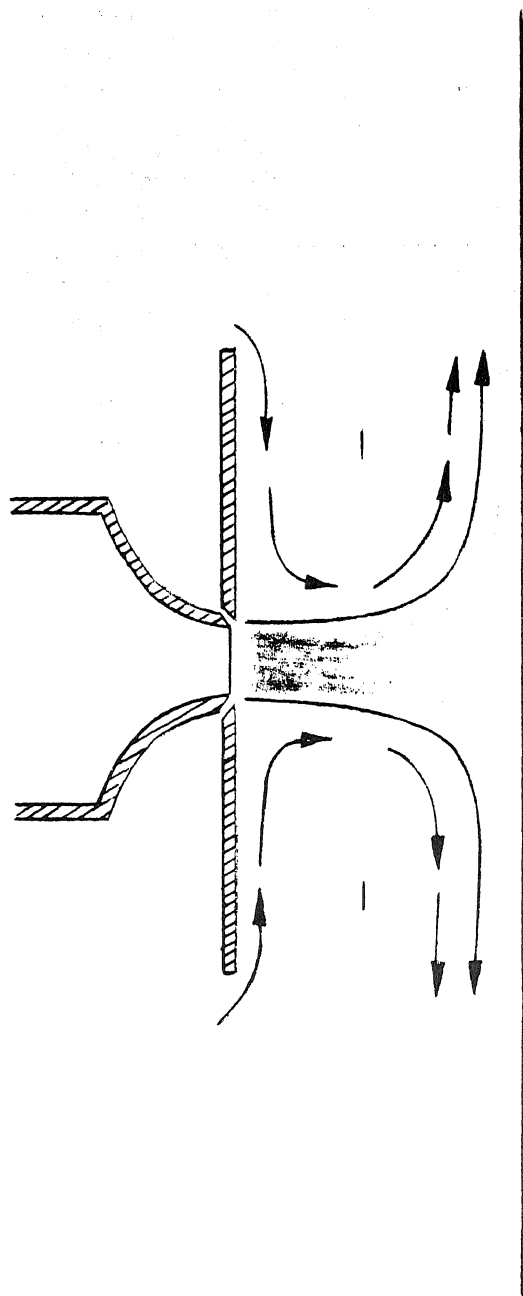


Figure 1

MULTIPLE JET ENTRAINMENT AND FOUNTAIN

220

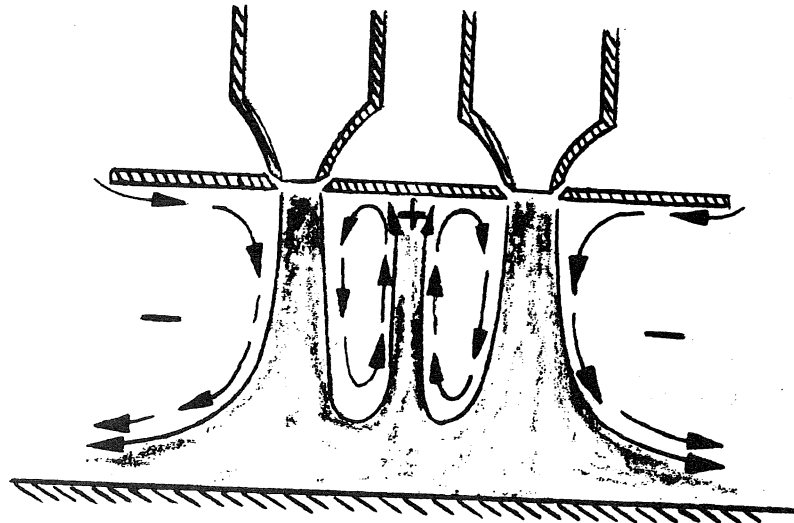


Figure 2



SCHEMATIC OF TEST SETUP

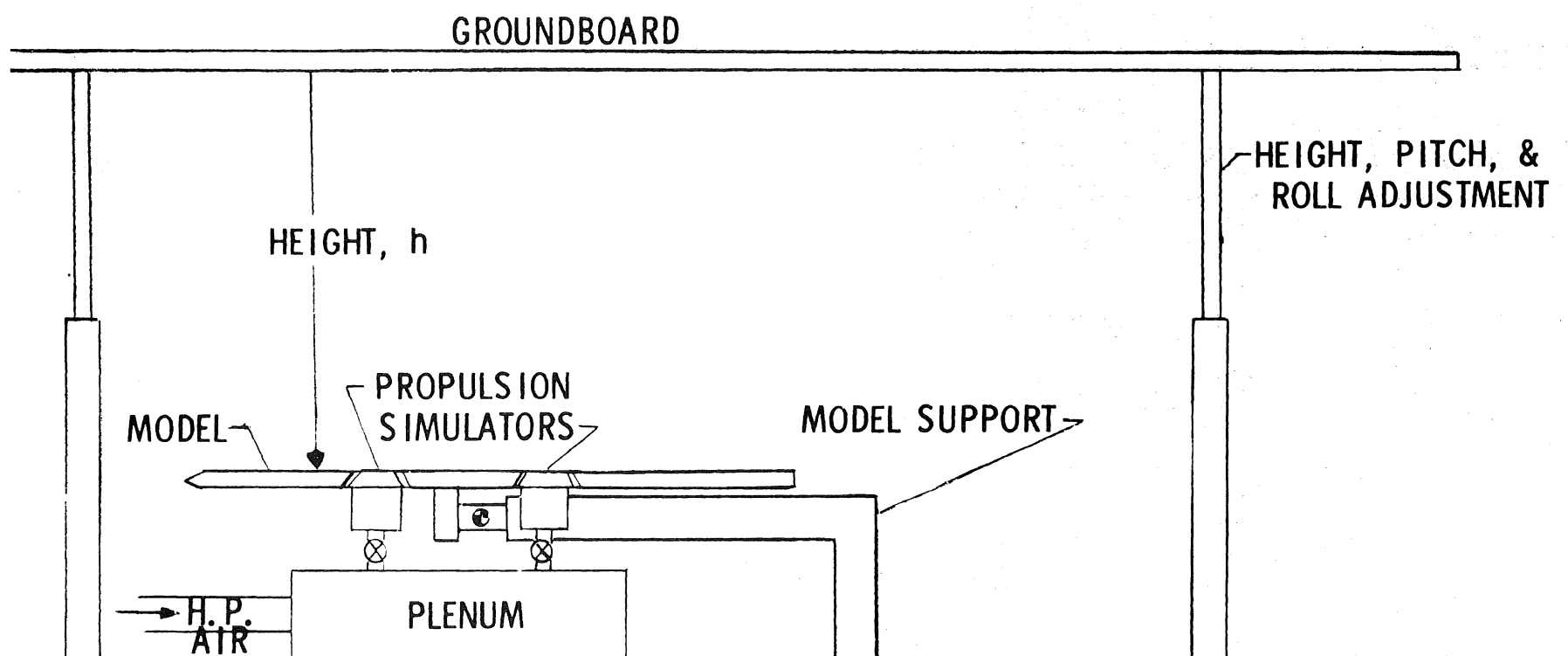
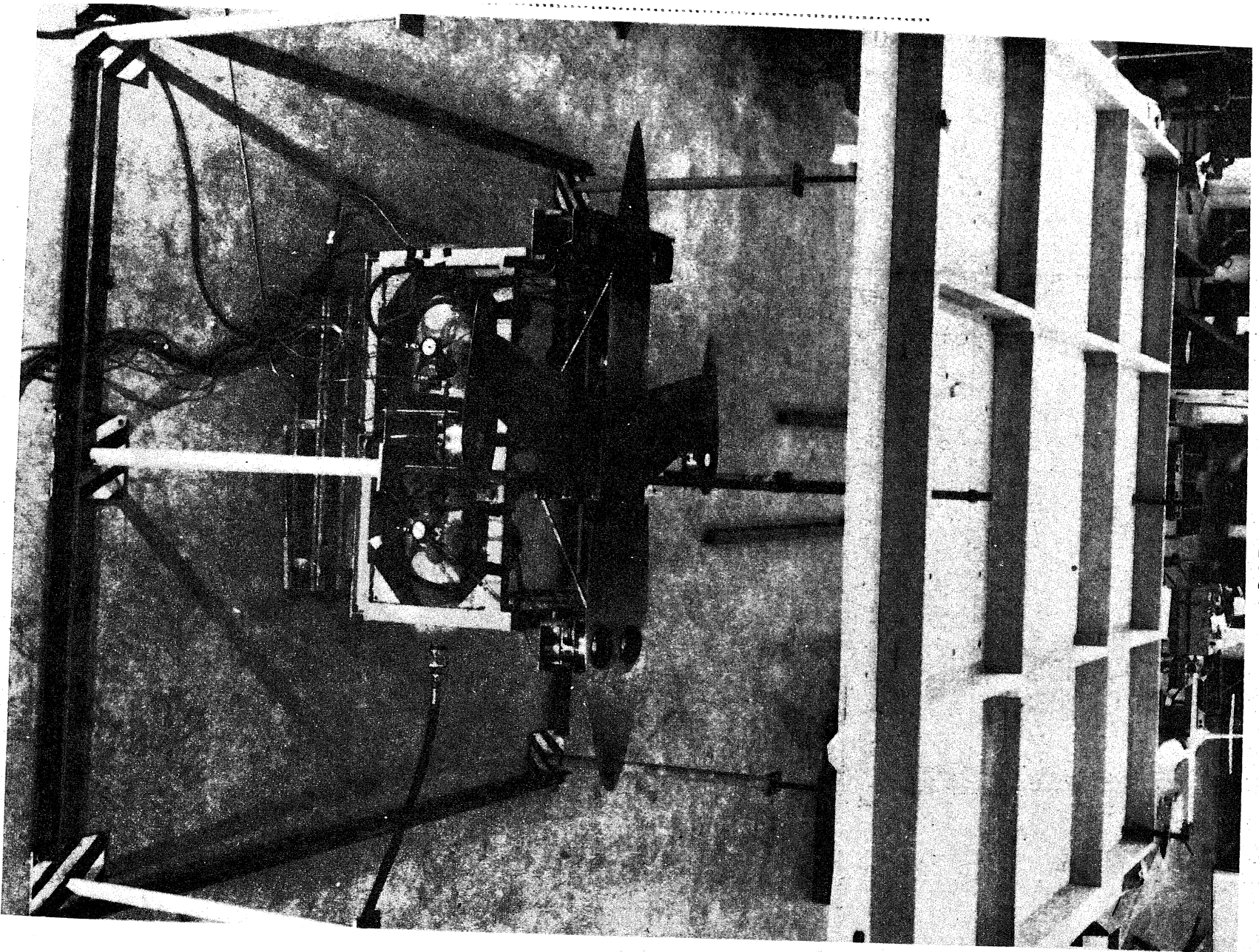


Figure 3



TEST SETUP

Figure 4
222

NASA
L-73-1770

LIFT-FAN TRANSPORT WIND-TUNNEL MODEL

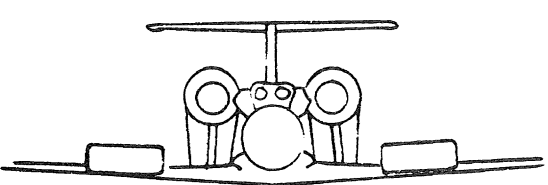
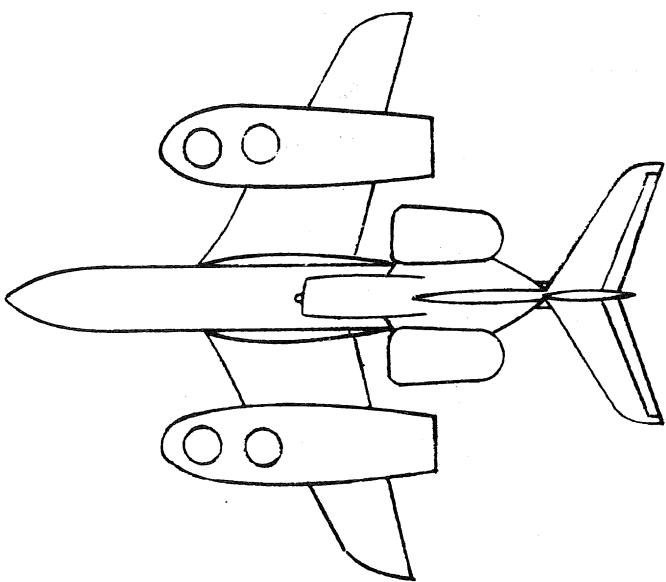


Figure 5

LIFT-FAN TRANSPORT FLAT PLATE MODEL

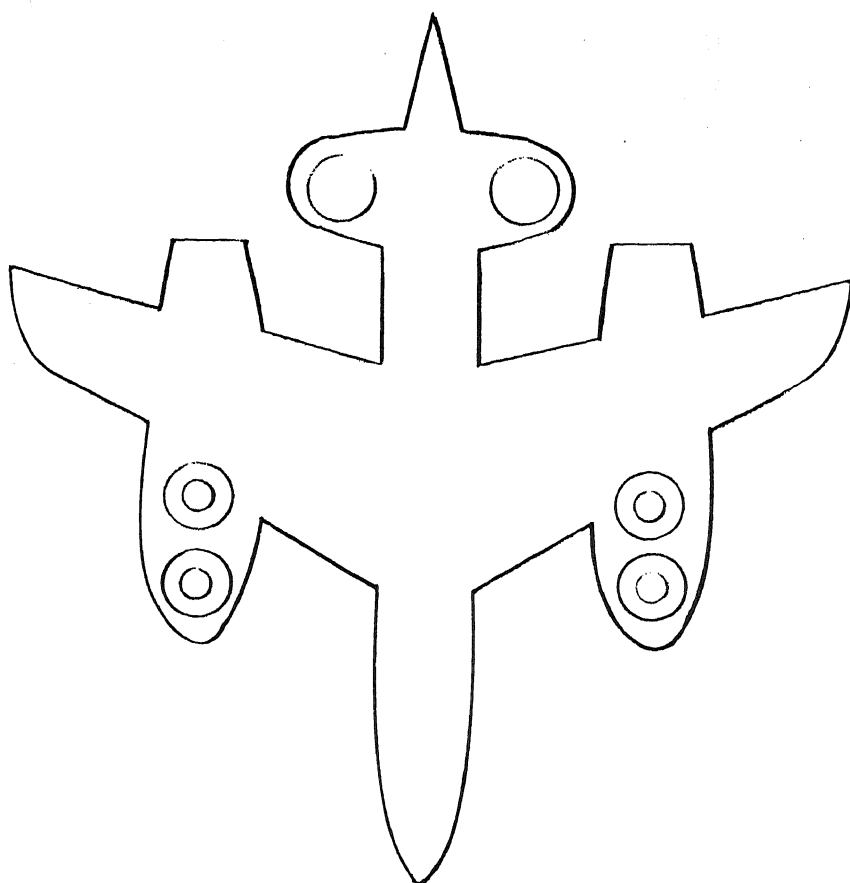


Figure 6

COMPARISON OF INDUCED LIFT IN HOVER

LIFT-FAN TRANSPORT CONFIGURATION

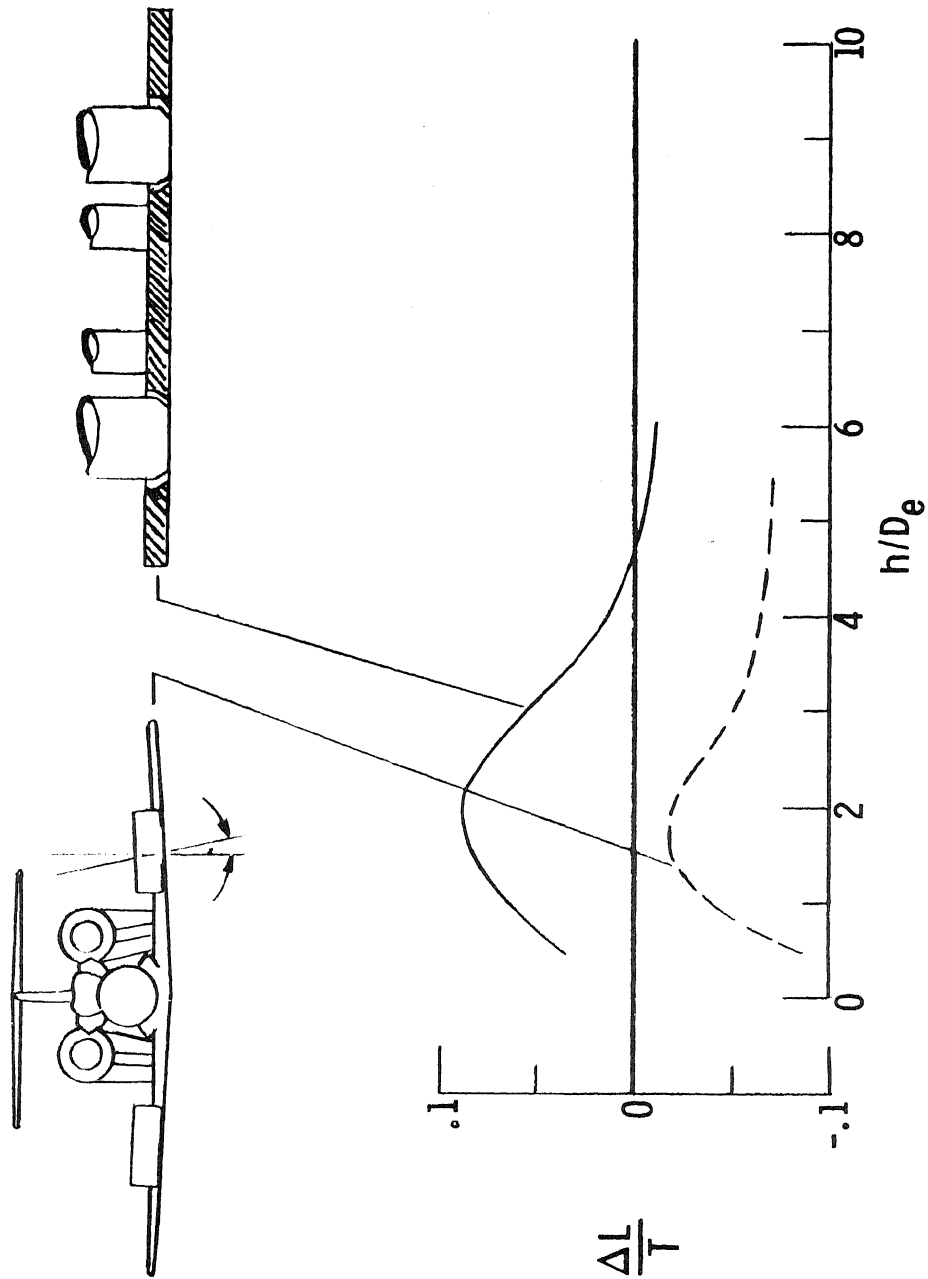


Figure 7



JET FIGHTER WIND-TUNNEL MODEL

226

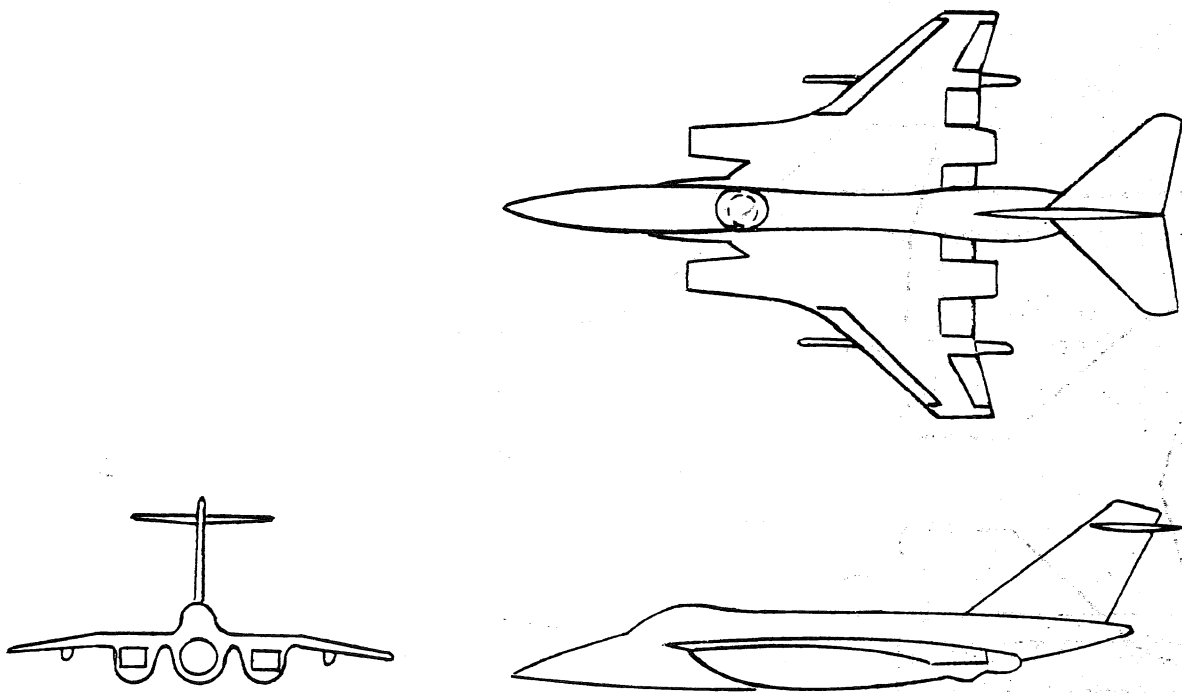


Figure 8



JET FIGHTER FLAT PLATE MODEL

227

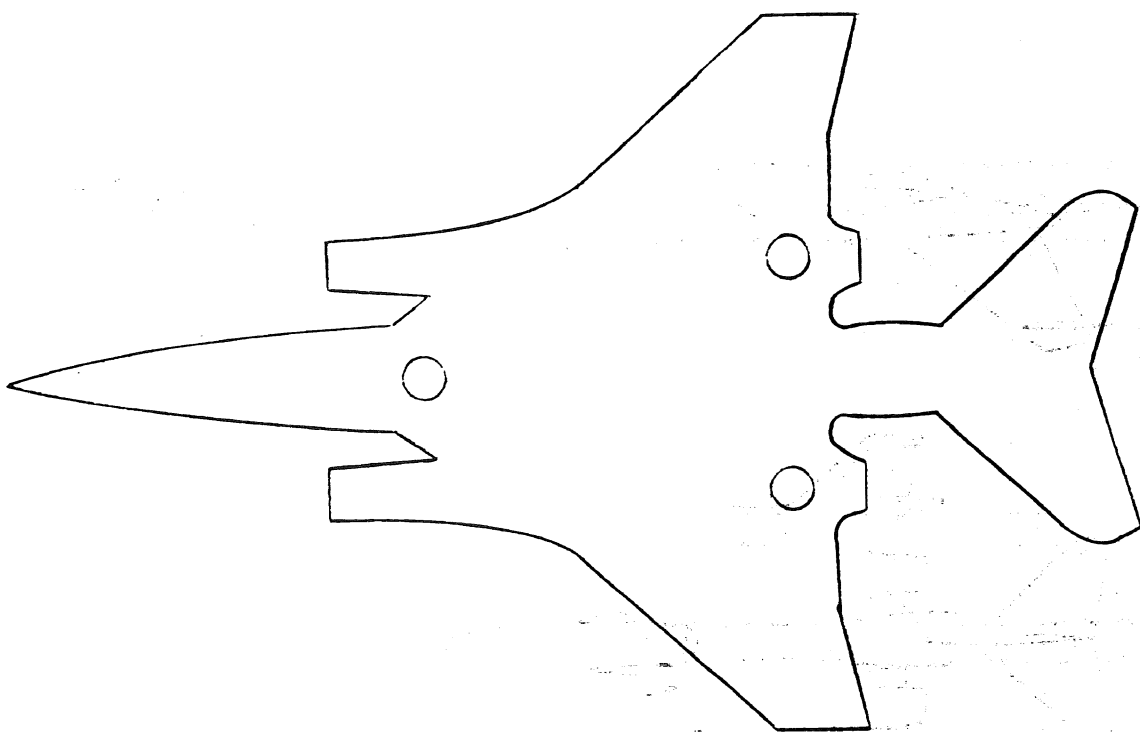


Figure 9



COMPARISON OF INDUCED LIFT IN HOVER

FIGHTER CONFIGURATION

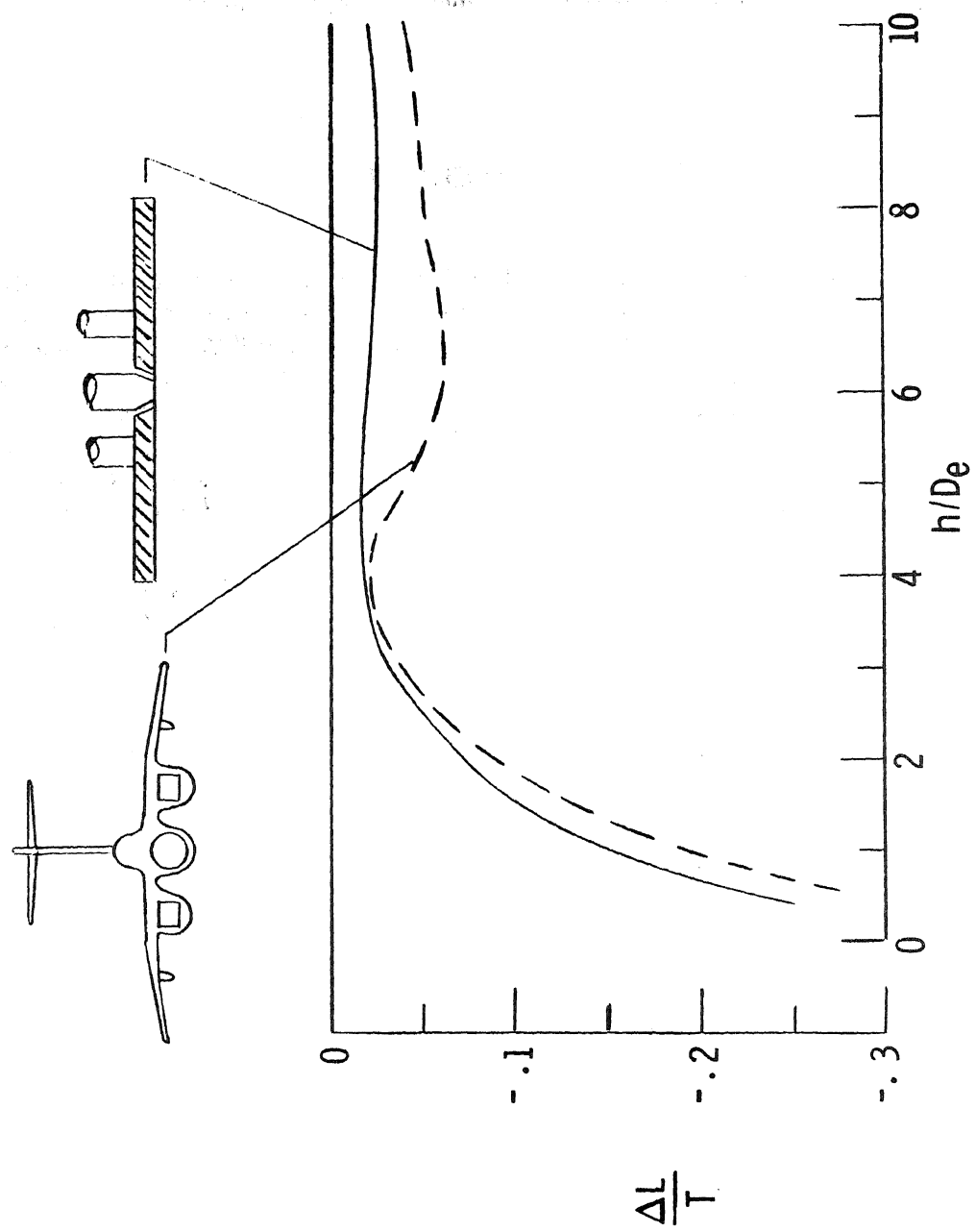


Figure 10

MODEL TESTS OF JET LIFT VTOL AIRCRAFT CONFIGURATION IN THE PROXIMITY OF A RAISED POROUS DECK

by

A. Karemaa

General Dynamics Convair Division

and

E. M. Lynch

Naval Air Systems Command, The United States Navy

ABSTRACT

The vectored thrust or lift-jet type VTOL aircraft may suffer varying degrees of lift degradation when operating close to the ground. Potential reingestion of hot gases during takeoff and landing may result in significant thrust losses, and the propulsion-induced flow about the aircraft may lead to aerodynamic forces or lift losses on the wing and fuselage surfaces. When we consider that the payload of a typical VTOL fighter airplane represents a relatively small percentage of the total weight, it is obvious that the proper control of the propulsion-induced effects and hot gas reingestion can have a significant impact upon the VTOL airplane payload capability. These losses can be reduced by various means including the treatment of the ground environment.

The objective of this program consequently was to generate test data on vectored-thrust and lift-jet type VTOL airplane model configurations operating over a porous surface. It was expected that this approach would reduce engine inlet proximity temperatures, engine induced aerodynamic effects, and improve the on-deck environment.

The test program included a four-jet configuration, a six-jet configuration, and a three-jet configuration, all in the presence of various porous deck arrangements. It appears that an effective porous deck must be designed primarily from the standpoint of hot gas reingestion. Propulsion-system-induced effects will impose certain constraints in respect to deck porosity and porous to solid deck spacing, while the below-deck environmental information will assist in the definition of loads on the deck structure.

The tests demonstrated that a properly designed porous surface with louvers will reduce the propulsion-system-induced effects to the out-of-ground effect levels and lead to significant decreases in the engine inlet proximity temperatures. However, the relatively high deck temperatures could lead to structural design problems. This is especially true when prolonged operation of engines over the porous surface is contemplated.

1. INTRODUCTION

The vectored thrust or lift-jet type VTOL aircraft may suffer varying degrees of lift degradation when operating close to the ground. The exact amount depends upon the aircraft configuration. Potential reingestion of hot gas during takeoff and landing may result in thrust losses on the order of 5 to 10% and the propulsion-induced flow about the aircraft may result in aerodynamic forces on the wing and fuselage surface on the order of an additional 5 to 10%. Consequently, the sum of the reingestion and induced interference effects can equal a significant percentage of the aircraft weight.

When we consider that the payload of a typical VTOL fighter airplane represents a relatively small percentage of the total weight, it is obvious that the proper control of the propulsion-induced effects and hot gas reingestion can have a significant impact upon the VTOL airplane payload capability. This control can be accomplished by flight vehicle design, varying operational techniques and takeoff and landing surface design. The tests conducted by the General Dynamics Convair Division dealt with the latter concept, which consists of a raised porous deck and constitutes one means of controlling these flow phenomena. This porous surface is supported a certain distance above a solid deck. The jet exhaust gases from the airplane operating above this deck pass through the porous surface and exhaust laterally along the solid deck.

Thus, the objective of this program was to generate test data on vectored-thrust and lift-jet type VTOL airplane model configurations operating over a porous surface deck. The program was specifically designed to obtain data on the effect of the various porous deck design parameters on aircraft-induced interference effects and reingestion trends and to obtain data on the ground jet about the porous deck for various VTOL configurations. This document summarizes these test results.

The test (no. 342) was conducted in the General Dynamics recirculation and impingement test facility located near the high-speed wind tunnel. Figure 1 shows an installation diagram of the model and the porous deck for this test program. A photograph of the test installation is presented in Figure 2. Heated high-pressure air was supplied to the model through the Airflow Laboratory Facility. Model interference forces and moments were measured by a six-component internal strain gage balance system. Inlet proximity temperature rise was measured in the vicinity of engine inlets with aspirated thermocouples. Ground jet pressures and temperatures were measured under and around the porous deck model for all configurations. Wind-over-deck conditions were simulated through the use of a wind generator. The test program was divided into four phases:

1. Single-jet study with porous deck arrangements
2. Four-jet configuration study with porous deck arrangements, including a wind-over-deck study and a deck rotation study
3. Six-jet configuration and a porous deck arrangement
4. Three-jet configuration and a porous deck arrangement

Each phase is discussed further in Section 3.

2. TEST EQUIPMENT

This section describes the airplane model arrangements used, the raised porous deck model, the inlet proximity temperature probes, and the wind generator.

2.1 AIRPLANE MODEL DESCRIPTION

The airplane model used during this test program was an existing VTOL research model designed to represent a multitude of fighter type VTOL aircraft.

The basic fuselage shell of the model was constructed of aluminum, steel, and wood. The fuselage shell was designed to be independent of the substructure components, which include the high-pressure plenums and nozzles. The fuselage shell was supported from the substructure by means of a six-component internal strain gage balance that measured the forces and moments on the fuselage and the aerodynamic surfaces.

The fuselage substructure as shown in Figure 3 consists of two high-pressure plenums, an internal balance, water cooling jacket, and a fuselage support bracket. Three sides of each plenum included several two-inch-diameter holes to allow for installation of the various nozzles. Cover plates were provided for the nonblowing positions during various propulsion arrangement tests.

High-pressure air was supplied to the plenums. Flow to each nozzle was throttled through an orifice plate to reduce the pressure level and to establish an even flow distribution. Nozzle calibrations were performed for all of the arrangements tested, which included the thrust, nozzle pressure ratio, weight flow, and plenum pressure relationships. The flow was discharged through a 30-degree conical half-angle nozzle as shown in Figure 4.

The model arrangement tested with four jets operating was composed of the basic fuselage, which had two side inlets faired into a smooth contour and a swept trapezoidal planform wing with 11 degrees of anhedral. The wing had an area of 1.56 square feet, a span of 28 inches, and an aspect ratio of 3.48. The wing was mounted high on the fuselage with the nozzles located below the wing near the wing leading and trailing edges. A horizontal stabilizer was located high on the fuselage aft of the wing. The horizontal stabilizer had a swept trapezoidal planform with a leading edge sweep of 40 degrees, an area of 0.43 square feet, a span of 14.4 inches, and an aspect ratio of 3.35 (Figure 5).

The model arrangement tested with six jets operating was identical to the four-jet arrangement except that the additional jets were added along the model centerline forward and aft of the four-jet arrangement (Figure 6).

The model arrangement tested with the three-jet arrangement was composed of the basic fuselage, a delta wing, and canard. The jet arrangement included two nozzles located forward of the delta wing and one nozzle located aft of the wing trailing edge along the model centerline. The delta wing had a leading edge sweep of 60 degrees, an area of 2.0 square feet, a span of 25.168 inches, and an aspect ratio of 2.2. The canard located above and forward of the delta wing had an area of 0.078 square feet per panel, a span of 3.78 inches per panel, and an aspect ratio of 2.452 (Figure 7).

2.2 POROUS DECK DESCRIPTION

The raised porous deck was nominally a 1/15-scale model of the NAEC (Naval Air Engineering Center) preliminary test design, miscellaneous drawing 0.9583. The deck was 70 feet wide and 70 feet long. To provide porous deck design evaluation, the following flexibility was designed into the porous deck model.

1. Ability to insert three screened grids of different porosities (40, 60, and 80% open)
2. Ability to adjust the porous surface height above the solid surface
3. Ability to install flow directing vanes so that airflow is discharged from both sides
4. Ability to set three vane angles (30, 45, and 60 degrees to the vertical)
5. Ability to change the vane pitch

The porous deck model was composed of four basic components: the interchangeable upper surface, the basic beam substructure, the deck support side panels, and the flow directing vane arrangement.

Figure 8 illustrates a planform view of the porous deck model. Figure 9 shows a side view of the porous deck model with the vane details. Figures 10, 11, and 12 show the porous deck with all of the components assembled, the vane assembly installed under the substructure, and the three screen grids with porosities of 40, 60 and 80% open.

2.3 INLET PROXIMITY TEMPERATURE PROBE DESCRIPTION

One of the objectives of the test program was to assess the effect of porous deck geometry on the flow field temperatures in the vicinity of the engine inlets. Since the model does not include an inlet flow simulation system, the flow field in the vicinity of the inlets was largely determined by a highly turbulent fountain upwash and ground jet recirculation. An unshielded thermocouple in this environment would be subject to unknown velocity errors and radiation effects. Aspirated thermocouples were used to record the inlet proximity temperatures to minimize these errors and to provide a more consistent local flow condition.

The probes were distributed at various heights and distances from the inlet opening location to sample different areas in the flow field that might be induced by an operating inlet. Figure 13 shows the thermocouples arranged for the six-jet-propulsion arrangement. The aspirating lines were connected to an ejector system, which provided the required suction.

2.4 WIND GENERATOR DESCRIPTION

To provide wind-over-deck conditions during the test program, a wind generator was constructed to provide a controlled wind environment in the open air facility. The ejector-driven wind generator is shown in Figure 14. The primary drive flow is supplied from the General Dynamics high-speed wind tunnel compressor system at plenum pressures up to 300 pounds per square inch. Thirty-six primary nozzles are connected to the plenum supply by extended pipes with individual choke plates. The mixing chamber is six feet square, four feet in length, with a square shaped inlet. A 3.5-degree sidewall diffuser leads to an eight-foot-square exit, providing a diffuser area ratio of 1.775 and maximum wind velocities of 60 mph.

3. TEST RESULTS

3.1 PROPULSION-SYSTEM-INDUCED EFFECTS

Lift jets and vectored cruise engines induce air currents about the fuselage and lifting surfaces of a hovering VTOL vehicle. This air movement will produce lift, drag and side forces on the airframe and moments about all airplane axes. The forces along the vertical axes (lift losses or gains) constitute the most important element, since they can add or subtract from the maximum VTOL gross weight. This document consequently addresses and summarizes only these induced lift forces.

The propulsion-system-induced lift forces are extremely sensitive to ground proximity. The lift gains or losses are usually most severe at airplane-to-deck spacing equal to or less than 15 engine nozzle diameters. At altitudes higher than about 17 diameters, most configurations considered will have become asymptotic to a lift loss level equal to a few percent, known as the

out-of-ground-effect loss. This loss persists regardless whether the airplane exhibits lift losses or gains at close proximity to the ground.

The remainder of this section summarizes the propulsion-system-induced lift losses on three VTOL configurations with four, six and three nozzles (see Section 2 for configuration descriptions). The reader will notice that these induced effects are relatively insensitive to the deck parameters such as porosity, louver angles, or porous-to-solid deck spacing. It appears that as long as the vehicle operates over any reasonable porous surface, an out-of-ground-effect condition will be achieved from the standpoint of the induced forces. To put it in other terms, as long as we specify a "porous surface" we can be reasonably assured that it will reduce our propulsion-system-induced effects at hover near the ground. As will be pointed out in Section 3.2, however, the same observation does not apply to inlet proximity temperatures. Consequently, the engine reingestion characteristics will dictate the porous deck design parameters such as porosity, louver angles, and porous-to-solid deck spacing.

All data presented in this section was obtained with exhaust gas temperatures at about 500F. The nozzle pressure ratio was 2.0 for all configurations except the three-nozzle case, where 2.6 was used. This spacing of louvers or vanes below the porous deck was a consistent 0.5 engine diameter (0.705 inch).

Induced Effects on a Model with Four Nozzles – The induced lift characteristics of a four-nozzle configuration operating over a solid surface are depicted in Figure 15. A level vehicle exhibits a strong positive ground effect (lift gain) for all shown distances higher than 2.8 diameters above the ground plane. This positive ground effect, however, decreases when we move from 12 to 15 diameters above ground, and we know from other tests that it will become slightly negative above 18 nozzle diameters.

The other significant effect exhibited by Figure 15 is that there is a large reduction in this positive ground effect with changes in airplane pitch or roll attitude. This means that a similar vehicle will experience lift losses when it executes pitch or roll maneuvers during hover close to the ground. Although the positive ground effect is beneficial in that it helps arrest the rate of sink during vertical landings, the lift losses with attitude are not.

This last problem is eliminated to a large extent by operating over a porous surface (Figure 16). As can be seen, the maximum deviations with attitude are about 1%. This stabilizing effect of the porous surface is demonstrated once more in Figure 17, where induced lift losses are plotted as a function of pitch angle.

Next let us investigate the effect of louvers. Louvers reduce the area between the porous and the solid deck. For example, louvers set at 45 degrees reduce the space by 0.71 nozzle diameters (the vanes have a chord equal to 1.0 nozzle diameter). Thus, for a porous-to-solid deck spacing of 2.0 diameters, the distance left for gas escape route is about 0.97 nozzle diameter (the beam substructure occupies another 0.32D; see Figure 9). Figure 18 again illustrates the effect of deck spacing. With the exception of 2.0 diameters, the spacing has no significant effect. Figure 18 indicates that the induced effects are minimized as long as we have a clearance between the two decks equal to at least 1.53 to 1.68 nozzle diameters. Note that this conclusion applies to 60% porosity.

The effect of wind is especially significant from hot gas reingestion considerations. Its impact on propulsion-system-induced effects is generally small. There were some interesting effects, however.

First let us examine the model over a porous deck at zero degree angle of attack and with wind approaching head-on (zero degree). Figure 19 indicates the usual data band for 0, 10 and 20 knots wind speed. We can say that these winds have no significant effect on the propulsion-system-induced lift losses or gains. (Note that the data does not include the aerodynamic lift on the wing and fuselage. Only incremental forces caused by propulsion system or nozzle operation are shown.) The 40-knot wind case, however, shows a sharp increase in lift losses. This effect, summarized in Figure 20, is consistent with similar results obtained by VFW in Germany, for example.

A check was made to determine if a model attitude change would significantly increase its sensitivity to wind (Figure 21). The findings were negative. Runs were also conducted with negative angles of attack with similar results. (See Reference 4.) Next the runs were repeated with the wind from 45 degrees off the starboard bow (Figure 22). The results again indicate small if any effect. Unfortunately, wind velocities above 20 knots were not used for these cases. It can be noticed, however, that the 20-knot data is on the negative side of the data band (Figure 22).

During the test planning, concern was expressed about the effect of the airplane model orientation in respect to the deck or the louvers. To determine if any adverse effects existed, the deck was rotated under the model to various angles (10, 30, and 90°). The position of the model over the center of the deck was maintained. The results of these tests, shown in Figure 23, indicate no significant effect as far as the induced lift forces are concerned.

The test results of the four-nozzle configuration over the porous surface can be summarized as follows. First, the porous surface will reduce significantly the changes in propulsion-system-induced effects with airplane attitude changes. This should lead to safer VTOL operations. The vane or louver angles and deck orientation had no effect on induced forces. Neither did the porous-to-solid deck spacing, as long as a minimum space equal to about 1.6-engine diameters was maintained. Low winds nor their direction had any significant effect on induced lift forces. For conditions in excess of 20 knots, there was found to be a further increase in induced-lift losses.

Perhaps the most significant conclusion of this test data is that from the propulsion-system-induced-effects standpoint, most of the porous deck design parameters are not critical. As long as there is a porous surface (perhaps 40 to 80% porosity) reasonably spaced above the solid surface (with about 1.6-engine exhaust diameters of clearance), the concept will largely reduce or eliminate propulsion-system-induced effects. This characteristic is to a certain extent fortunate, since the reingestion trends were found to be much more sensitive to the porous deck design parameters.

Induced Effects on a Model with Six Nozzles — The propulsion-system-induced effects of a configuration with six nozzles closely resemble the data from the four-nozzle case. Both exhibit a large positive ground effect over a solid surface and both are sensitive to airplane attitude changes (attitude changes lead to increased induced lift losses). These similarities can be determined from Figures 15 and 24. The positive ground effect disappears when the model was placed over a surface with louvers (Figure 25). When we consider that six nozzles produce about 50% more gas per given time, then we can estimate the minimum deck spacing as 2.72 engine diameters, based on the four-nozzle model data ($1.5 \times 1.6 + 0.32$). This trend seems to be verified to some extent by Figure 25. The porous-to-solid deck spacing at 2.5 engine diameters seems to be inadequate to produce a complete "out-of-ground-effect" condition.

The model with six nozzles was not tested in the presence of wind.

The six-nozzle concept, like the four-nozzle design, is relatively insensitive to the porous deck design parameters. For a deck with a 60% porosity and reasonable solid-to-porous deck spacing (estimated as a clearance equal to a minimum of 2.4 engine diameters), most propulsion-system-induced effects will be eliminated.

Increased Effects on a Model with Three Nozzles – The three-nozzle concept is the only arrangement that exhibited propulsion-system-induced lift losses for all distances above a solid deck (Figure 26). These losses were subsequently reduced to a nominal “out-of-ground-effect” level (1% or less in this case) by operating the model over a 60% porous deck with louvers. These results corroborate the data in Reference 4, where the same model was tested over 20, 40, and 60% porous surfaces without louvers and with a solid-to-porous deck spacing of 8.5 nozzle diameters. It appears that for this concept, a deck clearance of 1.48 nozzle diameters is more than adequate ($2.5 - 0.32 - 0.7 = 1.48$). The porosity should be kept at 40% or above, however.

3.2 ENGINE INLET PROXIMITY TEMPERATURES

Jet upwash temperatures in the vicinity of the engine inlets were recorded with aspirated thermocouples as described in Section 2.3. A sample of the graphical data (Figure 27) presents individual temperatures as a function of model height. The ordinate is inlet proximity temperature in excess of ambient temperature: $\Delta T_I = T_I - T_O$, where:

T_I = inlet proximity thermocouple readings (F)

T_O = ambient atmospheric temperatures (F)

The abscissa is nondimensional model height (H/D) where:

H = model height above deck (in.)

D = single nozzle diameter (in.)

Probe and inlet definitions are described in Section 2.3. The sample presentation (Figure 27) shows the trend of inlet proximity temperatures with model height for the four-nozzle configuration over a solid deck. The wide distribution of temperatures in each inlet vicinity is indicative of the high gradients experienced in jet fountains. The four-nozzle configuration develops a complex fountain interaction under the fuselage aft of the inlet area. A portion of the fountain flows forward under the fuselage, entraining ambient air in a highly turbulent mixing process. The resultant streams diffuse into the vicinity of the inlets, producing the thermal distributions indicated by the individual thermocouple readings. In addition to the high-temperature gradients experienced in each inlet area, there is a large differential in temperature between the left- and right-hand inlets. This imbalance indicates that the forward fountain flow direction deviates from the model axis. Flow direction is extremely sensitive to the balance in individual nozzle jet flow conditions; small deviations in nozzle size, nozzle angle, or pressure ratio would induce large fountain flow deflections.

Since the objective of this program is to provide an index of inlet reingestion temperatures, the individual thermocouples closest to each of the simulated inlet faces were averaged and used in the following discussion to measure the effect of test parameters on inlet proximity temperatures. Thus, for the four-nozzle configuration:

$$\Delta T_{I_{AV}} = \frac{(T_I)_5 + (T_I)_{10}}{2}$$

with thermocouples 5 and 10 defined in Reference 5. The choice of thermocouples for defining $\Delta T_{I_{AV}}$ is somewhat academic, since the temperature distribution collapsed with porous deck improvements and all temperature indications followed consistent trends. The three- and six-nozzle configurations exhibited comparatively low temperature distributions, and the same thermocouples were used for defining $\Delta T_{I_{AV}}$. All data was recorded at nominal jet temperatures of 450F, with the exception of one run. During that test, the jet temperature of the forward two nozzles in the four-nozzle configuration was varied over a range of 350F. Model height was held constant ($H/D = 4$), over a solid ground plane.

The variation of $\Delta T_{I_{AV}}$ with ΔT_{TE} (forward jet exhaust temperature) is shown in Figure 28. Decreasing forward jet temperature reduces the inlet proximity temperature in a consistent trend.

In the following discussion of the effect of configurational changes on $\Delta T_{I_{AV}}$, all comparisons are based on temperature readings at estimated landing gear height ($H/D = 2.5$) since, in most instances, these data points represented the highest level of temperature recorded.

Engine Inlet Proximity Temperatures on a Model with Four Nozzles – The four-nozzle configuration was tested over porous decks of various porosities and deck spacing (h_{pd}/D) as described in Section 2.2. Initially, no vanes were used. Of the combinations tested, 40% porosity with a two-nozzle-diameter deck spacing demonstrated the highest improvement by reducing $\Delta T_{I_{AV}}$ from 75F over solid deck to 10F over the porous surface (Figure 29). Well defined minimum temperatures were attained at 40% porosity with deck spacings of 2 and 2.5 nozzle diameters. The steep slope of both curves in the area of 40% porosity indicates that lower porosity (not tested) might have produced even lower temperatures. The flow mechanism that generates these results was not investigated in this program. The data indicates, however, that the low porosity range reduces fountain strength and that low deck spacing decreases ground jet entrainment. The two mechanisms combine to carry off hot gases beyond the inlet flow fields.

The addition of vanes changed the optimum deck spacing from 2 to 4 nozzle diameters, with temperature at 2.5-nozzle-diameter spacing being only slightly higher than the temperature at 4 nozzle diameters (Figure 30). Both minima occur at a vane angle setting of 45 degrees. Since the vane structure occupies a space of about one nozzle diameter below the porous deck, it is not surprising that the optimum deck spacing is higher than the corresponding value with the porous surface alone.

Comparing the best combination of deck parameters tested:

Without vanes (porosity = 40%, $h_{pd}/D = 2$), $\Delta T_{I_{AV}} = 10F$

With 45-degree vanes (porosity = 60%, $h_{pd}/D = 4$), $\Delta T_{I_{AV}} = 3F$

Model pitch attitude changes of five degrees in negative and positive directions reduced $\Delta T_{I_{AV}}$ over a solid ground plane and also over a 60% porosity deck (Figure 31). The addition of 45-degree vanes to the porous deck reversed this relationship. The pitched model temperatures were reduced by the porous deck, but the addition of vanes had only a small effect here. The angularity between jet flow and porous deck openings with the pitched model reduces the effective deck porosity. This effect would explain the lower temperatures observed for the pitched model with porous deck alone, since 40% porosity was optimum (Figure 29). The addition of vanes provides another reduction in effective porosity by turning the flow angle and may have reduced the effective porosity well below the 40% optimum level, so that $\Delta T_{I_{AV}}$ was increased (Figure 31). Winds of 10

and 20 knots cleared the gas flow away from the inlet flow fields, and negligible $\Delta T_{I_{AV}}$ was recorded at all model attitudes.

At 10 degrees of bank angle on the model over a solid ground plane, the $\Delta T_{I_{AV}}$ was reduced to 2F (Figure 32), from a value of 100F for a level model. Apparently, the bank angle diminished fountain strength to the point where the hot gases were entrained by the ground jets and swept away from the inlet flow fields. Porous decks alone were relatively insensitive to model bank angles. The addition of vanes improved porous deck performance considerably at the 10-degree model bank angle. The effect of wind was to reduce the recorded temperatures to the local ambient level.

Porous deck orientation with respect to the model was varied and data recorded at 0, 10, 30, and 90 degrees (Figure 33). The value of $\Delta T_{I_{AV}}$ rose considerably at the 10-degree setting, dropped to zero at the 30-degree setting, and rose slightly at 90 degrees to the zero-degree value. No $\Delta T_{I_{AV}}$ was recorded with winds at the 10- and 30-degree settings of porous deck orientation.

The effect of wind direction (ψ_w) was evaluated at head-on to the model (0 degree), at 10 degrees and at 45 degrees at various model attitudes (Table I). Temperature levels were low at both 10- and 20-knot wind velocities. The 45-degree wind azimuth produced slightly higher levels than the 0- and 10-degree azimuth settings.

Engine Inlet Proximity Temperatures on a Model with Six Nozzles – The six-nozzle configuration exhibited low values of $\Delta T_{I_{AV}}$ in the proximity of both cruise and lift inlets over a solid deck (Figure 34). Porous decks of 60 and 80% porosity vanes exhibited higher temperatures than those recorded over the solid deck. Data trends indicate the possibility that lower porosities (20 to 40%) may demonstrate temperature levels lower than those for the solid-deck case. The addition of 45-degree vanes to a 60% porosity deck improved temperature levels substantially. At an h_{pd}/D of four nozzle diameters, $\Delta T_{I_{AV}}$ was decreased below the solid-deck values.

The six-nozzle configuration was relatively insensitive to model attitude in pitch and roll when operated over a solid ground plane (Figures 35 and 36). Temperatures levels increased or held essentially constant with model attitude changes when operated over a deck of 60% porosity.

Engine Inlet Proximity Temperatures on a Model with Three Nozzles – Testing the three-nozzle configuration was limited to operation over a porous deck of 60% porosity at an h_{pd}/D of 2.5 with 45-degree vanes. At landing gear height ($H/D = 2.5$), both lift and cruise inlet proximity temperatures averaged 11F.

4. SUMMARY

The test results involving a porous deck and a model representing a VTOL vehicle with three propulsion system arrangements have been summarized under two categories: propulsion-system-induced effects and engine inlet proximity temperatures. It appears that a porous deck will be designed primarily from the standpoint of hot gas reingestion while propulsion-system-induced effects will impose certain constraints in respect to deck porosity and porous-to-solid deck spacing.

From the standpoint of propulsion-system-induced effects, any surface with the porosity in the 40 to 80% range will reduce these effects to out-of-ground-effect level. From other tests (Reference 4), we have determined that a surface with 20% porosity is marginal in this respect, especially with the airplane close to the deck or porous surface. Consequently, we have selected 40 to 80% as the preferred porosity range from induced effects standpoint (Figure 37).

The examination of the induced-effects data (Section 3.1) also reveals that although a wide variation in the porous-to-solid deck spacing has no significant impact here, there are certain minimum distances that should be maintained. Specifically, the clearance or space between the two decks is critical. This is the area occupied by gas or ground jet, and the evidence indicates that very closely spaced decks will lead to back-pressure conditions, especially when the model is close to the surfaces. To put it in other terms, adequate space must be allowed for the gases to escape between the two surfaces.

This minimum distance, based on data obtained from tests with various nozzle configurations, is shown in Figure 38. Note that the data assumes that the gas is escaping in two principal directions. Should the louvers deflect the flow in one direction only, the clearance values should be doubled.

The test results involving the engine inlet proximity temperatures produced several interesting results. First, a six-nozzle design had low temperatures here while a model with four nozzles produced extremely high temperatures (the reader is cautioned that the information in this report refers to approximate steady-state or hover conditions only. Other tests have indicated that a rapidly moving groundboard or model can reduce significantly the recorded engine inlet proximity temperatures). The location of a single high-velocity ground jet underneath the inlet locations (for the six-nozzle design) was found to be highly favorable. This can be seen from Figures 29 and 34 when we compare the data at zero % porosity.

Another significant result was obtained when the forward nozzle exhaust gas temperatures were reduced. The data in Figures 28 indicates that the engine proximity temperatures are a function of the forward nozzle exhaust gas temperature and are relatively insensitive to the aft nozzle exhaust gas characteristics.

The operation of the four-nozzle configuration over a porous deck can be summarized as follows. The deck without vanes leads to significant reductions in inlet proximity temperatures. A porous-to-solid deck spacing of 2 nozzle diameters was found to be especially favorable here (Figure 29). The addition of louvers showed an additional improvement. Compare the data in Figure 30 (with vanes and for 60% deck porosity) to the corresponding data (at 60% porosity) in Figure 29. With vanes, however, allowances must be made for the space occupied by these devices. The porous-to-solid deck spacing is consequently increased to 2.5 to 4 nozzle diameters. This provides a below-deck clearance at about 1.5 to 3 diameters. (This information is recorded as 1.75 in Figure 38.)

Tests involving the relative alignment of the model to porous deck (with louvers) indicated that a 10-degree misalignment leads to increased engine proximity temperatures. Other orientations reduced the temperatures. The wind also had a favorable effect. Before a porous surface is designed for a full-scale vehicle, these phenomena should be investigated further.

The porous deck without louvers had a completely unfavorable effect on the six-nozzle configuration. Engine inlet proximity temperatures increased for all porosity levels tested. Only the addition of vanes (at 60% deck porosity) lead to reduced temperatures as compared to operations over a solid surface. A solid-to-porous deck spacing of 4.0 nozzle diameters had to be maintained to get this effect.

The reingestion trends obtained from these tests indicate that vanes are necessary to obtain reduced temperature levels, that vanes set at 45 degrees work in a satisfactory manner, and that a porosity of 60% appears adequate (Figure 37). However, certain minimum clearances between the porous and the solid deck must be maintained (Figure 38).

The below-deck environment was also investigated during these tests in terms of peak velocity and temperature parameters. This data was nondimensionalized with respect to the nozzle exit and ambient conditions. Several observations can be made with respect to the ground jet below the porous deck. First, the peak gas velocities decrease about two to three times more rapidly than the peak temperatures. Changing deck design parameters such as vane angles, porosity and porous-to-solid deck spacing was found to have only a small effect on these ground jet characteristics. The wind also failed to have a significant impact here. The model attitude change from level conditions, however, was found to lead to higher peak temperature and velocities in the ground jet.

The highest temperatures and velocities recorded for each configuration have been summarized in Figure 39. The data shows that the configuration with four nozzles produced the most severe conditions. The reader is cautioned that this is directly related to the fact that a large data base exists for this specific configuration. Had the single-, three-, and six-nozzle configurations also been pitched and rolled over the porous surfaces, their maximum temperatures and velocities would have undoubtedly increased. We should also keep in mind the fact that the porous deck under consideration deflected the gas in two directions. Consequently, this data cannot be applied directly to deck concepts where the gas is deflected to one side only.

The examination of Figure 39 can only lead to one conclusion: the porous deck structural design could represent a major thermodynamic problem, especially when exhaust gases in the 1,000 to 2,000F range are to be transported and disposed.

6. REFERENCES

1. Tyler, S.P., "Pretest Report for Model Tests of Jet Lift VTOL Aircraft Configurations in Proximity to a Raised Porous Deck," General Dynamics Convair Report TR-74-CA-01(P), February 1974.
2. Weber, H.A., "Calibration of the Ejector-Driven Wind Generator," General Dynamics Convair Report T-VFA-073, July 1974.
3. Karemaa, A., Tyler, S.P., Weber, H.A., "Model Tests of Jet Lift VTOL Aircraft Configurations in Proximity to a Raised Porous Deck," General Dynamics Convair Report CASD-NSC-74-006, Volumes I through XIII, August 1974.
4. Karemaa, A., Ramsey, J. C., "Aerodynamic Methodology for the Prediction of Jet-Induced Lift in Hover," General Dynamics Convair Report CASD-ERR-73-012, December 1973.
5. Karemaa, A., Tyler, S.P., Weber, H.A., "Summary of Model Tests of Jet Lift VTOL Aircraft Configurations in Proximity to a Raised Porous Deck," General Dynamics Convair Report CASD-NSC-75-001, March 1975.

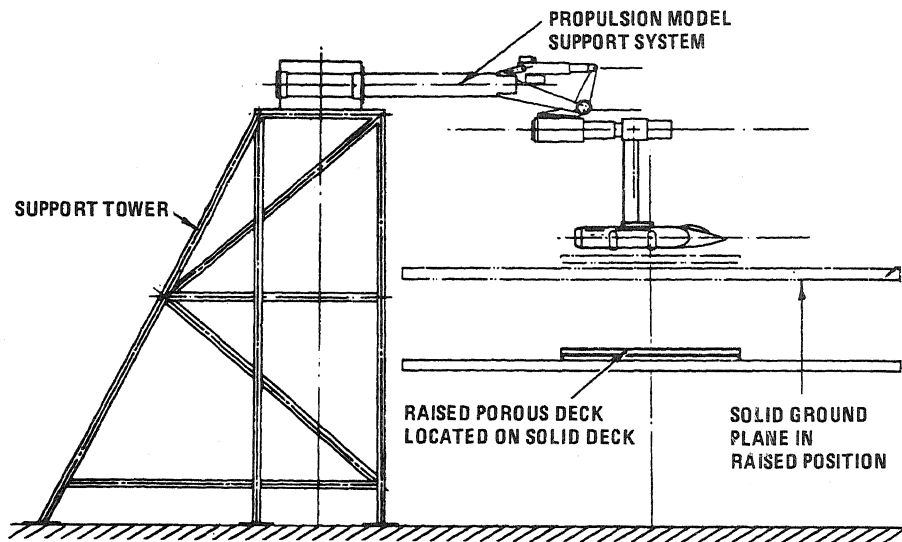


Figure 1. The test installation includes a movable ground plane and a model that can be pitched and rolled.

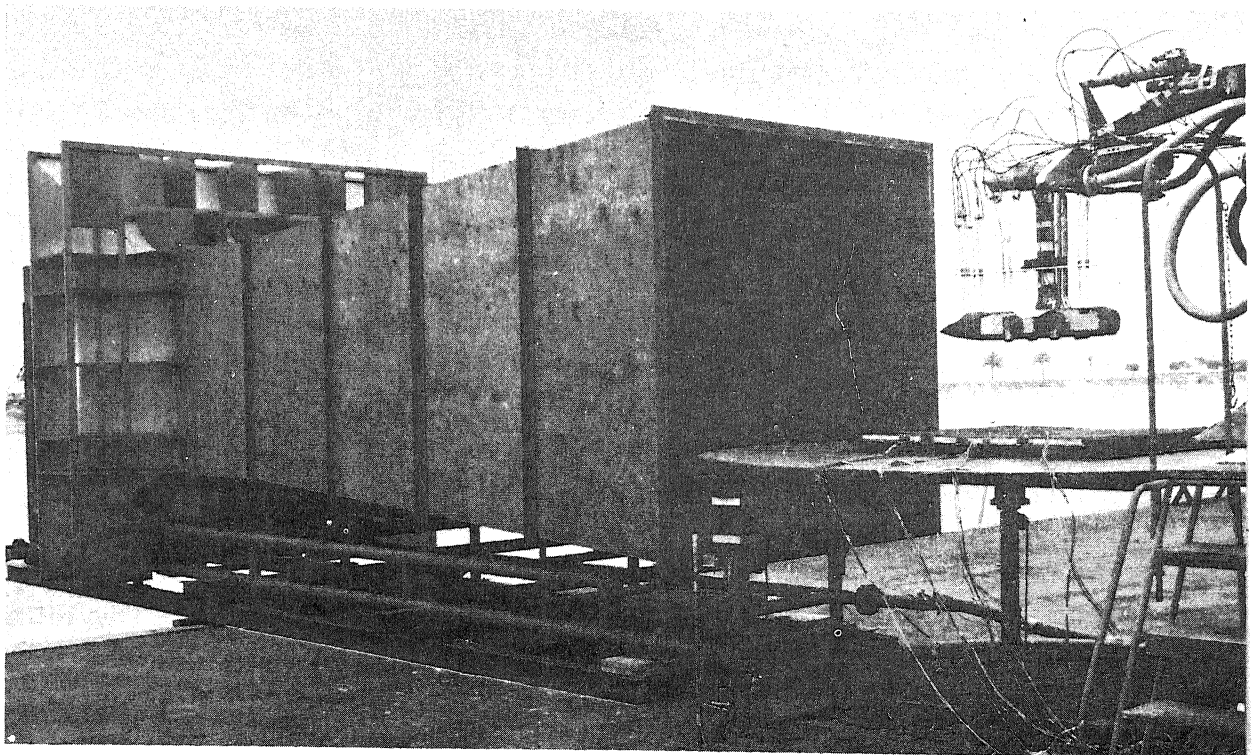


Figure 2. The test facility included a wind generator and a movable 12-foot-diameter ground board.

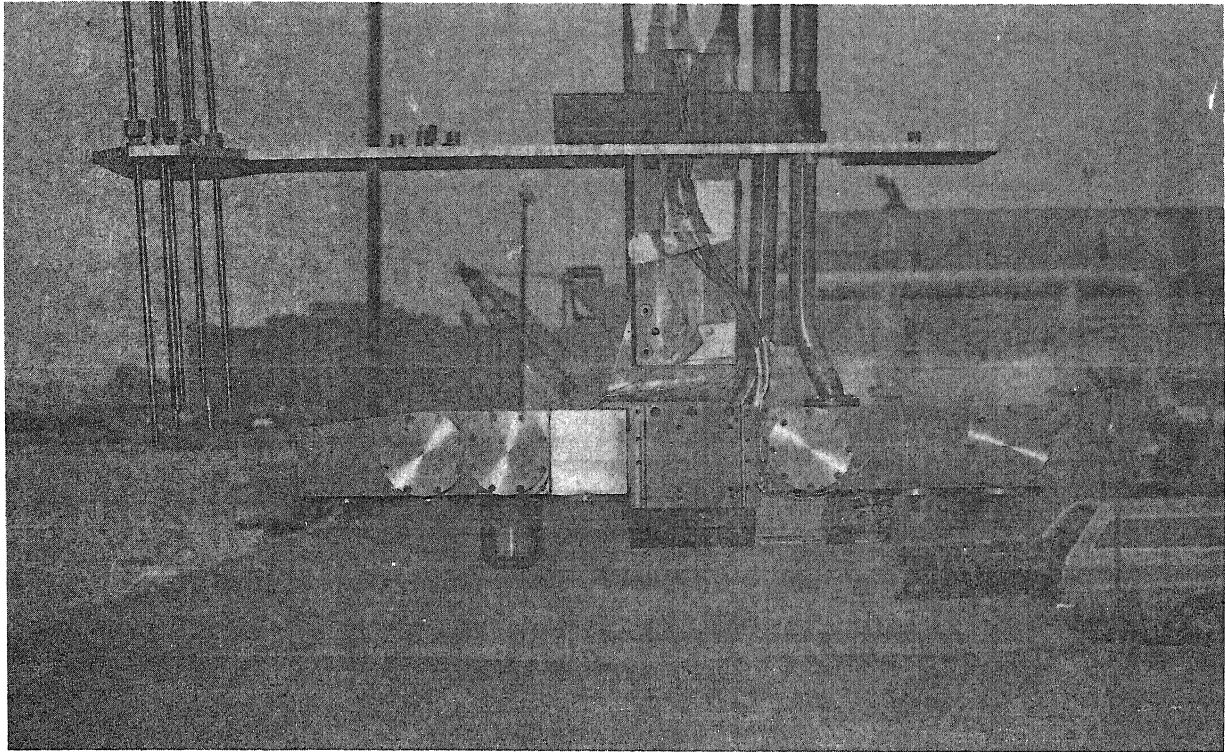


Figure 3. The fuselage substructure consisted of two plenums, an internal balance, water cooling jacket and fuselage support bracket.

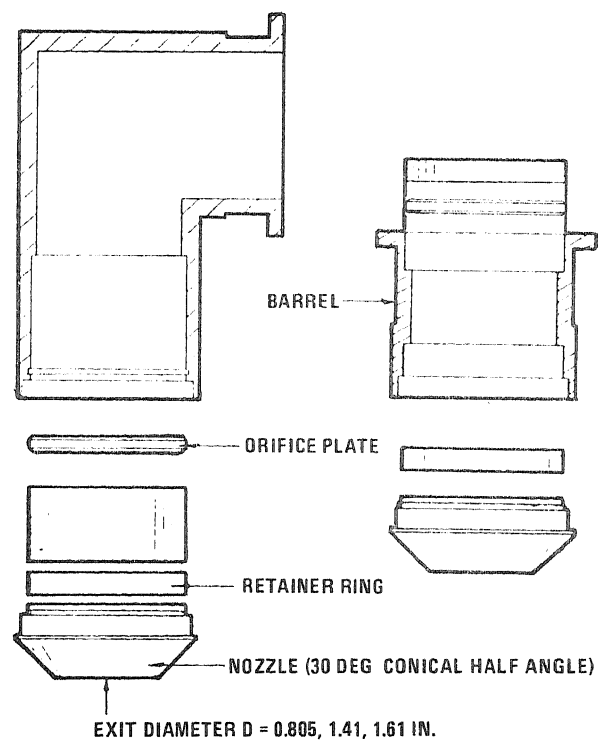


Figure 4. The jet flow was discharged through 30-degree conical half-angle nozzles.

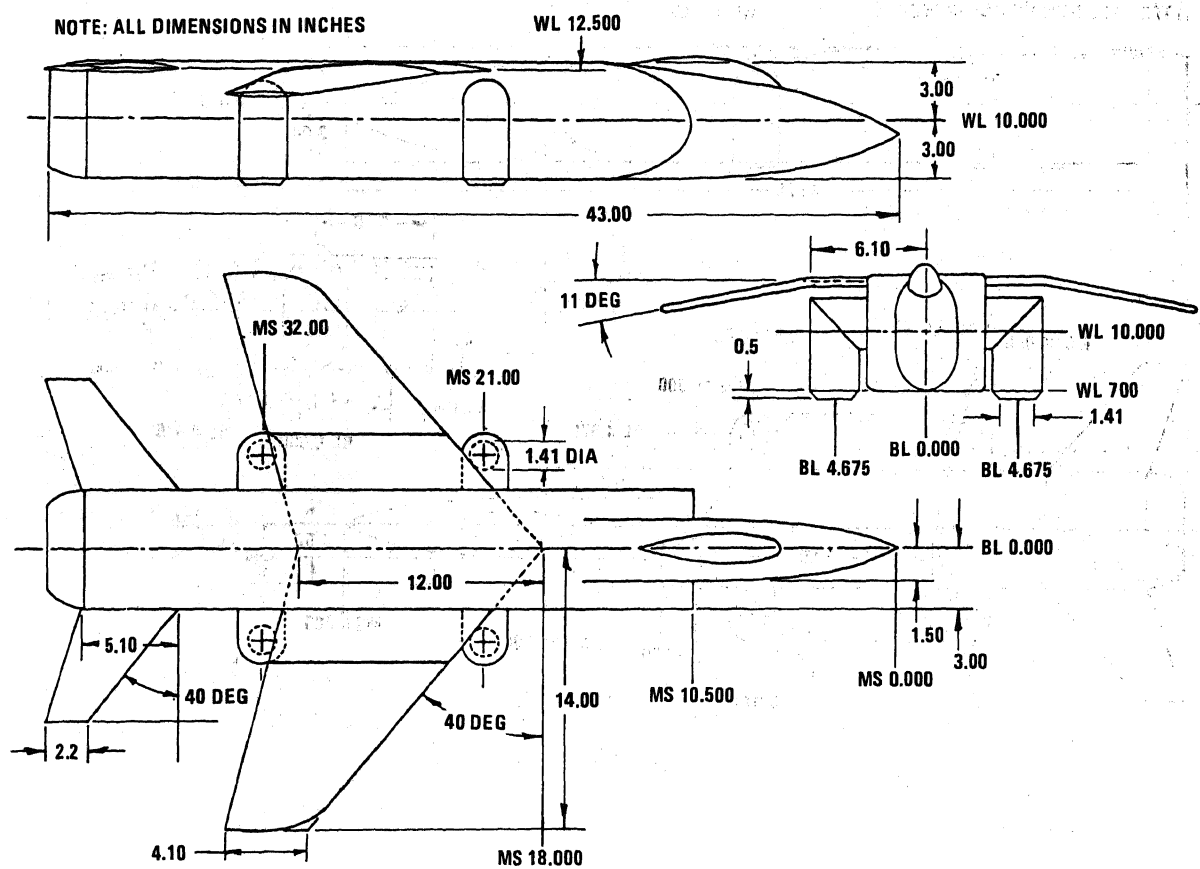


Figure 5. The model with the four-jet propulsion system was designed to represent a Pegasus engine type installation.

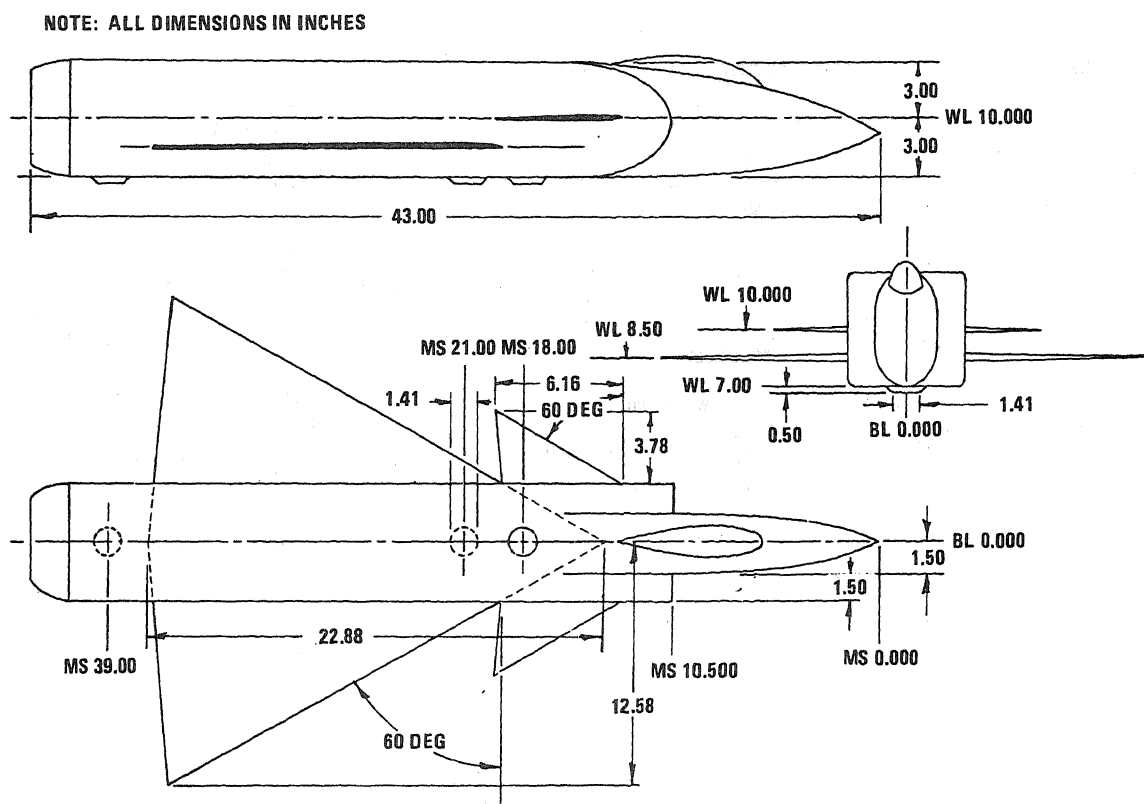


Figure 7. The model with the three-jet propulsion system represented an advanced supersonic fighter concept.

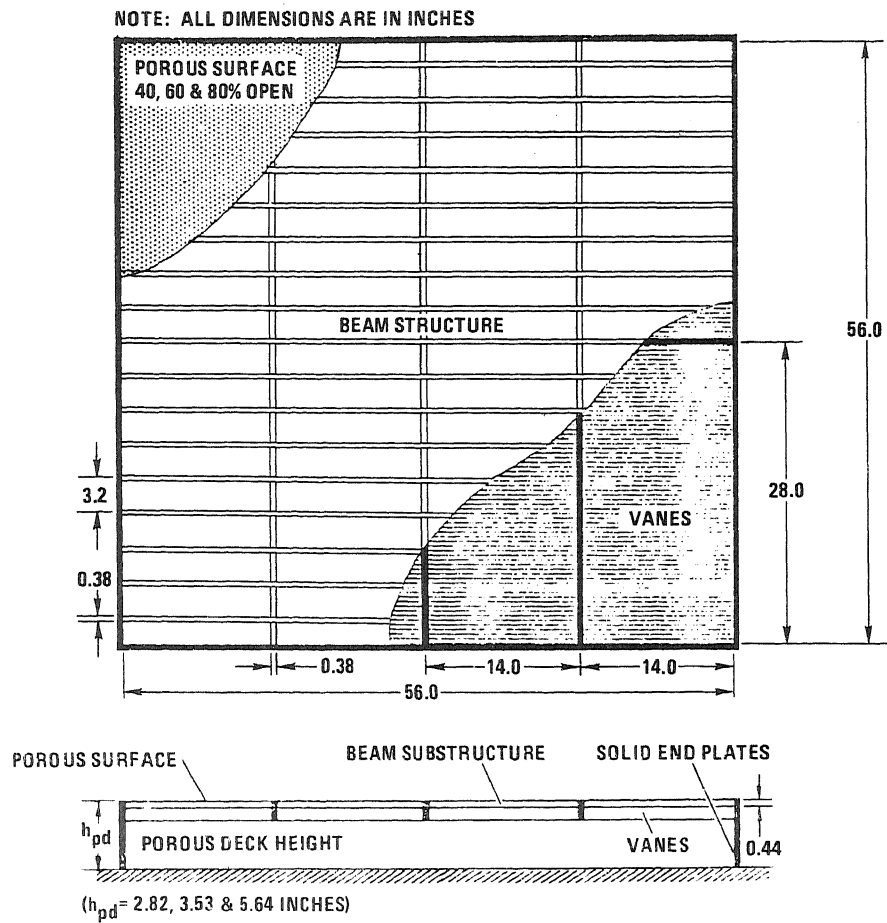


Figure 8. The porous deck model was composed of a porous surface, substructure and vanes.

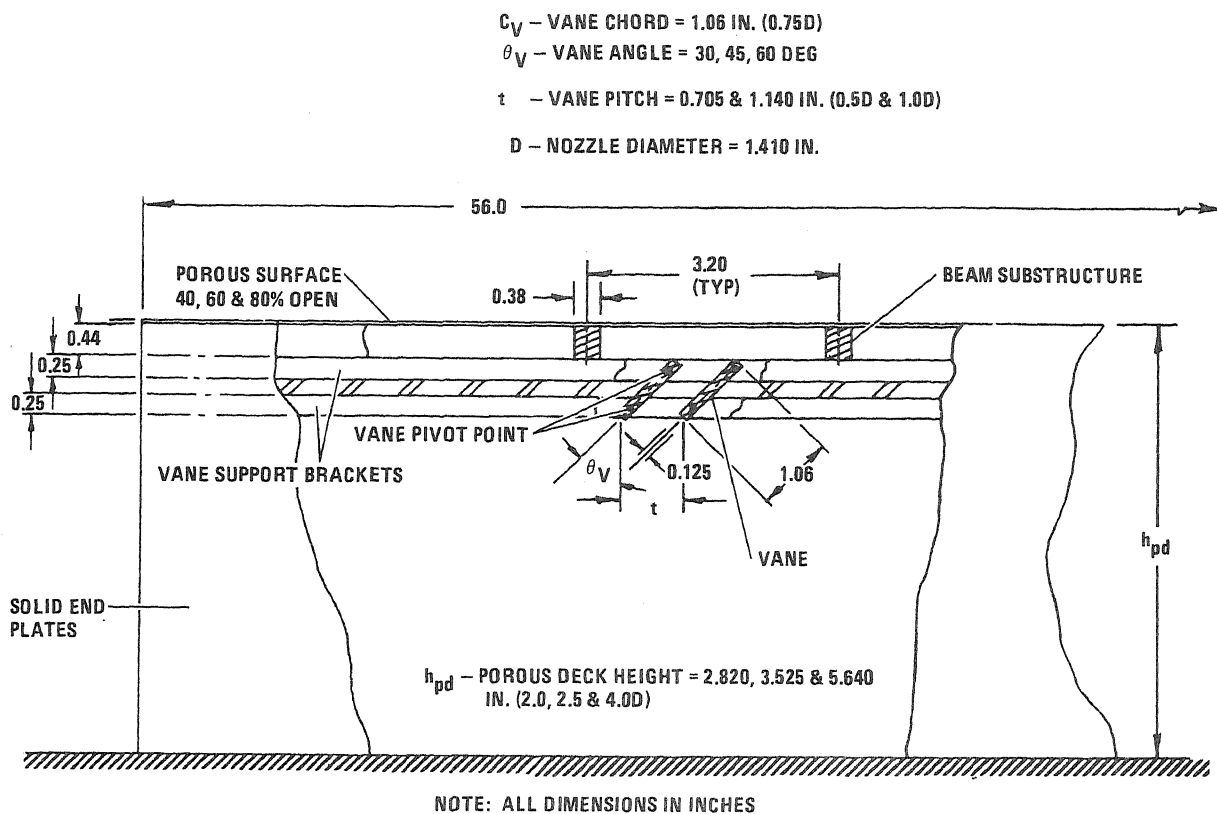


Figure 9. The porous deck model had vanes that could be deflected 30, 45 and 60 degrees.

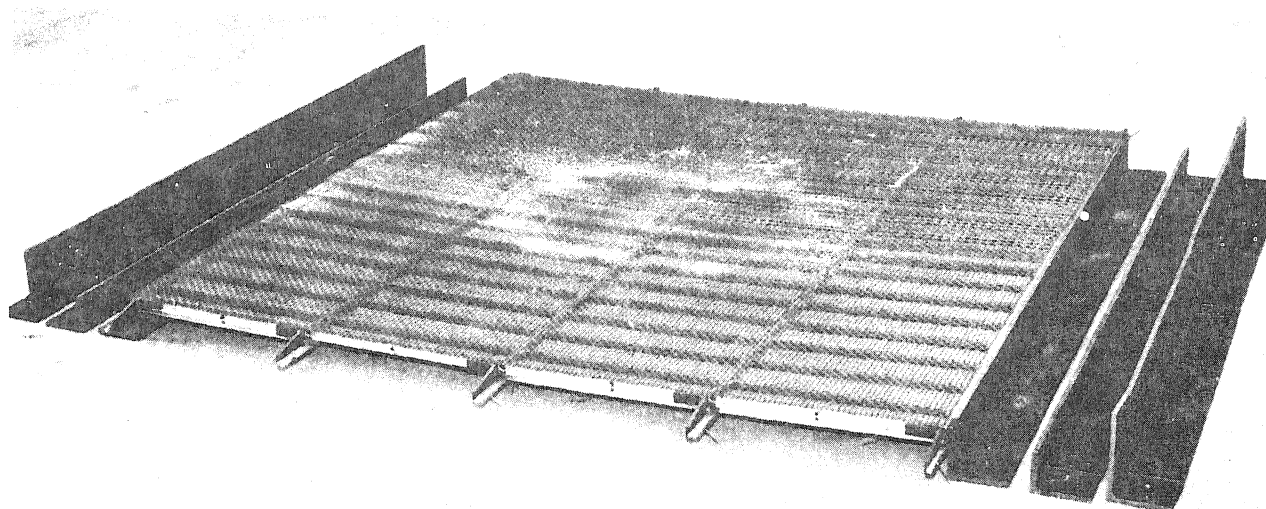


Figure 10. The porous deck model had supports for three deck heights.

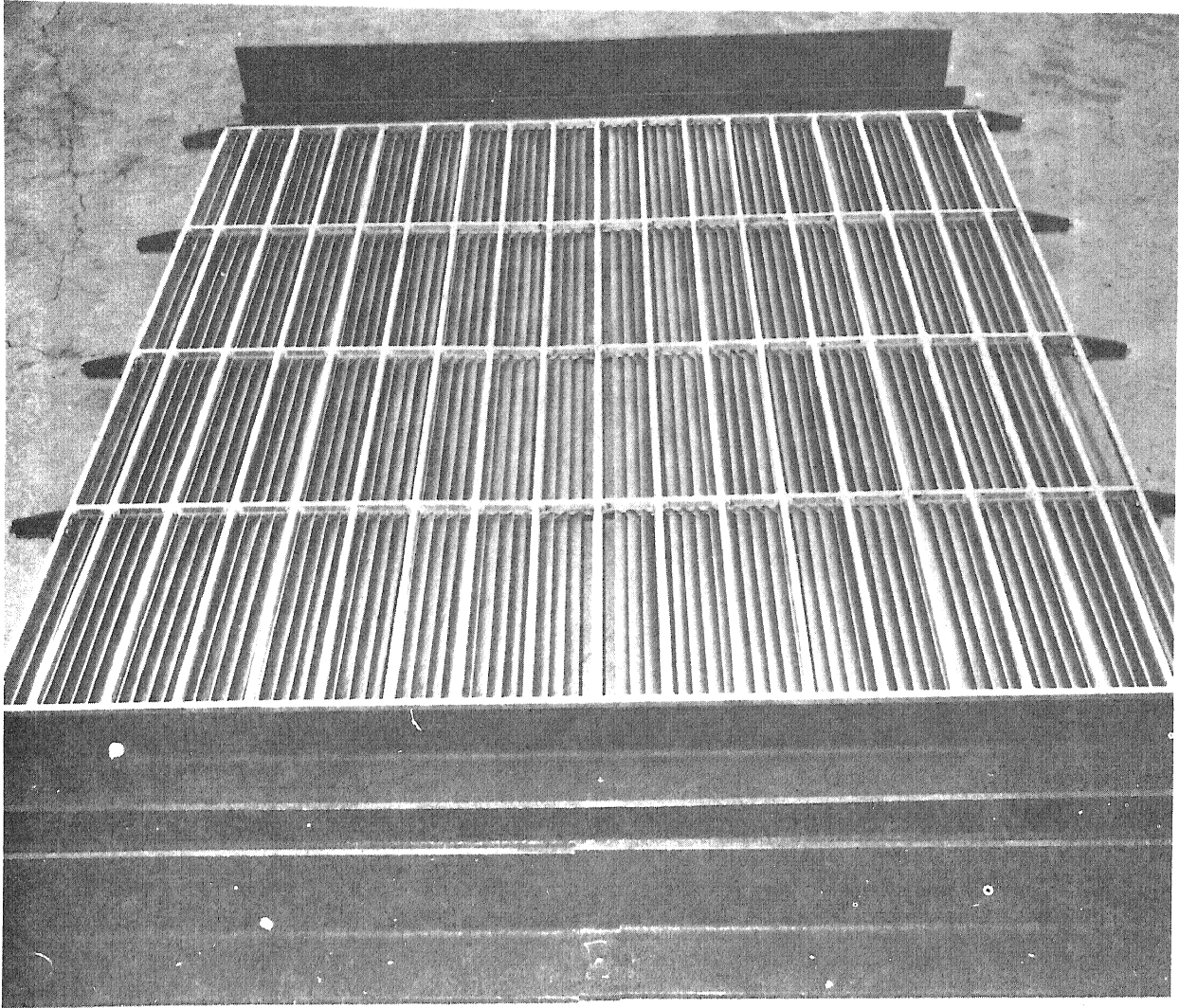


Figure 11. The vanes were deflected to port and starboard.

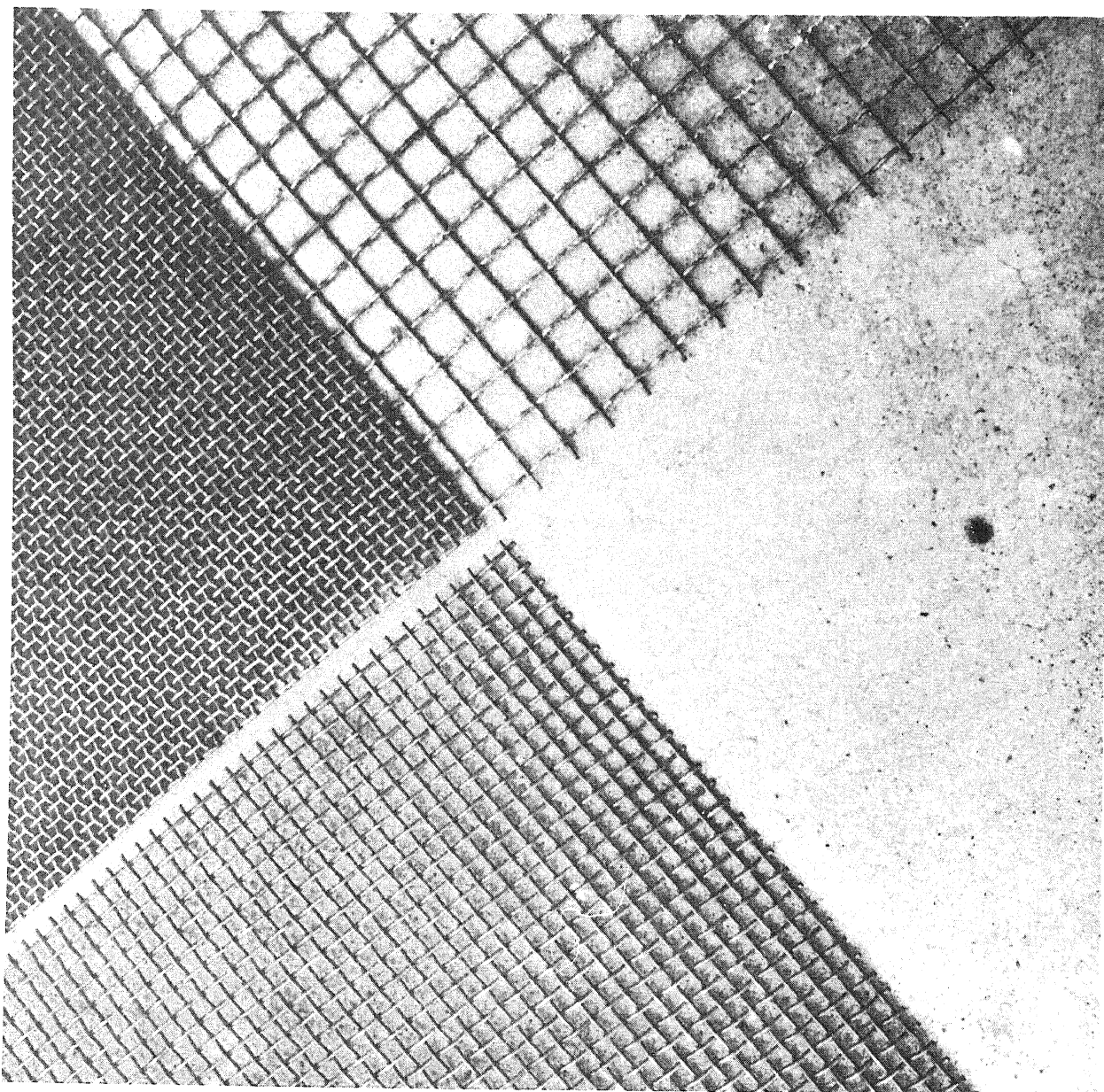


Figure 12. Three porous surfaces were tested: 40, 60 and 80%.

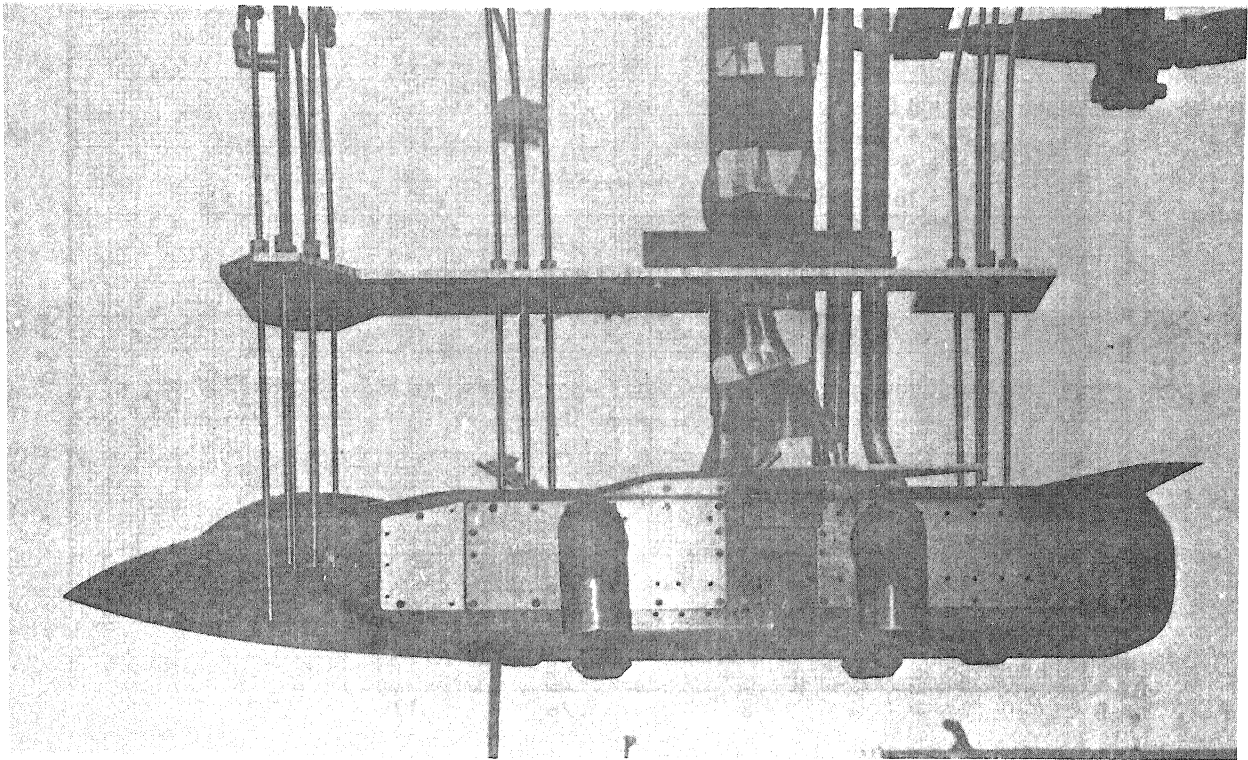


Figure 13. Inlet proximity thermocouples were installed above the model (six-jet propulsion arrangements shown).

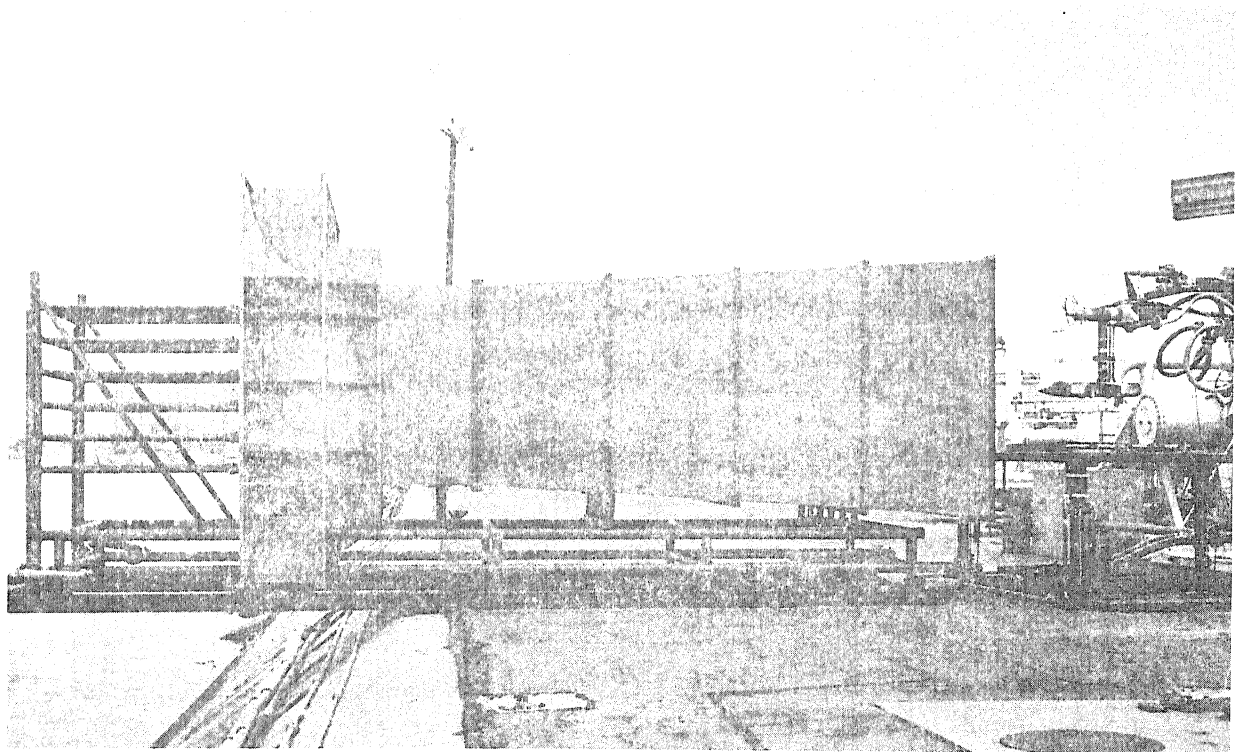


Figure 14. The wind generator was driven by an ejector system.

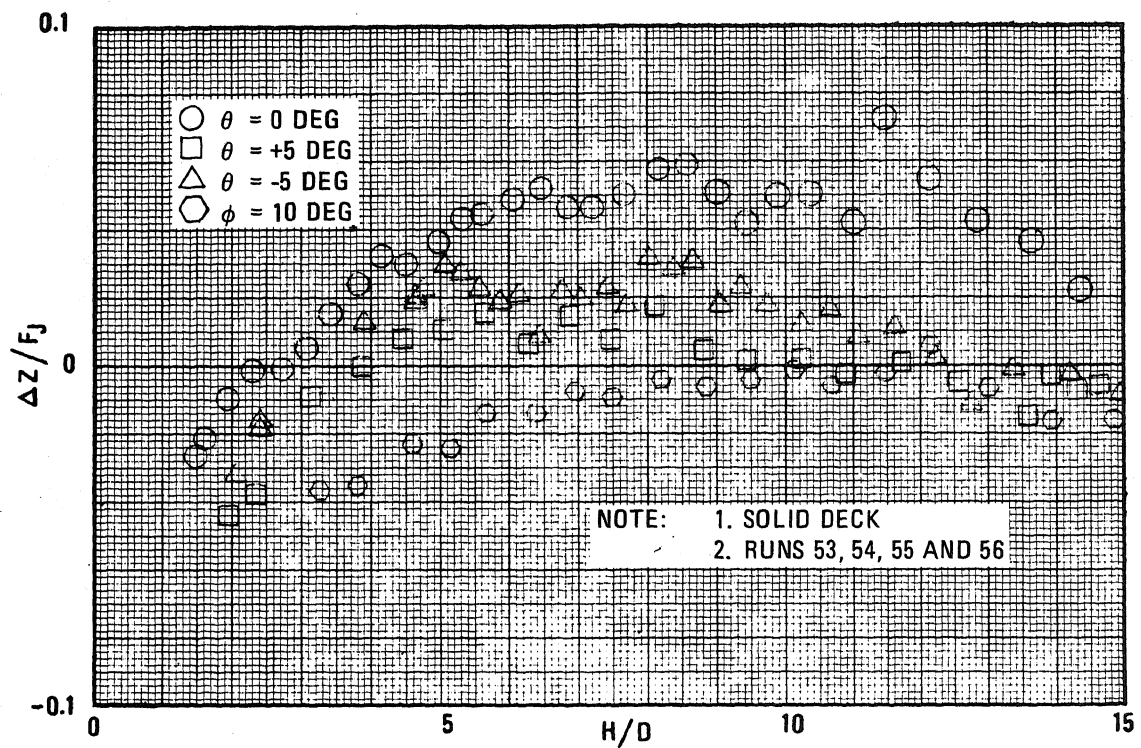


Figure 15. Changes in airplane attitude over a solid deck produce large variation in induced lift forces (four nozzles).

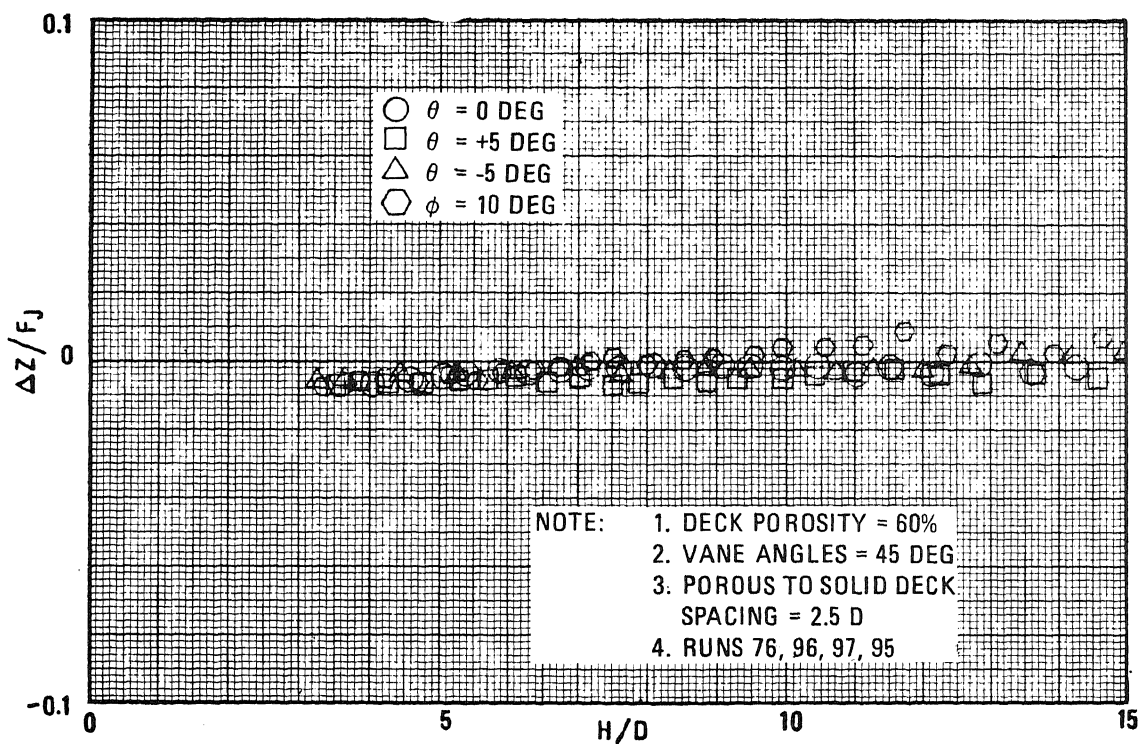


Figure 16. Changes in airplane attitude over a porous deck produce only small variations in induced lift forces (four nozzles).

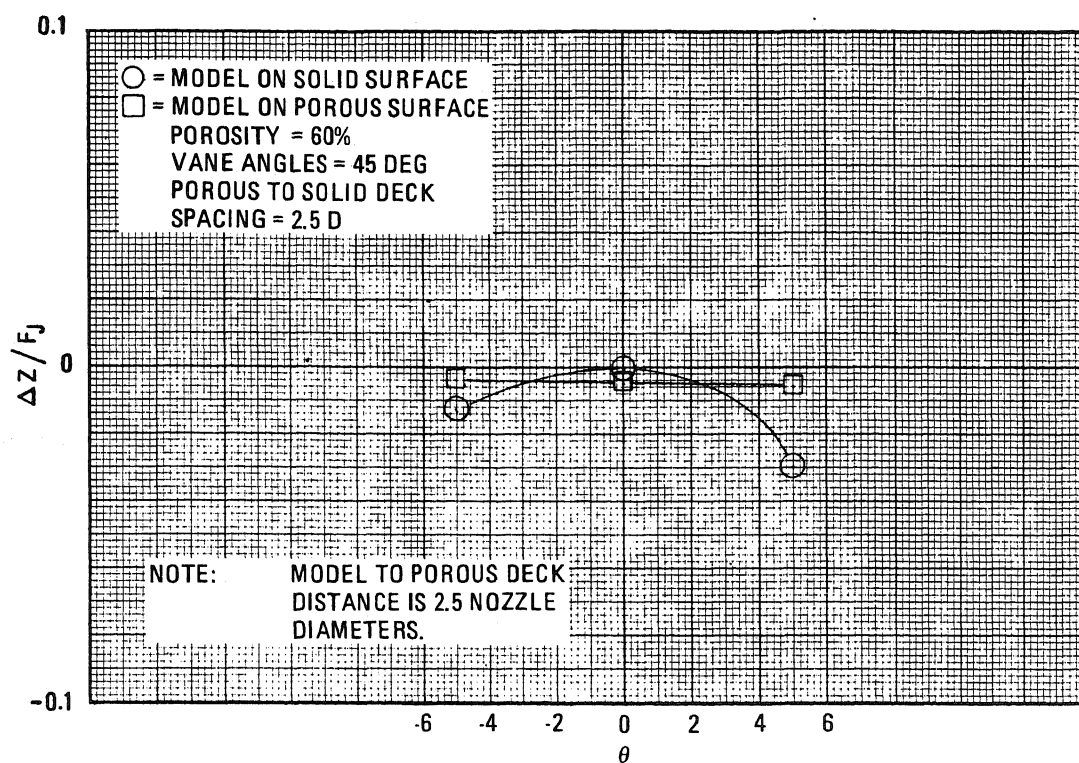


Figure 17. Changes in propulsion-system-induced lift with airplane attitude become negligible over a porous surface (four nozzles).

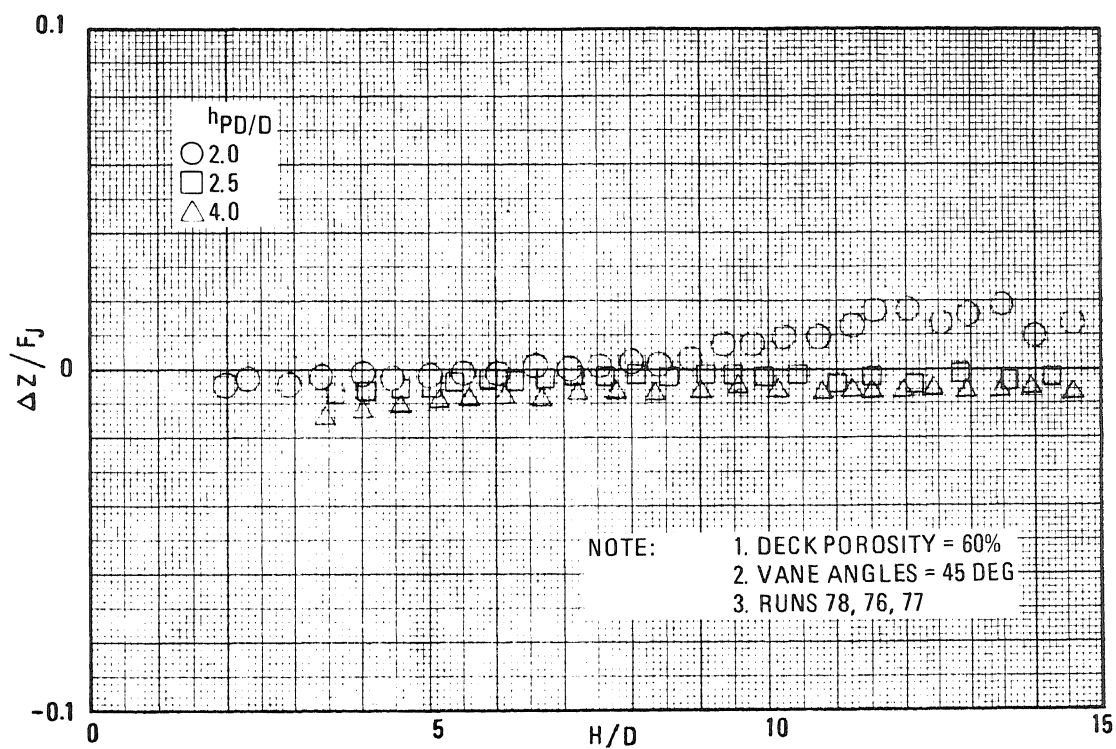


Figure 18. For a porous deck with louvers, the propulsion-system-induced effects are negligible for deck spacing equal 2.5 and 4.0 nozzle diameters (four nozzles).

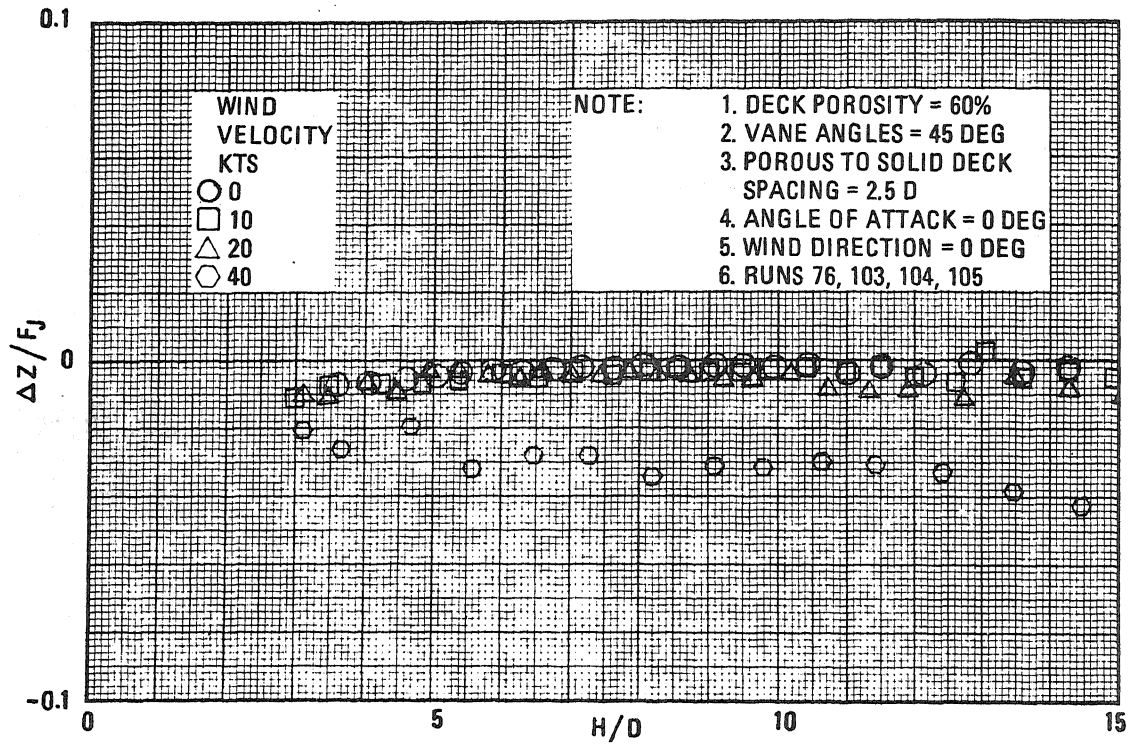


Figure 19. Wind velocities of 20 knots and less had only a small effect on propulsion-system-induced forces (four nozzles).

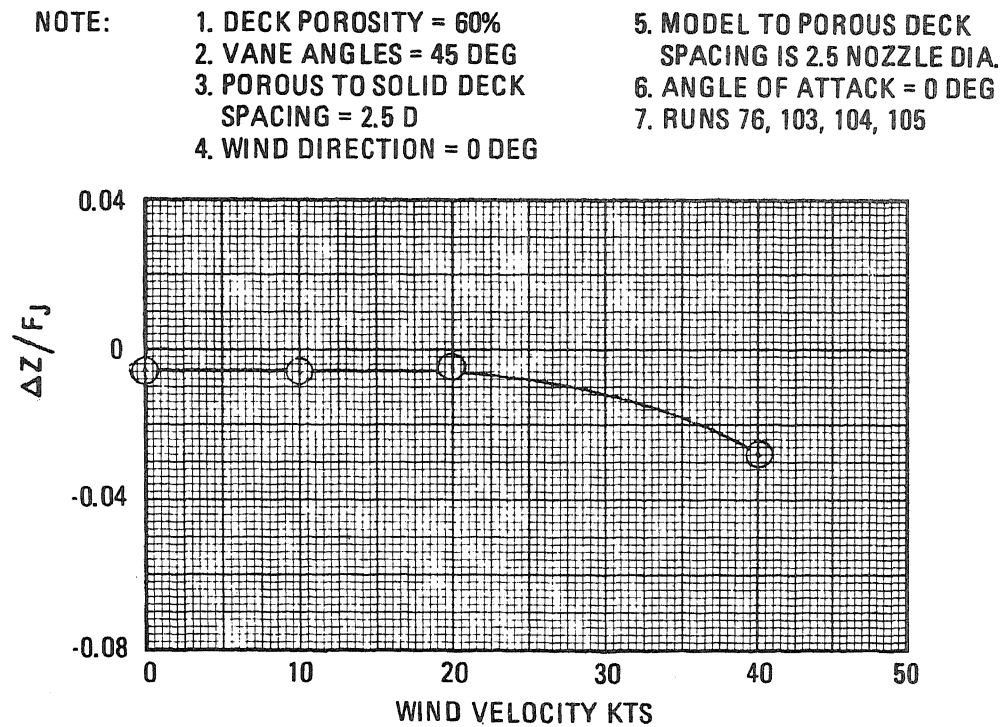


Figure 20. Up to 20 knots, the wind had very little effect on the induced lift forces (four nozzles).

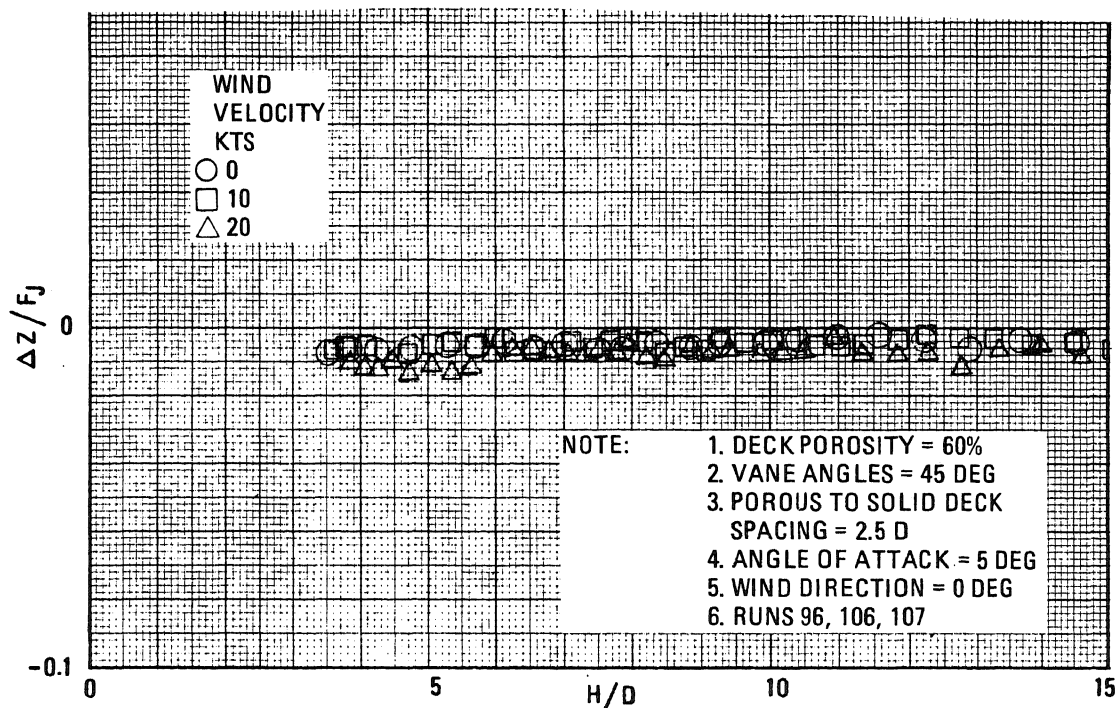


Figure 21. At a five-degree angle of attack, a 20-knot wind had no significant effect on propulsion-system-induced forces (four nozzles).

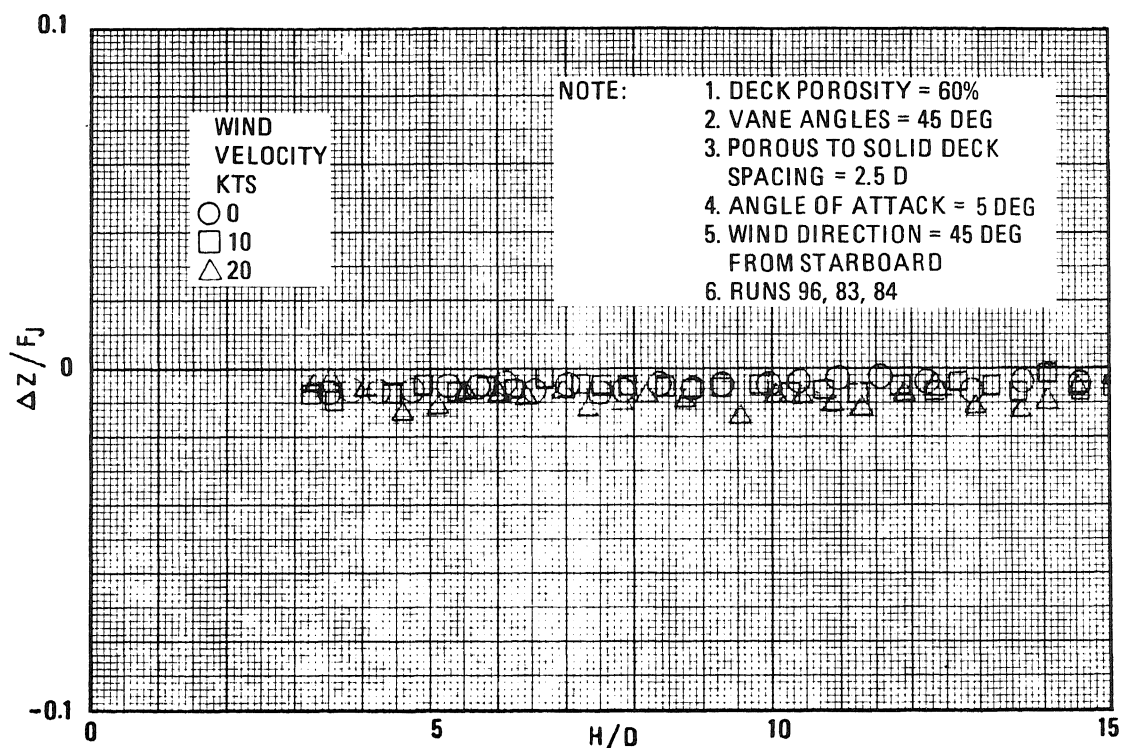


Figure 22. The effect of wind on propulsion-system-induced forces is small at a five-degree angle of attack (four nozzles).

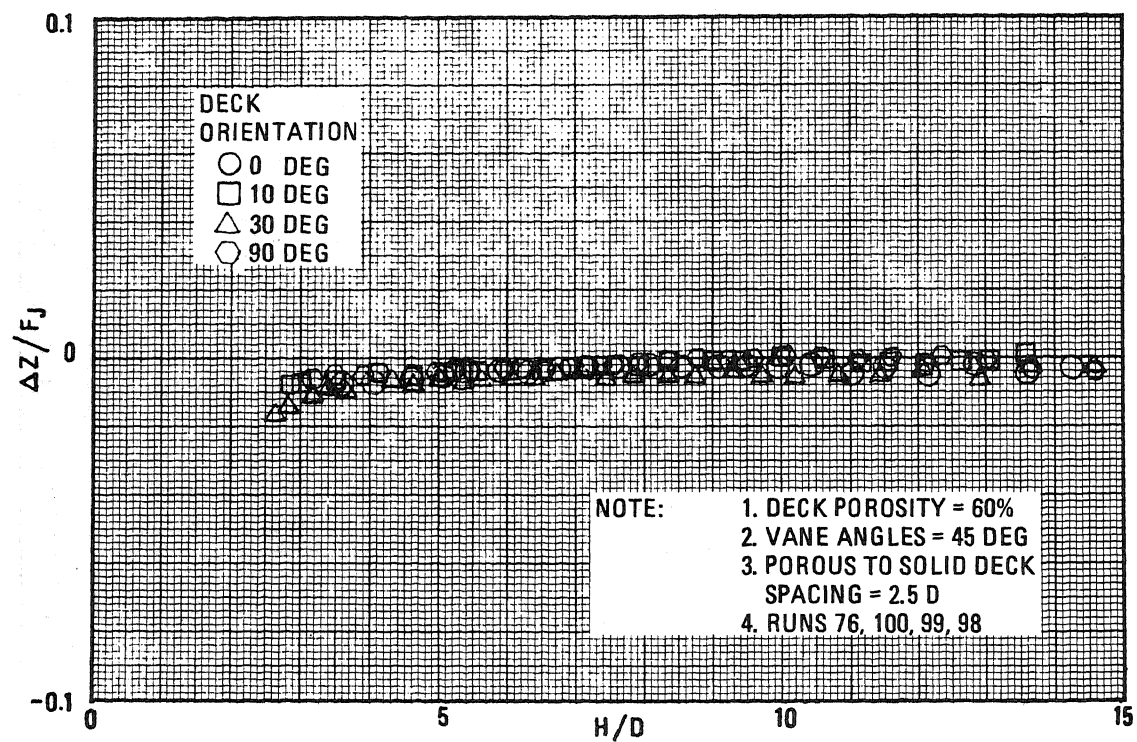


Figure 23. Changes in the model orientation on the porous deck had no significant effect on propulsion-system-induced forces (four nozzles).

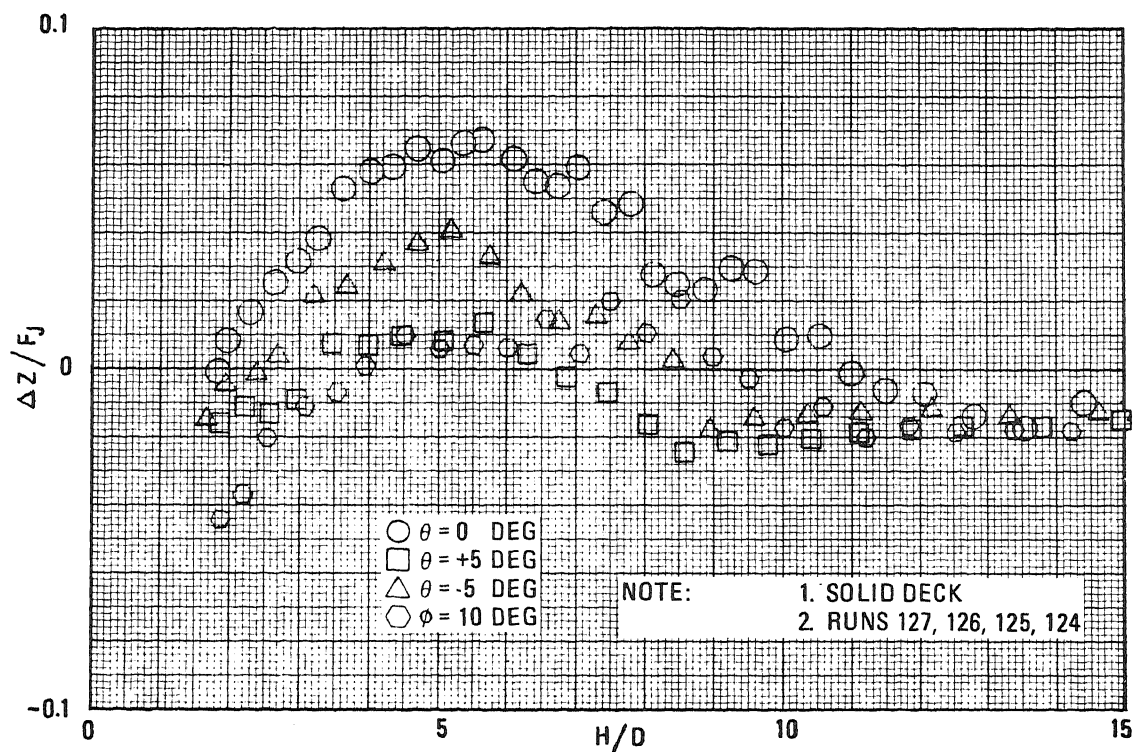


Figure 24. Changes in airplane attitudes over a solid deck produce large variations in induced lift forces (six nozzles).

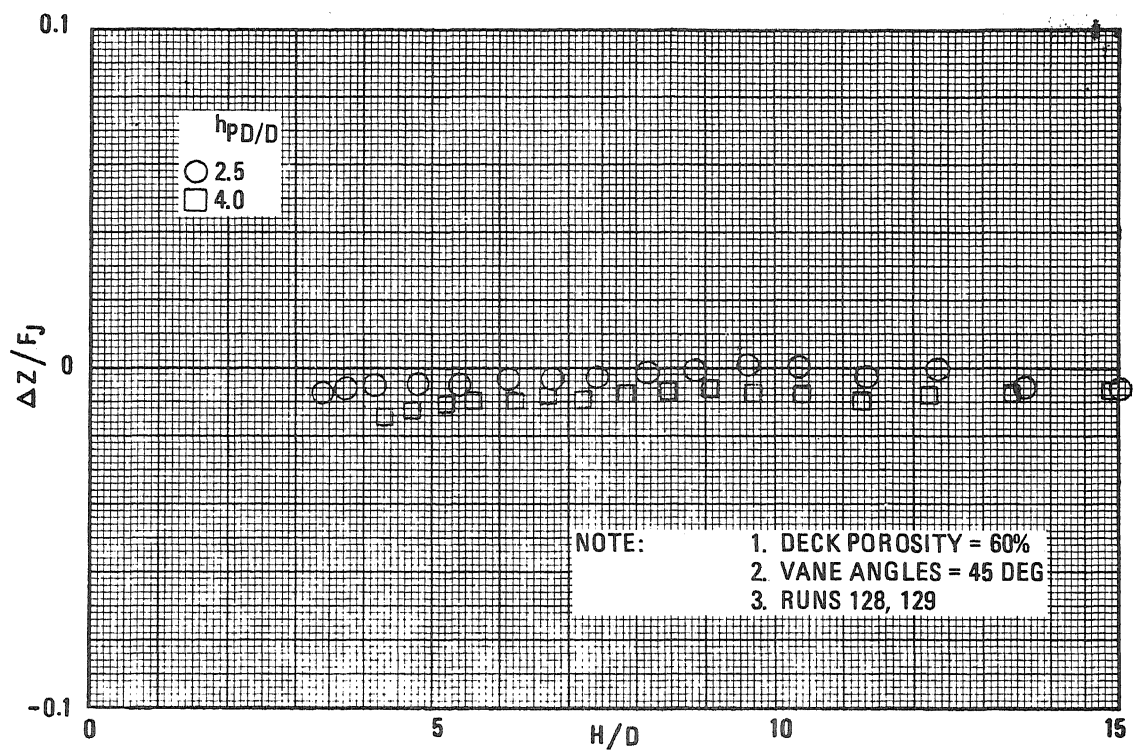


Figure 25. The porous deck with louvers caused the propulsion-system-induced effects to become small (six nozzles).

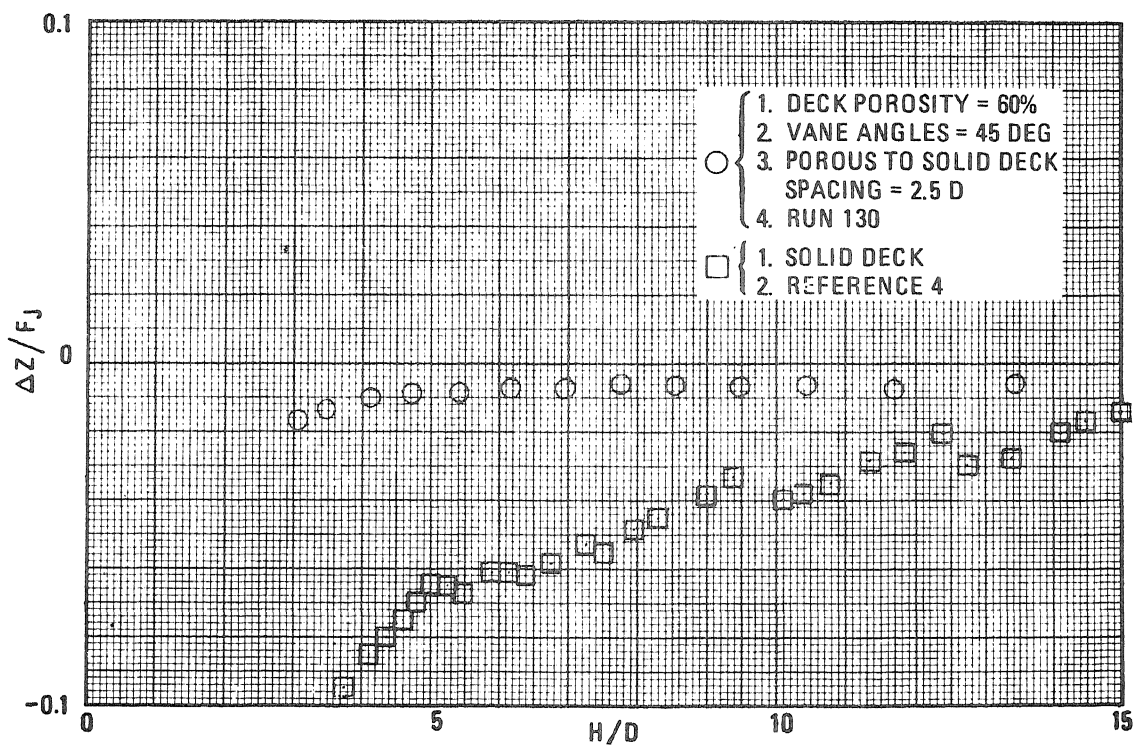


Figure 26. A porous surface with louvers eliminates most of the propulsion-system-induced effects (three nozzles).

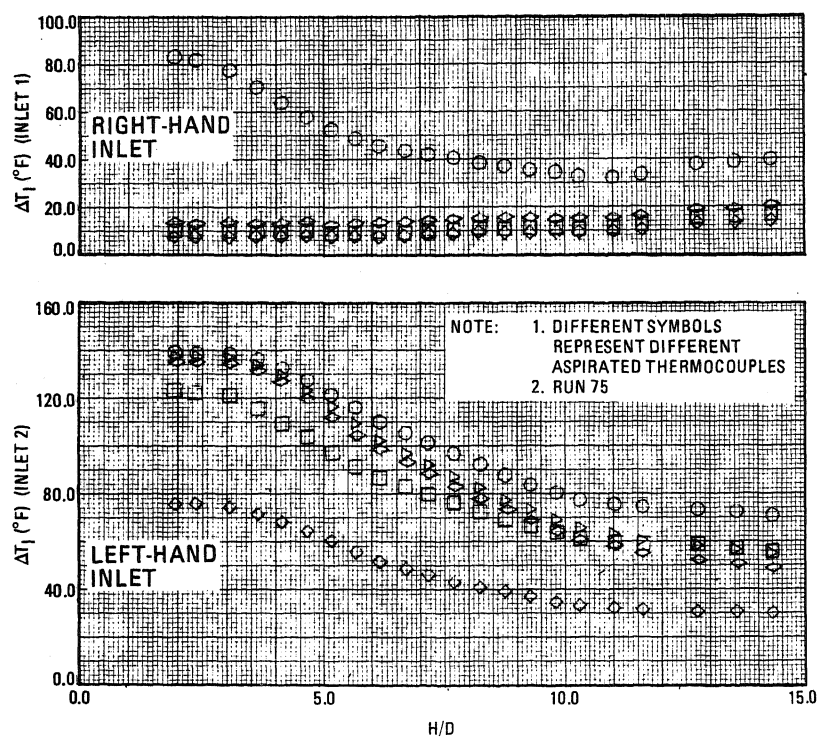


Figure 27. Typical engine inlet proximity temperature data decreased with distance above ground.

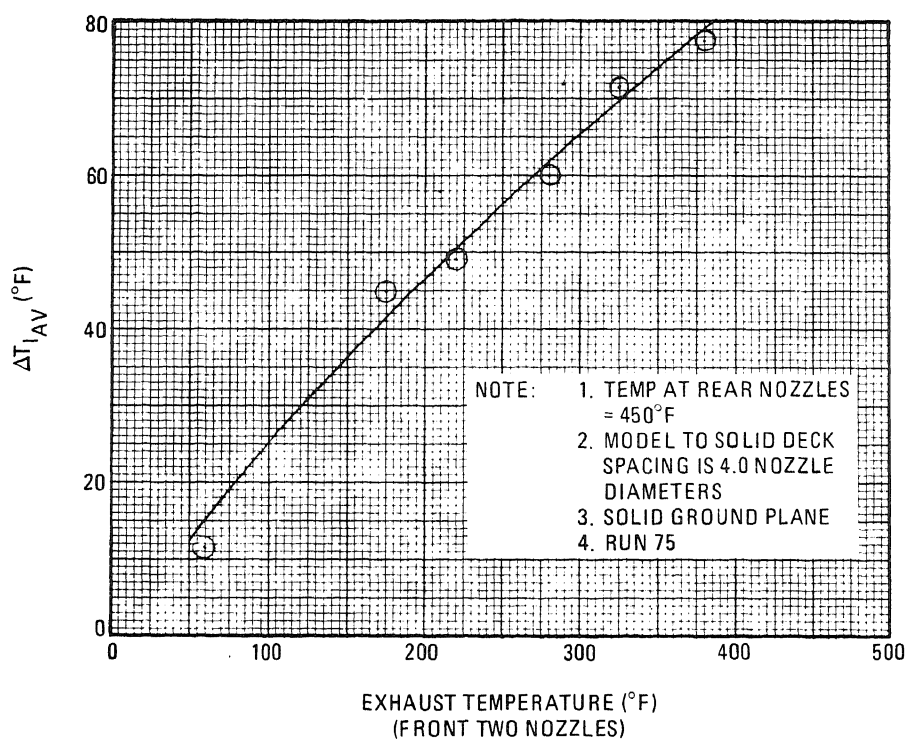


Figure 28. A decrease in the exhaust temperature of the front nozzles lead to a reduction in inlet proximity temperatures (four nozzles).

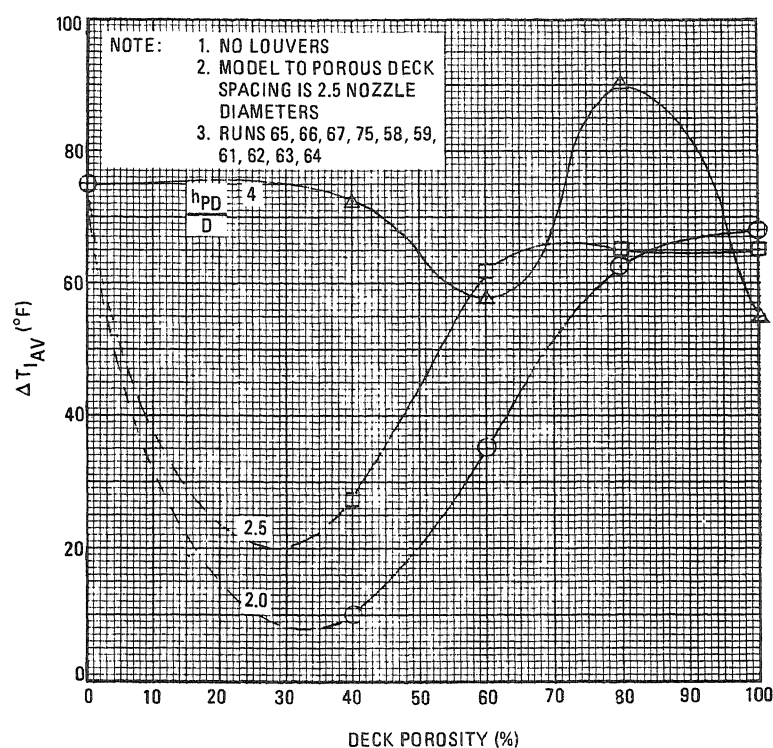


Figure 29. Forty percent porosity (or less) and a solid-to-porous deck spacing of two engine diameters (or less) was found to be best from engine inlet proximity temperature standpoint (four nozzles).

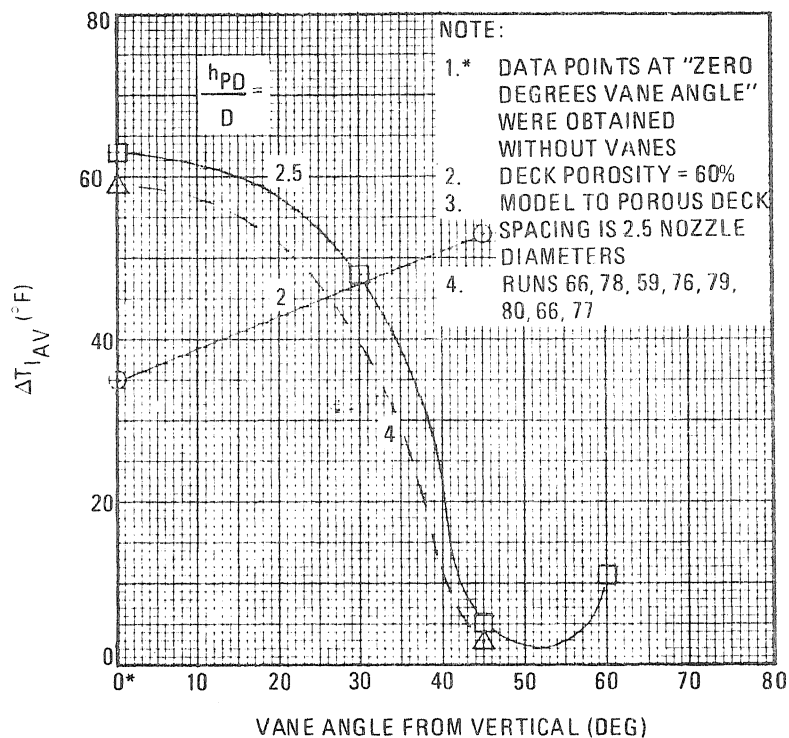


Figure 30. The vane angle of 45 degrees gave best results (four nozzles).

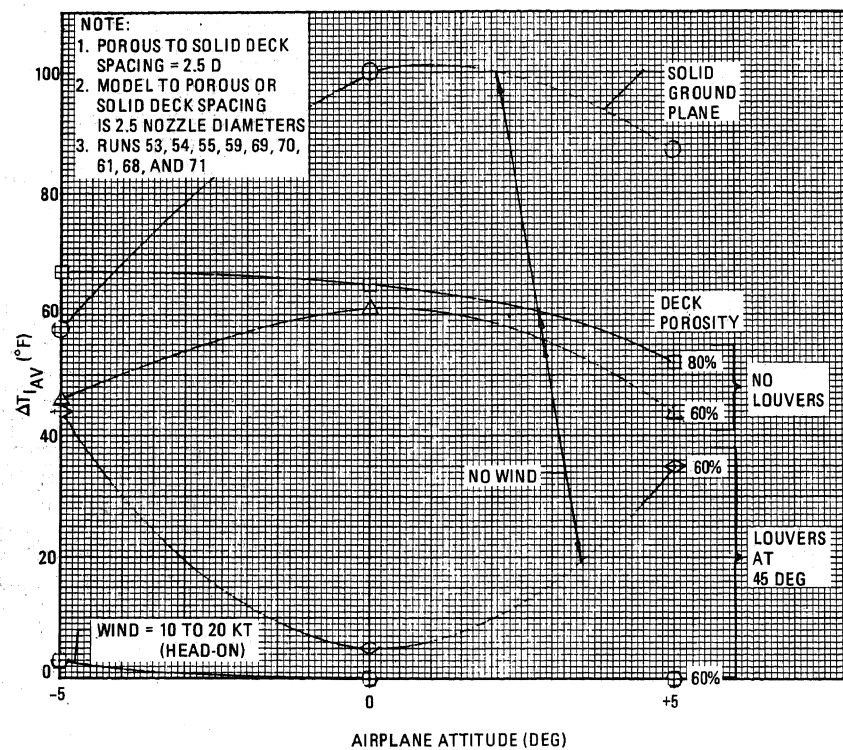


Figure 31. On a deck with louvers, pitch attitude changes lead to increases in inlet proximity temperatures, while on a solid surface and a porous surface without louvers, the opposite is true (four nozzles).

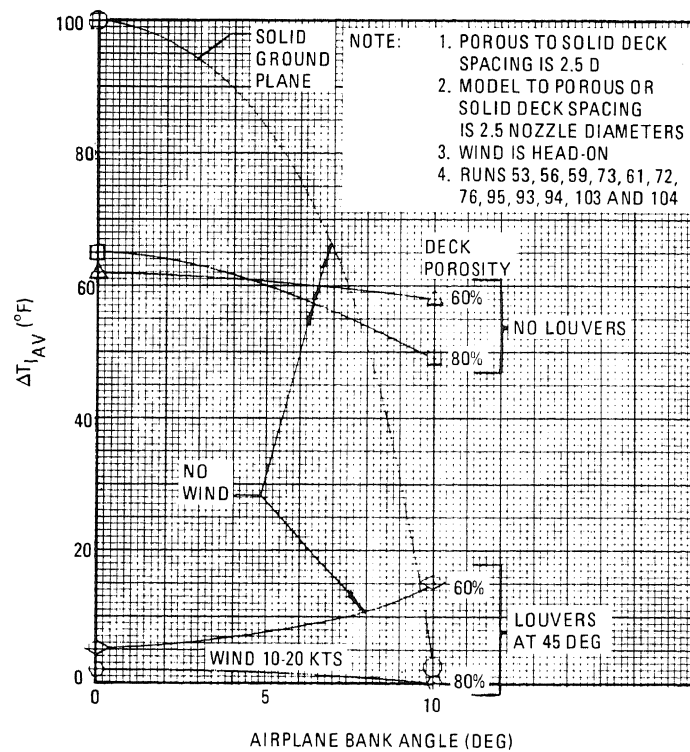


Figure 32. Bank angle and winds reduce inlet proximity temperatures (four nozzles).

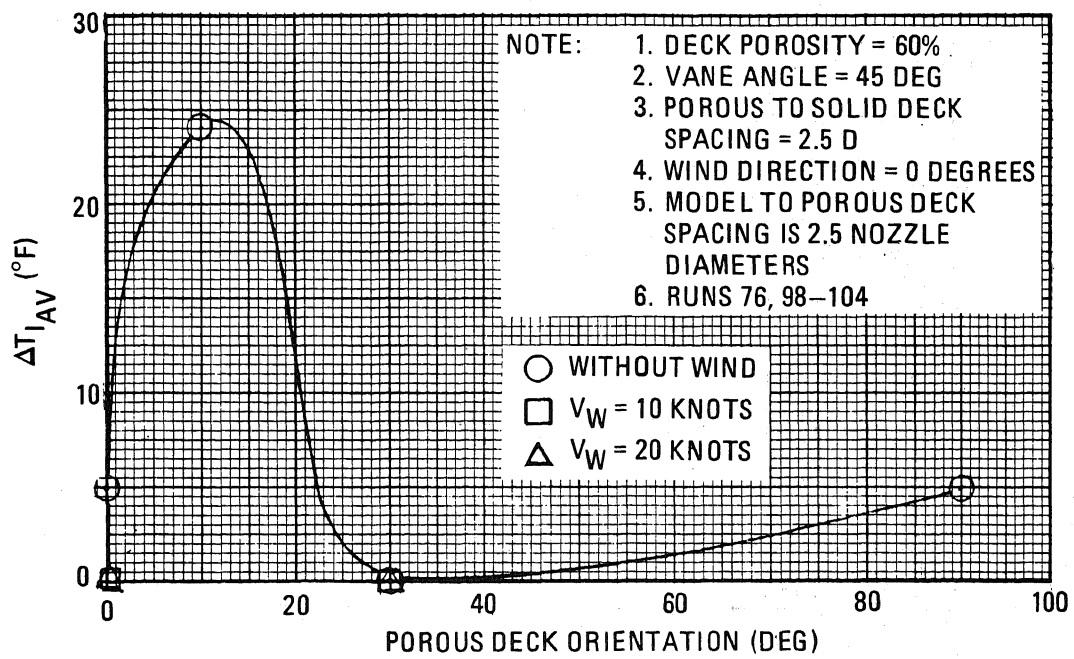


Figure 33. A 10-degree off-center orientation (yaw) of the model leads to increased engine inlet proximity temperature.

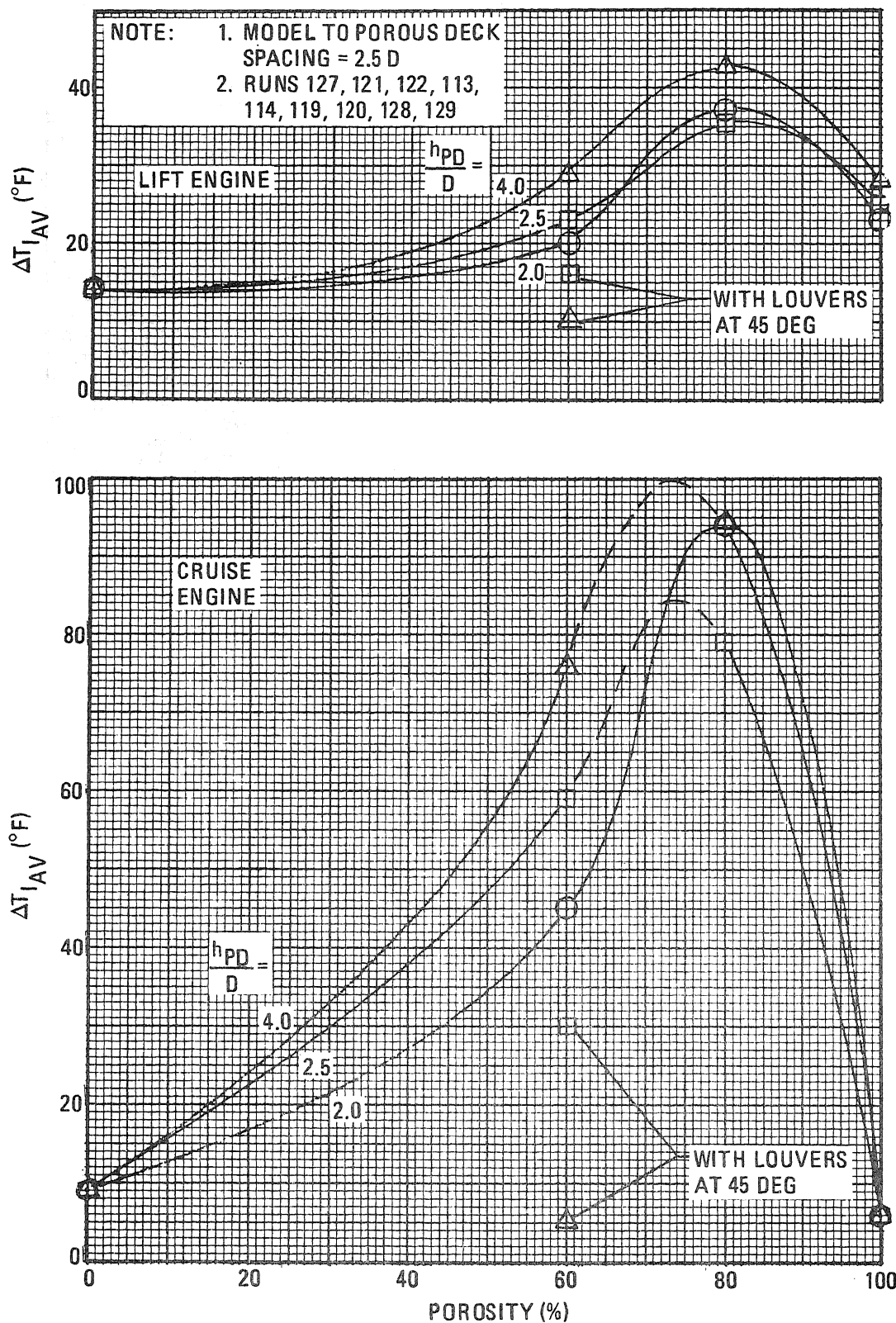


Figure 34. Porous deck with or without louvers degraded engine inlet proximity temperature in most cases. Sixty percent porosity at h_{PD}/D of four with vanes showed some improvement, however (six nozzles).

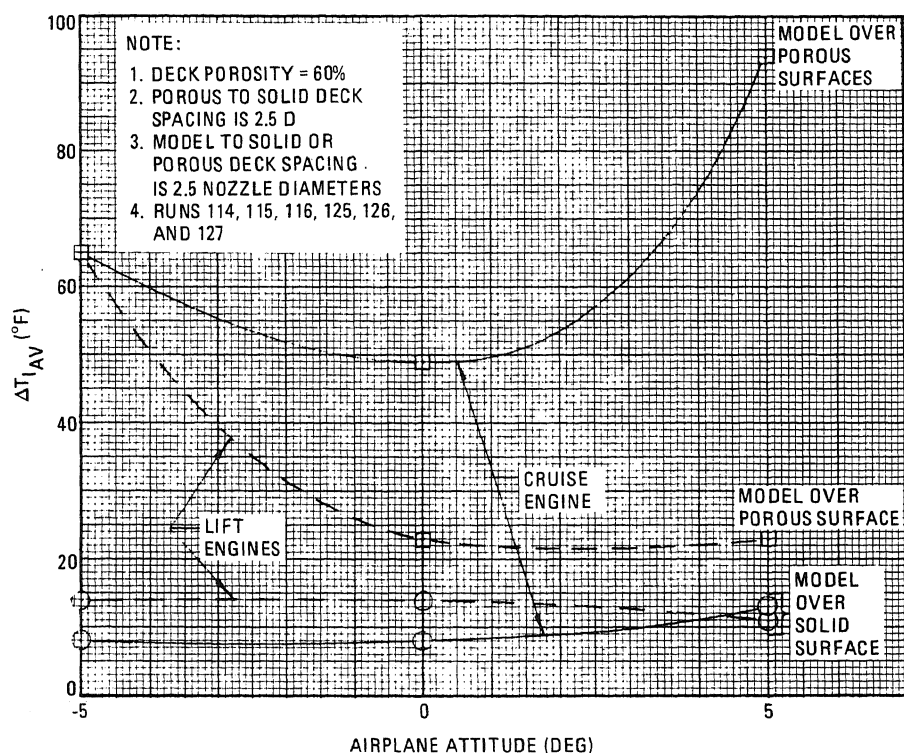


Figure 35. Excursions in pitch increased inlet proximity temperatures in most cases (six nozzles).

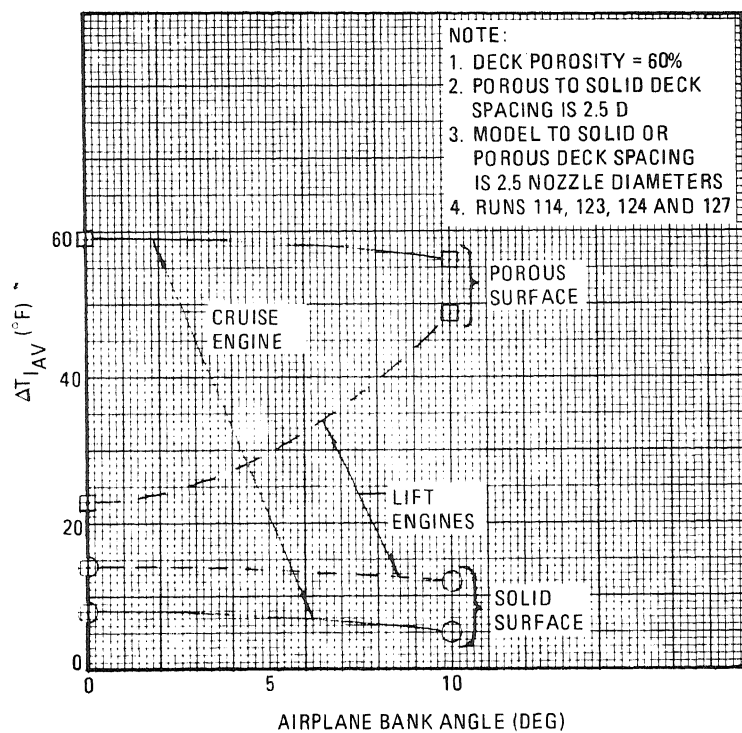


Figure 36. Excursions in bank had a mixed effect on inlet proximity temperatures (six nozzles).

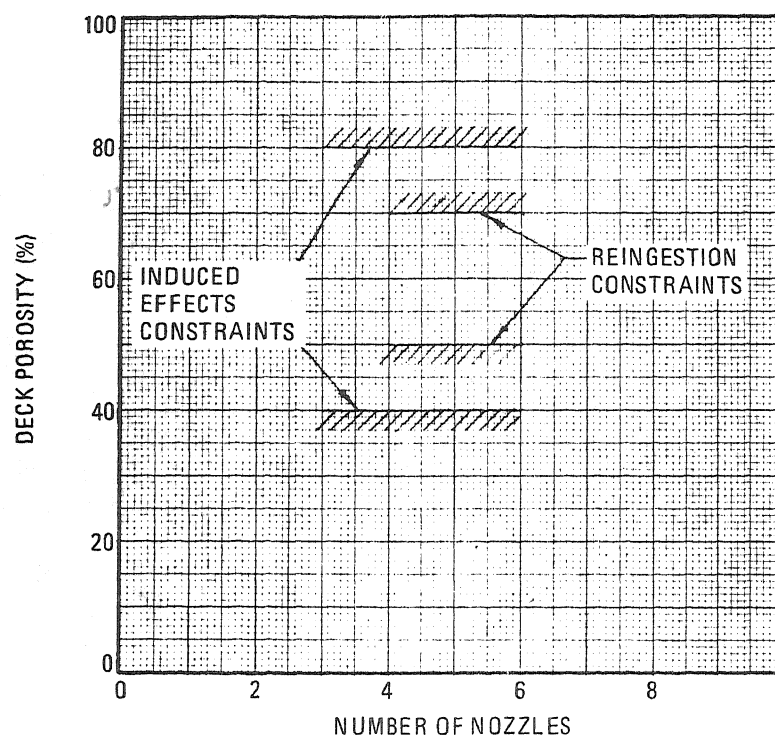


Figure 37. The recommended deck porosity is 50 to 70%.

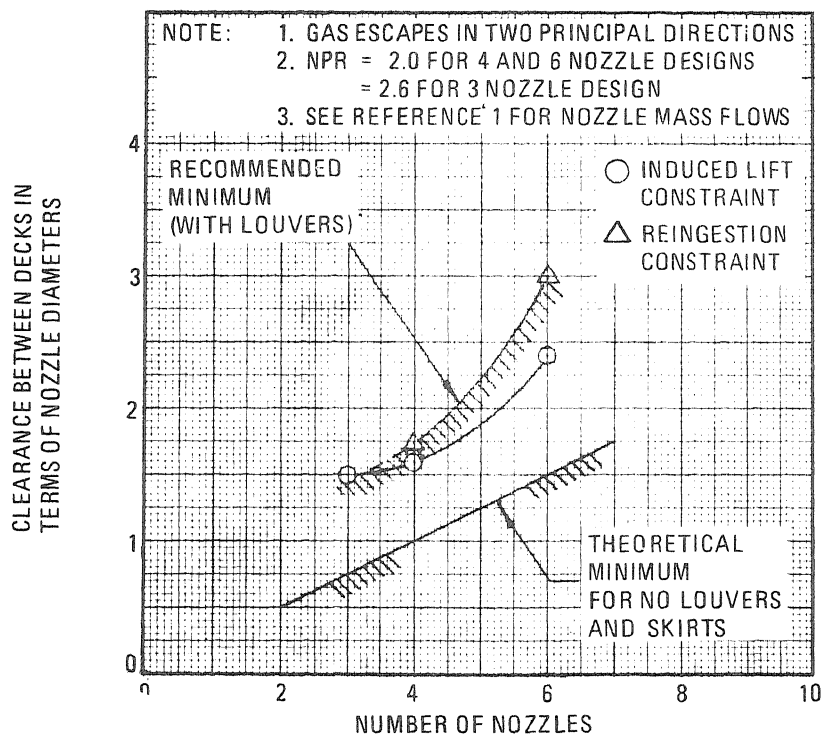


Figure 38. The porous-to-solid deck spacing is largely dictated by engine hot gas reingestion trends.

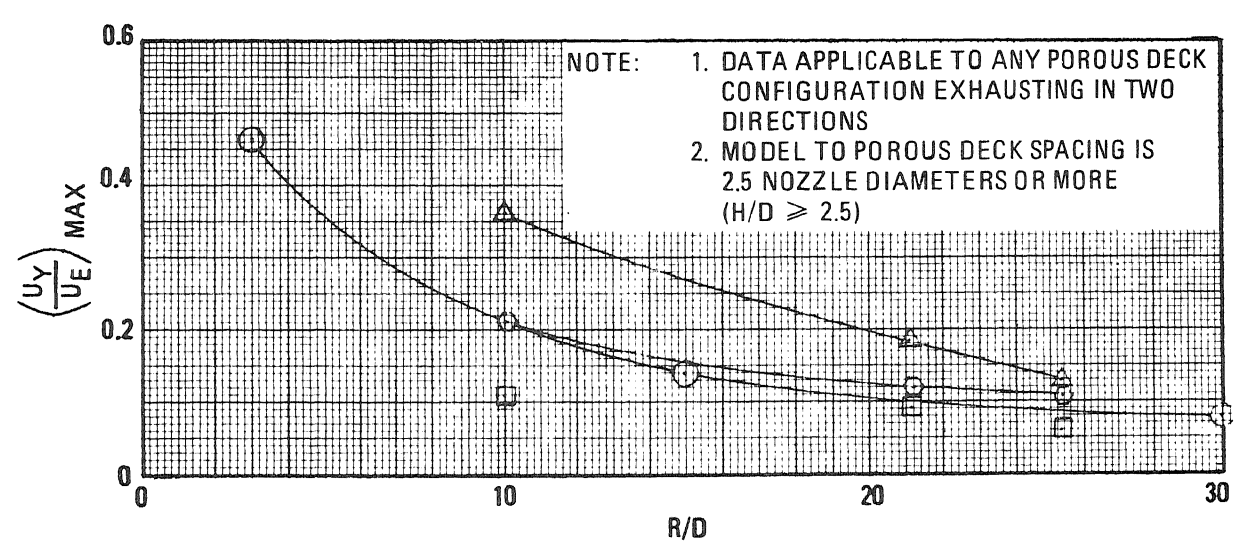
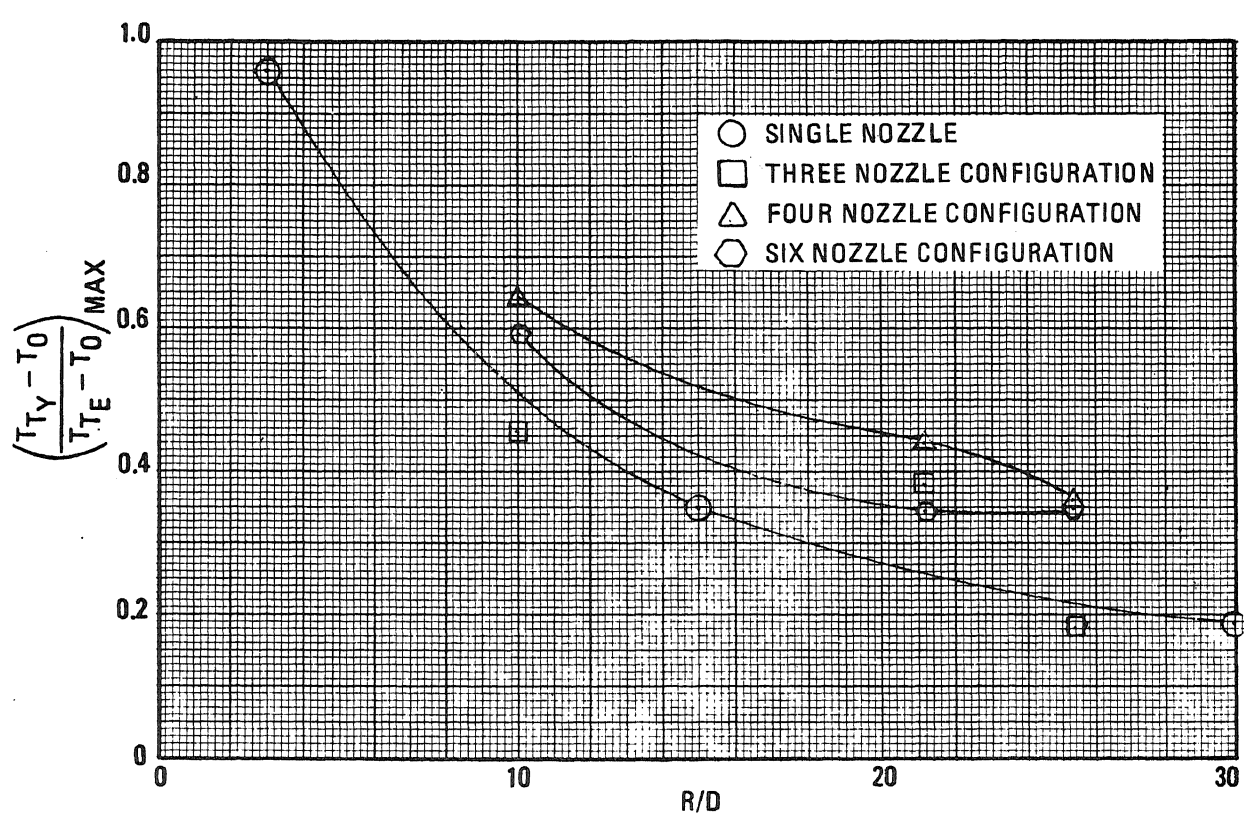


Figure 39. The maximum gas temperatures recorded below the porous surfaces were sufficiently high to cause concern from the structural standpoint.

Table I. Effect of wind direction on inlet proximity temperature (four nozzles).

Pitch/Roll (θ/ϕ) (deg)	Wind Speed (V_w)(kt)	Wind Direction (ψ)(deg)		
		0	10	45
0/0	10	0	2	0
	20	0	0	6
5/0	10	0	3	5
	20	0	2	3
-5/0	10	2	3	11
	20	2	2	7
0/10	10	0	0	Not Tested
	20	1	1	Not Tested

1. Deck porosity = 60%
2. Vane angle = 45 deg
3. Porous-to-solid deck spacing = 2.5 nozzle diameter
4. Deck orientation angle = 0 deg
5. Model-to-porous-deck spacing = 2.5 nozzle diameters

EXPERIMENTAL EVALUATIONS OF AERO/PROPULSION EFFECTS FOR LIFT PLUS LIFT/CRUISE V/STOL AIRCRAFT

Robert A. Cea & Robert E. Krepski
Grumman Aerospace Corporation
Bethpage, New York 11714

ABSTRACT

As part of a continuing effort to develop viable V/STOL aircraft for the 1980s, Grumman has conducted a number of experimental programs to evaluate the extent of jet-induced effects. This paper highlights results of recent test programs at the British Aircraft Corporation V/STOL wind tunnel and the VFW-Fokker hot-gas facility. The objectives of these programs were to evaluate aero/propulsion phenomena which have a strong influence on jet-induced lift, moments, and recirculation temperature rise in hover and transition flight regimes.

Model variations, the use of various non-dimensional coefficients, test techniques, and some test results are highlighted to aid in formulating more accurate prediction techniques.

INTRODUCTION

A thorough knowledge of jet-induced effects on forces, moments, and reingestion is required for the design of V/STOL aircraft. Figure 1 highlights the importance of jet-induced losses. This paper is divided into two separable but yet synergistic categories of jet-induced effects testing:

- Test programs to determine the extent of jet-induced forces and moments for two supersonic strike/fighter configurations
- Results of a test program to establish the extent of hot-gas reingestion during in-ground operation

JET-INDUCED FORCE & MOMENT TESTING

Grumman has been involved with several jet-induced tests at NASA/Langley, British Aircraft Corporation and its own V/STOL facility at Farmingdale, New York. The latest test series were conducted at BAC on Grumman Design 607A (a twin lift engine plus a single lift/cruise engine) and Design 623 (a single lift engine plus twin lift/cruise engines). Figures 2 and 3 show these models installed in BAC's 5.5M V/STOL wind tunnel.

Test Facility & Technique

The BAC facility is capable of performing tests applicable to hover, transition, and STOL flight regimes, as well as conventional power-off aerodynamic tests. Exhaust-flow simulation is provided by cold air supplied through the sting/mainfold from an external source.

Inlet flow is not simulated to reduce cost and model design/fabrication time. Proper inlet simulation may alter the level of results, but the trends should not be

affected. A moving ground belt with leading-edge suction provides the proper ground boundary layer simulation necessary for STOL testing.

Jet-induced forces and moments are obtained using an interference testing technique. The model balance measures only pure aerodynamic plus interference forces and moments. Therefore, the balance can be sized so that the anticipated loads are near the upper limits of balance capacity (where balance accuracy is greatest). This approach to testing necessitates a metric/non-metric method of model fabrication where direct thrust forces and moments are grounded. Figure 4 illustrates the non-metric sting/manifold/nozzle assembly which is precalibrated to measure the direct thrust forces. Figure 5 shows the metric model shell installed on this assembly. The metric/non-metric method of model fabrication is clearly illustrated by the double-door construction of the engine deflector door. Each of the front and rear deflector doors is composed of two parts. The inner components (which measure direct thrust effects) are secured to the non-metric outer shell. Therefore, any forces or moments acting on the outer door will be registered by the model balance.

Data Analysis Considerations

Data pertaining to the hover flight mode are usually presented in the format of jet-induced forces and moments as a function of height above ground. Forces and moments are non-dimensionalized by static gross thrust or, if applicable, model reference geometry. Height is non-dimensionalized by model reference span. Similarly, one is tempted to present forward speed effects (i.e., transition and STOL) using the same non-dimensionalized jet-induced incremental effect approach. Grumman has found that this approach may be somewhat misleading since the incremental data:

- Are dependent on the accuracy of the power-off reference data
- May ask relevant aerodynamic phenomena which are pertinent to aircraft design

The former point is illustrated by the hypothetical data shown in Fig. 6. Two sets of identical lift data are used except for the power-off reference points (the differences of which may be attributable to balance accuracy at low dynamic pressure). The totally different trends exhibited by the incremental data are due to the differences in the reference power-off data. This inaccuracy may very well lead to the incorrect assessment of a particular configuration modification. The second point is illustrated by the stabilizer effectiveness data shown in Fig. 7. Again, lift data have been chosen for the example. The upper portion of Fig. 7 shows incremental jet-induced lift non-dimensionalized by gross thrust as a function of effective velocity ratio for three different stabilizer settings. One curve may be faired through all three sets of data. Specifically, it appears that the application of power has no effect on stabilizer effectiveness. But an additional important piece of information comes to light when the data are analyzed by the total lift coefficient format. Evidently, there is no increase in stabilizer effectiveness for deflections beyond -20 deg. Thus, an important piece of information could be missed if the data are accessed solely on the basis of incremental jet-induced forces and moments. Hence, it is recommended that both the incremental force (or moment) and lift coefficient data format be used for data analysis at forward speed.

Test Results

During the course of experimental investigations conducted by Grumman Aerospace Corporation certain results have come to light which have general applications with respect to jet-induced interference effects testing. These are:

- Forward speed data are relatively invariant with tunnel speed

In forward speed (i.e., transition or STOL flight), aerodynamic and/or interference parameters can be expressed as functions of either of two thrust parameters:

- Effective velocity ratio

$$V_{EFF} = (V_{\infty} / V_j)_{EFF} = 2A_j q_{\infty} / T, \text{ or}$$

- Thrust coefficient

$$C_{\mu} = T / q_{\infty} S_{REF}$$

where: A_j = Nozzle exit area

q_{∞} = Freestream dynamic pressure

T = Gross thrust

S_{REF} = Reference wing area

In the wind tunnel, variation in either of these parameters may be attained by varying either thrust or dynamic pressure. It was found more advisable to keep freestream dynamic pressure constant (from both balance sizing and tunnel operating envelope considerations) and vary thrust. The question then arose whether a variation in thrust produces the same physical result as a variation in freestream dynamic pressure. Figure 8 illustrates the results of a series of tests conducted at three different values of tunnel speed. These results indicate that the variations in lift with power setting are relatively invariant with tunnel speed

- Out-of-ground effect jet-induced interference characteristics are relatively insensitive to angle of attack

Configurations evaluated experimentally by Grumman to date have exhibited jet-induced interference characteristics which are relatively invariant with angle of attack for the out-of-ground-effect (i.e., transition) flight mode. Typical results are shown in Fig. 9. Data are presented in both total aerodynamic coefficient and incremental jet-induced interference formats. Both show that for preliminary design purposes jet-induced interference effects may be assumed to be invariant with angle of attack

- Wind tunnel models must accurately simulate the jet-exit configuration

The effects of adding sideplates to the lift/cruise engine nozzles of Design 623 are shown in Fig. 10. Although the importance of accurately simulating nozzle exit geometric characteristics is obvious, these data are shown to illustrate the differences in levels of jet-induced interference characteristics which can be obtained if one is not careful in accurately simulating aircraft geometry.

An example of a large effect caused by a less obvious configuration component is illustrated by the effect of adding rear nozzle doors on Design 607A, as depicted in Fig. 11. Data presented in both formats show a noticeable detrimental effect at forward speed. Although one tends to overlook the refinement of such minor details as these during the initial stages of preliminary design, they might prove to have a significant effect on the levels of jet-induced interference

- The lift engine may be a major contributor to jet interference at forward speed

Figure 12 shows the contribution which the lift and lift/cruise engines make to the total loss in lift at forward speed. Examples are shown for two widely different V/STOL designs. The open symbols denote data for Design 623 (a single lift and twin-pod-mounted lift/cruise engine concept). The closed symbols correspond to Design 607A, a configuration having two lift engines and a single lift/cruise rear-mounted engine. The relative strength of the jets are widely different for the two designs (the ratio of lift to lift/cruise thrust being 1.33 for Design 607A and 0.57 for Design 623).

Despite these differences, both configurations exhibit flat variations in lift coefficient for the lift/cruise jet on case, as compared to the data for the lift jets on only. As a numerical example, consider data for Design 623 (the open symbols). At a thrust coefficient of 4.0, the total lift coefficient (aerodynamic plus jet-induced interference) is -0.055. To examine the separate contributions of each jet, one must select the thrust coefficient which was used to obtain the total for the aircraft. For a total thrust coefficient of 4.0, the corresponding values of lift and lift/cruise engine thrust are 1.45 and 2.55, respectively. At these values, one can note that almost twice as much degradation in lift is due to the isolated lift jet than the isolated lift/cruise jet. The remaining amount of lift degradation is attributable to interference effects between both engines.

Note that although both configurations have different contributions to total lift, the lift engine is the major contributor in both cases

HOT-GAS REINGESTION TESTING

Grumman has conducted several hot-gas reingestion and ground footprint test programs at VFW-Fokker for the VAK-191B and Grumman Design 623 aircraft. These discussions will highlight some of the latest reingestion results from the Design 623 test program.

Test Facility & Technique

A 1/12-scale model (Fig. 13), was tested in VFW-Fokker's gas dynamic facility in Bremen, Federal Republic of Germany. The facility is capable of providing supersonic hot-gas flow to simulate exhaust conditions and has suction capability to simulate inlet mass flow. The aircraft was mounted over a ground plane with a moveable door. A test run was conducted with the door open to get baseline temperature measurements, then with the door closed to get actual data, and then again with the door open to get a new baseline. Each test run averaged 2 min. Wind was provided by a fan located off the test rig. The facility is vented to avoid excessive increases in ambient temperature.

As with other jet-induced testing, significant detail must be paid to accurately simulating configuration details. However, reingestion tests are critically dependent on accurately simulating the exact inlet and exhaust flow conditions.

Earlier VFW testing indicated that the level of inlet temperature rise measured was related directly to inlet Mach number (see Fig. 14.) Other types of test techniques, such as aspirated thermocouples, may measure local ambient conditions very accurately but cannot affect the hot-gas flow passing by the inlet. In most cases inlet suction is required to "suck in" the masses of hot-gas flow which pass an inlet at significant speeds. Additionally, inlet suction should be varied with exhaust flow to accurately simulate full-scale conditions.

To simulate exhaust flow, each nozzle is calibrated to ensure that an accurate pressure profile exists, as shown in Fig. 15. The pressure distributions are integrated to establish thrust vector angle as a function of nozzle deflection angle. In addition, upstream pressure is correlated to exhaust pressure and is checked for each run.

Exhaust gas temperatures are measured both upstream of the nozzle and at the exhaust plane for each run. Thermocouple locations are chosen iteratively to ensure repeatability.

Data Analysis

Inlet temperature rise is measured by high-response (0.2 sec) thermocouples located at the engine face in each inlet. Figure 16 illustrates the thermocouple (T/C) location and distribution for each rake. All three engine rakes have 12 T/Cs positioned in inner and outer rings. More thermocouples were chosen for the outer ring where the largest difference in inlet ΔT is anticipated.

Inlet temperature rise is arrived at by conducting a regression analysis for each T/C to establish mean inlet temperatures. The T/C mean readings are then averaged by its region of influence to determine the average inlet temperature rise. Note that the outer T/Cs are responsible for one-half the area of the inner T/Cs. The average inlet temperature rise is then compared to the ambient temperature measured at several locations to establish inlet ΔT due to hot-gas reingestion.

Test Results

During the course of this investigation, certain demonstrated results have general application with respect to hot-gas reingestion testing:

- Inlet temperature rise may be a strong function of jet deflection angle

It is well known that reingestion decreases with jet deflection. Figure 17 highlights the significance of this trend. For a configuration like Design 623, inlet temperature rise reduces dramatically with jet deflection. Large jet deflection angles used for rolling VTOs or for STOs can reduce reingestion to a negligible amount as compared to a pure 90/90 case. More important, however, is the large reduction at smaller angles. A 10-deg jet deflection can reduce reingestion by 70-90%. That is, if a pure VTO experiences 100°F of reingestion, a 10-deg deflection can reduce that to a tolerable 10°F. In addition, a 10-deg deflection still results in an aircraft thrust/weight above one. Therefore, hot-gas reingestion can be avoided and still have a pure VTO

- Reingestion is sensitive to both wind and aircraft altitude

During the test program several variables were investigated, including the effects of wind and height. Figure 18 highlights some of these results. Most V/STOL designs are sensitive to wind direction and velocity. Design 623 has its hot-gas flow channeled underneath the fuselage along the podded nacelles. This arrangement makes it vulnerable to headwinds. Some of the high-speed gas flow passes the inlet under static conditions. However, increasing wind velocity can push these gases back into the inlet. The other criterion, height above ground, is also sensitive. Design 623, like most V/STOL aircraft, reaches a height where reingestion is greatest. Above that, reingestion will dissipate quickly

The point to be made is that in developing or testing a viable V/STOL design, one must ascertain the worst wind and height conditions, not just static conditions

- Reingestion is dependent upon thrust split

Lift plus lift/cruise aircraft will have a fountain and/or upwash somewhere between the forward and rear jets. The location and inclination angle of this fountain is associated directly with the level of reingestion experienced. Aircraft having weak (low-thrust) forward jets may experience a forward-facing fountain which provides a good source of hot gas close to the inlet. Figure 18 illustrates the trend with thrust split. The lift engine must contribute a significant portion of total thrust to minimize reingestion. This trend should be considered in the preliminary design of any V/STOL aircraft

- Auxiliary doors are necessary to reduce reingestion

Design 623 incorporates auxiliary doors on the top of each inlet to provide increased static pressure recovery. In line with the research considerations given to this type of testing, it was decided to close these doors to determine their effect on temperature rise. Figure 18 depicts one such condition where

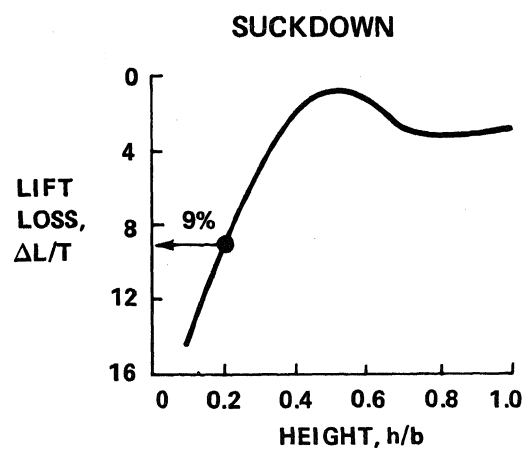
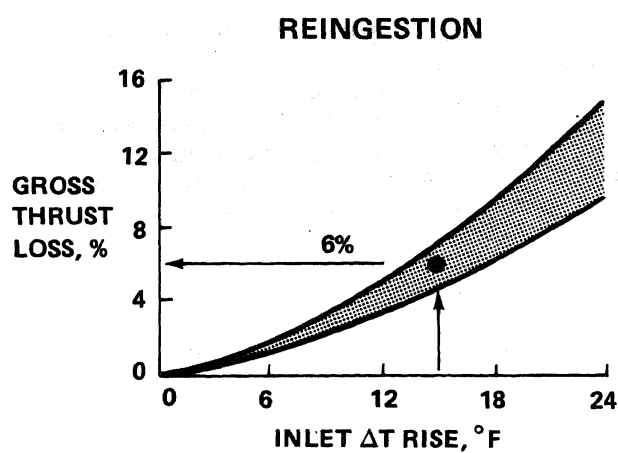
inlet temperature rise more than doubled with the auxiliary door closed. This trend was anticipated because a region of cool air existed above the nacelle. The message, however, is: test several locations for the auxiliary inlet to determine the optimum location but always keep the door open

- Temperature distortion is as critical as average inlet temperature rise

Figure 19 has been included to illustrate the magnitude of inlet temperature distortion which may be experienced during each takeoff or landing. These data indicate that severe circumferential and radial distortions can occur. Therefore, one must not only be concerned with absolute levels of reingestion but on how badly the inlet flow is distorted. To ensure the successful development of future V/STOL aircraft, more emphasis must be placed on the allowable temperature distortion for an engine and how it affects stall

CONCLUSIONS

Test programs designed to evaluate jet-induced effects are vital in a development program. Testing technique is well in hand but not universally adopted. More attention should be paid to data analysis, and classical trends are becoming evident. However, more needs to be done to analytically minimize test requirements. Grumman has been working on methodologies to predict these phenomena, but still lacks necessary empirical data. It is recommended, therefore, that more research-oriented tests be conducted to provide the required information on jet entrainment, scaling laws, and non-uniform nozzle exhaust flow, both in- and out-of-ground effect.



RESULT

A 30,000-LB AIRCRAFT WHICH HAS 15% THRUST
LOSS DUE TO JET-INDUCED EFFECTS:

- LOSES AVAILABLE VTO FUEL
→ 33% DECREASE IN RADIUS, OR
- MUST OVERSIZE EACH ENGINE
→ 15% INCREASE IN TOGW

THEREFORE

JET-INDUCED LOSSES MUST BE:

- MINIMIZED, AND
- ACCOUNTED FOR ACCURATELY

Fig. 1 Importance of Jet-Induced Effects

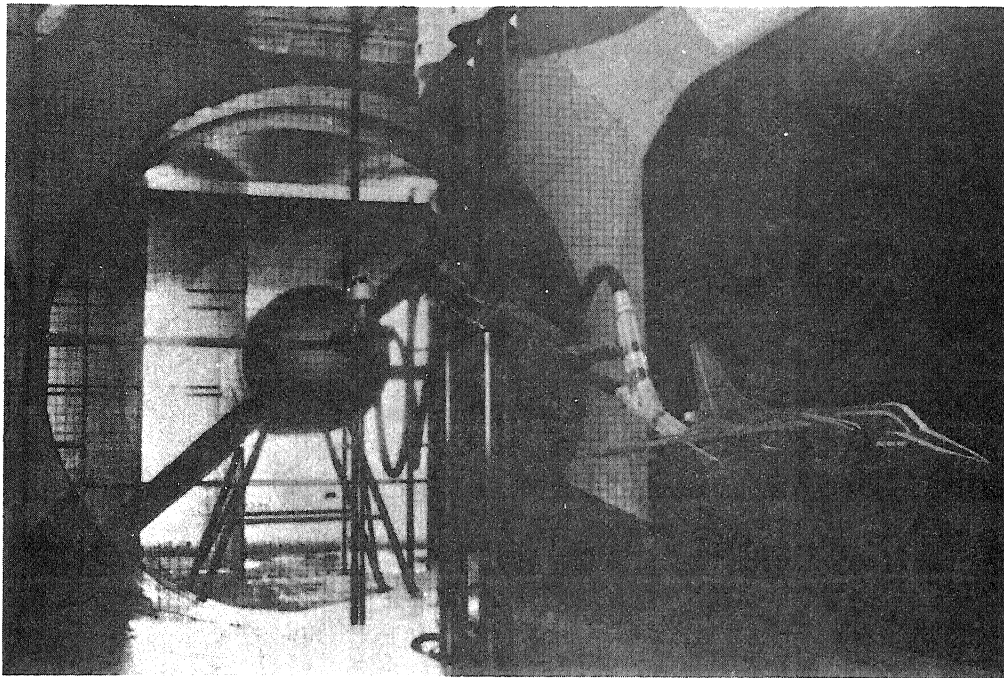


Fig. 2 1/8-Scale Model of Twin DLE, Single LCE Design 607A

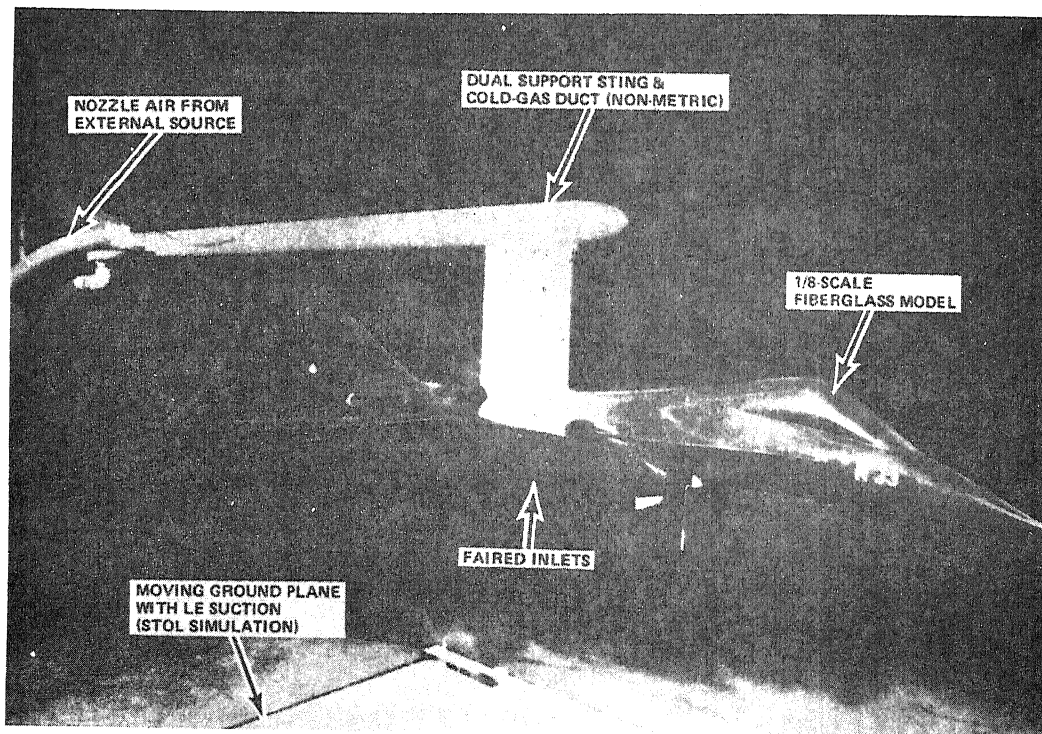


Fig. 3 Single DLE, Twin LCE Design 623 in BAC 5.5-m V/STOL Tunnel

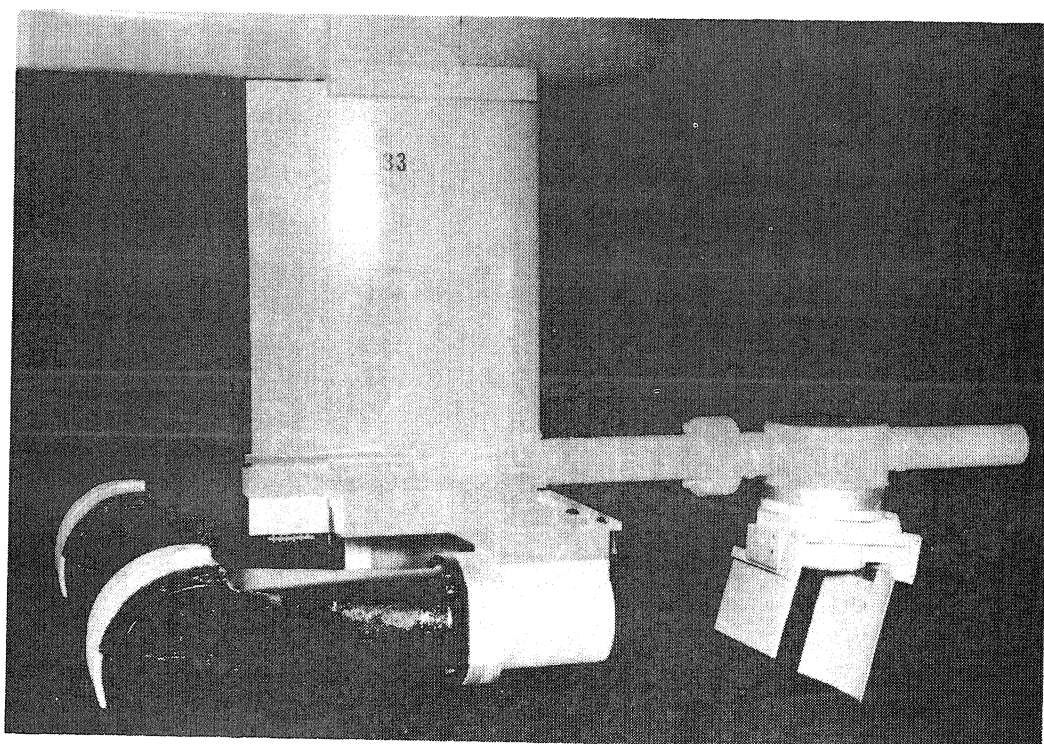


Fig. 4 Non-Metric Sting/Manifold/Nozzle Assembly

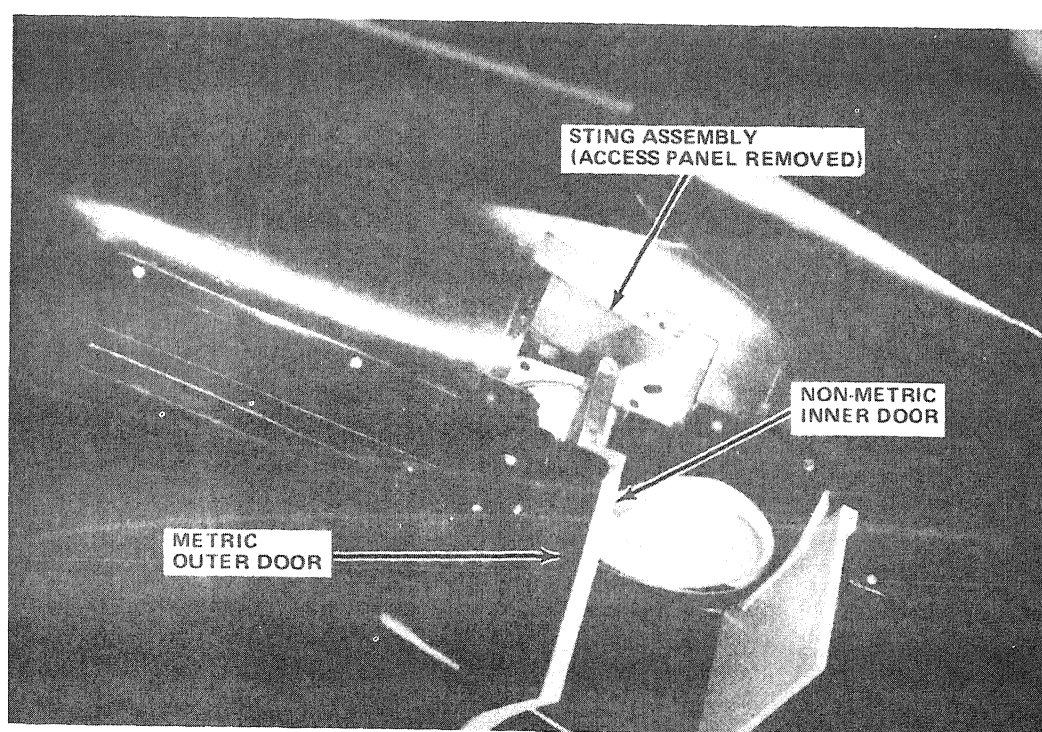


Fig. 5 Example of Metric/Non-Metric Model Construction

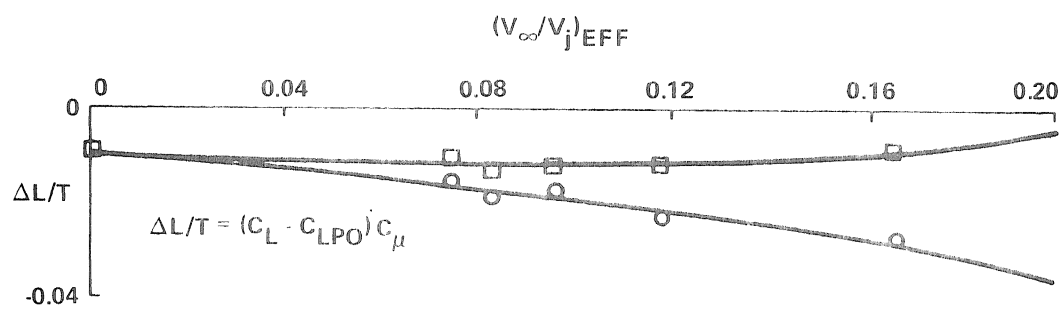
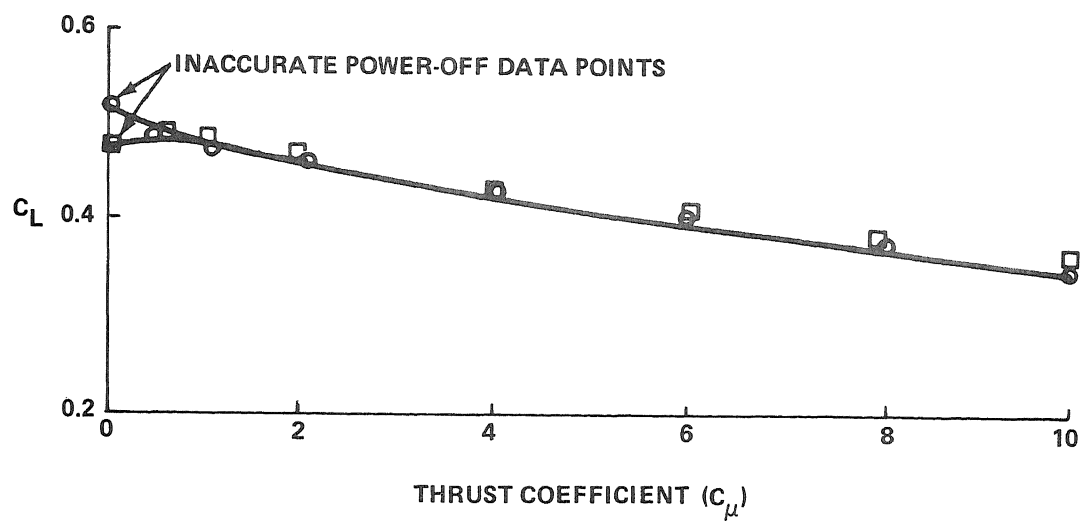


Fig. 6 Analysis of Incremental Data ($\Delta L/T$)

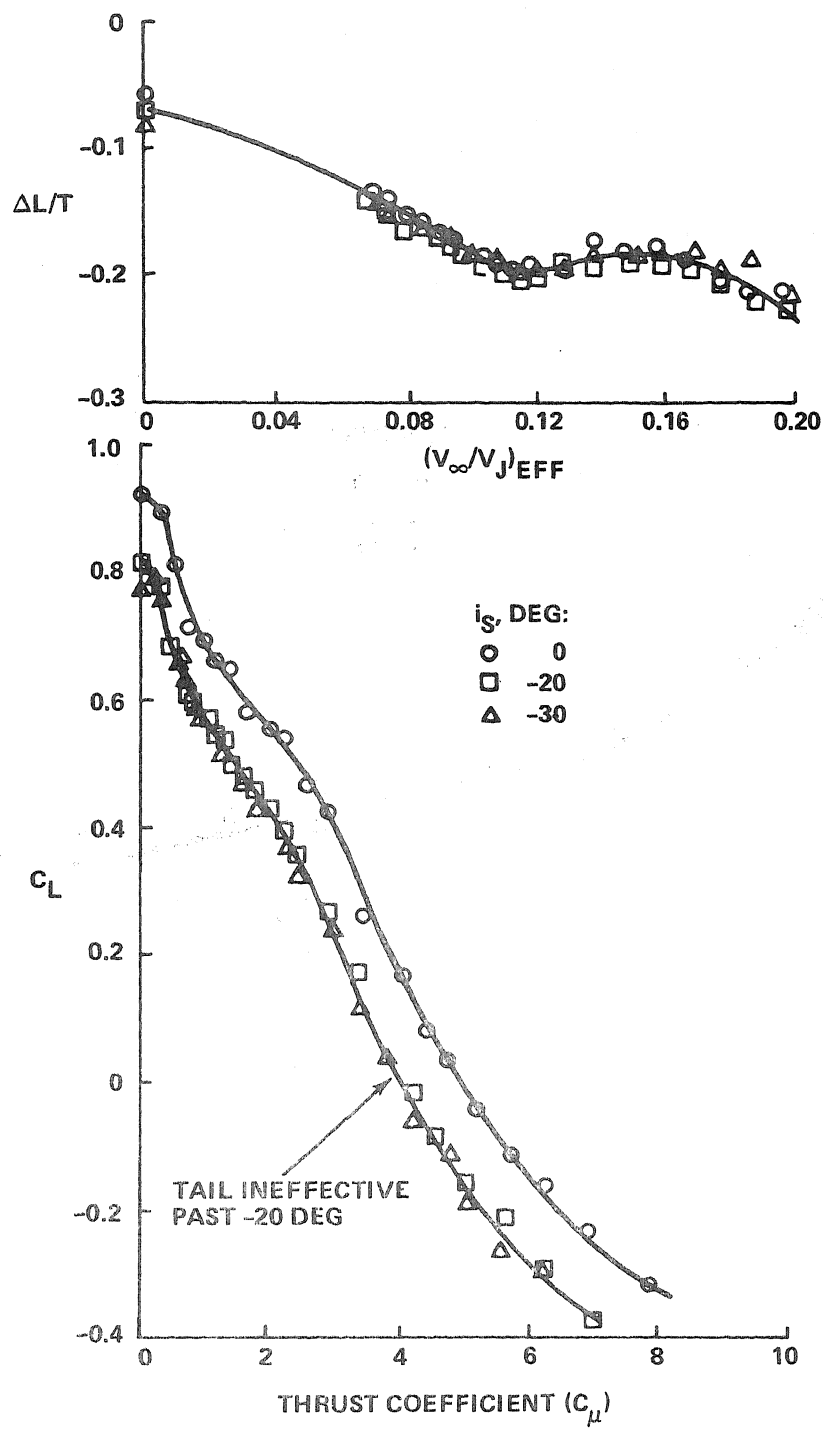


Fig. 7 Incremental Data Analysis

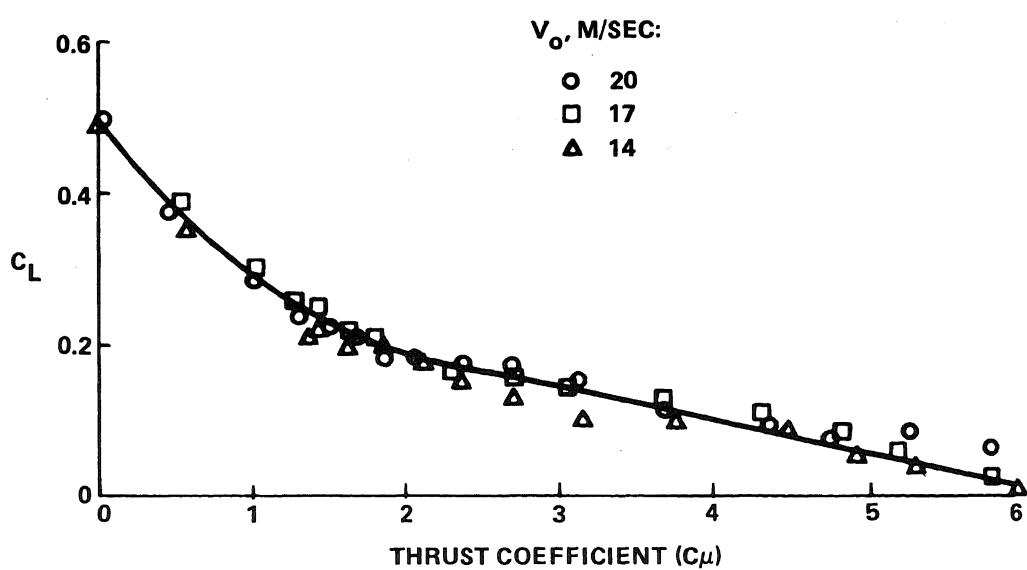


Fig. 8 Forward-Speed Data vs Thrust Coefficient

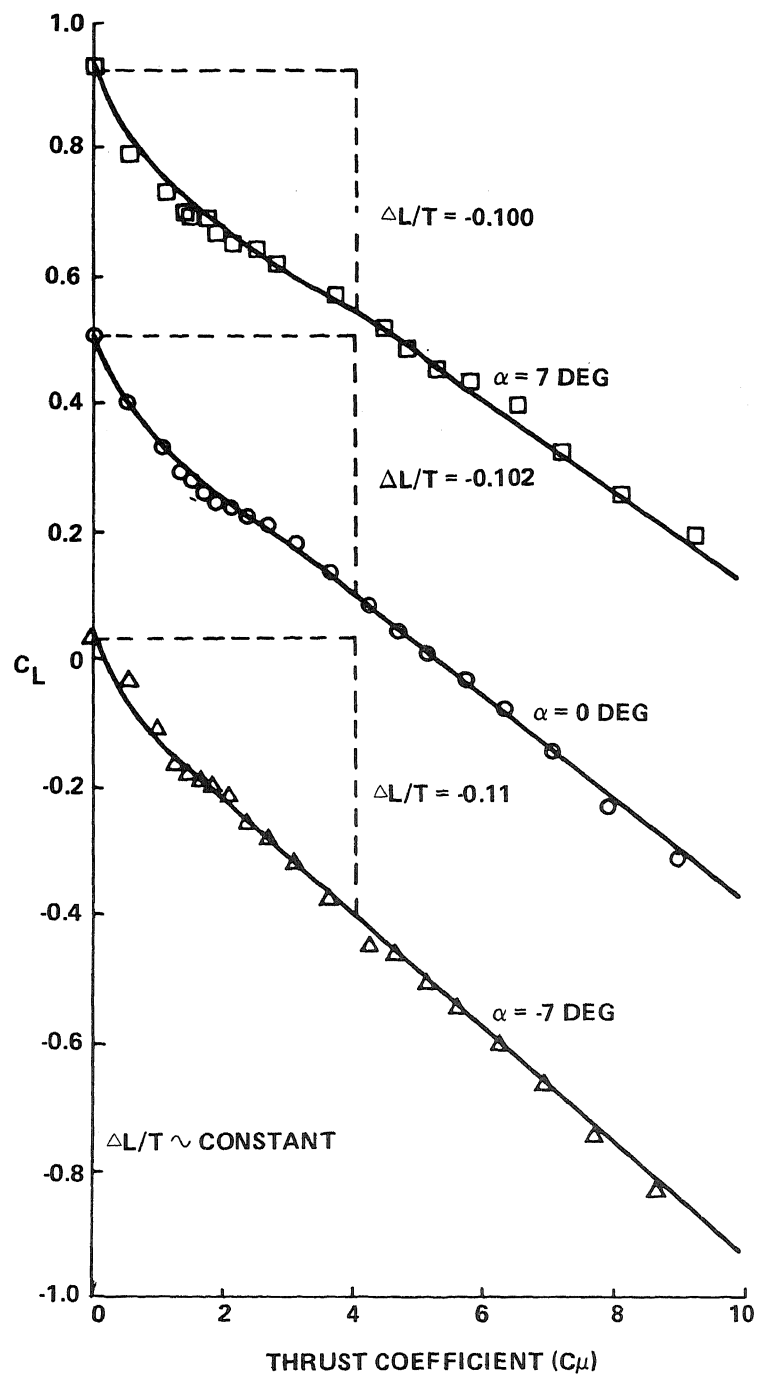


Fig. 9 OGE Angle-of-Attack Considerations

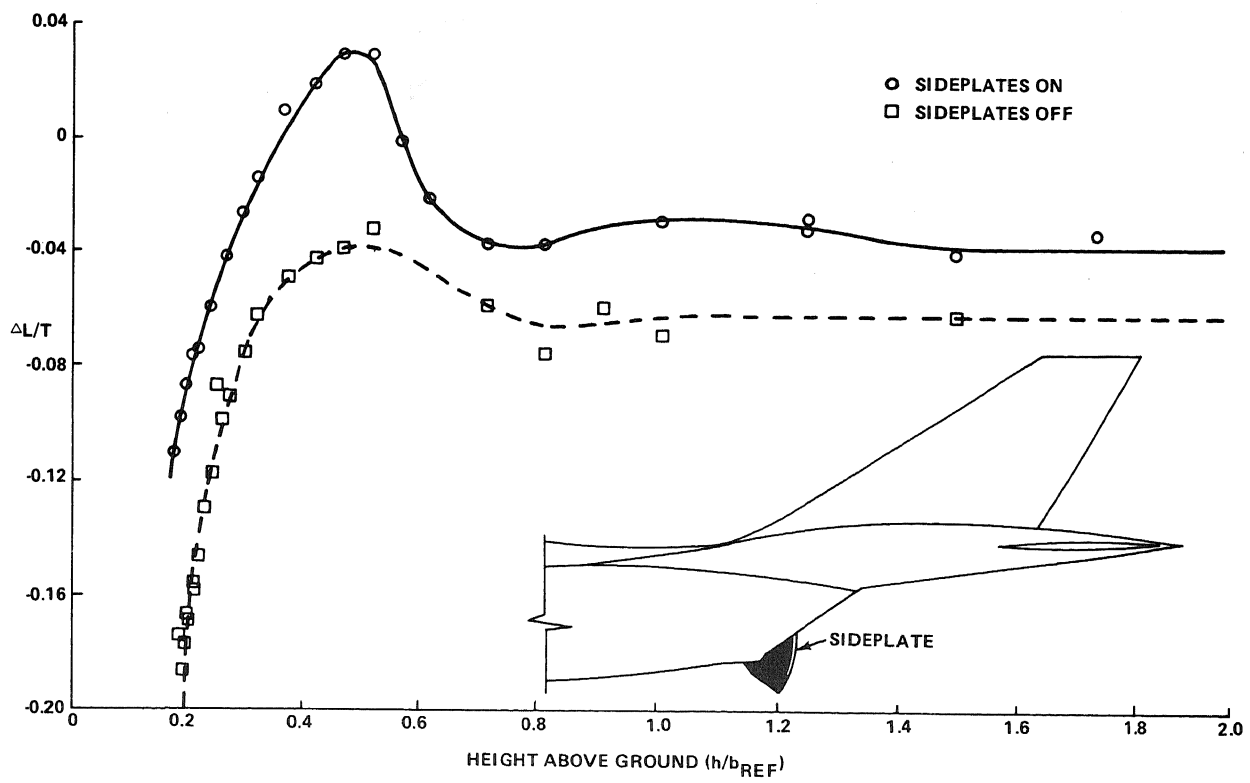


Fig. 10 Improperly Configured Model

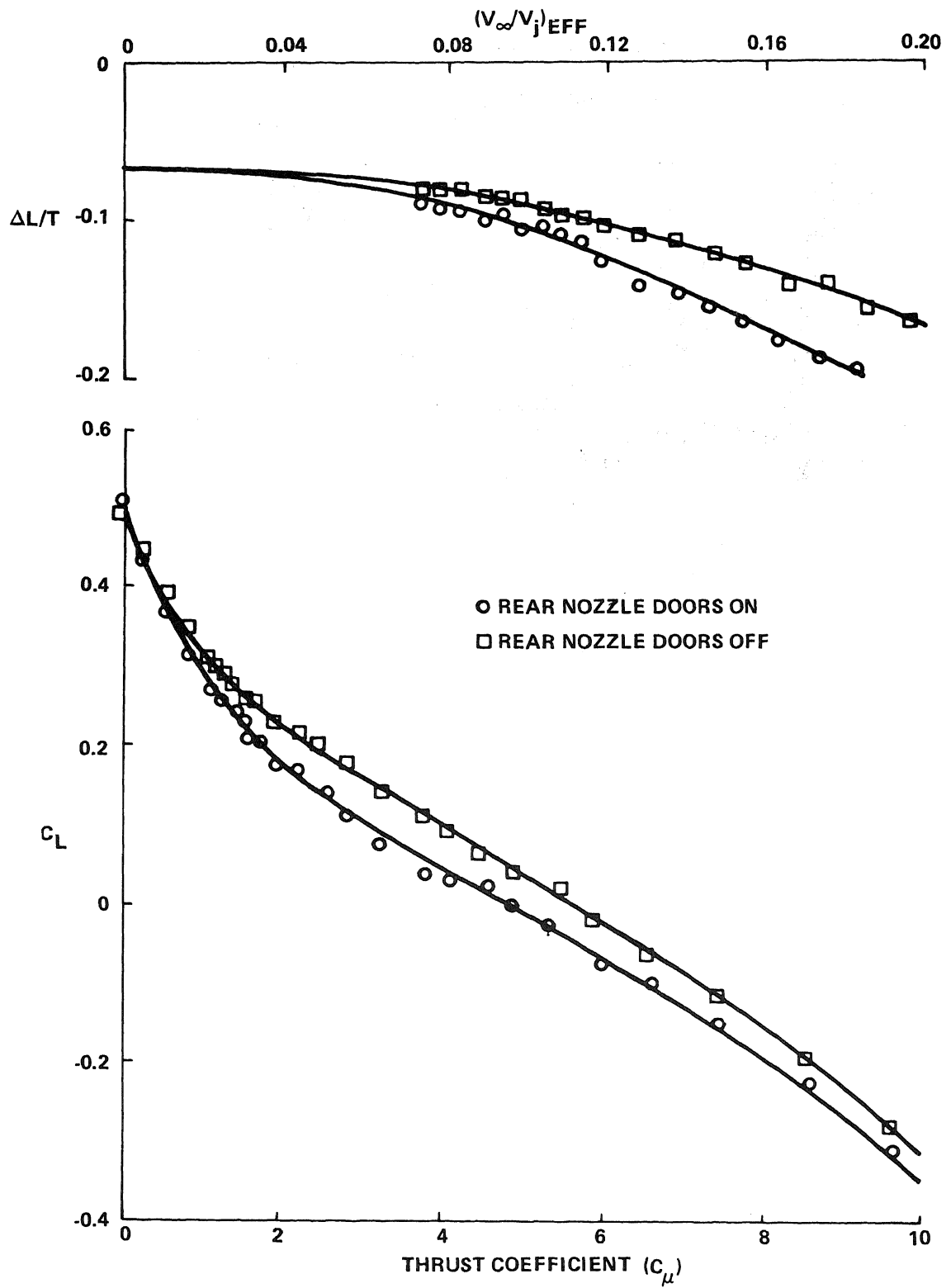


Fig. 11 Configuration Detail

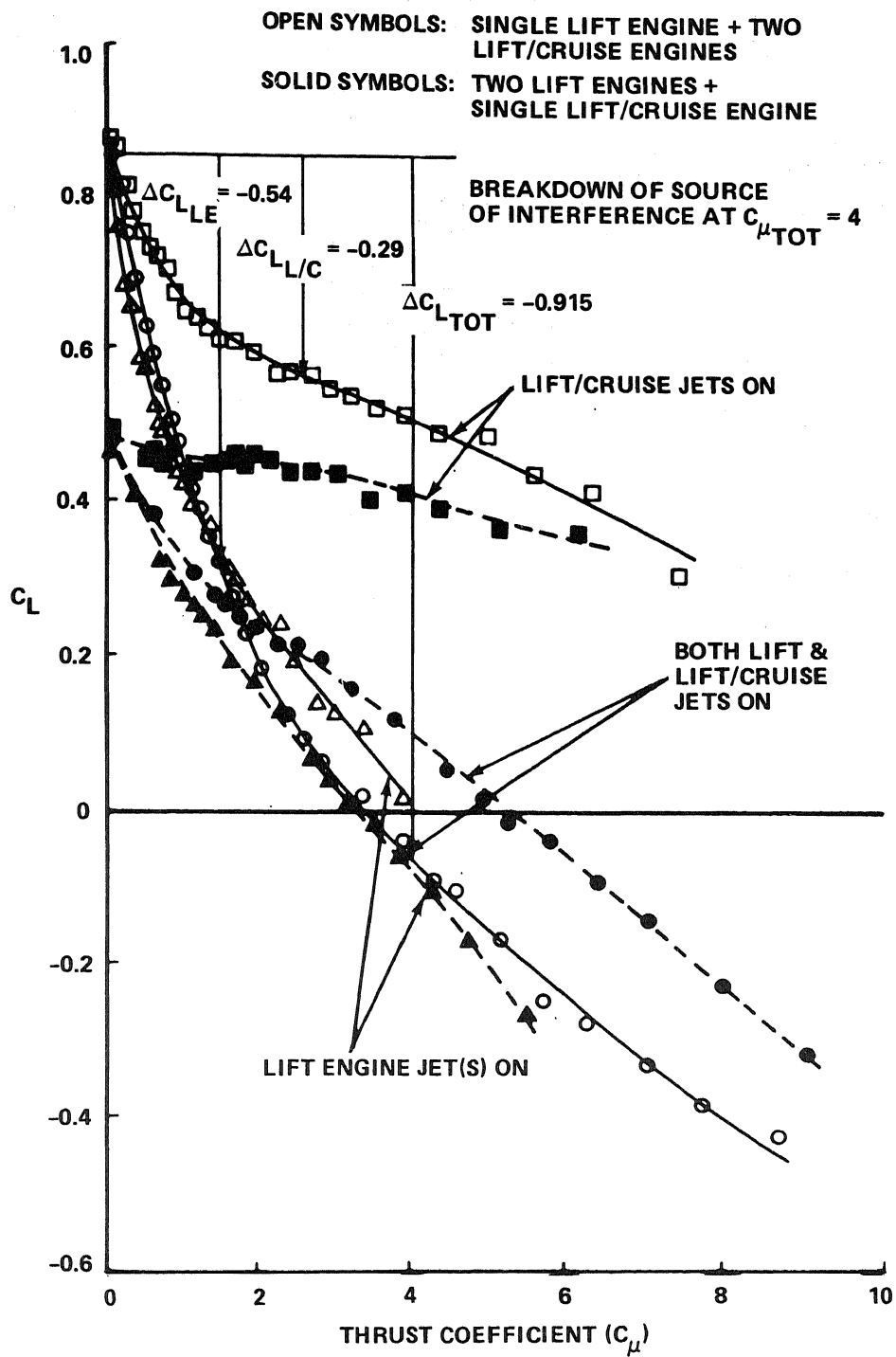


Fig. 12 Lift Engine Contribution

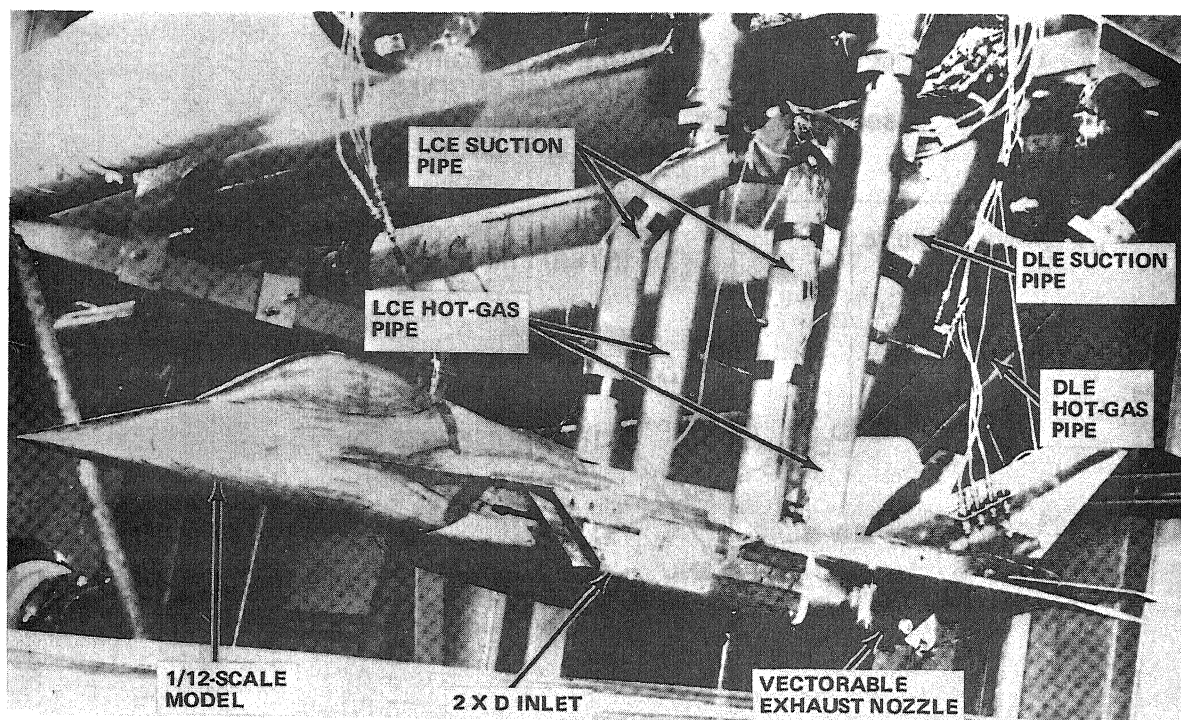


Fig. 13 Design 623 Hot-Gas Test Model & Rig

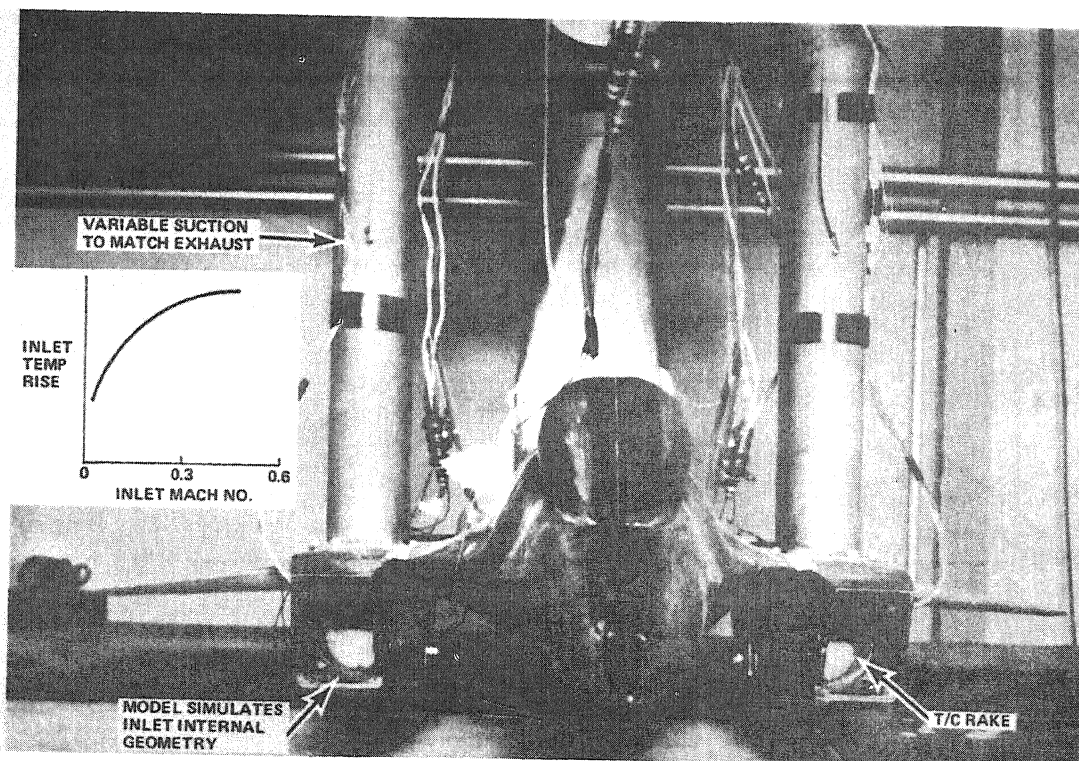


Fig. 14 Induction System Simulation

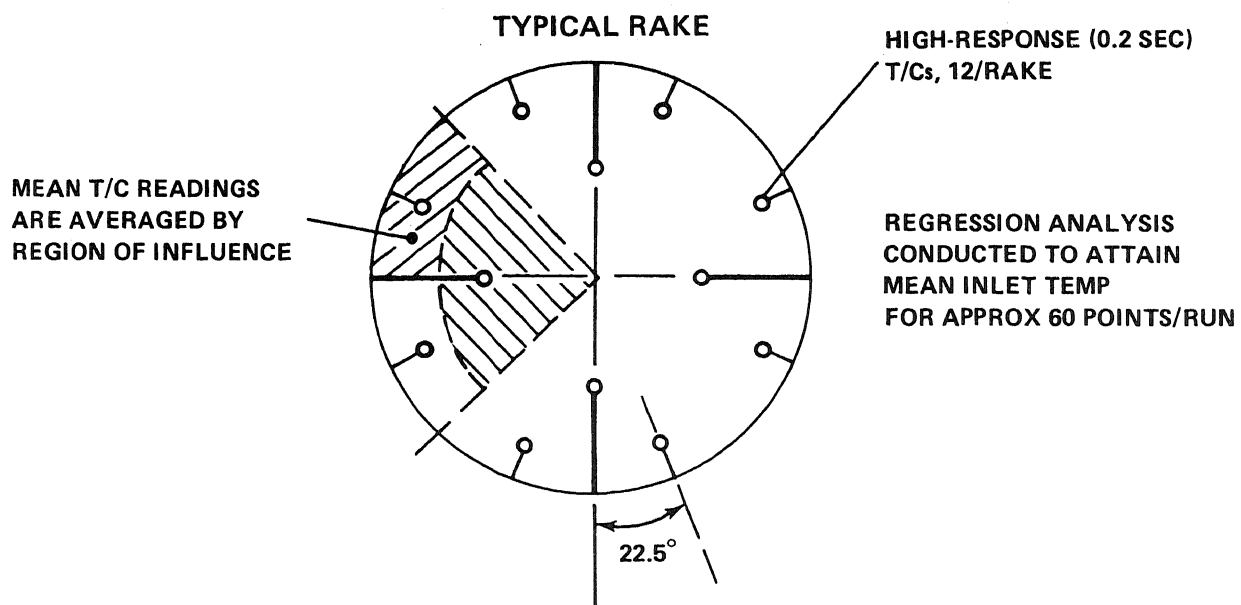
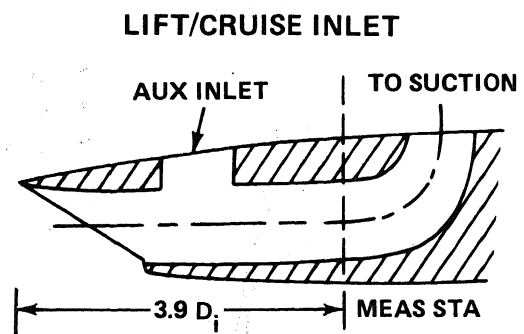
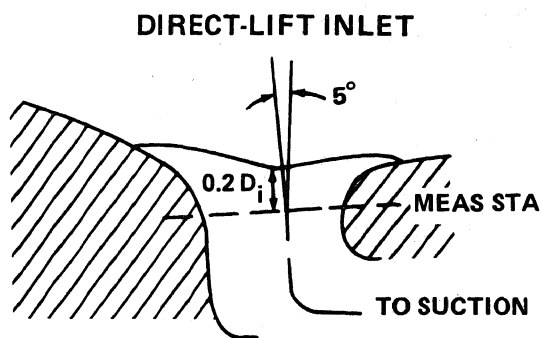


Fig. 16 Thermocouple Location & Distribution

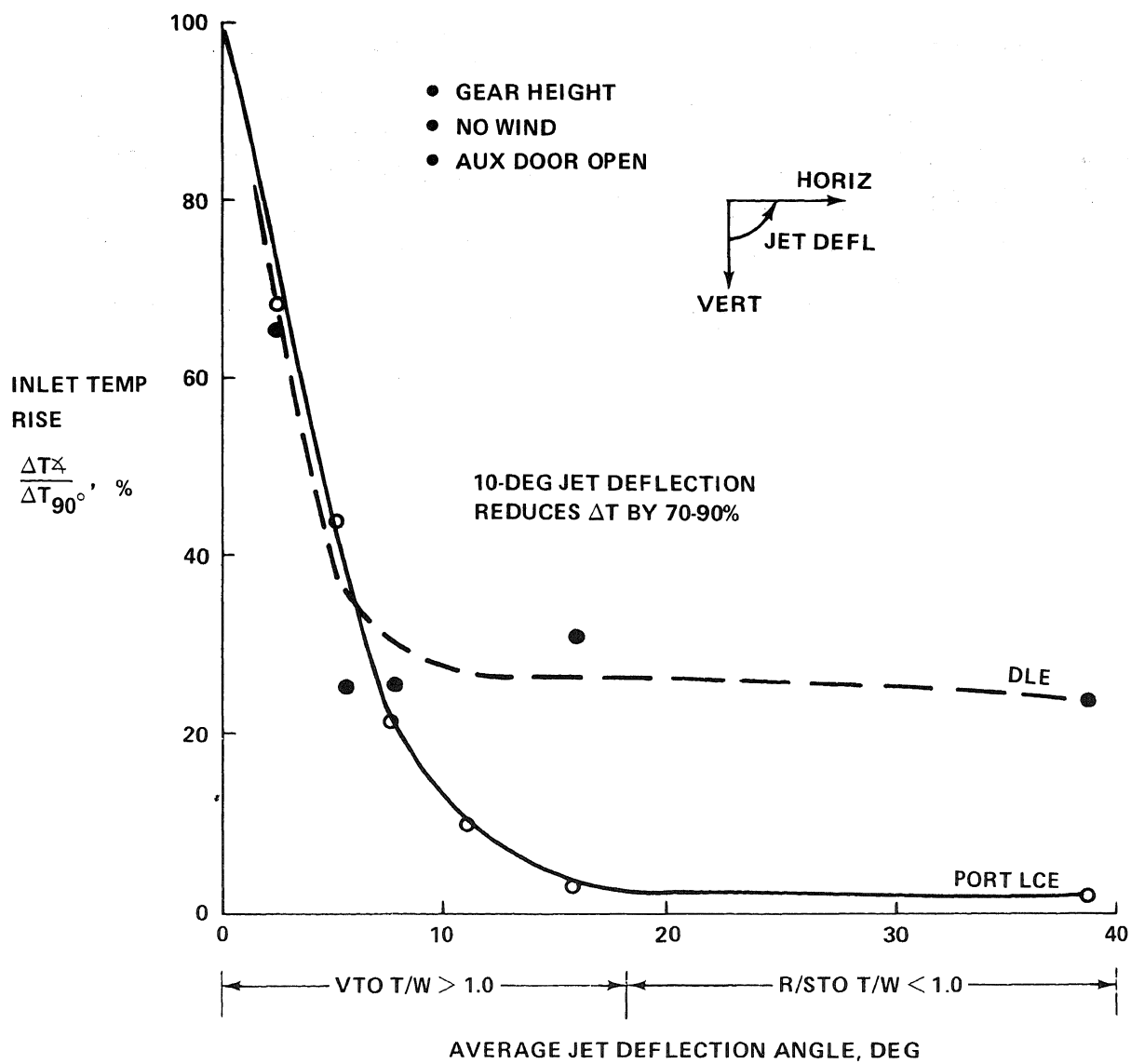


Fig. 17 Sensitivity to Jet Deflection

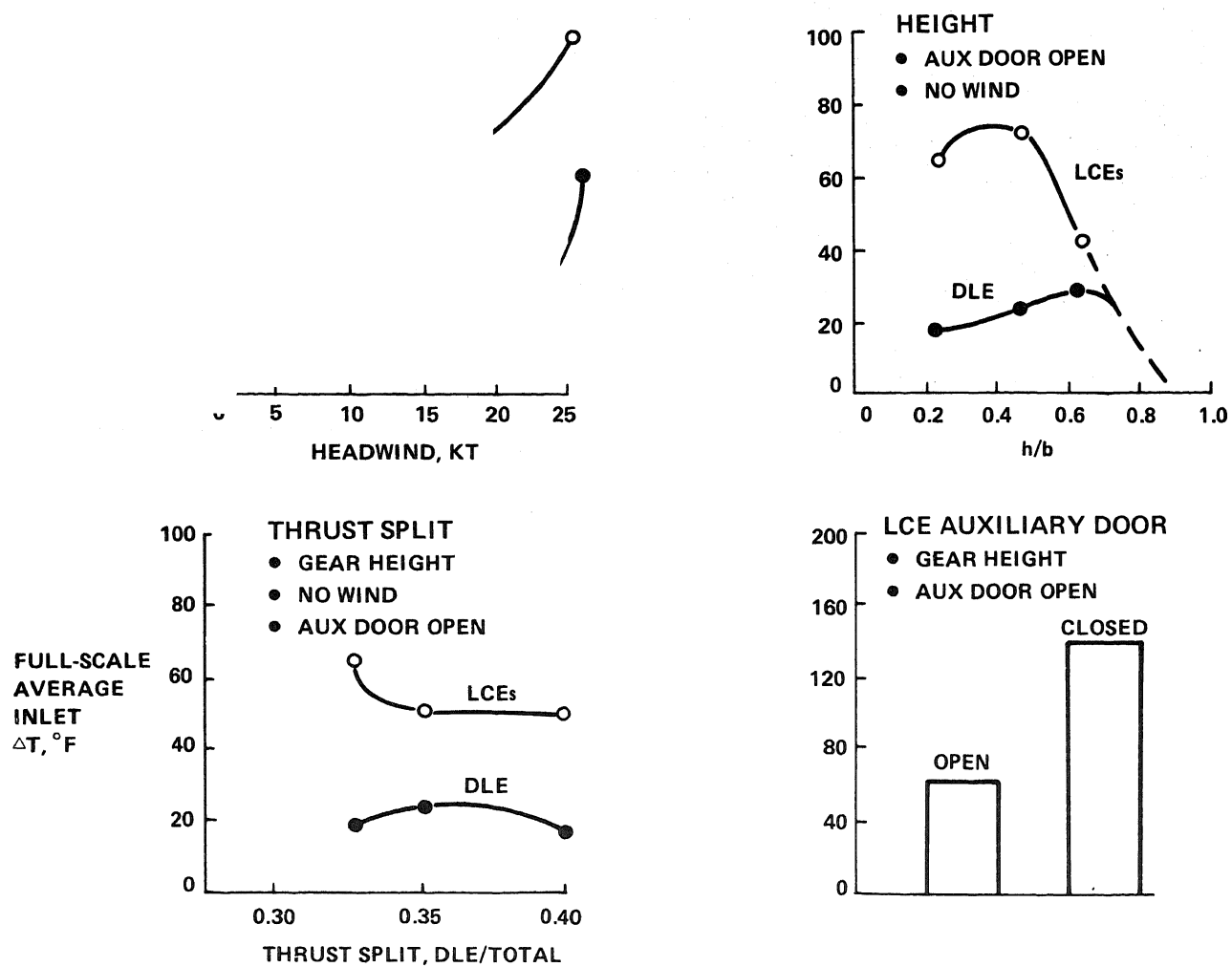


Fig. 18 Effect of Test Variables on Inlet ΔT

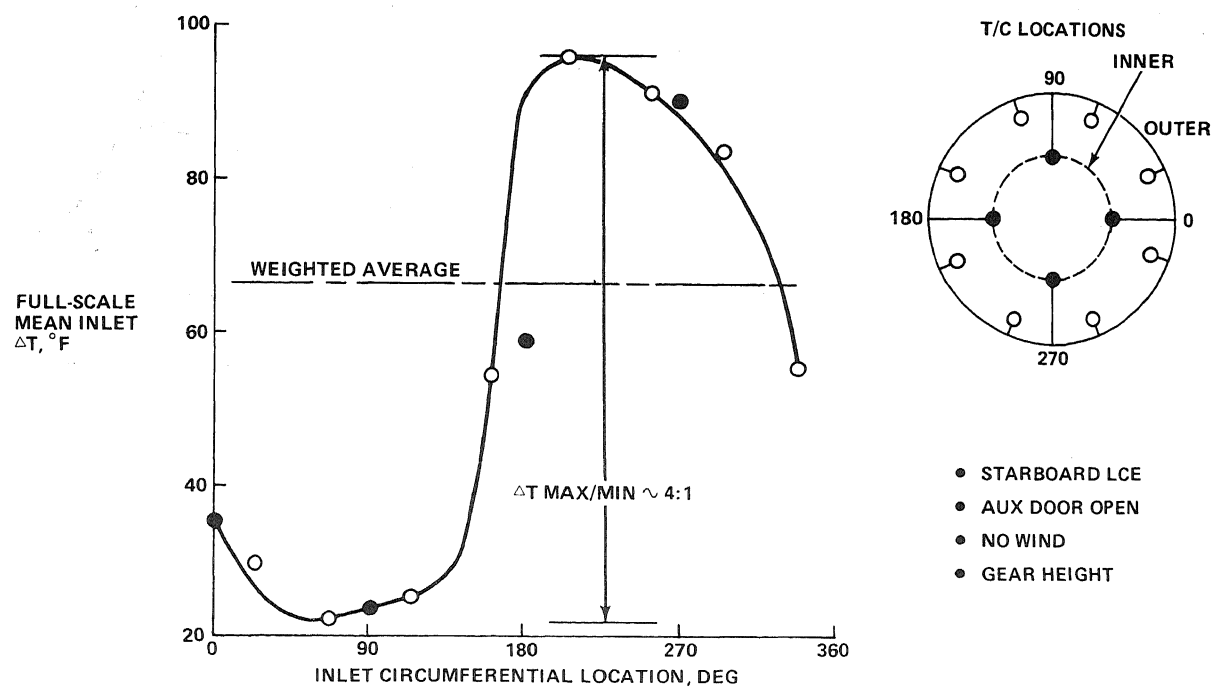


Fig. 19 Inlet Temperature Distortion

Forces and Moments Produced on a Two-Dimensional Body in a Strong Lift-Jet/Airframe/Ground Interaction*

by

D. R. Kotansky and W. W. Bower

*McDonnell Douglas Research Laboratories
McDonnell Douglas Corporation
St. Louis, Missouri 63166*

Abstract

The prediction of induced forces and moments on VTOL aircraft in close ground effect is critical to the sizing of propulsion systems, the specification of thrust vectoring requirements, and the design of aircraft control systems. Theoretical prediction of the required aerodynamic forces and moments is severely complicated by the strongly viscous (turbulent) nature of the flowfields and the complex geometries involved. In addition to these very fundamental complications, the effects of density variations, environmental cross-winds, and flow unsteadiness must frequently be considered.

In an effort to begin the development of comprehensive theoretical methods for the prediction of these types of flowfields, an experimental and theoretical investigation of the viscous flowfield, including forces and moments, produced on a two-dimensional body with a centered, vectorable lift-jet in close proximity to a ground surface has been initiated. The current objectives of this investigation are: (1) to compute the viscous flowfield about the physical model utilizing one or more currently available turbulence models in a finite-difference solution of the governing elliptic equations of motion, and (2) to measure significant flowfield properties and forces and moments on the physical model as a result of the lift-jet/model-surface/ground interaction in a two-dimensional static experiment. These initial efforts, both theoretical and experimental, are limited to two-dimensional and incompressible flow, but can be extended to include compressibility and cross-flow effects. Nozzle height above ground, h/D , lift-jet thrust vector angle, and jet Reynolds number are the primary variables, and emphasis is placed on the prediction and measurement of induced forces and moments for small values of h/D , i.e., $0.5 \leq h/D \leq 5.0$.

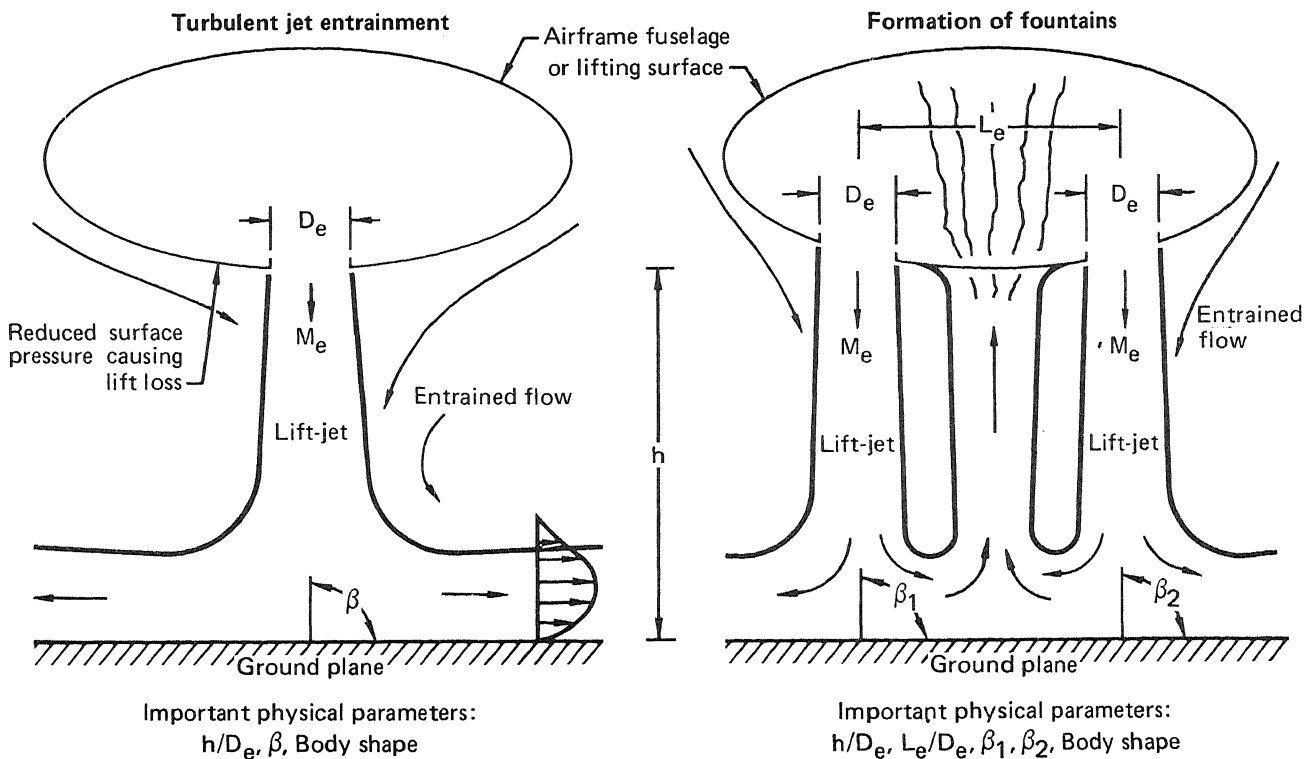
The rationale, specific objectives of both the theoretical and experimental programs, progress to date, and the long-range objectives are discussed. Emphasis is placed on the necessity for including a fully-elliptic solution to the viscous flowfield with an appropriate turbulence model and on the need for accurate, detailed experimental data on model forces and moments, turbulence properties, and external flow entrainment by the jet in the experimental model flowfield.

**This research was conducted under the McDonnell Douglas Independent Research and Development Program.*

Introduction

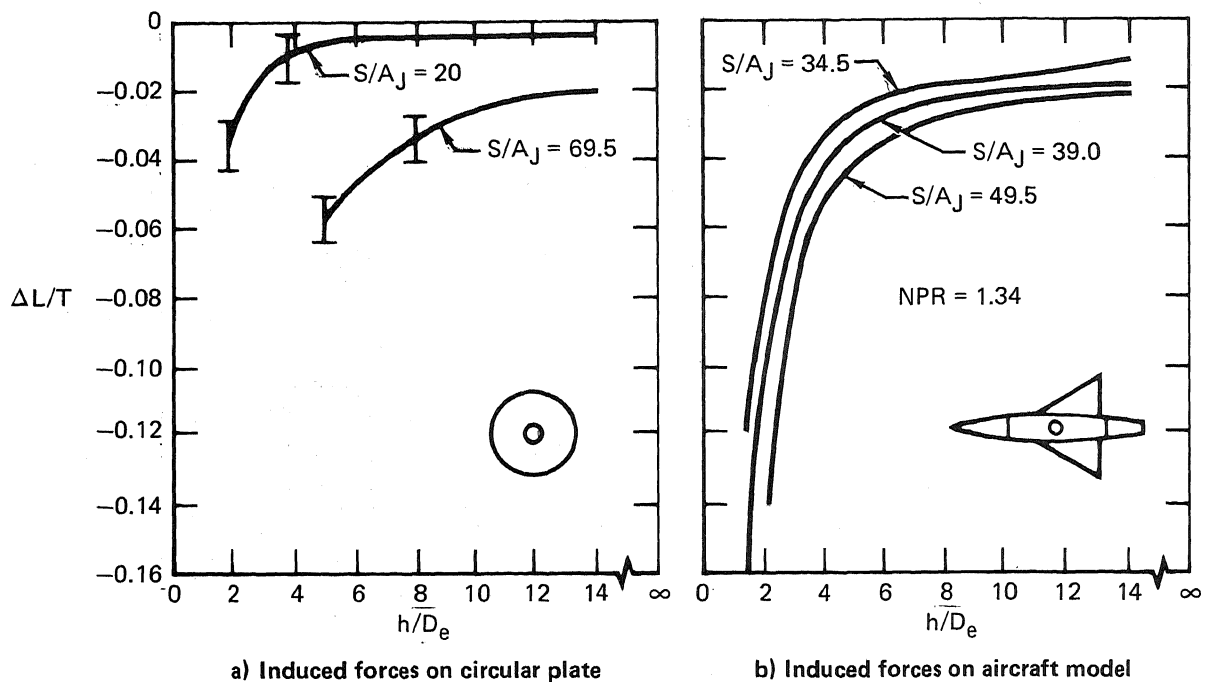
The design of VTOL aircraft equipped with powered lift-jet or powered lift-augmentation systems requires a knowledge of the complicated flowfield associated with the operation of these devices over a wide range of aircraft operating conditions. Of particular importance are the flowfield interactions resulting from the operation of these types of aircraft in proximity to the ground where strong interactions frequently occur between the lift-jet stream, airframe surfaces, and the ground. These interactions usually result in the introduction of generally unpredictable forces on the airframe which can be positive (providing additional lift) or negative, in which case a nominally designed propulsion system may not provide sufficient thrust for an adequately controlled take-off. In addition to these induced net loads, situations are encountered where unfavorable moments are produced on the airframe resulting in significant stability and control problems.

The induced forces (and moments) in ground proximity usually result from one of two reasonably well defined viscous flow phenomena, jet entrainment and the formation of jet flow fountains. These two basic interactions are indicated schematically in Fig. 1. Jet entrainment causes otherwise static air to be set into motion, resulting in locally reduced static pressures on nearby airframe surfaces and thus introducing aerodynamic loads. The jet entrainment effect occurs both in and out of regions influenced by the presence of the ground, but is frequently accentuated as the distance between the jet source (nozzle exit) and the ground is reduced. This effect is illustrated by basic data obtained by NASA on the induced loads on a circular plate through which a relatively small diameter jet emanates. The induced loads on the plate as a fraction of the jet thrust, $\Delta L/T$, are shown in Fig. 2a as a function of h/D_e , the ratio of jet exit height above ground to jet exit diameter. This is shown for two plate-surface to jet-exit area ratios S/A_j . The data clearly show the increase in magnitude of the negative induced force as the height above ground is reduced (and also as the surface area ratio is increased). The data shown were obtained by direct measurement of the forces on the plate by a force balance, as described in Ref. 1. Similar data for a delta-winged aircraft model are shown in Fig. 2b.¹ Other data supporting this general type of behavior with small-scale model tests with a single jet in ground effect can be found in Refs. 2 and 3. Hall⁴ has verified similar behavior utilizing a large-scale flat plate and a single lift jet supplied by a J-85 engine.



GP75-0592-1

Fig. 1 VTOL flowfield interactions in ground effect



GP75-0592-2

Fig. 2 NASA interaction test (Ref. 1)

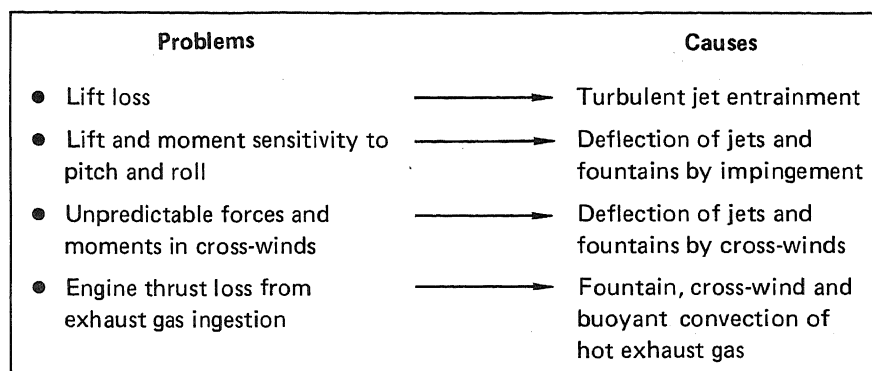
Although the jet entrainment effect occurs both in and out of ground proximity, the formation of jet flow fountains requires an impingement surface and, therefore, is peculiar to operation close to the ground. The formation of fountains is also configuration-dependent in that multiple jets are required and the relative location and spacing between the jets are strongly influential factors. The recirculation of jet flow caused by fountains sometimes results in a positive ground effect,⁵ which is a result of the positive pressurization of airframe surfaces containing and deflecting the upward flow of the fountains. Because of the upward convection of the lift-jet stream in the fountains, a degradation of propulsion system performance frequently results through exhaust-gas ingestion. In this respect, fountains can be seriously detrimental to VTOL aircraft performance in ground proximity. Induced aerodynamic force data on a number of VTOL aircraft configurations in ground effect with multiple lift-jets can be found in Ref. 6. These data are particularly interesting in that a double change in the sense of induced forces occurs for certain configurations with widely spaced lift-jets in close ground proximity.

In summary, the aerodynamics of VTOL aircraft are influenced by a number of geometric parameters and the viscous (turbulent) nature of the local flowfield. Significant VTOL flowfield interactions and their effects on aerodynamic performance in ground effect are summarized in Fig. 3. The general prediction of these flowfields and resulting aerodynamic forces for arbitrary aircraft configurations is undoubtedly many years off, and it may never be economically feasible to rely solely on theoretical predictions. However, it is possible with present state-of-the-art knowledge to synthesize useful solutions for well-defined viscous flowfields about airframe components of significant current interest. It is to this objective that the work described herein is directed: the prediction of viscous flowfields, including induced forces, about selected aerodynamic shapes with self-contained lift-jets in ground proximity for a well-defined set of flow conditions.

Approach

In view of the complexities of VTOL powered lift-jet/airframe/ground interactions, current design and development practice is to approach the investigation of these problem areas experimentally. This is necessitated by a general lack of prediction methods except for a few special cases which have been modeled empirically. These works include those of Wyatt³ for single lift-jets and a recently developed empirical method by Louise and Marshall⁷ for twin lifting jets which includes the favorable effect of a fountain. These methods are useful for the prediction of in-

duced loads on certain configurations but are limited to vertical flight conditions and otherwise static external flowfields. If generally useful prediction methods for VTOL flowfields are to be developed, they must be physically descriptive to allow parametric variation of significant aircraft and environmental variables, i.e., we must be able to study the effects of variations in basic aircraft geometry, height above ground, jet impingement angle, number of jets and nozzle exit spacing, aircraft pitch and roll, and cross-wind effects.



GP75-0592-3

Fig. 3 VTOL flowfield interactions in ground effect

To achieve these predictive capabilities, a number of approaches are possible; some are suggested in Fig. 4 with major advantages, disadvantages, and projected capabilities. No additional discussion of approaches (1) or (2) is required. Approach (3) basically consists of potential flow models of the *irrotational* flowfield induced by jet entrainment. This is accomplished using "sinks" whose strengths are determined from experimental measurements of jet entrainment. This technique has been applied by Wygnanski^{8,9} to infinite flat plates and elliptic cylinders in static external flowfields out of ground effects. Since experimental values of turbulent jet entrainment are required, application of this technique to VTOL flowfields in which strong interactions with the ground occur presents a difficult experimental measurement problem. Also, modeling of fountains by this method is impossible since flowfields containing jets and fountains are fundamentally rotational.

Approach (4) consists of modeling the lift-jet/airframe/ground interaction flowfield by patching together available analytical models for jet entrainment, jet impingement, wall jet boundary layers, etc. as required to complete the flowfield in question. This method would permit some viscous effects to be included, but in general would be very cumbersome and subject to serious questions about the accuracy of patching the various flowfield regions.

Approach (5) consists of solving the complete flowfield interaction together with appropriate boundary conditions using the fully-elliptic mathematical description of the fluid dynamics of the flow. This is accomplished by solving the partial-differential equations of continuity and momentum (time averaged Navier-Stokes equations) together with a one- or two-equation model of turbulence. Solutions of this type are discussed in detail by Gosman et al.¹⁰ This approach includes all the fluid dynamics of the physical problem in a time-averaged sense and is a great simplification over the ultimate solution, Approach (6), which at the present time is considered intractable.

McDonnell Douglas Research Laboratories (MDRL) has initiated a theoretical and experimental program to develop a computational technique for the prediction of VTOL lift-jet/airframe/ground interaction flowfields through the solution of the time-averaged elliptic flowfield equations as in Approach (5) of Fig. 4. The selection of this approach was based largely on the requirement for a solution of the complete subsonic flowfield with viscous effects without resorting to the patchwork method of Approach (4), and the additional requirement that the effort can be extended to include computation of cross-winds, compressibility, and temperature fields. The requirements of the initial effort are presented in Fig. 5.

The selected viscous interaction problem, shown schematically in Fig. 6, consists of a two-dimensional jet emanating from a body surface representative of an airframe component lower surface and located in proximity to a planar ground surface. The flowfield surrounding the interaction region far from the jet source is static, i.e., there is no translational velocity of the jet source. The entire flowfield is steady and two-dimensional in the mean sense, and density

differences are small such that the flowfield can initially be assumed to be incompressible. The major variables are (1) cross-sectional shape and characteristic length of the simulated airframe component, (2) height above ground of the jet exit, h/D_e , and (3) angle β of impingement of the jet on the planar ground surface. These major variables are included in both the theoretical and experimental investigations.

	① Model and full-scale testing	② Empirical prediction methods based on ①	③ Potential flow models	④ Patched flow- field models using available regional methods	⑤ Elliptic solution of complete viscous flowfield utilizing turbulence model	⑥ Complete Navier-Stokes solution for high Reynolds number
Major advantages	Only currently available method for evaluating VTOL aircraft configura- tions	Some parameter- ization possible through interpolation	Technology available	Elements of required technology available; some viscous effects can be included	Complete mathematical description of physical problem permitting parametric investigation of all pertinent variables	Complete mathematical description of physical problem permitting parametric investigation of all pertinent variables
Major disadvantages	Inflexible and expensive	Extrapolation usually not possible; requires voluminous test data	Empirical jet entrainment data required; no viscous effects included	Regional patching techniques very complicated, problem dependent, and require experimental verification; extremely difficult for complex geometries	3-5 Year development time required	10+ Year development time required
(eventual) Capability to predict						
a) Entrainment induced lift loss	Yes	Yes	Yes	Yes	Yes	Yes
b) Fountains	Yes	Yes	No	Yes	Yes	Yes
c) Complex geometries	Yes	Yes	Yes	No	Yes	Yes
d) Cross winds	Yes	Yes	Possibly with empirical jet path data	No	Yes	Yes
e) Temperature field	Yes	Yes	No	No	Yes	Yes

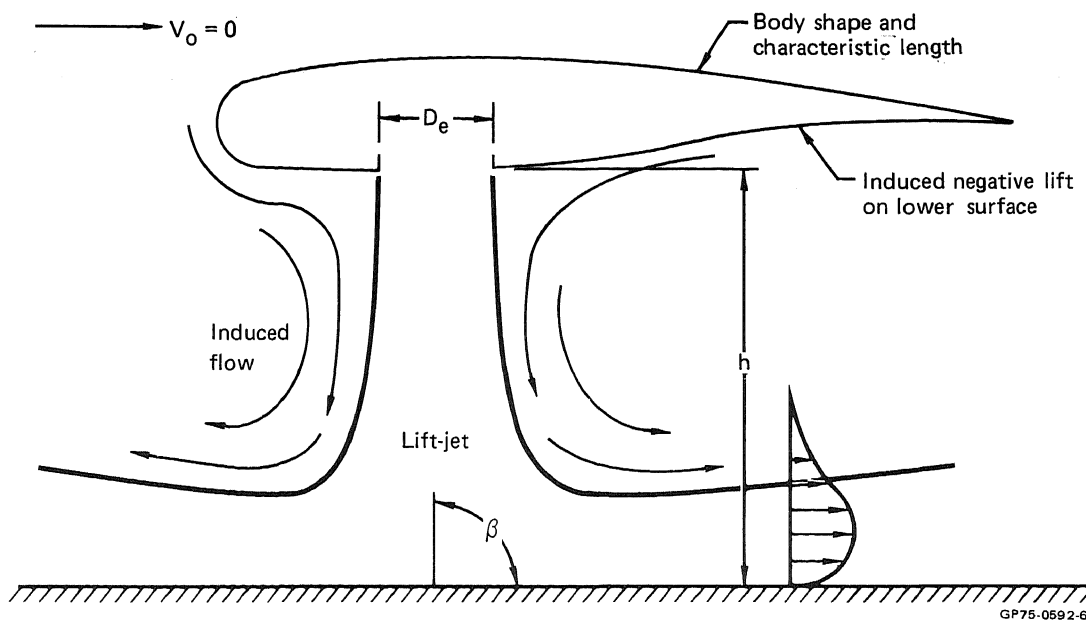
GP75-0592-4

Fig. 4 Prediction of lift-jet/airframe/ground interactions

- Prediction of jet entrainment
- Fully elliptic solution with no boundary layer type approximations
- Application to arbitrary body shapes
- Capability to include compressibility effects
- Inclusion of static pressure field in solution
- Application to two- and three-dimensional geometries

GP75-0592-5

Fig. 5 VTOL flowfield prediction; theoretical model requirements



GP75-0592-6

Fig. 6 Lift-jet/airframe/ground/interaction: interaction parameters

This study of the viscous lift-jet/airframe/ground interaction problem in two dimensions has been formulated to facilitate theoretical modeling of the interaction without the greatly increased effort required for the three-dimensional approach. The two-dimensional formulation also results in a simplified experimental test program, although care must be exercised to ensure two-dimensionality of the test model flowfield. It should be noted that only in a two-dimensional configuration of this type is it possible to vector the lift-jet and create an asymmetric jet impingement while maintaining two-dimensionality in the entire flowfield. This will provide an opportunity to investigate and model mathematically the effect of the asymmetry on jet entrainment. These theoretical and experimental efforts, in addition to proving the utility of the methods to be developed for three-dimensional flowfields, have a direct application to a number of VTOL interaction problems that are basically two-dimensional or not strongly three-dimensional. These include the following: (1) ejector-driven, augmentor-wing, high-lift systems, (2) direct lift systems with closely spaced, multiple jet exits in which the jet streams merge before ground impingement, and (3) wing trailing-edge slot blowing (jet flap) systems.

Experimental Program

An experimental investigation of the viscous flowfield occurring between simulated airframe undersurfaces and the ground in the presence of a two-dimensional lift-jet will be conducted. Specific objectives are (1) to explore the dominant characteristics of the viscous interaction flowfield and define acceptable free flowfield region boundaries and boundary conditions, (2) to obtain detailed measurements of mean and turbulent flow properties in the jet/static flowfield interaction region characterized by high turbulent entrainment rates, and (3) to measure the induced forces on simulated airframe undersurfaces in ground effect over a range of test variables known to significantly influence the magnitude of these forces. These measurements are required to implement and evaluate the theoretical modeling of the viscous interaction flowfield and to provide needed interaction data on induced forces in close ground effect.

Consideration of available in-house test facilities, the desirability of a fairly large model to facilitate the numerous experimental measurements required, and the requirement for a complete mathematical description of the two-dimensional flowfield, led to the selection of a model with a symmetrical, modified-oval cross section with a jet exit slot width of 1.5 in. The general arrangement of the test configuration is shown in Fig. 7. The length of the jet slot is 60 in. which results in a jet slot aspect ratio of 40:1 and a model aspect ratio of approximately 4.3:1. A cross-sectional view of the model which shows the selected outer profile shape is shown in Fig. 8. The two-dimensional nozzle and plenum assembly, as shown in this figure, can be vectored to 30 deg on either side of the model center-line. This is required to enable later testing of nonsymmetrical body shapes. Additionally, the high-pressure plenum assembly is structurally independent of the outer body to facilitate changes in body shape. The large aspect-ratio jet exit slot and model endplates are utilized to assure two-dimensionality of the turbulent jet and entrained flowfield in the region of measurement. As shown in Figs. 7 and 8, the center lower panel of the model is metric, and induced forces and moments on the simulated airframe undersurface will be measured directly with a two-component strain gage force balance installed within the model. Two-dimensionality of the flowfield will be established by static pressure measurements on the ground plane and on the nonmetric model surface. Additional checks of two-dimensionality will be made with jet flowfield rake pressure instrumentation. A summary of model parametric capabilities is presented in Fig. 9.

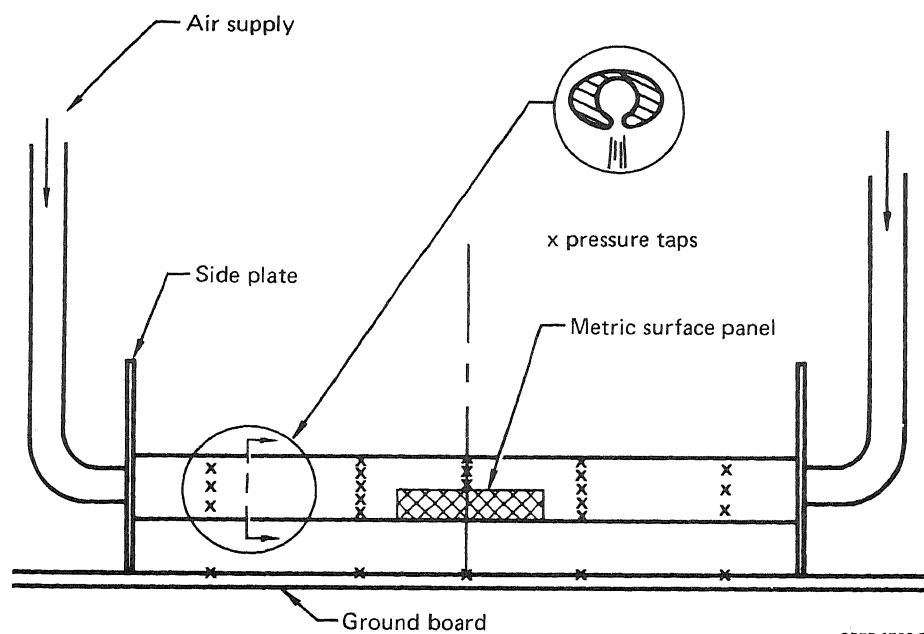
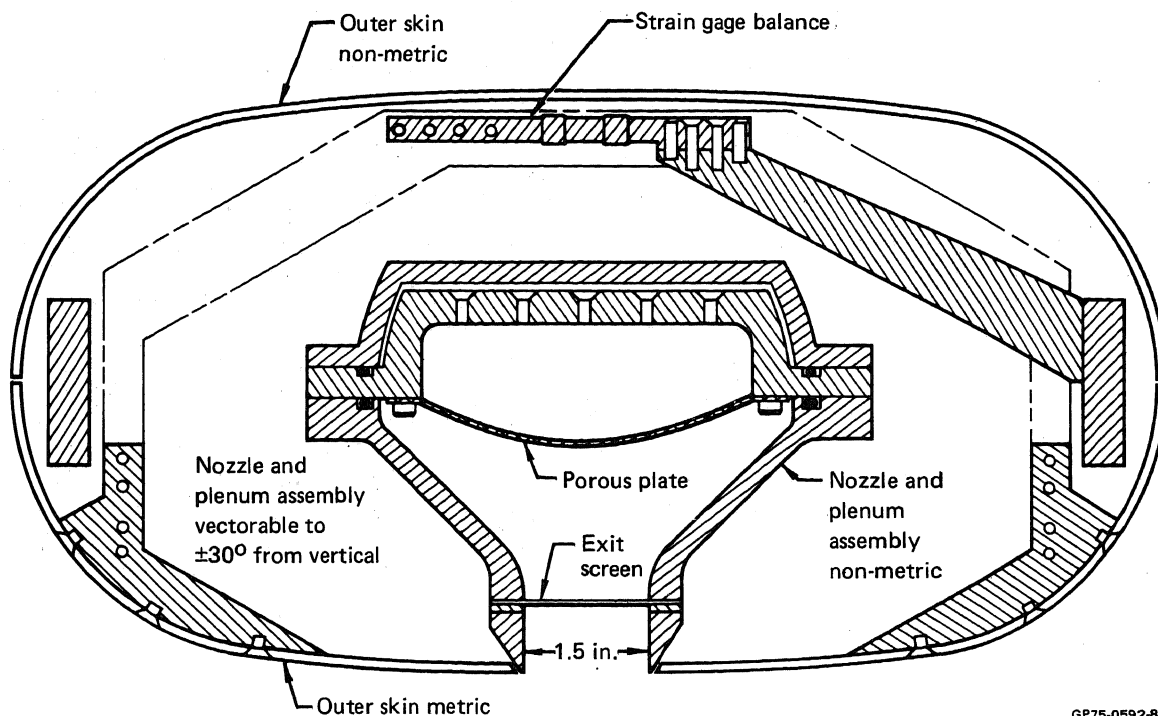


Fig. 7 Test detail and instrumentation: two-dimensional lift-jet/airframe/ground interaction experiment



GP75-0592-8

Fig. 8 Two-dimensional lift-jet/ground/interaction model; cross-section view

- Height-above-ground variable from $h/D_e = 0.5$ to $h/D_e = 30$
- Two-dimensional jet slot vectoring angle range -30° to $+30^\circ$ from vertical
- Jet exit Mach number up to 1.0
- Model outer shape as desired
- Cross flow velocity up to wind tunnel capability

GP75-0592-9

Fig. 9 Model parametric capabilities

The high-pressure plenum and nozzle assembly is supplied with clean air at a pressure in excess of 300 psig. This results in a low-velocity supply to the upper chamber eliminating large lateral velocities. The first stage of pressure reduction occurs through a heavy porous plate with approximately 4% open area. Subsequent pressure reductions occur through a second porous plate and a jet exit screen with approximate porosities of 30% and 60%, respectively.

The first test series will provide detailed flow measurements and induced forces on the model undersurface for height-above-ground to jet-exit-slot width ratios of 0.5 to 5.0 for jet-exit velocity-vector angles of 0 and 30 deg with respect to vertical. In addition to measuring the induced forces on the simulated airframe undersurface, detailed measurements of the viscous flowfield in the interaction region will be made. These will consist of local flow direction determinations using directionally sensitive "cobra" probes, static pressure measurements on the simulated airframe and ground surfaces, and hot-wire anemometer measurements of turbulent flow properties primarily in the regions of strong jet entrainment. The initial tests will be conducted in the incompressible flow regime with jet exit slot Reynolds numbers varying up to 250,000. Once two-dimensionality is established, emphasis will be placed on the detailed measurement of four or five experimental configurations including one flat plate configuration. Measurements will include surveys of the flowfield at some distance from the model to establish representative flowfield boundaries and boundary conditions. Nominal test conditions for the initial test runs are given in Fig. 10.

h/D_e	Body shape	β	R_{D_e}	T_{te}	Jet profile
2	Modified oval	90°	200,000	530°R	Uniform
2	Modified oval	90°	50,000	530°R	Uniform
4	Modified oval	90°	200,000	530°R	Uniform
4	Modified oval	60°	200,000	530°R	Uniform
2	Flat plate	90°	50,000	530°R	Uniform

GP75-0692-10

Fig. 10 Test conditions for initial experiments involving extensive flowfield measurements

Fabrication of the model was initiated in June 1975 and will be completed by the end of August. The first test series is planned for late September 1975. The model will be tested in the McDonnell Mini-Speed Wind Tunnel (MSWT) located in St. Louis, Missouri. The MSWT is an additional tunnel leg and test section added to the McDonnell Low-Speed Wind Tunnel (LSWT). It is an open-circuit, open-throat tunnel with the 15 ft high, 20 ft wide, and 20 ft long test section enclosed within a 50 ft high, 60 ft wide, and 50 ft long building. The test section includes an adjustable-height, moving-belt ground plane. Airflow provided by the LSWT drive motor and fan is diverted to the MSWT for testing in the 0 to 65 knots speed range. Continuous auxiliary air pressure of 300 psig and flow in excess of 20 lb/s, suction capability of 13 lb/s at 0.5 atm, or combinations of pressure and suction are available at the model. Model and balance data are recorded on a 20-channel CSC magnetic tape system with final data computed on the SEL 810A computer located on site.

Analytical Program

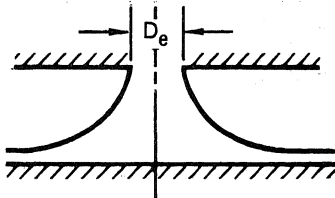
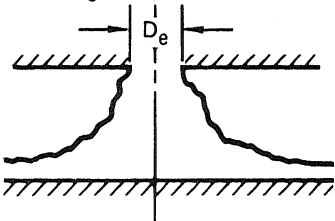
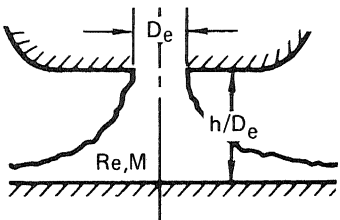
In order to obtain detailed and accurate distributions of the flow properties associated with a strong lift-jet/airframe/ground interaction, a numerical solution of the time-averaged Navier-Stokes equations is required. Inviscid analyses are inadequate, even with displacement thickness corrections, since the flowfield, which contains pressure gradients in both coordinate directions, is not compatible with the boundary layer approximations.

The present approach is to solve the time-averaged Navier-Stokes equations for steady, plane, incompressible flow to describe the mean motion of the fluid for a flowfield associated with a configuration such as that shown in Fig. 6. This effort involves two problems: formulating a system of equations to describe the turbulence and developing a numerical procedure to accurately solve the flowfield equations.

In the current work, the turbulent kinetic energy equation derived by Wolfshtein¹¹ will be used in combination with constitutive equations to relate the turbulent kinetic energy to the turbulent stresses that arise in the time-averaged Navier-Stokes equations. This turbulence model incorporates a turbulent viscosity length scale, a turbulence energy dissipation length scale, and five empirical constants, and it relates the square root of the turbulent kinetic energy directly to the turbulent viscosity. The accuracy of the turbulence model will be established on the basis of comparisons of computed flow properties and those measured in the complementary ground interaction test program.

The second problem, the development of numerical procedures to solve the flow equations, has received the most attention to date in the theoretical portion of the lift-jet/airframe/ground interaction study. The coupled elliptic partial differential equations which describe the flow are nonlinear, and numerical procedures are necessary to obtain a solution. The method of approach that has been adopted is illustrated in Fig. 11. Initially attention has been focused on solution of the governing equations for laminar jet impingement problems in rectangular domains. This has involved

calculation of the stream function and vorticity distributions and the associated distributions of velocity and pressure for a range of Reynolds numbers. The next step in the analysis is to solve the turbulent flow equations for the same rectangular domains and, finally, to extend the procedures to domains with an irregular upper boundary that simulates an airframe undersurface.

Configuration	Analysis steps	Result evaluation method
<p>Task I - Solution of laminar-flow equations for parallel-plate configuration</p> 	<ol style="list-style-type: none"> 1. Solution of the vorticity transport equation and Poisson equation for stream function 2. Calculation of the velocity components and solution of the Poisson equation for pressure 	Comparison of results with numerical calculations of Gosman et al. ¹⁰
<p>Task II - Solution of turbulent-flow equations for parallel-plate configuration</p> 	<ol style="list-style-type: none"> 1. Solution of the time-averaged vorticity transport equation, Poisson equation for stream function, and turbulent kinetic energy equation 2. Calculation of the time-averaged velocity components and solution of the time-averaged Poisson equation for pressure 	Comparison of results with numerical calculations of Gosman et al. ¹⁰ and test data of MDRL
<p>Task III - Solution of turbulent-flow equations for a configuration with a contoured upper surface</p> 	<ol style="list-style-type: none"> 1. Conformal mapping of geometry into a rectangular domain 2. Solution of the time-averaged vorticity transport equation, Poisson equation for stream function, and turbulent kinetic energy equation 3. Calculation of the time-averaged velocity components and solution of the time-averaged Poisson equation for pressure 4. Parametric variation of Re, M, and h/D and calculation of the corresponding static pressure distributions 	Comparison of results with test data of MDRL

GP75-0592-11

Fig. 11 Development of the lift-jet/airframe/ground interaction calculation scheme

The first task, the solution of the laminar-flow equations for a parallel-plate configuration, has been completed. The governing equations are the vorticity transport equation and the Poisson equation for the stream function. The former equation is derived by differentiating the x-momentum equation with respect to y , subtracting from this the y-momentum equation that has been differentiated with respect to x , and introducing the defining equation for vorticity. The Poisson equation for the stream function is obtained by substituting the defining equations for the

stream function into the defining equation for the vorticity. The two equations are normalized and then discretized using the augmented-central-difference finite-difference algorithm derived by Hoffman.¹² The resulting nonlinear finite-difference equations are solved through iteration using relaxation procedures.

Once the vorticity and stream function distributions are calculated, the problem of computing the distributions of the velocity components and static pressure remains. The latter, of course, is the property of greatest interest in the lift-jet/airframe/ground interaction analysis. The velocity components are easily calculated from the discretized forms of the defining equations for the stream function, but the pressure field is not solved so easily. This is reflected in the observation made by Roache¹³ that many papers on Navier-Stokes solutions published as late as the 1960's do not contain pressure solutions, and others contain pressure solutions that are erroneous. The latter point deserves elaboration.

The most straight-forward approach in calculating the pressure field is to start at an arbitrary point in the flow with an arbitrary pressure level and numerically integrate the pressure gradients in the two coordinate directions as given by the discretized x- and y-momentum equations. In theory, the solution should be independent of the path of integration, but in practice this is not the case since quadrature errors can lead to different answers for different paths.

A more accurate solution can be obtained through solution of the Poisson equation for pressure. This equation is derived by adding the x-derivative of the x-momentum equation to the y-derivative of the y-momentum equation. The complexity associated with the solution of this equation is that the magnitude of the pressure is not known at the boundaries; only the pressure gradients as given by the two momentum equations are known. That is, the Poisson equation for pressure must be solved subject to Neumann rather than Dirichlet boundary conditions, and using iterative techniques the level of the solution drifts. To avoid this problem, a "direct-solver" approach has been developed at MDRL which provides a computationally rapid and accurate solution of the pressure field without iteration.

The two configurations investigated in the laminar-flow studies are shown in Fig. 12. The geometry shown in Fig. 12a is the one analyzed by Gosman et al.¹⁰ A developed jet, for which the normal velocity distribution is specified as a function of x, enters the upper free boundary and strikes the ground at a distance of one entrance jet diameter from the upper boundary. The right and left boundaries are each one entrance jet diameter from the jet centerline. With the normal velocity component specified analytically and with the tangential velocity component taken as zero, the vorticity and stream function distributions at the jet entrance plane follow immediately from their defining equations. Along the remainder of the upper boundary, the flow is taken to be irrotational and normal to the free surface. At the right boundary the flow is taken to be parallel to the wall, which provides homogeneous Neumann boundary conditions on the vorticity and stream function. Along the wall, Dirichlet conditions on ω and ψ result from the

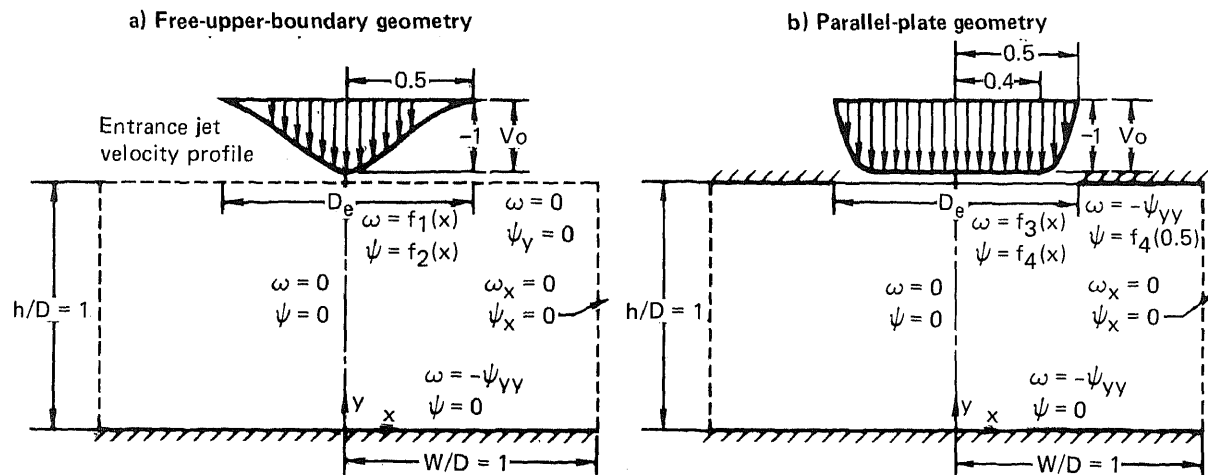


Fig. 12 Flow configurations and boundary conditions

GP75-0592-12

no-slip and impermeable wall velocity constraints, and along the jet centerline, Dirichlet conditions on ω and ψ result from the flow symmetry. Since the flowfield is geometrically symmetric about the jet axis, only the region to the right of the centerline need be solved.

The geometry shown in Fig. 12b is similar to the one described except for the presence of a wall bounding the jet at the upper surface. The entrance normal velocity component is taken to be uniform over 80% of the entrance jet width and then to decay to zero with a cubic variation; the tangential component is taken as zero. The boundary conditions are the same as for the previous geometry except at the upper wall where the no-slip and impermeable wall conditions lead to Dirichlet conditions on ω and ψ . The flow is solved only for the half-plane to take advantage of geometric symmetry.

Figure 13 illustrates the comparison of the vorticity and stream function distributions for the configuration shown in Fig. 12a as computed in the present work and by Gosman et al.¹⁰ The solutions are shown for Reynolds numbers of 1 and 1000 (based on the width and properties of the jet at the entrance plane) and illustrate good agreement between the two different finite-difference schemes.

The distributions of the velocity components and static pressure (which Gosman et al. did not report in Ref. 10) are shown in Fig. 14 for $Re = 1000$. The x-component of velocity is negative near the upper right-hand corner of the solution domain. The relatively large gradients of the x-component of velocity near the wall reflect the development of a boundary layer. The plot of the y velocity component clearly depicts the decay of normal velocity as the jet nears the ground. In the calculation of static pressure through a direct solution of the Poisson equation, the jet centerline pressure at the upper boundary is set to zero. The contour plot illustrates the increase in pressure going toward the stagnation point.

Figure 15 shows the flow properties computed in the present work for the laminar jet impingement flow between two parallel plates at a Reynolds number of 1000. The contour plot of the x-component of velocity shows the boundary layer growth on the upper and lower surfaces, with separation occurring on the upper surface. Compared with the profile shown in Fig. 14, the flow with the nearly uniform entrance profile results in the flow experiencing greater normal velocities throughout the field. The corresponding static pressure contours are shown for a value of zero pressure at the upper boundary jet centerline. The pressure is, of course, lower in the vicinity of the upper right corner for the flow geometry with a bounding upper surface as compared with the geometry with a free boundary.

The next step in the analysis, which is currently in progress, is to solve the turbulent-flow equations for the geometries shown in Fig. 12. Comparisons will be made with the solutions of Gosman et al.¹⁰ for the configuration in Fig. 12a and with data to be acquired in the MDRL test program for the configuration in Fig. 12b. The final step in the planned sequence is to solve the turbulent flow equations using conformal mapping procedures for the modified-oval upper boundary shape investigated in the experimental program.

Concluding Remarks

Following completion of the experimental and analytical studies of the two-dimensional configuration, comparisons will be made between the measured and predicted flow properties to determine the scope of further required analytical efforts. Poor agreement will necessitate developing a more detailed turbulence model.

Future experimental work will be conducted to determine the influence of the jet impingement angle, Reynolds number, and nozzle height above ground on the flowfield in a more extensive parametric study. Future analytical efforts in this area include incorporation of the two-dimensional energy equation in the analysis to predict compressibility effects and a feasibility study of extending the procedure to simple three-dimensional geometries.

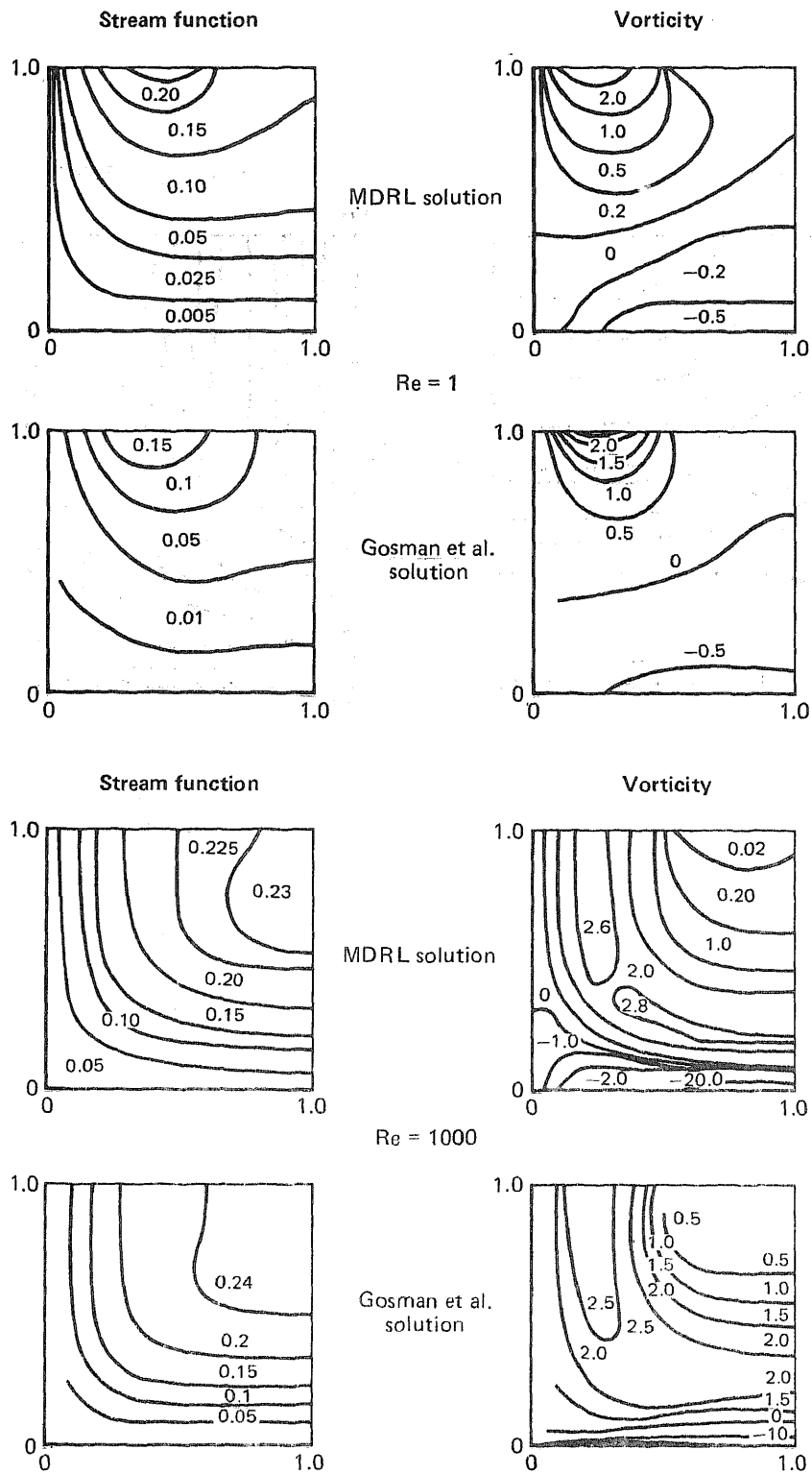
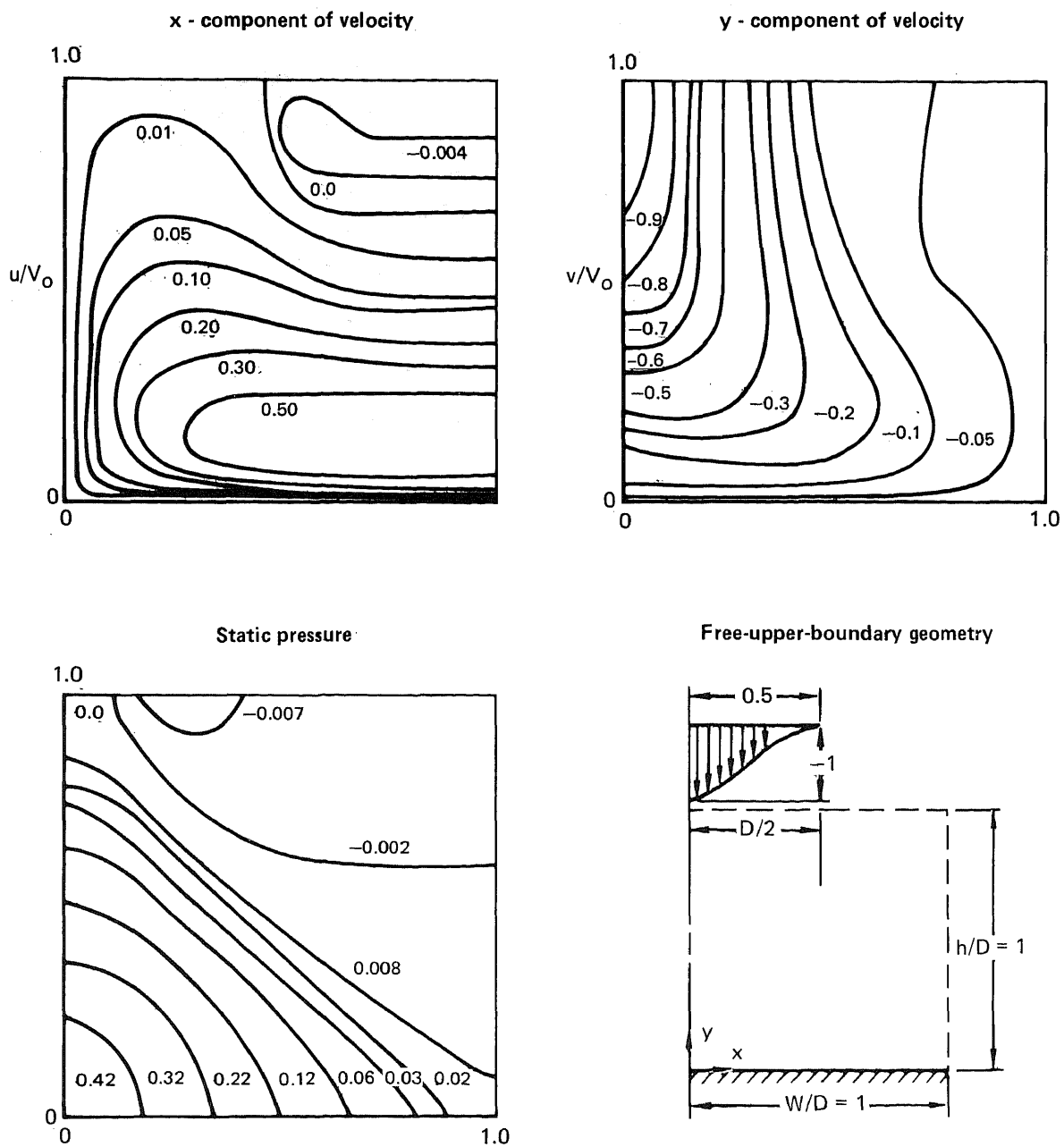
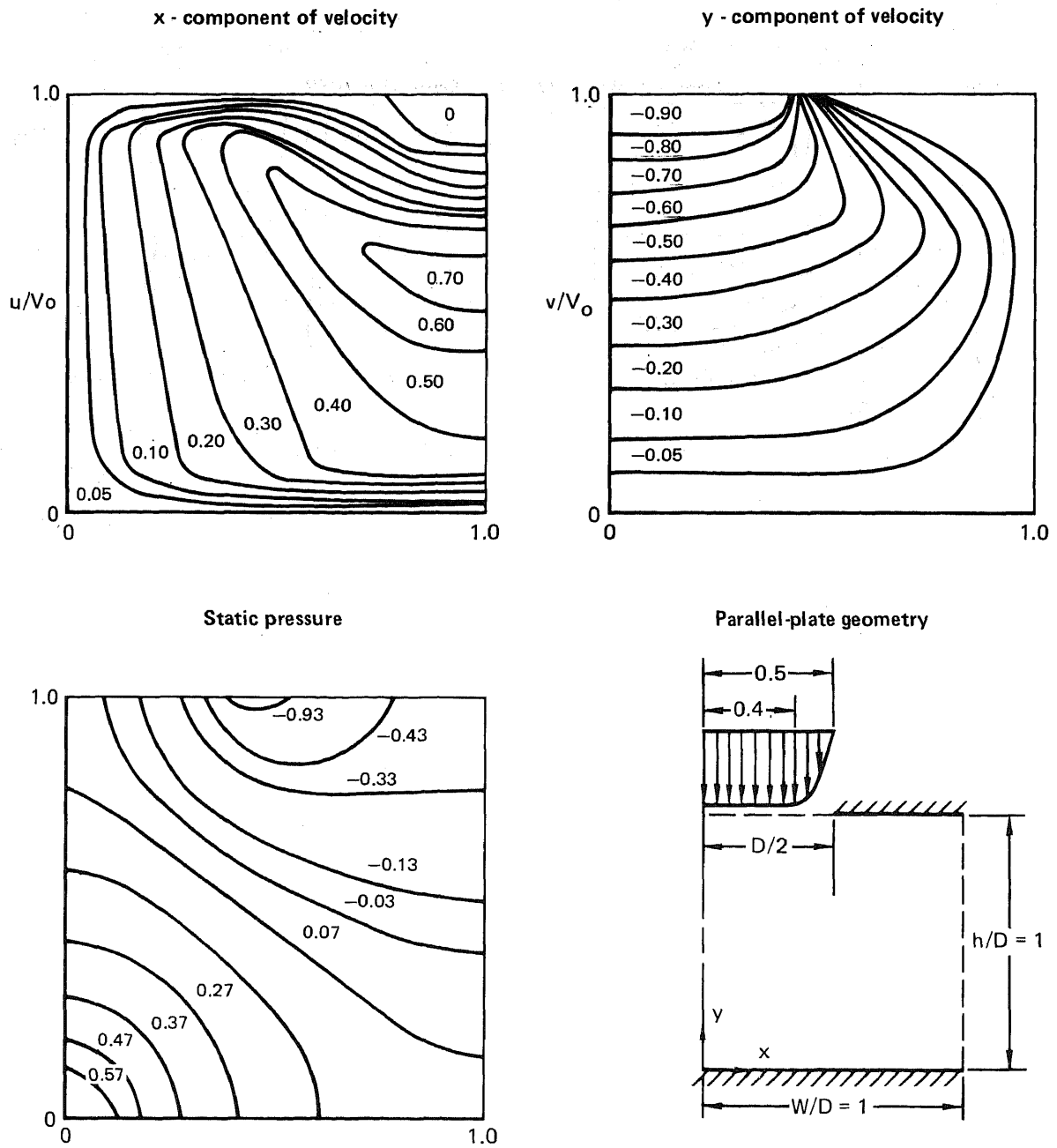


Fig. 13 Comparison of MDRL laminar-flow solutions with those of Gosman et al.¹⁰



GP75-0592-14

Fig. 14 Laminar velocity and static pressure contours for the free-upper-boundary geometry, $Re = 1000$



GP75-0592-15

Fig. 15 Laminar velocity and static pressure contours for the parallel-plate geometry, $Re = 1000$

References

1. G. L. Gentry and R. J. Margason, "Jet-Induced Lift Losses on VTOL Configurations Hovering in and out of Ground Effect," NASA TN D-3166, February 1966.
2. K. P. Spreemann and I. R. Sherman, "Effects of Ground Proximity on the Thrust of a Simple Downward-Directed Jet Beneath a Flat Surface," NACA TN 4407, September 1958.
3. L. A. Wyatt, "Static Tests of Ground Effect on Planforms Fitted with a Centrally-Located Round Lifting Jet," Ministry of Aviation C. P. 749, Brit. A.R.C., 1964.
4. G. R. Hall, "Scaling of VTOL Aerodynamic Suckdown Forces," *J. Aircraft* 4, 393 (1967).
5. Rahim Lavi, "Parametric Investigation of VTOL Ground Proximity Effects," AIAA Paper No. 67-440, 1967.
6. Wilhelm Seibold, *Untersuchungen über die von Hubstrahlen an Senkrechtstartern Erzeugten Sekundärkräfte*, Jahrb. 1962 WGLR.
7. J. Louisse and F. L. Marshall, "Prediction of Ground Effects for VTOL Aircraft with Twin Lifting Jets," AIAA Paper No. 74-1167, 1974.
8. I. Wygnanski, "The Flow Induced by Two-Dimensional and Axisymmetric Turbulent Jets Issuing Normally From an Infinite Plane Surface," *Aero. Quarterly* Vol. 15, 373 (1964).
9. I. Wygnanski, "The Effect of Jet Entrainment on Loss of Thrust for a Two-Dimensional Symmetrical Jet Flap Aerofoil," *Aero. Quarterly* 17, 31 (1966).
10. A. D. Gosman, W. M. Pun, A. K. Runchal, D. B. Spalding and M. Wolfshtein, Heat and Mass Transfer in Recirculating Flows (Academic Press, New York, 1969).
11. M. Wolfshtein, "Convection Processes in Turbulent Impinging Jets." Report SF/R/2, Department of Mechanical Engineering, Imperial College of Science and Technology, London, November 1967.
12. G. H. Hoffman, "Calculation of Separated Flows in Internal Passages," Workshop on Prediction Methods for Jet V/STOL Propulsion Aerodynamics, Arlington, VA, 28-31 July 1975.
13. P. J. Roache, Computational Fluid Dynamics, (Hermosa Publishers, Albuquerque, New Mexico, 1972).

Session D

FLOW AND THERMAL EFFECTS

Chairman: R. E. Kuhn, NASA Langley Research Center

Session D

FLOW AND THERMAL EFFECTS

Chairman: R. E. Kuhn, NASA Langley Research Center

EXHAUST GAS REINGESTION STUDIES ON LIFT-ENGINE VTOL FIGHTER CONFIGURATIONS

Jerry V. Kirk* and Jerry P. Barrack†
Ames Research Center, NASA
Moffett Field, California 94035

ABSTRACT

Recirculation of exhaust gas from a lifting engine back into the engine inlet, called reingestion, has proven to be one of the difficult operating problems for jet-powered VTOL aircraft. This paper summarizes the results of studies of the reingestion characteristics of two different lift-engine mounting arrangements on a configuration simulating a supersonic VTOL aircraft. The investigation includes static tests and wind-tunnel tests in ground effect of a large-scale model powered by J-85 engines. The results indicate that the reingestion environment in both cases is very severe and will probably require the development of special facilities and techniques for successful flight operations.

NOTATION

D	inlet or exit diameter, in. (cm)
H	height of model above ground, in. (cm)
rpm	corrected engine rpm
V	velocity, f/s or knots
α	angle of attack, deg
ρ	density, slugs/ft ³
σ	engine angle from horizontal, deg

Subscripts

AV	average		
c	lift-cruise engine	max	maximum
j	jet	min	minimum
L	lift engine	o	free stream

*Operations Manager, Large-Scale Aerodynamics Branch.

†Aerospace Engineer, Advanced Aircraft Studies Office.

INTRODUCTION

Flight Research on experimental aircraft with jet engines to provide lift revealed that reingestion of exhaust gases is a major problem that cannot only cause a hover performance reduction but is potentially dangerous because of the possibility of a catastrophic loss of the lift engines. As a result, considerable experimental research on this problem was conducted in the 1960's. Some of this research is presented in references 1-3. This paper summarizes the reingestion research done statically and at forward speed on a large-scale model of a lift-engine-powered VTOL fighter aircraft, using J-85 engines to simulate the lifting powerplants. The effect of various parameters on reingestion and techniques for reducing reingestion are discussed and research on reingestion prediction techniques is suggested.

STATIC REINGESTION

Reingestion Flow Fields

Flow from multiple engine VTOL aircraft can be broken into two types, the far field and the near field. The far field is that flow which escapes the immediate location of the airplane, then, because of its buoyancy due to a relatively high temperature, rises. The rising flow is constantly being replaced by new, hot exhaust gas, so that a large-scale recirculation pattern, several airplane dimensions in size is set up. Thrust losses while hovering in a fixed position increase as the local hot air mass degrades engine performance. This type of reingestion is sensitive to wind conditions. The other type, near field ingestion, behaves somewhat differently and can have more serious results. In the near field of the jet flow, the exhaust stream lies close to the ground unless it meets a stream from another engine. When this occurs, a fountain is formed (fig. 1). This fountain of high velocity hot air is directed up and may find its way into an engine inlet. In this case, engine surge may occur because of the inlet temperature distortion caused by the fountain of hot air. The fountain is neutrally stable, thus the location is affected by very small winds, difference in power settings, or other anomalies that may occur. This fountain, as it impinges on the airframe may cause an upload that provides positive ground effect. However, because of the fountain's lack of stability, this may appear as buffeting to a pilot and be objectionable. Because of this lack of stability, the flow from the fountains into the inlet can be periodic and the actual temperature rise difficult to predict.

Test Setup

Figures 2 and 3 are photographs of the model with the two lift-engine arrangements mounted on the Ames Static Test Facility. Details of the models can be found in references 1-3. The model had a wingspan of 24 ft (7.32 m). Figure 2 shows the swiveling lift-engine arrangement with four J-85's for the lift engines, and two J-85's for the lift/cruise engines. Figure 3 shows the same arrangement excepting that the three internally mounted J-85's were substituted for the four swiveling engines. This version of the model had conical, bifurcated, and slot nozzles available for the lifting engines.

The model propulsion system was fitted with dynamic instrumentation to measure exhaust gas pressure and inlet temperature. Because of the periodic nature of the flow, thermocouple response time can be a problem. In this case, the finest thermocouple wire that could withstand the environment was used [5 mils (0.00013 m) with a time constant of 30 milliseconds].

The technique used for the static tests was to start all engines and set the engines at 70% rpm. All engines were then accelerated together rapidly (about 3 seconds) to full throttle. Data were then taken for 30 seconds before power was reduced.

Reingestion Test Results

Swiveling lift engines. — Figure 4 shows the variation with time of exhaust gas pressure and the reading of one thermocouple in the lift-engine inlets. The thermocouple chosen was the one with the largest transient response. In this case, both the lift and lift/cruise engines were exhausting vertically, and the model was at a height-to-diameter ratio of 5. The number 4 engine stalled at 3½ seconds, with a measured average temperature rise of 144°F (65°C), but the maximum temperature gradient was about 1000°F/s (539°C/s). If thermocouple response is accounted for (ref. 4), the numbers are 157°F (67°C) and 1700°F/s (925°C/s). Maximum temperatures were recorded in the 3 to 6 o'clock portion of the inlet. The other three engines appeared to have no problem.

Similar results, with the swiveling engines at 80° from horizontal, are shown in figure 5. In this case, engine number 4 ran for 11 seconds before surge, however engine thrust degradation began several seconds earlier, as shown by the exhaust pressure trace. The measured average temperature rise was 90°F (32°C) with a temperature gradient of 1200°F/s (648°C/s). Allowing for thermocouple lag, these figures become 132°F (56°C) and 2100°F/s (1150°C/s). Again, the other three engines had little problem.

Figure 6 shows data with the swiveling engines at 70° from horizontal. There was very little reingestion and no problems.

Figure 7 shows the variation with time of rpm, average inlet temperature, and distortion index for engines 1 and 2, with the lift engines at 80°, and with 5° cant. The inlet temperature of both engines were about the same for 5½ seconds when a transient gust of hot air entered the inlet of engine 2. Subsequently, number 2 engine stalled in 1 second. The measured average inlet temperature was 180°F (83°C) at stall and the distortion index was 0.2.

With the swiveling lift engines, numbers 2 and 4 surged much more often than 1 and 3, indicating that the fountain came up the side of the fuselage and was deflected off the lower surface of the wing into inlets 2 and 4. These engines, ingesting the hot gas, protected engines 1 and 3. On the other hand, the wing protected the cruise engines so that they were not a problem.

Figure 8 shows the temperature rise, thrust loss, and lift loss as a function of swivel angle for an $H/D = 5$. The large temperature rise with the swivel engines at 90° causes a 25% thrust and lift loss. By changing the swivel angle to 80°, the temperature rise is greatly reduced and the thrust loss is significantly lessened. As shown by the curve, the swivel angle for maximum lift is 70° to 80° rather than 90°. This suggests that a slant rather than vertical takeoff may be the desirable operational procedure for some lift-engine fighter designs.

Internally-mounted lift engines. — Figure 9 shows the conical, bifurcated, and slotted nozzles used on the model with internally-mounted lift engines. With the conical nozzles, reingestion was so severe that the engines could not be accelerated without surge of at least one engine. Figure 10 shows the temperature and exhaust gas pressure time history with bifurcated nozzle 90° from the horizontal. Engine number 1 stalled 2 seconds from time zero, and then engine number 2 began to reingest and stalled 14 seconds later. Approximately 0.4 second prior to stall, engine number 1

experienced measured gradients of 1000°F/s (539°C/s) with a temperature rise of 60°F (15°C), however, at stall, the corresponding figures were 500°F/s (260°C/s) and 26°F (-3°C) [1450°F/s (787°C/s) and 44°F (7°C) with thermocouple lag corrected]. Vectoring the exhaust to 75° from horizontal essentially removed the reingestion problem (fig. 11).

Temperature rise and thrust loss as a function of exhaust vector angle for the model with internally-mounted lift engines is shown on figure 12. With the conical nozzles, it was impossible to get data at 90° vector angle, so that curve stops at 80° . With bifurcated and slot nozzles, the temperature rise at 80° and 90° vector angles produced a 10 to 15% thrust loss with a corresponding lift loss. Since the engines could not be operated continuously at 80° and 90° , this result depends on providing engines with improved compressor stall margin. Addition of doors to the bottom of the fuselage with the bifurcated nozzles reduced thrust loss about 4%. As with swiveling lift engines, it appears that slant takeoff operations are feasible.

Engine tolerance to temperature rise. — Figure 13 relates temperature rise at stall inception with temperature rise rate at stall (ref. 5). The two curves are for full admission and half admission of hot gases at the compressor face. The data points on the figure are from the stalls shown in figures 4 through 11 of this investigation. Good agreement is shown for one of the stalls. The other three stalls show lower rates of temperature rise but tolerance to high average temperature rise before stall. This discrepancy may have been caused by the highly distorted flow across the compressor face, or different compressor characteristics. In some cases, high localized temperatures were measured at the compressor face of the J-85 without stall. The shift of the operating line caused by small localized "hot spots" was probably small enough to allow the compressor to adjust to the mismatch. On the other hand, lower distortion levels occurring over a large portion of the compressor face appeared to induce compressor stall more readily.

Effect of height and exhaust vectoring. — Figure 14 summarizes static reingestion characteristics with both swiveling and internally-fixed lift engine mountings. The lightly shaded area represents the combinations of vector angle and height where engine surge would be expected. The heavily shaded area represents where ingestion is heavy and surge may occur. Only the swiveling, retractable configuration could be vectored forward (90° to 110°). Of the four ground heights tested ($H/D = 2.5, 5.0, 7.5,$ and 9.7), height-diameter ratios between 5 and 7.5 were the worst for ingestion. Results shown are general and are for a no wind condition. The engine toe-out angle for the swiveling-lift engines was 15° , but the results at 0° are similar. Of the three exhaust nozzles tested with the internally-fixed lift engines, the slotted sound-suppressor nozzles produced somewhat lower temperature gradients and average inlet temperatures than the conical or bifurcated nozzle; however, with exhaust vector angles of 80° and 90° , the engines stalled regardless of exhaust nozzle installation.

Although no forward vectoring (90° to 110°) was accomplished with the internally-fixed configuration, due to a limitation in the thrust vectoring system, there is no reason to believe the results would be different from those shown for the swiveling, retractable configuration.

Proper vectoring of the lift engines forward and lift-cruise engines aft to balance moment, provided thrust-to-weight ratios are adequate, should provide VTOL capability to both configurations, however, both arrangements could also perform slant takeoffs with a vector angle of about 75° .

Design for Low Reingestion

Reference 6 presents studies of the effect of inlet location and wing placement on reingestion characteristics. These results indicate that a low wing is beneficial in suppressing flow from the fountain, which will protect cruise-engine inlets located above the wing as well as the lift-engine inlets. Several inlet arrangements with low static reingestion were found, thus it should be possible, with appropriate configuration control, to eliminate static reingestion as a major problem, which leaves the question of reingestion at low forward speeds.

EFFECT OF FORWARD SPEED ON REINGESTION

Test Arrangements and Procedures

Figures 15 and 16 show the model mounted in the Ames 40- by 80-Foot Wind Tunnel at two different heights. The model arrangement is the same as in the static reingestion study. The reingestion instrumentation is also the same. Reingestion data were obtained by running the wind tunnel at a velocity where reingestion did not occur, setting engine power, then decreasing wind tunnel velocity continuously while continuously recording inlet thermocouple and exhaust gas pressure data. These data were obtained for two ground heights, several exhaust gas deflection angles, and several power settings.

Reingestion Flow Patterns at Forward Speed

Reingestion flow patterns vary considerably with speed. Figure 17 shows exhaust flow patterns at relatively high forward speeds where ingestion does not occur. At these speeds, the exhaust gas is rapidly mixed with surrounding air and is swept back under the aircraft without causing a problem. At somewhat lower speeds (fig. 18), the exhaust gas flows forward, rises, and blows back into the engine inlets. This type of ingestion becomes more severe down to a certain speed and then improves as the circulation path becomes larger and approaches the far field flow discussed for static reingestion. Finally, as shown in figure 19, for some configurations fountains are found at low speed so that the flow field closely resembles that of near field static reingestion.

Reingestion at Forward Speed

Figure 20 shows the typical variation of tunnel speed and temperature from lift-engine inlet number 1 as a function of time for lift engines at 90° . Figure 21 shows the variation with time of temperature distortion index and average temperature for inlet number 1 with the same configurations as for figure 20. This reingestion appears to be more regular in character than reingestion at zero velocity. Although not shown, reingestion continued and distortion increased until at 17 knots, the average temperature rise was $177^\circ\text{F}(85^\circ\text{C})$ and distortion was 0.16.

Figure 22 shows similar data for engine 2. The high distortion from onset is believed to be ingestion of compressor bleed air, which could be eliminated.

It is apparent that high values of average temperature and distortion can occur when lift-engine VTOL aircraft operate near the ground. Figure 23 shows reingestion boundaries for the model aircraft studied here. The points chosen to define the boundaries are illustrated in figure 20 and are labeled "reingestion first occurred". The lift-engine angle as a function of nondimensional momentum ratio for reingestion onset is shown for two ground heights. At lift-engine angles of about 73°

and 84° , reingestion can be completely avoided at ground heights of 5.6 and 12.7 nozzle diameters, respectively. As the lift engines were vectored more vertically, reingestion occurred. Therefore, to avoid reingestion completely, transition would have to be made at a height greater than 12.7 nozzle diameters, thereby increasing the transition time required and fuel burned, which may compromise the aircraft mission.

THEORETICAL PREDICTION OF REINGESTION

Prediction of reingestion is in its infancy. Both far-field and near-field flows involve turbulent mixing and the aerodynamics of separated flow, thus detailed definition of flow characteristics such as distortion index or even average temperature rise is not possible at this time. Possible theoretical approaches are suggested in the following discussions.

Far-Field Reingestion

The flow field of the exhaust gas along the ground resembles a wall jet. Turbulent mixing and stability calculations may be used to predict the separation of the jet from the ground and buoyancy, and heat-transfer calculations may provide estimates of the characteristics of the surrounding air and thus provide a temperature rise and corresponding thrust loss as a function of time. Adding atmospheric anomalies such as winds and the ground boundary layer would further complicate the calculations. For hover conditions, this calculation may not be worth the effort, however, the calculation also bears on ingestion at forward speed, which can have serious effects. It then would seem that the important factors which need to be included in a theoretical calculation are airplane speed and height and the far-field characteristics of the gas being ingested. This would provide predictions of reingestion at forward speed near the ground.

Near-Field Reingestion

Study of an aircraft configuration will give an indication of the location of fountains and thus a gross indication of a reingestion problem that may cause engine surge. However, to define the strength, turbulence, and temperature content of the fountains is impossible at the present time. A first appropriate step may be a potential flow analysis that includes a finite element representation of the aircraft, ground, and jets. This flow model could be expected to define fountain strength, location, and possibly the ratio of free air to exhaust gas ingested in the inlet. Perhaps then sources could be added to the jet representation to simulate turbulent mixing and temperature reduction. With information such as this, it would be possible to analytically study the relative ingestion problems of different configurations. Representation of the periodic nature of the fountain flow is beyond the current state-of-the-art. Analytical work to describe near-field reingestion flow fields is seriously lacking. Efforts in this direction should be encouraged.

CONCLUDING REMARKS

The results presented in this paper show that exhaust gas reingestion for lift-engine-powered VTOL aircraft can severely limit VTOL operational capability. The aircraft must be designed to minimize reingestion, the operation must be restricted to specially prepared sites, or operational techniques must be developed to avoid reingestion. These studies showed that a zero-length slant takeoff rather than a VTOL takeoff can probably avoid reingestion at takeoff. However, techniques for a zero-length landing are not clear. Aircraft configured as those studied herein may be incapable of VTOL landings, indicating that design of lift-engine VTOL fighters to minimize reingestion may be essential unless it is acceptable to limit operation to specially prepared sites.

Analytical evaluation of reingestion characteristics will be extremely difficult because turbulent mixing, periodic, and separated flows are involved. Nevertheless, techniques using simplifying assumption can yield valuable information and should be developed.

REFERENCES

1. Kirk, J. V.; and Barrack, J. P.: Reingestion Characteristics and Inlet Flow Distortion of V/STOL Lift Engine Fighter Configurations. Paper No. 68-78 presented at AIAA 6th Aerospace Sciences Meeting, Jan. 1968.
2. Barrack, Jerry P.; and Kirk, Jerry V.: Low-speed Characteristics of High-Performance Lift-Engine V/STOL Aircraft. SAE Paper 68-0644.
3. Kirk, Jerry V.; and Barrack, Jerry P.: Reingestion Characteristics and Inlet Flow Distortion of V/STOL Lift-Engine Fighter Configurations. NASA TN D-7014, Dec. 1970.
4. Hall, G. R.; and Bogdanovic, J. A.: Reponse of Bare Engine Intake. *Journal of Aircraft*, Vol. 4, No. 6, 1967, pp. 394-396.
5. Wallner, L. E.; Useller, J. W.; and Saari, M. J.: A study of temperature transients at the inlet of a turbojet engine. NACA RM E57C22, 1957.
6. Tolhurst, William H., Jr.; and Kelly, Mark W.: Characteristics of Two Large-Scale Jet-Lift Propulsion Systems. NASA SP-116, Paper 15, April 1966.

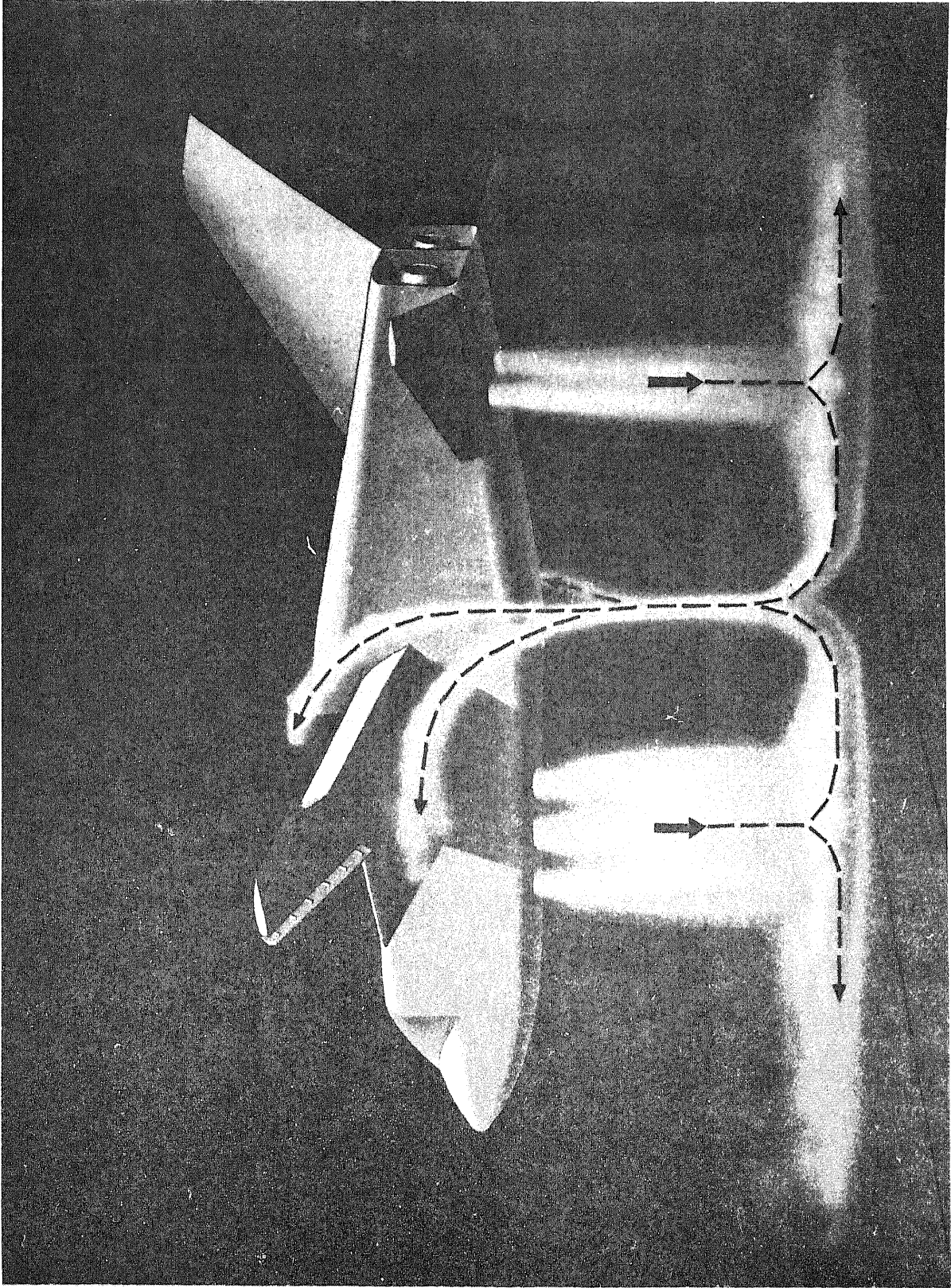


Figure 1.— Short-path, high-temperature rise flow patterns (fountain effect).

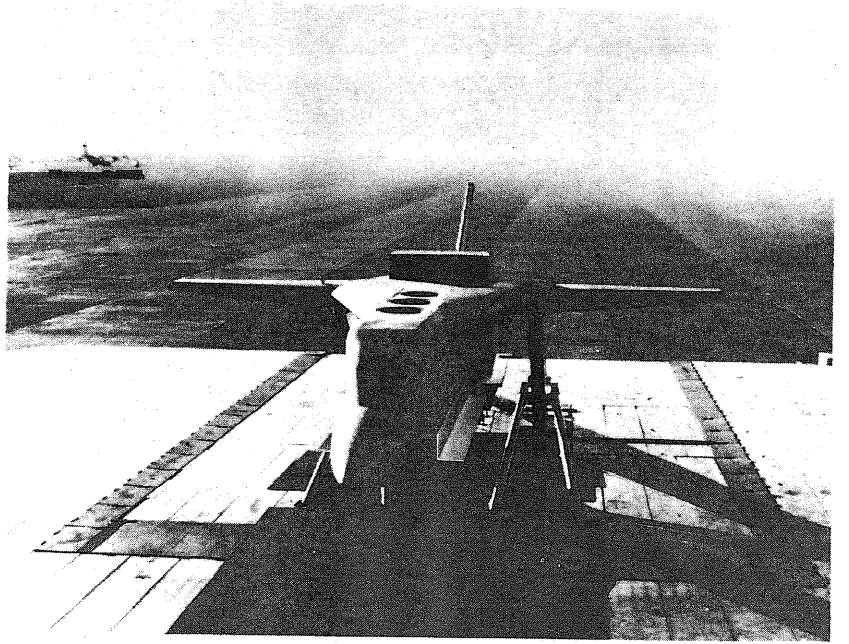
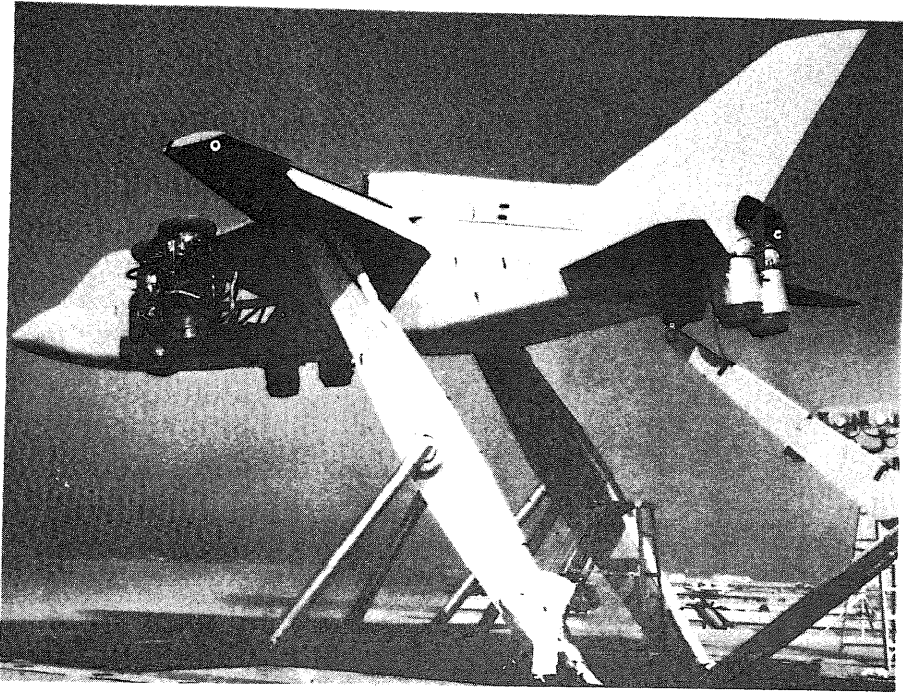


Figure 2.— Model with swiveling retractable lift engines mounted on Ames static test stand.

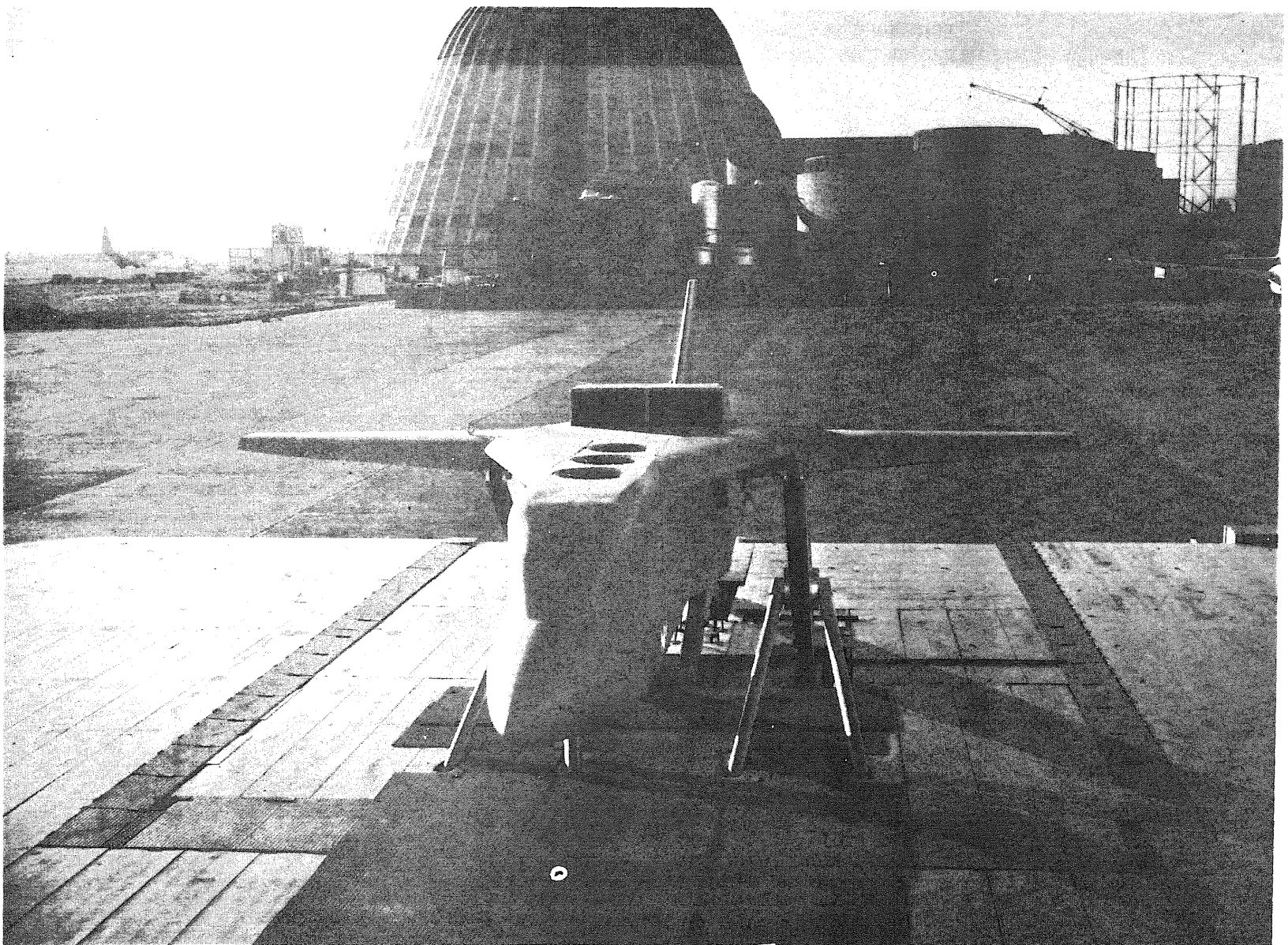


Figure 3.— Model with internally-fixed lift engines mounted on Ames static test stand.

ENGINES 90° FROM HORIZONTAL, HEIGHT/DIAMETER = 5.0

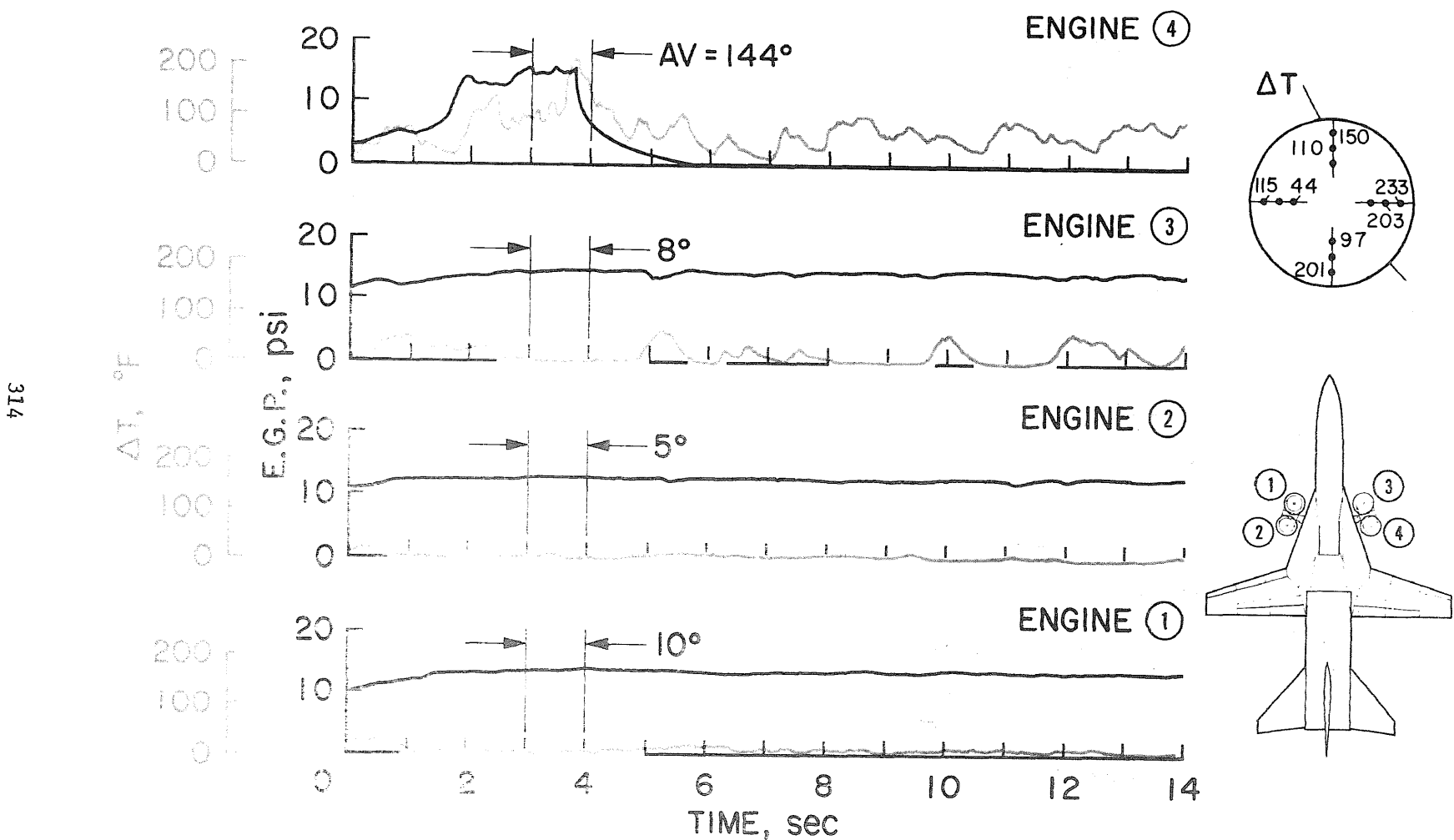


Figure 4.— Time history of exhaust gas pressure and inlet temperature for the swiveling retractable configuration with high ingestion.

ENGINES 80° FROM HORIZONTAL, HEIGHT/DIAMETER = 5.0

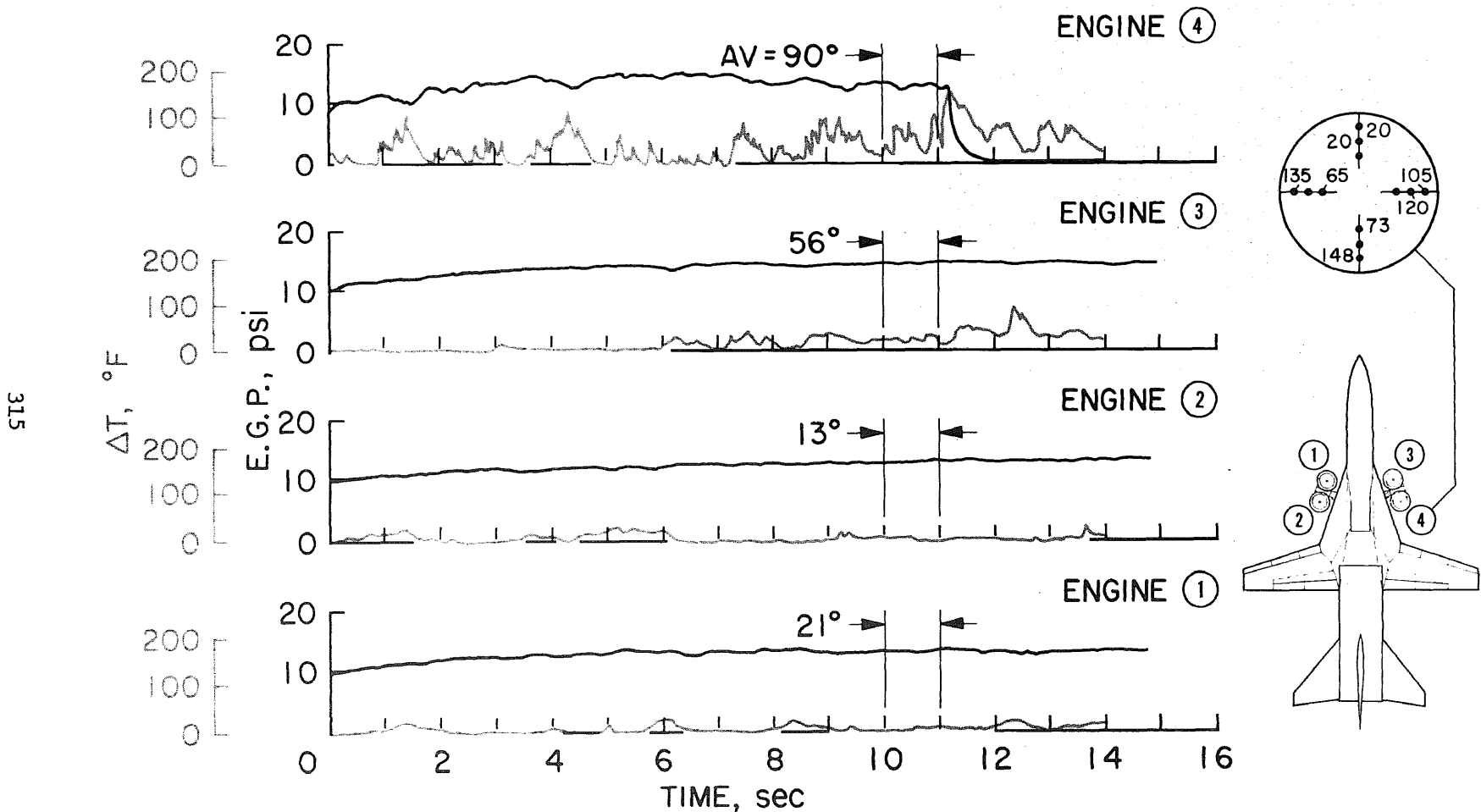


Figure 5.— Time history of exhaust gas pressure and inlet temperature for the swiveling retractable configuration with high ingestion.

ENGINES 70° FROM HORIZONTAL, HEIGHT/DIAMETER=5.0

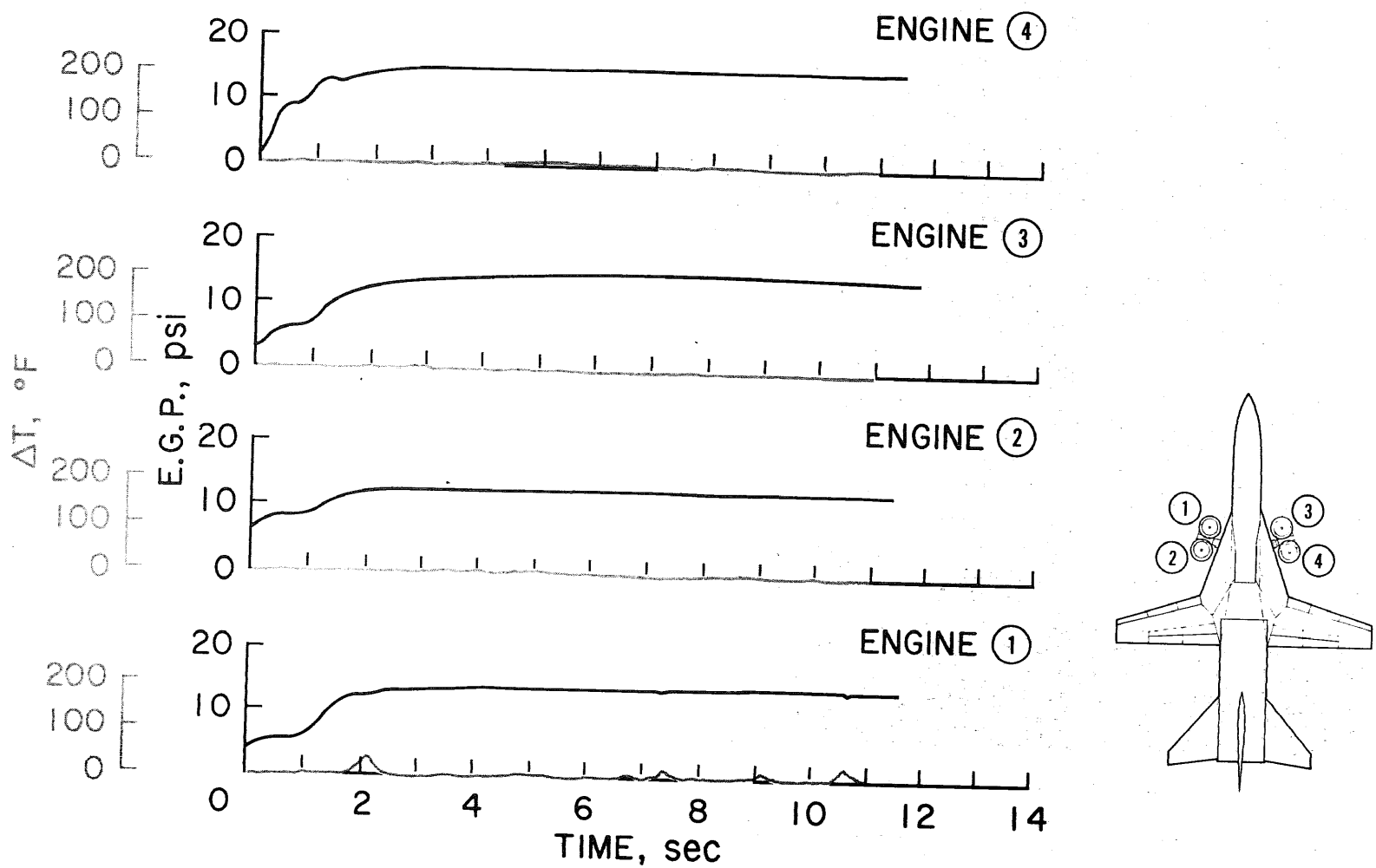


Figure 6.— The history of exhaust gas pressure and inlet temperature for the swiveling retractable configuration with low ingestion.

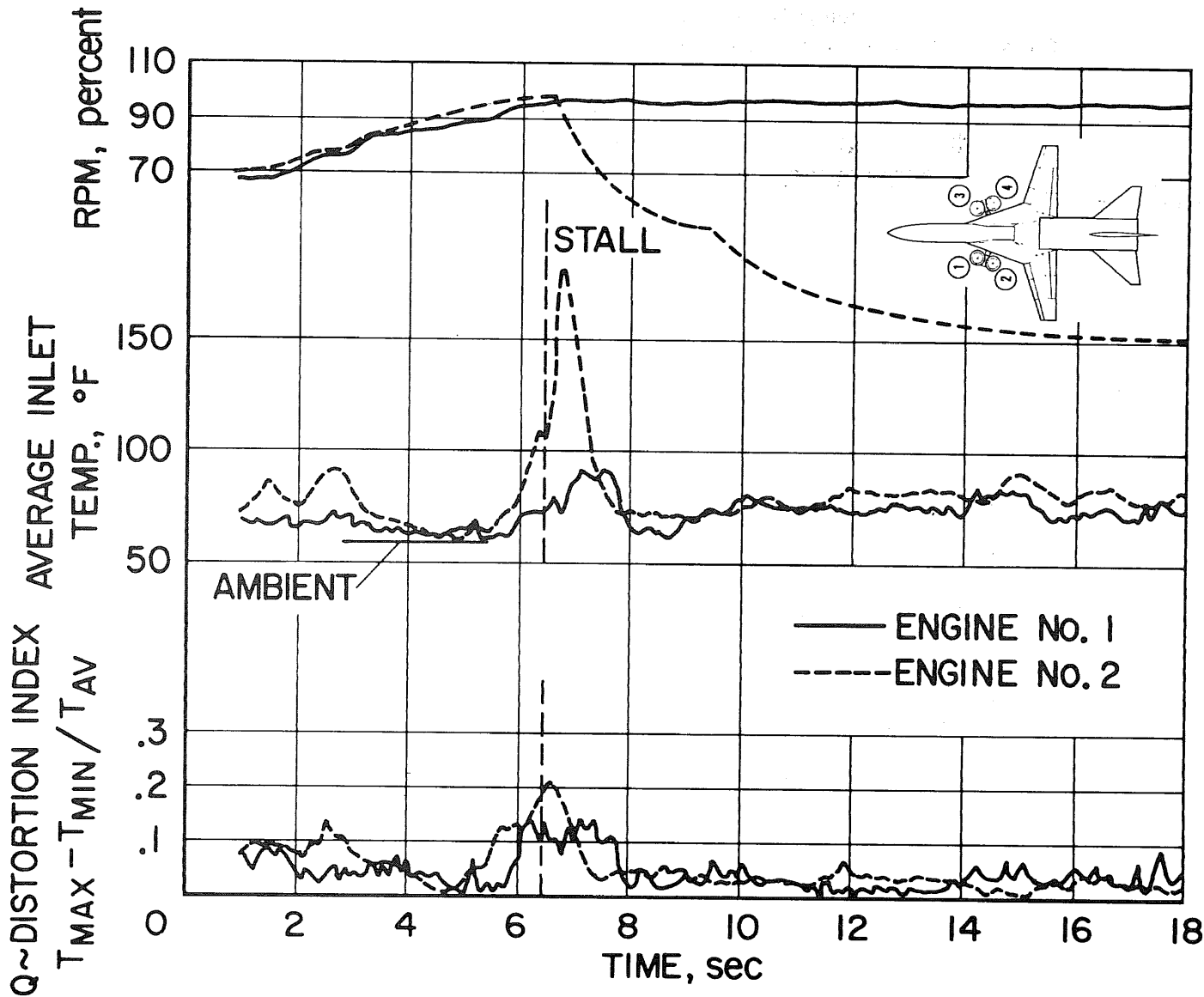


Figure 7.— Variation with time of rpm average inlet temperature and distortion index for engines 1 and 2 for the swiveling retractable configuration, at $\sigma_L = 80^\circ$ and engine cant angle = 5° .

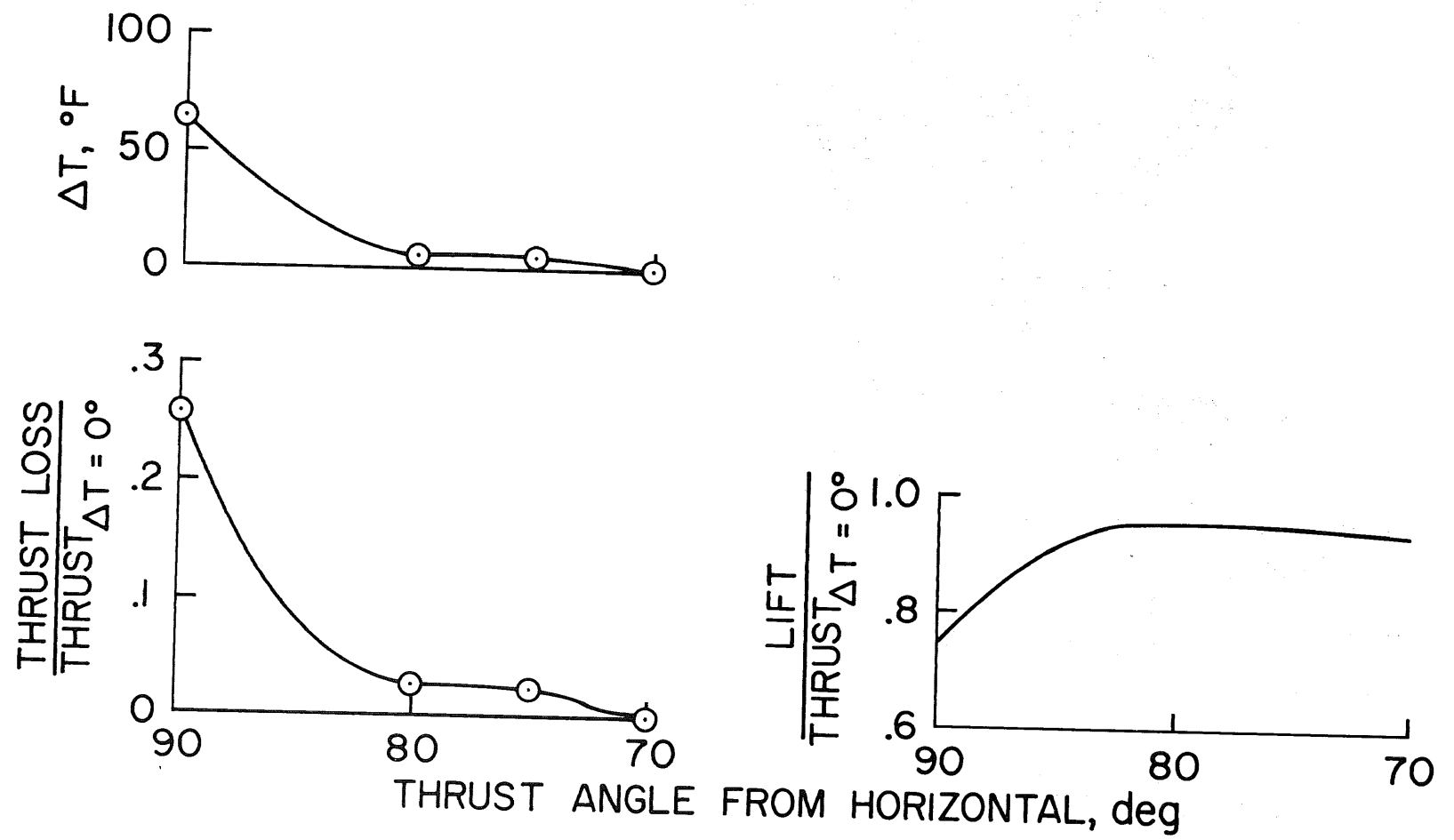


Figure 8.— Temperature rise, thrust loss, and lift loss as a function of swivel angle, at $H/D = 5.0$.

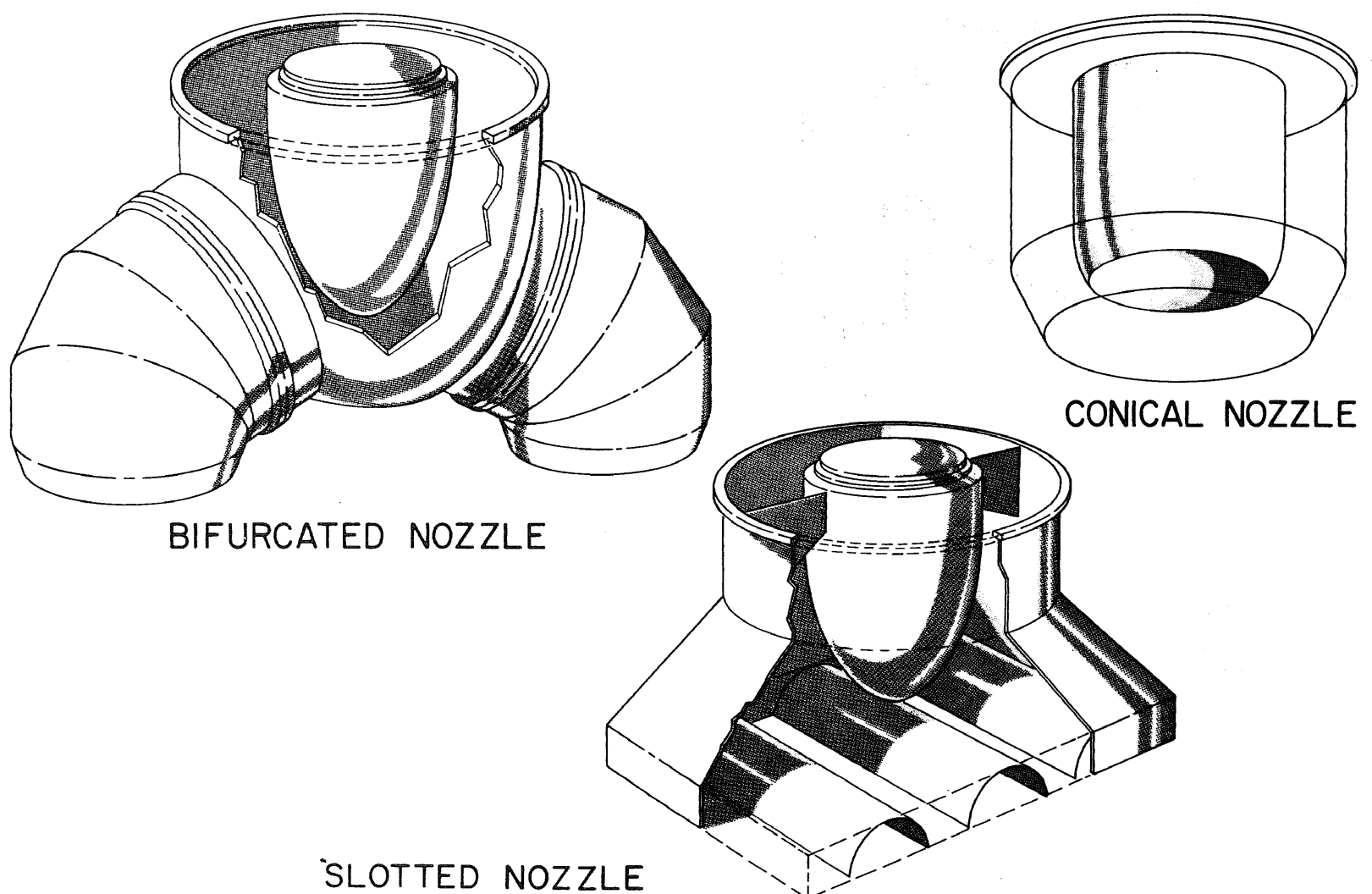


Figure 9.— Exit nozzles tested with internally-fixed lift-engine configuration.

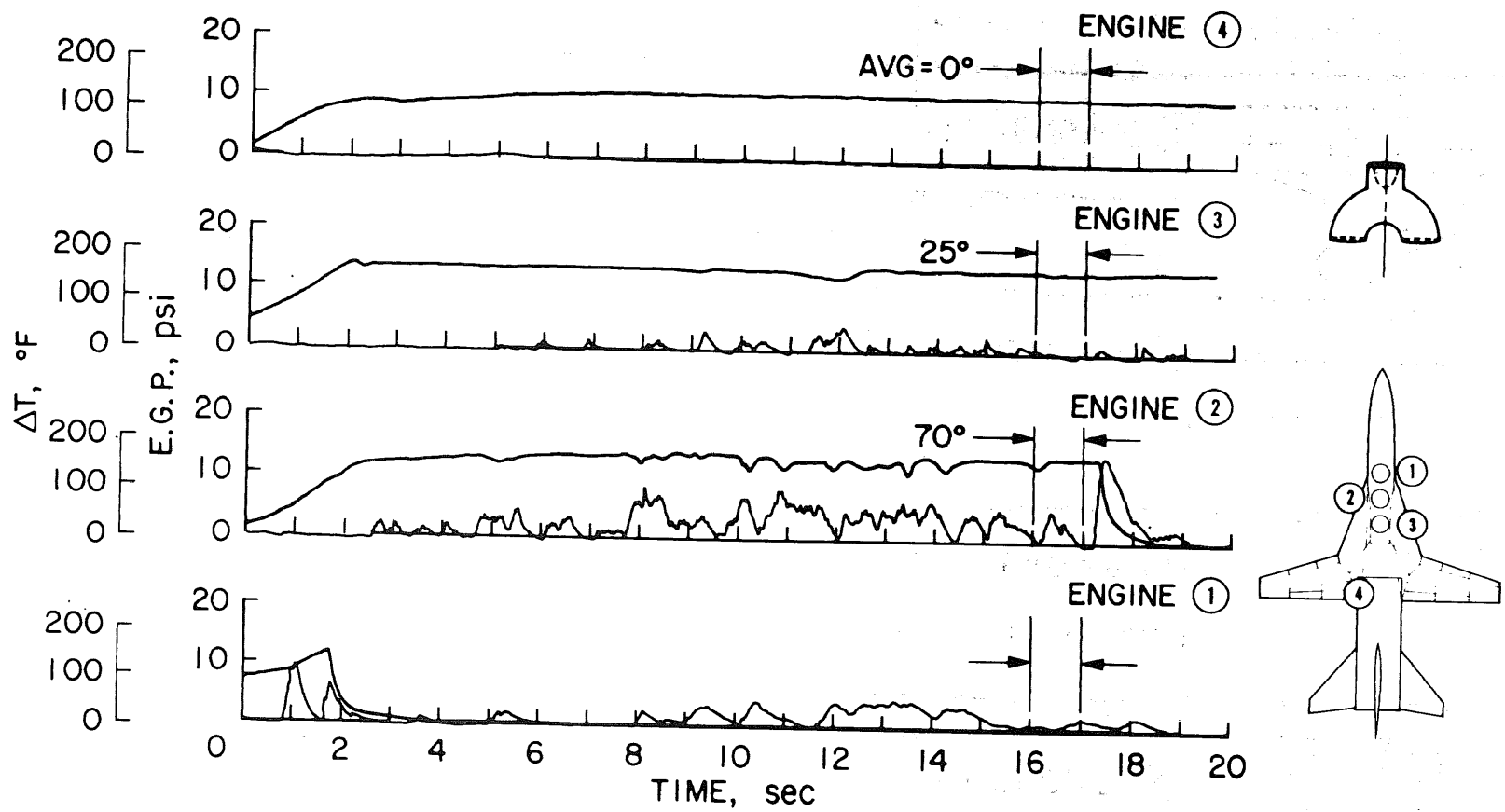


Figure 10.— Time history of exhaust gas pressure and inlet temperature for the internally-fixed configuration with high ingestion.

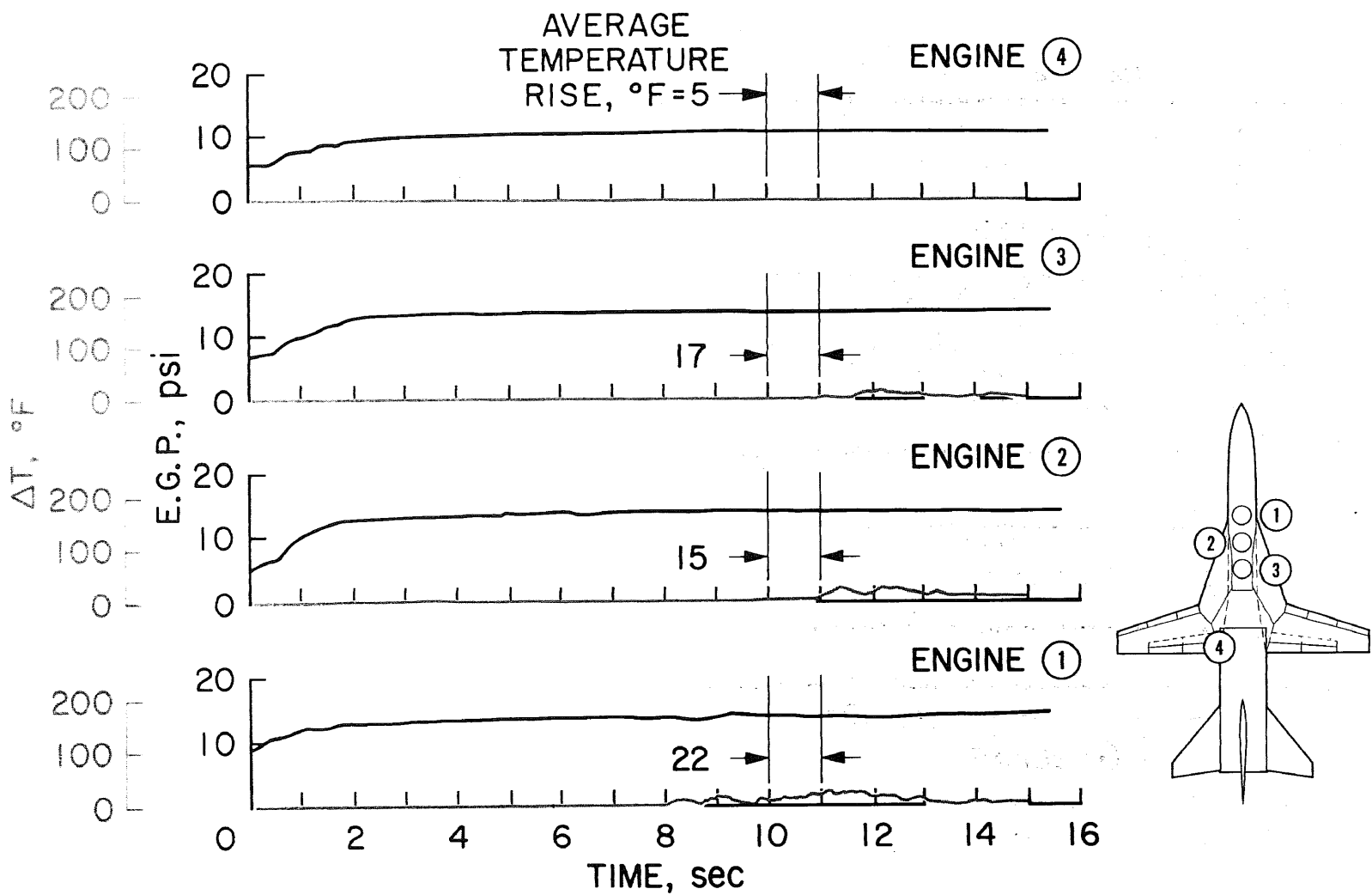


Figure 11.— Time history of exhaust gas pressure and inlet temperature for the internally-fixed configuration with low ingestion.

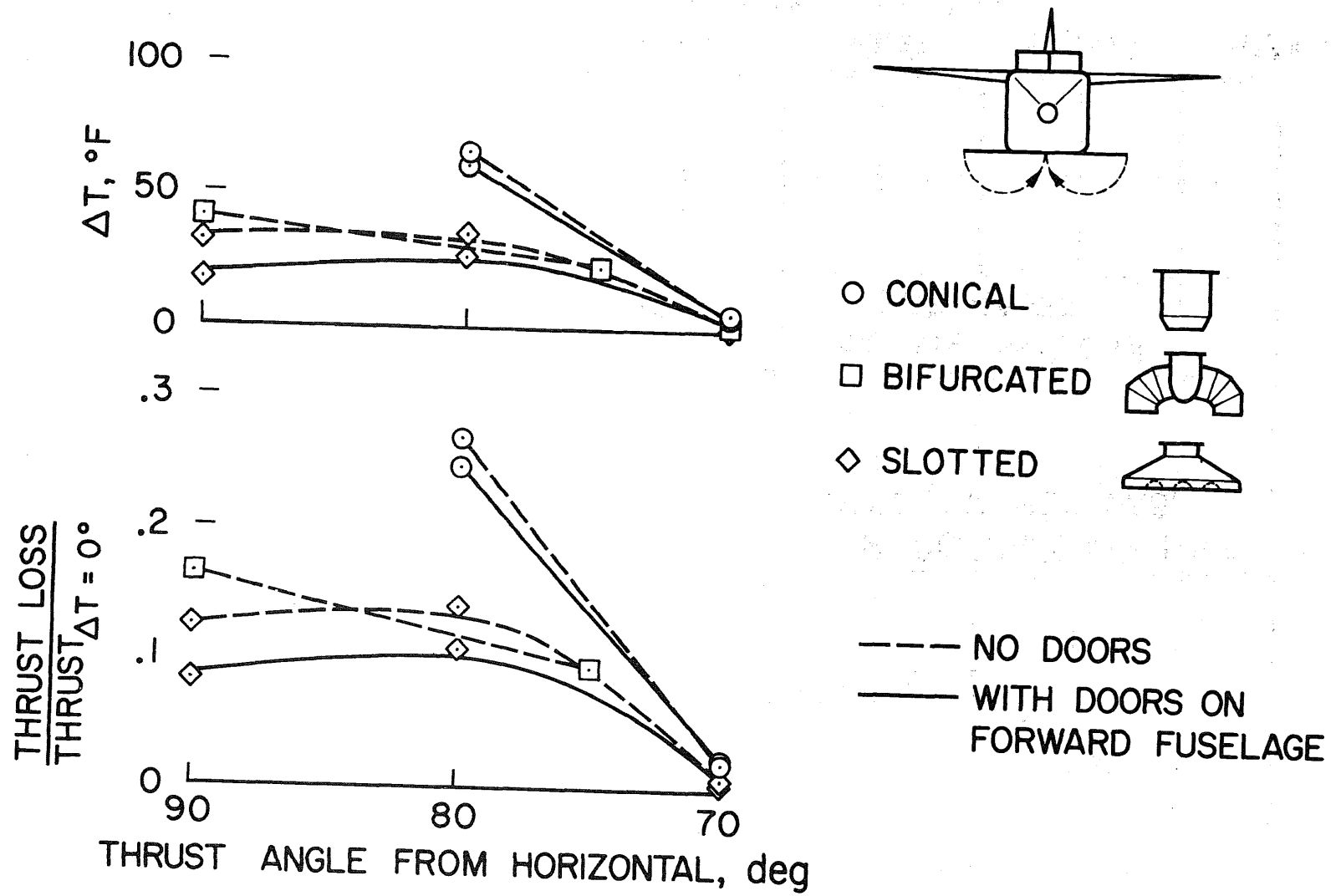


Figure 12.— Temperature rise and thrust loss as a function of exhaust vector angle for the internally-fixed configuration.

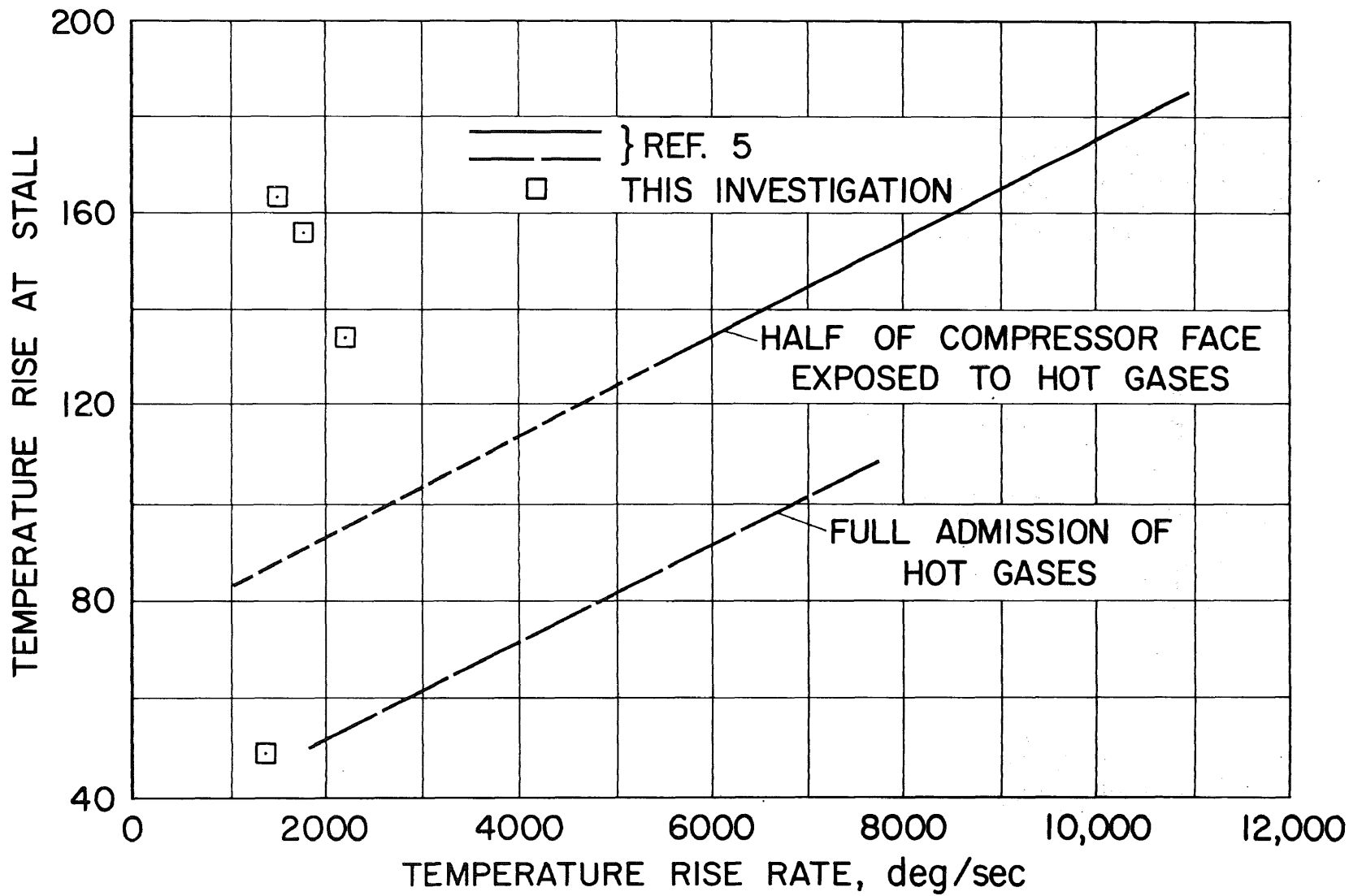


Figure 13.— Influence of temperature rise rate and temperature rise on compressor stall.

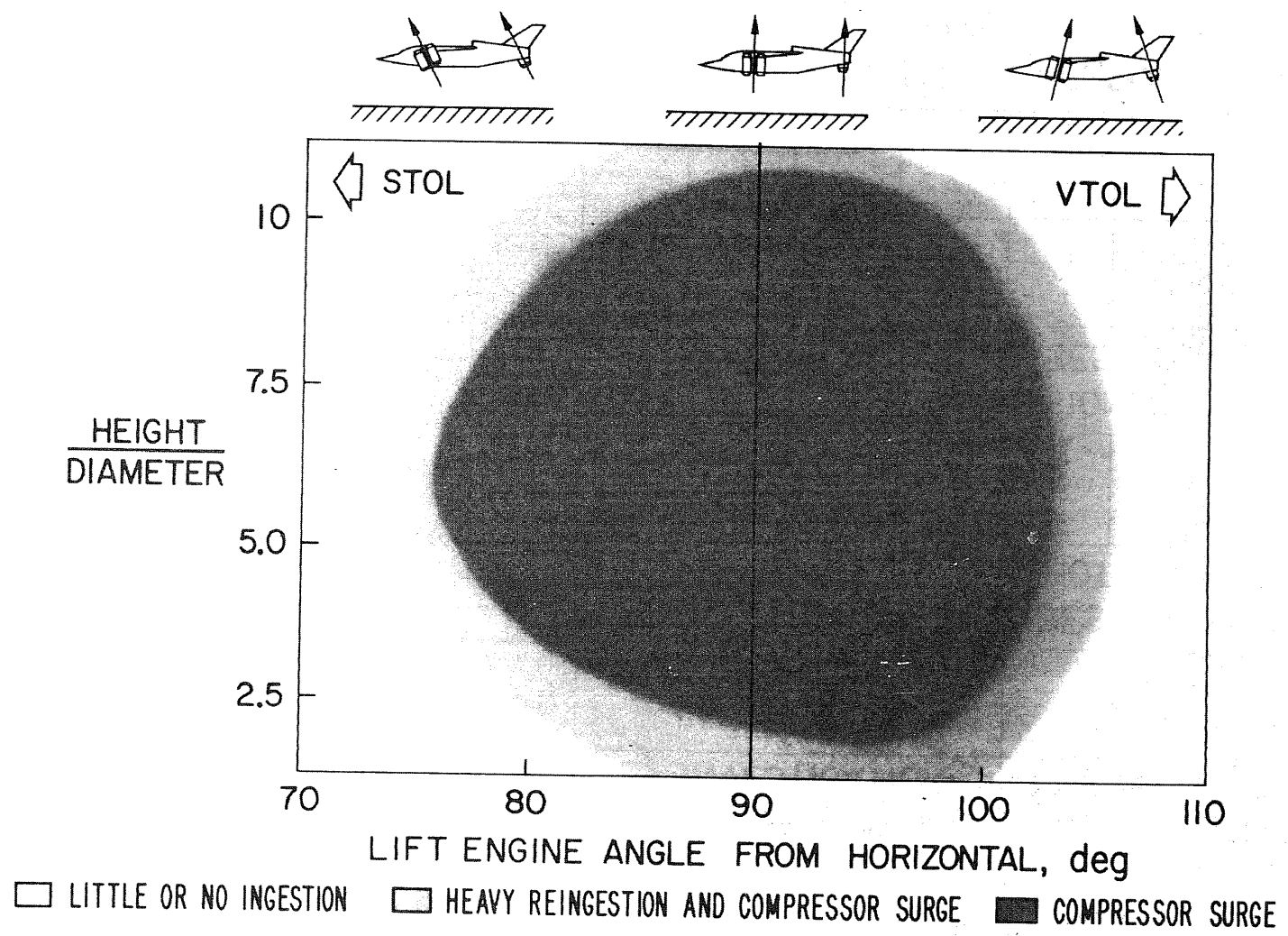


Figure 14.— General operating boundaries for lift engine fighter model.

NATIONAL AERONAUTICS AND SPACE ADMINISTRATION
AMES RESEARCH CENTER, MOFFETT FIELD, CALIFORNIA

H/D = 5.6



H/D = 12.7

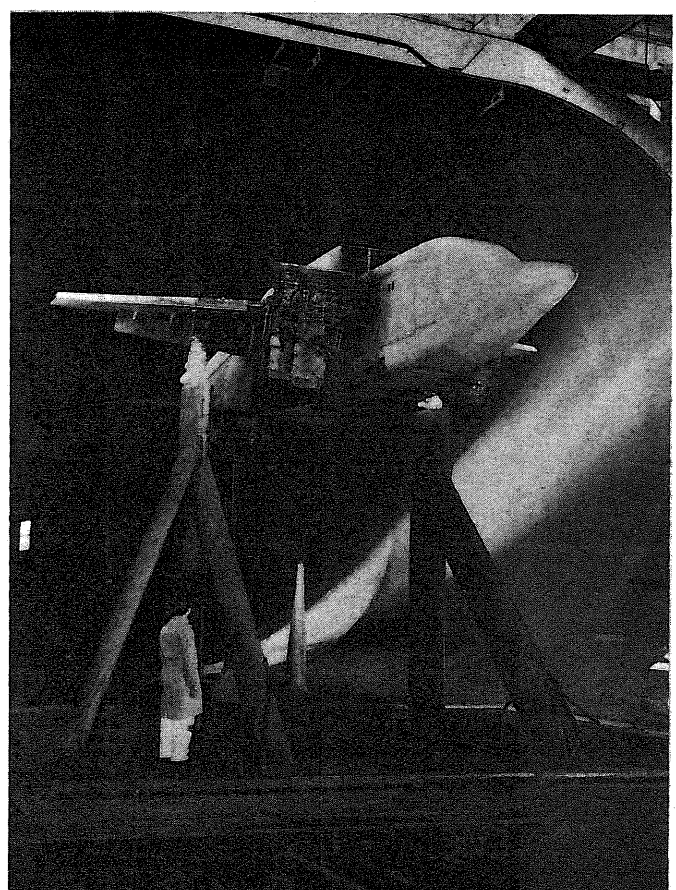


Figure 15.— Swiveling-retractable lift-engine model mounted in Ames 40-by 80-Foot Wind Tunnel.

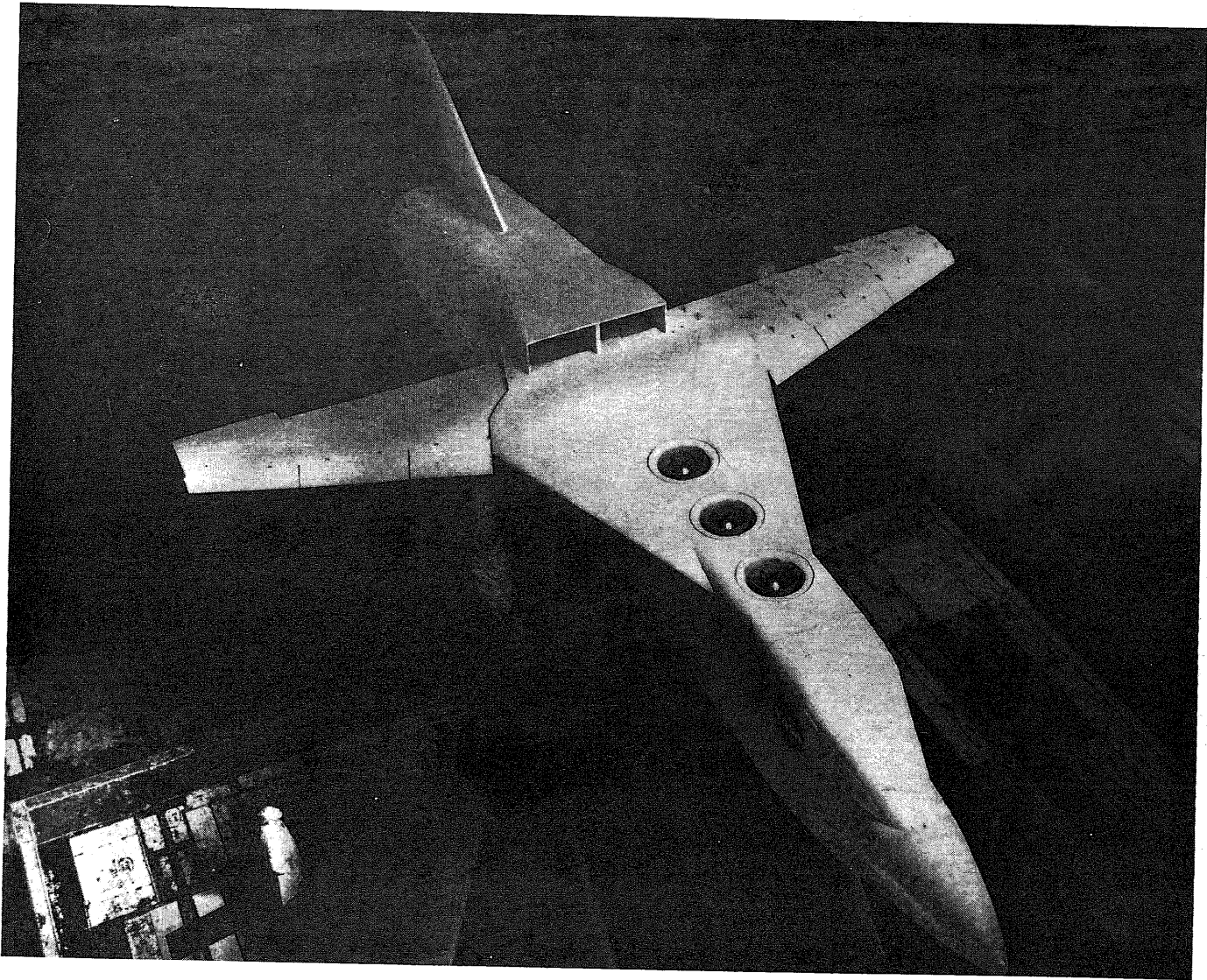


Figure 16.— Internally-fixed lift-engine model mounted in Ames 40- by 80-Foot Wind Tunnel, at $H/D = 12.7$.

NATIONAL AERONAUTICS AND SPACE ADMINISTRATION
AMES RESEARCH CENTER, MOFFETT FIELD, CALIFORNIA

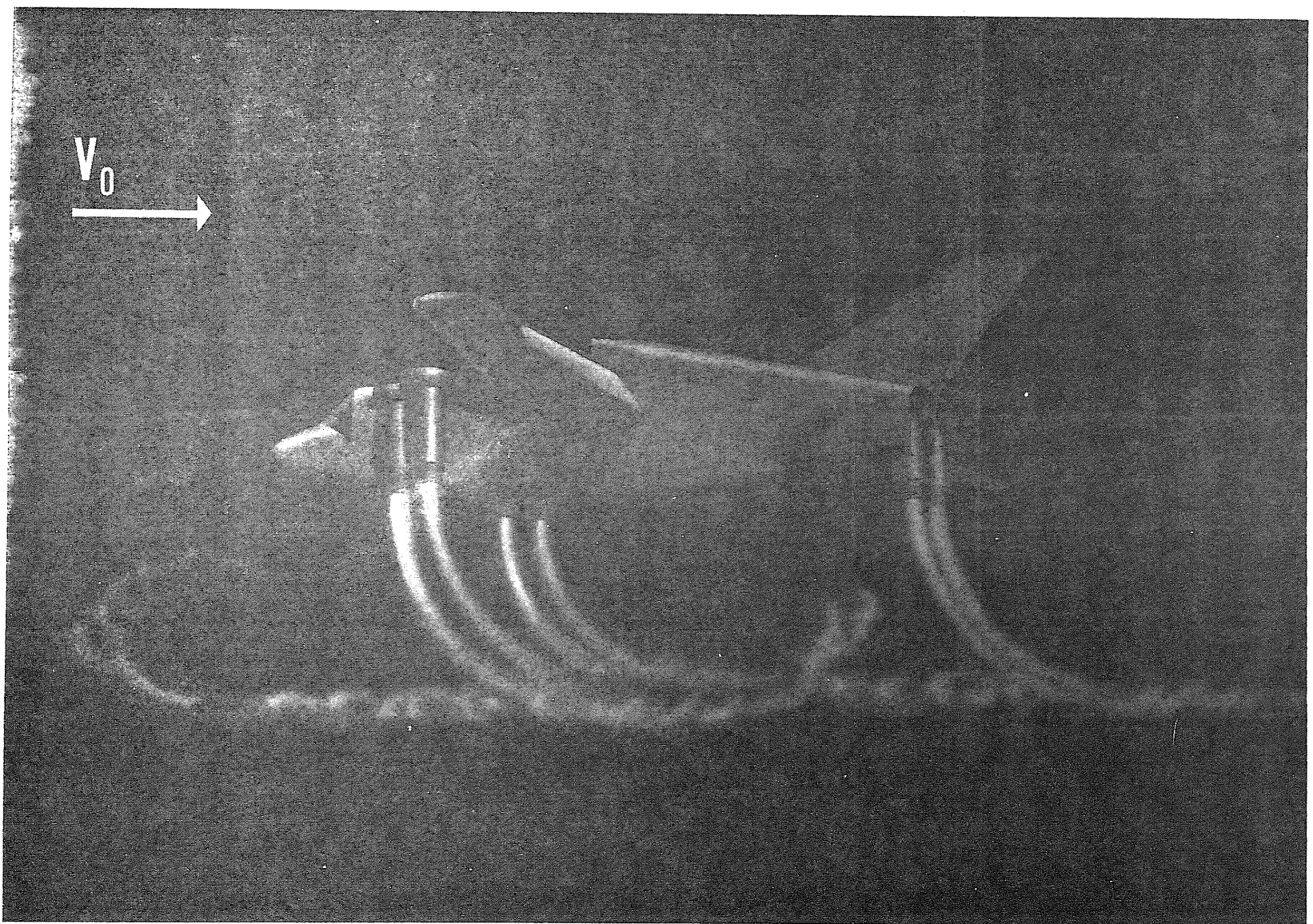


Figure 17.— Mechanism of reingestion: with high forward speed, no reingestion.

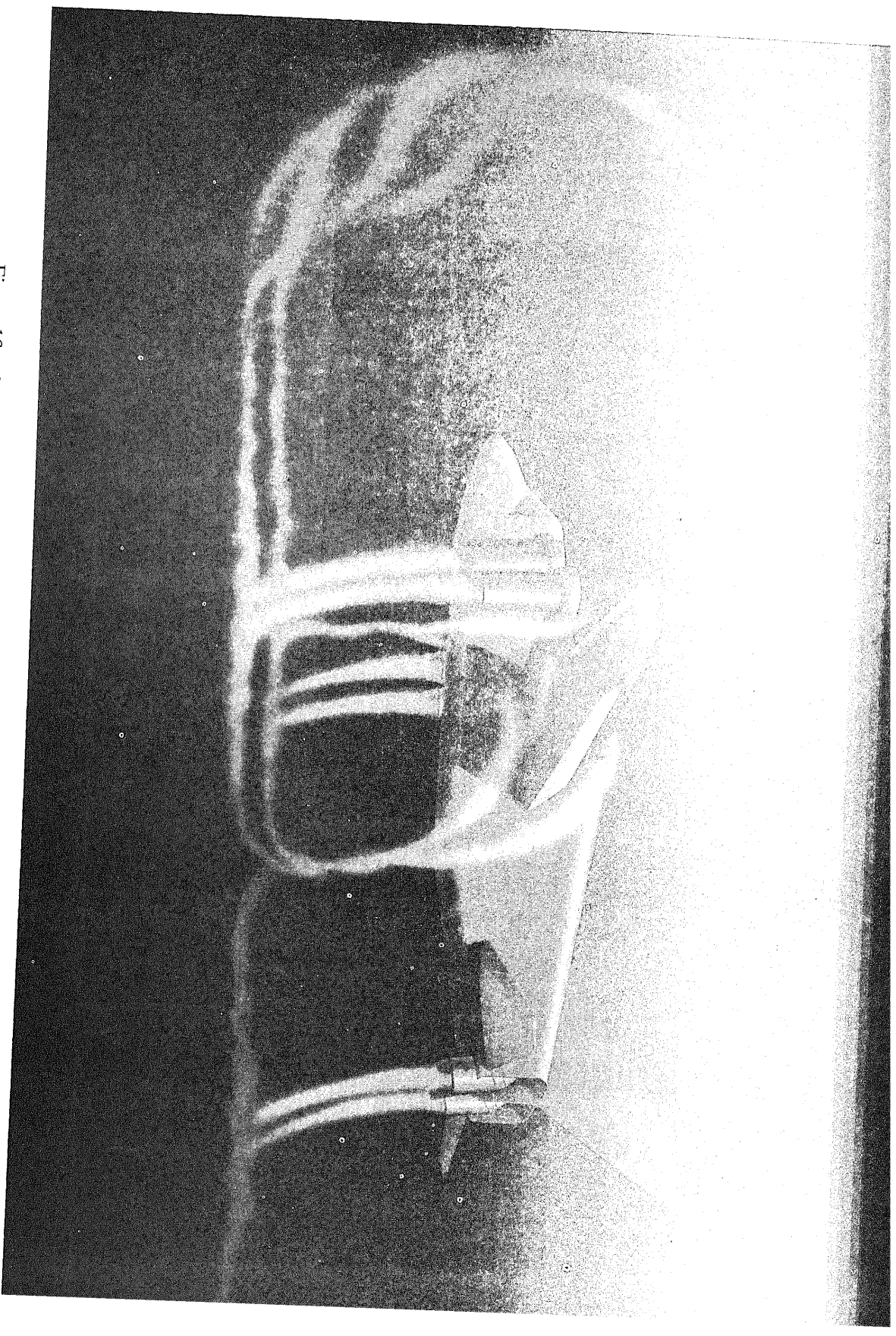
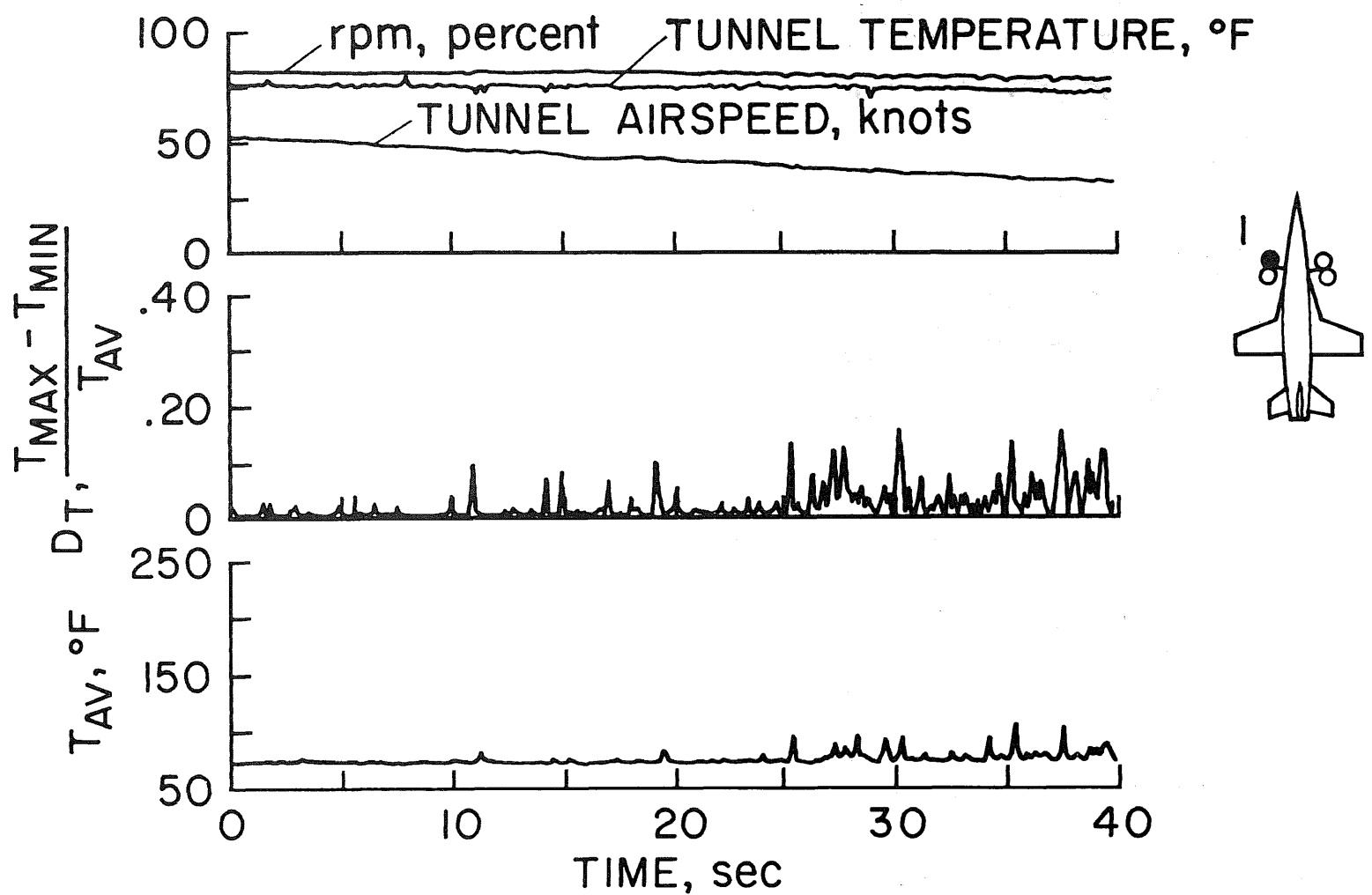
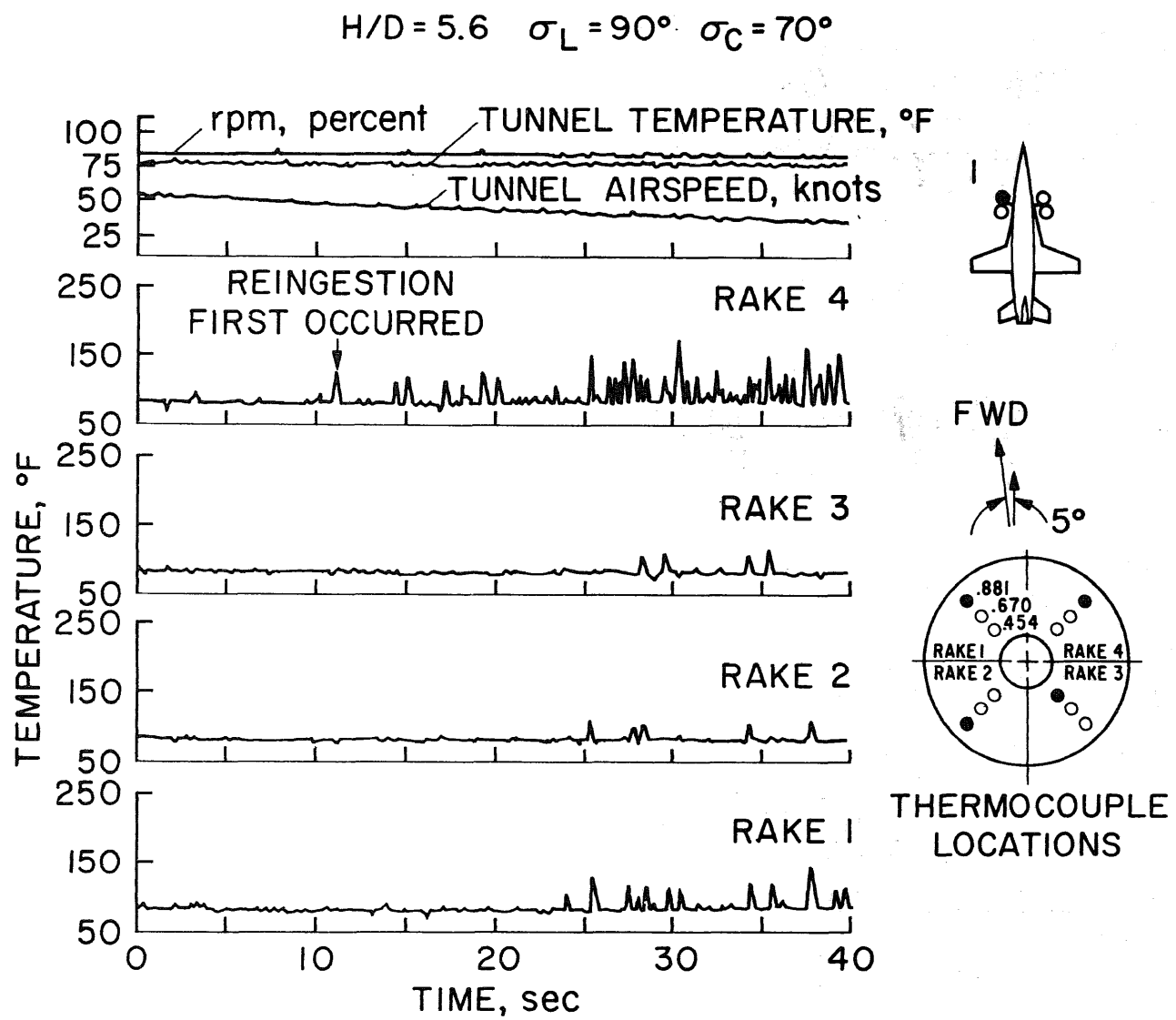


Figure 19. — Mechanism of reingestion: with low forward speed, short-path reingestion.



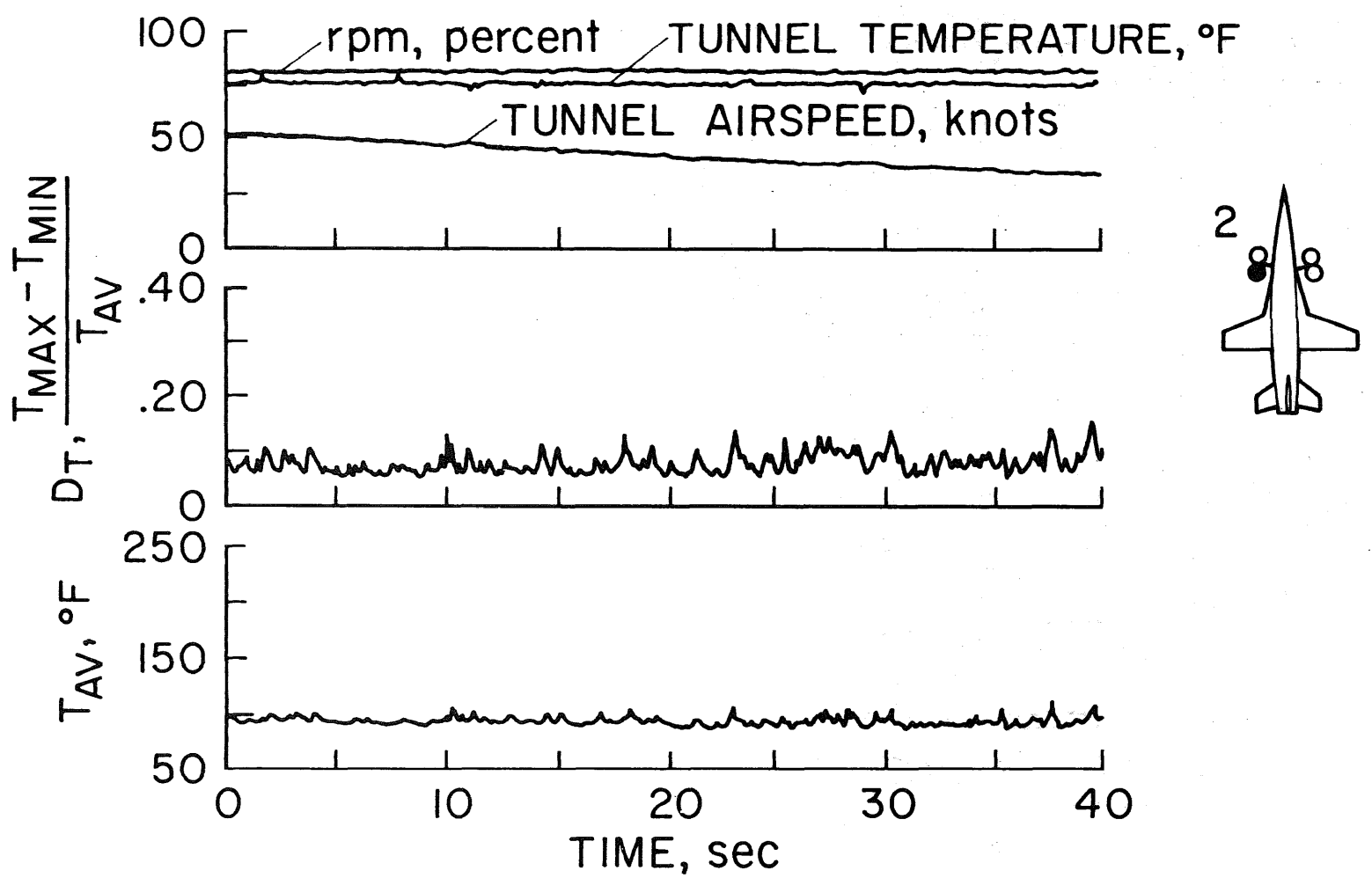


Figure 22.— Variation with time of temperature distortion index and average temperature for inlet number 2 as a function of time, at $\sigma_L = 90^\circ$ and $H/D = 5.6$.

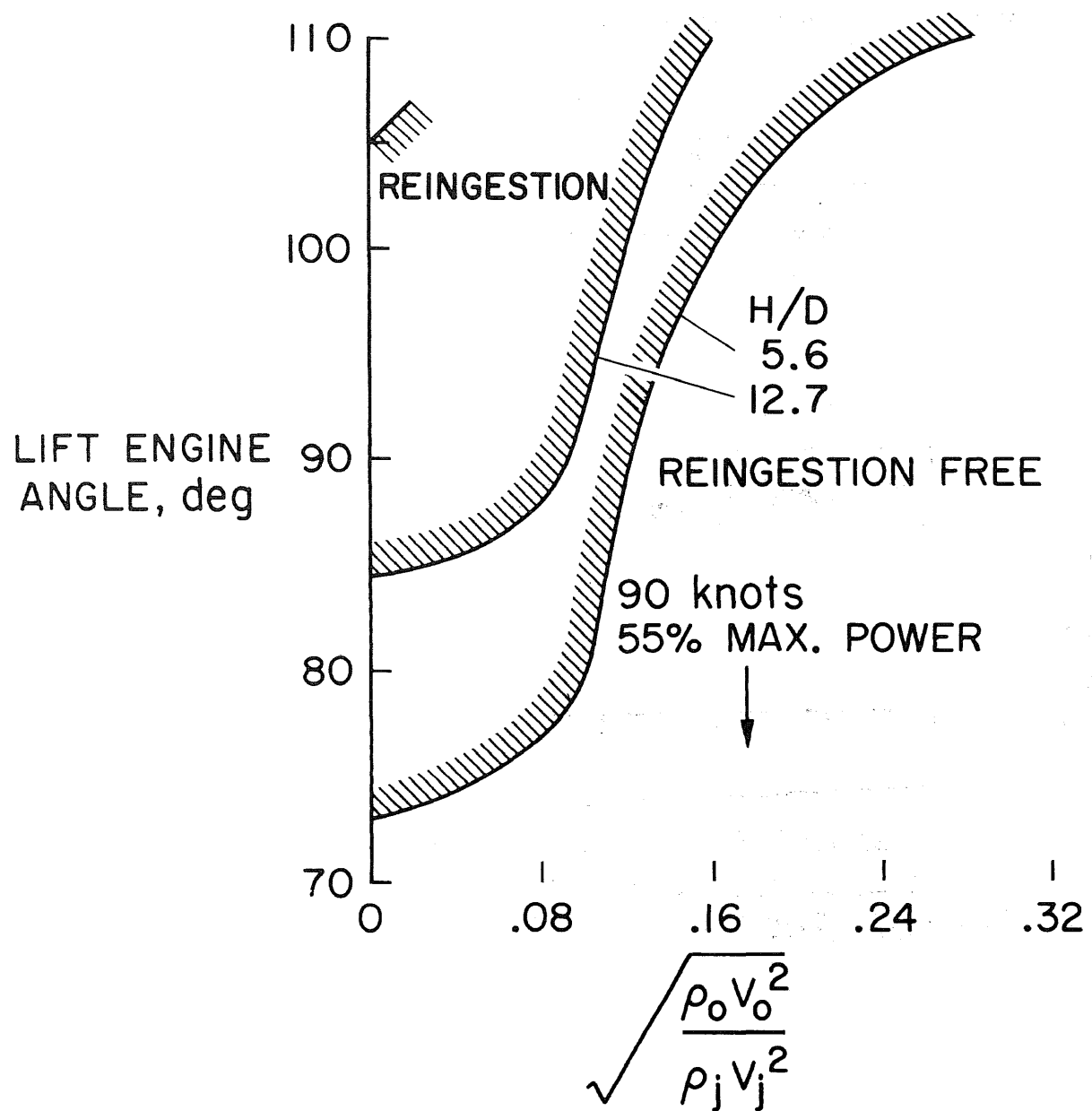


Figure 23.— Reingestion boundaries for the model of this investigation.

GROUND FOOTPRINT THEORETICAL & EXPERIMENTAL STUDIES

W. Barron & H. Frauenberger
Grumman Aerospace Corporation
Bethpage, New York 11714

ABSTRACT

The development of a general methodology is outlined for analyzing the jet-induced ground footprint and hot gas upwash characteristics of V/STOL aircraft. Some unique features of the methodology are noted and its analytical and experimental basis are discussed. A comparison is made of predicted vs test data. Requirements for additional test data are indicated, to improve prediction capabilities. The results of hot gas tests of V/STOL scale models are also shown, noting the effects of aircraft design and operational variables on footprint characteristics.

SYMBOLS

a	=	nozzle characteristic function
C	=	cosine distribution coefficient
C_D	=	nozzle mass discharge coefficient
C_H	=	nozzle heat discharge coefficient
D	=	nozzle diameter
H	=	nozzle height above ground
I	=	Momentum
K_M	=	Constant (Exhaust Nozzle Geometry)
K	=	Constant
k	=	Constant
ΔPt	=	$(P - P_\infty)/(P_J - P_\infty)$
Pr	=	P_J/P_∞
R	=	Radial distance from impingement point
ΔT_t	=	$(T - T_\infty)/(T_J - T_\infty)$
Tr	=	T_J/T_∞
X	=	distance from nozzle exit
ϕ	=	azimuth angle

σ	= inclination angle
θ_g	= ground impingement angle
θ_t	= ground turning angle
γ	= C_p/C_v
ζ_p	= axial correlation parameter
ζ_T	= axial correlation parameter
μ	= crosswind ratio

SUBSCRIPTS

J	= jet exit
p	= pressure
T	= temperature
t	= total
∞	= ambient

INTRODUCTION

Grumman realizes the importance of developing prediction techniques for analysis of complex jet-airframe interaction problems and has actively supported these efforts through Independent Research and Development (IR&D) funding.

This presentation concerns itself with prediction techniques for jet-lift V/STOL aircraft ground footprints and upwash. The problem of inlet re-ingestion is intimately related to ground footprint and is a part of our methodology development but is not treated in this presentation due to space and time limitations. Several objectives, Fig. 1, are considered in the presentation. These are addressed in subsequent illustrations.

FLOW FIELD DESCRIPTION

Figure 2 depicts a jet-lift V/STOL aircraft hovering in ground effect, together with its recirculating exhaust gas flow field. The complete flow field is comprised of a number of subregions as defined below:

- Inner Region - A region externally bounded by the lines connecting the jet impingement points on the ground plane
- Outer Region - The entire flow field excluding the inner region

- Free Jet - The region immediately downstream of the exhaust nozzles where a jet plume is developed. The free jet excludes the region in proximity to the ground where ground plane and turning effects exist
- Stagnation Region - (Ground Impingement Region) Characterized by a small region of zero velocity and a significant directional change of the inflowing mass
- Wall Jet - The wall jet is characterized as a radially spreading flow outward along the ground plane from the jet impingement stagnation region. Separation from the ground eventually results from wind and/or buoyancy effects (outer region) or the interaction with other wall jets
- Far Field - The region originating at the wall jet separation point in which the hot gases rise in a diffuse "cloud" due to buoyancy. Winds strongly influence the location of this region and may cause reingestion by blowing the separated hot gases toward the inlets
- Stagnation Line - A locus defining the stagnation points of interacting wall jets. The wall jets separate from the ground along this locus into a two dimensional upwash.
- Fountain - A region of relatively strong upwash located at the intersection of inner region stagnation lines

METHODOLOGY DEVELOPMENT

Approach

Grumman's approach to methodology development is indicated in Fig. 3. Starting with the semi-empirical methodologies of Ref. 1 and 2, their scope was extended through the development of characteristic functions for rectangular nozzles, application to general aircraft configurations, scaling, etc. The resulting methodology was then computerized. Correlation with new data (component, model and full scale) is used to improve the methodology. Modifications are made on the basis of these correlations and the need for additional experimental data is determined. The iterative process continues until satisfactory correlation is achieved.

Data Sources

Data for methodology verification and/or modification has been obtained from several sources. (See Fig. 4.)

Grumman's Research Department conducted tests on multi-nozzle arrangements at low pressure ratios. Impingement pressures were in very good agreement with predicted values. Details of these tests are available in Ref. 3.

The Grumman Advanced Development V/STOL Nozzle Test program provided free jet decay data for nozzles with aspect ratios of 1.0, 2.0, and 3.5 and several approach Mach numbers. These data correlated well for circular nozzles and were used to develop decay relationships for aspect ratios up to 3.5 and approach Mach number effects for flow turning at the nozzle inlet.

A series of flow field tests utilizing the Grumman V/STOL hover test rig with a 1/8-scale model of Design 607A were conducted. Pressure data for free-jets and wall jets agreed well with predictions (Fig. 9 and Ref. 4).

Extensive hot gas testing at VFW-Fokker in Bremen, Germany on models of the VAK-191B and Grumman Design 623 has produced considerable flow-field data. Details of the tests and correlations of some data are presented later. Additional testing of Design 623 is scheduled to start in September. Limited full scale VAK-191B test data has also been received.

Analysis Elements

To develop a methodology for generalized configurations, a systematic approach to the flow field analysis is required. The elements of the Grumman methodology are indicated in Fig. 5. Configuration independent calculation techniques for each of these elements are outlined in Fig. 6 and discussed below. An additional element of the complete methodology relates to inlet temperature rise prediction.

FLOW FIELD ANALYSES

Free & Wall Jets

Equations for free jet and wall jet decay of circular nozzles are available. Those used in the methodology are presented in Fig. 7. The following are items of interest in the analysis.

Free jet calculations for high aspect ratio nozzles and approach Mach number/turning effects are accomplished utilizing circular nozzle decay equations and an appropriate coordinate shift in the dimensionless distance from the jet exit plane (X/D). The coordinate shift relationships are empirical.

An inclined jet impinging on the ground distorts the ground plane isobars and isotherms. By applying the proper cosine distribution to the wall jet decay equations isobars and isotherm profiles are predictable, showing reasonably good agreement with test data.

Analysis of wall jet test data from Design 623 model tests and external sources indicates significantly lower temperature decay rates in wall jets approaching stagnation lines. Additional data is required to evaluate the influence of stagnation lines on wall jet pressure and temperature decay.

A preliminary model for high aspect ratio wall jets has been developed. The analysis uses basic wall jet decay equations and an approximation of the mass flow split on impingement to predict isobars and isotherms. Additional test data is needed to verify this model. Such data will be obtained in the Design 623 model test series beginning in September.

Two sets of equations are presented for the free jet and wall jet regions in Fig. 7. The initial set are basically those of reference 1, modified for inclined jets. Consistently good correlation with test data has been obtained with the free jet equations while correlation with wall jet temperature data has been somewhat inconsistent. Changing the exponent $-.09$ to $-.15$ and multiplying the entire equation by a factor of 1.413 yields better correlation with some data.

The equations presented as alternates are those used by VFW-Fokker. It is interesting to note that both pressure ratio and temperature ratio appear in the wall jet relationships. The constants K_1 , K_2 , K_3 , and K_4 must be determined empirically.

Stagnation Lines

The locus of stagnation lines between interacting wall jets is obtained by balancing wall jet total pressure components normal to the stagnation line. Since initially the stagnation locus is unknown an iterative procedure is required. The temperature at any point of a stagnation line is determined from an energy balance of the inflowing wall jet temperatures at that point. These inflowing wall jet temperatures are based on an equation for inner region wall jet decay.

Separation Locus

Neglecting buoyancy effects the upwind wall jet separation radius is defined by equal total pressures of wall jet and wind. At zero and low wind velocities buoyancy should be considered. By utilizing an empirical approach the interaction of buoyancy and winds is inherent in the equations. The shape of the separation locus for angles within ± 90 of the upwind direction can be approximated by a cosine distribution.

The equations for wall jet separation radius in Fig. 7 are derived from those presented in Ref. 1. A comparison of predictions with test data revealed large discrepancies at pressure ratios at or above 1.4. Correcting the equation by introducing the pressure ratio to the $1/4$ power yielded good agreement with test data for pressure ratios up to 1.9. The profile of the separation radii for angles within ± 90 degrees of the upwind direction ($\theta = 0$) also agrees well with available data.

Two-Dimensional Upwash

Decay of the two-dimensional upwash originating at the stagnation lines is calculated as an imaginary free jet whose nozzle exit plane (virtual origin) is located some distance below the ground plane. The location of the virtual origin is a function of the temperature at a specific point on the stagnation line and the assumed exit conditions of the imaginary free jet. Slipstream and upwash mass flows are defined by considering momentum vectors coupled with the radially-spreading wall jet mass flow of the impinging free jets.

The momentum relationships for two dimensional upwash are obtained from the VFW-Fokker recirculation methodology. The upwash and slipstream momentums are calculated for intervals along the stagnation line, with a summation process to determine the total slipstream momentum in an interval. The upwash direction at a point is a function of the jet and slipstream momentum ratios at that point.

Fountain

The mutual interaction of three or more wall jets produces a three-dimensional upwash or fountain located at the intersection of the inner region stagnation lines. At its origin the fountain mass flow equals the summation of the inner region slipstream mass flows. The fountain is modeled and consequently analyzed as an equivalent free jet utilizing the same basic techniques used for two-dimensional upwash. Fountain

pressure and temperature decay rates are significantly less than those for two dimensional upwash. Inclination of the fountain is determined from the ratio of the inflowing momentum of the stagnation lines. Assuming symmetry of thrust levels about the aircraft center-line only fore and aft stagnation line momentum components need be considered.

TEST DATA COMPARISONS

A comparison of free jet pressure decay for the 1/8-scale hover test model of Design 607A is presented in Fig. 8. Rake measurements for five nozzles each with an aspect ratio of 1.33 were made for non-dimensional distances from the jet exits of approximately 5 to 20. Predicted values compare favorably with measurements, averaging slightly higher. The scatter in the data is attributed to difficulties in locating the jet center with the rake coupled with the effects of a choke plate immediately upstream of the nozzle exit.

Figure 9 presents upwind wall jet separation radii test data for three wind velocities and a range of nozzle pressure ratios from 1.4 to 1.9. The corresponding predictions using the methodology discussed earlier show reasonable agreement with the data with a consistent trend to predict slightly smaller separation radii than measured. Agreement of predictions with test data improves with increasing wind velocity and pressure ratio.

A comparison of the calculated and measured wall jet separation locus for angles between 0 and ± 90 degrees is presented in Fig. 10. Values have been normalized by the upwind separation radius. Excellent agreement is achieved over the entire range of angles utilizing the indicated cosine distribution.

A comparison of predicted and measured pressure and temperature decay with height above the ground plane for a central fountain of a four jet group is presented in Fig. 11. Prediction techniques were those described previously for fountains. Generally good agreement is achieved for pressure with some underestimation near the ground for the lower H/D case. Temperature decay predictions are excellent for both cases at all elevations.

MODEL TEST DATA

Grumman has run extensive V/STOL hot gas model test programs during 1974 jointly with the VFW-Fokker Company of Bremen, Germany, on a 1/8-scale model of the VAK-191B and a 1/12-scale model of Grumman Design 623. The VAK-191B has one direct lift engine (DLE) forward and one aft with a four-jet lift-cruise engine (LCE) centrally located. Design 623 has one DLE forward and two LCE's with aft nozzles. Photographs of these models are shown in Fig. 12 and 13. They are rigidly supported above a movable ground plane adjustable for airplane height, pitch and yaw. Both models include the capability for nozzle thrust vectoring over a wide range of angles. They are instrumented with high response thermocouples in the inlets, fuselage, nacelles and on the ground. Suction is provided in the inlets to simulate inlet Mach no's. Maximum jet temperatures varied from 500°F to 1300°F in different tests, providing a broad base of temperature data. Nozzle pressure ratios were varied to simulate different engine thrust conditions. Cold flow tests were also run to provide flow visualization on the ground plane and to provide smoke and tu/t surveys of the flow around the models.

Ground Temperatures

Test results on VAK-191B model ground plane temperatures with the LCE only operating are shown in Fig. 14. These are compared with predictions based on the methodology outlined in the paper. Agreement between test and theory is good both inside and outside the region bounded by the impinging jets.

Ground Flow Visualization

Figure 15 shows two ground footprint flow visualization pictures made for Grumman Design 623 at two sets of jet deflection angles. These determine the two-dimensional stagnation line patterns and fountain locations and also verify model thrust balance and jet alignment. The results show that aft deflection of the DLE and LCE jets from the original $90^\circ/90^\circ$ position causes a significant rearward bending and movement of the stagnation lines, and a corresponding aft shift of the fountain. This, together with fountain aft inclination, would cause more rearward impingement of the upwash on the fuselage and reduce the impingement gas temperatures.

Figure 16 shows a comparison of calculated and measured stagnation line patterns for another jet deflection condition for Design 623. Close agreement in the line shapes and locations is evident, lending confidence to the calculation procedure.

Ground Temperatures vs Jet Deflection

Maximum ground temperatures at the simulated nose gear location for Design 623 are shown in Fig. 17 for various rearward deflections of DLE and LCE jets. The deflection angle combinations were selected for aircraft thrust balance. The reduction in the forward wall jet flow due to rearward jet inclination causes a significant decrease in these temperatures. The predominant influence is deflection of the DLE jet due to its location relative to the nose gear. The calculated and measured temperature trends are similar, but temperature magnitudes differ significantly. From other ground temperature measurements, it appears that the nose gear thermocouple readings are somewhat high.

Fountain Characteristics

Figure 18 presents an analysis of the central fountain region of Design 623 for a series of tests in which jet nozzle exhaust angles were varied at constant thrust levels. As the DLE and LCE nozzles are rotated aft the location of the central fountain shifts rearward. The fountain inclination angle, initially canted forward 131.5° from the horizontal, changes significantly with nozzle angle assuming a nearly vertical (99°) inclination at the 68/80 position. The predicted mass flow entering the fountain from the inflowing slipstreams decreases markedly from the initial 80/90 position. The fountain base temperature increases only slightly as the fountain location moves closer to the hotter lift-cruise engine jets. The overall effects as expected, is a significant reduction in inlet ingestion levels with rearward nozzle rotation which was confirmed in the test program.

Fuselage Temperature vs Jet Deflection & Thrust

A comparison of measured and calculated maximum fuselage gas temperatures for Design 623 is shown in Fig. 19. These occur in the region where two-dimensional upwash between the LCE nozzles has a major influence on the results. The calculations underestimate the fuselage temperatures when nozzle angles are more nearly vertical

but agree well at greater nozzle rearward deflections. The change in the trend appears to be due to interaction between fountain and two-dimensional upwash in this region.

Design 623 test data on fuselage temperature distributions vs DLE and LCE jet deflection angles is shown in Fig. 20. A large change in temperatures occurs over the range of deflection angles shown. Peak fuselage temperatures occur well aft of the airplane C.G. at all angles, but shift further aft as the jets are deflected aft. This is caused by the increasing aft inclination of both the central fountain and the two-dimensional upwash between the two LCE jets. This upwash makes a major contribution to the peak temperatures due to its higher temperature and shorter flow path to the fuselage vs that of the fountain.

Figure 21 shows that increasing the DLE thrust level of Design 623 decreases the fuselage temperatures. The effects are small for the range of thrust levels tested. An increase in the DLE thrust has an effect equivalent to deflecting a jet of unchanged thrust, rearward. Fuselage temperature effects are therefore similar. The relationship between thrust change and equivalent jet deflection angle can be evaluated from the wall jet momentum relationships for inclined jets. The results of this calculation are shown in Fig. 22.

Model Temperature Scaling

An evaluation of temperature scaling was made during a series of Design 623 model test runs. The range of LCE nozzle exit test temperatures was 655°F to 1305°F. The gas temperatures at several locations on the ground and fuselage were scaled up to a 3000°F equivalent full scale LCE nozzle temperature for each test condition. The results are shown in Fig. 23 as percentage changes in full scale temperature with changes in model test temperature, using the 655°F temperature as a reference baseline. Scaling is good, with only small percentage changes up to the maximum test temperature.

REFERENCES

1. Gray, L., and Kisielowski, E., "Practical Engineering Methods for Predicting Hot Gas Reingestion Characteristics of V/STOL Aircraft Jet Lift Engines", NASA-CR-111845
2. Behnert, R., "Bodeneffekt bei Strahlgestutzen Senkrechtstartern", VFW-Fokker Report EA380 ZTL, August 4, 1971
3. Hill, W., "Experimental Studies of Multi-Jets In Ground Effect", NAVAIR Workshop on Prediction Methods for V/STOL Aerodynamics, July 28-31, 1975
4. Wohllebe, F., "The Design and Development of a Hover Rig for Model Tests", NAVAIR Workshop on Prediction Methods for V/STOL Aerodynamics, July 28-31, 1975

- DEFINE RECIRCULATING FLOW FIELD
- DISCUSS GRUMMAN METHODOLOGY FOR GENERAL CONFIGURATIONS
- PROVIDE COMPARISONS OF CALCULATIONS WITH TEST DATA
- DISCUSS MODEL TESTS OF DESIGN 623 & VAK-191B

Fig. 1 Objectives

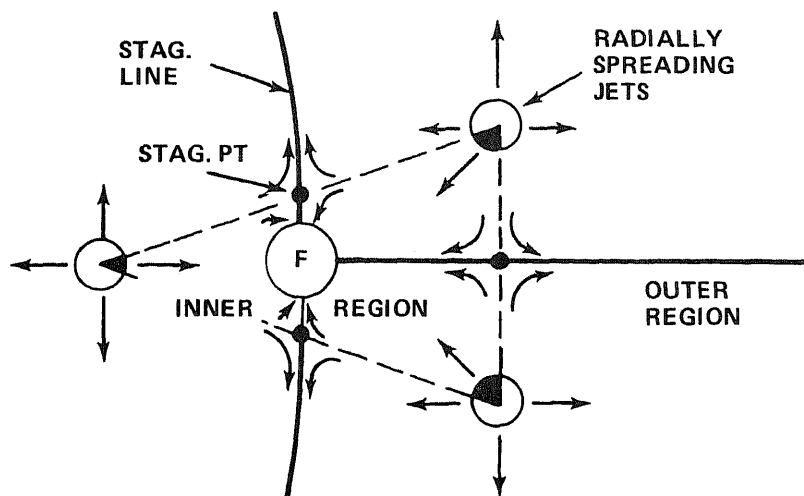
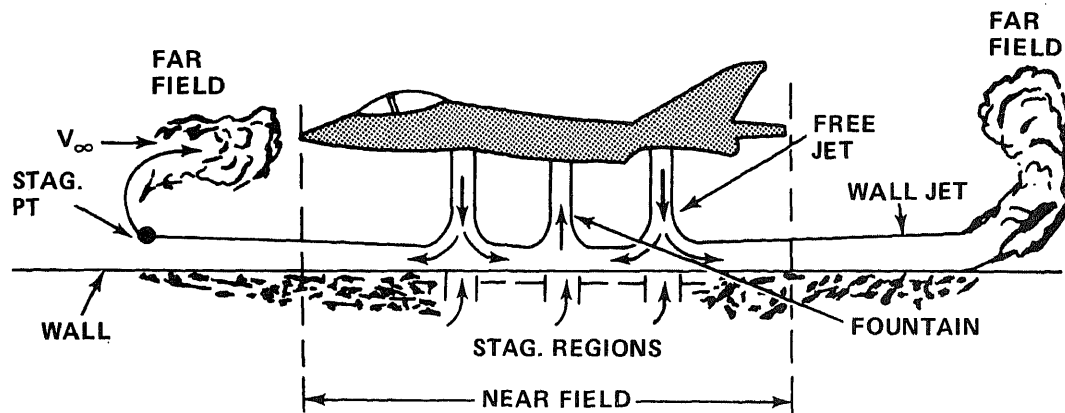


Fig. 2 VTOL Aircraft Flow Fields

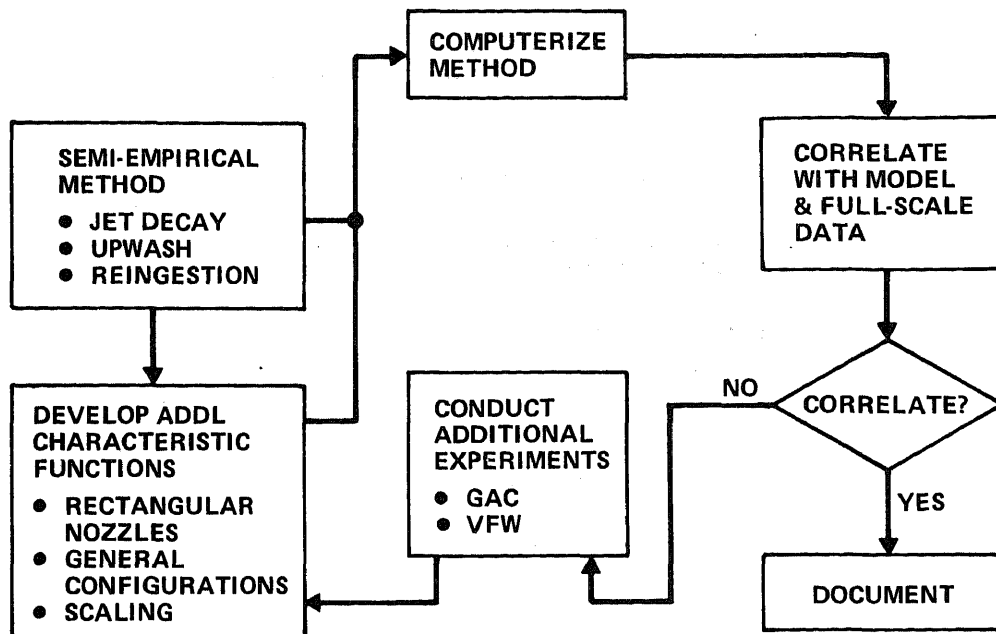


Fig. 3 Grumman Methodology Approach

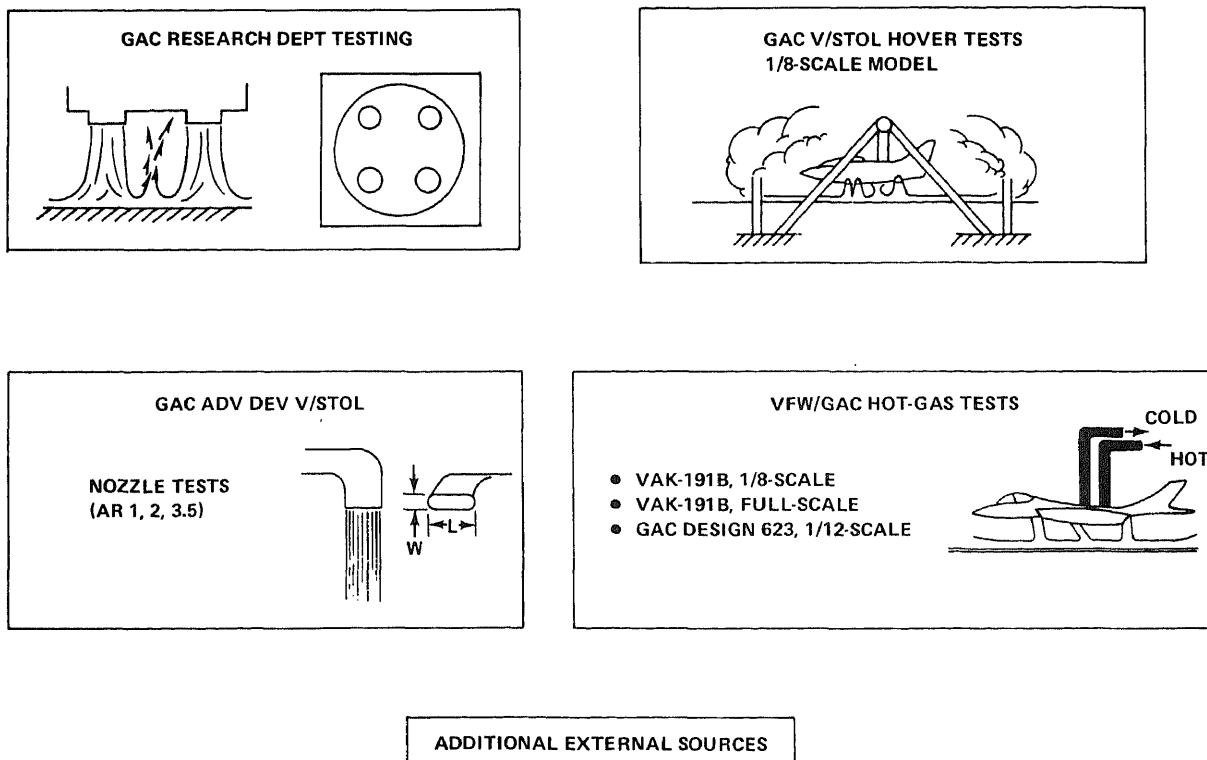


Fig. 4 Program Validation—Data Sources

- FREE-JET & WALL-JET P&T DECAY
- STAGNATION-LINE LOCUS FOR MULTI-JET ARRANGEMENTS
- WALL-JET SEPARATION LOCUS (WIND EFFECTS)
- 2D UPWASH DECAY & DIRECTION
- FOUNTAIN LOCATION, DIRECTION, & DECAY

Fig. 5 Analysis Elements

FREE JET

- P&T DECAY $f(P_r, T_r, AR, M, X/D)$
- CALCULATIONS FOR $AR > 1$ & HIGH APPROACH M

WALL JET

- P&T DECAY $f(P_r, T_r, H/D, R/D, \sigma, \phi)$
- INCLINED JET EFFECTS/COSINE DISTRIBUTION
- INFLUENCE OF STAGNATION LINES ON P&T DECAY
- HIGH-ASPECT-RATIO NOZZLE WALL JETS

STAGNATION LINES

- LOCATION BY WALL-JET PRESSURE BALANCE
- TEMPERATURE BY ENERGY BALANCE

SEPARATION LOCUS (WIND EFFECTS)

- NEGLECTING BUOYANCY – WHEN $\Delta P_{t_w} = \Delta P_{t_\infty}$
- EMPIRICAL APPROACH INCLUDES BUOYANCY EFFECTS
- COSINE DISTRIBUTION FOR ANGLES $\leq \pm 90$ DEG FROM UPWIND DIRECTION

2D UPWASH

- DECAY FROM MODIFIED FREE-JET EQUATIONS & VIRTUAL-PATH TECHNIQUE
- SLIPSTREAM/UPWASH M & DIRECTION FROM JET MOMENTUM VECTORS

FOUNTAIN

- AT INTERSECTION OF INNER REGION STAGNATION LINES
- $\dot{M}_F = \sum (\text{SLIPSTREAM } \dot{M})_{\text{INNER REGION}}$
- MODELED AS EQUIVALENT FREE JET
- DECAY BY VIRTUAL-PATH TECHNIQUE
- INCLINATION BASED ON MOMENTUM RATIO OF INFLOWING MASS

Fig. 6 Calculation Techniques

FREE JET

$$\zeta_P = (P_r)^{-0.07} (T_r)^{0.25} \frac{X/D}{K_n \sqrt{C_D}}$$

$$\zeta_T = (P_r)^{-0.86} (T_r)^{0.5} \frac{X/D}{C_H}$$

$$\Delta P_t = f(\zeta_P)$$

$$\Delta T_t = f(\zeta_T)$$

WALL JET

$$\Delta P_{t_w} = C^2 \frac{K_1^2 C_D (H/D)^{2(K_2-1)}}{(R/D)^{2K_2}}$$

$$\Delta T_{t_w} = C [2.109 - 0.0123 (\theta_t)] \frac{(H/D)^{-0.09}}{(R/D)}$$

$$C = 1 + (4/\pi) \cos(\sigma) \cos(\phi)$$

$$\theta_t = \cos^{-1} [-\cos(\theta_g) \cos(\phi)]$$

ALTERNATES (X/D > 4)

$$\Delta P_T = \frac{K_1}{T_r^{1/4} P_r^{(2\gamma-1)/2\gamma} (aX/D)^2}$$

$$\Delta T_T = \frac{K_2}{T_r^{1/4} P_r^{1/2} (aX/D)}$$

ALTERNATES

$$\Delta P_{t_w} = C^2 \frac{K_3}{T_r^{1/8} P_r^{(2\gamma-1)/2\gamma} (aR/D)^2}$$

$$\Delta T_{t_w} = C \frac{K_4}{T_r^{1/4} P_r^{1/2} (aR/D)}$$

$$C = 1 + (4/\pi) \cos(\sigma) \cos(\phi)$$

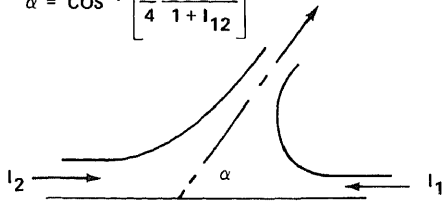
SEPARATION RADIUS

$$\Delta P_{t_w}^{1/2} (P_r)^{1/4} / \cos(\phi/2) = 2\mu/1 + 5\mu$$

$$\mu = \left[\frac{P_\infty}{2G T_\infty (P_J - P_\infty)} \right]^{1/2} V_\infty$$

FOUNTAIN

$$\alpha = \cos^{-1} \left[\frac{\pi}{4} \frac{1 - I_{12}}{1 + I_{12}} \right]$$



UPWASH 2D

UPWASH

$$I_{Fi} = (I_1 \sin \phi_1 + I_2 \sin \phi_2)_i$$

SLIPSTREAM

$$I_{Si} = \sum_{\text{STAG}}^i [I_1 (1 - \sin \phi_1) + I_2 (1 - \sin \phi_2)]_m$$

DIRECTION

$$I_{1-2i} = \frac{[1 - (4/\pi) \cos \phi_1] I_{1i}}{[1 + (4/\pi) \cos \phi_2] I_{2i} + I_{Si}}$$

$$\alpha_i = \cos^{-1} \left[\frac{1 - I_{1-2i}}{1 + I_{1-2i}} \right]$$

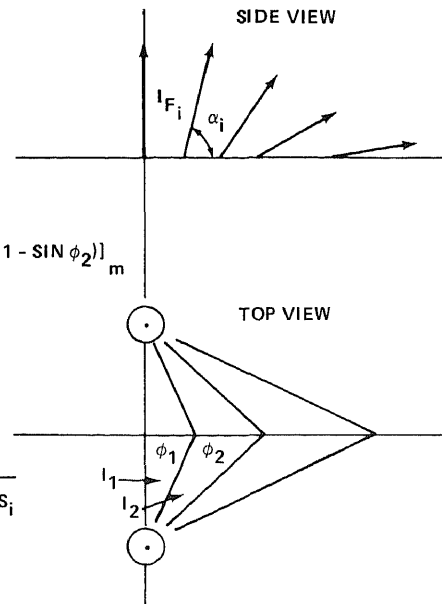


Fig. 7 Typical Equations

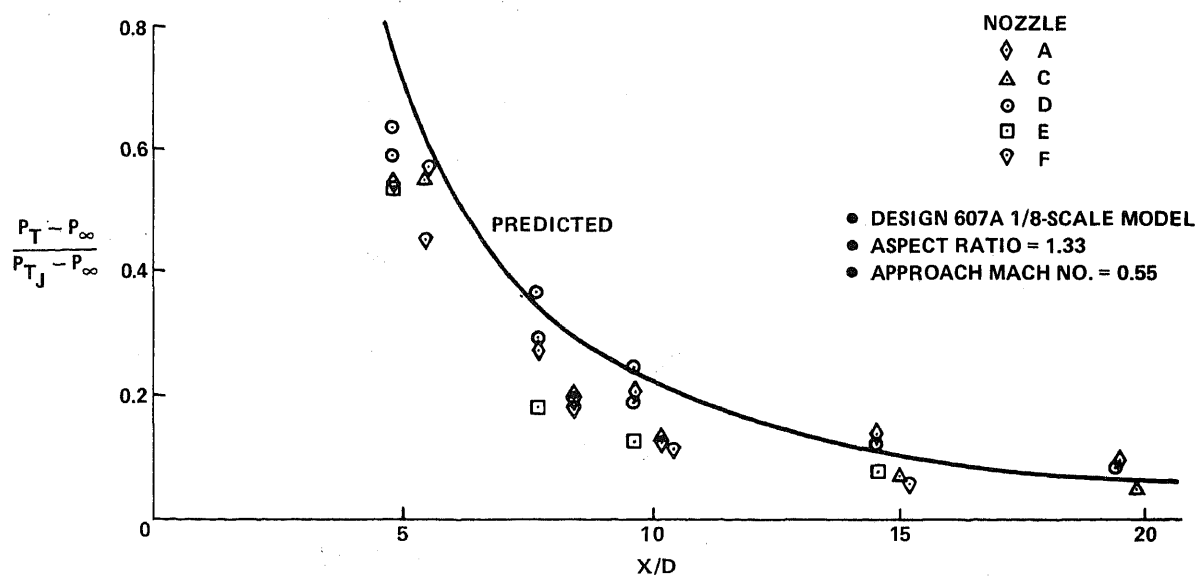


Fig. 8 Free-Jet Total Pressure Decay

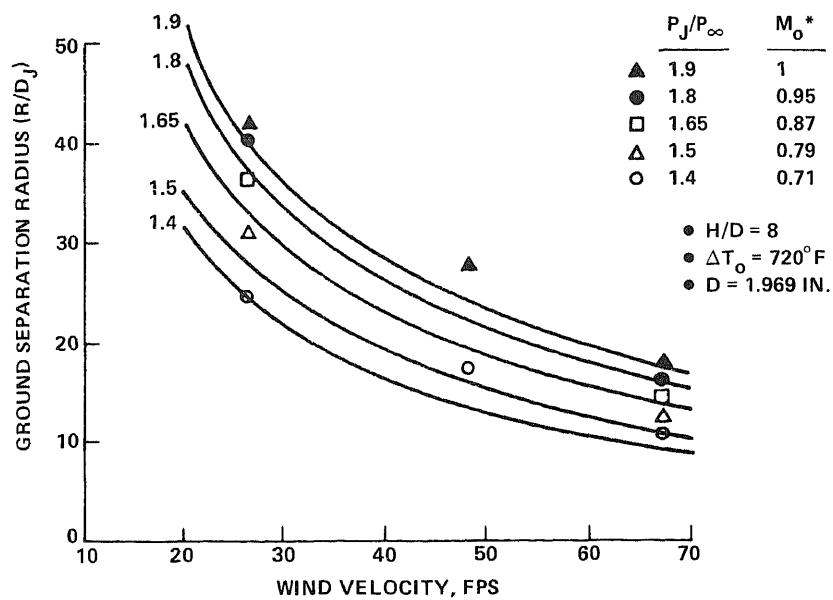


Fig. 9 Upwind Wall-Jet Separation Radius

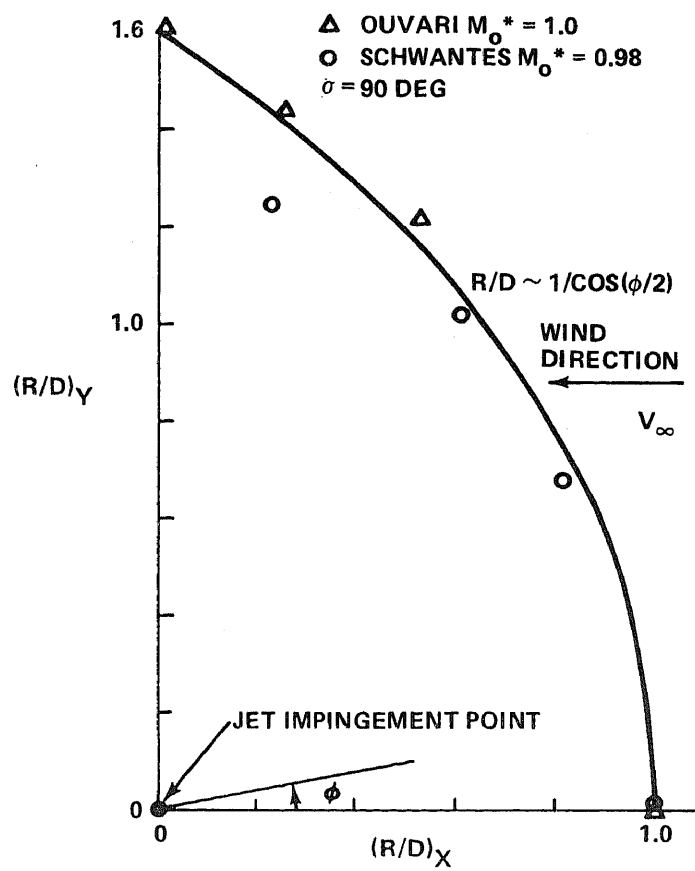


Fig. 10 Wall-Jet Separation Locus

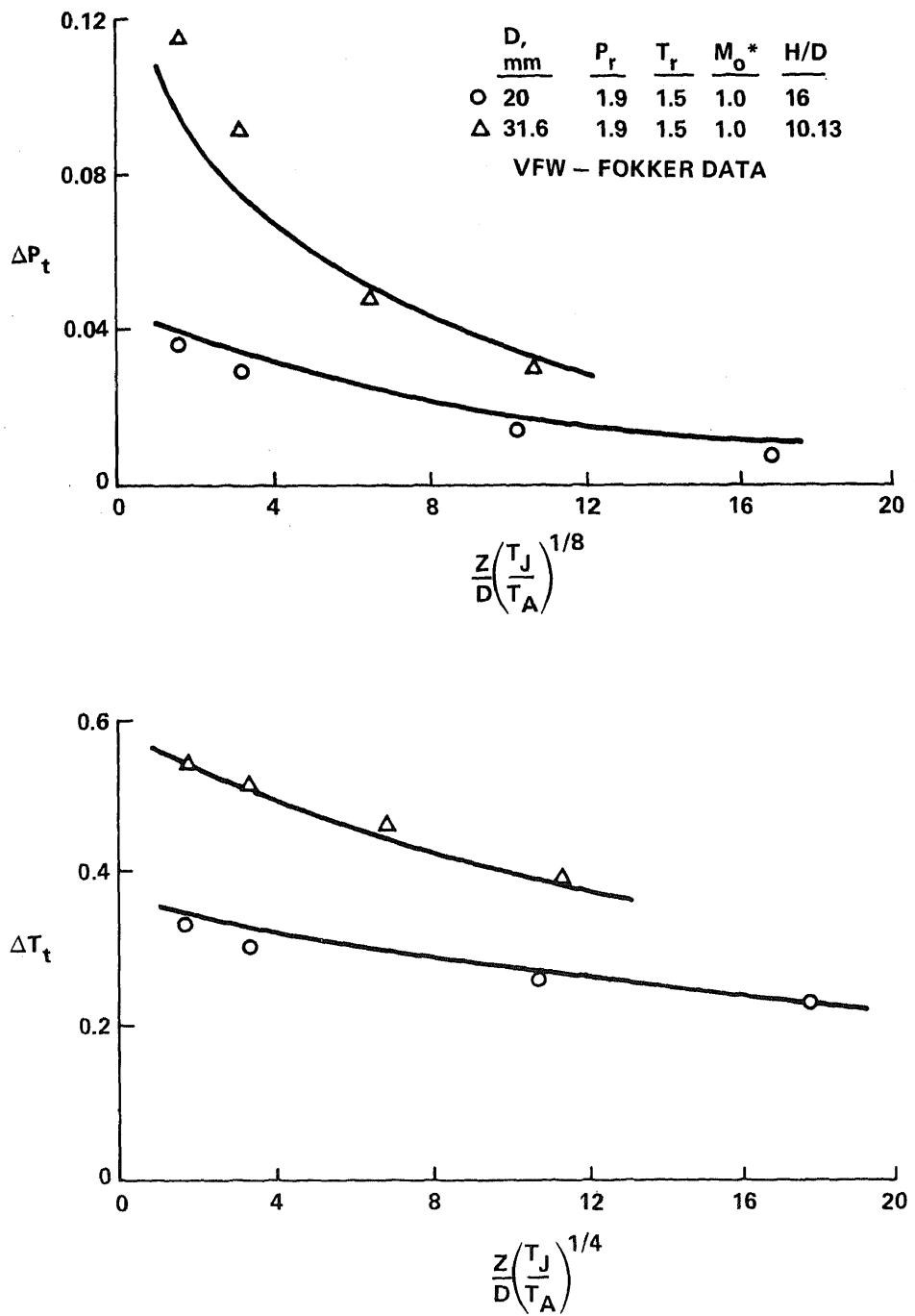


Fig. 11 Central Fountain, 4-Jet Group

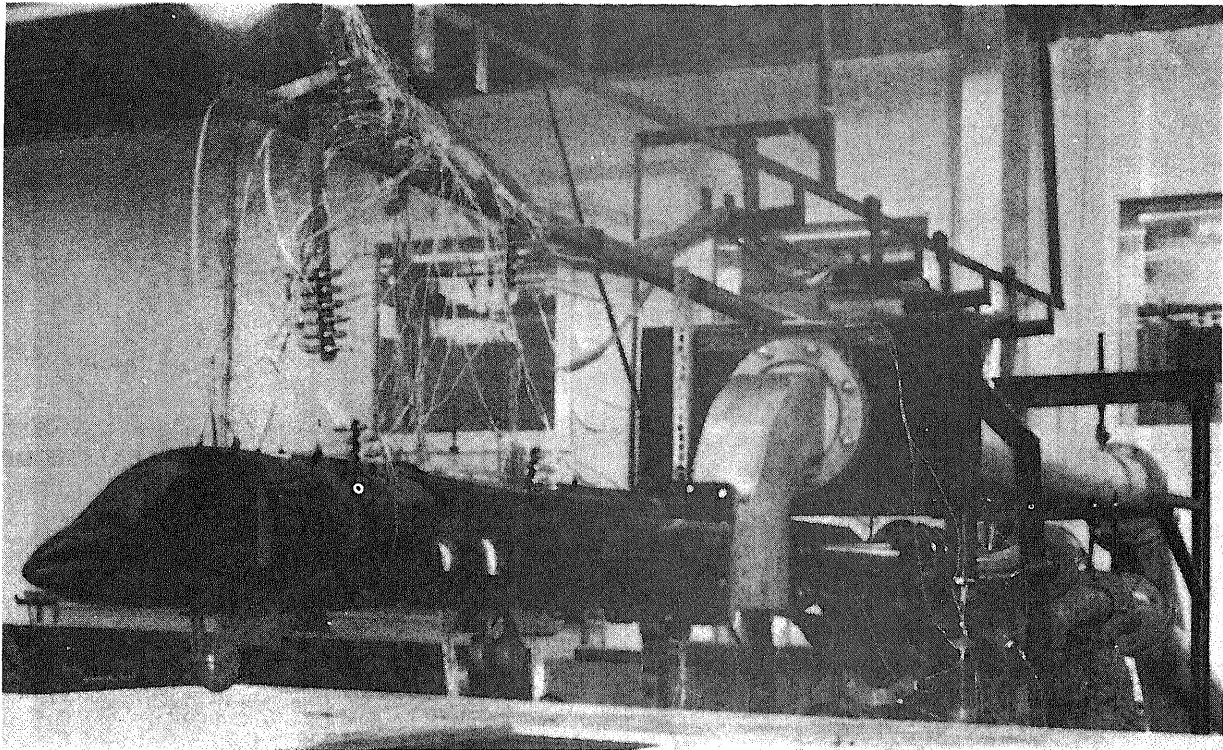


Fig. 12 VAK-191B Model Test

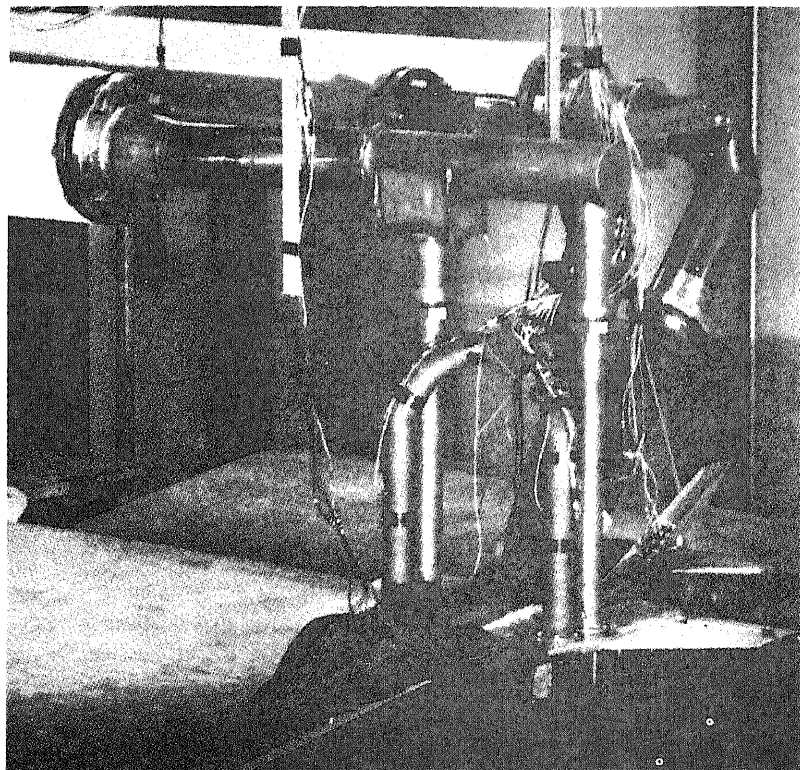


Fig. 13 Grumman Design 623 Hot-Gas Model

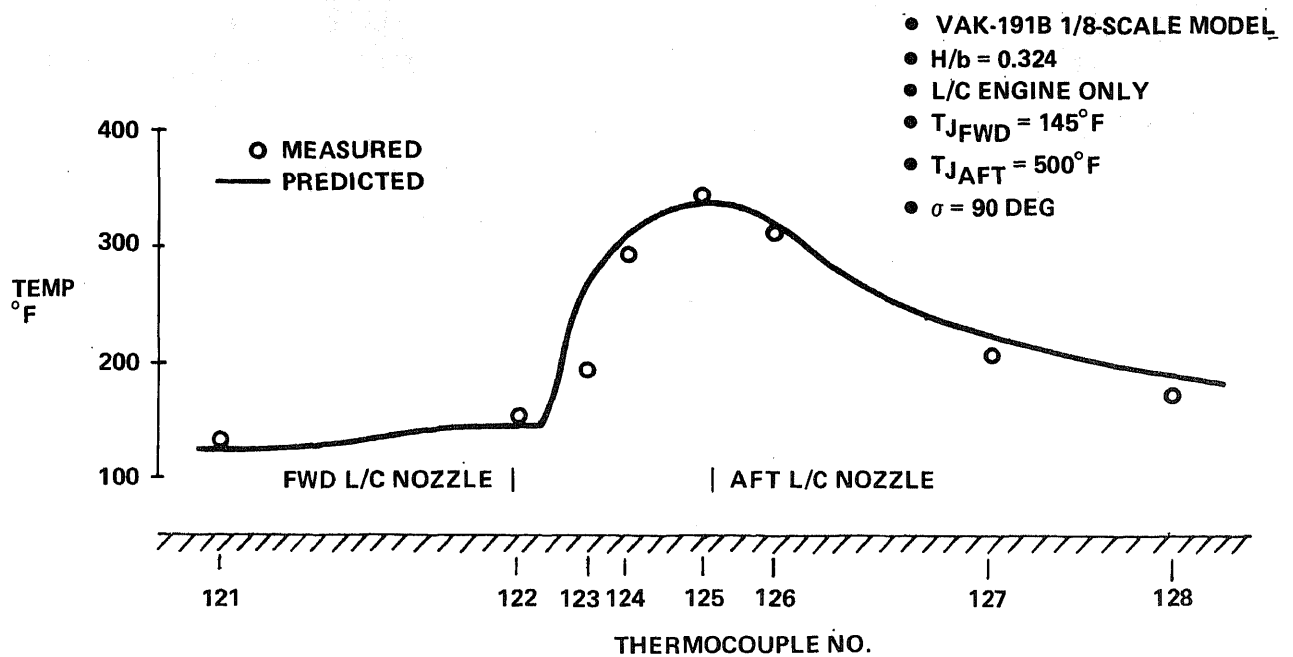
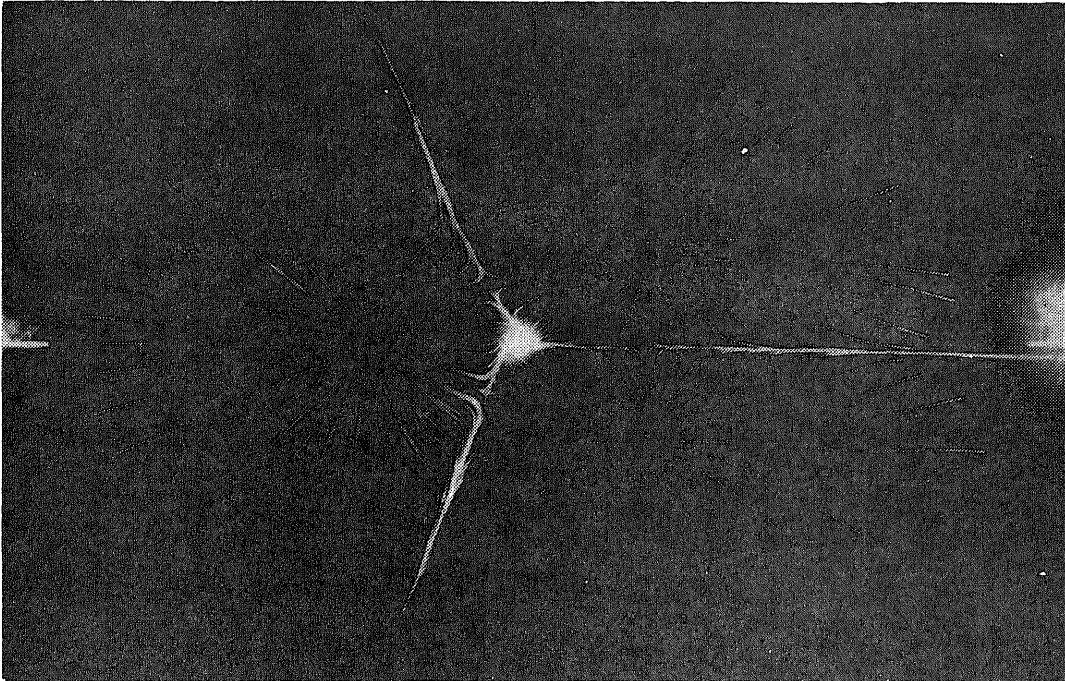


Fig. 14 Ground Plane Centerline Stagnation Temperatures

$\delta_{DLE}/\delta_{LCE} = 90/90 \text{ DEG}$



$\delta_{DLE}/\delta_{LCE} = 75/80 \text{ DEG}$

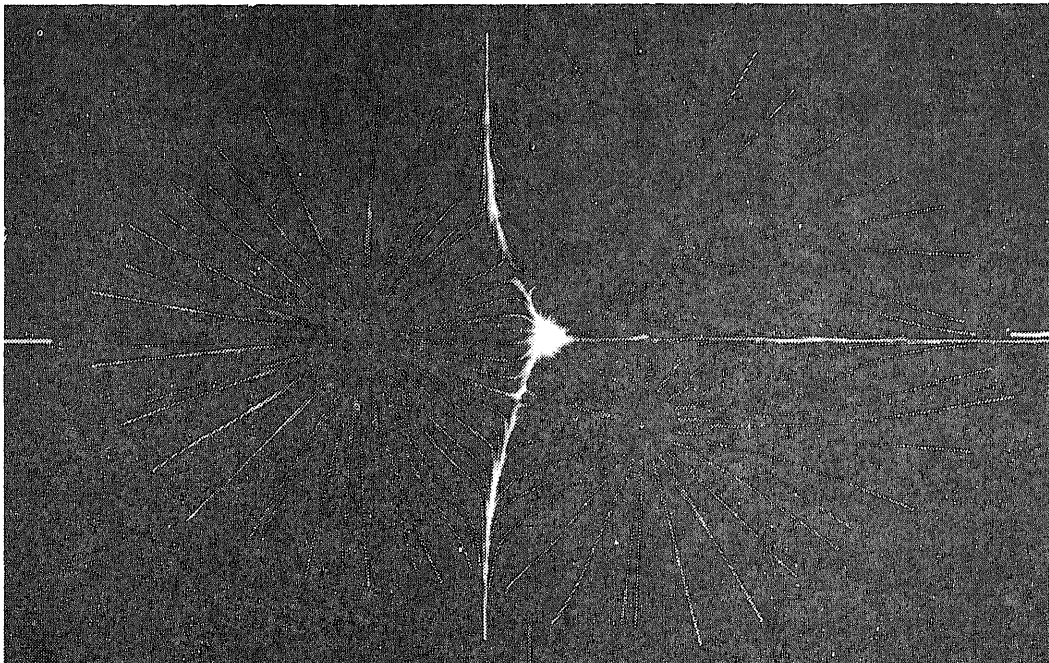
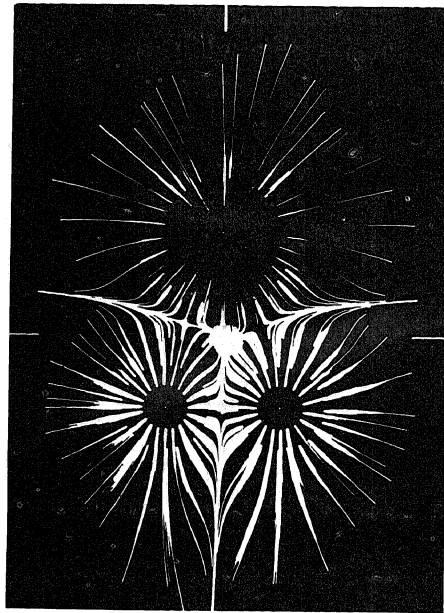


Fig. 15 Ground Footprints, Grumman Design 623 Tests



$$\begin{array}{c}
 +483 \\
 \swarrow \quad \searrow \\
 719 + (434) \quad 424 + 719 \\
 \downarrow \\
 () \text{ VFW, MEASURED TEMP, } \\
 \text{ } ^\circ\text{F}
 \end{array}$$

Fig. 16 Calculated Stagnation Locus & Temperature

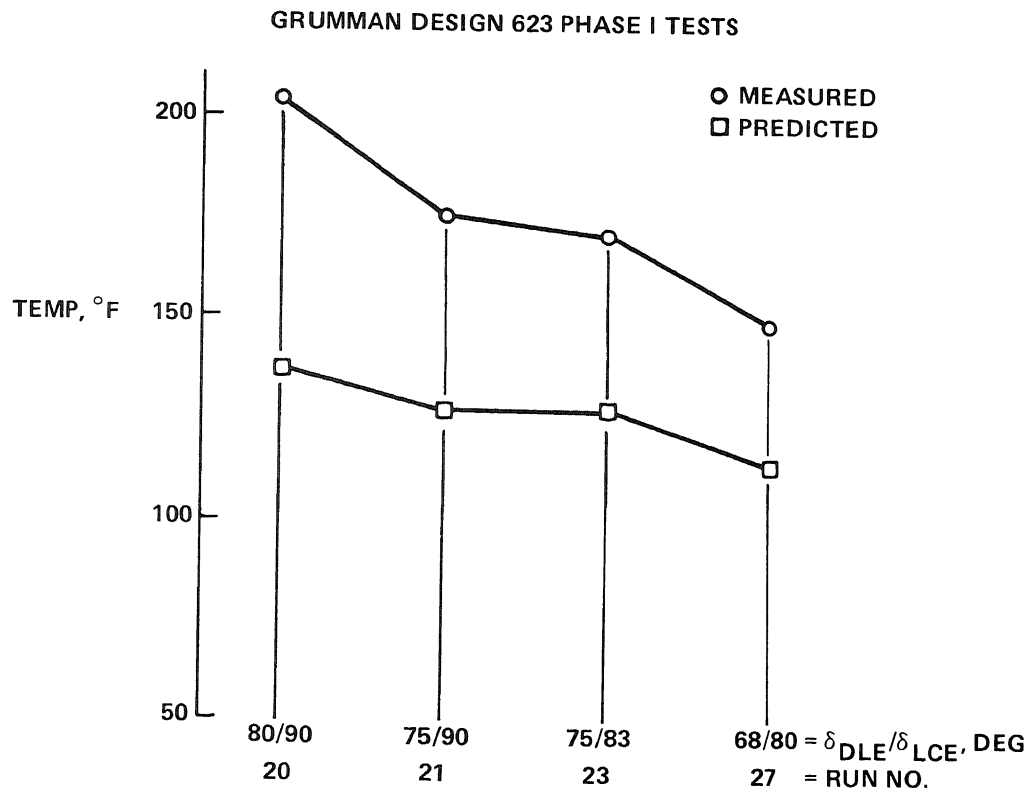


Fig. 17 Gas Temperature at Nose Gear

GRUMMAN DESIGN 623 PHASE I TESTS

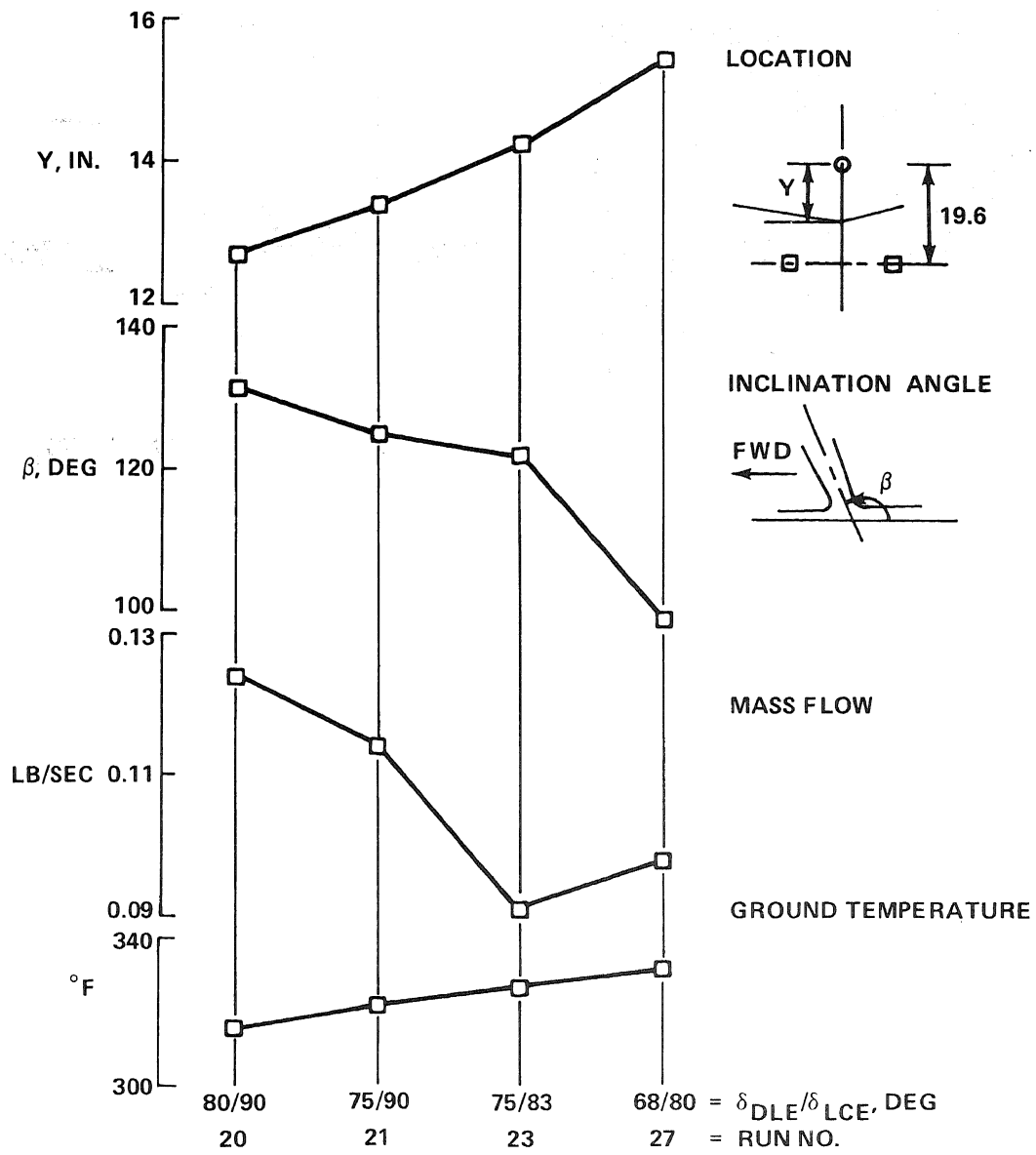


Fig. 18 Predicted Fountain Data

GRUMMAN DESIGN 623 PHASE I TESTS

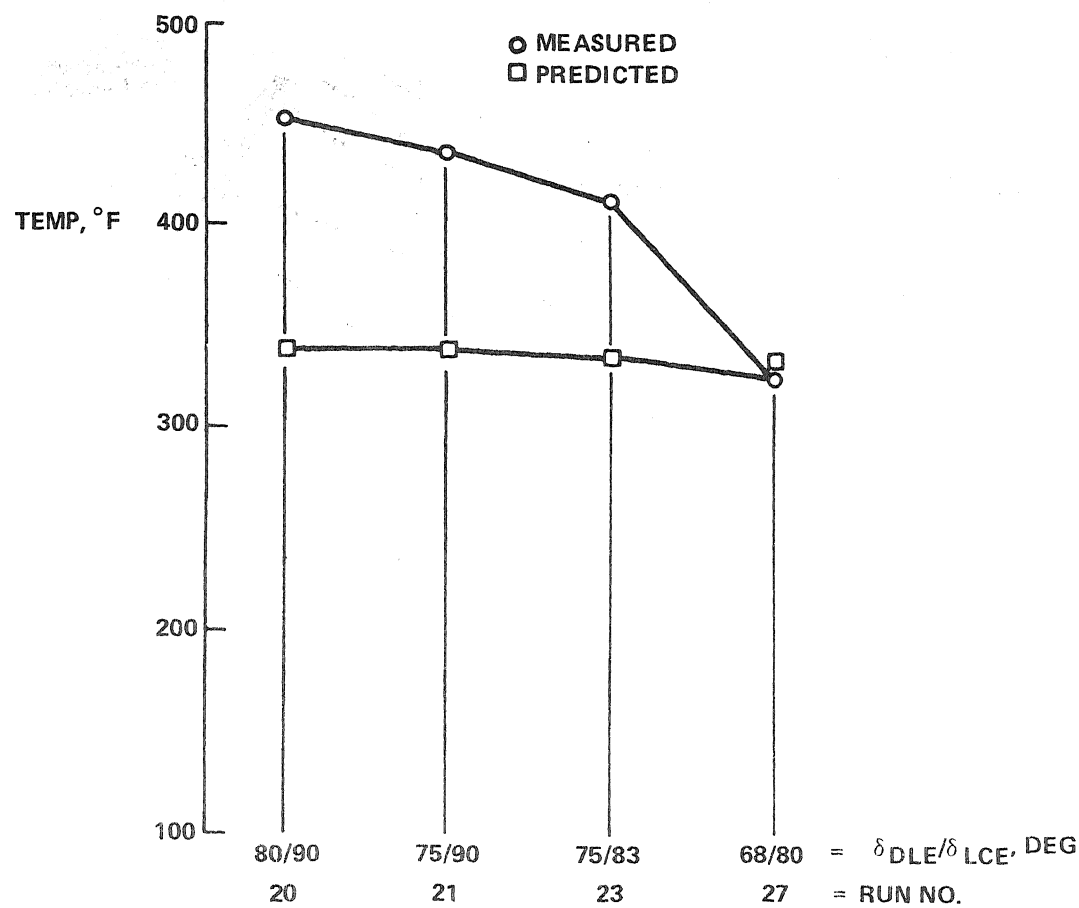


Fig. 19 Fuselage Maximum Gas Temperature

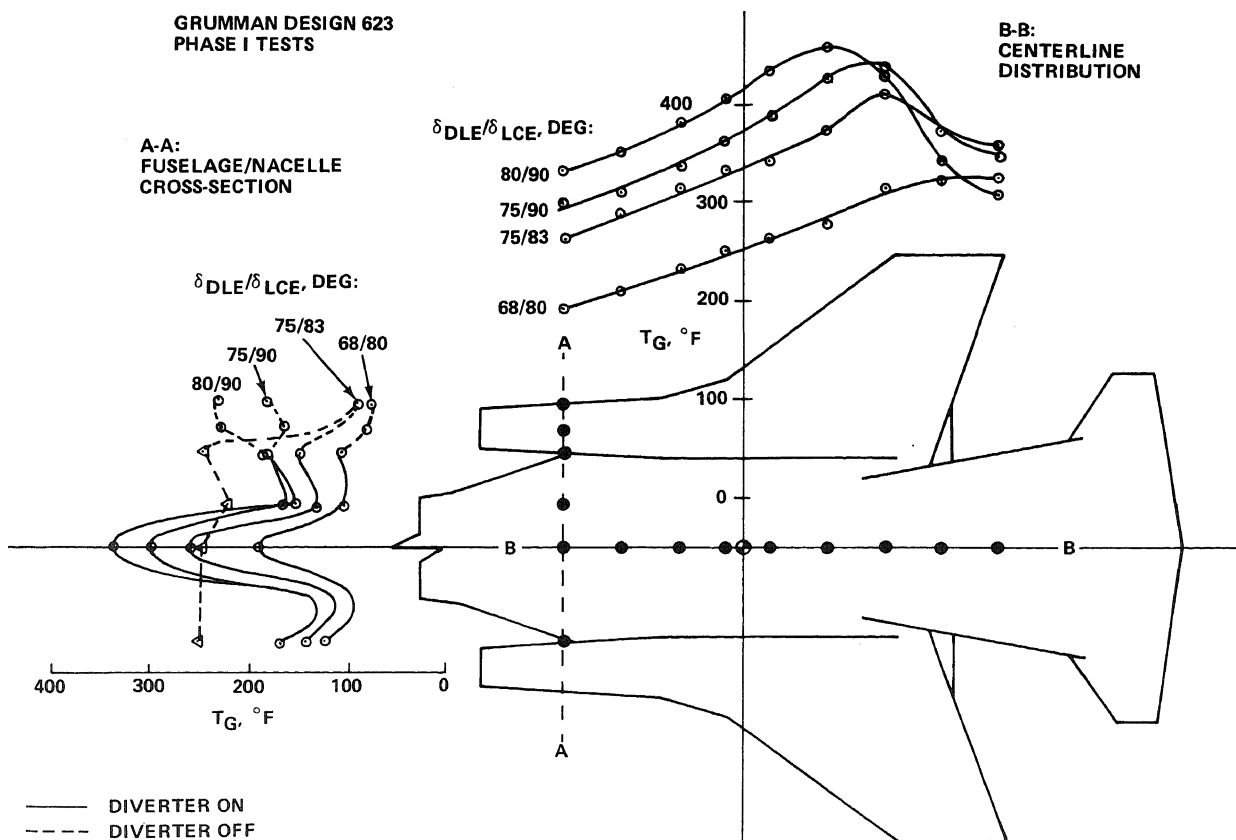


Fig. 20 Fuselage Gas Temperature vs Nozzle Deflection Angles

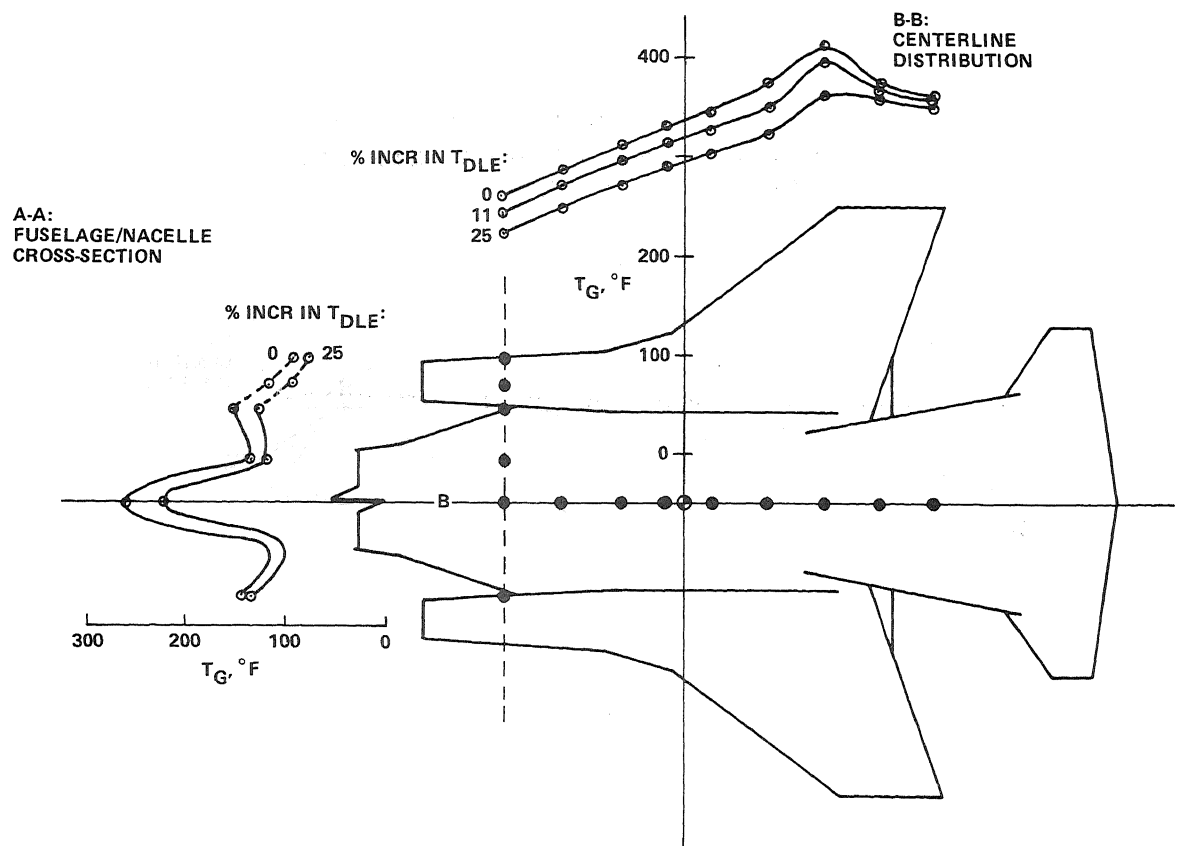


Fig. 21 Fuselage Gas Temperatures vs DLE Thrust Level

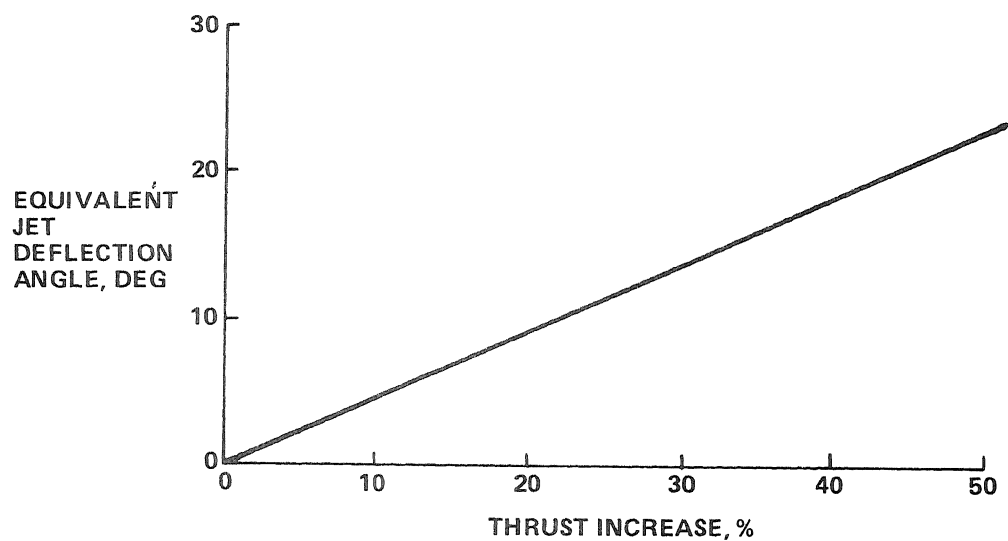


Fig. 22 Jet Deflection Equivalent of Increased Thrust

- GRUMMAN DESIGN 623 PHASE I TESTS
- MODEL REFERENCE = 655° F (0% CHANGE)
- DATA SCALED TO 3000° F

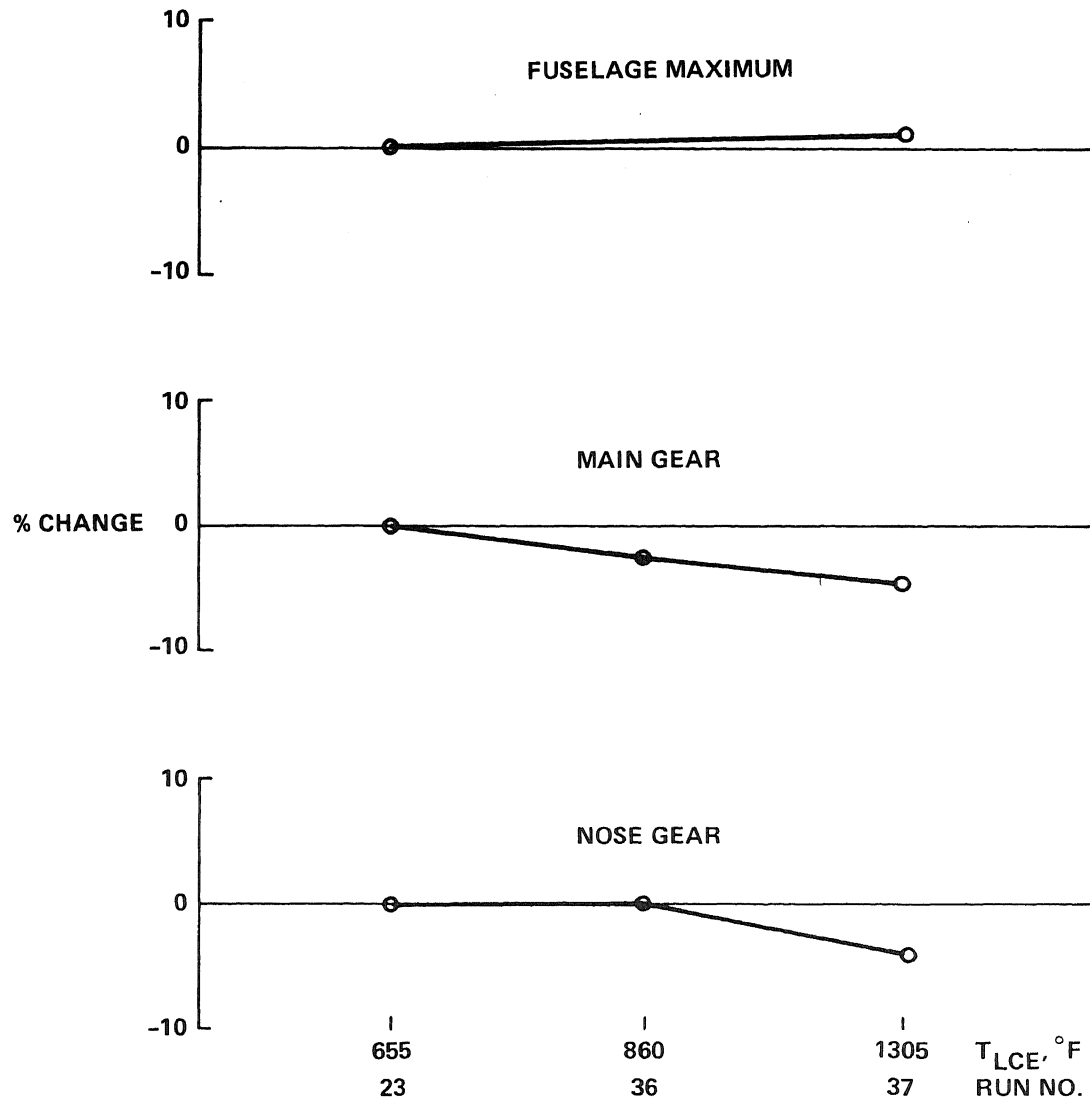


Fig. 23 Temperature Scaling Comparison

VTOL REINGESTION MODEL TESTING OF FOUNTAIN CONTROL AND WIND EFFECTS

**Henry A. Weber
A. Gay
General Dynamics Convair Division
San Diego, California**

ABSTRACT

VTOL aircraft operating in ground effect are subject to hot gas reingestion, which induces thrust loss and/or engine stall. Direct measurements of intake reingestion levels have been made over a wide range of operating conditions and wind environments, using a powered aircraft model to reproduce typical VTOL aircraft reingestion patterns. In addition, a test program of a more fundamental nature was initiated, with the objective of obtaining a better understanding of the flow field processes involved, by a detailed study using relatively simple impinging jet geometries. The ultimate goal of this research is the development of an analytical methodology applicable to general configuration evaluations using a semi-empirical approach.

NOMENCLATURE

D	Diameter inches
H	Height of aft lift nozzle exit plane above ground level, inches
H_c	Vertical height of recirculation cloud, inches
k	Ratio of inlet to nozzle flow rate
NPR	Nozzle pressure ratio
P	Pressure, psia
q	Total pressure above ambient ($P_T - P_\infty$)
R	Radius, inches
T	Temperature, F
V	Velocity, feet per second
X	Distance along model centerline, inches
Y	Distance lateral to model centerline, inches

Greek Letters

ΔT	Temperature rise, F
ϕ	Wind source direction, degrees
∞	Ambient condition

Subscripts

E	Nozzle exit
I	Inlet
M	Maximum value in ground jet profile
N	Nozzle
O	Capture stream tube
S	Point of ground jet separation
T	Total
WG	Wind generator

INTRODUCTION

VTOL aircraft operating in ground flow field effect are subject to hot gas reingestion that can cause thrust loss and/or compressor surge. This phenomenon has been demonstrated on full-scale aircraft and on models representing various aircraft configurations and propulsion system arrangements. Previous investigators have shown that the external flow field established in ground effect is configuration-dependent and has a strong influence upon reingestion characteristics. Thus far, attempts at analytical determination of the flow field have been unsuccessful and correlation of empirical data has been limited to specific configurations. The problem is amplified by the strong influence of many operating parameters: aircraft height and attitude, ground surface geometry, and ambient wind direction and velocity. Development of an analytical methodology is required to minimize the expense of model testing of candidate VTOL aircraft/propulsion system configurations. To achieve this methodology, a semi-empirical approach is planned, using data from a variety of models tested under a broad range of test conditions.

The General Dynamics Convair recirculation and impingement model and initial data obtained with the model were described in Reference 1. Since that report, a wind generator has been constructed to extend the test matrix to include wind speed and direction. A parallel program, of a more fundamental nature, has been initiated to investigate the general properties of flow fields created by relatively simple impinging jet geometries. Flow field pressure probes, temperature probes, and flow visualization devices are used to obtain flow field surveys. Some initial results from this program that relate to the understanding of the reingestion problem are included, together with the recent results from the recirculation and impingement model.

FLOW FIELD DESCRIPTION

Figure 1 is a schematic representation of the flow of a single jet impinging on the ground. The free jet and the radially spreading ground jet entrain ambient air at the free boundaries. The mixing of entrained air with the hot gas thickens the jet and a decay in peak temperature and velocity occurs with distance. It must be noted that the jet flows are highly turbulent in nature and all references made here to local values of pressure, velocity, and temperature will be to the time-averaged mean values.

Figure 2 shows schematically the flow field for a two-jet system. An interaction occurs in the opposing ground jets at the intersection of the x-y axes. The interaction flow is vertical between the nozzles but at some distance along the y axis the flow becomes virtually horizontal to form a "reinforced" ground jet. Confining attention to the region close to the x-y intersection, where the interaction flow has a strong vertical component, it can be noted that this upwash "fountain" acts like another free jet as it entrains surrounding fluid, thickens, and experiences a decay of peak total pressure (and peak velocity) and temperature. Other multijet systems will form similar interaction regions.

Hot gas ingestion problems are generally considered to arise from near-field and far-field flow recirculation. The near-field problem is caused by interactions such as shown in Figure 2. Some of the hot fountain gases may reach the intake region after impinging on the aircraft undersurfaces and spreading (in a ground jet fashion) over the surfaces. Certain configurations are more prone to near-field ingestion than others. For example, top-mounted inlets protected from the upwash by large surfaces are generally more free from the problem than side intakes.

Hot gas ingestion caused by near-field flows can be affected by ambient winds, since the velocity of the upwash flow may be considerably decayed from the nozzle exit velocity. In addition, changes in aircraft attitude relative to the ground may alter the direction of the upwash. Near-field ingestion problems must be eliminated or controlled by general design considerations of inlet-nozzle-vehicle geometry. In addition, it is possible to control or modify the near-field flows in certain cases by the use of deflecting surfaces on the vehicle.

Far-field ingestion represents a different problem than can be explained by the single-jet example of Figure 1. The ground jet flowing radially outward from impingement experiences a decay in velocity and temperature as ambient air is entrained and the jet thickens. In the absence of winds, a heated jet will eventually separate from the ground since the decay characteristics are such that buoyancy forces will eventually overcome the radial momentum, and the separated gases may drift toward the intake due to the induced flow field (caused mainly by the ink action of the entraining jets and, to a lesser extent, the inlet sink). The temperature of the recirculated gases in this case will be considerably lower than for typical near-field ingestion. Moreover, the time taken from start-up to establish far field recirculation of this type will be several orders of magnitude greater than the near-field recirculation ingestion; thus, far-field ingestion at zero or low headwind velocity may be overcome by vehicle operational procedures.

The effect of winds on far field recirculation is considerable. The ground jet separates closer to the impingement region as wind velocity is increased, and separates at higher temperatures, since

decay of velocity and temperature in the ground jet is minimally affected by winds up to near the separation region. The recirculation gas cloud formed has a complex geometry, as it is subjected to wind forces and the sink action of the ground jet flows. Some properties of the recirculation flows are obtained in the next section.

BASIC FIELD TESTING

Extensive data on turbulent jets and analytical results is presently available in the literature for the free jet and wall jet regions, mainly for subsonic jets and cold flow. To extend this data to nozzle exit conditions more representative of V/STOL nozzles, and since only limited data is available in other important regions, a test program was conducted in the present research to investigate the general flow fields created by relatively simple geometries. These comprised mainly single jet impingement, although some double-jet cases have also been studied. The major equipment for the test was existing hardware and models, but additional instrumentation was developed, comprising mainly sensitive field probes to include total pressure and temperature measurements. Approximately 60 to 80 point locations were monitored in most tests to specify characteristics of the flow field. Some tests were conducted in a controlled wind environment using the wind generator. Most of these experiments were conducted using 30-degree conical nozzles with exit diameters of 1.41 inches. In addition to extensive probing of the flow fields, smoke flow visualization tests were undertaken and movie records obtained to investigate certain aspects of the recirculation gas flow in the presence of headwinds. Results of these tests relating to the reingestion problem are summarized below.

Figures 3 and 4 show the decay in peak property values of pressure and temperature in the ground jets created by single vertical jets. The ranges of conditions covered are indicated in the figures. Each point indicates a mean value from 24 experiments for the peak pressure decay curves and 12 experiments for the temperature curves. The data bands shown indicate the spread over all experiments. The curve of Figure 3 was derived analytically from profile shape and jet spread measurement and is represented by

$$[q_M/q_N]^{1/2} = 1.55 (R/D_N)^{-1.13}$$

The curve of Figure 4 was derived from the limiting case of zero heat transfer to the ground plane, low exit velocity, and small nozzle total temperature increase above ambient and is represented by

$$\Delta T_M/\Delta T_N = 1.124 (R/D_N)^{-0.87}$$

Figure 5 shows two "stills" from the smoke visualization movies to illustrate flow field recirculation due to headwinds. The figure shows the ground jet separating or "peeling" when the decay of dynamic pressure in the ground jet is sufficient so that the ground jet radial momentum is overcome by the wind. Figure 5A was taken with vertical impingement, nozzle pressure ratio of 2.0, and wind velocity of 50 fps. Figure 5B represents an inclined jet case at a nozzle pressure ratio of 2.0 and a wind velocity of 20 fps. Inclining the jet results in a weak forward jet wash, which is relatively easily overcome by the wind forces. Figures 6 and 7 show the results of measurements of the important geometric parameters, separation distance R_S , and cloud height H_C . Figure 6 shows that the separation distance is represented by,

$$R_S/D_N = 0.61 (q_N/q_\infty)^{1/2}$$

The mean separation distance R_S was fairly well defined for a given set of conditions, but the upper boundary of the cloud was generally not well defined. This was due to the diffuse nature of the smoke away from the separation region in addition to the high turbulence levels. Thus, a wide band is shown in Figure 7 within which the cloud upper boundary was contained when projecting the film records at high speed.

AIRCRAFT MODEL TESTING

A 1/10-scale powered model of a typical lift-plus-lift-cruise VTOL fighter-attack aircraft (Figure 8) was constructed to obtain empirical data on the flow field parameters influencing reingestion. The model simulates an airplane having a delta wing-canard planform with two lift engines located in the forward section of the fuselage and a deflected cruise engine nozzle aft. To obtain maximum simulation capability, the model is designed to duplicate engine exhaust jet pressure conditions (nozzle pressure ratio of approximately 2.8) with scaled inlet and exhaust flow rates. Jet temperature levels are in the order of 1,000F in the cruise jet and 1,900F in the lift jets.

The flow field generated by this lift-plus-lift-cruise model configuration is a composite of the ground jet interactions previously described for basic flow fields (Figures 9 and 10). In this case, an aft fountain is formed between the cruise and the aft lift jet. Another fountain may be formed between the lift jets, depending upon nozzle/ground geometric and flow parameters. The external flow field influencing inlet reingestion is thus characterized by: (1) three-dimensional ground jets (simple and reinforced), (2) fountain flows, (3) ambient air induced into the flow streams by entrainment, (4) interactions among all above elements, and (5) wind effects.

The model built in 1974 (Figure 8) is a refurbished version of the 1972 model, reported in Reference 1. Results obtained with the 1972 model clearly indicated that a fountain formed between the lift jets caused high reingestion temperatures. Temperature level was minimized by converging the flow direction of the lift jets. In the 1974 model, the lift jet spacing was reduced from 1.9 to 1.55 nozzle diameters to reduce fountain strength (Figure 11). The lift jets were shifted forward and canard position lowered to reflect full-scale aircraft design modifications.

The recirculation and impingement test facility¹ is used for testing the model over a ground plane with adjustable height and attitude. An ejector-driven wind generator, used to simulate ambient wind velocity, develops a 60-knot wind over an eight- by eight-foot area with consistent flow uniformity.

The model is tested over a matrix of specific test parameters within the following ranges:

Model height above ground:	3.1 to 10.5 lift nozzle diameters
Model pitch:	±5 degrees
Model roll:	±5 degrees
Wind speed:	0 to 60 knots
Wind direction:	90 degree to head-on

Conventional wind tunnel instrumentation is used to record the test conditions as listed above. Flow field instrumentation includes high-response thermocouples at the engine inlets and at other selected locations in the external flow field. The external thermocouples are of the aspirated type to minimize radiation error. Electrical outputs of the individual thermocouples are traced on dynamic recorders so that a temperature-time history of the flow field is generated.

During initial testing of the basic configuration (Figure 8), cruise inlet temperatures in the order of 100F were recorded at the lowest model height tested (landing gear almost touching the ground plane). A comparison of the 1972 and 1974 model results (Figure 12) was disappointing since the reduced lift jet spacing had been expected to reduce fountain strength and, hence,

reingestion temperatures. Probing the external flow field with aspirated thermocouples revealed that, in fact, the forward fountain had been eliminated and that the current source of reingestion was the aft gases flowing forward under the fuselage. It is theorized that shifting the lift jets forward (Figure 11) reduced the entrainment strength of the lift jets in the critical area between wing and canard, thus allowing the aft fountain gases to flow forward into the cruise inlets.

This hypothesis was confirmed in a series of tests that involved varying the canard setting angle and installing various types of deflectors under the fuselage (Figure 13). The deflectors were designed to divert the aft fountain gases laterally and away from the inlets. By rotating the canard so that the forward portion was brought closer to the lift jets, a local flow field was established that entrained the diverted aft fountain gases. The resulting effect on inlet temperature levels (Figure 14) indicates that both canard rotation and gas deflection are required to achieve manageable reingestion temperatures. The 25-degree value of canard rotation is the optimum setting achieved after evaluating settings from 0 to 45 degrees.

The revised model (Figure 13) was then tested at various model heights, wind speeds, and directions using the wind generator. The resulting wind envelope (Figure 15) shows the relationship of inlet temperature rise for each inlet as a function of the major test variables. Most of the curves follow the expected trend – an initially low value of reingestion at zero wind speed is increased at intermediate wind speeds as the wind forces ground jet separation and carries hot gases back to the engine inlets. In most cases, wind speeds greater than 50 knots swept the hot gases under the model, diverting them from the inlet flow field. All four inlets demonstrate similar patterns and essentially the same temperature levels. This characteristic indicates that the gases returned by the wind are well mixed in a large enveloping cloud.

The effect of pitch and roll on reingestion temperature level was minimal (Figure 16) for the revised configuration whereas previously reported characteristics¹ for the 1972 model showed large increases in temperature – particularly for +5-degree model pitch. The implication is that the flow field control established by this configuration overpowers distortions caused by model attitude changes within the test range.

Inlet flow of the basic configuration was varied from 0% to 100% of design flow to determine whether reingestion temperature levels were influenced by the inlet flow field strength (Figure 17). Aspirated thermocouples were used to minimize thermocouple radiation error at the zero-flow condition. Results indicated a relatively flat characteristic down to 40% of design flow with fair correlation between throat and aspirated thermocouples. The zero-flow readings, however, were considerably lower, indicating that test results from models without inlet flow fields should be viewed with caution.

Lift jet temperature was varied from 500 to 1,200F and the resulting reingestion temperature level measured for both the basic configuration (Figure 8) and the revised configuration (Figure 13). The temperature lines are linear within the range investigated for lift and cruise inlets, as shown in Figure 18. The level and slope of each line is different, suggesting that the extrapolation of test results from low jet temperature models is an uncertain procedure.

ANALYSIS OF WIND EFFECT

An order-of-magnitude analysis based on the above results was made for the headwind conditions of the reingestion tests. Only the forward-facing side intakes were considered.

The far-field recirculation source is the forward lift jets. The side intakes obtain air from an equivalent stream tube of diameter D_o . It is assumed that $D_o \ll R_s$ and that the flow field is nearly two-dimensional close to the longitudinal axis head of the intakes. If the excess heat above ambient in the nozzle gases is conserved in the flow field, the recirculatory gases provide a mean excess temperature above ambient (ΔT_I) of order

$$\frac{\Delta T_I}{\Delta T_N} \approx \frac{1}{k} \frac{D_O}{2\pi R_S}$$

where k is the ratio of intake flow rate to nozzle flow rate.

The variable D_O is related to the nozzle reference diameter, D_N , for small intake temperature rise by

$$D_O/D_N = \left[k \frac{V_E/V_\infty}{T_E/T_\infty} \frac{p_E}{p_\infty} \right]^{1/2}$$

where the nozzle reference diameter and exit conditions are taken for an equivalent conical nozzle to apply the previous results for the recirculation flow fields.

Since there are two in-line lift jets, the question arises to the strength of the forward ground jet propagation. It was found during the basic flow field tests that for such closely spaced jets, the ground jet pressure decay is close to that for the forward jet impinging independently for low H/D ; i.e., as in Figure 3. For high H/D , the pressure decays less rapidly, tending to the characteristics of an equivalent nozzle diameter passing the combined mass flow. Thus, for this analysis, it is assumed that for the lowest H/D the hot gas source flow corresponded to a single lift-jet nozzle mass flow and for the highest H/D to both lift nozzles.

By applying the conditions of the present reingestion tests in headwinds, with the value of R_S obtained from Figure 6, the curve of ΔT_I versus wind velocity is obtained as shown in Figure 19. For operation at sufficiently high wind velocity, the curves of Figure 7 indicate that the recirculation gas cloud will pass below the intake capture tube. Thus, by taking the applicable ratio at the intake region of H_C/R_S from Figure 7 as approximately 0.3, this effect was included in Figure 19 by taking a linear fall in ΔT_I as the cloud decreased in height from above to below the capture tube. The comparison with test data indicates that the order of magnitude estimates and trends agree to some extent with the test data shown. Intermediate values of H/D obtained during the tests indicated more scatter, however – particularly at $H/D = 4.9$, where values of ΔT_I around 45F were measured at 10 and 20 knots before a fall-off to zero occurred at 40 knots. It is considered that a residual near-field reingestion problem persisted in the model configuration which possibly was amplified at $H/D = 4.9$.

It is of interest to note that the intake temperature rise was considerably less than that obtained from the peak gas temperature values from Figure 4 at the separation radius.

The cloud geometry data here shows comparable results to that of Abbott,² using a different experimental technique, although in the present tests the wall jet penetrated somewhat further against the wind before separation occurred. Abbott obtained a recirculation cloud height of about $\frac{1}{2} R_S$, which is similar to the maximum value indicated in Figure 7. Further tests were performed by Abbott,² using a twin-jet configuration with an opposing wind along the reinforced ground jet axis. This produced a recirculation cloud of about twice the height obtained with a single jet. This result seems to be confirmed from the intake temperature rise measurements obtained in the present tests, where a wind blown at 90 degrees to the model longitudinal axis created an approximately constant intake temperature rise over the wide range of model H/D at each wind speed.

CONCLUSIONS

1. Fountain deflectors and canard rotation provide a powerful means of redirecting fountain gases and reducing inlet reingestion.
2. A wind envelope has been generated. The results reflect a strong dependence of inlet temperature upon wind speed and direction. For this lift-plus-lift-cruise aircraft configuration, quartering and beam-on wind effects were more severe than head-on. Both wind speed and direction effects were nonlinear functions of model height.
3. Pitch and roll effects were minimal for the revised configuration within the 5-degree tilt angle range evaluated.
4. Inlet flow systems are required on reingestion models to obtain representative test data. The results generated in this test indicate that a 60% reduction in design flow provides consistent values of inlet reingestion temperatures.
5. The effect of jet temperature on inlet temperature was linear within the range tested. The slope of this relationship is a function of reingestion level and/or model configuration.
6. This test series has demonstrated the capability of the recirculation and impingement model test facility to provide a broad matrix of inlet reingestion data. The information obtained is establishing an empirical base from which more detailed analytical modeling of the external flow should be undertaken.

REFERENCES

1. Weber, H.A., "VTOL Recirculation and Impingement Model Testing," AIAA Paper 73-1183, November 1973.
2. Abbott, W.A., "Studies of Flow Fields Created by Vertical and Inclined Jets when Stationary or Moving Over a Horizontal Surface," Ministry of Aviation, A.R.C. C.P. No. 911, October 1964.

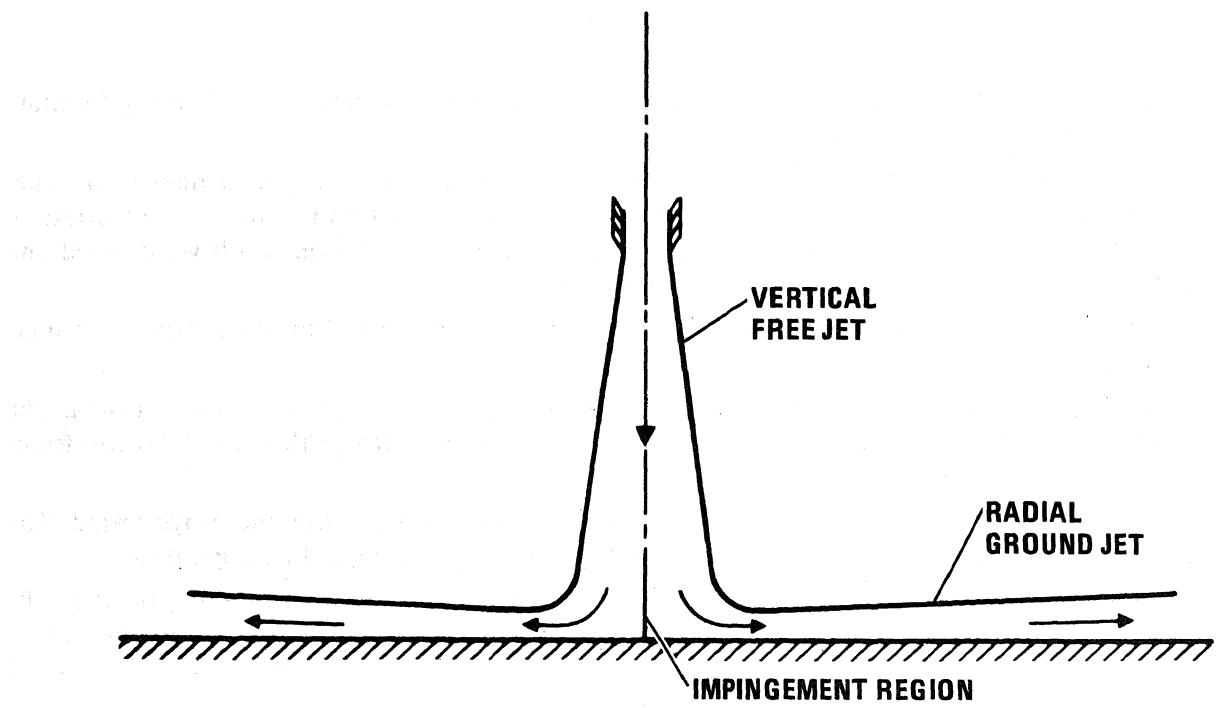


Figure 1. Single jet impingement.

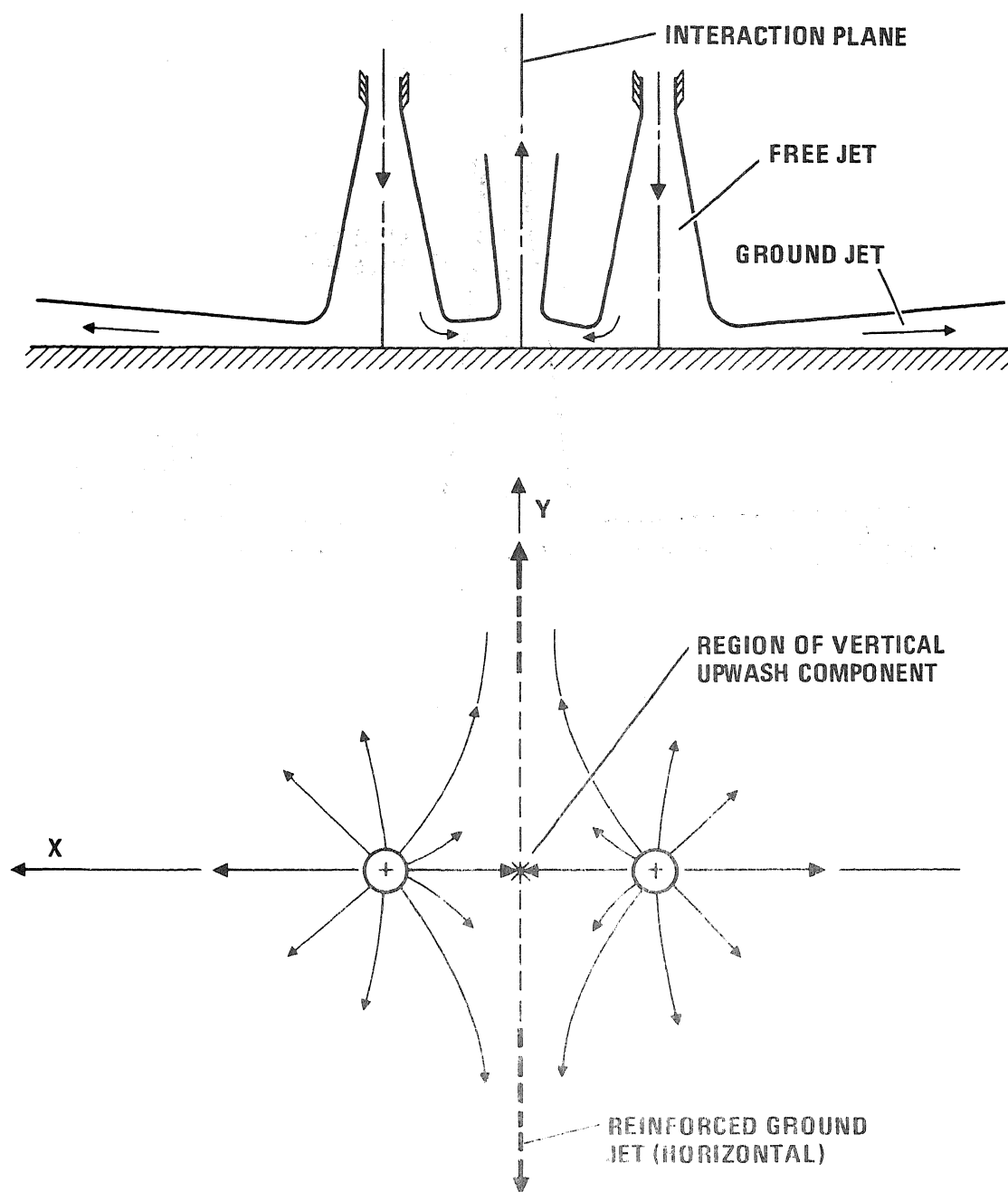


Figure 2. Double jet impingement

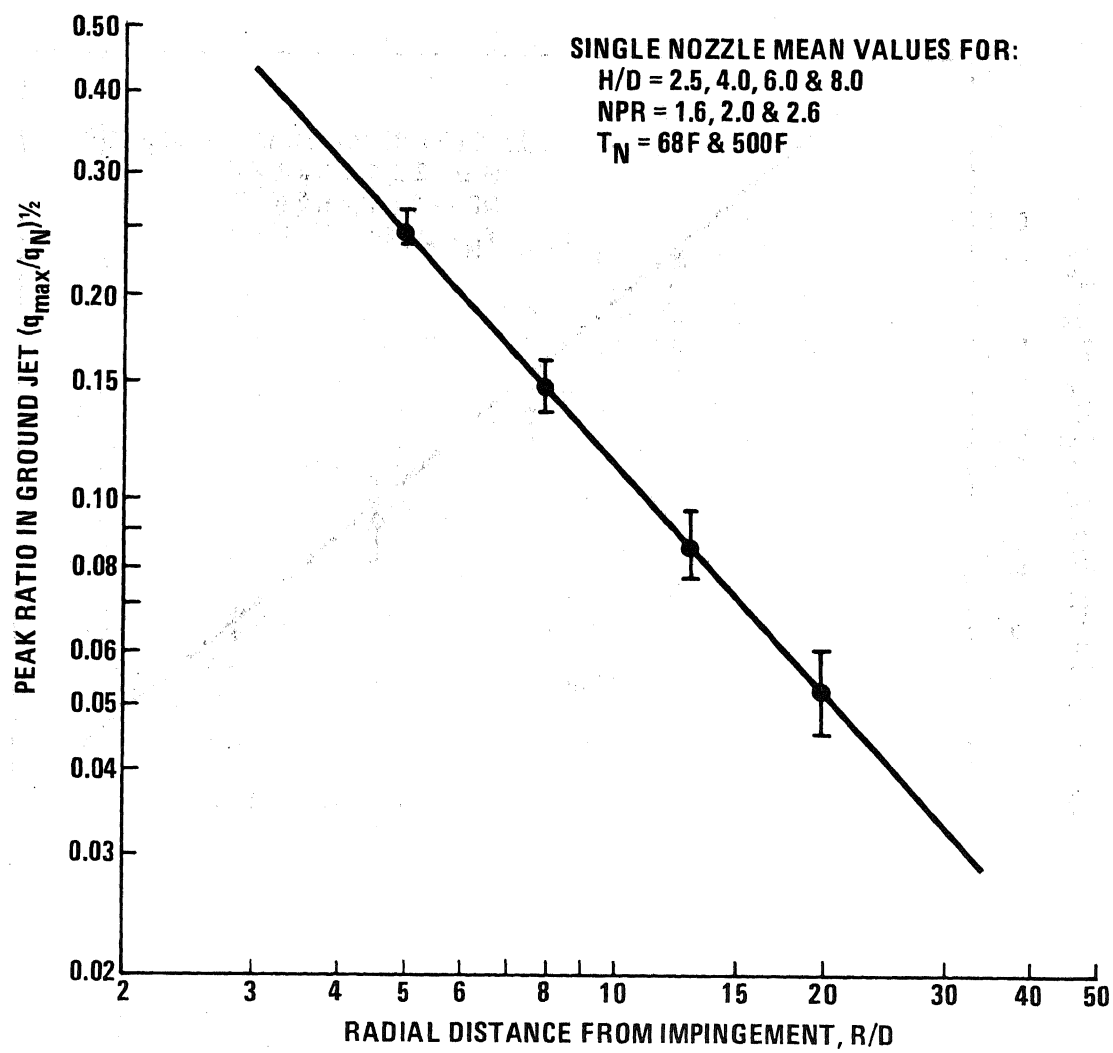


Figure 3. Ground jet peak total pressure decay.

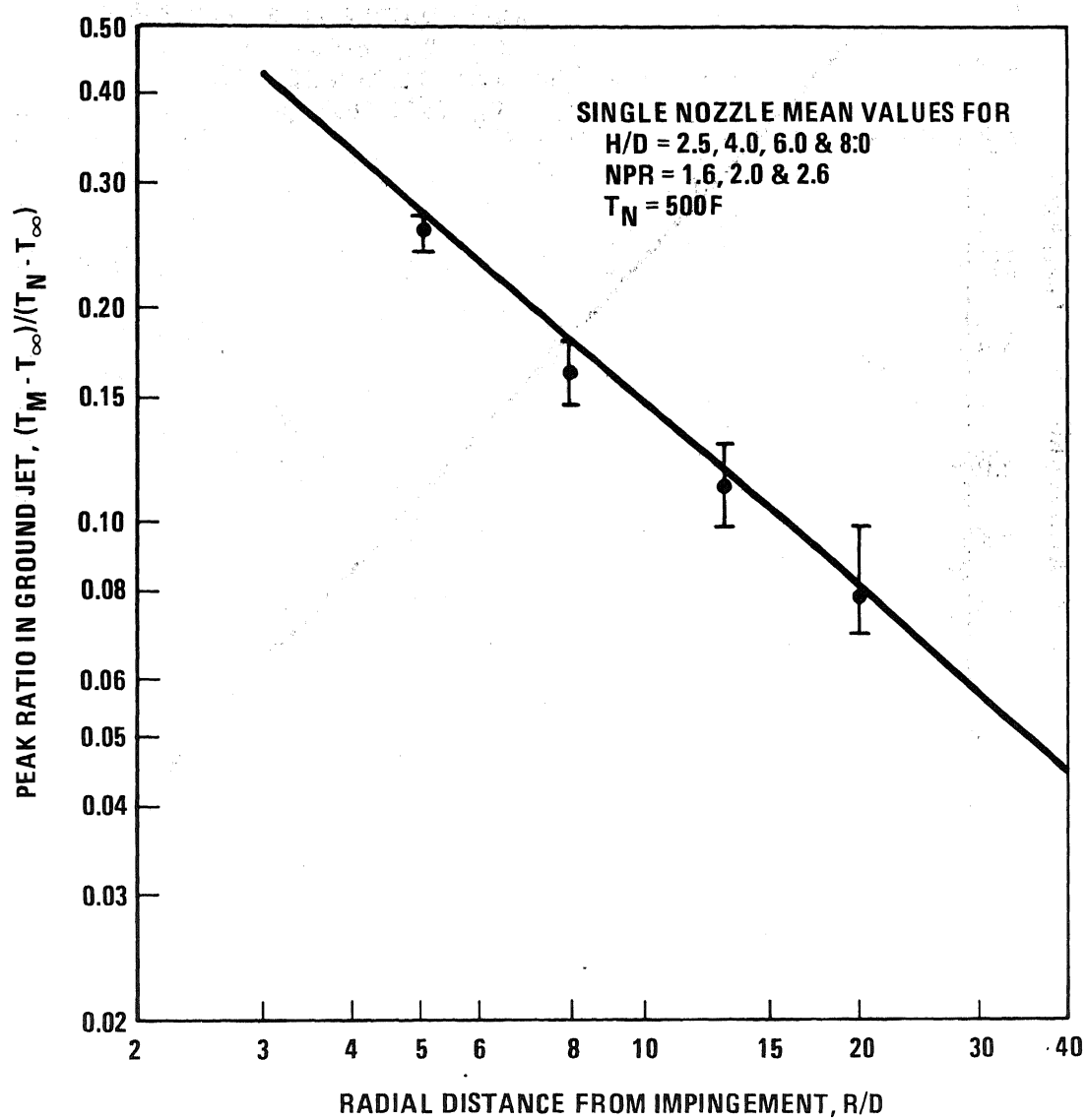
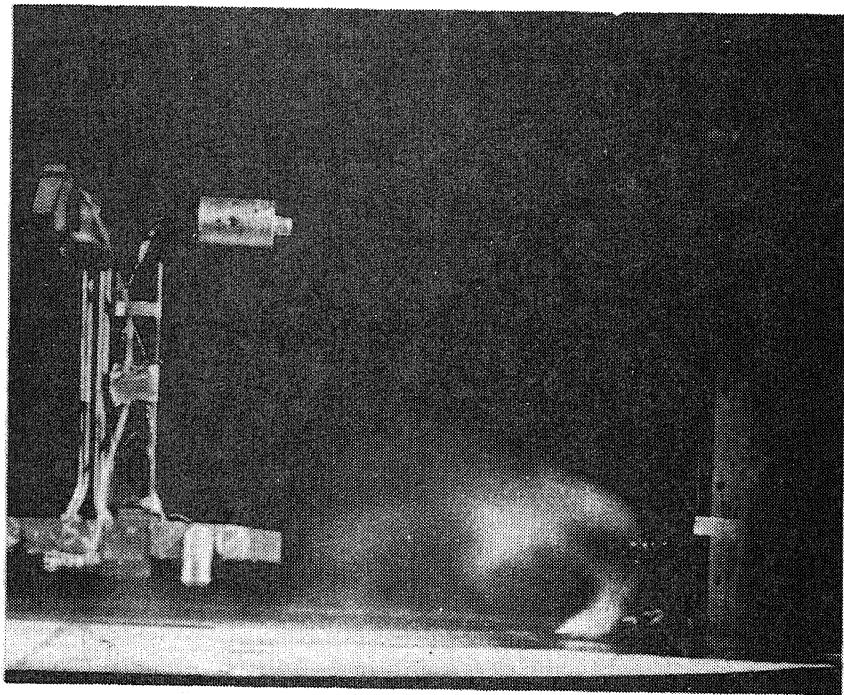
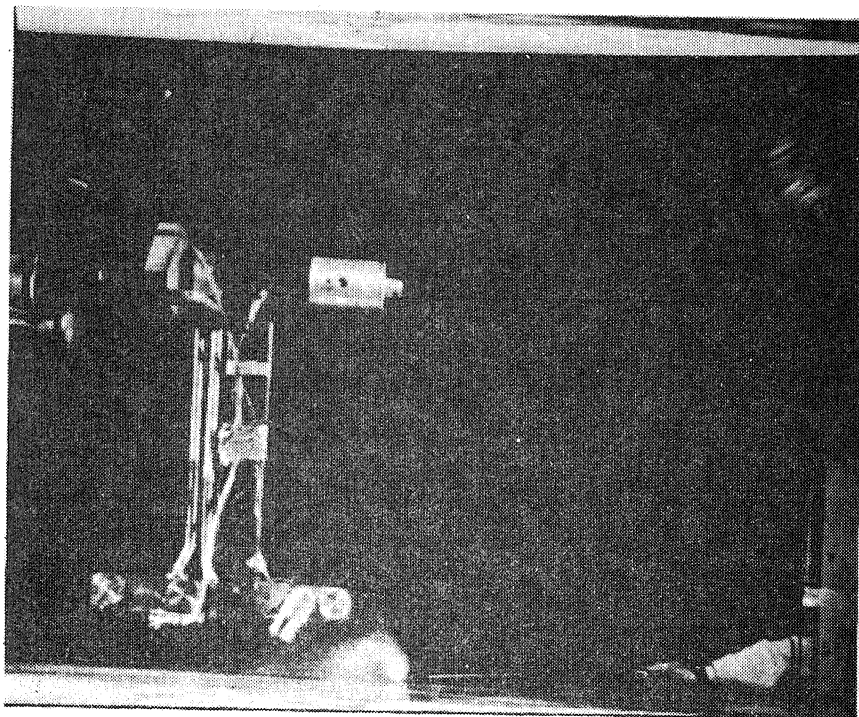


Figure 4. Ground jet peak temperature decay.



VERTICAL JET, $H/D = 2.5$, $NPR = 2$, $V_{WIND} = 50$ FEET/SECOND



JET INCLINED 30 DEGREES, $H/D = 2.5$, $NPR = 2$, $V_{WIND} = 20$ FEET/SECOND

Figure 5. Stills from smoke flow visualization film.

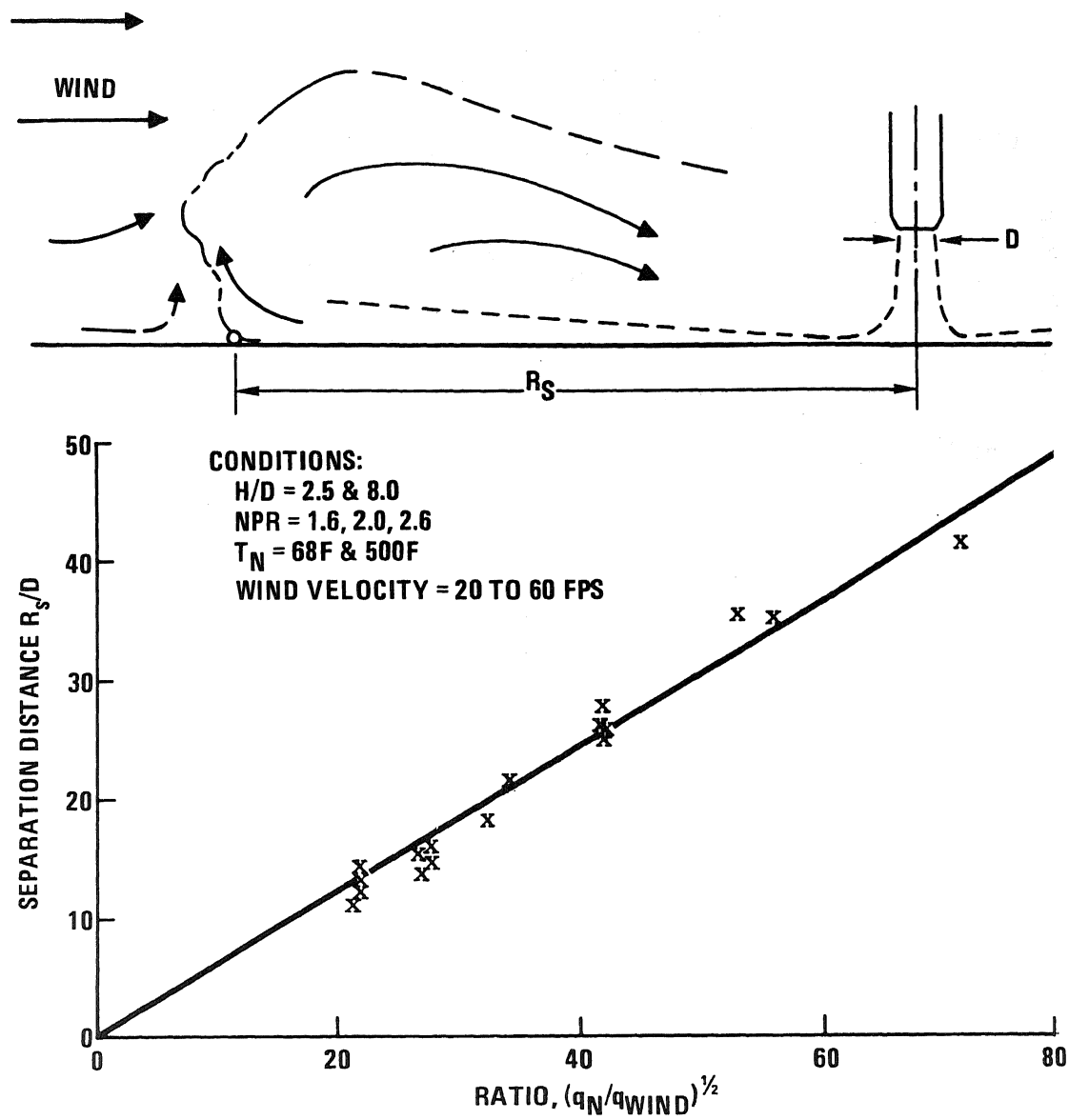


Figure 6. Ground jet separation distance.

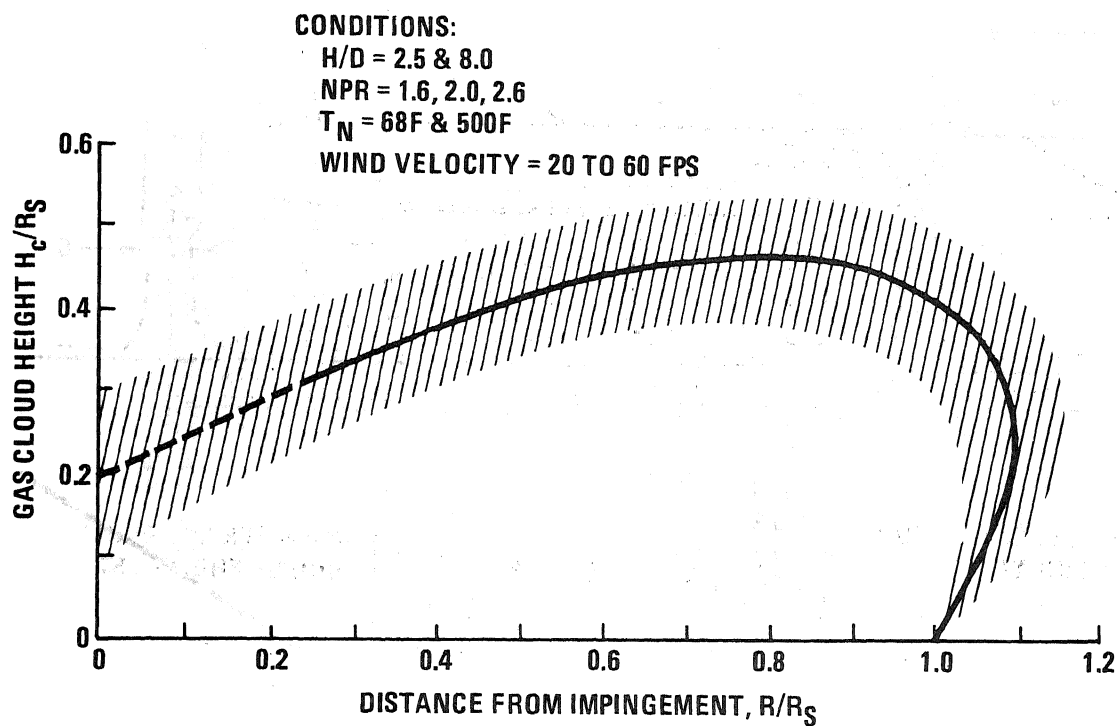


Figure 7. Recirculation gas cloud geometry.

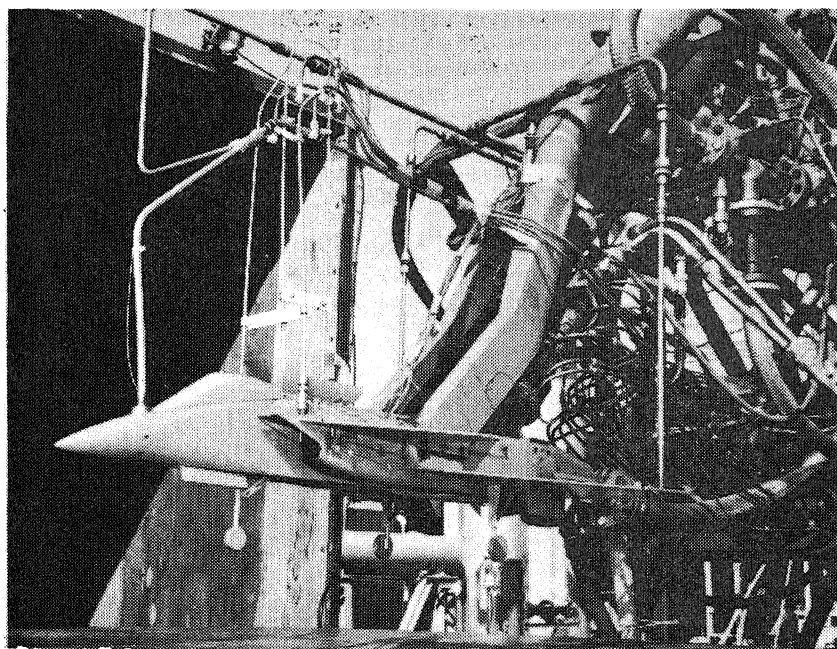


Figure 8. Hot gas model basic configuration.

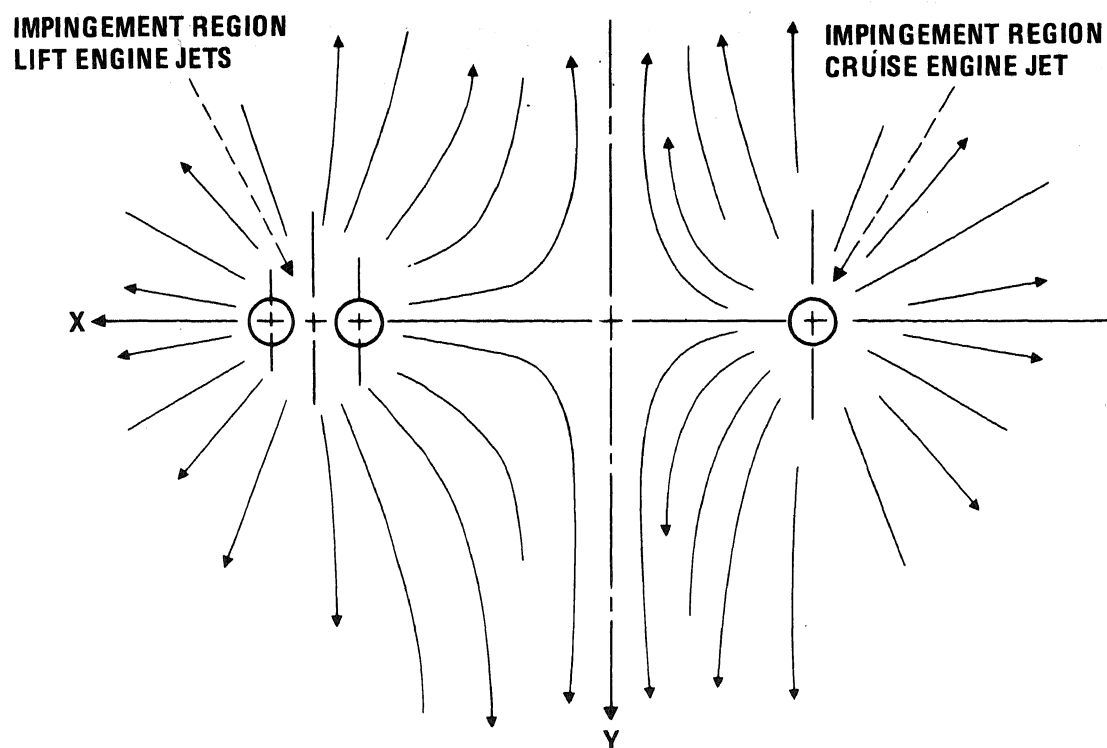
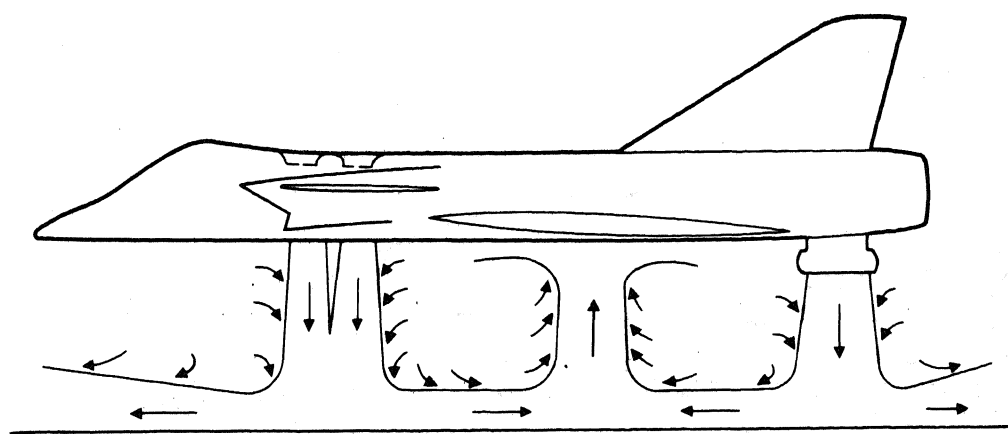


Figure 9. Near-field jet flows.

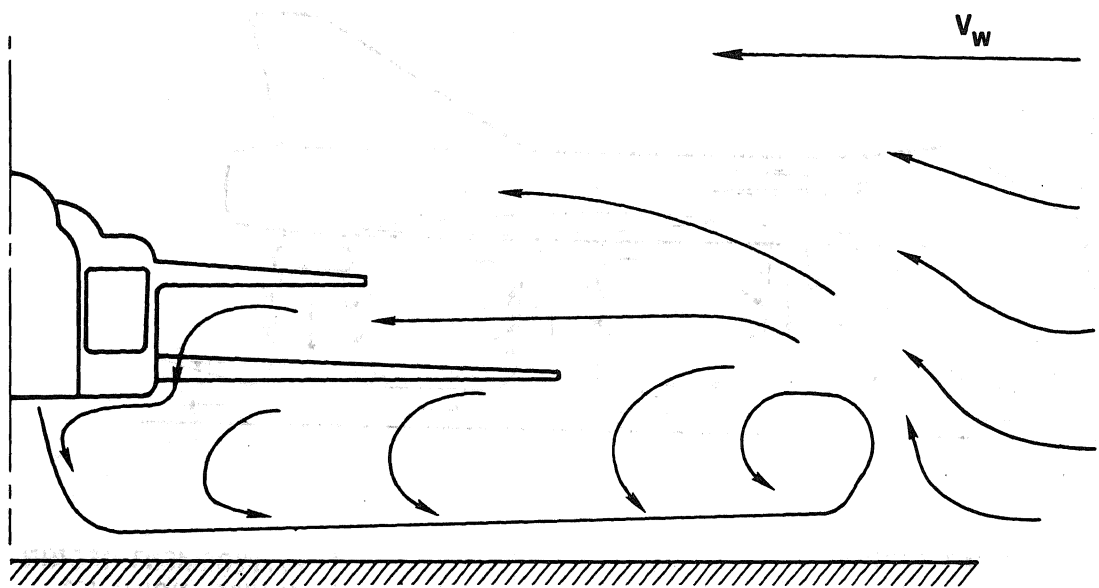


Figure 10. Far-field wind effect.

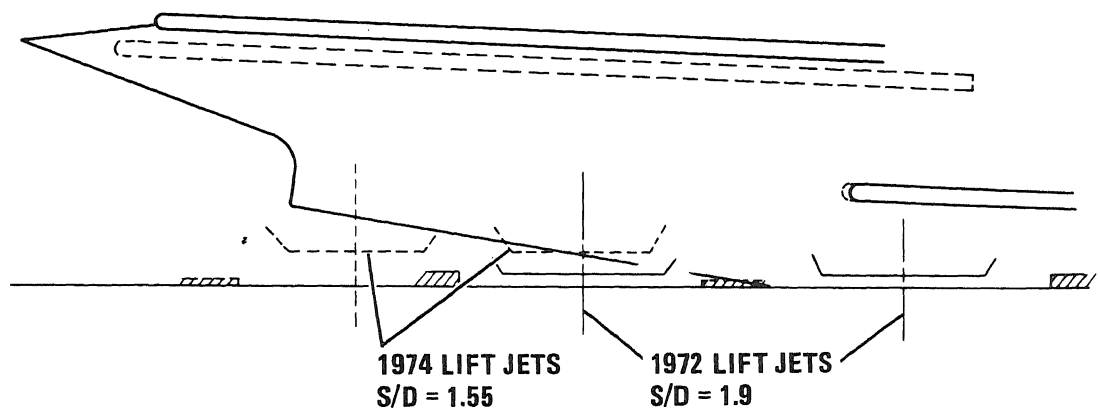


Figure 11. Comparison of 1972 and 1974 models.

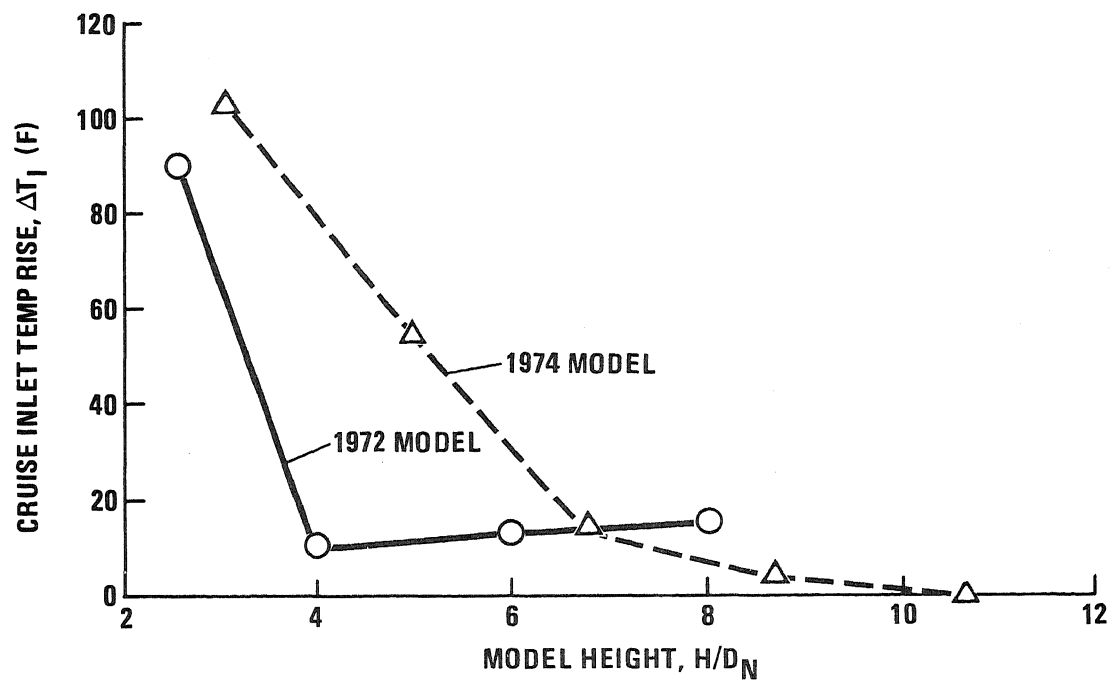


Figure 12. Effect of model update revision.

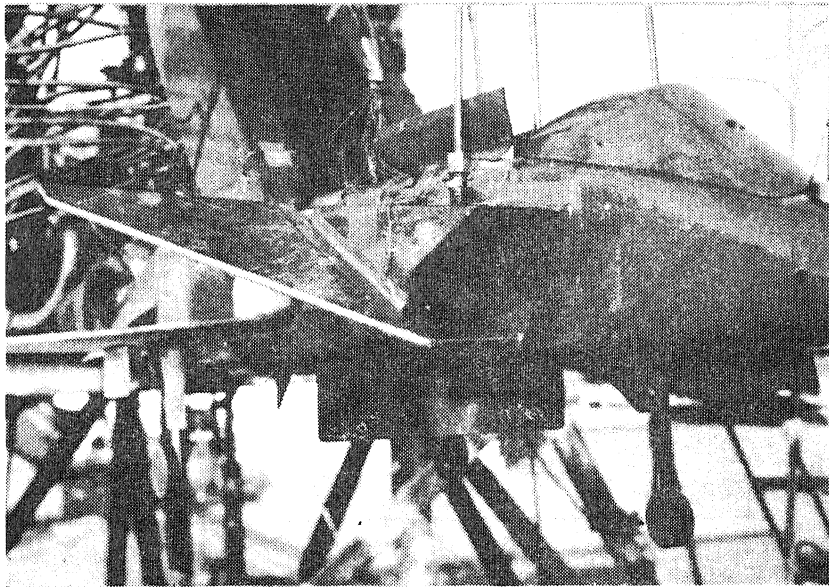


Figure 13. Hot gas model revised configuration.

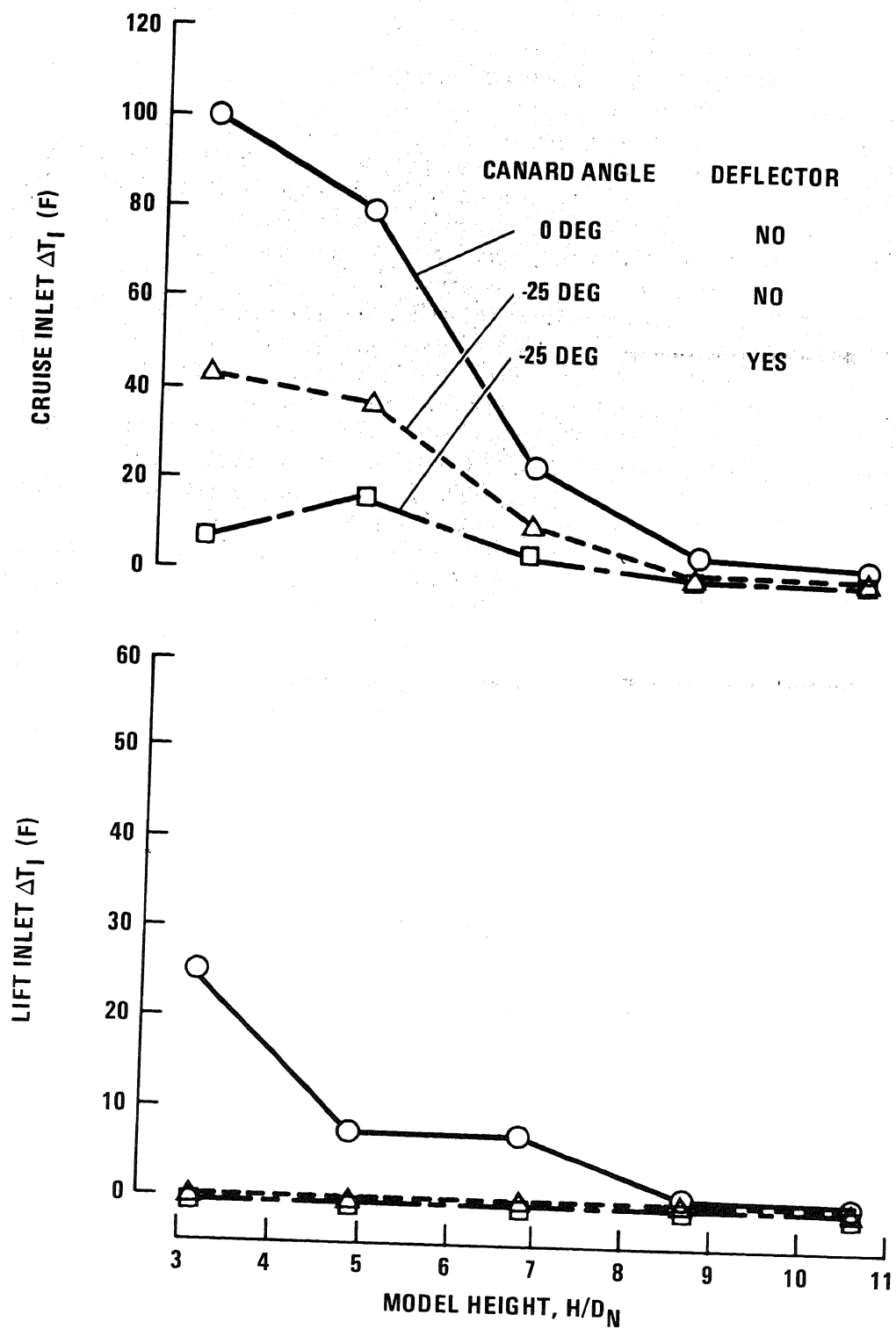


Figure 14. Effect of canard rotation and deflection.

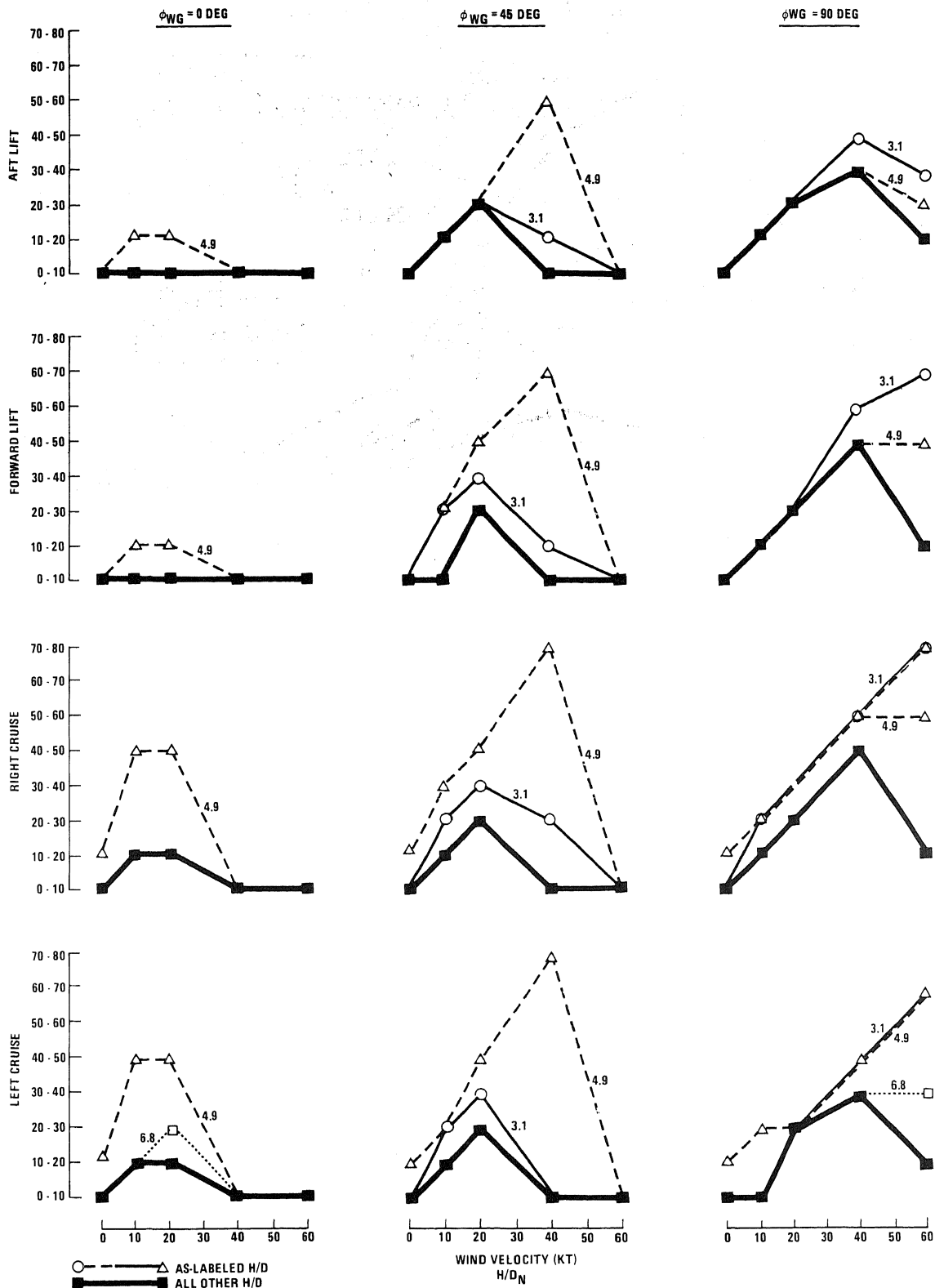


Figure 15. Effect of wind velocity.

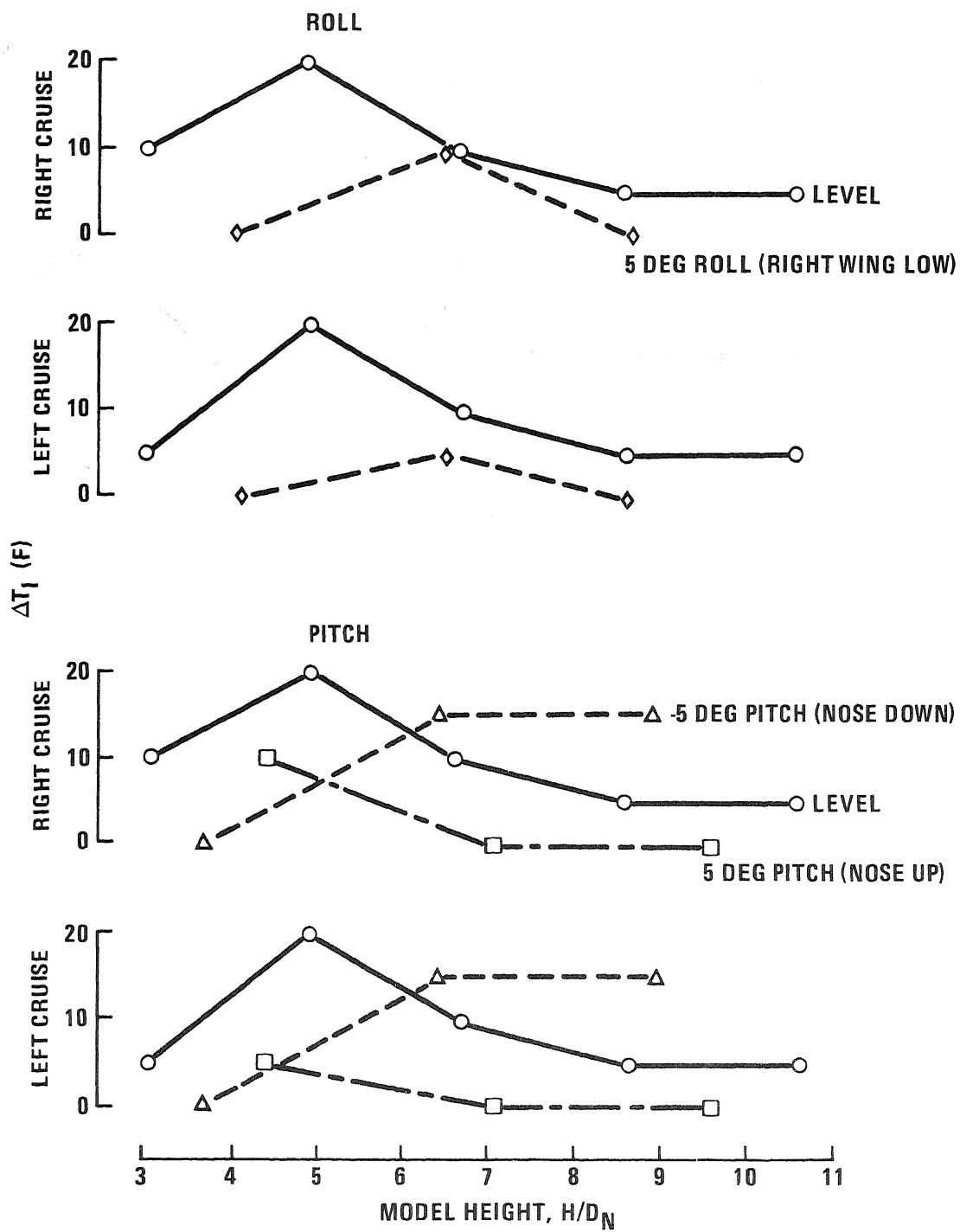


Figure 16. Effect of model attitude (revised configuration).

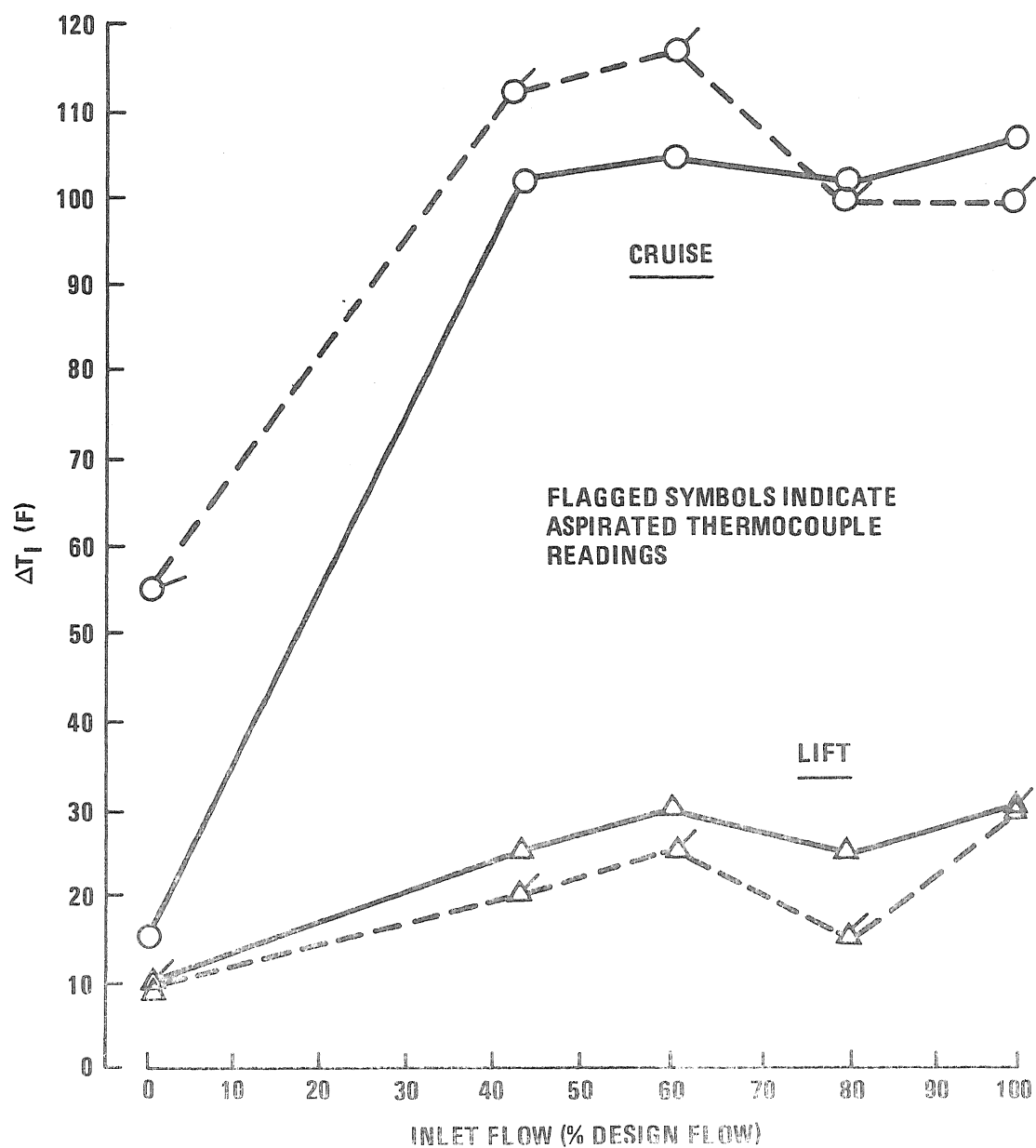


Figure 17. Effect of inlet flow.

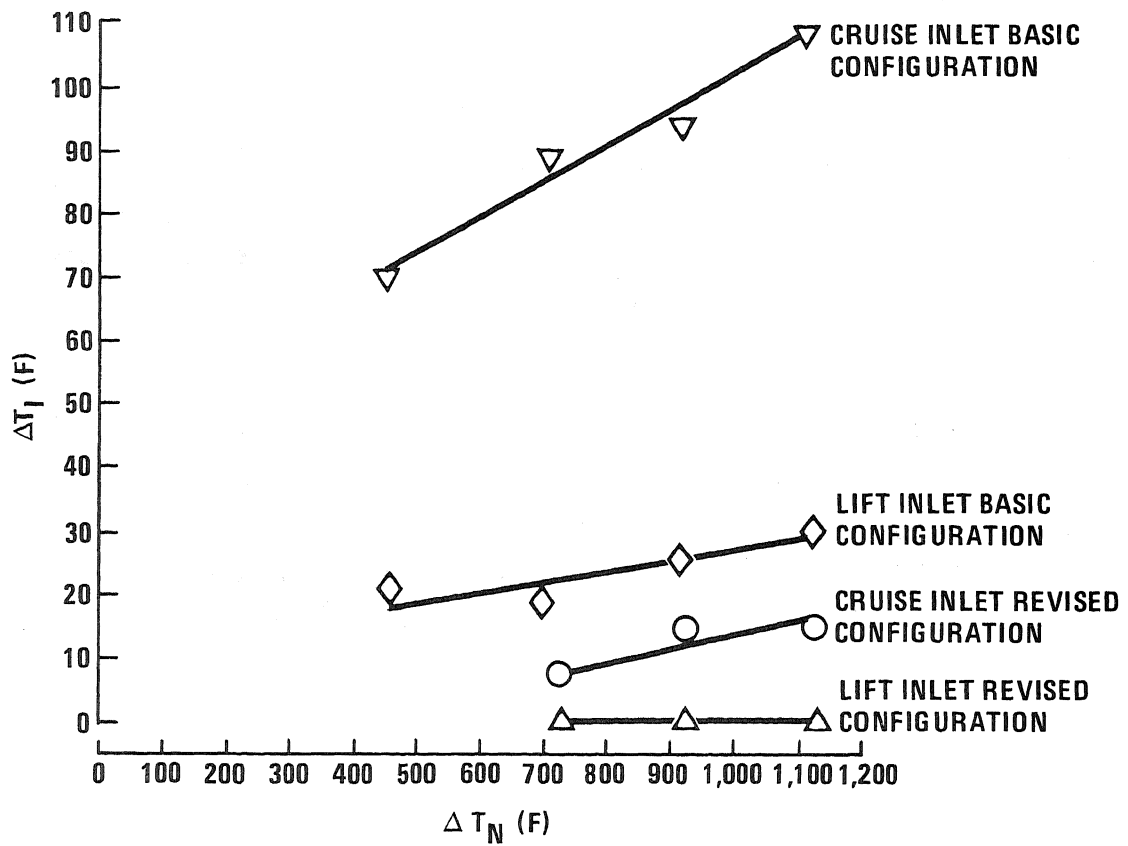


Figure 18. Effect of jet temperature.

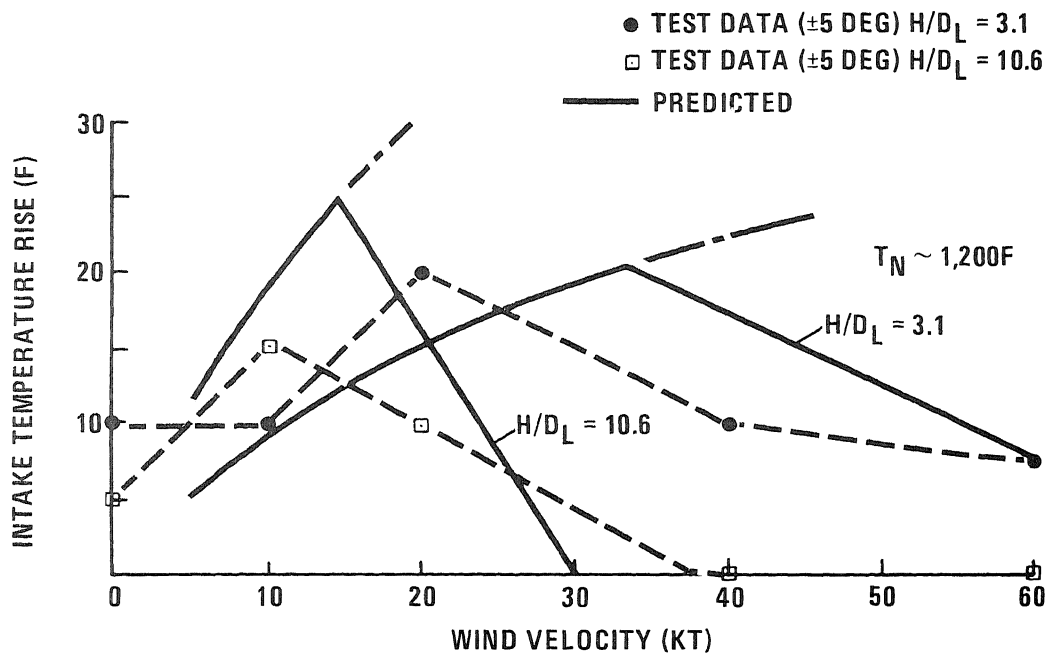


Figure 19. Reingestion in headwinds

EXPERIMENTAL STUDIES OF MULTI-JETS IN GROUND EFFECT

William G. Hill Jr., Theodore Luzzi, & Richard C. Jenkins
Grumman Aerospace Corporation
Bethpage, New York 11714

ABSTRACT

An experimental investigation of the flow fields created by multiple jets impinging on a ground plane, with primary emphasis on flows pertinent to VTOL aircraft, was conducted in Grumman's jet mixing laboratory. Experimental flows were produced by one, two, or four axisymmetric subsonic air jets. Initial tests were conducted to evaluate free mixing of multiple jet clusters without ground impingement. Whereas the multiple jets operating out-of-ground-effect were found to have very little influence on each other, significant mutual interference was found during ground impingement.

Axial variation of the ground plane pressure distribution caused by single-jet impingement was found to follow a two-part scaling rule. When the jet-exit-to-ground-plane distance was in the fully developed jet regime, the pressure distributions agreed with previously developed scaling laws. For closer jet-to-ground-plane spacing, a new correlation of impingement pressures was developed. A simple relationship was also found between the axial variation of maximum ground plane pressure and free-stream pitot pressure on the centerline of the jet. Impingement tests with two jets produced a bistable flow field caused by mutual interference on the ground plane. Four-jet impingement produced a markedly more unstable flow field. In studying the instability of this flow field, a three-dimensional manometer array was developed which allowed determination of the nature of the oscillations. With this understanding of the flow-field oscillations, a "jet shield" was developed which stabilized the flow and also produced the beneficial side effect of higher pressures on the aircraft surface.

A theory was developed to predict the ground plane stagnation lines and fountain location for multijet arrays. Good agreement was achieved between theory and experimental ground plane oil flows.

INTRODUCTION

Propulsion system designs for a VTOL aircraft generally employ several jet nozzles for vertical thrust, with aircraft stability being maintained during ascent and descent by differential control of the jet exhausts. Operation of three or more vertically directed jets close to the ground produces a complex flow pattern around the aircraft that can both degrade the net upward force and complicate aircraft stability problems. Lift losses in ground effect can be attributed to the recirculation pattern produced around the aircraft by the engine exhausts and the ambient air which they entrain. The interaction of the engine exhausts with the ground involves two opposing effects. Ground impingement enhances ambient flow entrainment, significantly lowering the pressure underneath the aircraft (suckdown). In addition, the multiple jets impinging on the ground meet and send fluid spurting upward to collide with the aircraft underside and increase lift (fountain effect). (See Fig. 1.)

The influence of the ground effect flow on vertical force and stability may be strongly dependent on the shape of the aircraft underside and the jet exhaust

configuration. The simplest possible aircraft and jet geometries were employed to gain a basic understanding of surface pressure variations and flow stability encountered in multiple jets operating in-ground-effect, and of the interaction between suck-down and fountain effects. In addition, subsonic jet exhaust velocities with no heating or gas composition variations were employed. These choices were made to enable thorough measurements and probing of several geometries to be accomplished at low cost.

While VTOL aircraft liftoff forces and surface pressure levels in-ground-effect must be influenced by jet exit properties (Mach number, temperature, etc), the general pattern of the recirculating flow field that exists between the aircraft and the ground may not be significantly altered by jet properties, providing a fully turbulent shear layer is developed at the jet exit. Results presented in Ref 1 indicate that essentially the same suckdown and fountain behavior exists under an aircraft for sonic jets as for subsonic jets, indicating a relatively small effect of jet Mach number. Results presented in Ref 2 indicate that an equivalent flat-plate model can give a correct indication of the induced lift on a three-dimensional model, due to a fountain.

During the investigation, extremely unsteady conditions in the multiple jet impingement flows were also observed. After much experimentation a means was developed of stabilizing the flow pattern, which is referred to as "jet shields." These shields prevent the impinged fountain from disturbing the jet exit conditions and in addition, increase the pressure on the aircraft underside. The jet shield's performance suggests the mechanism of a radial wall-jet system formed by the fountain on the aircraft underbody that interacts strongly with the primary jets as they emerge from the aircraft.

EXPERIMENTAL APPARATUS

The jet flow fields were developed from a nozzle array mounted on the front face of a 2-ft-square settling chamber (Fig. 2) pressurized by a centrifugal fan. Low turbulence levels were obtained by using a honeycomb flow straightener and turbulence damping screens downstream of the diffuser. The jet nozzles were 1-in. I.D., thin-wall pipes arranged in a square array. The entrance of each nozzle was flush with the 2-ft-square front wall of the settling chamber. Each nozzle consisted of a 1-in.-diameter ASME flow metering section (elliptical entrance contour shape) followed by a 6-in.-long constant-area section. The spacing between adjacent nozzle centerlines was 2 in. Flows were developed from either one or two of the jets from this array by sealing the entrance and exits of unused nozzles and slightly constricting the inlet of the centrifugal fan so as to obtain the same jet exit velocity with either one, two, or four jets in operation. The jet Reynolds number based on nozzle diameter was nominally 10^5 .

A 6-in.-square flat plate, installed flush with the nozzle exits and instrumented with surface-pressure taps, was used to simulate an aircraft underside for most of the tests. For some tests, a much larger plate was used with an aircraft planform shape (Fig. 2). The ground plane was a 1-1/2-ft-square plexiglass sheet, also instrumented for pressure measurements, mounted normal to the flow with provisions for axial and transverse motion relative to the jet array.

The experimental work consisted of field probe measurements of a single free jet and surface-pressure measurements with this jet operating in-ground-effect. The former work was undertaken to document the free-jet velocity profiles operating out-of-ground effect. Hot-film probes were used for most of the free-jet measurements. These probes were mounted on a motorized traverse mechanism to obtain axial and transverse surveys of both mean velocity and turbulent intensity. The probe signals were linearized and displayed on an X-Y pen recorder, using a voltage signal from the probe spatial position sensor to drive the X-component of pen motion. This data recording technique was also used with a pressure transducer to obtain free-jet pitot-probe profiles.

For multiple jets operating in-ground-effect, concentration was focused primarily on surface-pressure instrumentation for both the ground plane and the airplane plate. Oil-flow patterns on the ground plane were also observed. The main interest in this work was to determine the nature of the flow field between the jet exhausts and the ground plane, particularly for the multiple-jet case. While field measurements above the ground plane would have been most helpful in this investigation, efforts to obtain such measurements were, with one exception, unsuccessful because the flow fields of most interest (multiple-jet impingement) were not stable and the presence of a probe and its support significantly altered the entire flow field. The lack of flow-field stability could be seen from fluctuations in the ground plane pressure distribution, which were displayed on a manometer array constructed to visualize the instantaneous pressure contours on either the ground plane or the airplane plate.

SINGLE-JET IMPINGEMENT

Impingement of a single axisymmetric jet on a flat plane surface normal to the axis of the jet produces several distinct zones. If the distance above the ground, h , is large compared to the nozzle diameter, d , the flow near the exit will contain an undisturbed region of primary flow that ends several diameters downstream of the exit plane. This undisturbed core is surrounded and followed by a mixing zone-shear layer into which ambient air is entrained. This entrainment and mixing continues to occur along the free boundaries of the remainder of the flow. In a region above the ground plane opposite the jet exit, but much larger in diameter, designated the interaction zone, the flow turns parallel to the ground plane. Beyond this zone the flow remains basically parallel to the ground plane in a radially directed wall jet.

The details of the flow field depend on the ratio h/d and also to some extent on the jet exit velocity. Surface-pressure measurements on the ground plane provide a useful description of this type of flow field. Figures 3, 4, and 5 show pressure distributions measured on the ground plane at different axial locations. These measurements were obtained without a flat plate at the nozzle exit plane.

Figure 3 shows ground plane pressure profiles obtained for $h/d = 1.5, 3$, and 5 , together with the results of Brady and Ludwig (Ref 3) and Snedeker and Donaldson (Ref 4). The profiles for all ground plane locations show approximately the same width, with only minor variations in shape. These results all indicate that the pressure distributions are essentially independent of h/d for the entire close-in region ($h/d \leq 5$).

Figure 4 shows ground plane pressure profiles obtained for $h/d = 10$ and 15 . In this figure, the pressures are plotted versus r/δ , where δ represents the radius at which the velocity in the jet, without the ground plane, has dropped to half the center-line level. Values of δ were found from surveys of the free jet at the same h/d . As

noted by Bradbury (Ref 5), pressure profiles normalized in this fashion are independent of ground plane location providing it is located far enough from the jet exit for freestream velocity profiles to exhibit similarity, i. e., well beyond the potential core. Comparison of the data obtained with the generalized curve presented by Bradbury shows the ground plane pressure profiles following the same behavior.

It was found, as did Bradbury, that the ground plane pressure on the jet centerline (P_O) was higher than the free-jet pitot pressure on the centerline (P_{TO}) at the same h/d . Figure 5 presents a comparison of P_{TO} with P_O as a function of x/d . The variation of P_O was obtained by moving the ground plane. The two pressure profiles appear almost identical, except for an axial displacement of approximately $0.75d$. Results of shifting the ground plane pressure distribution $0.75d$ upstream are shown in Fig 5. The close agreement between these curves for $4 < h/d < 15$ suggests that this technique may be used to determine the maximum ground plane pressure from a centerline pitot pressure survey, rather than Bradbury's rule, $P_O = 1.12 P_{TO}$.

To summarize, the following method was developed for correlating ground plane impingement pressures with free-jet flow properties for a subsonic jet. For ground plane locations close to the jet (nominally $h/d = 5$ or less), the mean radial pressure distribution shown in Fig. 3 is used. For ground plane locations far from the jet exit, where freestream velocity profiles exhibit similarity ($h/d > 10$), the radial pressure distributions shown in Fig. 4 are used. In this case, the ground plane centerline pressure is set equal to the free-jet centerline pitot pressure at $0.75d$ above the surface (Fig. 5).

MULTIPLE-JET IMPINGEMENT

The flow pattern formed by two jets impinging on the ground plane was visualized using oil-flow techniques. Figure 6 shows a typical pattern formed after a 1-min exposure of a smear of oil on the ground plane. Note the double line pattern formed between the impact zones of the primary jets. The appearance of two lines in this region rather than a single line probably indicates that the ground flow separates before it reaches the plane of symmetry and turns upward, much as it often separates ahead of a solid wall. The distance between the centers of the two halves of the flow pattern was 2 in., corresponding to the centerline separation of the pair of 1-in. jets. This indicates that the interaction of the two jets does not alter the location of the centerlines.

Ground plane pressure surveys were conducted with the solid exit plane plate installed. Using two of the diagonal jets from the four-jet array to increase jet centerline separation, large fluctuations were found that were apparently caused by the presence of the solid exit plane plate. The nature of the fluctuations was unique because they revealed a bistable pressure distribution on the ground plane (Fig. 7). The pressure distribution along a line connecting the jet centerlines was not symmetric; higher ground plane pressures were measured around the periphery of one of the jet impact points. After a moment or two the ground plane pressures would suddenly change to enhance the pressure around the other jet impact point. However, the ground plane pressures on both jet centerlines remained constant and equal during this change indicating that the impingement of the jets was not affected, but that the meeting of the two ground plane flows was unsteady.

This random changeover from one unsymmetric distribution to its mirror image existed only with the solid-exit-plane plate installed, and could be stabilized at either one of the two distributions by deliberately tilting the ground plane. This bistable behavior was observed for ground plane locations from $h/d = 1.5$ to 5.0 . Within this displacement range, the ground plane pressures on the jet centerlines remained equal to the jet-exit-plane stagnation pressure.

Impingement tests with the four-jet array indicated a more complex flow field. Unsteady pressures were observed at all points on the ground plane, even without the solid-exit-plane plate. The presence of this exit-plane plate greatly magnified the pressure fluctuations.

A typical oil-flow pattern on the ground plane is shown in Fig. 6. The double line pattern isolating one quadrant of the impact zone is typical of many such photos, but the quadrant isolated varied from one moment to the next.

To investigate the nature of these pressure fluctuations, a three-dimensional manometer array (Fig. 8) was constructed with tubes laid out spatially in the same pattern as the ground plane pressure taps. The most extreme pressure fluctuations were found on the centerlines of the four jets. These pressures varied from a maximum value close to the settling chamber pressure down to a minimum value almost a factor of 10 lower. The nature of these fluctuations was random, with at least one of the centerline pressures always being well below the maximum value. The time scale of these fluctuations was of the order of 1 sec; they were accompanied by lower-amplitude pressure variations at all other points on the ground plane.

Observation of pressure disturbances on both the ground plane and the aircraft plate led to the conclusion that variations in the direction of the fountain were causing unsteady surface pressures. Movement of the fountain impact point on the aircraft plate will produce an unsteady flow along this surface and cause a time dependence of conditions at the jet exits. Variations in jet exit conditions will, in turn, affect the direction of the fountain. This close coupling between jet exit conditions and the direction of the fountain appears to be responsible for the unsteadiness in the flow field because it provides a mechanism for enhancing the turbulent fluctuations that exist in the mixing zone of a free jet. This interaction was broken, and the flow field almost completely stabilized, by installing small shields around the inner quadrant of the jet exits to effectively isolate the jets from fountain disturbances. With the shields installed, there were still small oscillations in ground plane pressures, but the amplitude was decreased by a factor of 10. In addition to stabilizing the fountain, it appears that this type of shield would create a favorable effect on aircraft lift. Figure 9 shows the variation of pressure on the aircraft with distance from the ground for one point on the exit plane plate. Similar behavior was observed at all other points measured in the region between the jets.

The shields increased the pressures on the exit plane surface between the jets over the entire range of distance above the ground (h/d less than about 3). Since the interference forces that occur close to the ground play a very important role in the performance capability of a VTOL aircraft, the positive effects produced by these shields hold the promise of being very beneficial and should be studied further.

Figures 10, 11, and 12 are photographs of the oil-flow pattern for other four- and three-jet arrays. In these photos, two-jet momentum strengths were used (relative

strength 0.5 and 0.344). In all cases the stagnation lines were concave toward the lower-strength jet. The intersection of the stagnation lines with the axis of symmetry indicates the ground location of the center of the fountain.

A theory was developed to determine the location of the stagnation lines and fountain positions. This theory assumes that the wall-jet flow from a single jet is radial and the magnitude of the total momentum at any radius is equal to the momentum at the jet exit plane. The momentum flux (momentum per unit arc length) of each vertical jet is a function of the radius only. Two radial wall jets formed from two vertical jets will meet and form a stagnation line at the ground. It is assumed that a stagnation line will form at the location where the components of the two local wall-jet momentum fluxes normal to the stagnation line are equal. From this, an expression for the direction that the stagnation line will take can be derived. The direction is a function of the strength of the two jets and the radial vectors to the point on the stagnation line from the two jets. An expression for the location of the stagnation point on the line connecting two jets was also derived. This location is the starting point for the solution for the stagnation line. At the known initial location, the direction of the stagnation line is calculated. A new point on the stagnation line is determined from this direction. Fountains will form at the coincidence point of two stagnation lines that fall within the inner region. To form a fountain, momentum flux must be directed in both the positive and negative directions along the axis of symmetry at the coincidence point. This can occur only in the inner region, which is contained within the lines connecting all jets. (The theory is developed in detail in Ref 6). A computer program was developed to generate and graphically display the stagnation line and fountain location for multi-jet arrays. This program is reported in Ref. 7.

These theoretical curves are compared to the experimental data in Fig. 10, 11, and 12. Figure 10, which shows a four-jet array with the two smaller jets on the axis of symmetry, shows two fountains on the axis close to the smaller jets. Figure 11 shows a three-jet array with one small jet on the axis of symmetry and indicates a single fountain near the small jet. Figure 12, which shows a three-jet array with the single large jet on the axis of symmetry, does not indicate a fountain because the coincidence point of the two stagnation lines lies outside the inner region.

The ground flow field is quite complicated. There is considerable interaction between the free and wall jets, fountains, ground, and aircraft underbody. Our methodology for attacking this complicated problem is to isolate individual phenomenon, study each experimentally and theoretically, and then incorporate their effects into an overall flow study. The work presented in this paper is a start of the study of a few ground flow phenomena.

REFERENCES

1. Gentry, G. L., and Margason, R. J., "Jet-Induced Lift Losses on VTOL Configurations Hovering In and Out of Ground Effect," NASA TN D-3166, February 1966.
2. Albany, L. F., "Analysis of Spread Multijet VTOL Aircraft in Hover," Old Dominion University, Norfolk, Va., Technical Report 74-T8, December, 1974, prepared under contract NAS1-11707 NASA/Langley, Va.
3. Brady, G. W., and Ludwig, G., "Theoretical and Experimental Studies of Impinging Uniform Jets," IAS Paper 63-29, January 1963.

4. Snedeker, R. S., and Donaldson, C. du P., "Experiments on Free and Impinging Underexpanded Jets from a Convergent Nozzle," Report 63, Aeronautical Research Associates of Princeton, Inc., September 1964.
5. Bradbury, L. J. S., "The Impact of an Axisymmetric Jet Onto a Normal Ground," Aeronautical Quarterly, May 1972, pp 141-147.
6. Luzzi, T., "Development of An Analytical Procedure for Determining the Stagnation Lines, Fountain Position, and Fountain Liftoff Angle of a Multijet VTOL Configuration in the Inground Mode," Grumman Research Department memo, to be published.
7. Siclari, M. J., Barche, J., and Migdal, D., "V/STOL Aircraft Prediction Technique Development for Jet-Induced Effects, Vol II, Users Guide to Compute Programs," Grumman Report PDR-623-18, April 15, 1975, final report under contract N00140-74-C-0113, Naval Air Propulsion Test Center, Trenton, N. J.

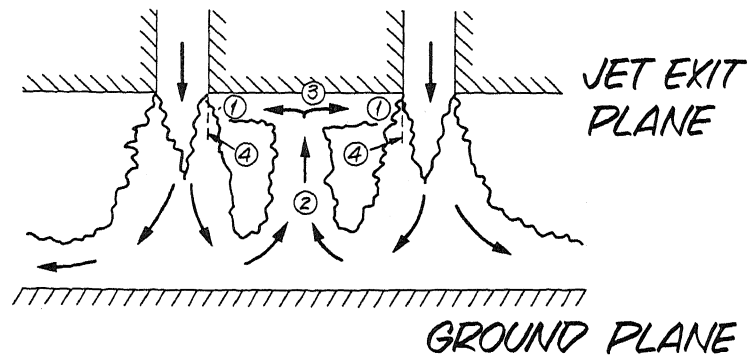
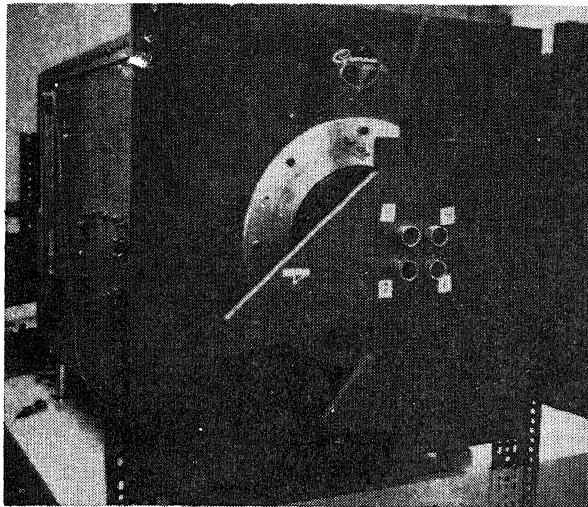
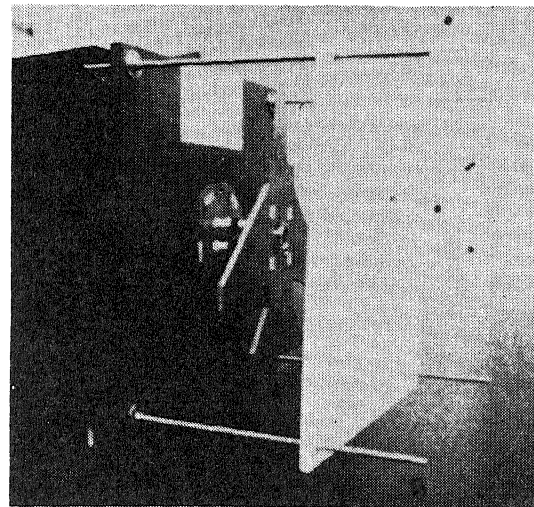


Fig. 1 Model Determined for 4-Jet Fountain Flow



WITH AIRCRAFT PLANFORM



PLANFORM WITH GROUND PLANE

Fig. 2 Experimental Facility

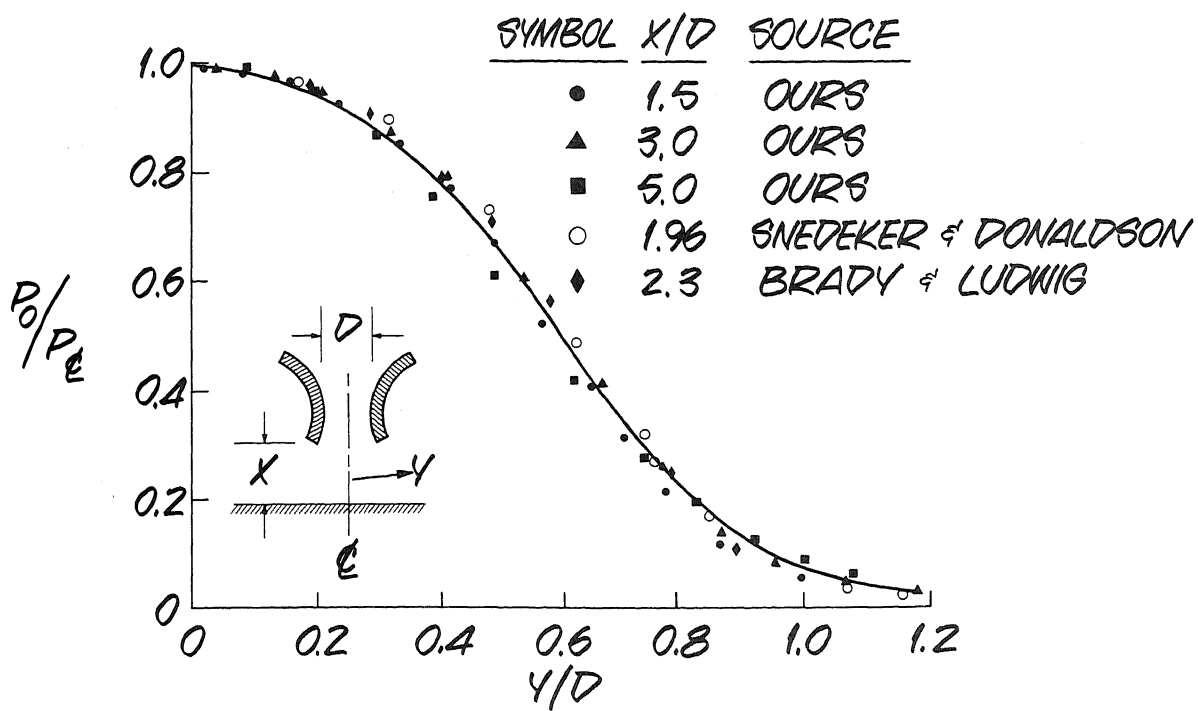


Fig. 3 Ground Plane Pressure Distributions from Single-Jet Impingement

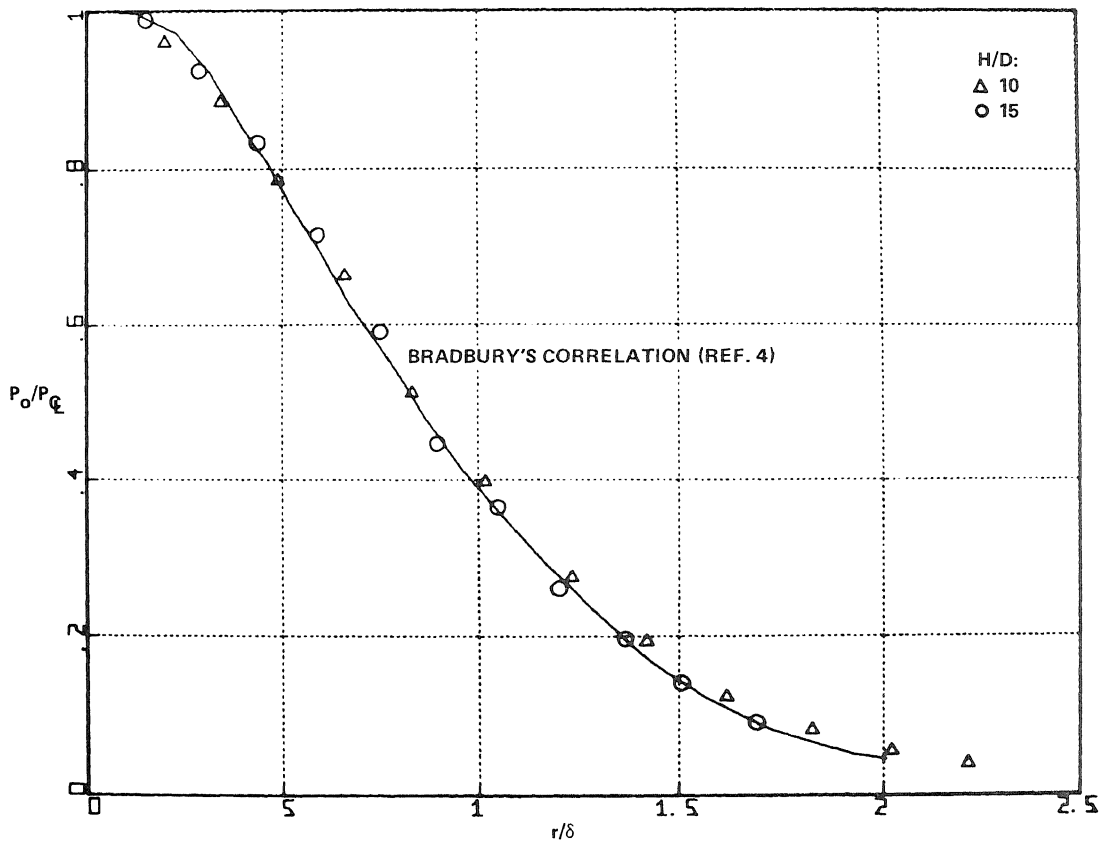


Fig. 4 Radial Impingement Pressure Distribution for Large H/D

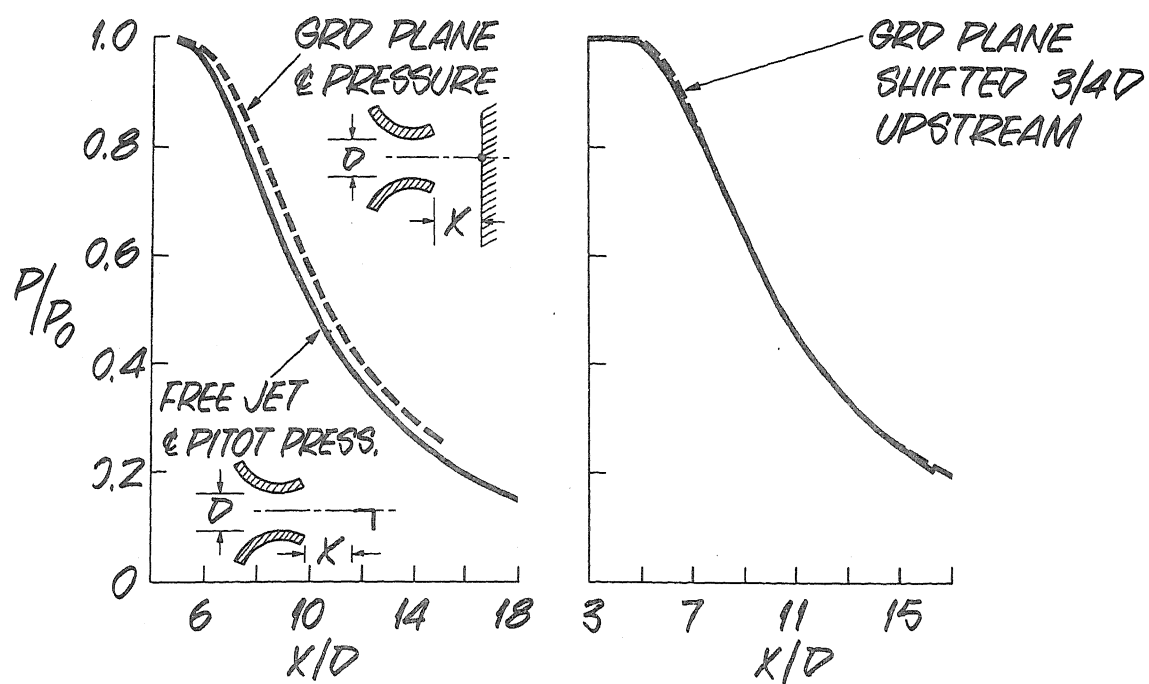
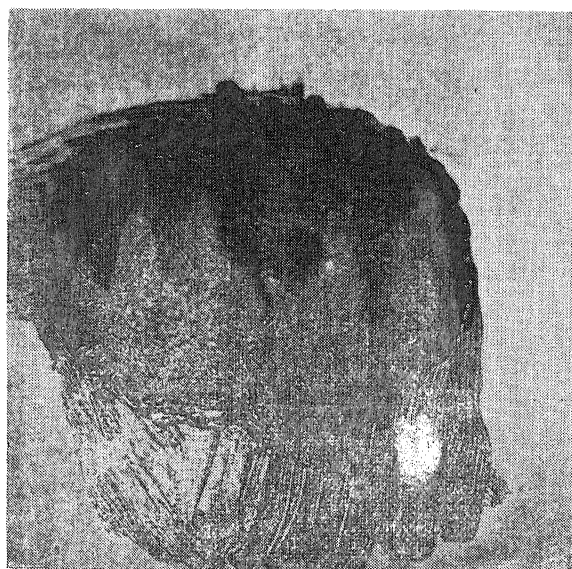
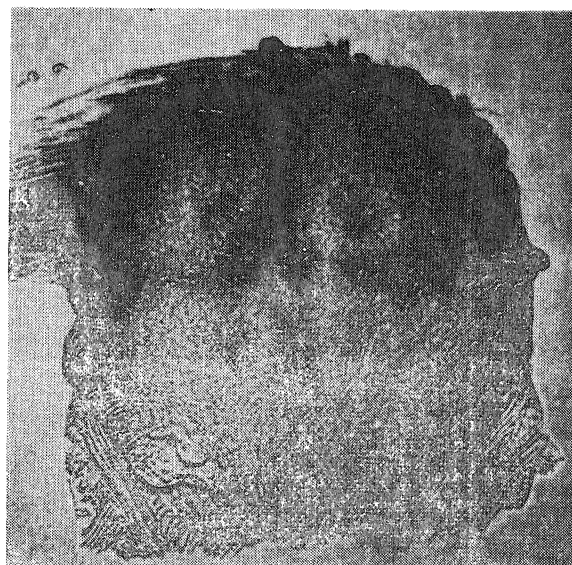


Fig. 5 Ground Plane Pressures Compared to Pitot Pressure



2-JET IMPINGEMENT



4-JET IMPINGEMENT

Fig. 6 Ground Plane Oil Flows

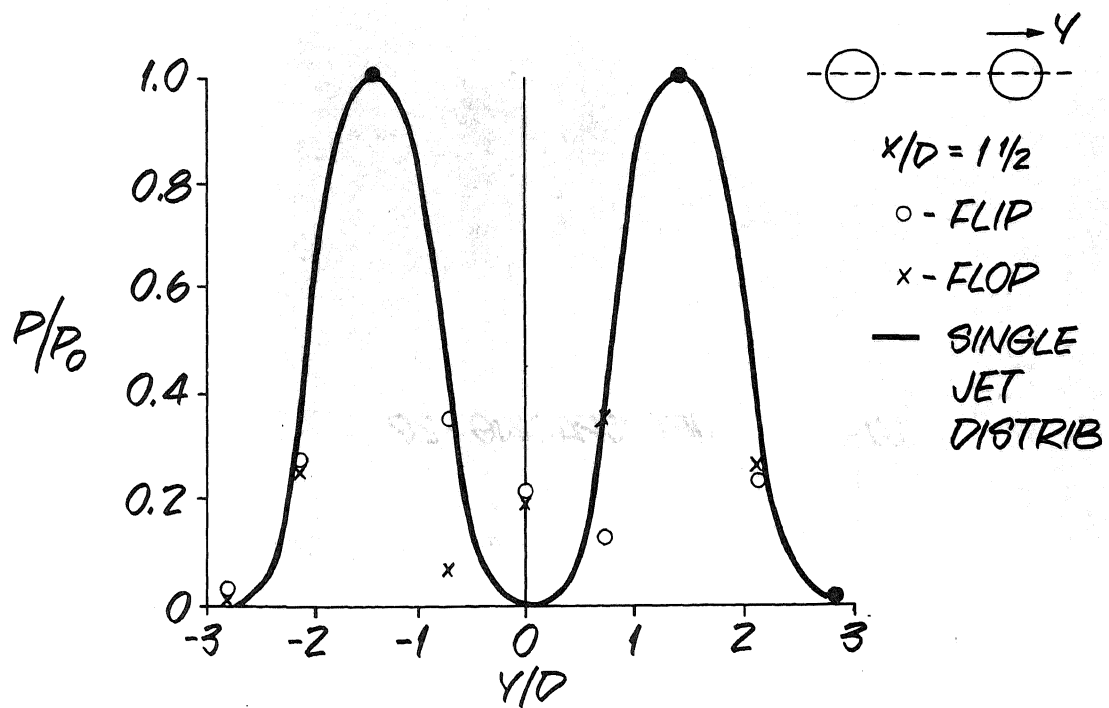
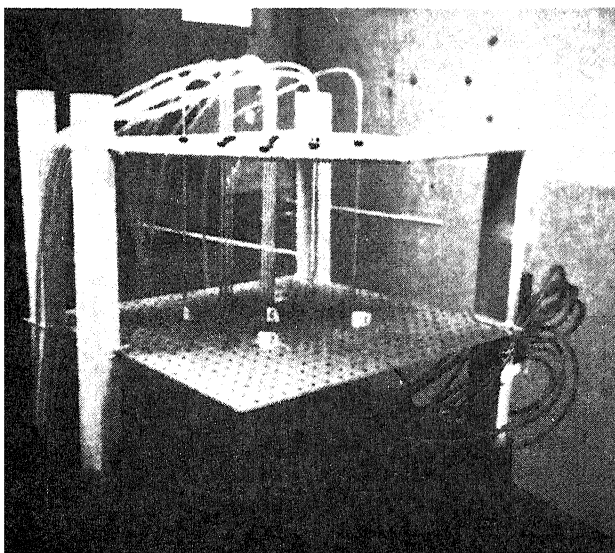
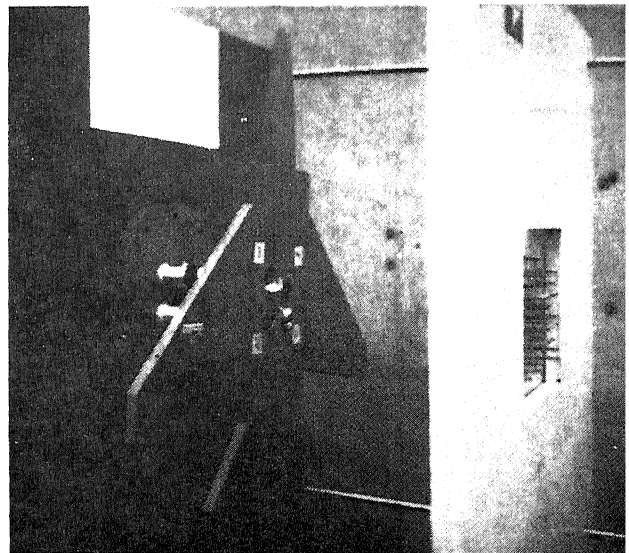


Fig. 7 Pressure Distributions Caused by Twin Jets



MANOMETER ARRAY



SHIELDS INSTALLED AT JET EXITS

Fig. 8 3D Manometer Array Shields

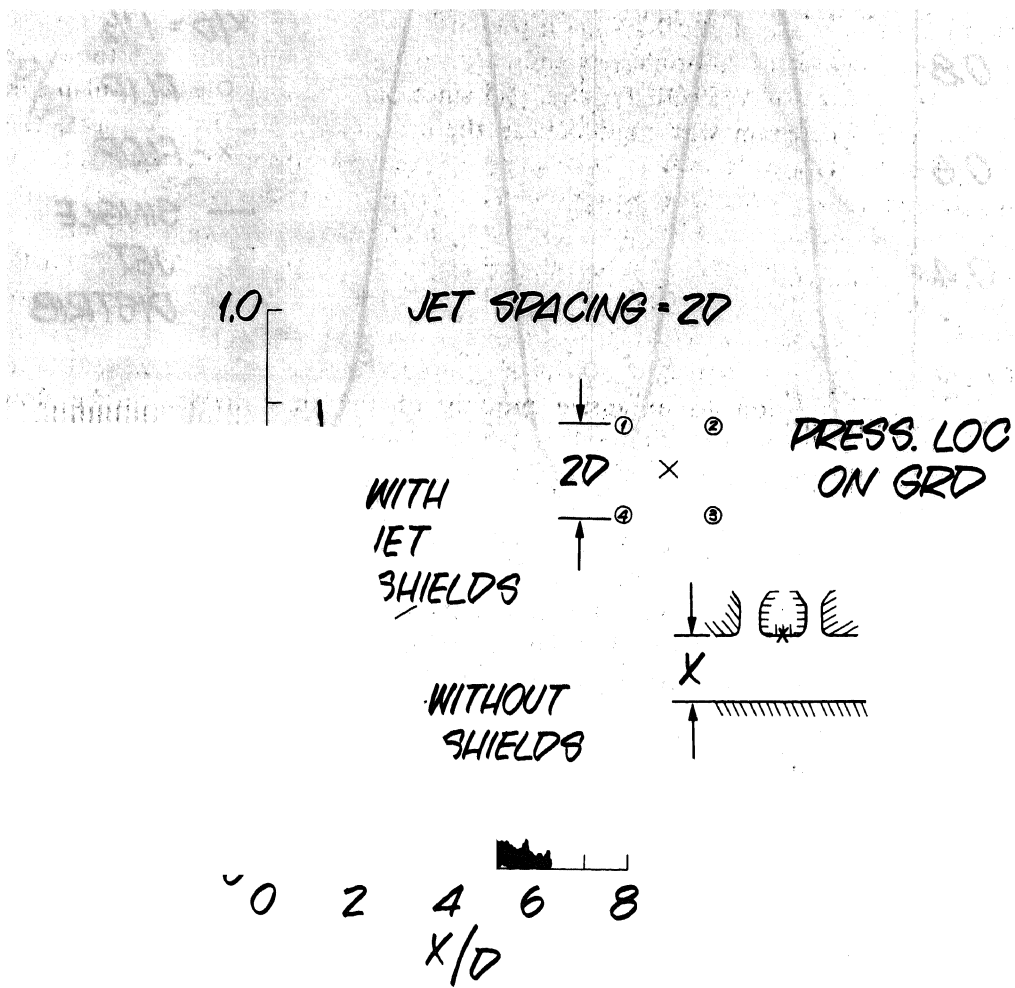


Fig. 9 Effect of Jet Shields on Fountain Stability & Levels

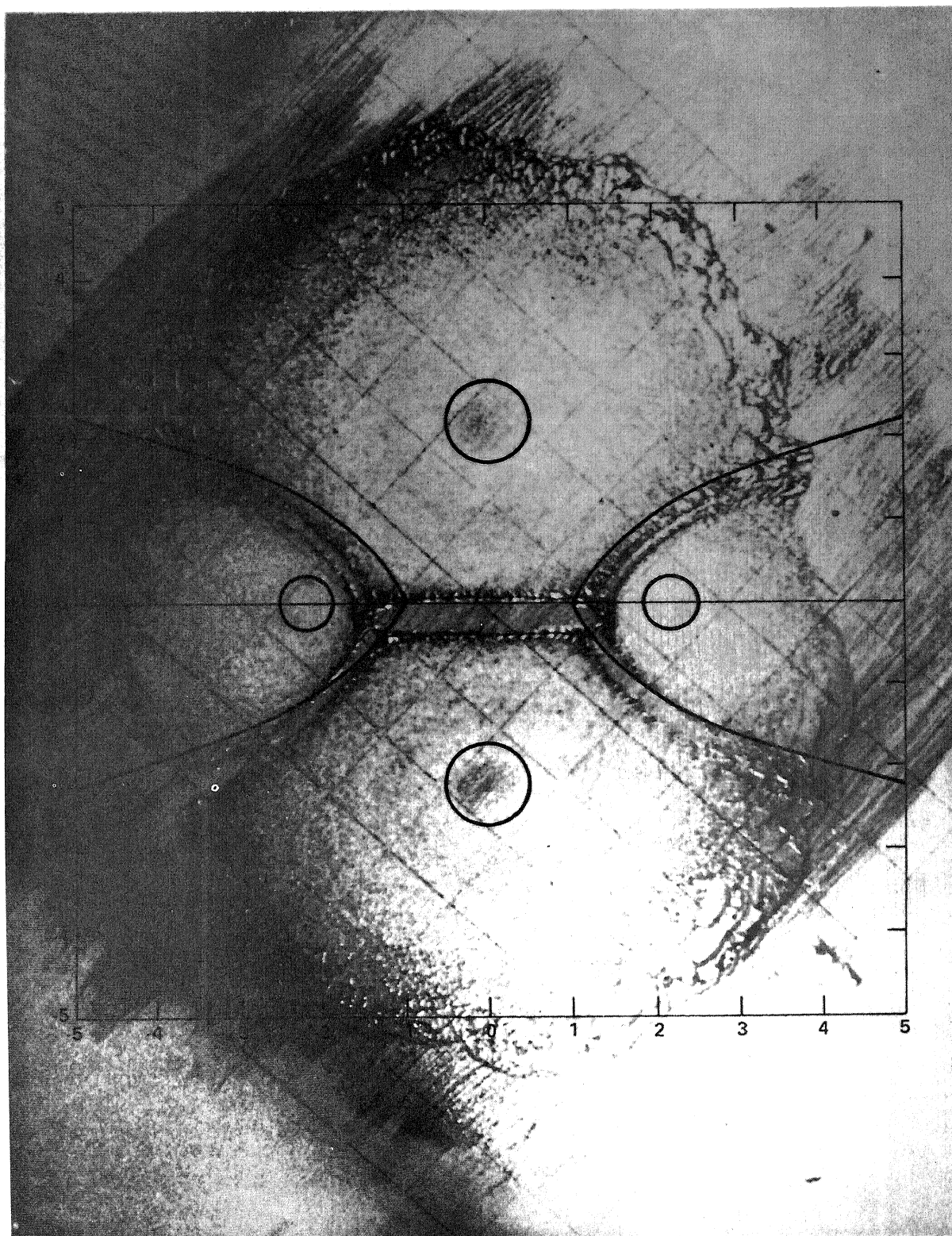


Fig. 10 Four-Jet-Array Ground Plane Oil Flow

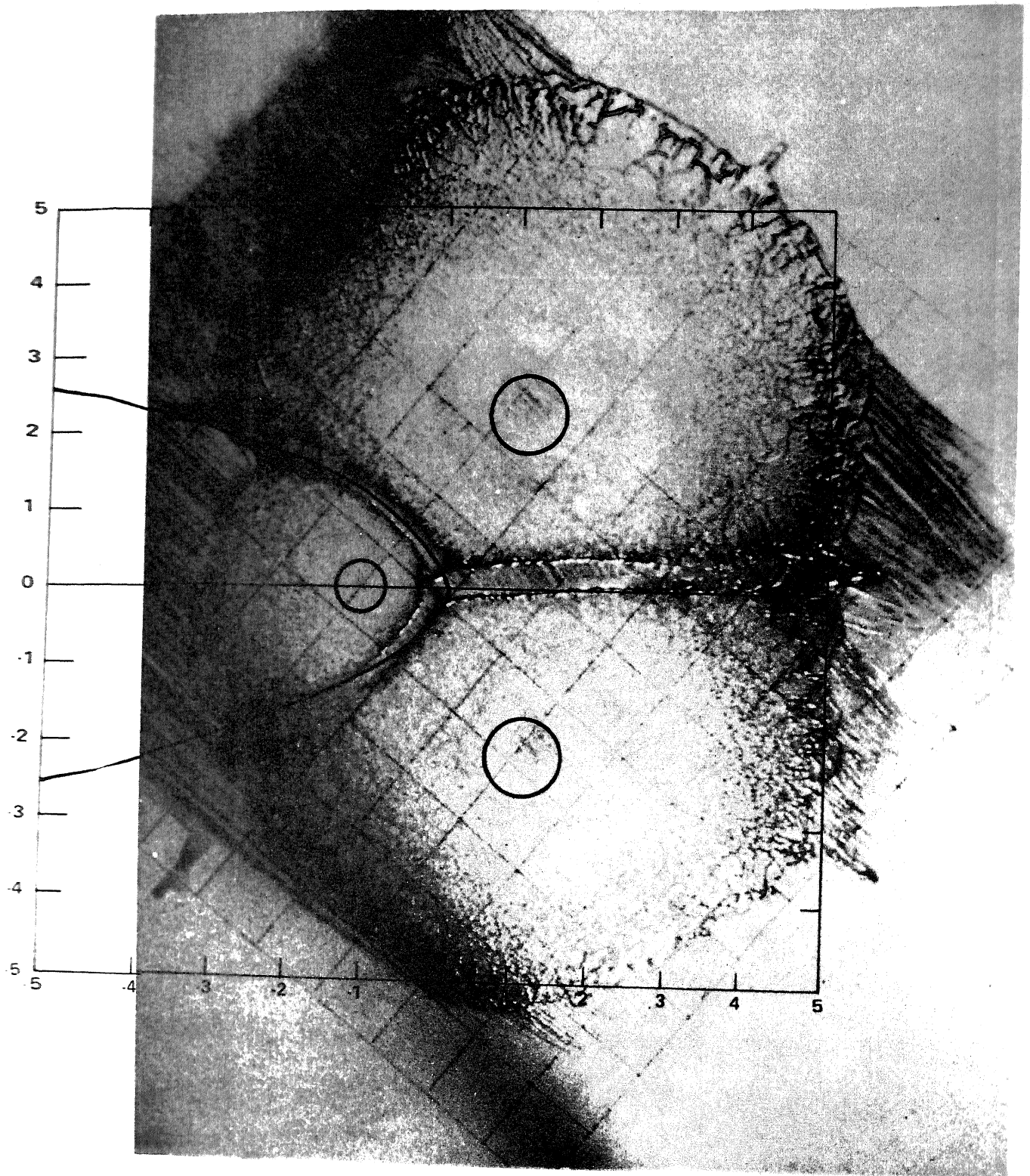


Fig. 11 Three-Jet-Array Ground Plane Oil Flow

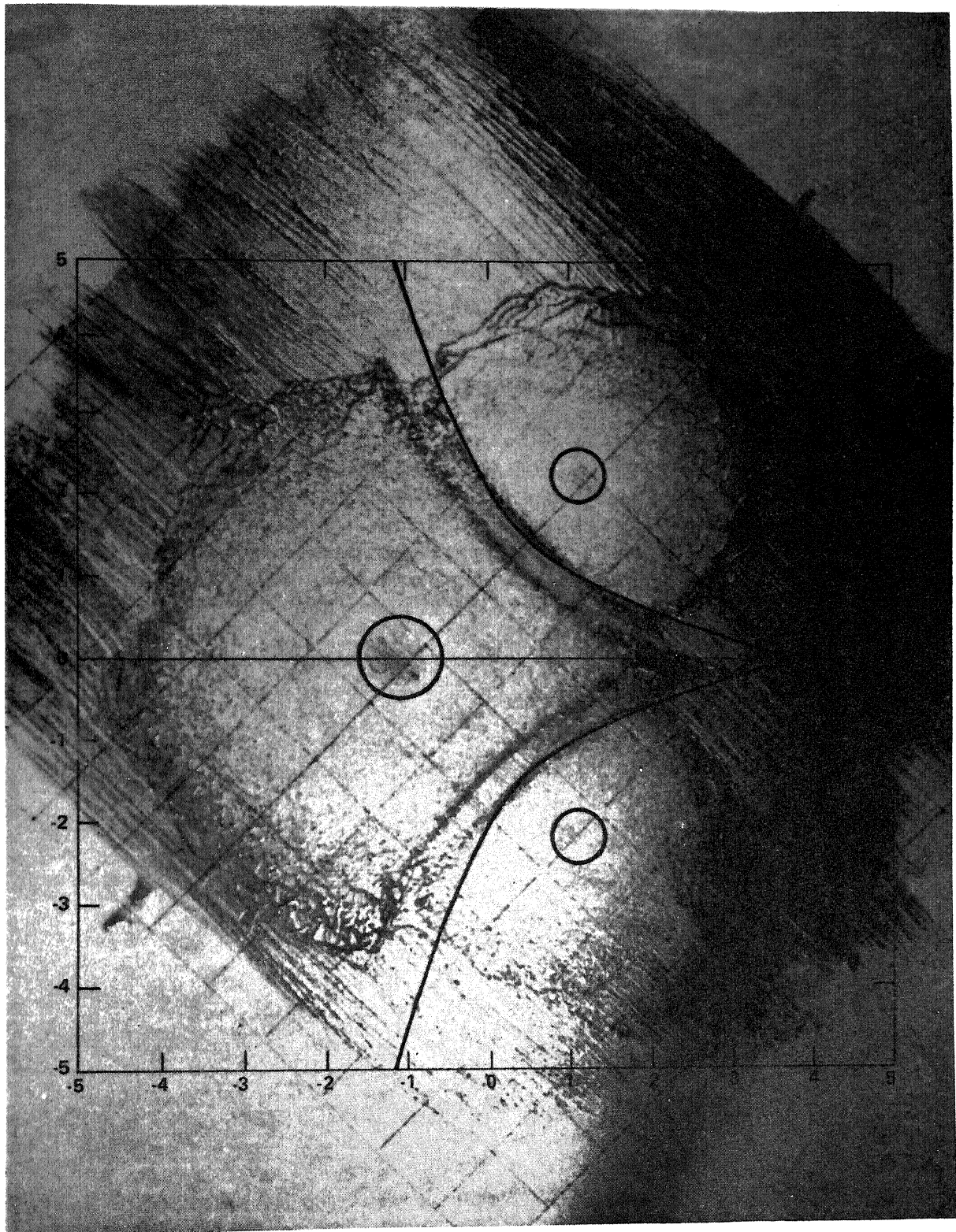


Fig. 12 Three-Jet-Array Ground Plane Oil Flow

CORRELATION OF LOW-SPEED WIND-TUNNEL AND FLIGHT TEST DATA

FOR A VTOL AND STOL AIRCRAFT

David H. Hickey* and Woodrow L. Cook[†]
Ames Research Center, NASA
Moffett Field, California 94035

ABSTRACT

Correlation of wind-tunnel data with flight data is an ongoing process designed to improve and verify wind-tunnel test techniques. One approach, which eliminates such questions as Reynolds number or scale effect in correlations, is to test the actual airplane in the Ames 40- by 80-Foot Wind Tunnel. Results of such correlations on five V/STOL aircraft were presented at an AGARD meeting in 1965.

Since that last report, two additional research aircraft have been tested in the Ames 40- by 80-Foot Wind Tunnel: the XV-5B fan-in-wing aircraft and the YOV-10 RCF (rotating cylinder flap) aircraft. The tests were conducted specifically to provide for correlation between wind-tunnel and in-flight aerodynamics and noise test data. This paper presents the correlation of aerodynamic data and discusses testing techniques that are related to the accuracy of the data or the correlations. Wind-tunnel and flight test data correlated well for both aircraft for unaccelerated flight conditions.

*Assistant Chief, Large-Scale Aerodynamics Branch.

[†]Chief, Flight Research Projects Office.

NOMENCLATURE

A_L	area of V/STOL lifting element, $n(\pi D_L^2/4)$
A_M	momentum area of aircraft, $\pi b^2/4$
A_T	wind-tunnel cross-section area
a	acceleration, g
b	wingspan
b_t	tunnel width
C_D	drag coefficient, D/q_s
C_L	lift coefficient, L/q_s
D	aircraft drag
D_L	diameter of lifting element, fans or propellers
L	lift
N_{down}	aircraft nose down
N_{up}	aircraft nose up
n	number of fans or propellers
q	dynamic pressure
S	wing area
T	fan or propeller thrust
V	velocity
W_F	aircraft weight
α	angle of attack, deg
β_V	fan-louver vector angle, deg
γ	aircraft flight-path angle, deg
δ_e	elevator deflection
δ_f	flap deflection

ΔL lift increment

θ aircraft angle to horizon, deg

Subscripts

a aerodynamic

F flight aircraft

j jet

n normal

s static

t horizontal tail

T wind tunnel

x horizontal

INTRODUCTION

At the Rome AGARD Flight Mechanics Panel Meeting in September 1965, a paper (ref. 1) was presented reporting the correlation of wind-tunnel aerodynamic test data with flight test data for several V/STOL aircraft. Four of the aircraft were tested, both in the Ames 40- by 80-Foot Wind Tunnel and in flight. More recently, additional specific data have been obtained for the XV-5B fan-in-wing aircraft (fig. 1) and the YOY-10 RCF (rotating cylinder flap) STOL aircraft (fig. 2). Although data for the XV-5 have been presented before (ref. 1), the data were questioned because of the necessity for limiting power because of control flexibility. Data from the YOY-10 have also been presented before in reference 2, which reported poor correlation between wind-tunnel and flight longitudinal control requirements. The additional tests were conducted to examine the discrepancies, if any, and, in the case of the XV-5B, to expand the performance envelope of the correlation to descending and decelerating flight.

Specific aerodynamic data test points simulating level flight and decelerating, descending flight conditions for the two aircraft were obtained in the Ames 40- by 80-Foot Wind Tunnel over the low-speed range for correlation with similar flight test points. This approach reduced the interpolation of the data and the reliance on parametric information for correlation purposes. Correlation of the aerodynamic results is presented and some of the problems in correlating wind-tunnel and flight test results are discussed.

CORRELATION OF TEST RESULTS

Table I shows some of the characteristic features (reported in refs. 2, 3, and 4) of the XV-5B and YOY-10 RCF aircraft.

XV-5B V/STOL Fan-In-Wing Aircraft

Tip-turbine-driven 1.1-pressure-ratio fans were used in the XV-5B wings, with each fan providing approximately 6800 lb (3090 kg) of thrust. A similar fan, but with a 3 ft (0.91 m) diameter, was installed in the nose of the aircraft. A thrust reverser in this fan exhaust provided pitch control.

The XV-5B aircraft was mounted in the Ames 40- by 80-Foot Wind Tunnel in the conventional manner, with a tail strut support as shown in figure 3. Wind-tunnel measurements were made of specific flight test points for steady, level flight, and 1-g conditions, and for decelerating flight at 10° descent angle.

Steady level flight. — The results of the wind-tunnel tests, compared to flight test results for several level-flight speed conditions, are shown in figure 4, where aircraft power, angle of attack, and louver angle were set at the same values as during flight test. Longitudinal control was then set to the necessary position for trimmed moment conditions in the wind tunnel, resulting in a measured total lift and drag of the aircraft. Good correlation of stick position for trim conditions was obtained. The results also indicate that the lift in the wind tunnel for the lower speeds, 30 to 70 knots (16–37 m/s), was less than 1% greater than the flight values. However, at 85 knots (43 m/s), the wind-tunnel lift was measured at a value 4.7% greater than the total lift obtained from the flight test results, perhaps this discrepancy was partially due to a known problem with one of the lift recording systems. Although equivalent to a difference in angle of attack of 1.2°, this discrepancy is within the accuracy expected from reference 1. These results may seem surprising in view of rather large wind-tunnel wall correlations predicted for an aircraft of this size in the wind tunnel. However, at these speeds, the aerodynamic lift on a direct lift vehicle such as the XV-5B is a small portion of the total, thus the wind-tunnel wall corrections must be very large to produce significant changes. This point is illustrated in figure 5, where the lift error referenced to aircraft gross weight is shown for two angle-of-attack errors. For the XV-5B at 40 knots (20 m/s), the error must be 5° to provide a total lift error of 4%. Similar results for pitching moment are shown in figure 6. Here, again for the XV-5B, a 10° error in horizontal tail angle of attack is a small portion of the total control available at speeds as high as 60 knots (30 m/s). These results point out that, for direct-lift aircraft flying at low speed, the prediction of overall aircraft performance and control is only slightly effected by wind-tunnel wall corrections.

Descending, decelerating flight. — In figure 7, the wind-tunnel and flight test data for the XV-5B in decelerating, descending flight at $\gamma = -10^\circ$, are compared. Comparisons are shown for longitudinal control-stick position, normal and axial acceleration for the aircraft with the same power conditions, fan exit louver angles, and angle of attack. For these data, the aircraft axis was approximately parallel to the flight path and the aerodynamic lift coefficient was about 0.5. A similar comparison is shown in figure 8 with the aircraft axis approximately horizontal during decelerating approaches at $\gamma = -10^\circ$. The aerodynamic lift coefficient was about 1.2 for the latter approach condition. Good correlation is shown for stick position and normal acceleration with the aircraft deck parallel to the flight path; however, the axial deceleration values measured in the wind tunnel are 0.05 to 0.1 g less (the greater differences occurring at higher forward speeds) than those obtained in flight test for the same power and louver-angle conditions. Some of this difference may be due to the inability to determine strut interference effects, which would have a larger effect on the aerodynamic drag at the high forward velocities. The wind-tunnel support struts were directly in front of the XV-5B landing gear and, hence, could have reduced the gear drag and accounted for part of the deceleration differences.

Better correlation was obtained with the aircraft deck parallel to the flight path and with lower aerodynamic lift coefficient than with the aircraft deck horizontal during the descending flight tests. Normal and horizontal deceleration values measured in the wind tunnel differed by as much as 0.15 g from the flight test results for the latter condition.

YOV-10 RCF STOL Research Aircraft

The YOY-10 RCF aircraft was operated in landing approach up to lift coefficients of about 4.3. The trailing-edge flaps had four 12-in. (0.305 m) diameter rotating cylinders mounted at the forward edge of the flaps. The cylinders were driven by hydraulic turbines at the end of each of the four cylinder sections at speeds of 7500 rpm.

Longitudinal control. — Figures 9 and 10 show the YOY-10 aircraft mounted in the Ames 40-by 80-Foot Wind Tunnel on two separate mounting systems. The mounting system shown in figure 9 was used prior to the flight test, primarily for functional check out, under air load, of such systems as the rotating cylinder flaps, modified propeller, and interconnect systems for the Lycoming T-53 engines. The strut system shown in figure 10 was used specifically for the flight and wind-tunnel test data correlation. As shown in figure 9, the tail strut is mounted on the lower surface of the horizontal tail, fairly close to the quarter-chord point, and could have caused an adverse disturbance in the flow field on the lifting side of the tail where high negative pressure gradients exist. The horizontal tail elevator setting requirements for trim are shown in figure 11, both for the flight results and the tests with the aircraft mounted on the two strut systems. The first wind-tunnel test data show large differences in elevator requirements for longitudinal trim and in static stability compared to flight test results; on the other hand, elevator requirements for longitudinal trim and static stability for the second wind-tunnel test show close correlation with flight test results. The flight test data indicate elevator requirements for trim that fall between uncorrected wind-tunnel data and wind-tunnel data incorporating conventional wind-tunnel wall corrections.

The difference between the first wind-tunnel test and the second wind-tunnel test could have been caused by any one or a combination of three factors. One is the aforementioned effect of interference between the tail strut and the horizontal tail. A second possibility is the different means of taking the wind-tunnel data. In the first test, the data were taken in parametric fashion with reliance on thrust coefficient for correlation with flight test results. In the second test, the wind tunnel was operated to simulate flight; dynamic pressure and propeller blade angle were varied with angle of attack to precisely simulate flight conditions. The third possibility is an error in longitudinal moment arm in the test set up on the first test. No single factor adequately explains the discrepancy between the two wind-tunnel tests, therefore, it seems likely that the discrepancy was caused by a combination of problems.

Lift and drag. — Figure 12 shows flight test and wind-tunnel data for lift, drag, and angle of attack (based on $\alpha = \theta - \gamma$) at given conditions of steady flight and propeller thrust. Good correlation with lift coefficient and angle of attack is shown with the second strut set up; although not shown, good correlation was also obtained with the tail strut mounted at the horizontal tail for all parameters except the previously discussed longitudinal control and static longitudinal stability. Introducing conventional tunnel-wall corrections appears to over correct the data when it is compared with flight test results. As shown in figure 13, the angle of attack, α , measured by the vane on the nose boom, was approximately 6° higher than the angle determined by the $\theta - \gamma$ method; the difference was due to the high upwash effects on the vane at these high lift coefficients. Using this uncorrected vane angle of attack would greatly reduce the correlation.

CONCLUDING REMARKS

Wind-tunnel sizing parameters for testing V/STOL aircraft or models, figure 14, were suggested (ref. 1) for unaccelerated flight conditions. The XV-5B and YOY-10 aircraft were sized within the test parameters shown in the figure. The size of the aircraft, span-to-tunnel width, the lifting element area, and the momentum area parameters appear to be reasonable, based on the correlation results for level, unaccelerating flight test conditions of these types of V/STOL aircraft in the 40- by 80-Foot Wind Tunnel. Although the measurements made for decelerating, descending flight were less conclusive, it appears that if all factors (such as strut interference drag effects) could be accurately accounted for, fairly good prediction of flight-path descent angle, power requirement, deceleration, and vectoring requirement could be made from wind-tunnel test results with models sized within the parameters outlined in reference 1.

REFERENCES

1. Hickey, David H.; and Cook, Woodrow L.: Comparison of Wind-Tunnel and Flight Test Aerodynamic Data in the Transition Flight Speed Range for Five V/STOL Aircraft. AGARD Report 520, 1965. (Also available in Conference on V/STOL and STOL Aircraft, NASA SP-116, 1966.)
2. Gerdes, Ronald M.; and Hynes, Charles S.: Factors Affecting Handling Qualities of a Lift-Fan Aircraft During Steep Terminal Area Approaches. Presented at the 27th Annual National V/STOL Forum of the American Helicopter Society, May 1971.
3. Cichy, D. R.; Harris, J. W.; and Mackay, J. K.: Flight Tests of a Rotating Cylinder Flap on a North American YOY-10 Aircraft. NASA CR-2135, Nov. 1972.
4. Weiberg, J. A.; Giulianetti, D.; Gambucci, B.; and Innis, R. C.: Takeoff and Landing Performance and Noise Measurements of a Deflected Slipstream STOL Airplane with Interconnected Propellers and Rotating Cylinder Flaps. NASA TM X-62,320, Dec. 1973.

CHARACTERISTICS	XV-5B	YOV-10 RCF
GROSS WEIGHT, lb (kg)	12,100 (5500)	11,700 (5320)
WING AREA, ft ² (m ²)	260.3 (24.17)	244 (22.67)
WING SPAN, ft (m)	29.8 (9.07)	34.0 (10.36)
FAN OR PROPELLOR DIAMETER, ft (m)	5.16/3.0* (1.574)/(0.915)	9.42 (2.87)
T/W RATIO, UNINSTALLED	1.25 (TOTAL)	0.45
FAN PRESSURE RATIO	1.1	—
ROTATING CYLINDER, RPM/HP	—	7500/30
DIAMETER, ft (m)	—	1.0 (0.305)
APPROACH VELOCITY, knots	100 → 0	57.0
APPROACH C _L	V/STOL	4.3
APPROACH γ, deg	-10 to -20	-3 to -8
SIDELINE NOISE LEVEL, PNdB (500 ft [152.5m])	113	99
TAKEOFF LANDING	112	93

*WING FAN/NOSE FAN DIAMETERS

TABLE 1. RESEARCH AIRCRAFT CHARACTERISTICS



Fig. 1

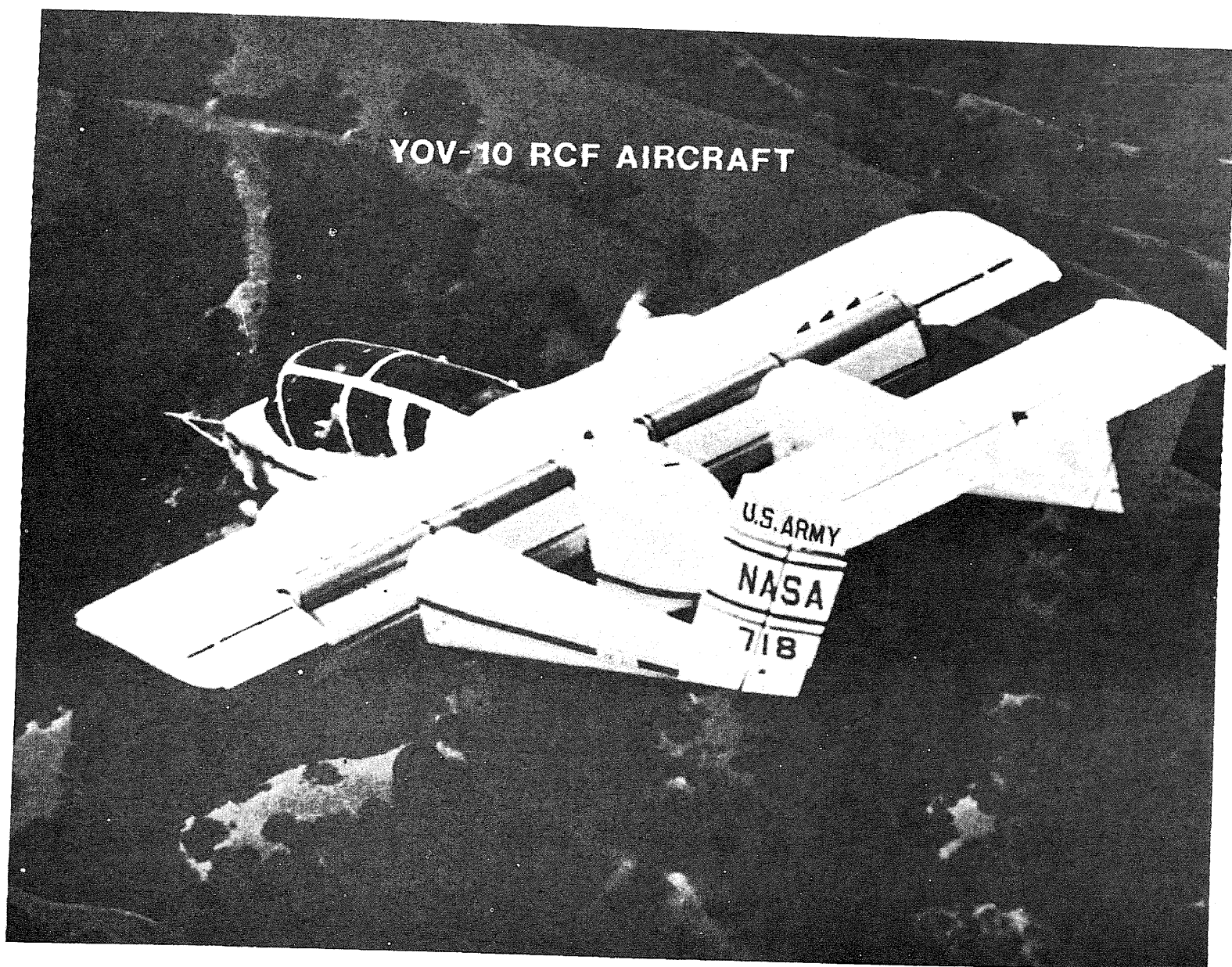


Fig. 2



Fig. 3

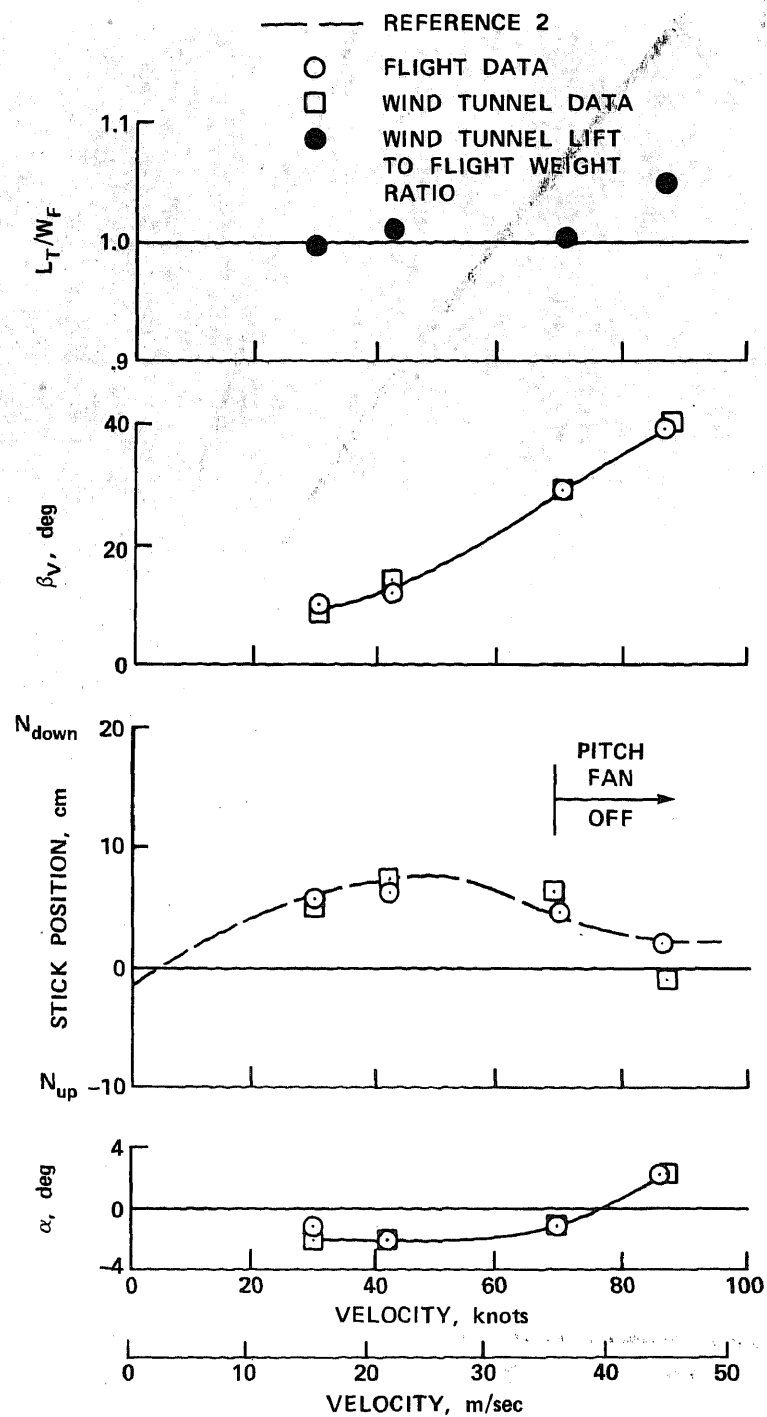


Figure 4.— Comparison of XV-5B flight and wind-tunnel data for level-flight conditions.

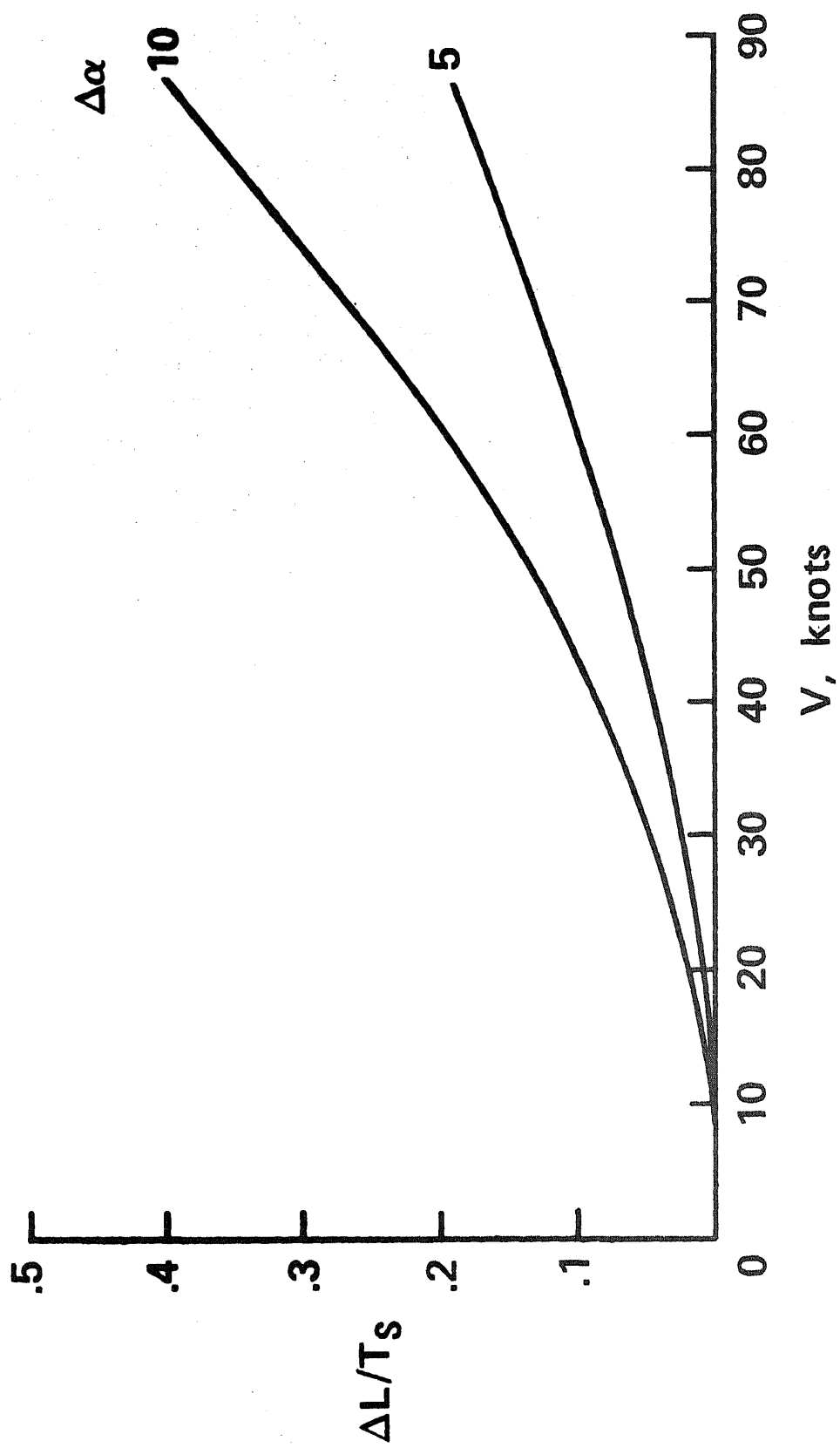


Figure 5.— Effect of error in angle of attack on lift-thrust ratio for the XV-5B.

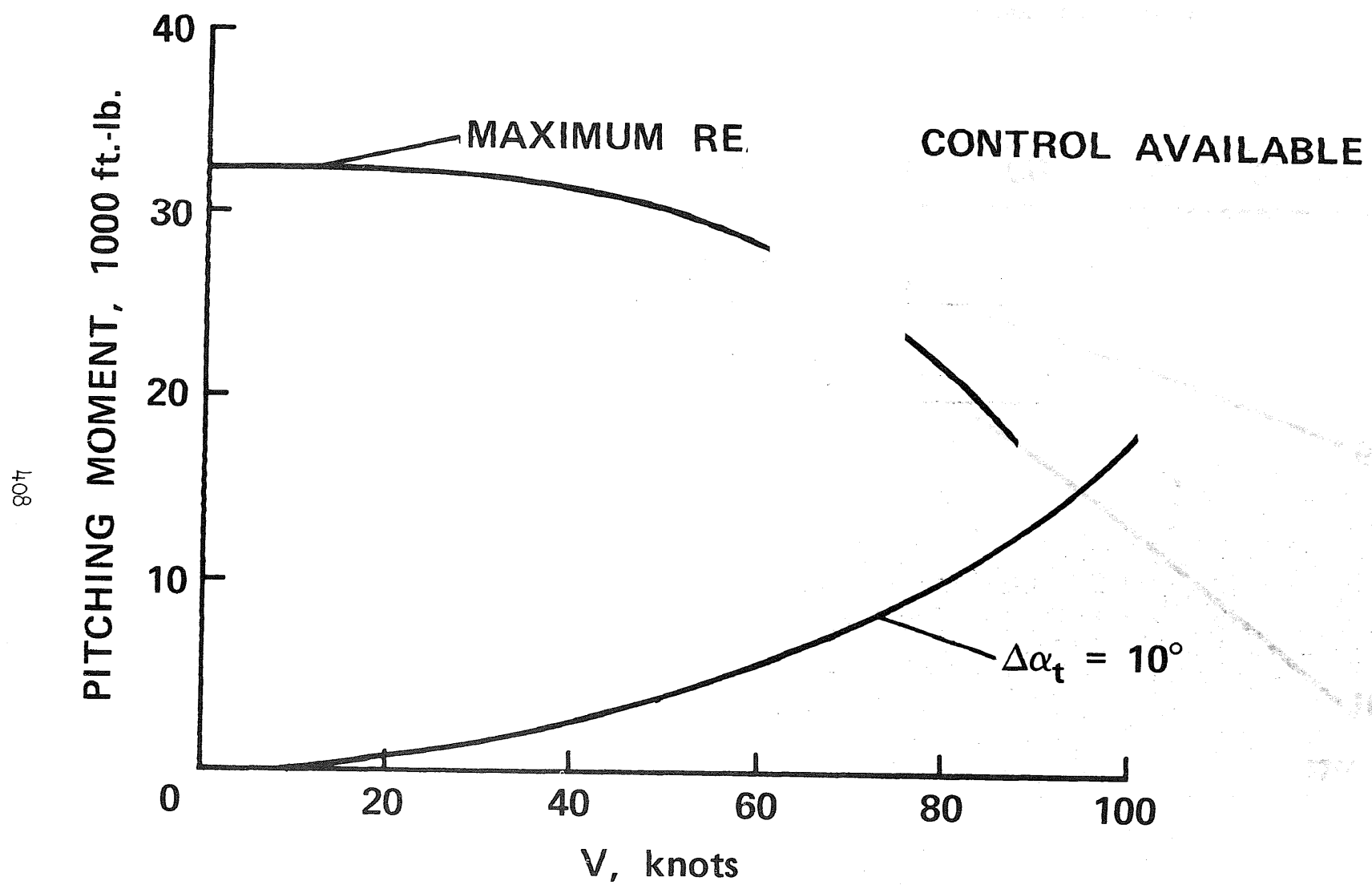


Figure 6.— Comparison of longitudinal reaction control power with aerodynamic control power.

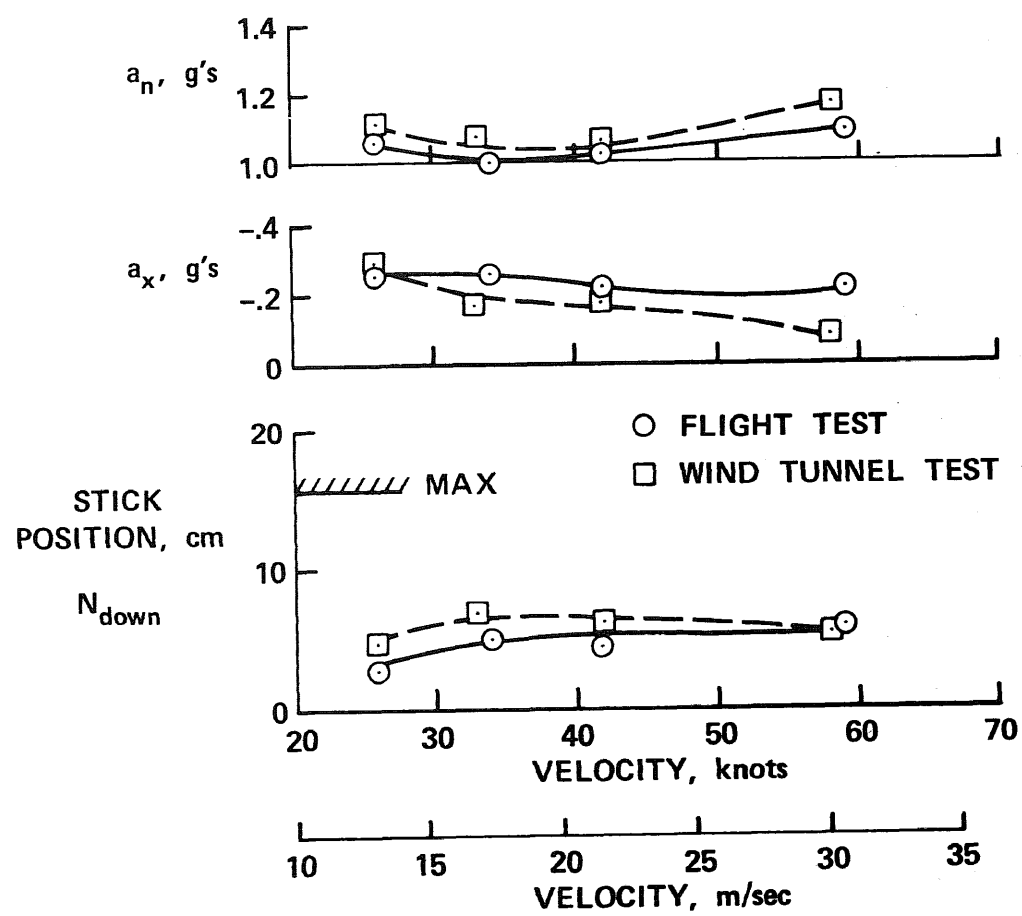


Figure 7.— Comparison of XV-5B decelerating descent data at $\gamma \cong -10^\circ$ for aircraft deck parallel to flight path, with $C_{L_2} \cong 0.5$.

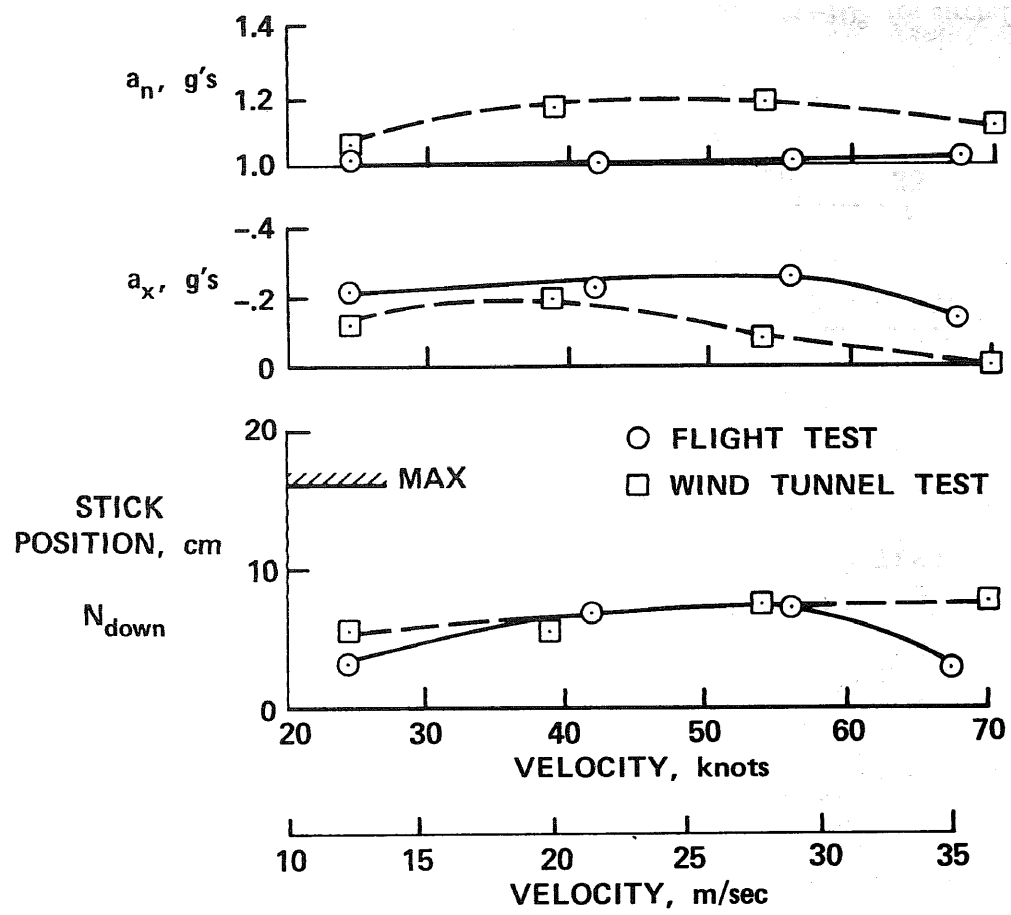


Figure 8.— Comparison of XV-5B decelerating descent data at $\gamma \approx -10^\circ$ for aircraft deck horizontal, with $C_{L_\alpha} \approx 1.2$.

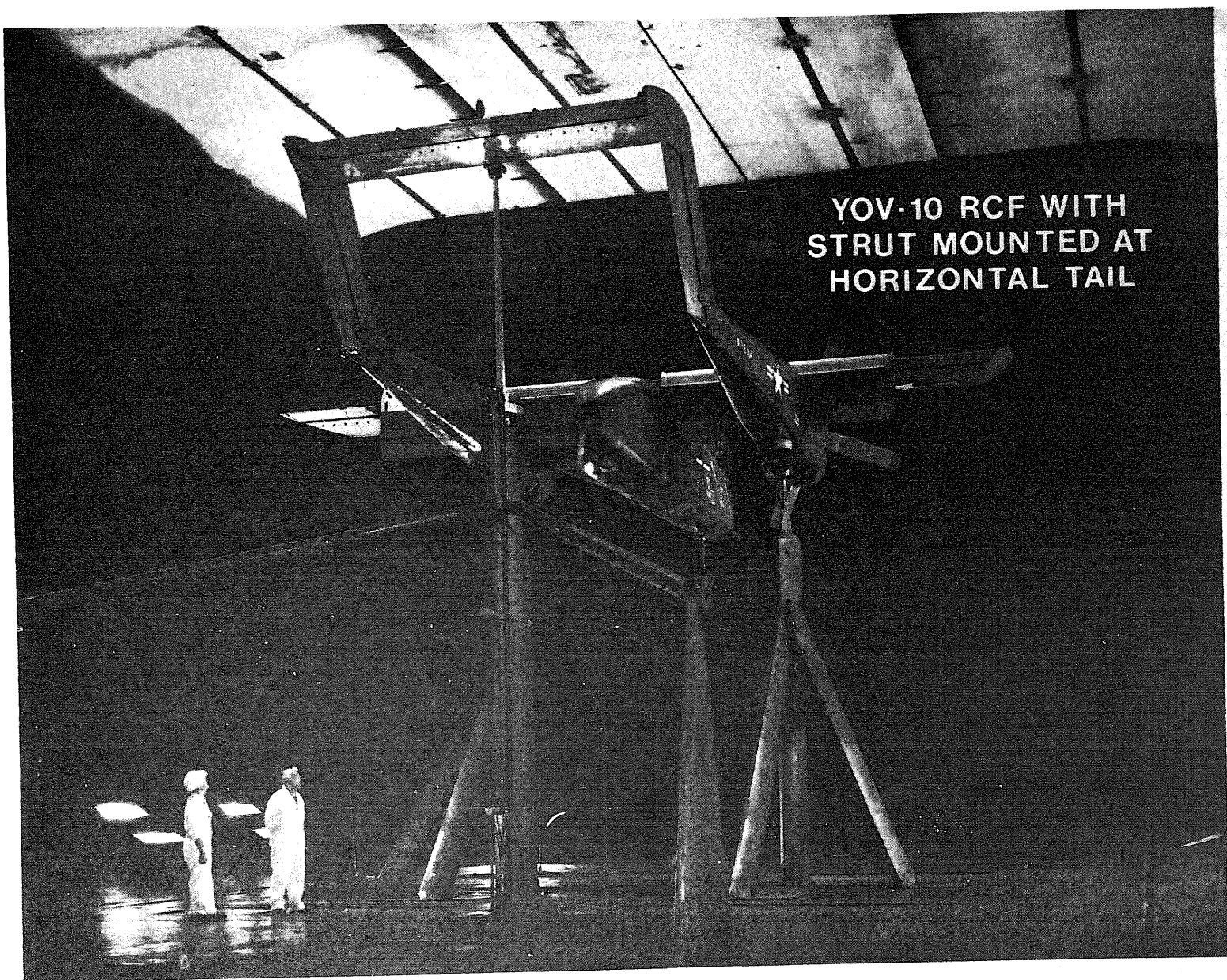


Fig. 9

YOV-10 RCF WITH STRUT MOUNTED AT
FORWARD FUSELAGE

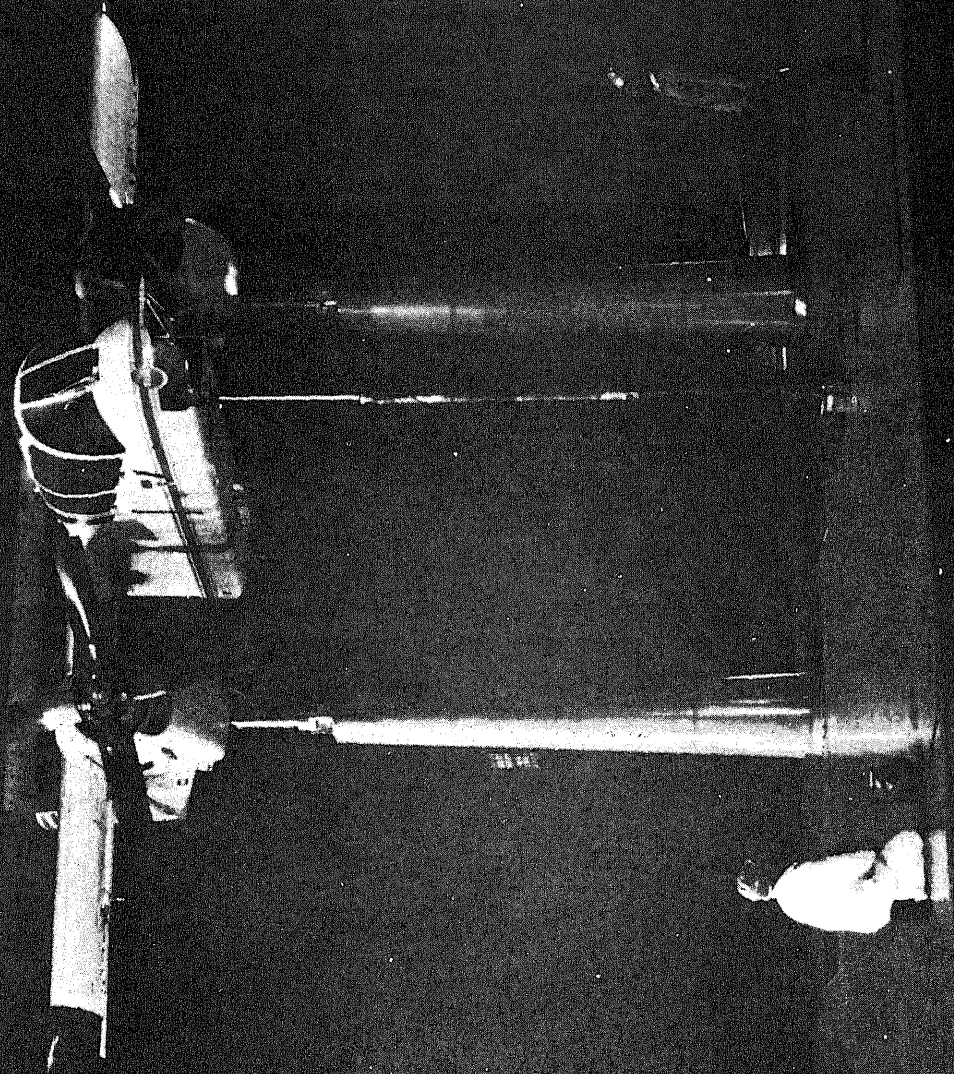


Fig. 10

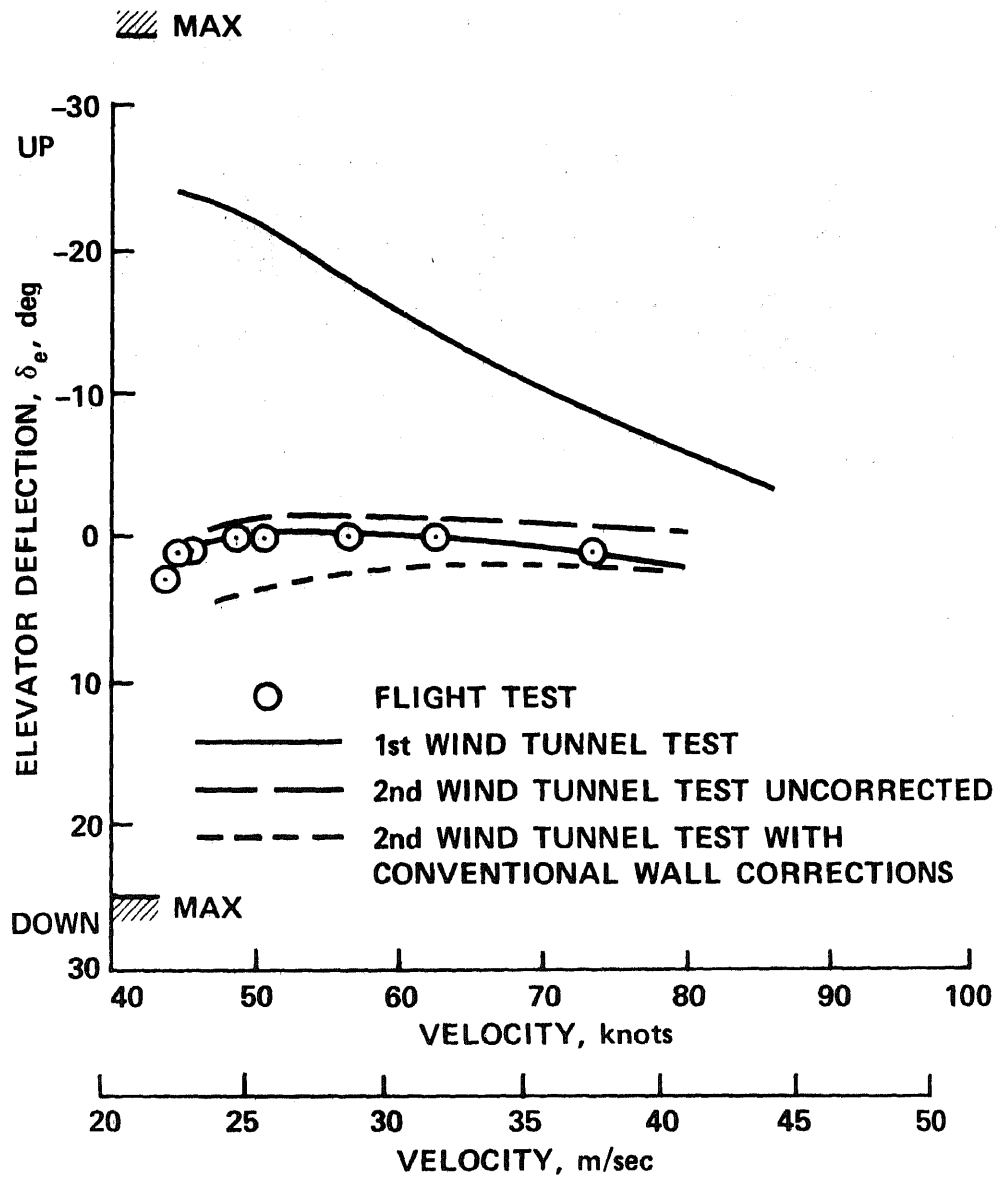


Figure 11.— Comparison of flight and wind-tunnel measured elevator deflection for trim YOY-10 RCF aircraft, with $\delta_f = 50/25$.

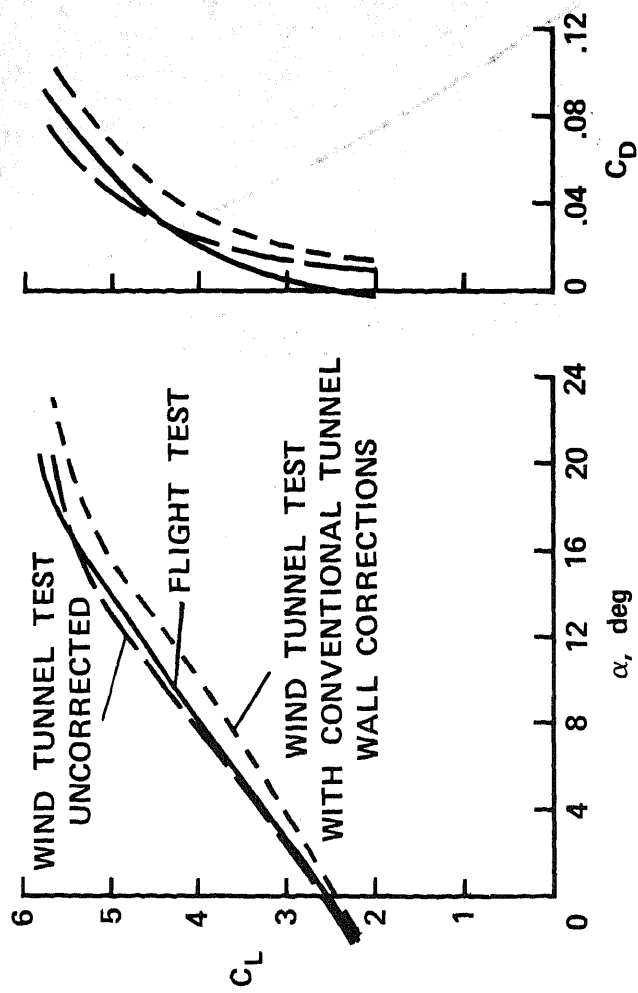


Figure 12.— Comparison of flight and wind tunnel measured lift and drag data for YOY-10 RCF aircraft, with $\delta_f = 50/25$.

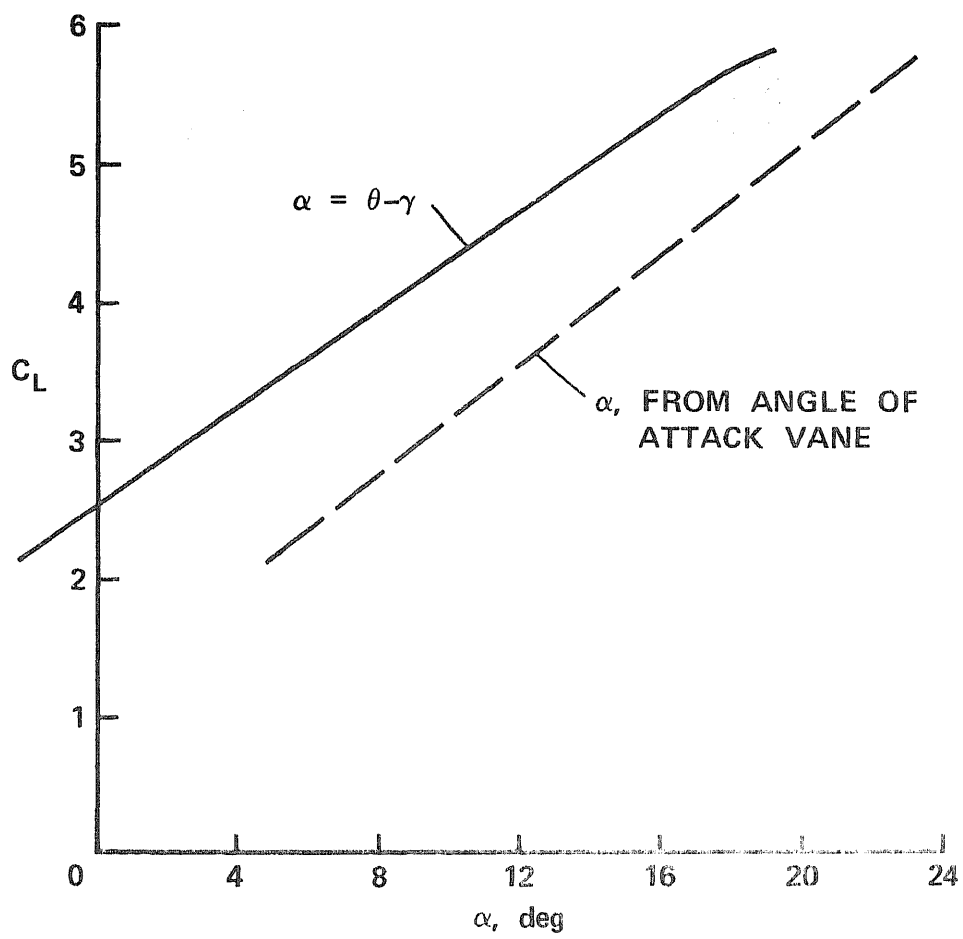


Figure 13.— YOY-10 RCF STOL aircraft upwash effects on angle of attack vane, with $\delta_f = 50/25$.

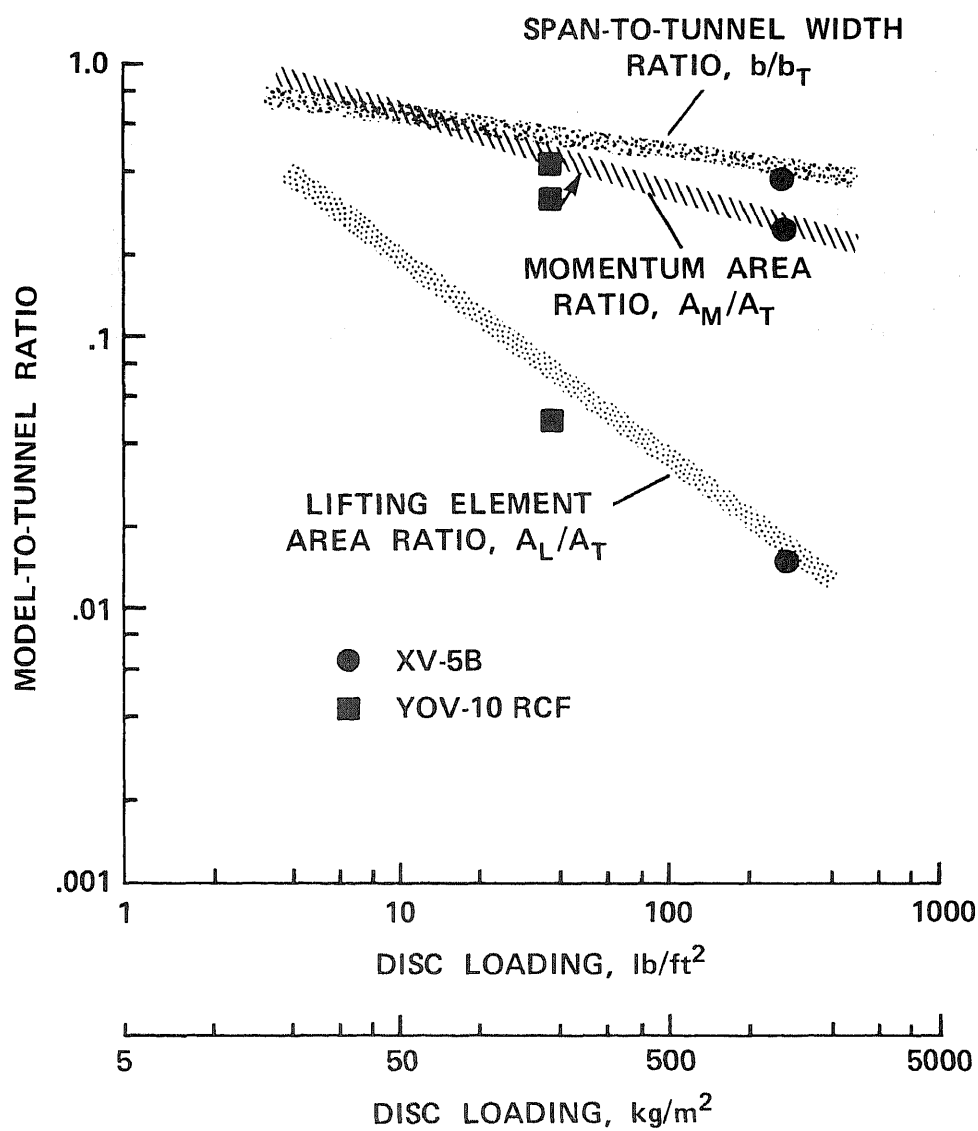


Figure 14.— Three model-to-wind-tunnel sizing parameters.

GROUND PLATFORM THERMAL FOOTPRINTS FOR VTOL AIRCRAFT

A. L. Rosenblatt
Grumman Aerospace Corporation
Bethpage, New York 11714

ABSTRACT

A self-plotting computer program has been developed to generate the nonsteady generalized ground platform temperature distributions resulting from impingement of engine exhaust gasses during VTOL operation. The program handles operations consisting of: ground idle, power advance, takeoff, hover, descent, power reduction, and shutdown. The duration of any of these stages can be changed or eliminated. The program contains a nodal map of the platform area under and beyond the aircraft. Separate prediction methods are used to provide local total temperature and velocity of the exhaust gas at each node (i.e., ground footprint) as well as thermal properties of the platform. Heat transfer coefficients and recovery temperatures are calculated, and a thermal balance performed to obtain platform isotherms at selected time intervals. Typical results are displayed for a lift-plus-lift/cruise configuration that depicts the effect of VTOL procedures on the platform temperature distribution.

SUMMARY

For jet-lift VTOL aircraft, the ground platform temperatures may be severe. The prediction of these platform temperatures, thermal gradients, and presentation of results is very time consuming and laborious. This paper describes a computer program that minimizes the time and effort needed to calculate these temperature profiles, and provides automatic plotting of the footprints at selected time increments.

The program was applied to Design 623 (one lift engine and two lift/cruise engines) operating from a 3/4-in. steel deck. Peak temperatures depend on takeoff and landing procedures and ground idle time. For example, increasing lift engine idle time on Design 623 (from 1 to 6 min) increases the peak deck temperature from 480 to 910°F. The computer program described can be applied readily to other platforms and other operating procedures.

DISCUSSION

The entire routine presented here is the adaptation of five existing Grumman thermodynamic programs, tied together with the necessary algorithms.

To allow flexibility, the procedure is not completely automated. When a particular aircraft design/platform configuration combination is being investigated, the necessary modifications can be readily written to have an automated program extending from inputs of impingement gas total temperature and velocity at each node to outputs of plotted platform isotherms.

The procedure can handle operations consisting of ground idle, power advance, liftoff, hover, descent (abort), power reduction, another ground idle, and shutdown. Any of these stages can be eliminated, or its duration changed. The following severe operation is used to exemplify the calculation results:

<u>Stage</u>	<u>Duration</u>
● Idle (lift engine at 45 deg and lift/cruise engines straight aft)	6 min
● Advance to VTO power and rotate all engines straight down	3 sec
● Ascend to 25 ft	5.6 sec
● Hover	1 min
● Descend	10 sec
● Reduce power	3 sec
● Idle (as above)	1 min
● Shutdown	

These conditions represent an aborted landing, over the same spot, with a large amount of idle time. Wind effects were also neglected.

DESCRIPTION OF ANALYSIS

The analysis is based on a Grumman Design 623 VTOL aircraft on a 3/4-in. steel deck. Figure 1 shows an outline of the aircraft superimposed on the deck nodal network. The lift engine impinges on node 9 during VTO. Exhaust total temperatures are 1060°F for idle and 1920°F for VTO. The lift/cruise engine, pointed straight aft during idle, does not impinge on the platform; during VTO it impinges on node 158 with a total temperature of 3040°F.

The plume ground pattern (total temperature and velocity) was derived from the work described in Ref 1. The test results are presented by W. Barron and H. Frauenberger elsewhere in this workshop. The convective rates for the stagnation area are taken from Heat Transfer by Chapman; for the flat plate areas the Bell curves were used. These were compared to the results described in Ref. 2; the agreement was within 6%.

RESULTS OF ANALYSIS

The results of the analysis are presented in the form of footprints at selected time slices. Figure 2 shows the platform thermal footprint at the end of the 6-min ground idle (preflight check). The hottest point is not at the engine locations because lift engine is pointed aft 45, deg and the lift cruise engine plume is not impinging on the platform. The maximum temperature occurs on node 9. Since the isotherms are at 50°F intervals, and due to the coarseness of the nodal grid, the footprint plot may not record the peak temperatures: however, it locates the hottest nodes and these can be examined from Calcomp plots, such as Fig. 3, which shows the temperature-time history of node 9 for the total mission. Good agreement is found with the footprint in this case; it shows 910°F as the peak temperature. It is interesting to examine the local recovery temperature on this node. During the ground idle, the plume impinges directly on this node at a temperature of 1040°F; when the power is raised and the

plume rotated, the direct impingement moves to node 1. At this time the local recovery temperature reduces and levels off at 380°F, during hover. During descent and rotation of the plume back to idle position, the plume temperature at this node rises to the original idle value, and exists until shutdown.

It should be pointed out that the bump that appears in the 150°F isotherm near the wing trailing edge (half-way out) is due to noise in the plotting routine. An investigation was made to ensure that this was not due to the heat transfer analysis. This bump will be seen to persist in later footprint plots. Some of the waviness is also due to noise in the plotting program.

Most of the platform reaches its maximum temperature at touchdown. Figure 4 shows the footprint at this instant. Three hot spots are centered around nodes 1, 9, and 158. For direct (90 deg) impingement, the stagnation nodes do not become the hottest; in this case, they are 2, 9, and 157 shown in Fig. 5 for the entire mission. Comparing Fig. 4 and 5, observe that for nodes 2 and 9 (Stations 311 and 405) the footprint agrees well with the node plots, but at node 157 (Station 526.5) the footprint nodes were too coarse to record the 700°F maximum shown on the node plot.

The differences in shapes of the curves in Fig. 5 are due to the motion of the impinging jets. The recovery temperature for node 157 is shown with the temperature response for that node in Fig. 6; comparing the recovery temperatures in Fig. 6 with that of node 9 in Fig. 3 indicates the reason for the differences in shapes of the nodal responses.

Figures 7 and 8 show the platform temperature at 5.24 and 10.6 min after touchdown. Note that the massive steel deck cools slowly.

The study was expanded to examine the more normal situation of no abort. Figure 9 shows maximum footprint temperatures for this operation. The temperature histories of the hottest nodes are given in Fig. 10.

Comparing Fig. 10 with 5, note that since the ground idle check time is still 6 min, the maximum temperature of 910°F is the same; however, the temperatures of the deck under the lift/cruise engine and the lift engine have been reduced from 700 to 480°F and 410 to 240°F, respectively.

The next alteration of the program reduced the ground idle time to 1 min (considered by some to be more practical). This is also a no-abort case. The results of this analysis are shown in the footprint, Fig. 11, and the time history in Fig. 12. Here, node 9 is reduced significantly to 445°F, and the lift/cruise and lift engine areas are reduced to 310 and 182°F, respectively.

CONCLUSION

The results presented in this paper show that the operational procedures have a dominant effect on platform temperatures.

The highest-temperature spot could be reduced readily by moving the aircraft a few feet periodically or by changing its heading. In regard to the other hot areas, if the aircraft did not take off and descend over the same spot, these temperatures would also be reduced.

Recent test data show that, from the standpoint of engine ingestion, it is advantageous to have a small forward velocity. This also reduces platform temperatures.

It is concluded, therefore, that the deck temperatures are very much a function of operational procedures, and with proper control of these procedures exhaust gas temperatures as high as 3000°F can be utilized for VTO aircraft.

REFERENCES

1. Gray, Kisielowski, "Practical Engineering Methods for Predicting Hot Gas Reingestion Characteristics of V/STOL Aircraft Jet-Lift Engines," NASA-CR 111845, 1971.
2. Donaldson, Snedeker, and Margolis, "A Study of Free Jet Impingement, Part 2, Free Jet Turbulent Structure and Impingement Heat Transfer", Journal Fluid Mechanics (1971), Vol 45, pp 477-512.

ACKNOWLEDGEMENT

The author acknowledges the major contributions made to the creation of the program described in this paper by the following personnel of Grumman's Thermodynamics Section: R. Bocchicchio, J. Palmieri, and Dr. K. Rathjen.

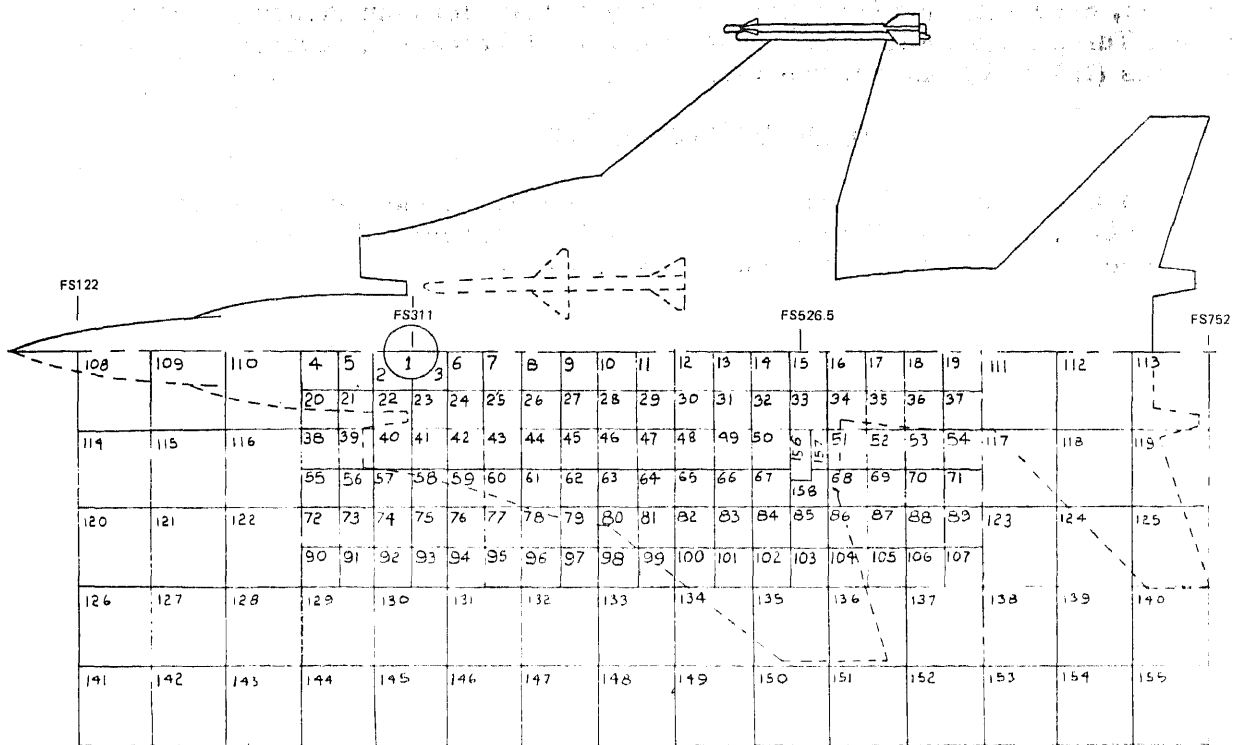


Fig. 1 Platform Nodal Pattern, Design 623 Model

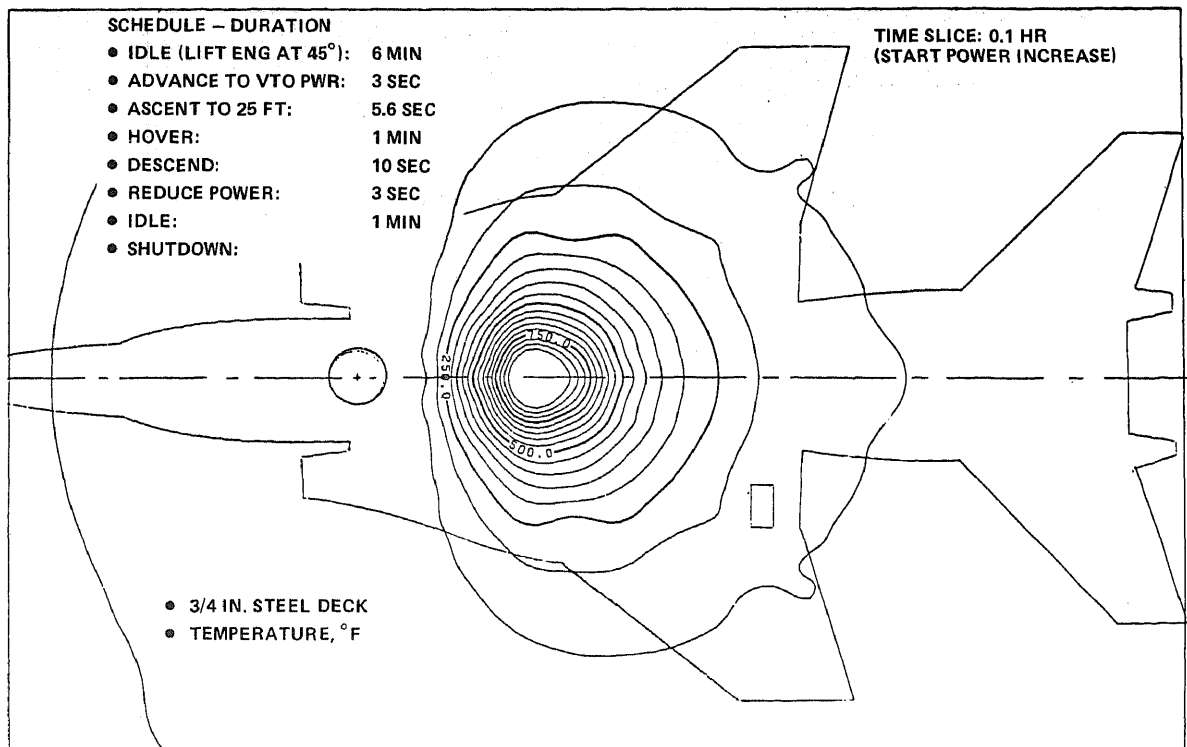


Fig. 2 Platform Temperatures, Design 623 Model

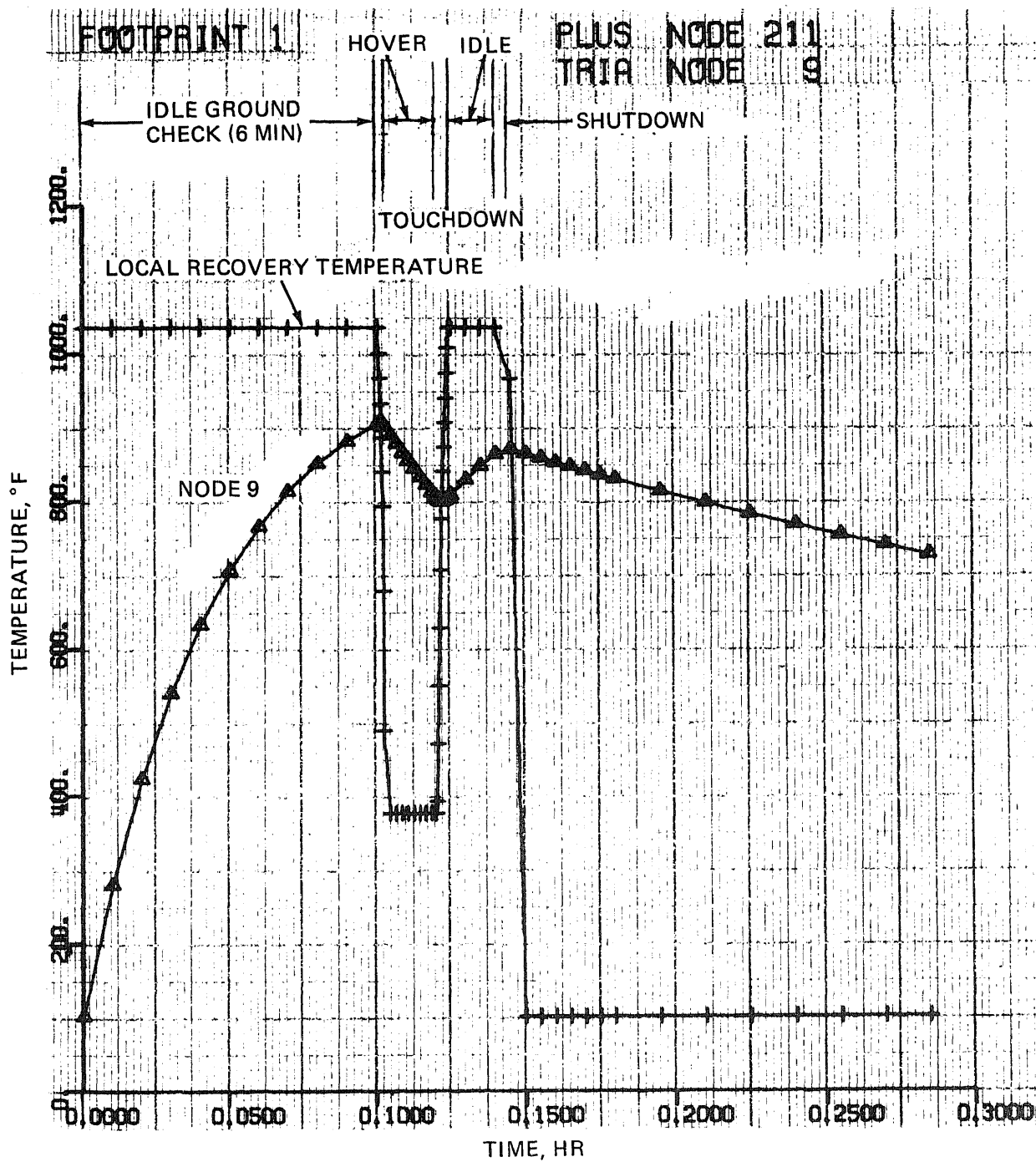


Fig. 3 Node 9 Time-Temperature History

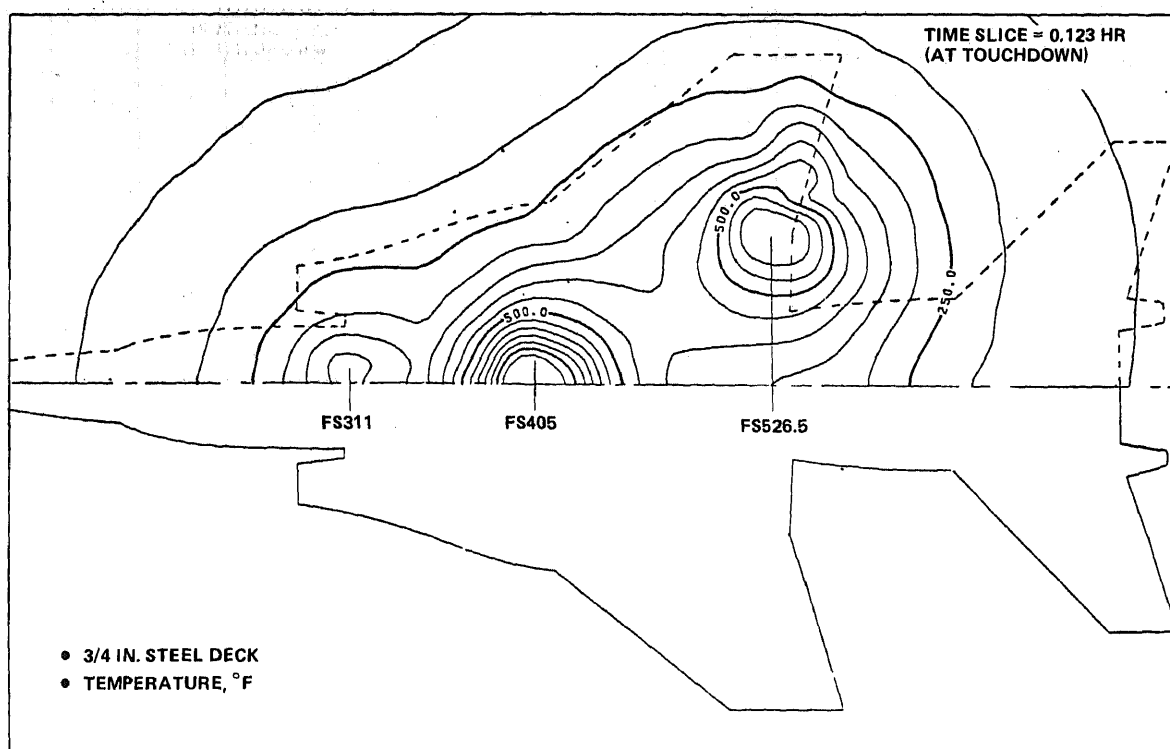


Fig. 4 Platform Temperatures, Design 623 Model

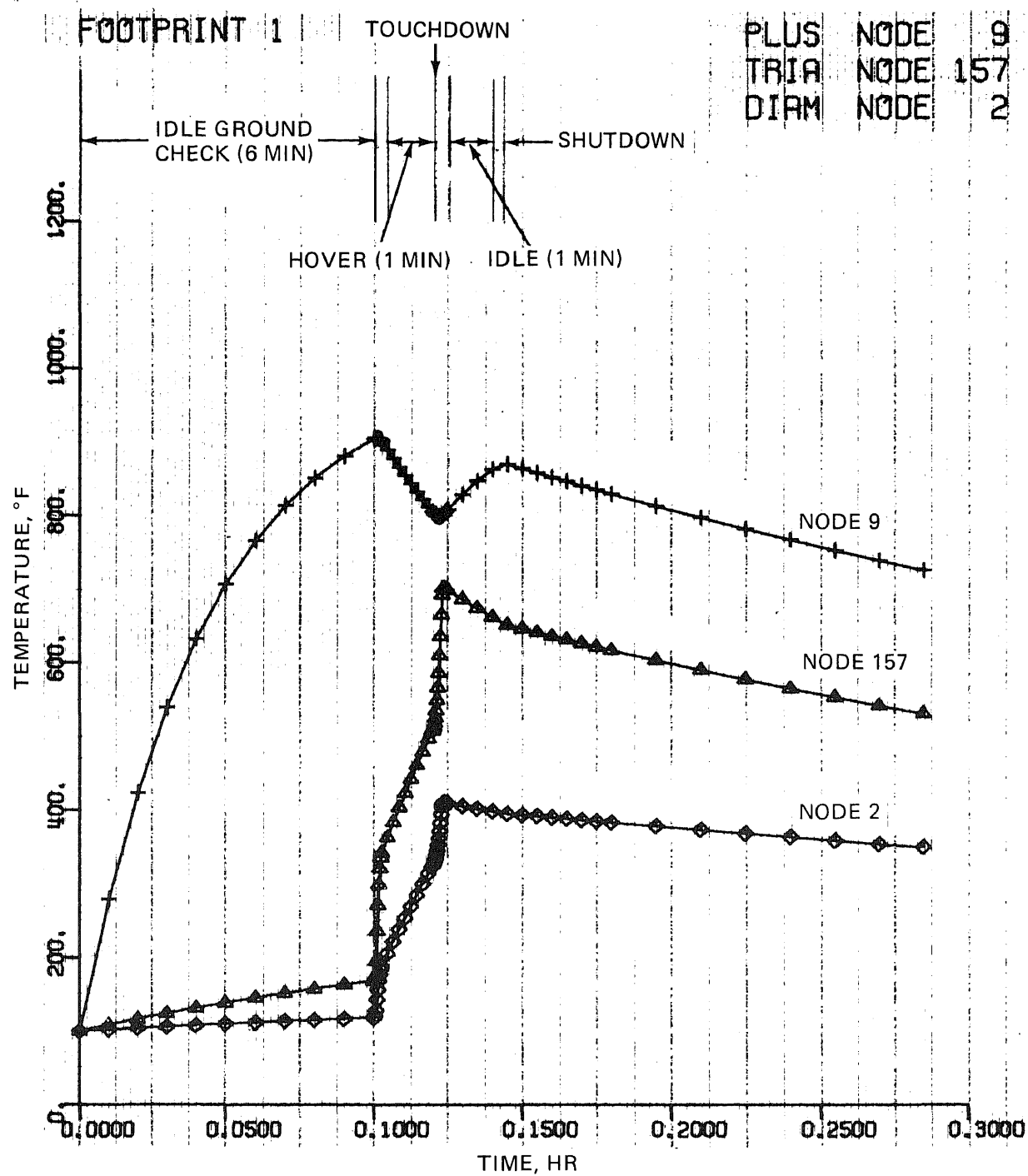


Fig. 5 Stagnation Nodes 2, 9 & 157

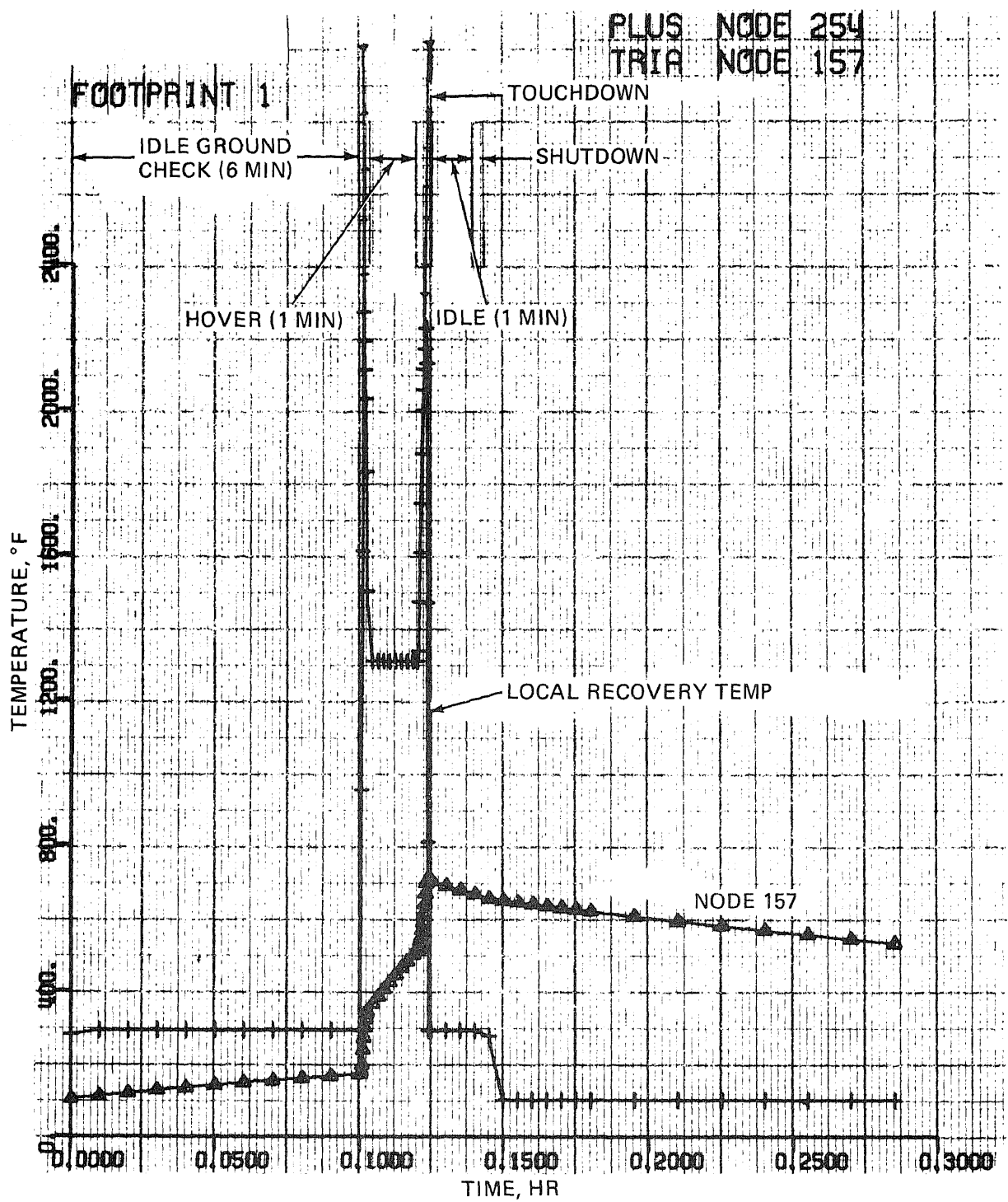


Fig. 6 Node 157 Recovery Temperature & Response

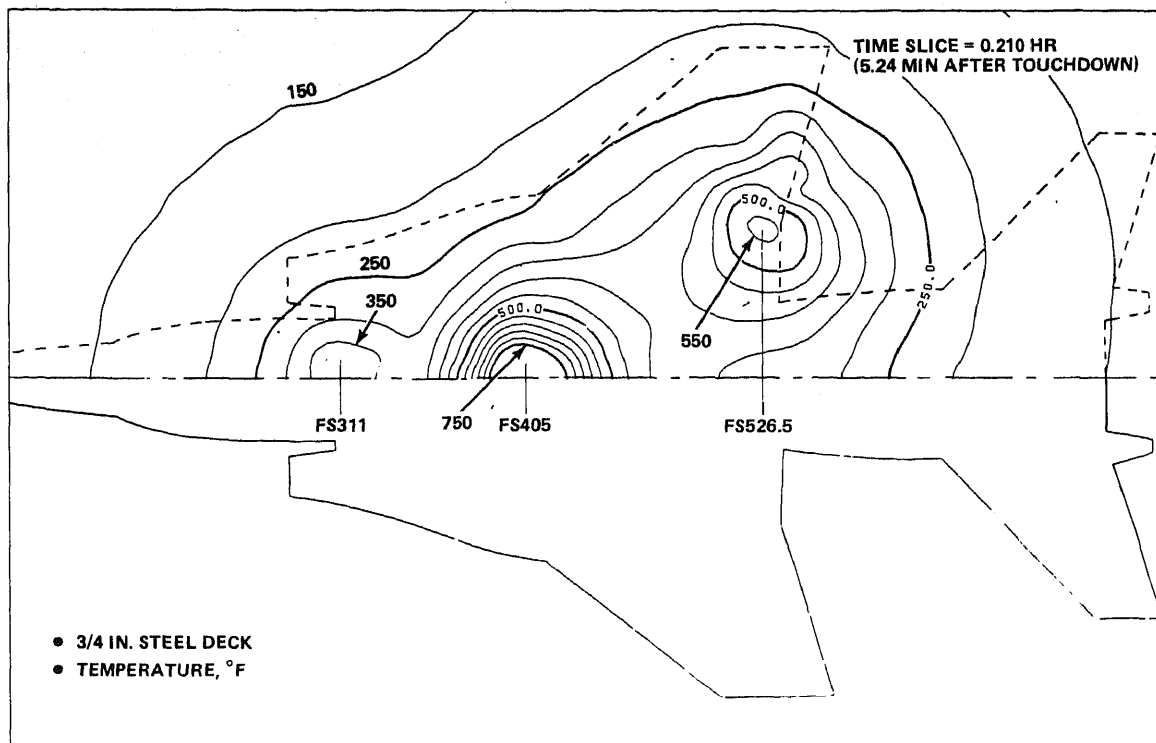


Fig. 7 Platform Temperatures, Design 623 Model

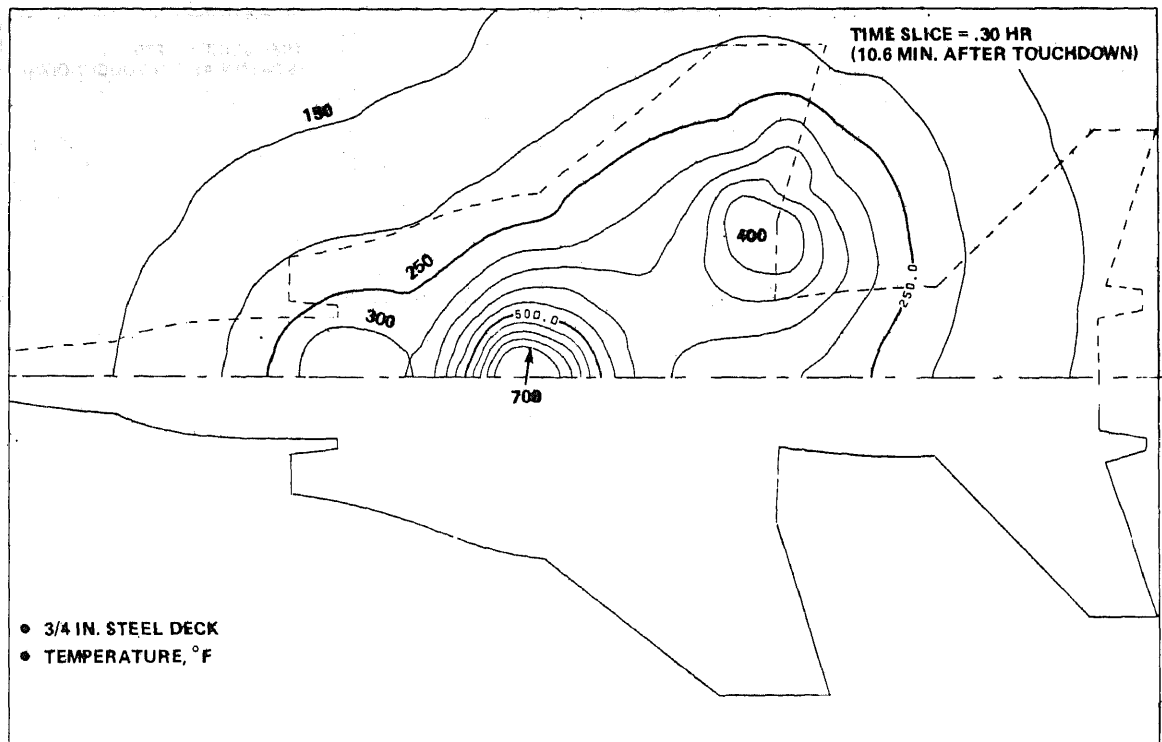


Fig. 8 Platform Temperatures, Design 623 Model

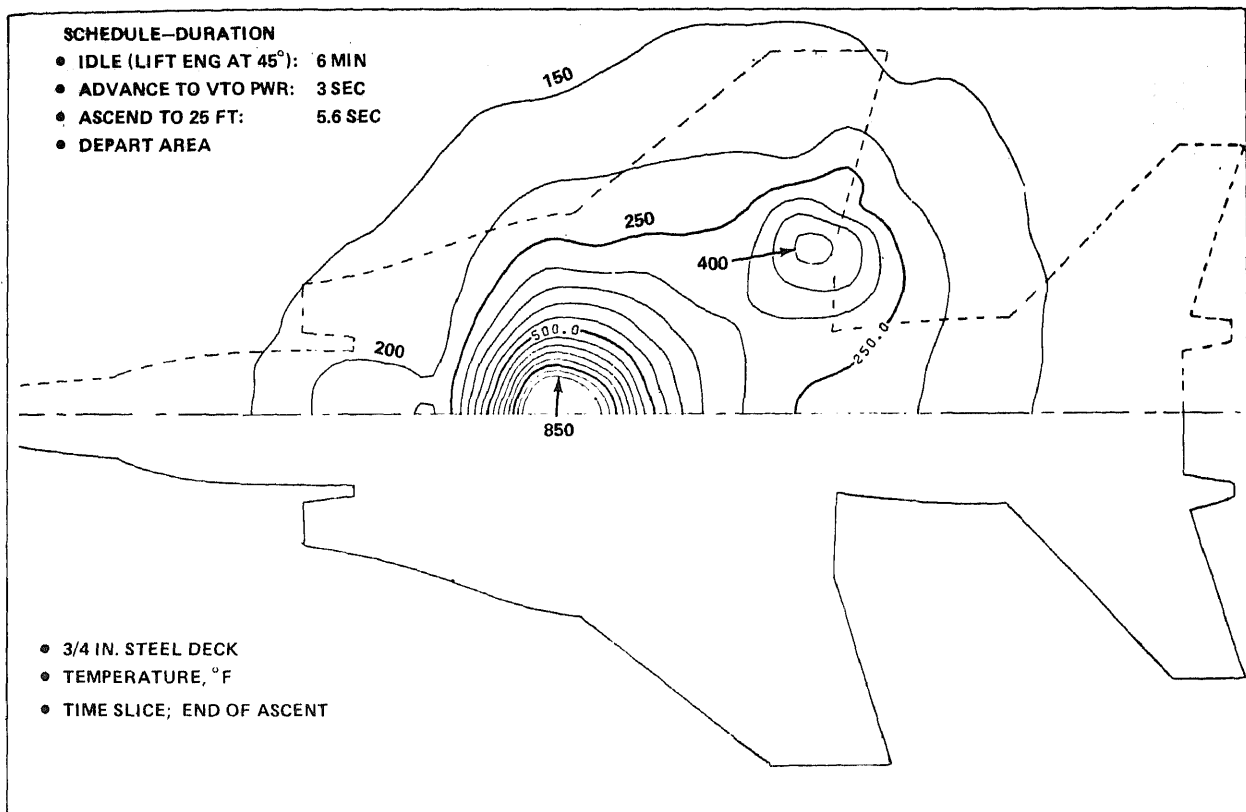


Fig. 9 Platform Temperatures, Design 623 Model

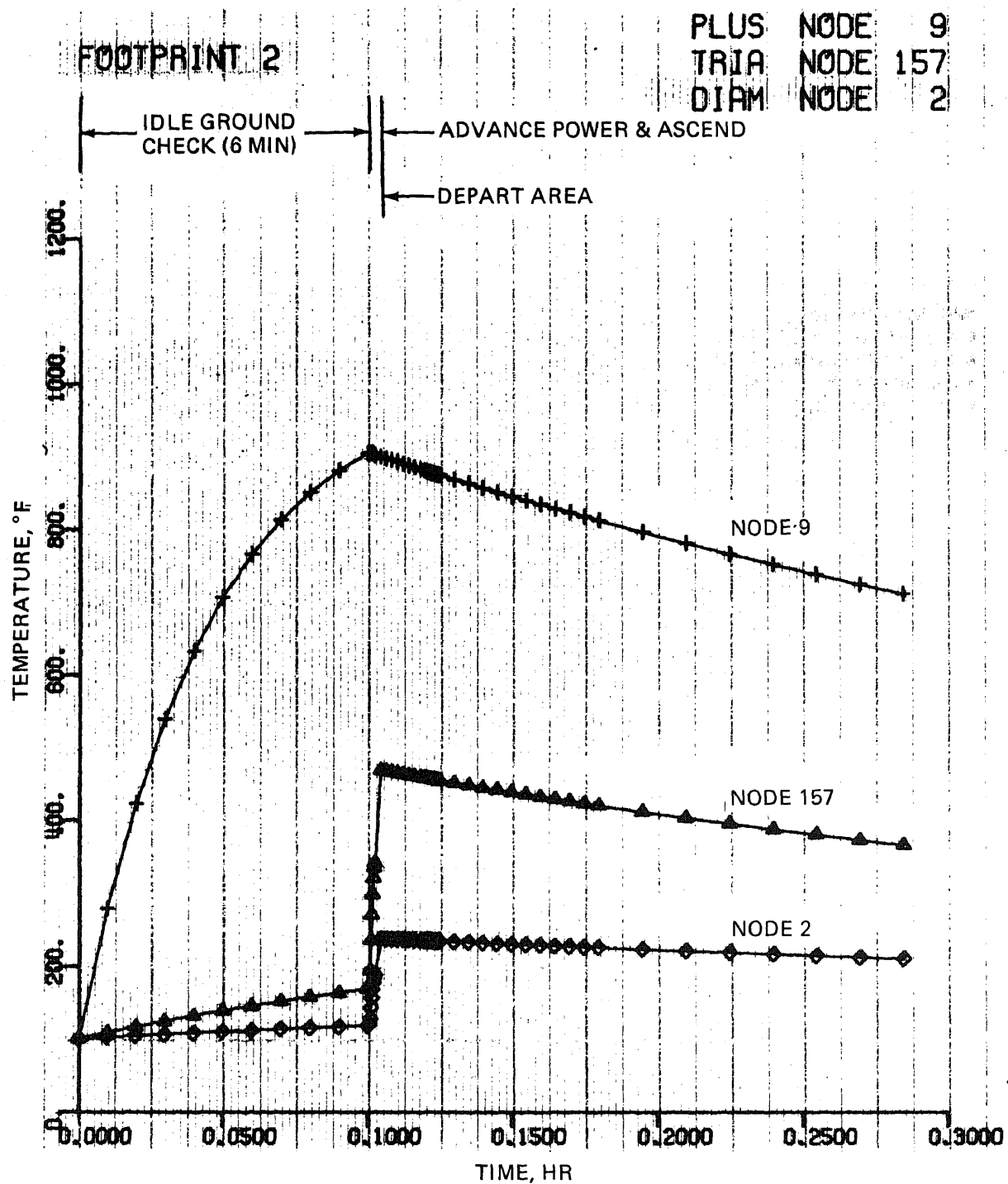


Fig. 10 Nodes 2, 9 & 157 Temperature Histories

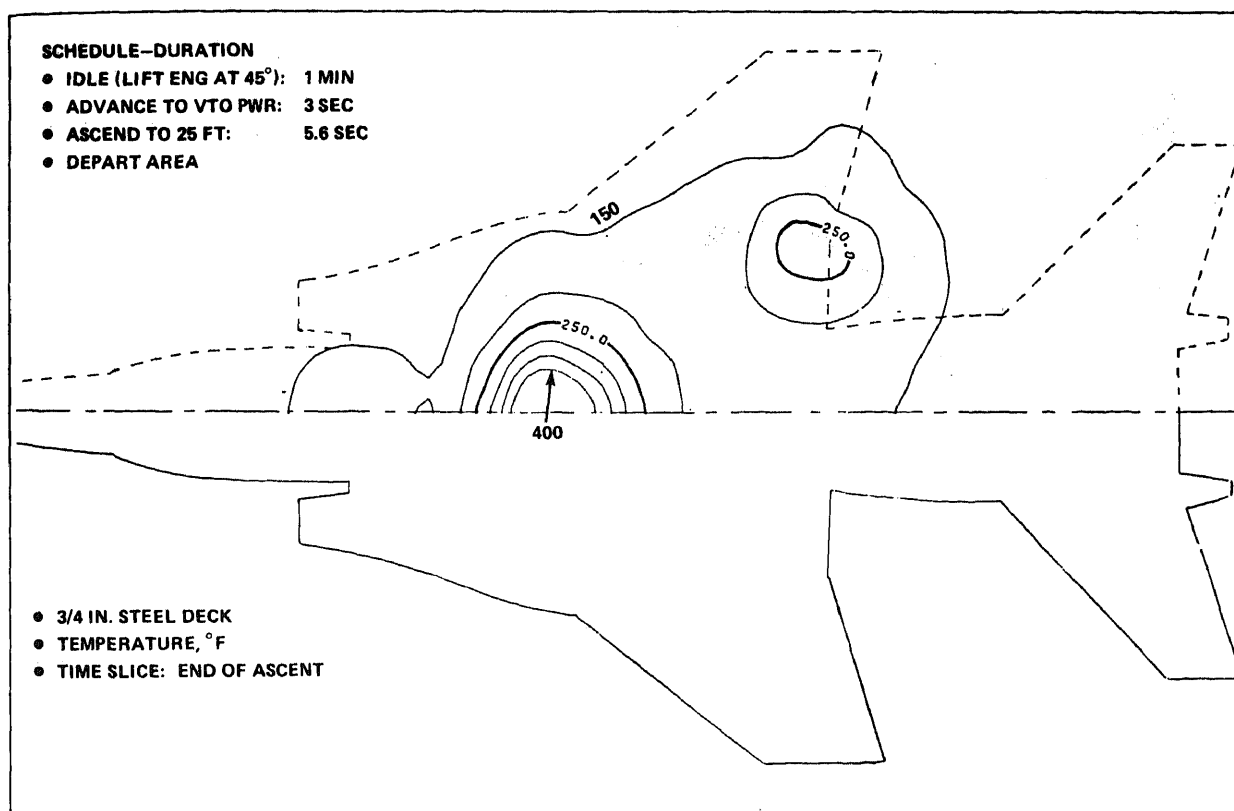


Fig. 11 Platform Temperatures, Design 623 Model

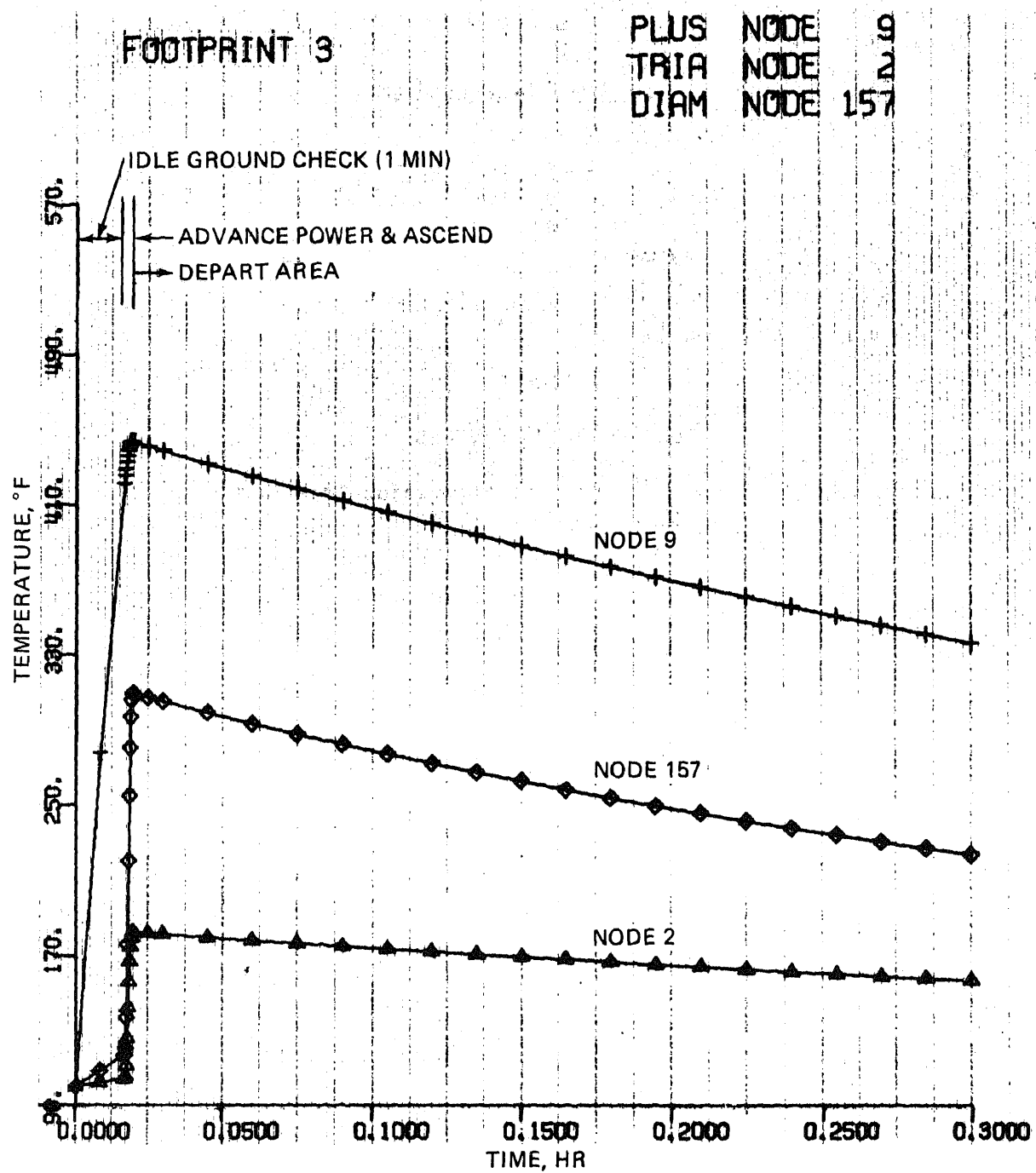


Fig. 12 No-Abort Time History

Session E

FLOW VECTORING DEVICES

Chairman: J. Curry, Naval Air Propulsion Test Center

DEVELOPMENT OF VECTORING DEVICES FOR JET V/STOL AIRCRAFT

Eugene H. Miller
Grumman Aerospace Corporation
Bethpage, New York 11714

ABSTRACT

A two-phase test program was conducted to select high-performance vectoring systems suitable for lift engines of V/STOL aircraft. The first phase examined four configurations: cut-off plug, single bearing swivel-tee plenum, single bearing swivel-scroll plenum, and flap nozzles. The models were 1/6.5-scale of representative V/STOL fighter designs. Extensive use was made of oil-flow techniques to obtain diagnostic patterns of internal flow fields and to locate areas of possible flow separation. Component pressure drops were converted to thrust losses to determine overall system performance levels.

The second phase studied nozzle design for the single bearing swivel systems with regard to optimization of nozzle thrust performance and downwash characteristics compatible with V/STOL aircraft. Nine nozzles were tested, varying exit area aspect ratio and inlet Mach number.

SYMBOLS

A_e	Nozzle exit area, sq in.
A^*	Nozzle throat area, sq in.
AR	Aspect ratio
C_d	Discharge coefficient, actual weight flow/ideal weight flow
C_v	Thrust coefficient, actual thrust/ideal thrust
C_{v_n}	Thrust coefficient for rotating portion of nozzle
D	Diameter, in.
F_G	Gross thrust, lb
L	Length, in.
M_e	Mach number at nozzle exit
NPR	Nozzle pressure ratio, P_T/P_∞
P_T	Total pressure, psia
P_e	Static pressure at nozzle exit, psia
P_∞	Ambient pressure, psia

T	Temperature, °R
W	Weight flow, lb/sec
X	Distance downstream of nozzle exit, in.
θ	Plug nozzle outer wall angle, or flap angle, deg
α	Ratio of specific heats

INTRODUCTION

The Navy is currently developing the V/STOL support ship from which V/STOL aircraft of various types will operate. The concept of jet V/STOL aircraft has been demonstrated successfully with the development of the subsonic Harrier aircraft. In the development of advanced high-performance supersonic lift plus lift/cruise aircraft, the exhaust systems must be vectorable during transition flight. Vectoring might also be accomplished with lift engines if they are to provide horizontal thrust in case of loss of lift/cruise engine thrust, or with the lift/cruise engine to provide additional lift. A supersonic configuration (Fig. 1) employing such concepts contains a hybrid propulsion system of two lift turbojets and one lift/cruise turbofan, with all engines utilizing pairs of vectorable nozzles. The nozzle swivel planes are canted inward to have the nozzles splayed outward as they rotate rearward, thus avoiding impingement on the fuselage. The requirement of thrust rotation, therefore, presents the problem of minimizing thrust loss in systems where loss mechanisms such as separation and shocks are likely to occur as the exhaust gases transist from an annulus to a circle and rotate up to 90 deg.

Possible candidates for V/STOL vectorable nozzles include the triple bearing swivel, cascades, flap, and bifurcated single bearing swivel (Fig. 2). The triple bearing swivel nozzle encounters ground clearance problems. The cascade nozzle is unattractive because of unwanted loss of thrust due to resulting side forces. The bifurcated swivel nozzle presents an attractive configuration in its ability to produce the fountain effect (Ref 1), i. e., buoyancy which can effectively counteract suckdown. Multiple jet patterns reduce lift loss for both in-ground and out-of-ground effects. The inherent high performance and simplicity of the flap nozzle make it attractive for V/STOL application. However, this configuration has drawbacks, such as heating the underside of the aircraft as the exhaust gases are vectored toward 90 deg.

An experimental program was conducted to obtain both performance figures and basic insight into a number of promising nozzle configurations. The configurations were designed basically for lift-engine technology, but lift/cruise engine applications are possible with some of the designs.

NOZZLE MODELS

The first phase of the test program examined four basic nozzle systems (Fig. 3 through 6):

- Cut-off plug
- Single bearing swivel-tee plenum

- Single bearing swivel-scroll plenum
- Flap

All but the cut-off plug were made of fiberglass. The nozzle models were 1/8.5-scale of representative fighter designs. Wooden patterns were used to form the fiberglass layups. (See Fig. 7.) The nozzle models were built in such a fashion as to enable splitting them after a test, thus permitting inspection of oil and lampblack patterns. A typical oil-drop study is shown in Fig. 8, depicting areas of separation and recirculation. (Vanes were later added to attach the flow to the nozzle wall.) The single bearing swivel configurations had nozzles which rotated in the swivel plane. They had grooves molded into the contour to enable accommodation of zero, one, two, three, or five vanes, providing equal areas. (See Fig. 8D.) Total-pressure rings were located at the entrance to the rotating nozzles, enabling a performance estimate of the losses in the plenum and nozzles separately: calculation of C_v could be based on engine total pressure or C_{v_n} based on total pressure to the rotating nozzle. The nozzles also had extensions to vary the flow enclosure (Fig. 8A).

In the second phase, nine nozzle configurations applicable to the single bearing swivel system were studied. Aspect ratio ranged from 1:1 to 3.5:1. Mach number ranged from 0.2 to 0.55. The nozzles were cast from stainless steel. Each was equipped with a removable airfoil-type turning vane.

FACILITY DESCRIPTION

The test program was conducted at the Grumman test facility complex (Fig. 9). The tests were run statically, i.e., with a free-stream Mach number of zero. The V/STOL thrust stand (Fig. 10) is composed of a three-component balance system: one self-contained force-link flexure (x direction) and two flexures on a separate beam to measure vertical force (z direction) and moment (M_y). Therefore, the thrust vector's magnitude, direction, and location are measured. Air flows into the rig from a high-pressure bottle bank (2400 psia) and is throttled down to less than 50 psia ($NPR = 1.4-3.0$). The air then goes through a turbine flowmeter to measure weight flow. The flowmeter provides a discharge coefficient accuracy of $\pm 0.3\%$.

The flow enters the model by flex hosing perpendicular to the plenum, thereby removing the x (axial) momentum component of the incoming flow, and then proceeds through a choke plate section composed of a screen and backup straightening vanes. In the next section, the flow accelerates to a simulated engine turbine exit.

CALIBRATION

The balance system was calibrated in the instrumentation laboratory using weights; the same procedure was repeated on the thrust stand. The entire system was then pressure-checked. A reference convergent nozzle was used to obtain rig corrections which were applied after the rig demonstrated good repeatability and no zero shifts in the measurements.

DATA ACQUISITION & REDUCTION

Pressure measurements were recorded by differential transducers and then filtered through a 5-cps passive filter. The signals were then applied to an SEL 810A

digital computer, which performed both data acquisition and data reduction. An analog plotter provided completely reduced and plotted data within minutes of a run.

Actual weight flow was obtained by measuring static pressure upstream of the flowmeter, temperature downstream of the flowmeter, and rotor cps. Force measurements were read from strain gauges in the x-component force link and z-component flexures. Weight-flow measurements were converted to discharge coefficient (C_d), and force measurements converted to thrust coefficient (C_v).

PHASE I TEST RESULTS

Cut-Off Plug

The cut-off plug was established as a reference goal because of its inherent high performance. Fig. 11 shows the plug with no outer nozzle, i.e., an annular nozzle, and an outer nozzle with a wall angle of 27 deg and an L/D of 0.15. A performance increase of 3.73% is obtained by addition of the outer nozzle. Similar results were obtained (Ref 2) with the optimum length-to-diameter ratio between 0.11 and 0.18 and the optimum angle between 20 and 40 deg. The thrust performance (C_v) results are high. However, it must be noted that the exhaust gases were not vectored in this configuration.

Single Bearing Swivel-Tee Plenum

Performance of the single bearing swivel-tee plenum nozzle is shown in Fig. 12, and can be broken into its components. For this configuration, the nozzle exhaust gases flow through a plenum from the turbine and then pass through the swivel nozzle. Therefore, two possible areas of loss are present: the turbine plenum and the rotating nozzle. The exhaust plenum pressure loss is a function of Mach number, and is shown in Fig. 13. The plenum total pressure loss can be converted to thrust loss for constant weight flow through a convergent nozzle by:

$$\frac{\Delta F_G/F_G}{\Delta P_T/P_T} = \left[\frac{P_\infty/P_T}{\left(\frac{P_e A_e}{P_T A^*} (1 + \gamma M_e^2) - \frac{P_\infty A_e}{P_T A^*} \right)} \right] W\sqrt{T} = \text{CONST}$$

$$= \frac{1}{\frac{1.269}{P_\infty/P_T} - 1} \quad (\text{for a choked nozzle and } \gamma = 1.4)$$

For example, at an NPR of 2.0, $(\Delta F_G/F_G)/(\Delta P_T/P_T) = 0.65$

For configuration 2 of Fig. 12, it is seen that for an NPR of 2, $C_v = 0.922$. From Fig. 13, with an inlet Mach number of 0.6, the plenum total pressure loss is 6.9%. This converts into a C_v loss of 4.48%. The C_v loss of the rotating nozzle itself at an NPR of 2 is 4.40% (C_v adds up to more than 1.00 when the losses are added due to the inaccuracy of the measurements). One major reason for the nozzle loss is the non-uniformity of the flow entering the nozzle due to the flow transition from an annulus to a circle.

The total pressure distribution across the flow area at the plenum inlet and exit is seen in Fig. 14. A more uniform distribution was obtained by channeling the flow to the nozzle by the addition of an insert (Fig. 15). A study of performance change with number of vanes is seen in Fig. 16 for the single bearing swivel-tee plenum nozzle without a boot extension. Without vanes, the flow separates completely from the nozzle wall, and performance is poor. (See Fig. 8D.) Addition of one vane results in a C_V of 0.825 at NPR = 3.0. There is another substantial increase in C_V with three vanes ($C_V = 0.895$), but performance increases only to $C_V = 0.905$ with five vanes.

The effect of rotating the nozzle is seen in Fig. 17. A loss of 2% in C_V occurred for a 90-deg rotation at an NPR of 2.2.

Single Bearing Swivel-Scroll Plenum

The scroll pattern was formed to guide the exhaust flow from the turbine annulus to the nozzle opening. Performance of this configuration with the boot extension and Mach 0.3 nozzle is shown in Fig. 18. However, plenum oil flows indicated large areas of separation and recirculation (Fig. 19). Performance levels in C_V were 2.85% below that of the tee plenum at an NPR of 3.0. It is believed that the scroll performance was low because the flow into the scroll had zero swirl, i.e., it was assumed that the lift engine turbine exit guide vanes would remove the swirl. However, if the incoming flow was to swirl, it would more easily follow the contour of the transition from the turbine annulus to the nozzle opening. Previous studies (Ref 2 and 3) alluded to two possibilities of loss in thrust coefficient due to swirl: (1) loss of energy resulting from tangential velocity and (2) low base pressures on the turbine base resulting from free vortex motion. However, they were not applicable to this configuration. In the first case, the scroll would guide the flow into the rotating nozzle making use of the tangential velocity; the second case is not possible since the base would be enclosed by the scroll contour. Thus, if the engine had modified or omitted exit guide vanes, performance would have been improved with this configuration. Lack of engine guide vanes would also result in engine weight reduction, elimination of vane component pressure drop, and shortening of engine length.

Flap Nozzle

The flap nozzle provided high-level thrust coefficient performance (Fig. 20) as it was vectored from 0 through 45 deg. A higher C_V level was reported (Ref 4), but those data were taken only for one isolated flap. The present configuration included the transition from the turbine exit and four flaps emanating from two slots (Fig. 6). There was no discernable difference in C_V as the flap was vectored from 0 to 15 deg. A 1% drop in C_V at a NPR of 3.0 was experienced when the flap was vectored from 15 to 30 deg. The actual thrust angle varied as a function of NPR. (See Fig. 21.) The correction was linear for 15, 30, and 45 deg; however, it was non-linear at 0 deg.

PHASE II TEST RESULTS

In this phase, performance and plume characteristics were examined for right-angle-turn nozzles used in conjunction with the single bearing swivel plenums. Nine configurations were tested in which the aspect ratio varied from 1:1 to 3.5:1, and the nozzle inlet Mach number varied from 0.2 to 0.55. (See Fig. 22.) Plume

data were recorded by a multiple-probe pressure rake as it was moved axially downstream of the nozzle exit. (See Fig. 23.) The total pressure-decay characteristics were then compared for the various configurations.

Nozzle Performance

Thrust coefficient (C_F) was found to be a function of nozzle inlet Mach number. (See Fig. 24.) The nozzle inlet Mach number was varied by changing the ratio of nozzle exit area to inlet area. The exit area was the minimum nozzle area; therefore, at NPRs greater than 1.89, the nozzles were choked and the inlet Mach number was determined by the area ratio. The nozzle thrust coefficient was a maximum, 0.985, through the Mach number range of 0.2-0.35. It decreased to 0.95 at an inlet Mach number of 0.55. The nozzle data appeared to be independent of exit area aspect ratio. The exceptions to this were the Mach 0.35 and 0.55, aspect ratio = 3.5, nozzles. Their decrease in performance can be explained by the substantial divergence angles on the two narrow sides of these nozzles, 10.7 and 20.5 deg, respectively. Data from the previous tests (Ref 5) are also plotted in Fig. 24. It is seen that the circular nozzle of Ref 5 (aspect ratio = 1) exhibited high thrust coefficient values, comparable to the present test. However, the high-aspect-ratio nozzle (aspect ratio = 5) exhibited significantly lower values. This is not the entire story. These nozzles actually were of lower performance than the present ones, since they both had low discharge coefficients due to flow separation off the inner nozzle wall. (See Fig. 25.)

With an extension of the inner nozzle wall, the discharge coefficients (Fig. 25) of the present configurations showed a marked improvement over the previous test (Ref 5). They displayed independence of aspect ratio, and a decrease in performance from a C_d of 0.95 through the Mach number range of 0.2-0.35, to 0.92 at Mach 0.55.

Overall, the velocity coefficients were at a constant level over the pressure ratio range of 1.4-2.6. The discharge coefficients were flat for the Mach 0.55 configurations throughout the pressure ratio range. However, with the remaining configurations, the discharge coefficient increases until a NPR of 2.0, and then is constant. Evidently, for the latter cases, the exit flow area increases until the throat is choked. This is most likely a vena contracta effect, since the Mach 0.2 and 0.35 series have appreciable convergence at the exit.

Figure 26 shows the internal pressure distribution of the aspect ratio 3.5:1 nozzle for a typical choked nozzle pressure ratio. The inner wall experiences a rapid expansion followed by a recompression. There appears to be no separation within the nozzle at both unchoked and choked conditions.

Exhaust Plume Characteristics

The primary reason for use of high-aspect-ratio nozzles in V/STOL aircraft is the rapid decay of the exhaust properties in the plume (downwash suppression), thereby minimizing field or carrier-deck erosion and personnel hindrance. A summary of the data for the various configurations is shown in Fig. 27. Shown with the present data are results from tests (Ref 6) of high-aspect-ratio nozzles which did not vector the exhaust flow. It is seen that the aspect ratio = 3.5 nozzle with a 90-deg bend provides a greater total pressure degradation than the Ref 6 nozzle of aspect ratio = 6. The 90-deg turn could quite possibly generate turbulence in the nozzle, thereby accelerating

the total pressure decay. It is seen that the Mach 0.55 nozzles always provide greater degradation in exhaust properties than the Mach 0.22 nozzles. Here, again, the greater losses probably generate turbulence and promote rapid mixing.

CONCLUSIONS

The test results demonstrated that good thrust performance can be achieved for a fully developed, bifurcated, single bearing swivel nozzle and a partially vectored flap configuration.

The following results were determined for V/STOL nozzle design:

- A uniform Mach number distribution must be maintained entering the rotating nozzle for maximum thrust performance
- The turbine exhaust gas must be diffused fully, i.e., the Mach number lowered prior to vectoring to obtain maximum performance
- Variations of exit area aspect ratio from 1:1 to 3.5:1 showed no significant effect on nozzle performance
- Nozzle thrust coefficients of 0.985 were obtained at nozzle inlet Mach numbers of 0.2-0.35. At higher Mach numbers (0.55), these values declined to 0.95
- Discharge coefficients of 0.95 were obtained at nozzle inlet Mach numbers of 0.2-0.35. At higher Mach numbers (0.55), they decreased to 0.92
- Decay of nozzle exhaust plume total pressure occurred most rapidly with the high-aspect-ratio nozzle. Total pressure decay is also accelerated by use of a nozzle that turns the flow and has a high inlet Mach number

REFERENCES

1. Margason, R., "Review of Propulsion Induced Effects on Aerodynamics of Jet V/STOL Aircraft," NASA TN D-5617, February 1970.
2. Baker, V. D., et. al., "Experimental Results with Lift Engine Exhaust Nozzles," AIAA Paper 65-574, AIAA Propulsion Joint Specialist Conference, Colorado Springs, Colorado, June 4-18, 1965.
3. Kentfield, J., "Nozzles for Jet-Lift V/STOL Aircraft," AIAA Journal of Aircraft, Vol 4, No. 4, July 1967, pp 283-291.
4. Midgal, D., "Design and Experimental Studies of Thrust Deflectors for V/STOL Direct Lift Engines," SAWE Paper 841, 29th Annual Conference on Mass Properties, May 1970.
5. Huenniger, E., and Miller, E., "Results of Tests on Various Nozzle Configurations Designed for V/STOL Aircraft Applications," Grumman Report ADR 14-02-73.2, October 1973.

6. Higgins, C., and Wainwright, T., "Dynamic Pressure and Thrust Characteristics of Cold Jets Discharging from Several Exhaust Nozzles Designed for VTOL Downwash Suppression," NASA TN D-2263, April 1964.

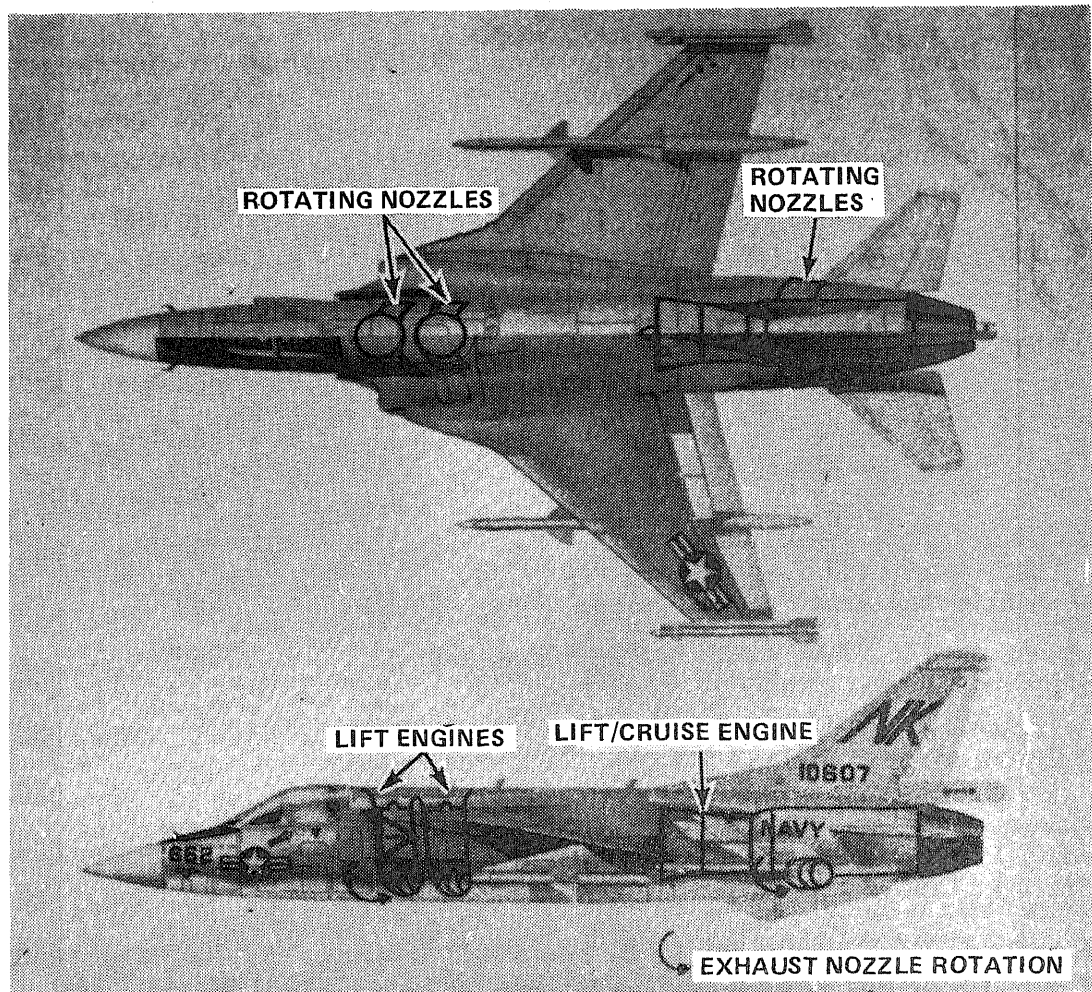
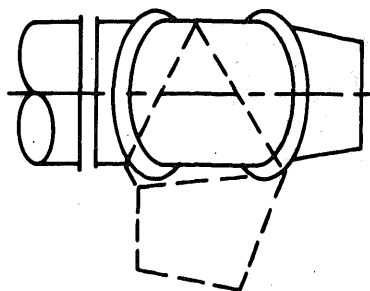
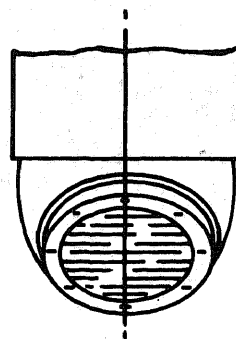


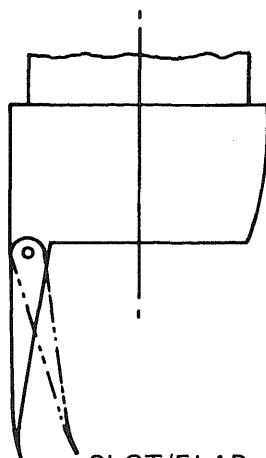
Fig. 1 Supersonic V/STOL Aircraft



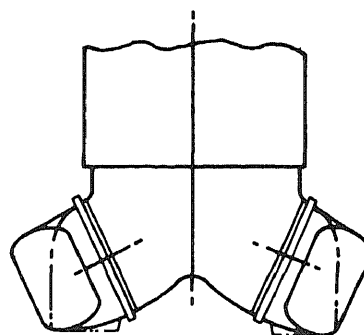
TRIPLE BEARING SWIVEL



TWIN ROTATING CASCADES



SLOT/FLAP



SINGLE BEARING SWIVEL

Fig. 2 V/STOL Nozzle Types

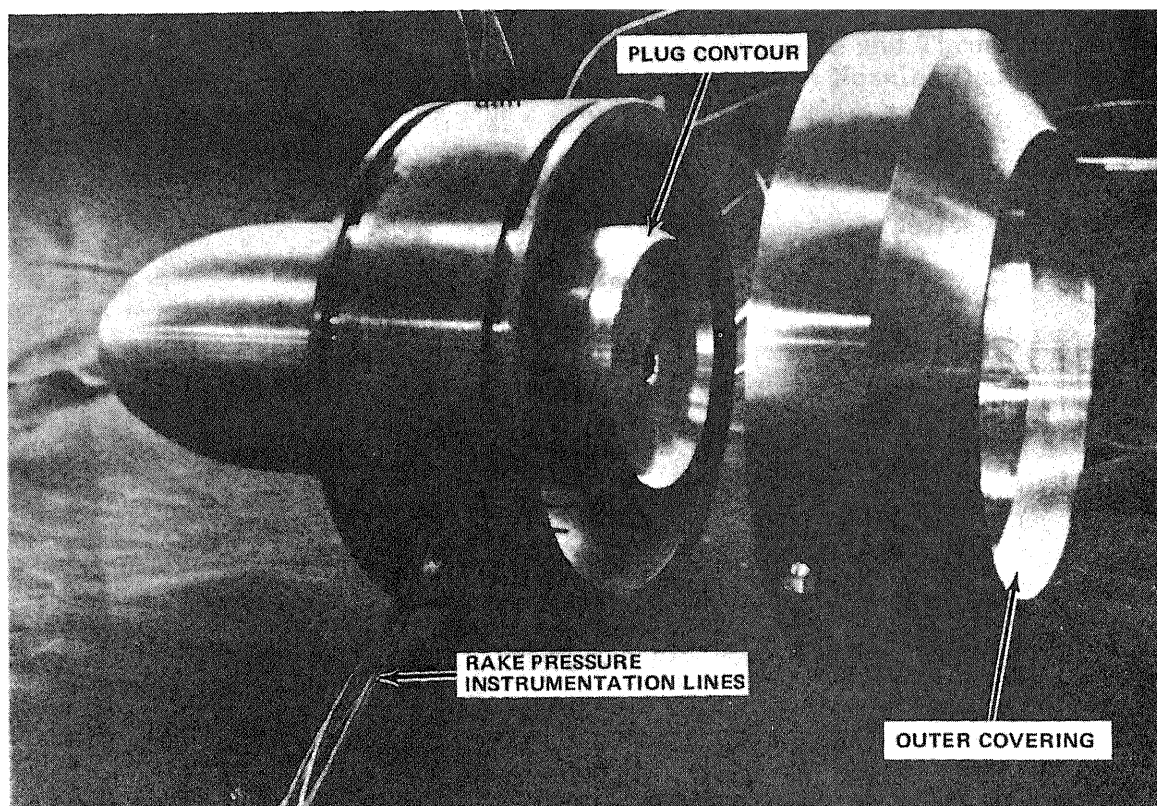


Fig. 3 Cut-Off Plug Nozzle

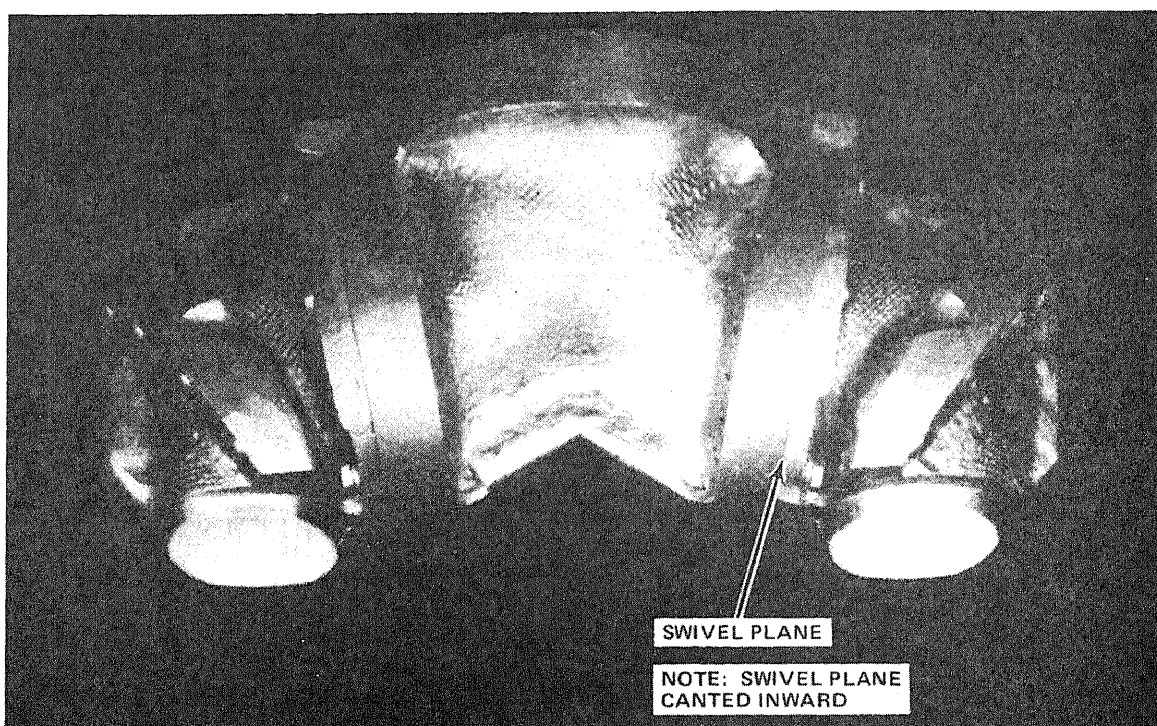


Fig. 4 Single Bearing Swivel-Tee Plenum Nozzle

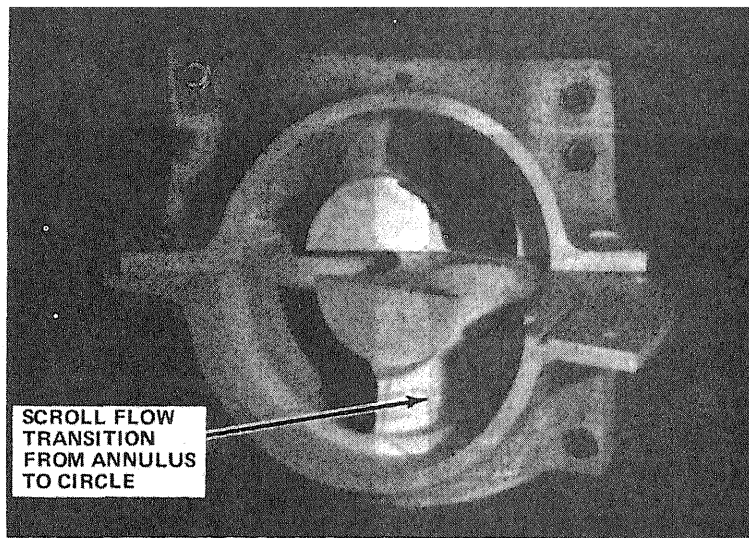


Fig. 5 Single Bearing Swivel-Scroll Plenum Nozzle

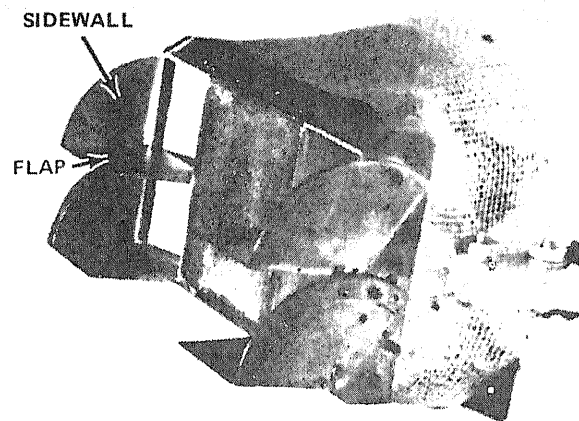


Fig. 6 Flap Nozzle

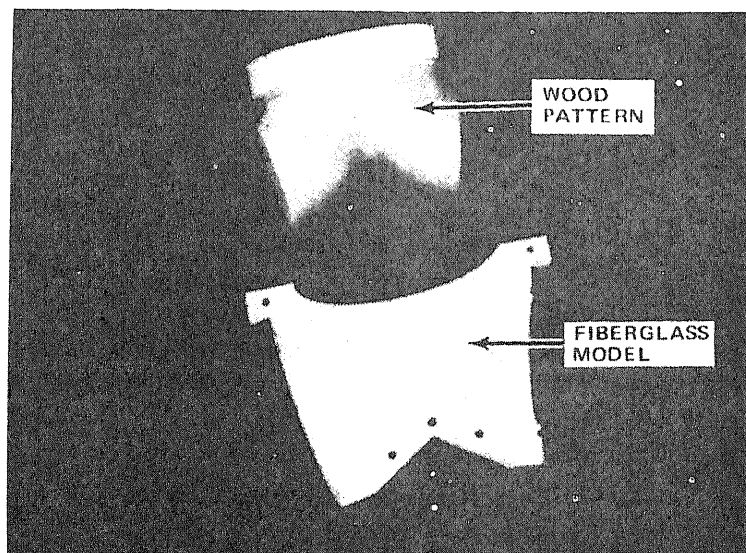
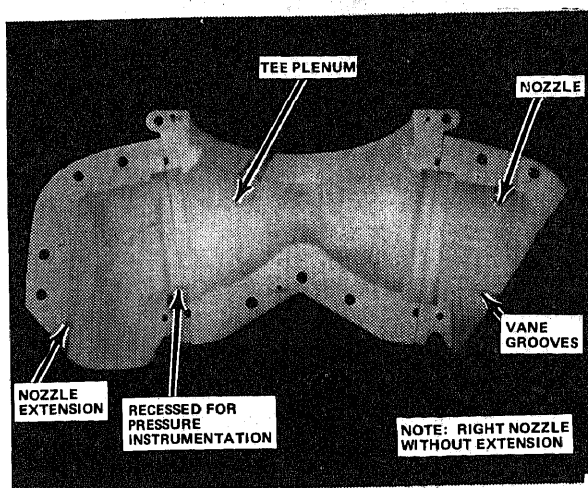
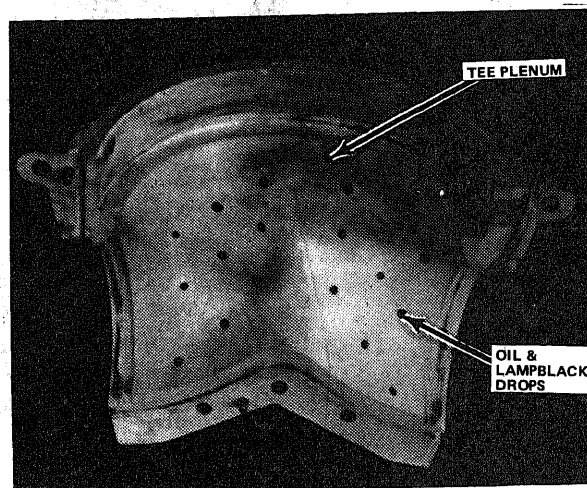


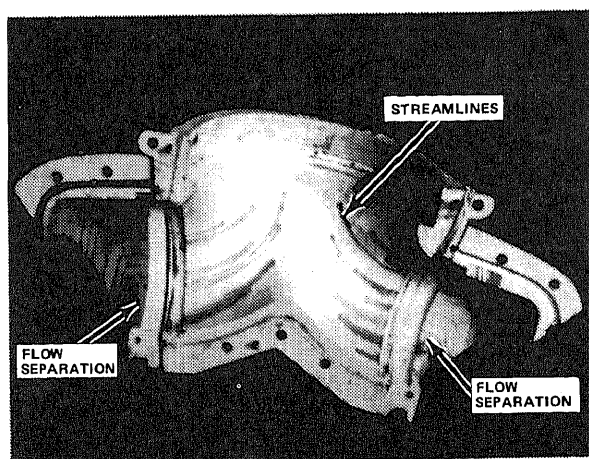
Fig. 7 Nozzle Model & Pattern



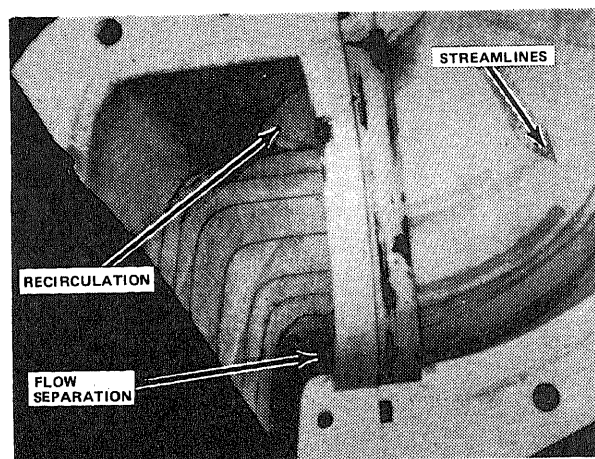
(A) NOZZLE CONTOUR BEFORE FLOW TESTING



(B) TEE PLENUM WITH OIL DROPS



(C) AIRFLOW PATTERNS



(D) CLOSEUP OF AIRFLOW PATTERNS

Fig. 8 Nozzle Oil-Drop Study

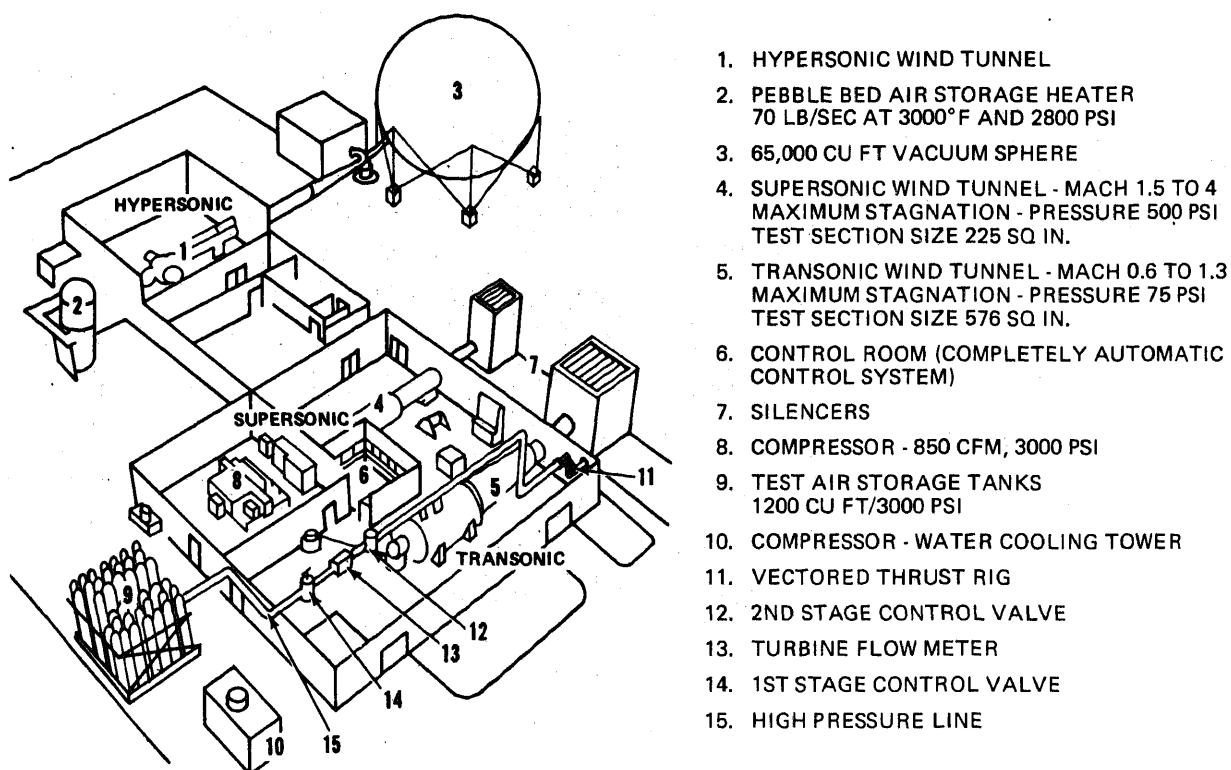


Fig. 9 Wind Tunnel Facilities

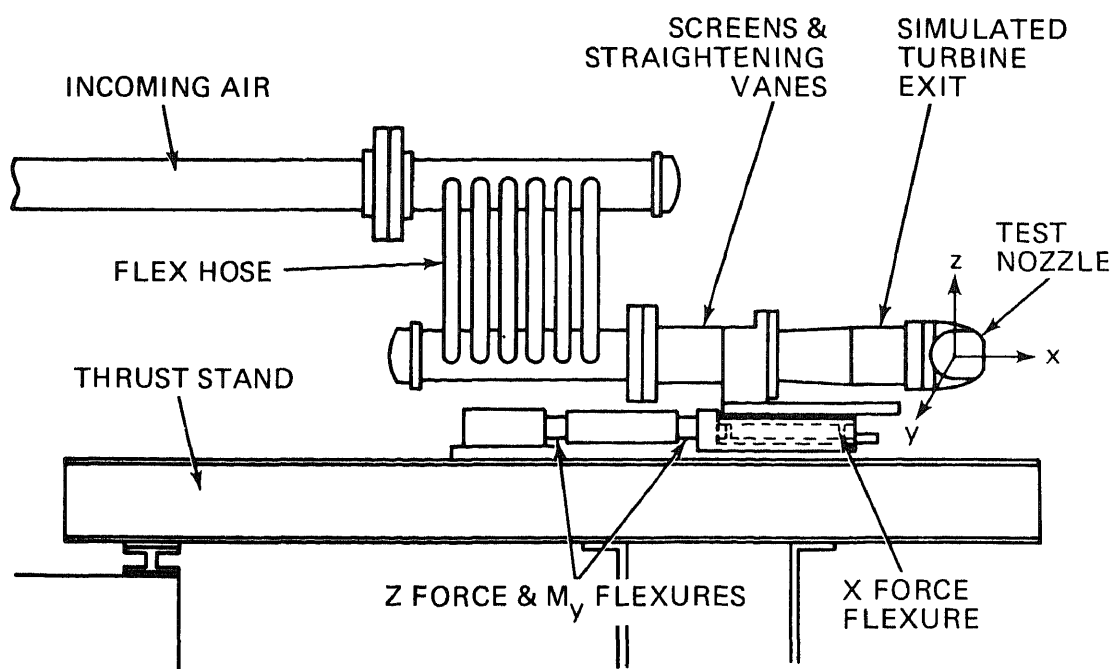


Fig. 10 V/STOL Nozzle Test Stand

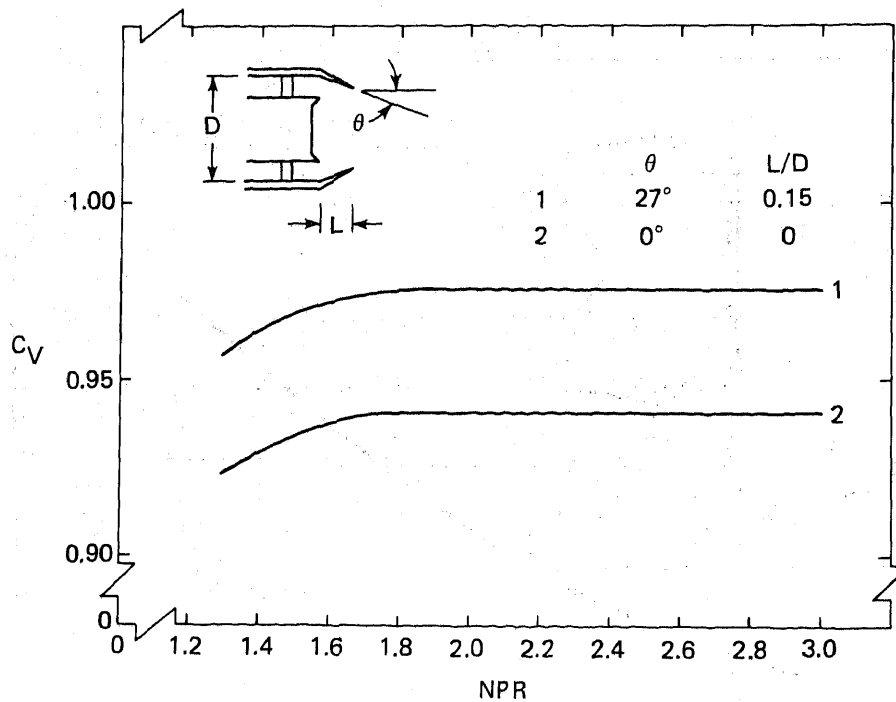


Fig. 11 Cut-Off Plug Performance

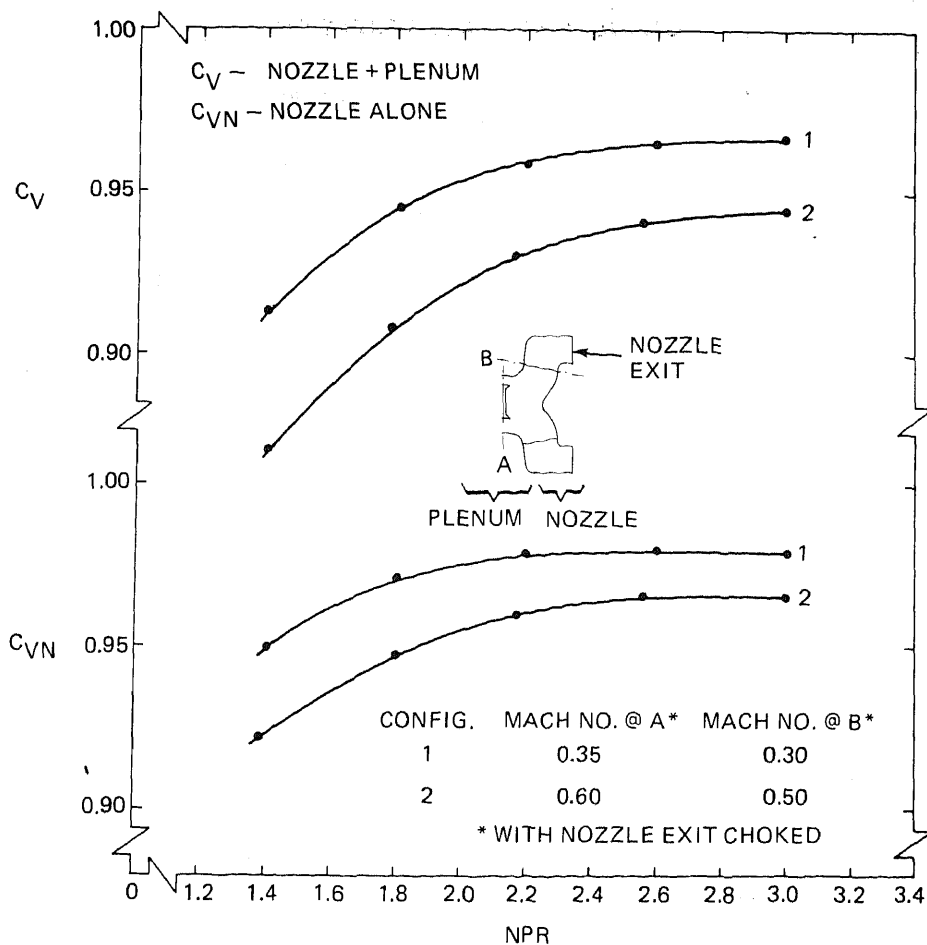


Fig. 12 Single Bearing Swivel-Tee Plenum Nozzle Performance

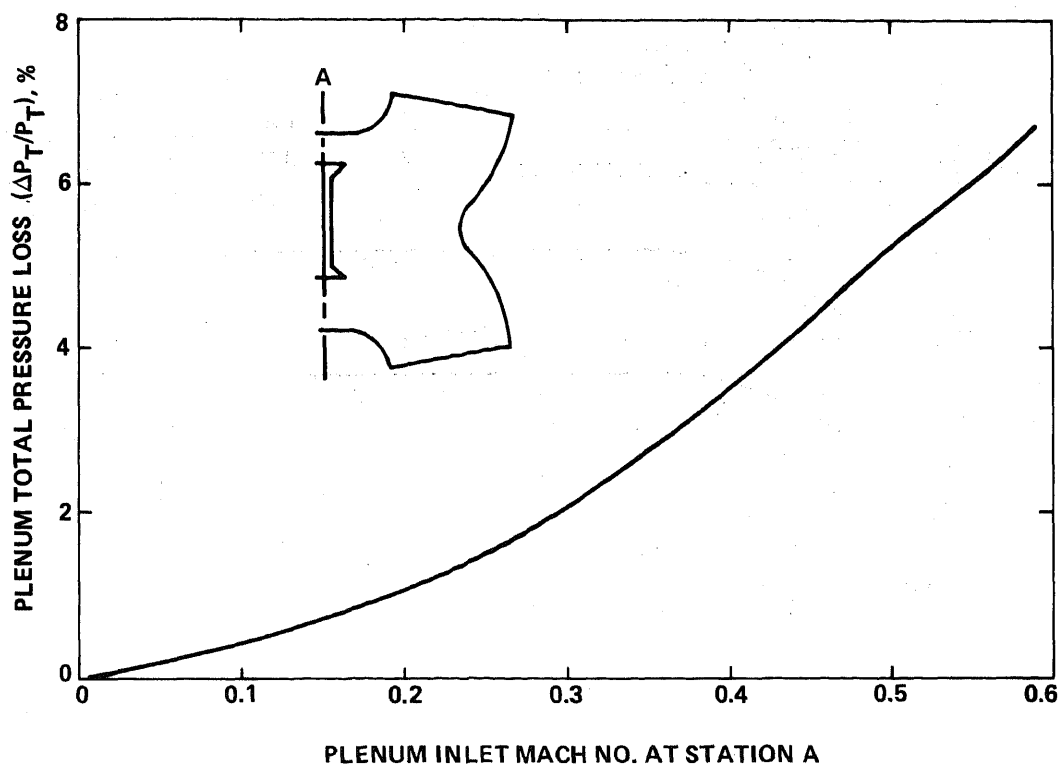


Fig. 13 Tee Plenum Pressure Loss vs Mach Number

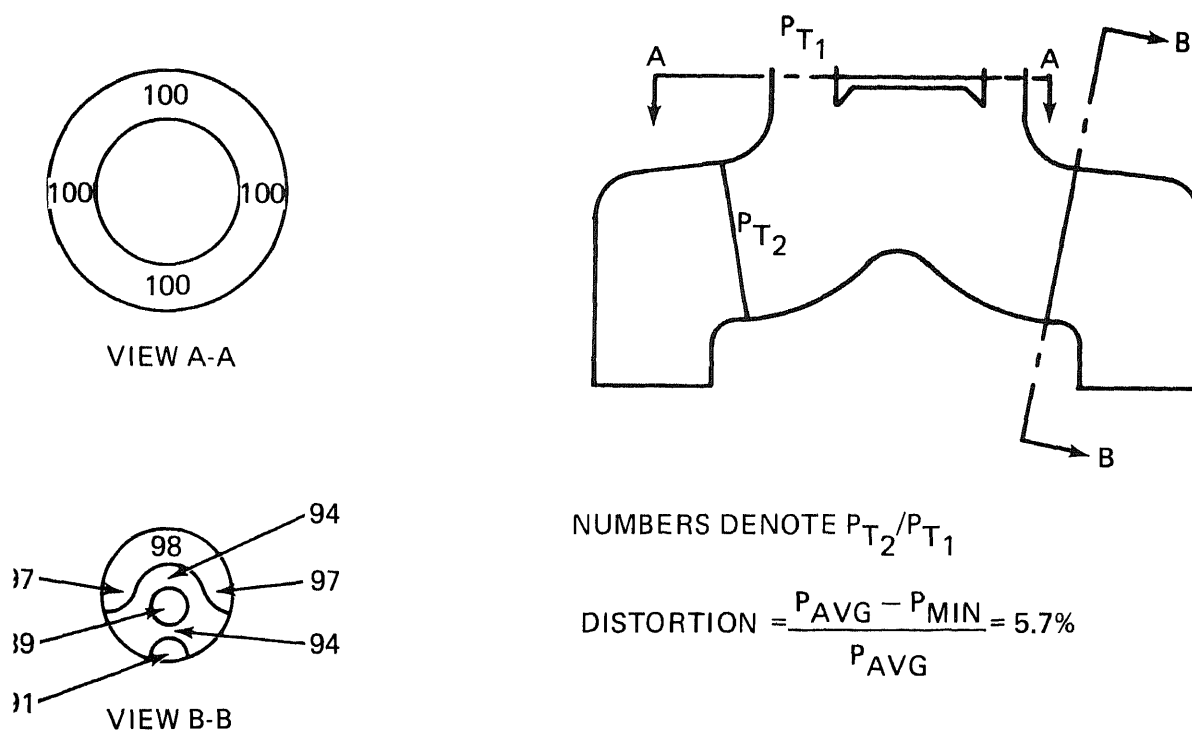


Fig. 14 Flow Distortion upon Transition from Annular to Circular Flow

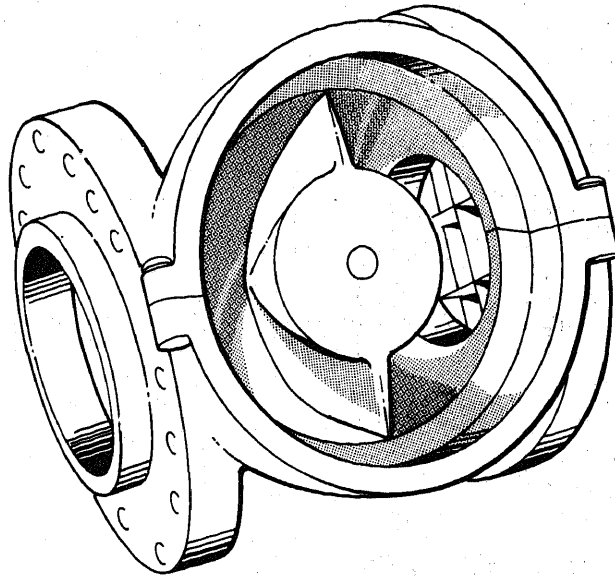


Fig. 15 Tee Plenum with Insert

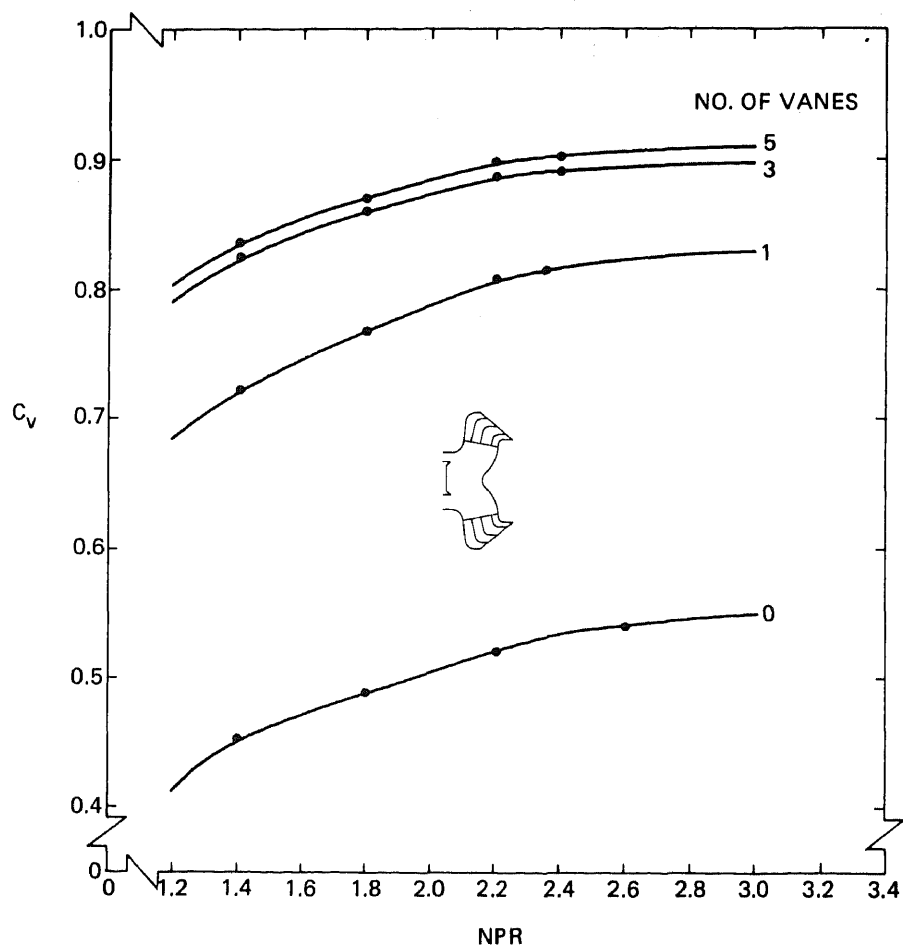


Fig. 16 Vane Comparison for Single Bearing Swivel-Tee Plenum Nozzle

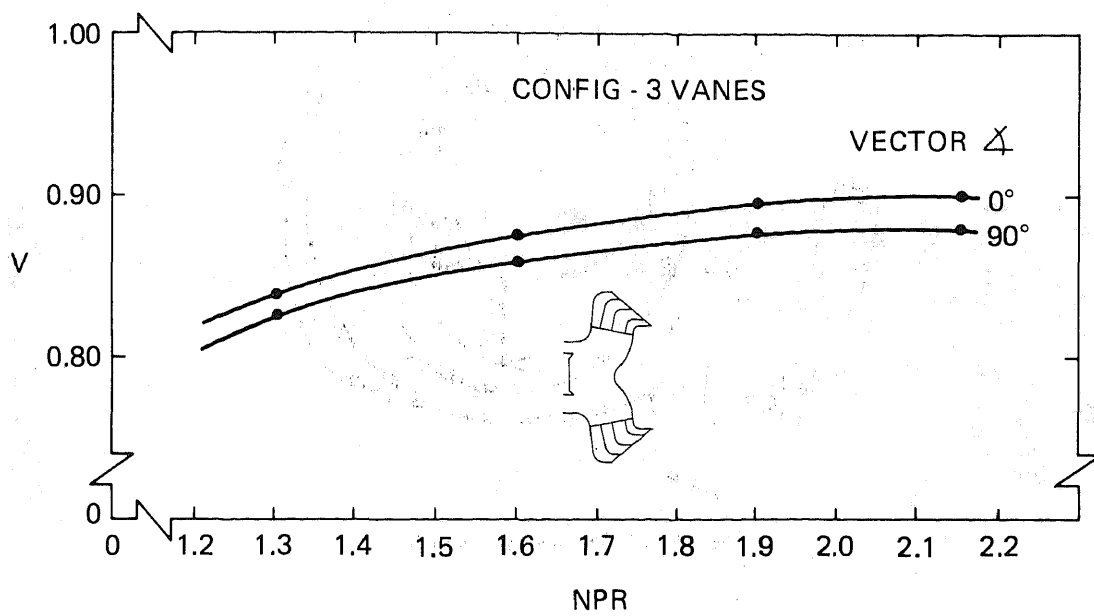


Fig. 17 Vectoring Effect on Single Bearing Swivel-Tee Plenum Nozzle

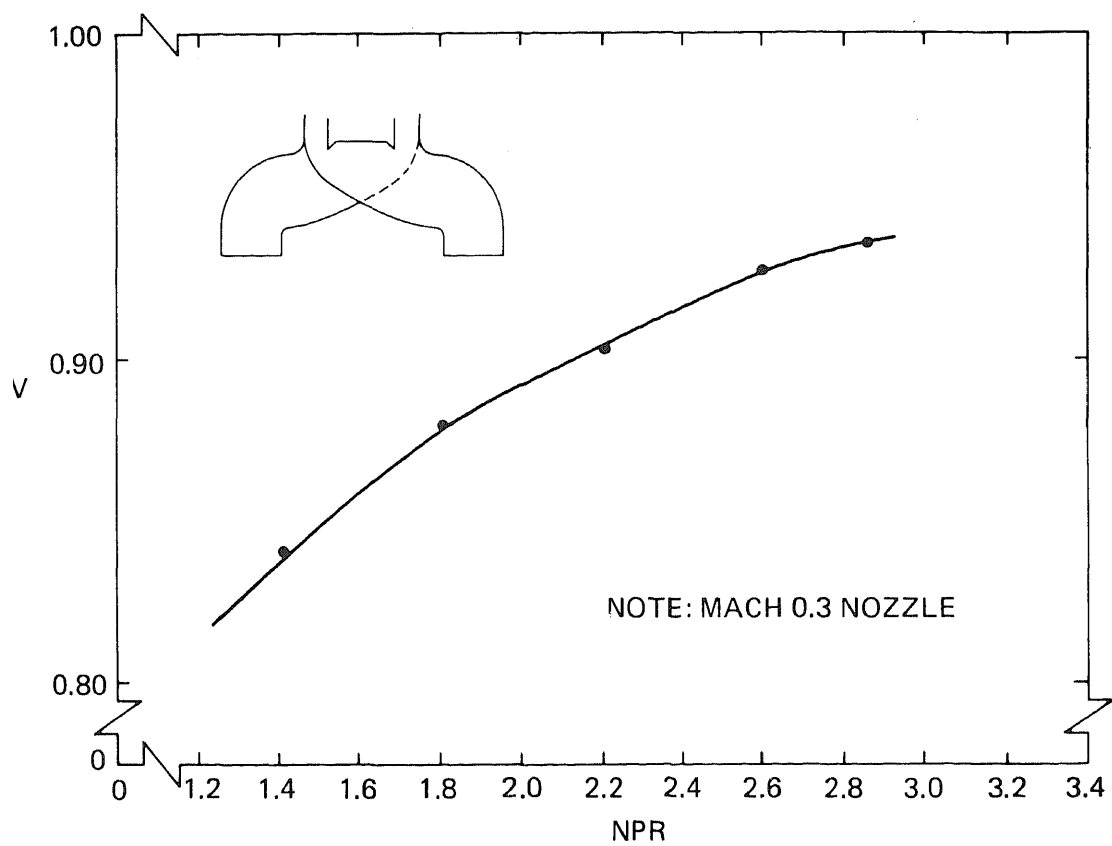


Fig. 18 Single Bearing Swivel-Scroll Plenum Nozzle Performance

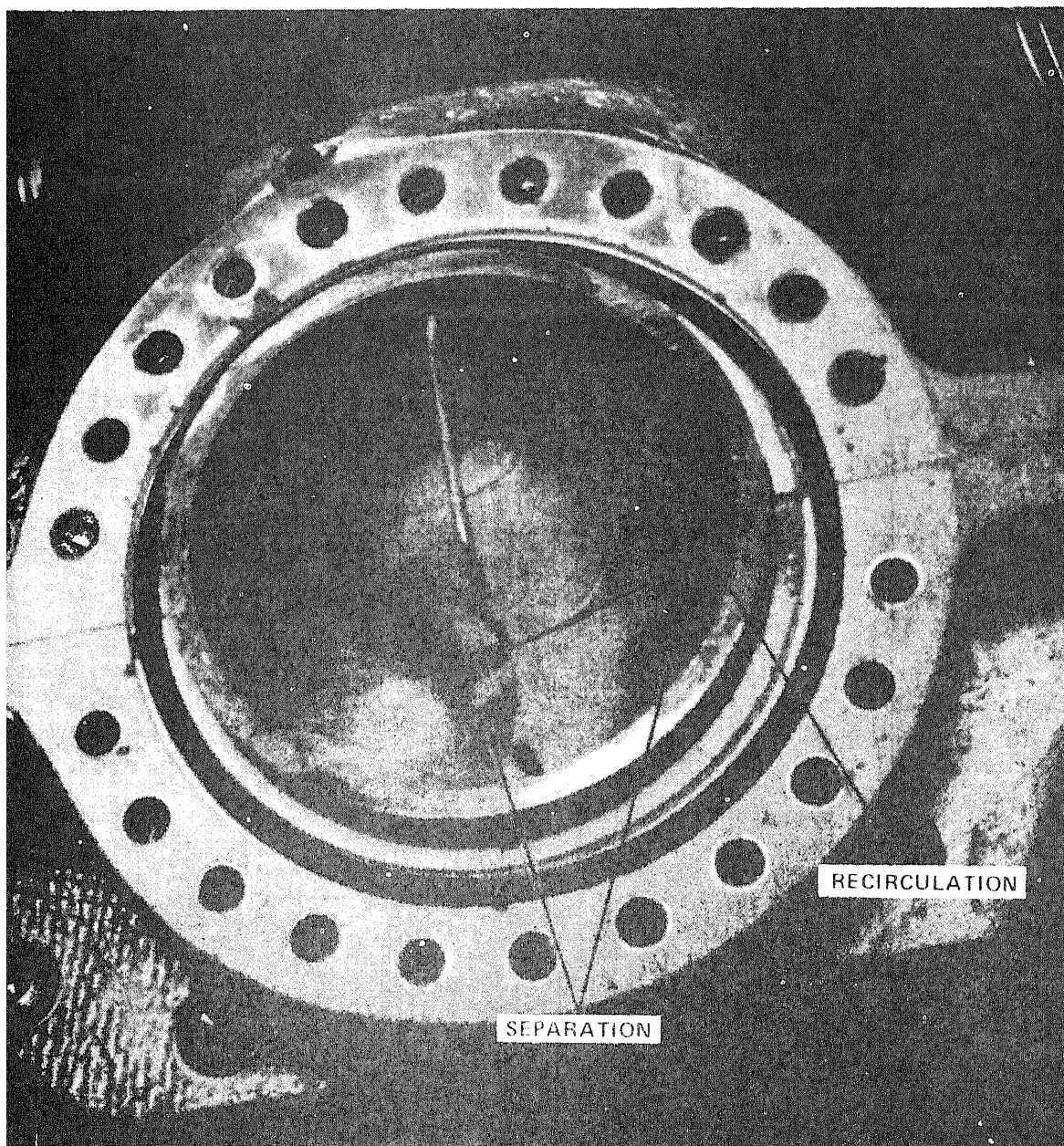


Fig. 19 Oil-Flow Pattern with Scroll Plenum

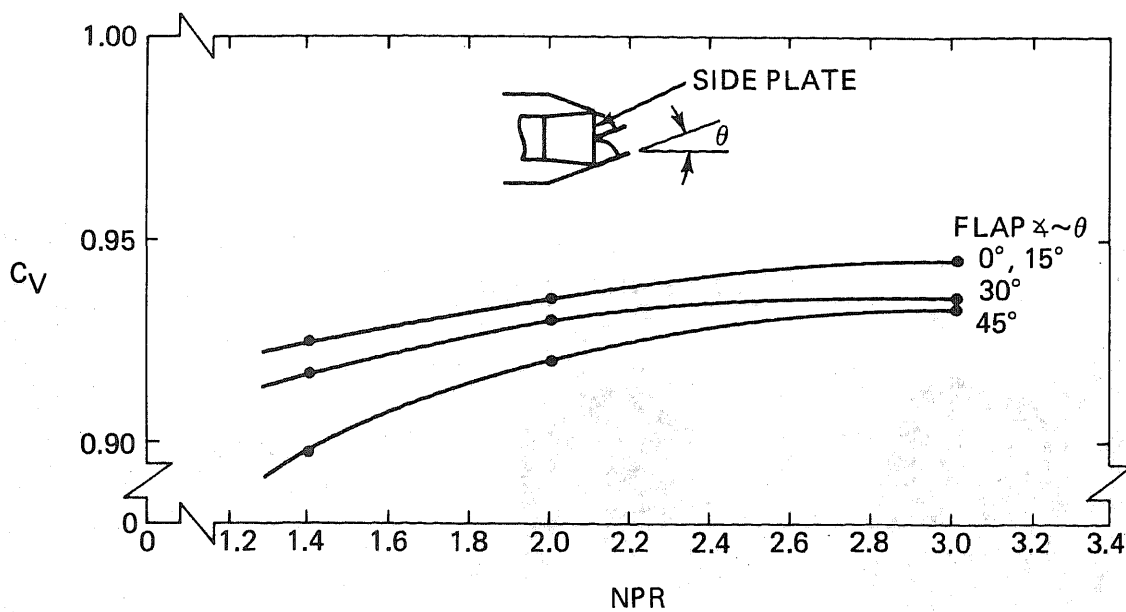


Fig. 20 Flap Nozzle Performance

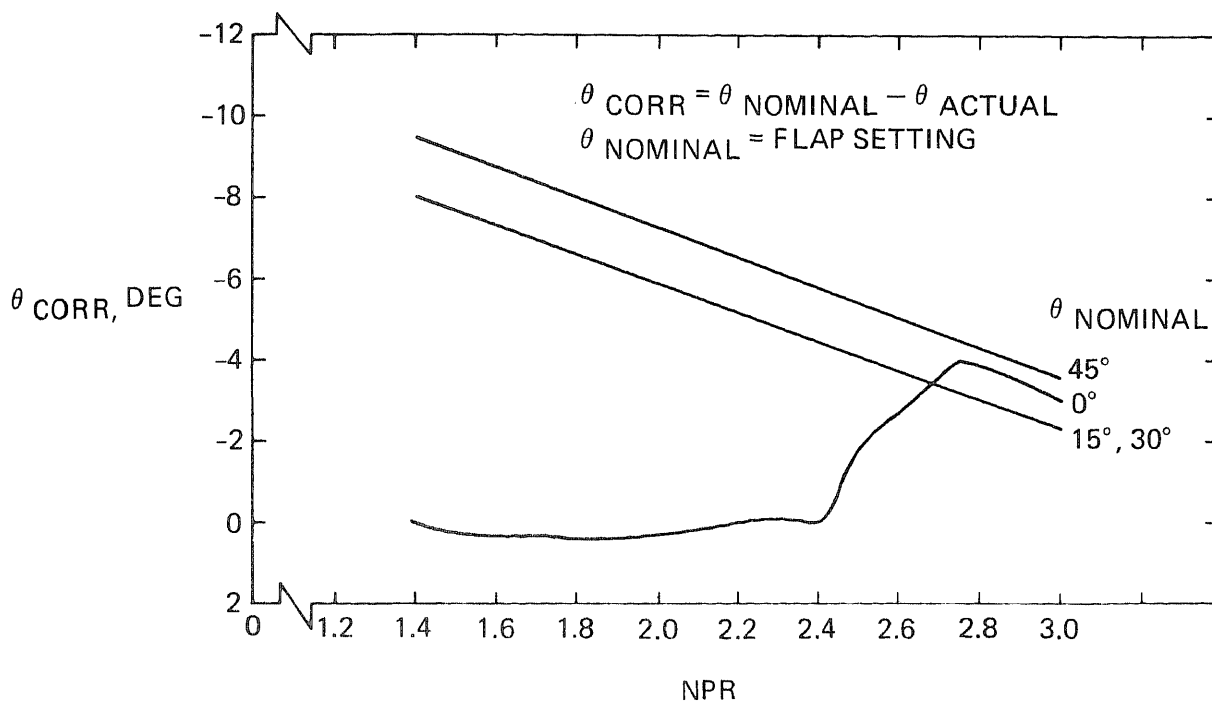


Fig. 21 Flap Nozzle Thrust Vector Correction

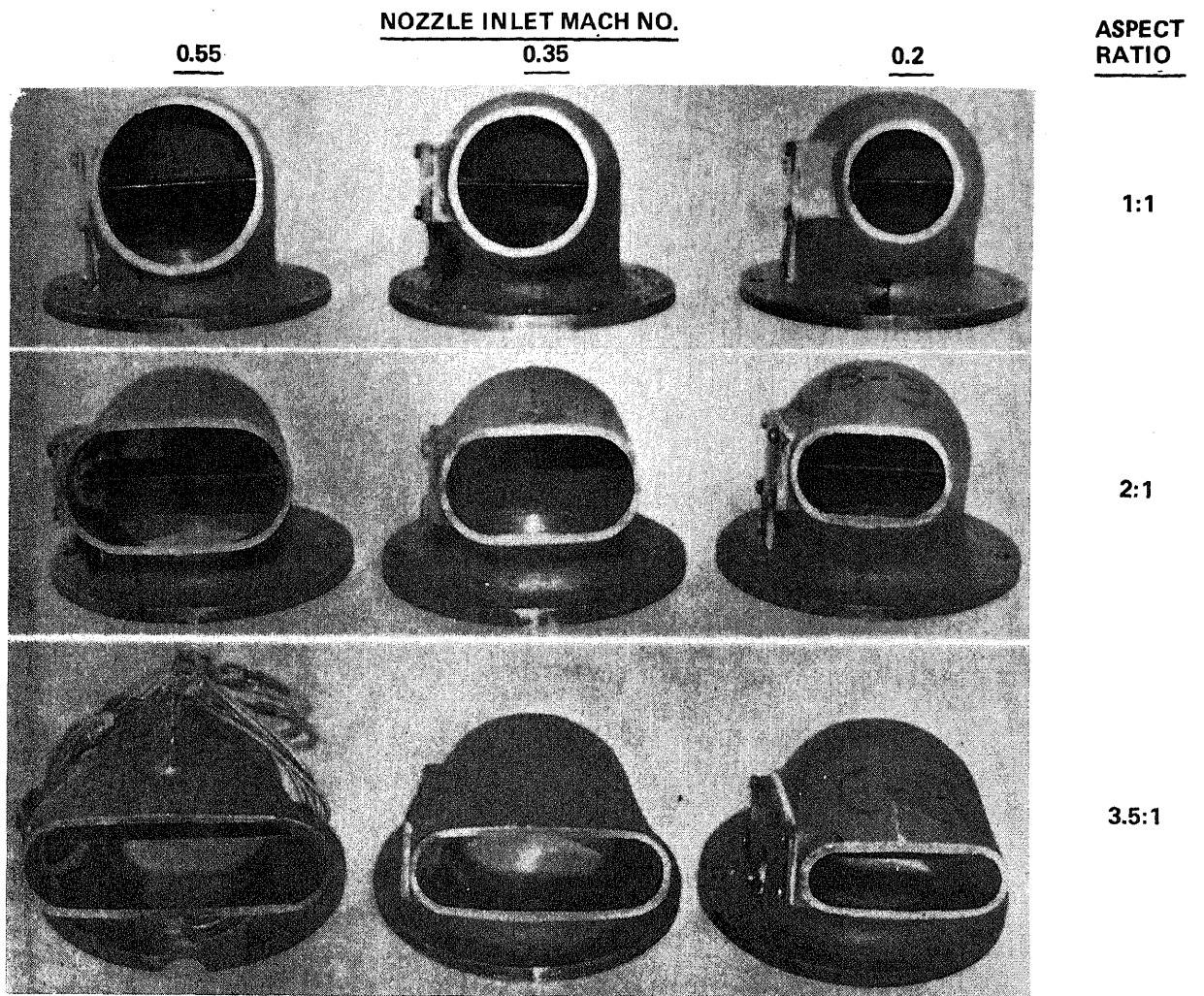


Fig. 22 V/STOL Nozzle Types

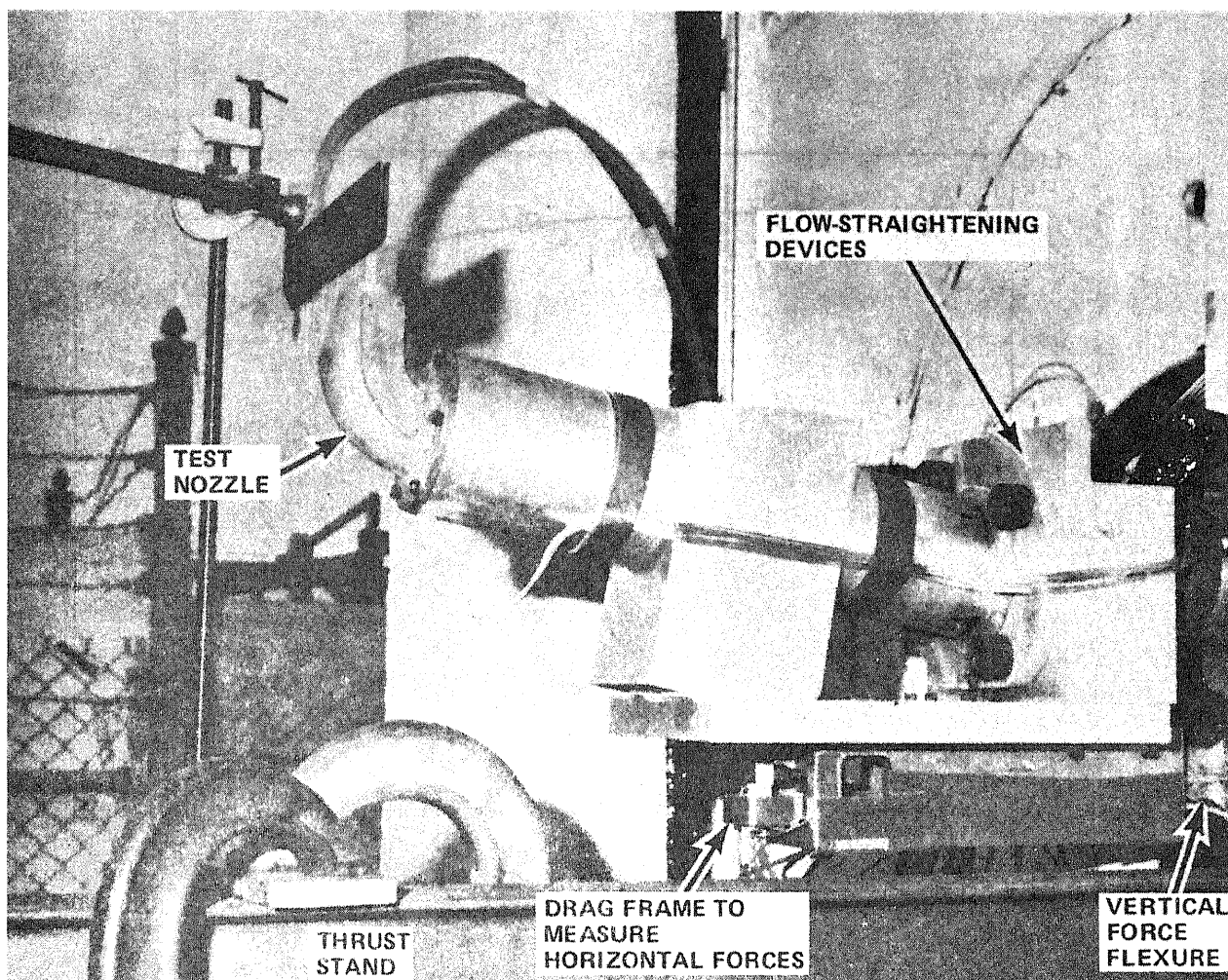


Fig. 23 Performance & Plume Characteristics Test Setup

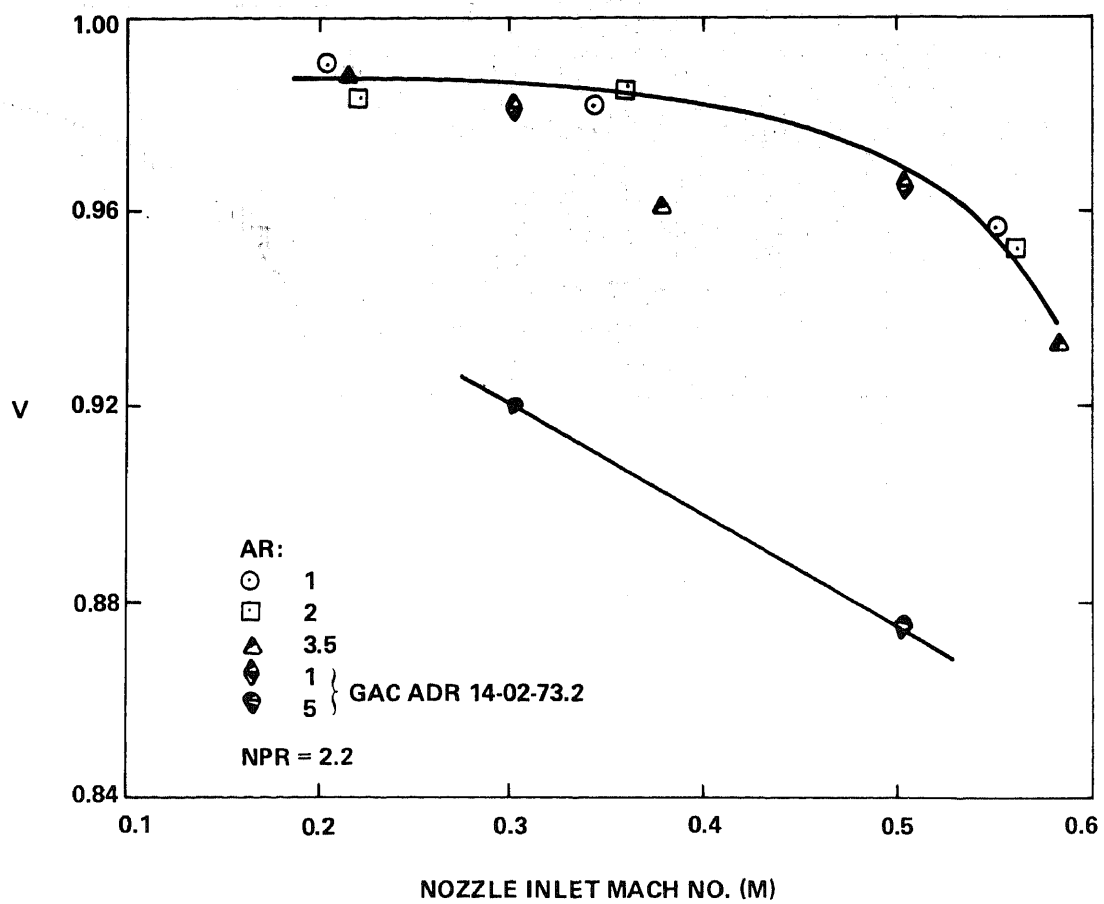


Fig. 24 V/STOL Nozzle Thrust Coefficient vs Nozzle Inlet Mach Number

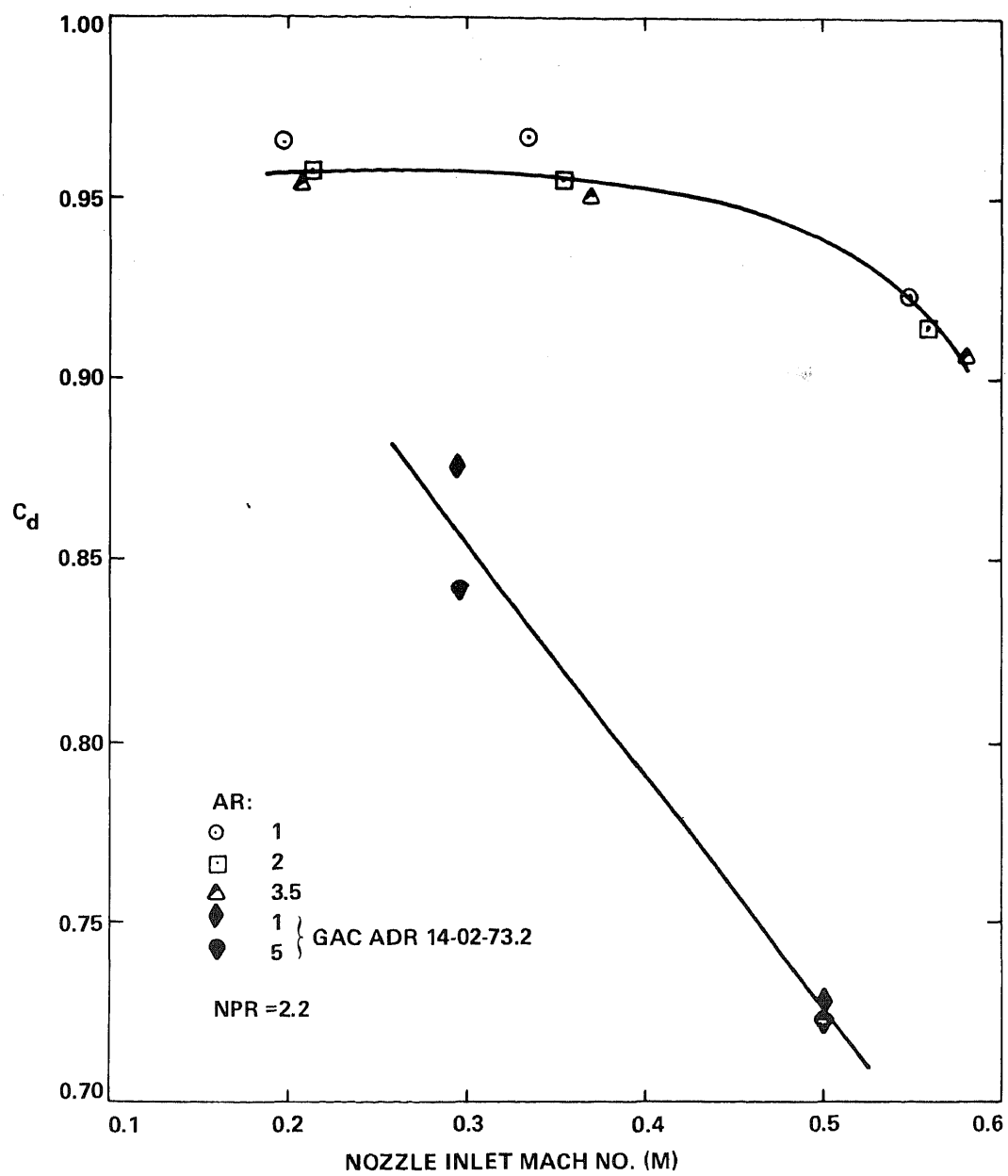


Fig. 25 V/STOL Nozzle Discharge Coefficient vs Nozzle Inlet Mach Number

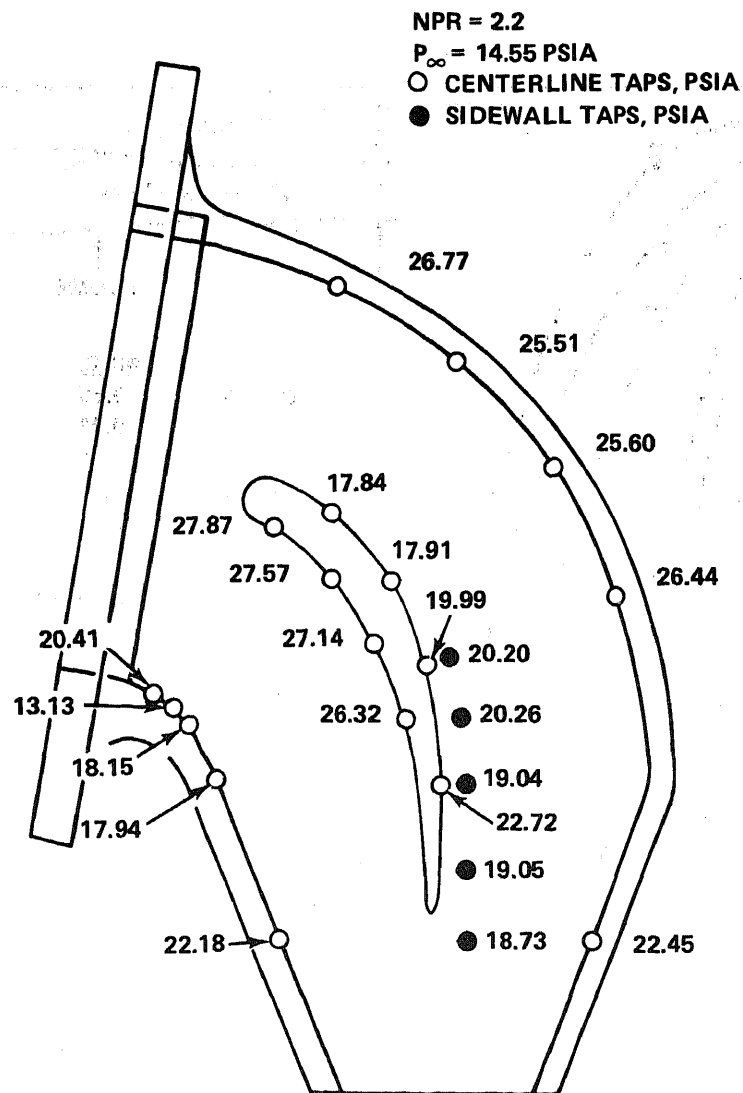


Fig. 26 3.5:1 AR Nozzle Internal Static Pressure Distribution

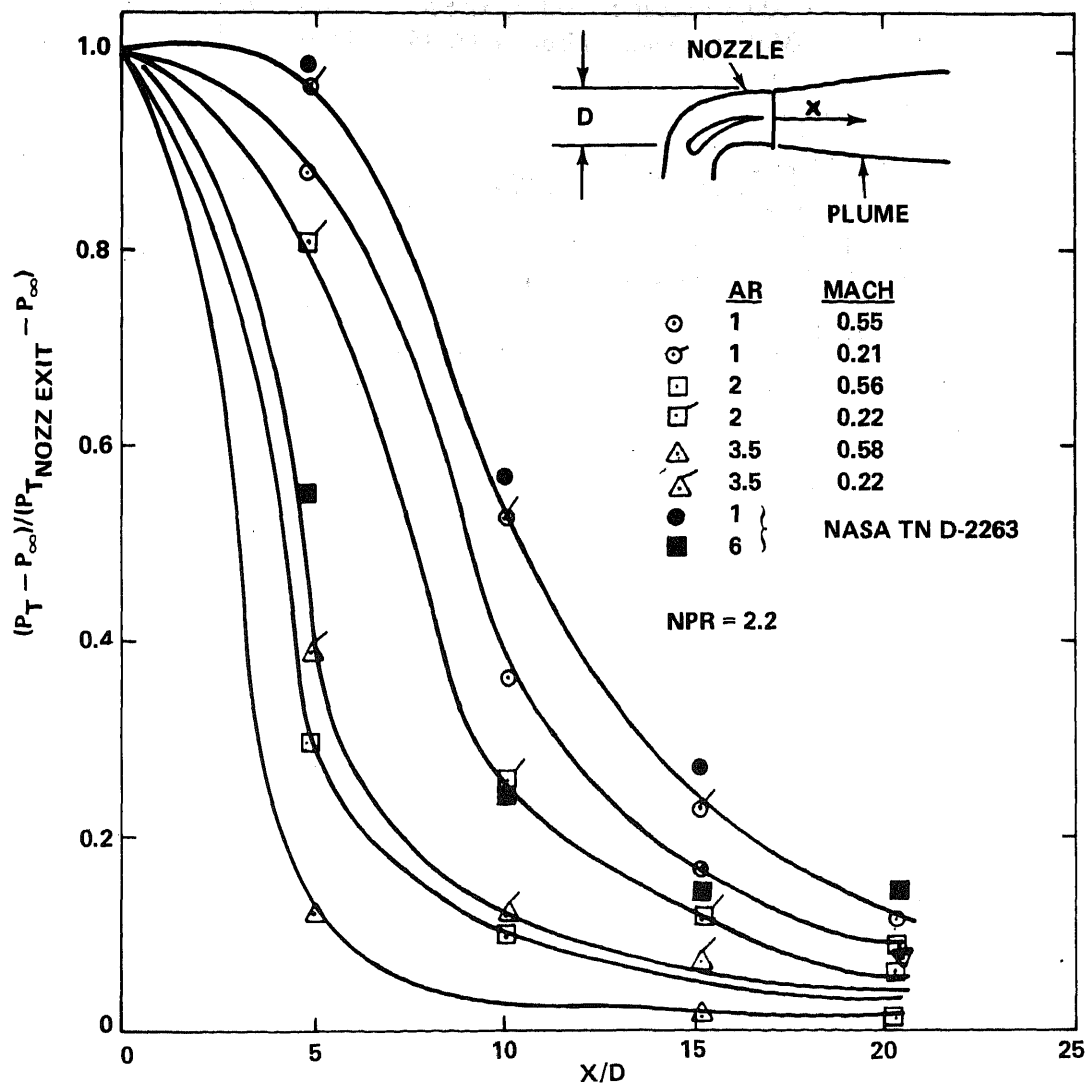


Fig. 27 V/STOL Nozzle Exhaust Plume Centerline Decay

LARGE-SCALE STUDIES OF PROPULSION-FLOW TURNING DEVICES FOR FAN-POWERED V/STOL AIRCRAFT

Brent K. Hodder*
U.S. Army Air Mobility R&D Laboratory
and

Jerry V. Kirk†
Ames Research Center, NASA
Moffett Field, California 94035

ABSTRACT

A brief review of large-scale experimental research on thrust deflectors for lift/cruise and lift fan-propulsion systems for VTOL aircraft is presented. The data presented encompass investigations conducted at Ames Research Center from the early 1960's to the present day. Overall system performance for a variety of configurations is compared and a brief description of each configuration is given. The majority of data presented was obtained with the particular thrust deflector system coupled with a full-scale tip-turbine-driven lift fan of 1.1 or 1.3 pressure ratio.

*Aerospace Engineer.

†Operations Manager, Large-Scale Aerodynamics Branch.

INTRODUCTION

Most VTOL aircraft have powerplants that must serve the dual function of lift for VTOL and thrust for cruise operation. This means that a flow deflector must be provided to direct the exhaust from the horizontal thrusting direction to the vertical. Other powerplants which may be used primarily for lift also need flow-turning devices to provide additional thrust for low-speed flight. These devices usually take the form of cascades of exit vanes.

This paper will summarize the work done at Ames Research Center on flow-turning devices for lift/cruise and lift fan-powered aircraft.

FLOW-TURNING DEVICES FOR LIFT/CRUISE FANS

Acceptable flow-turning devices must be light, compact, efficient, and, preferably, must fold out of the way during cruise operation to minimize cruise thrust loss. Some STOL-powered lift aircraft use flaps as flow deflectors, but it is apparent from figure 1 (ref. 1) that these devices do not maintain a high efficiency to the higher turning angles that are required for VTOL operation. A limited effort has been maintained at Ames, both by in-house and contractor programs, to design and test thrust-deflecting concepts with efficiencies more suitable for VTOL operation.

Figure 2 shows photographs of several deflectors investigated at Ames. The cascade deflector (ref. 2), figure 2a, had a cascade of variable camber exit vanes leaned 45° with respect to the nozzle exit plane. The cascade was tested on a wind-tunnel model with a 1.1 pressure ratio, tip-turbine-driven lift fan. The fan is powered by a T-58 gas generator. If flow-turning angles greater than 90° are required, a second cascade is necessary. This deflector was designed and fabricated by the General Electric Co.

The hooded D-shaped deflector (fig. 2b) was designed at Ames (ref. 3) and tested with the LF-336 1.3-pressure-ratio lift-fan. The LF-336 is powered by a J85-5 gas generator. This hooded configuration represented a conservative base-point design from which to judge the potential of additional development work. The design benefited from earlier work in this area reported in reference 4.

Figure 2c shows a single-swivel nozzle that was designed by Rockwell International (ref. 5) under contract to NASA Ames. This design, also tested with the LF-336, reduced mechanical complexity, not only for the method of thrust deflection, but also for providing control functions such as thrust spoiling and yawing moments.

Finally, figure 2d shows the conceptual design of an improved, vented D-shaped deflector designed by McDonnell-Douglas under contract to Ames. This design reflects additional development work on the hooded concept and has resulted in a design which promises to reduce system weight. This is accomplished by decreasing the amount of duct diffusion, the duct r/D and, subsequently, the number of rotating hoods. Small-scale tests indicate that good performance has been maintained by venting the interior bend of the duct (see ref. 6). A "boiler plate" model of this configuration is scheduled for testing with the LF-336 lift fan in late calendar year 1975.

Figure 3 shows the large-scale test results for turning efficiency out of ground effect for three deflectors (figs. 2a, b, and c). It should be remembered that all of the configurations tested

represent initial designs and none have benefited from an optimization program. The single-swivel nozzle deflector had a 14% thrust loss in the VTOL mode and a 3% nozzle loss in the cruise mode. The variable camber cascade had a 6% thrust loss in the VTOL mode, but the presence of the cascade without turning produced a 5% loss, thus the turning was very efficient. Finally, the hooded deflector with a radius-to-diameter ratio of 0.78 had a VTOL thrust loss of 5%. From strictly a vectoring performance point of view, either the cascade or the hooded deflector would appear to be adequate with their present state of development. However, one must consider the impact on overall aircraft performance. Both the variable camber cascade and the hooded deflector (fig. 2b) would significantly increase aircraft weight and probably mechanical complexity. The hot-gas tip-turbine drive feature of conventional lift fans accentuates the weight aspect of deflectors, since duct wall temperatures necessitate heavier metals for structural integrity. Flow mixers to reduce wall temperatures have been considered, but the weight-performance tradeoffs have not been studied.

The final but critical area of VTOL operation is deflector performance in an installed environment. The degree to which the deflector operates in ground effect obviously depends on the particular aircraft configuration, but it seems certain that fan-nozzle ground clearance in the VTOL mode will not exceed 1 to 2 nozzle diameters. Therefore, the impact of ground effect on deflector performance must also be investigated.

Figure 4 shows the effect of ground clearance on fan performance for the Ames hooded deflector. Even at h/D of 2, the hooded deflector experienced a 10% thrust loss. No attempt to vary nozzle area while in ground effect was made; however, it may prove to be beneficial. It should not be assumed that every deflector system will produce similar results in ground effect, but it is essential to include this aspect in the final determination of overall system performance. For reference, the ground effect on the LF-336 in a lift-fan configuration is shown in figure 5.

FLOW-TURNING DEVICES FOR LIFT FANS

Fans oriented to provide lift are usually shut down when airspeed is sufficient for wing-supported flight. However, at airspeeds between hover and that for wing-supported flight, the fan must provide both lift and thrust, thus flow-vectoring devices are required. These devices may also be required to act as a cover for the fan cavity during conventional flights.

Figure 6 contains photographs of the lift-fan flow-deflector systems studied at Ames. The 17.8 cm (7 in.) chord vanes, shown in figure 6a, have been used in the majority of the lift-fan aircraft configuration studies. The vanes are cambered to provide the largest turning in the thrust direction. The solidity of the cascade is 1.4. Figure 6b shows a cascade with 35.6 cm (14 in.) chord vanes. The airfoil section and solidity are the same; only the chord is changed. This system was modified at midspan by installing a flap with a linkage that provides a schedule between the flap angle and the vane deflection. A photograph of the flapped vane is shown in figure 6c. The articulated trailing-edge flap represents an attempt to widen the range over which efficient flow turning could be obtained. The 35.6 cm (14 in.) chord vanes were also modified into a chevron shape (fig. 6d) in an attempt to avoid fan backpressure at higher deflection angles. Finally, in figure 6e, a swiveling cascade is shown (ref. 7). In this case, the vanes are mounted on a rotating ring so that the vanes can be both rotated and deflected. By canting the fan exhaust, another degree of freedom is obtained for the vectoring system. Details of this system are given in figure 7.

Performance of these lift-fan flow-turning devices is given in figure 8. With the exception of the swiveling cascade data, in all vane cascade systems shown, the lift is referenced to the 17.8 cm (7 in.) chord vanes. The efficiency of the standard 17.8 cm (7 in.) chord louver system falls off beyond 30° of flow turning. Although not shown, the efficiency at the negative end would be expected to fall off beyond -10° . The 35.6 cm (14 in.) vane extended the turning range for equal efficiency about 3° and reduced the overall thrust slightly, whereas the flapped vanes increased the high efficiency range about 5° more. However, the flapped vane increased the total range of the system a great deal, since the flap was programmed to reverse the camber built into the airfoil. The swiveling cascade appears to have the best turning performance of the cascades studied. However, this result must be viewed with caution, since the actual resultant thrust force in hover is less than the value for other cascade swivel angles.

PREDICTION METHODS

Prediction of the performance of flow measuring devices rests mainly on empirical data. In addition, the vectoring device may backpressure the fan and thus affect performance further. For lift-fan flow-turning cascades, experimental cascade data are used, and the attendant turning losses are factored back into fan performance to provide the overall estimate of performance. For cruise-fan flow-turning devices, data on pipe bend losses are used. The ability of pipe bend losses to accurately predict system losses is hampered by the following: the lack of loss coefficients for the actual duct cross-sections used and the limited data for loss coefficients for bends with decreasing cross-sectional area, appropriate for designs in which the duct bend and exhaust nozzle are close-coupled. In either case, the prediction of flow-turning performance is not likely to be precise.

For best results, large-scale experimental data should be used. Figure 9 shows flow-turning performance for the full-scale 17.8 cm (7 in.) chord cascades and a one-sixth scale model of the same cascade. Although the turning angles were about the same, the scale-model cascade was much less efficient.

CONCLUSIONS

A review of experimental data from Ames Research Center indicates that flow-turning devices for VTOL aircraft do have adequate uninstalled performance. The flow-turning devices for VTOL propulsion systems that are used primarily for lift have sufficient performance for present-day applications. However, in the regime of thrust deflection for lift/cruise systems, there is a definite payoff for further work to fully realize the potential performance that has been demonstrated by full-scale tests. This additional work must provide a system which can handle the installed environment, be lightweight and mechanically feasible, yet maintain the basic performance proven with earlier designs. Furthermore, without a doubt, prediction methods could be improved.

REFERENCES

1. Hickey, D. H.: V/STOL Aerodynamics: A Review of the Technology. AGARD Conference Proceedings No. 143 on V/STOL Aerodynamics, 1974.
2. Kirk, J. V.; Dickinson, S. O.; Hall, L. P.; Coffman, M. G.: Aerodynamic Characteristics of a Large-Scale Lift-Fan Transport Model with Podded Fans Forward and Lift/Cruise Fans Mounted Above the Wing. NASA TM X-62,151, 1972.
3. Kirk, J. V.; Hall, L. P.; Hodder, B. K.: Aerodynamics of Lift-Fan V/STOL Aircraft. NASA TM X-62,086, 1971.
4. Brendal, D. H.: Vectored-Thrust Cruise Propulsion System Development Program. Part I, Vol. 1, AFAPL TR-68-18-Pt-1-Vol-1, 1967.
5. Schlundt, D. W.: Testing of Lift/Cruise Fan Exhaust Deflector. NASA CR-137682, 1975.
6. McDonnell-Douglas Aircraft Corp. Report. Design of a Thrust-Vectoring Nozzle for V/STOL Transport Lift/Cruise Fans. NASA CR-114,754, 1974.
7. Atencio, A.; Hall, L. P.; Kirk, J. V.: Low-Speed Wind Tunnel Investigation of a Large-Scale Lift-Fan STOL Transport Model. NASA TM X-62,231, 1973.

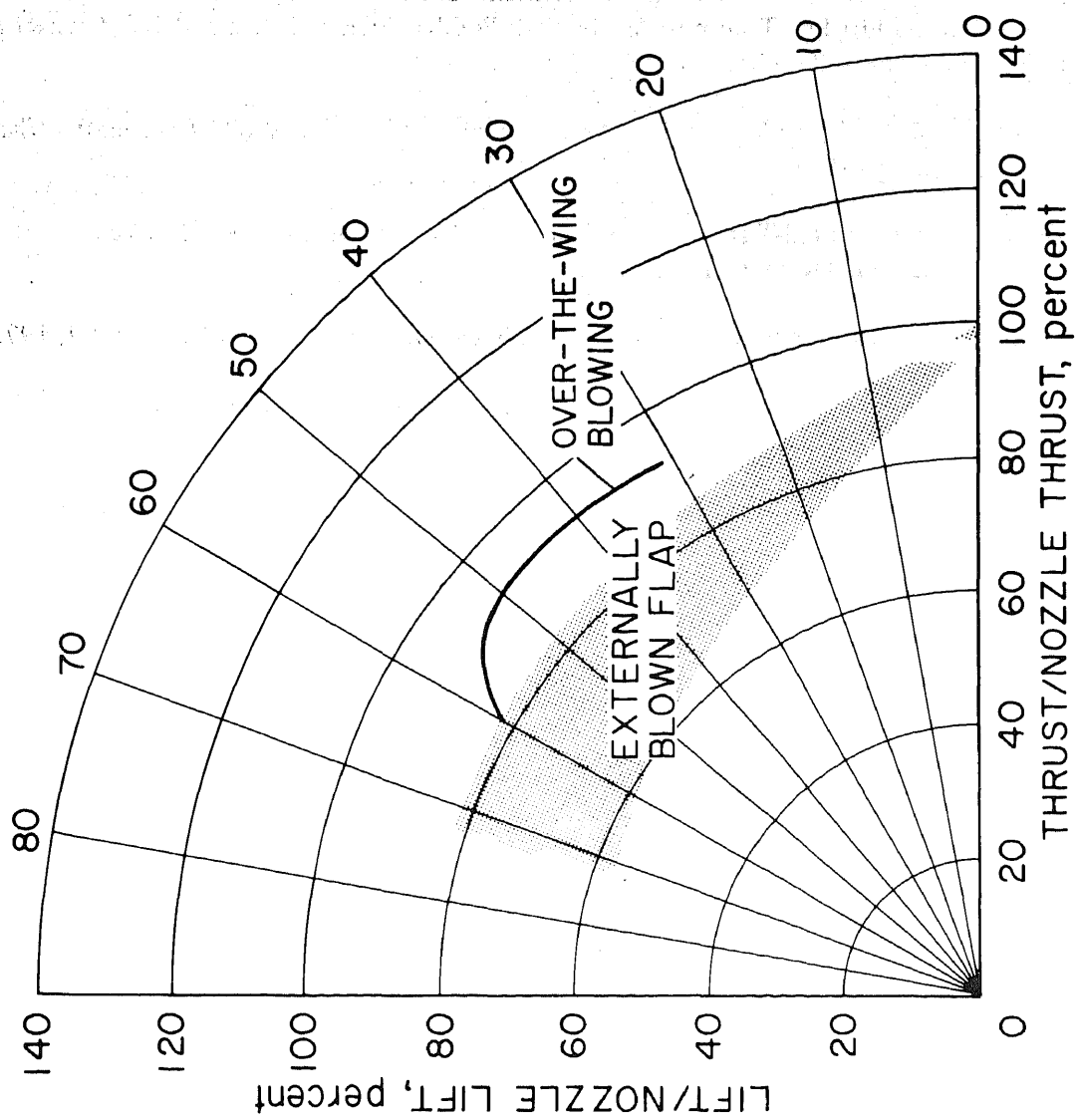
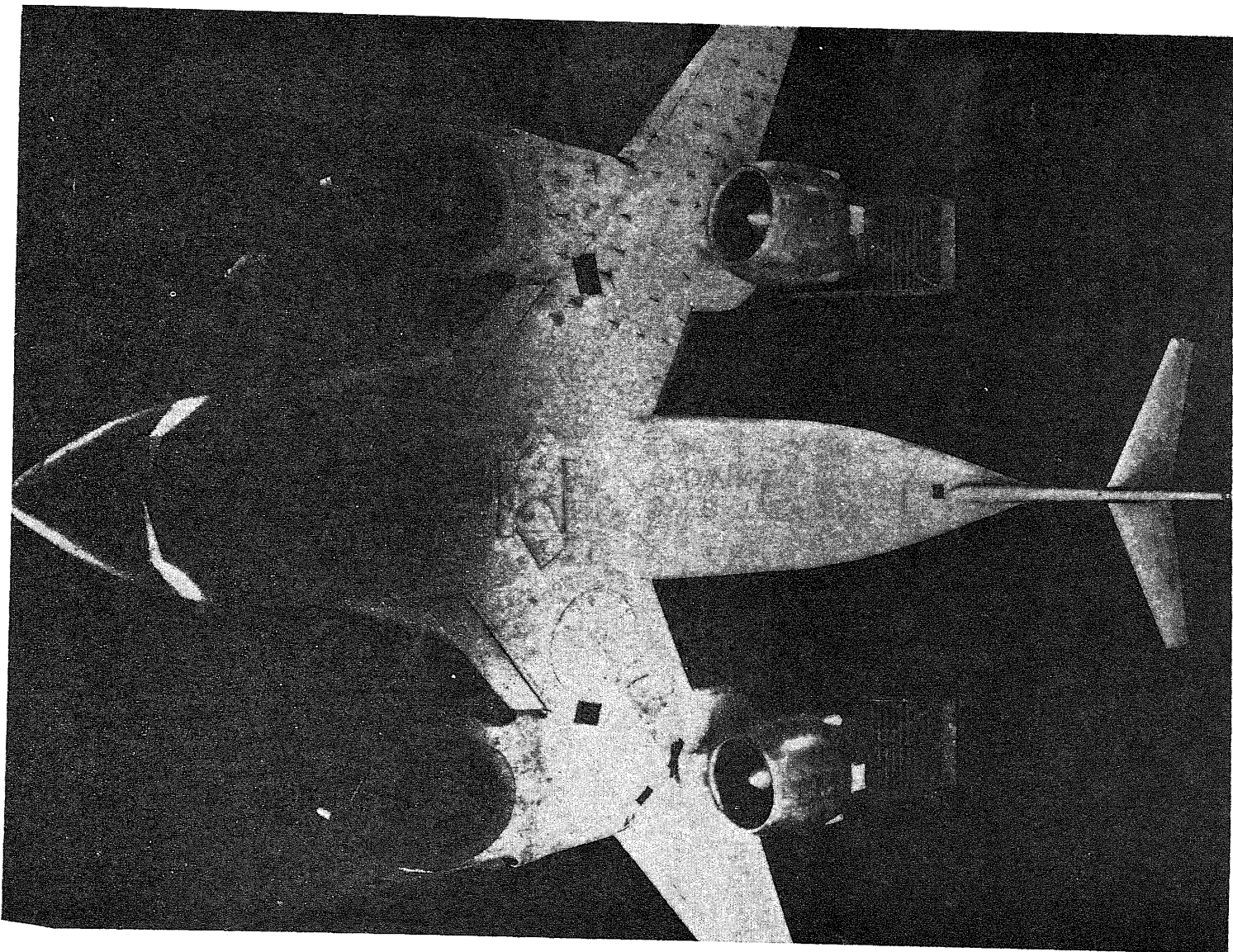


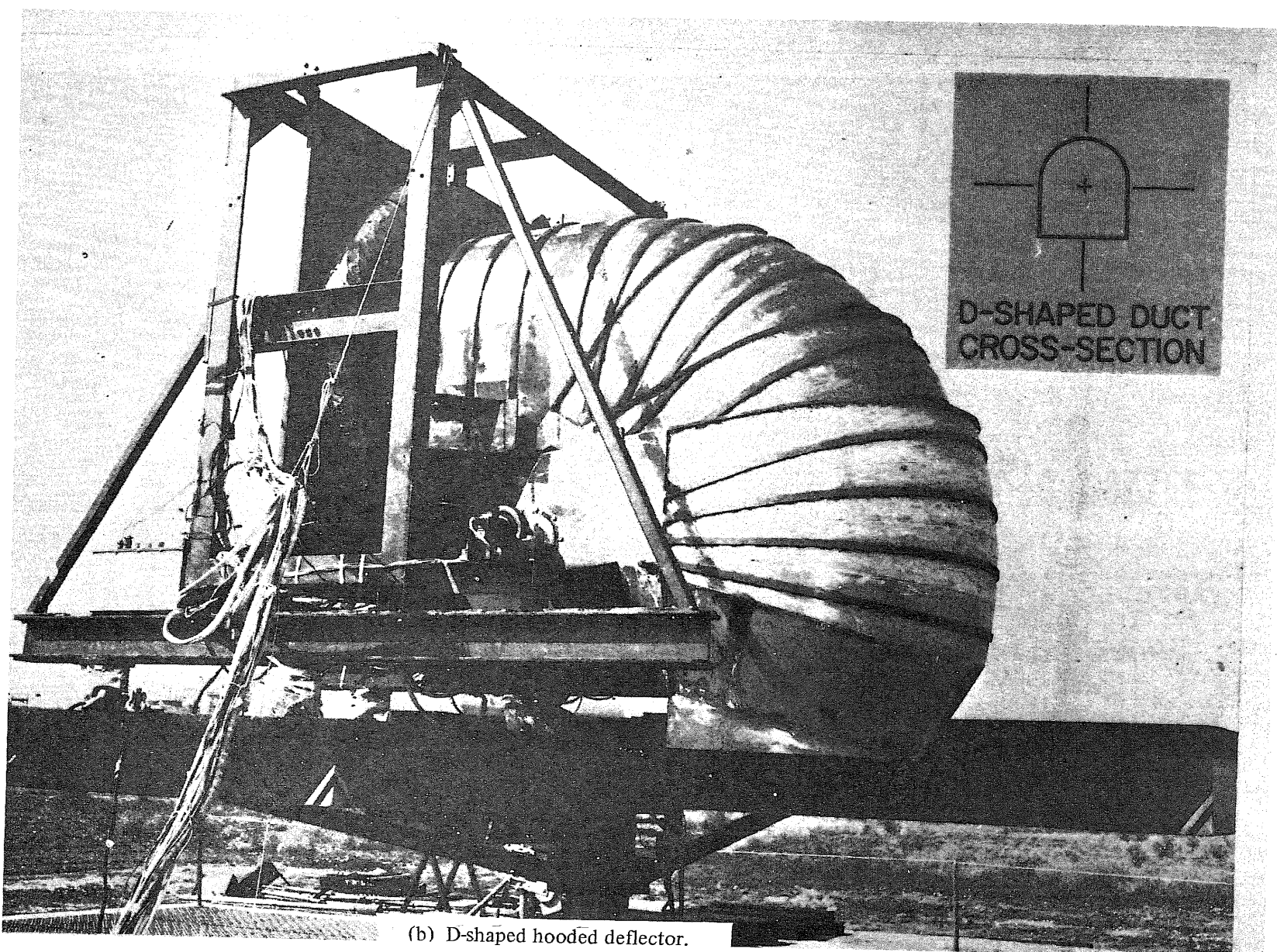
Figure 1.— Turning efficiency of STOL wing flap systems.



(a) Variable camber vane cascade.

Figure 2.— Photographs of several flow-turning devices investigated.

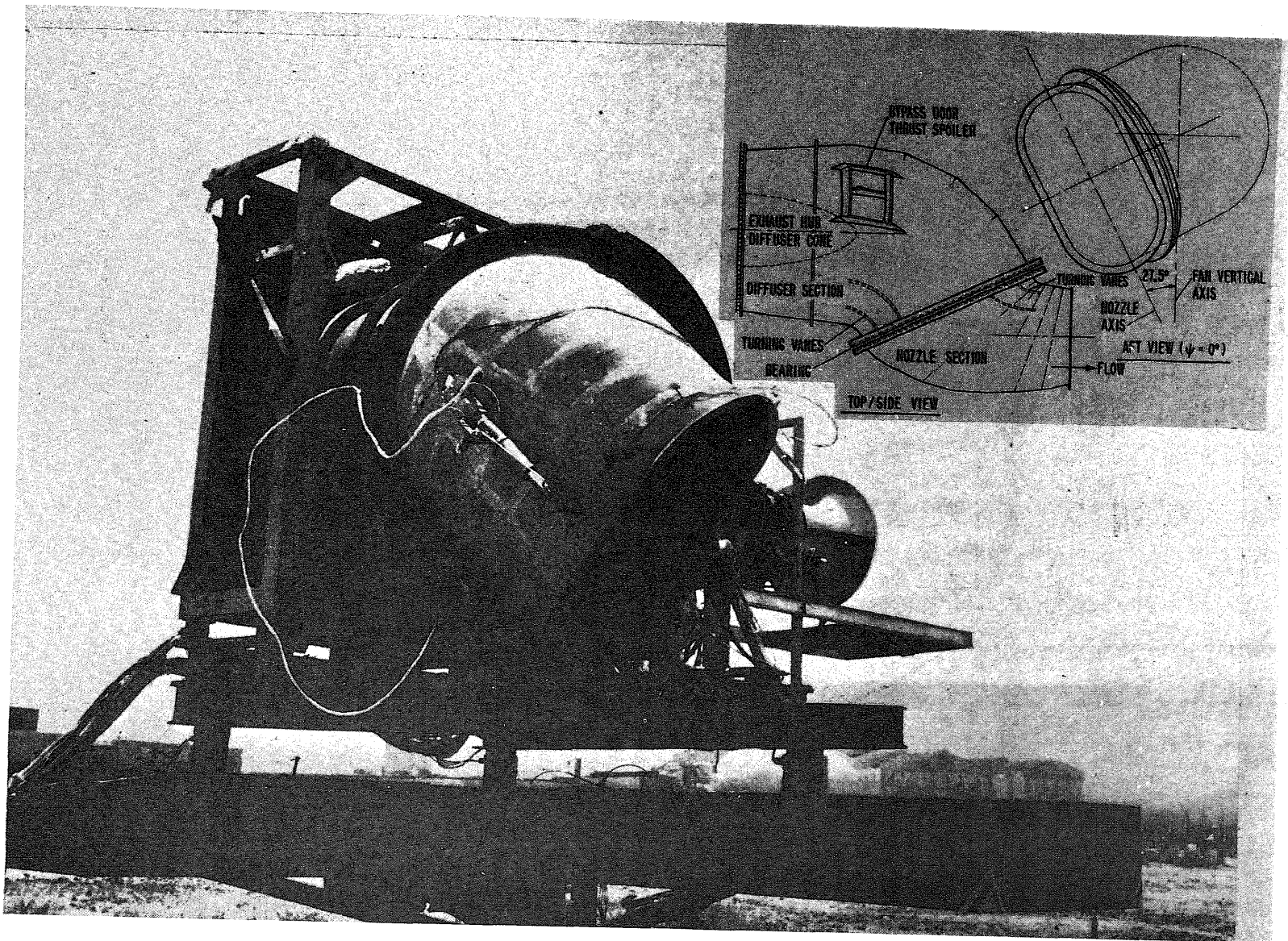
464



(b) D-shaped hooded deflector.

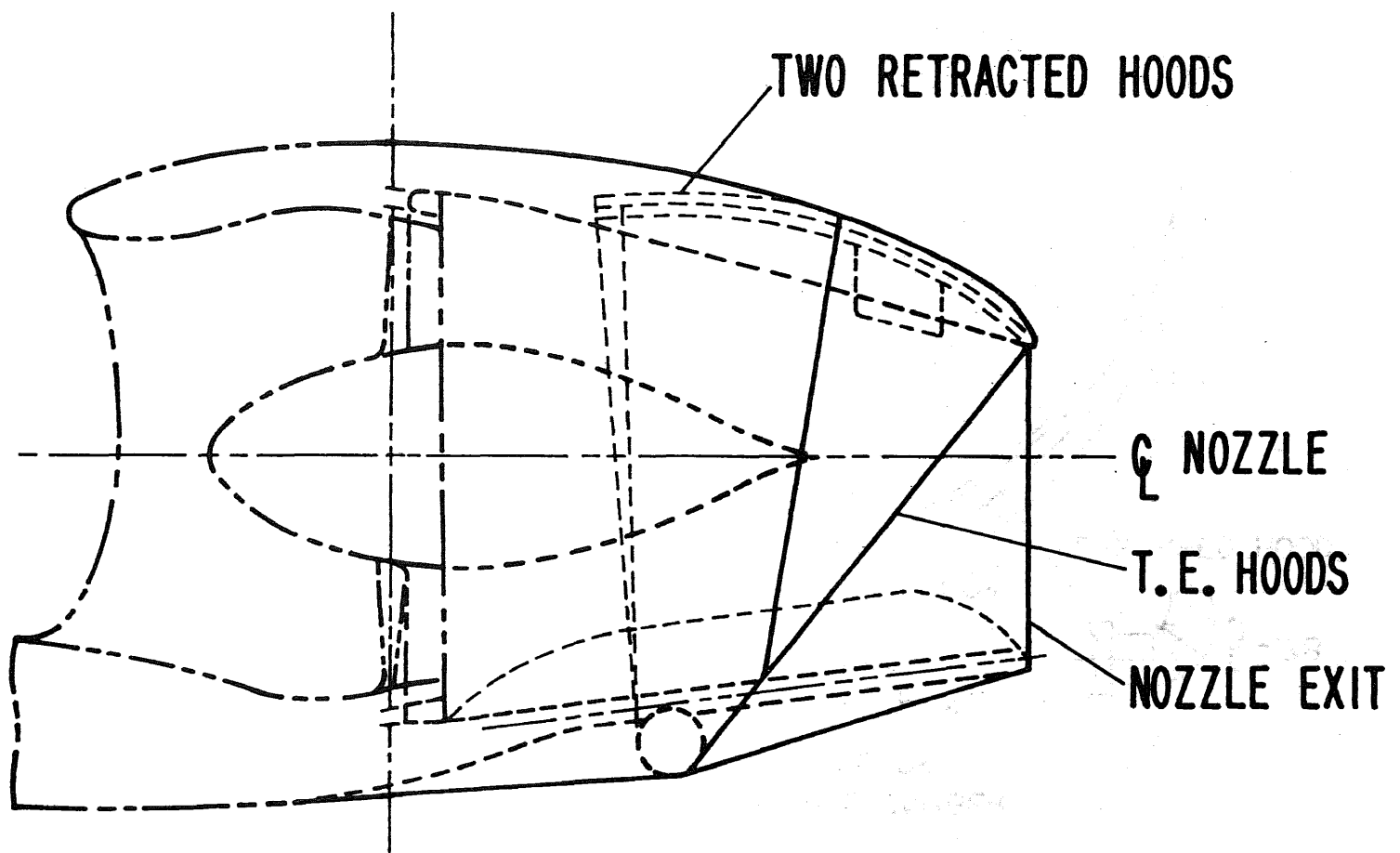
Figure 2.— Continued.

465



(c) Single-swivel nozzle deflector.

Figure 2.— Continued.



(d) Vented D-shape hooded deflector.

Figure 2.— Concluded.

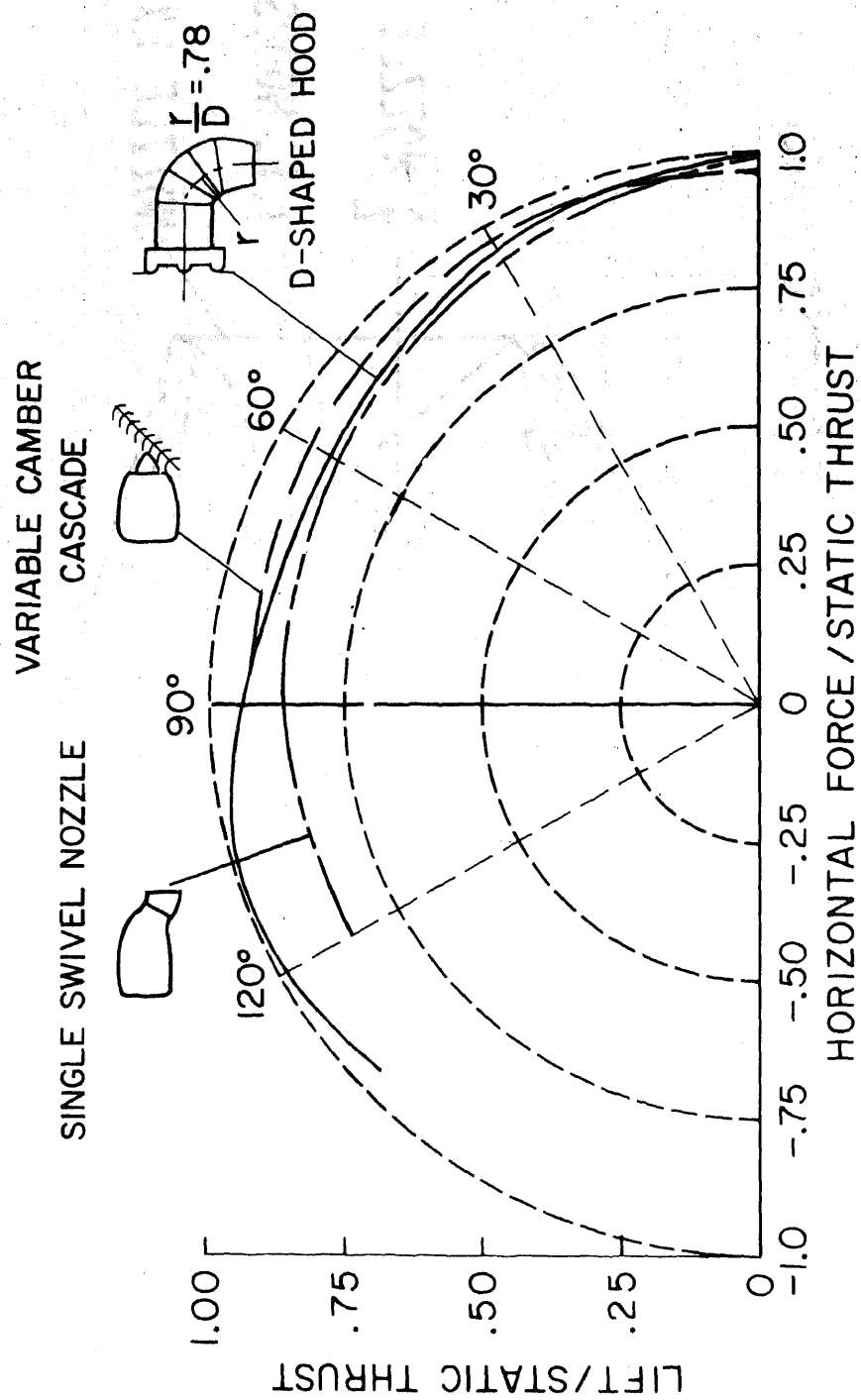


Figure 3.— Summary of turning efficiency for full-scale lift/cruise thrust deflectors.

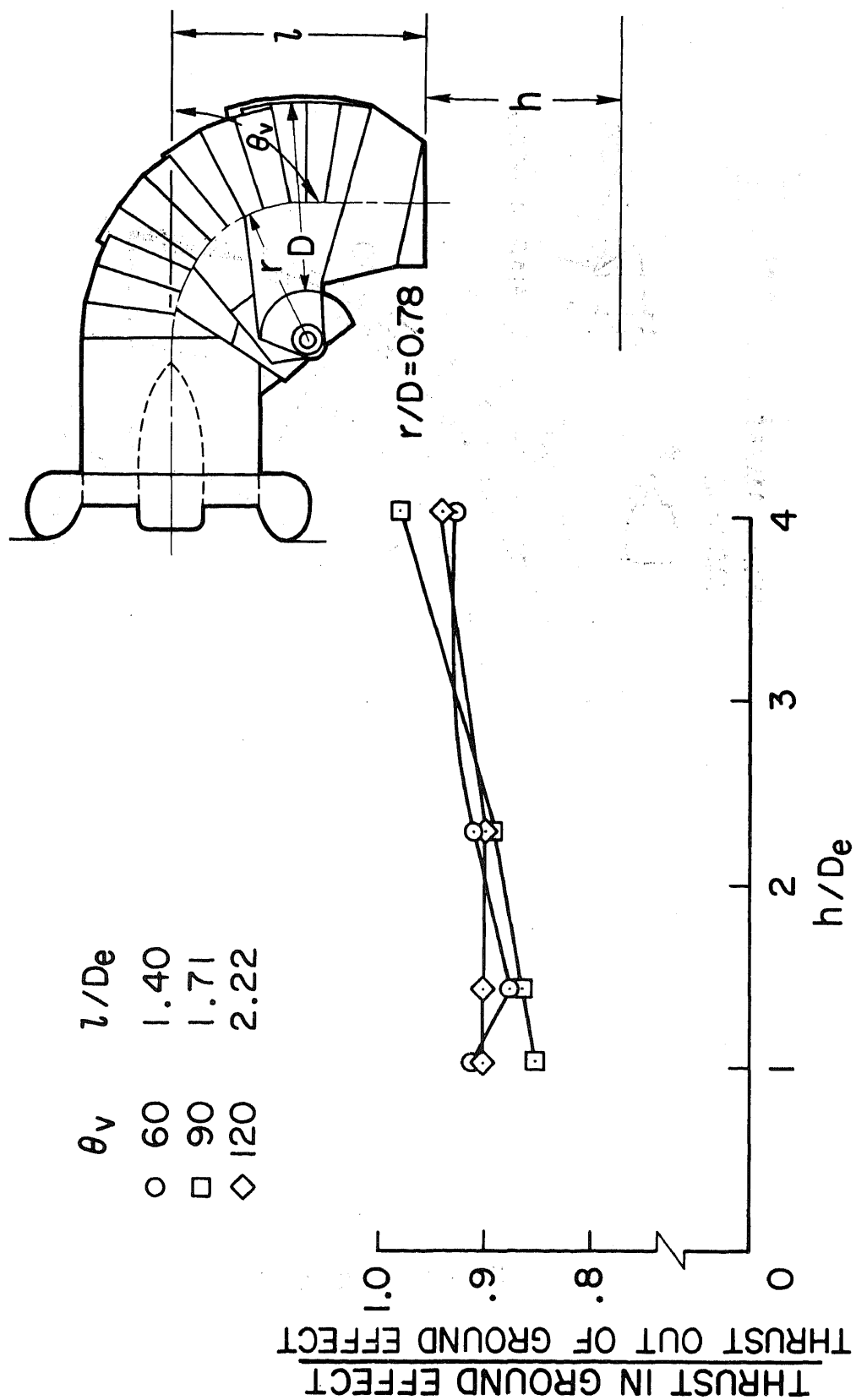


FIGURE 4 — Effect of ground height on VTOL thrust with the "D"-shaped hooded deflector.

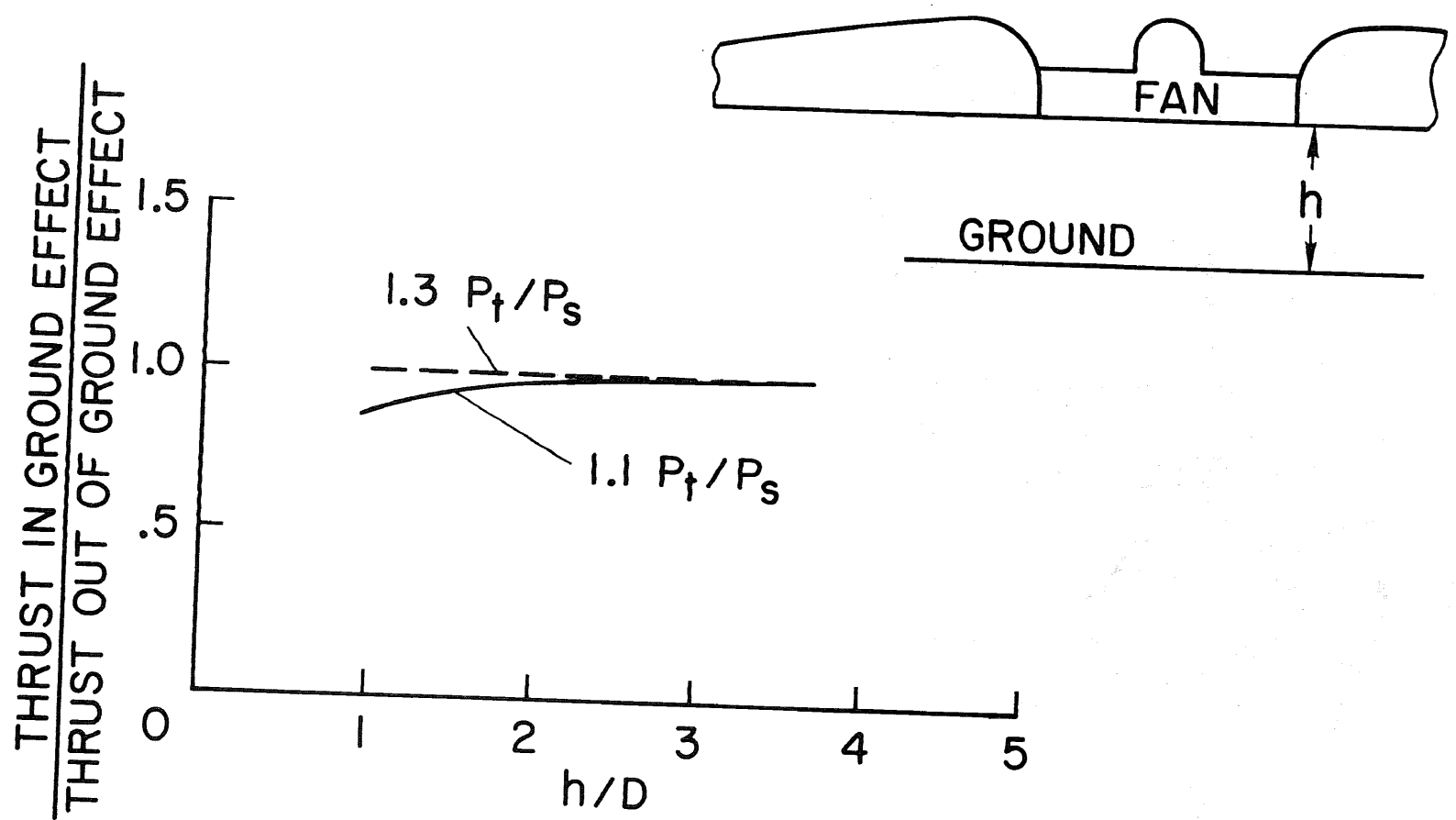
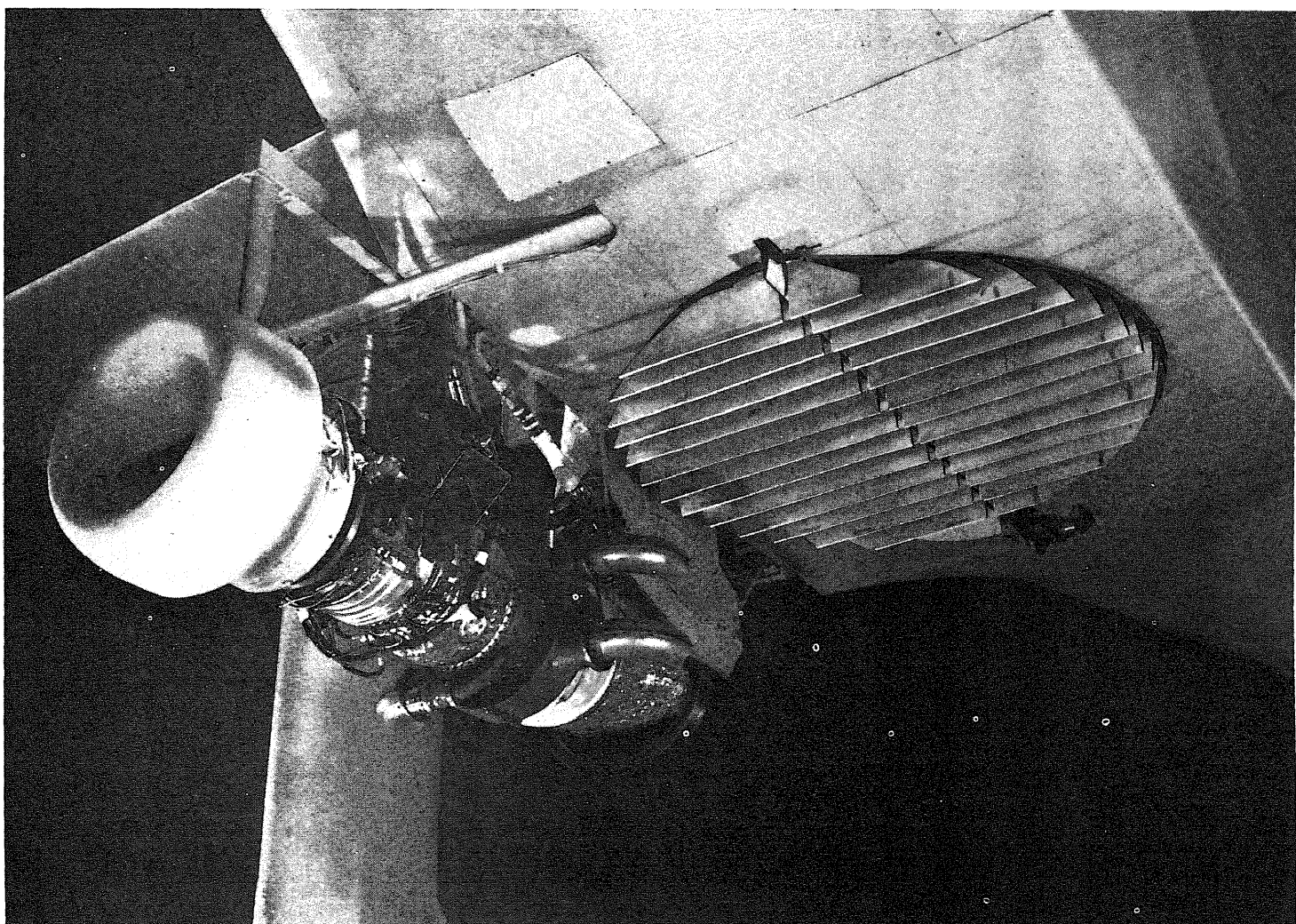
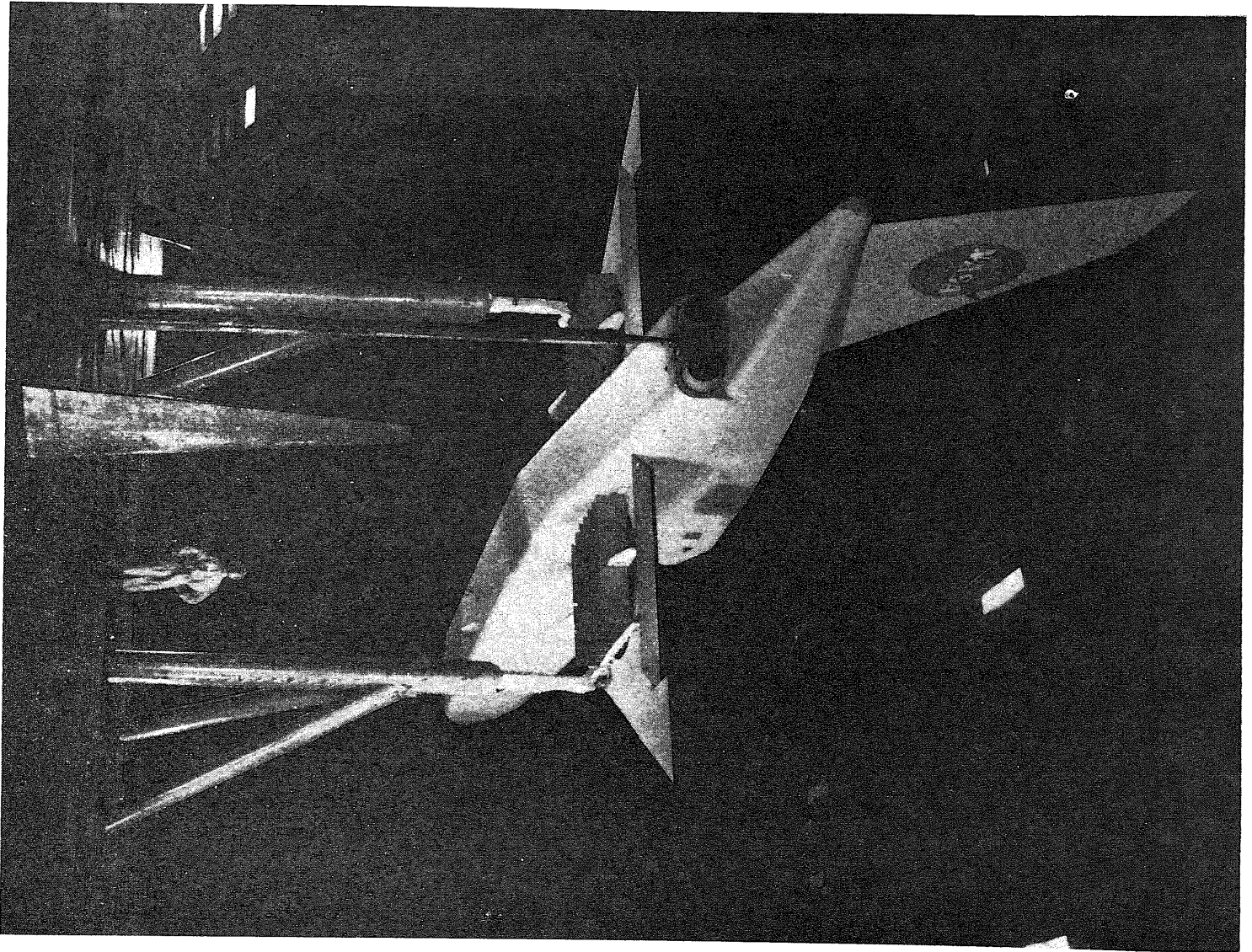


Figure 5.— Effect of ground on fan thrust in a wing installation.



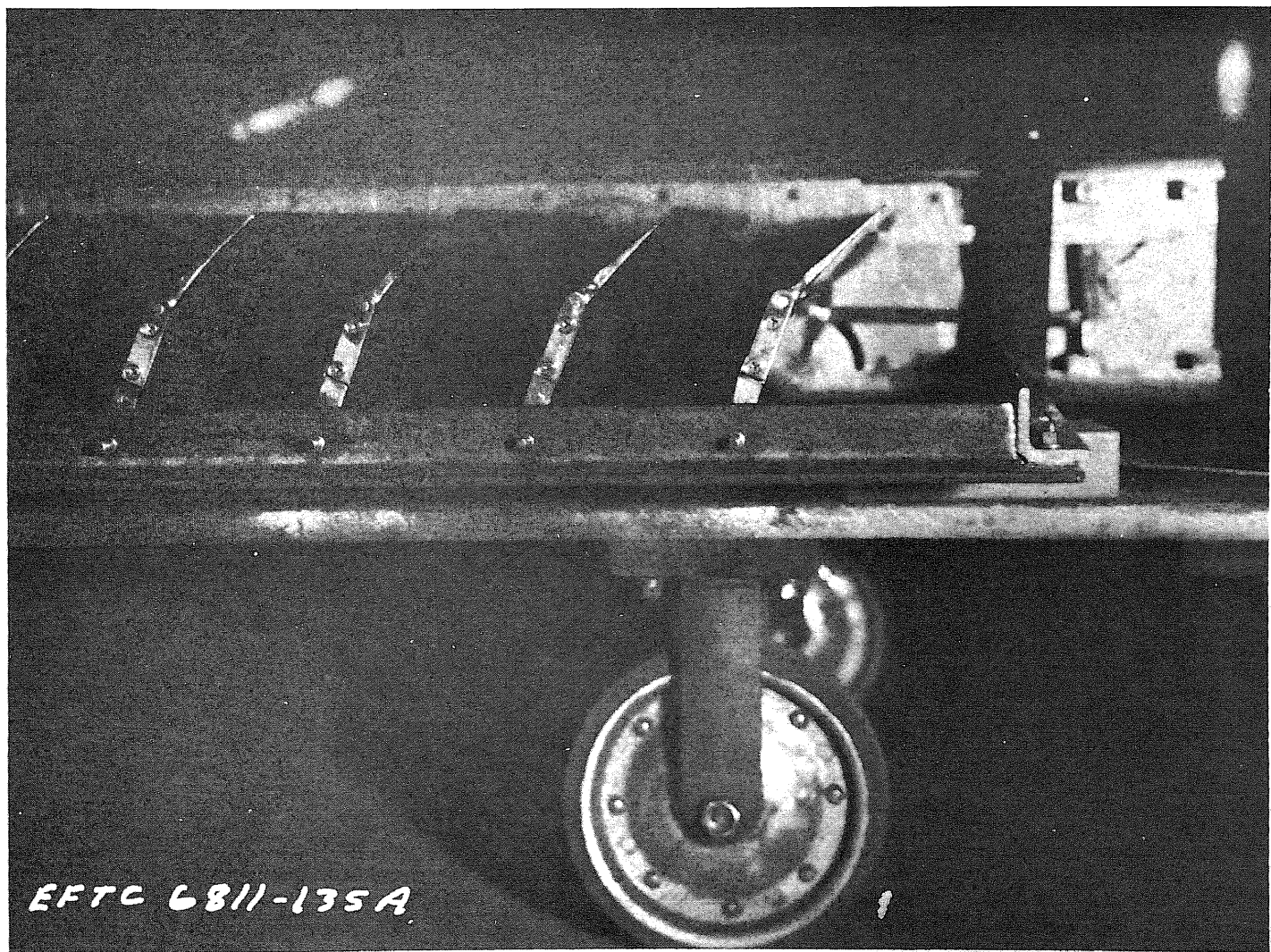
(a) 17.8 cm (7 in.) chord vane cascade.

Figure 6.— Photographs of various lift fan vane cascades for flow turning.



(b) 35.6 cm (14 in.) chord vane cascade.

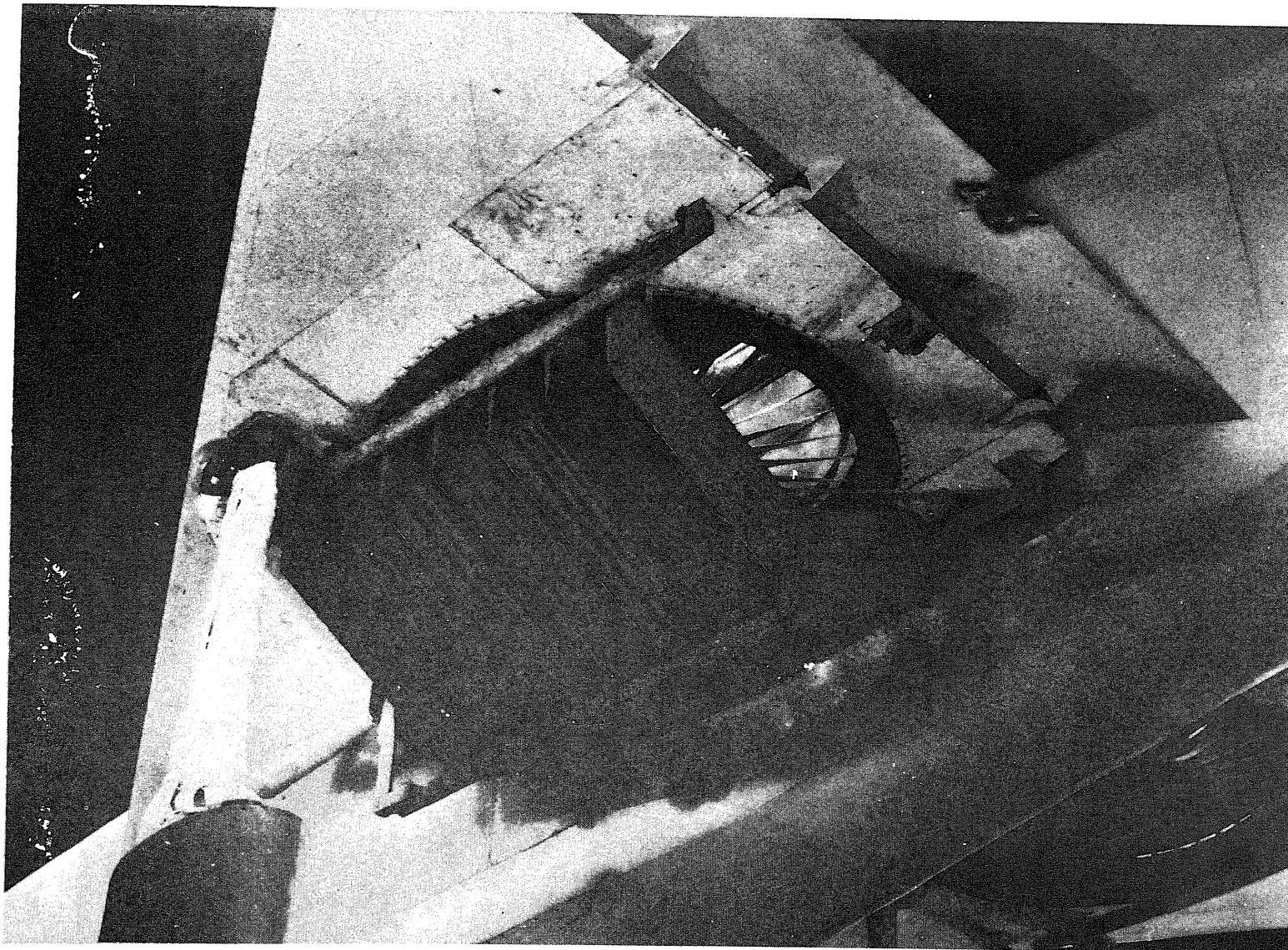
Figure 6.— Continued.



(c) 35.6 cm (14 in.) chord flapped vane cascade.

Figure 6.— Continued.

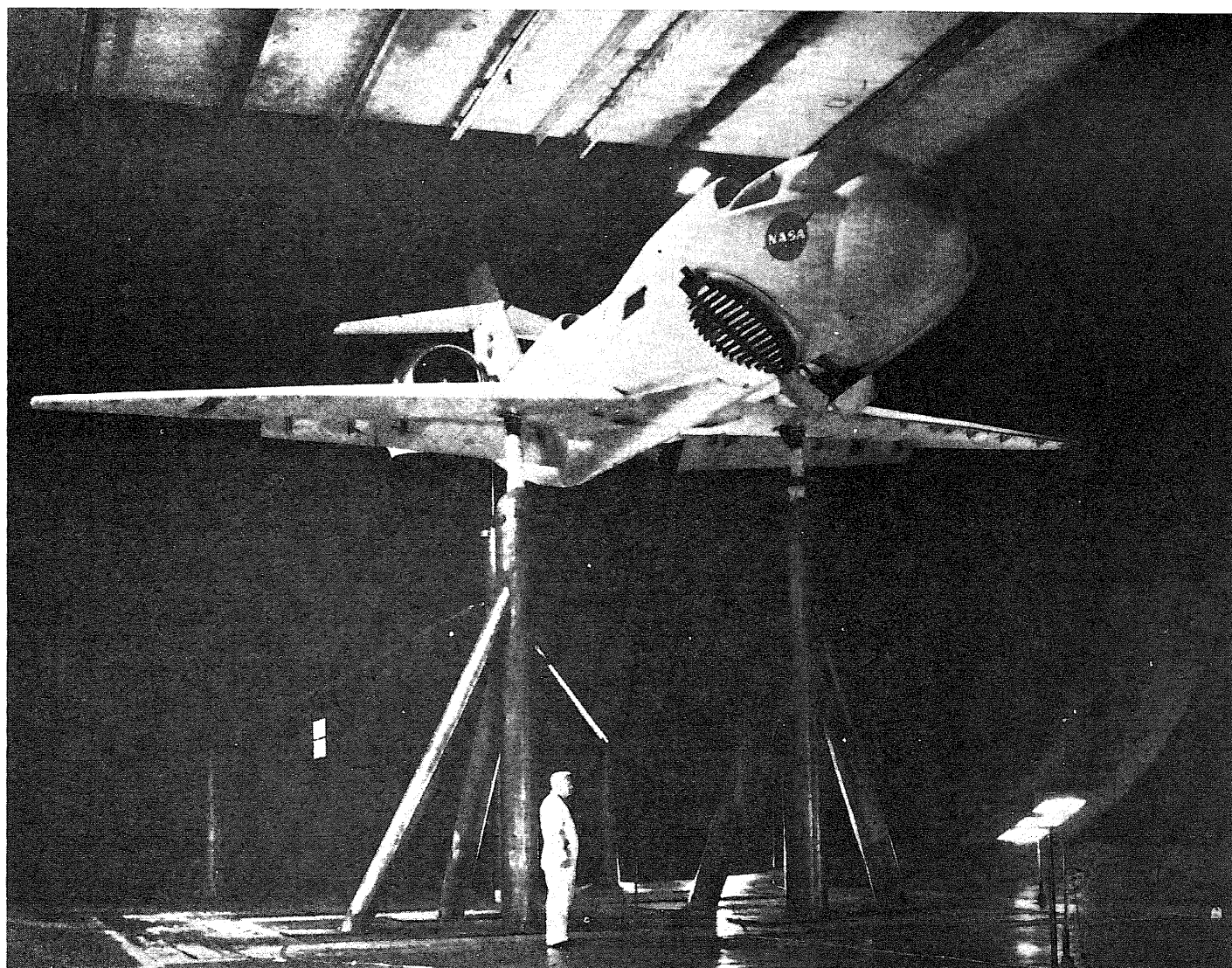
474



(d) 35.6 cm (14 in.) chord swept-vane cascade.

Figure 6.— Continued.

475



(e) Swiveling cascade.

Figure 6.— Concluded.

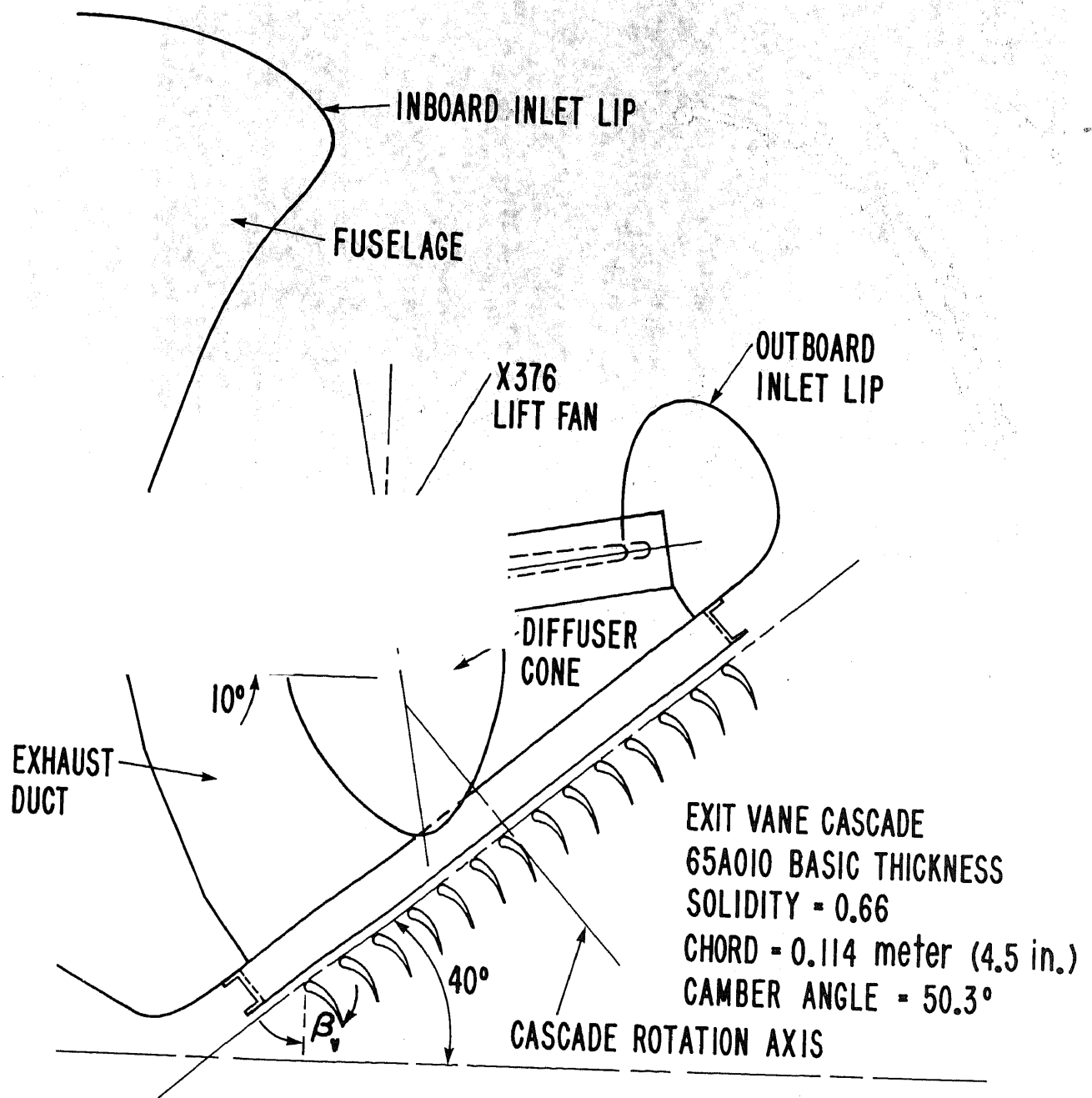


Figure 7.— Arrangement of swiveling cascade.

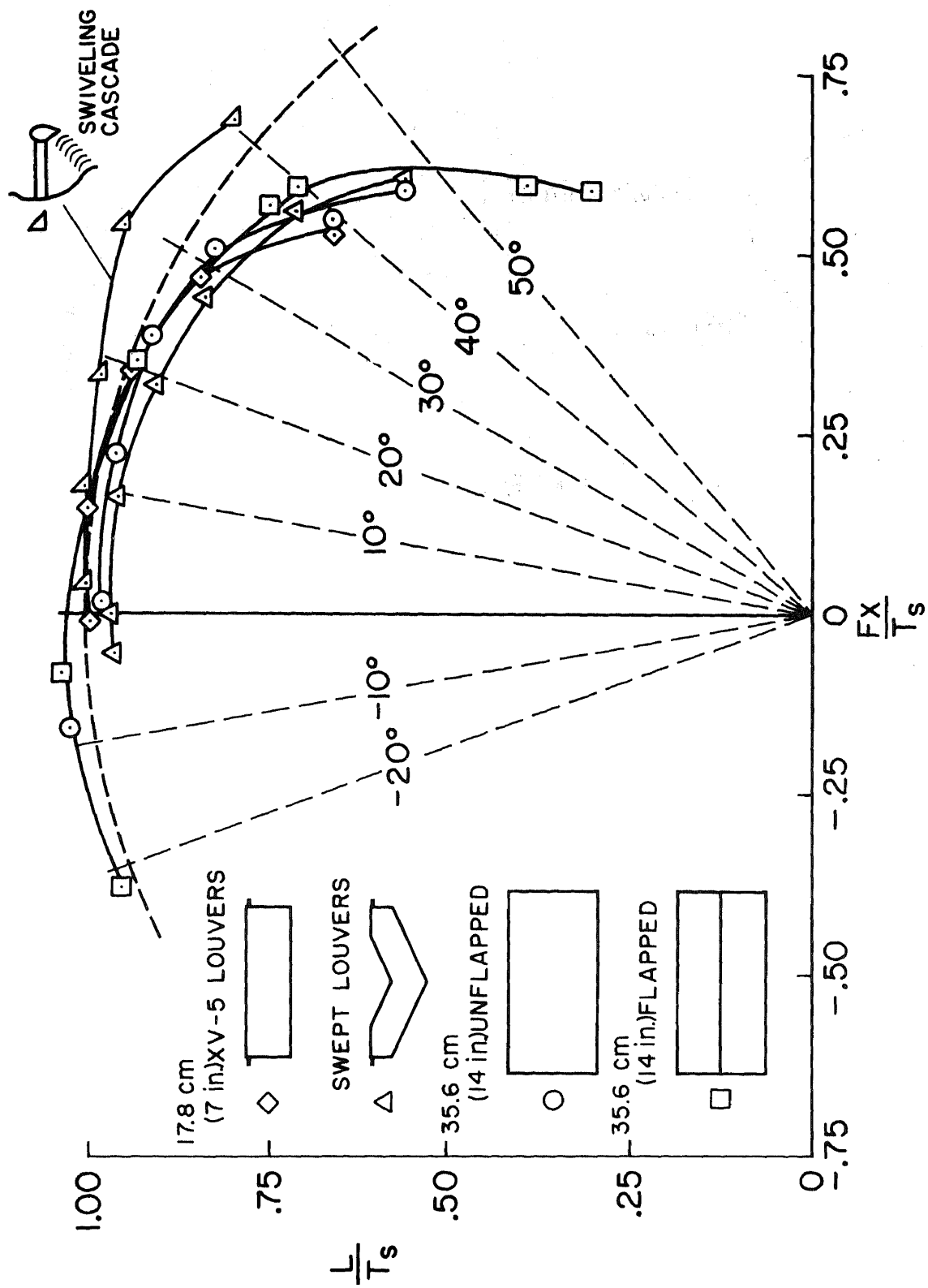


Figure 8.— Summary of turning efficiency for lift-fan thrust deflectors.

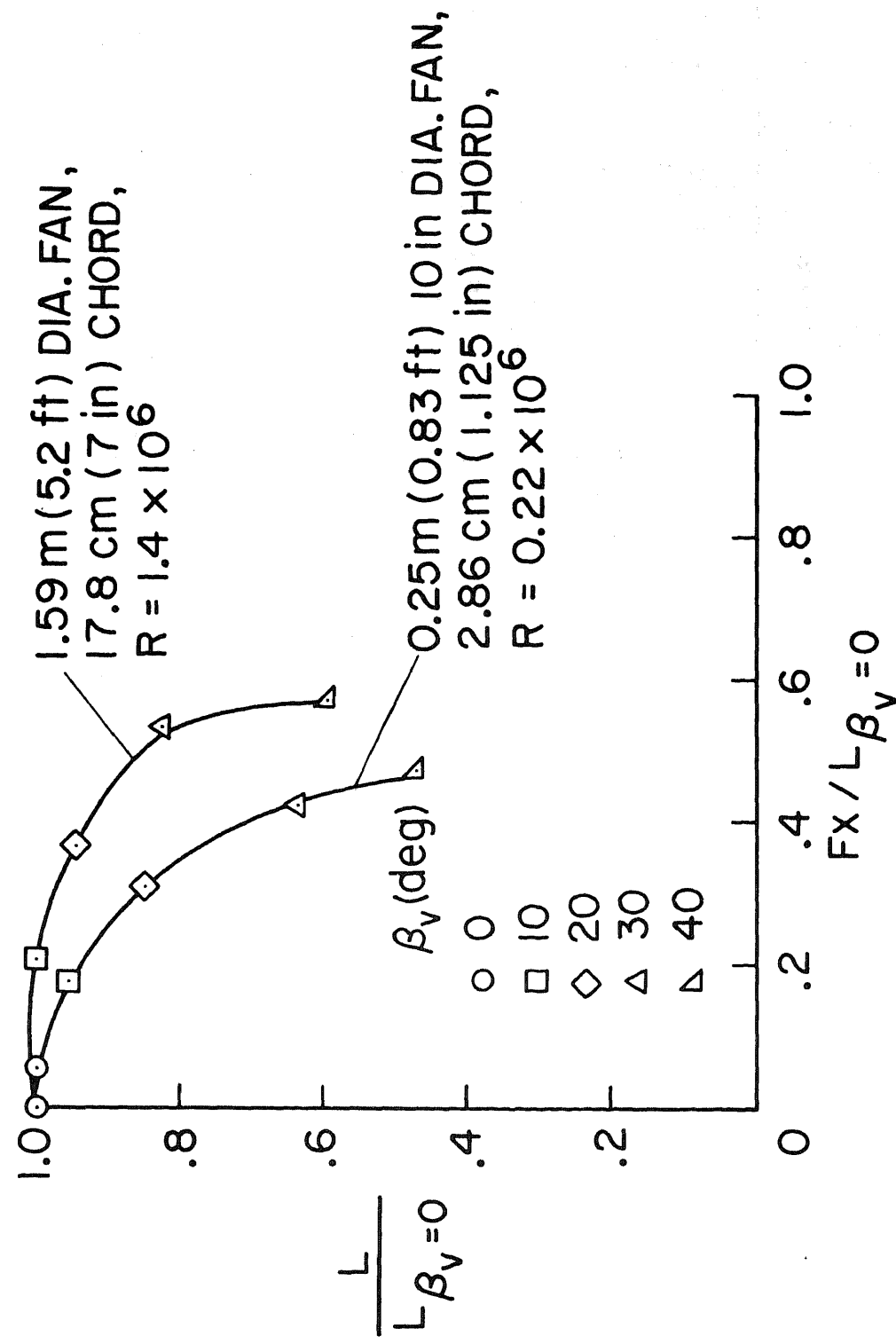


Figure 9. — Performance of large- and small-scale exit-vane systems.

ABSTRACT

A two-dimensional Augmented Deflector Exhaust Nozzle (ADEN) has been selected as a high potential exhaust system for advanced multi-mission V/STOL aircraft. The ADEN selection was based on the results of a Navy Advanced V/STOL Propulsion Component Development Program. This program included a comprehensive series of aerodynamic and mechanical design studies, aircraft system studies and scale model experimental test programs. ADEN detailed mechanical design has been completed and hardware fabrication for a full size ADEN demonstration test on G.E. J101 engine is underway. This paper presents the aerodynamic and mechanical features of the ADEN and describes the upcoming full scale demonstrator program.

INTRODUCTION

The United States Navy, recognizing the advanced technology needs to develop a superior multi-mission V/STOL fighter aircraft initiated an advanced V/STOL Propulsion Component Development Program. In mid 1972 the General Electric Company was awarded the Exhaust Nozzle/Deflector portion of the program.

The Nozzle/Deflector Component Development Program consisted of three parts: Part (1) was a comprehensive evaluation of the performance, design and installation parameters required for the identification of a Nozzle/Deflector system having the greatest potential for application to a Navy

V/STOL fighter. Part (2) included the detail design and component testing of the selected Nozzle/Deflector and Part (3) was the procurement of a full size engine demonstrator assembly of the selected Nozzle/Deflector

Based on the results of Part (1) and Part (2) of the program, the Naval Air Propulsion Test Center, Trenton, New Jersey, selected the Augmented Deflector Exhaust Nozzle (ADEN) for continued development, manufacture and demonstration on a General Electric J101 engine.

V/STOL PROPULSION SYSTEM REQUIREMENTS

Advanced V/STOL fighters require high specific thrust (afterburning) engines to best achieve multi-mission objectives. Results of aircraft system studies conducted in Part (1) indicate that the combat and P_S mission points size the main propulsion system such that all the required vertical thrust is potentially available from the cruise engines. From a total system weight standpoint, it is desirable to maximize the amount of onboard cruise engine thrust and minimize direct lift engine/devices size and thrust requirements during vertical operation. The capability to operate at afterburning power settings in vertical mode is therefore a desirable feature of an advanced nozzle/deflector system.

Advanced V/STOL aircraft configured to utilize the maximum amount of cruise engine thrust during vertical operation tend towards mid fuselage propulsion system installation to meet pitch balance constraints. Studies

ABSTRACT

A two-dimensional Augmented Deflector Exhaust Nozzle (ADEN) has been selected as a high potential exhaust system for advanced multi-mission V/STOL aircraft. The ADEN selection was based on the results of a Navy Advanced V/STOL Propulsion Component Development Program. This program included a comprehensive series of aerodynamic and mechanical design studies, aircraft system studies and scale model experimental test programs. ADEN detailed mechanical design has been completed and hardware fabrication for a full size ADEN demonstration test on G.E. J101 engine is underway. This paper presents the aerodynamic and mechanical features of the ADEN and describes the upcoming full scale demonstrator program.

INTRODUCTION

The United States Navy, recognizing the advanced technology needs to develop a superior multi-mission V/STOL fighter aircraft initiated an advanced V/STOL Propulsion Component Development Program. In mid 1972 the General Electric Company was awarded the Exhaust Nozzle/Deflector portion of the program.

The Nozzle/Deflector Component Development Program consisted of three parts: Part (1) was a comprehensive evaluation of the performance, design and installation parameters required for the identification of a Nozzle/Deflector system having the greatest potential for application to a Navy

V/STOL fighter. Part (2) included the detail design and component testing of the selected Nozzle/Deflector and Part (3) was the procurement of a full size engine demonstrator assembly of the selected Nozzle/Deflector

Based on the results of Part (1) and Part (2) of the program, the Naval Air Propulsion Test Center, Trenton, New Jersey, selected the Augmented Deflector Exhaust Nozzle (ADEN) for continued development, manufacture and demonstration on a General Electric J101 engine.

V/STOL PROPULSION SYSTEM REQUIREMENTS

Advanced V/STOL fighters require high specific thrust (afterburning) engines to best achieve multi-mission objectives. Results of aircraft system studies conducted in Part (1) indicate that the combat and P_S mission points size the main propulsion system such that all the required vertical thrust is potentially available from the cruise engines. From a total system weight standpoint, it is desirable to maximize the amount of onboard cruise engine thrust and minimize direct lift engine/devices size and thrust requirements during vertical operation. The capability to operate at afterburning power settings in vertical mode is therefore a desirable feature of an advanced nozzle/deflector system.

Advanced V/STOL aircraft configured to utilize the maximum amount of cruise engine thrust during vertical operation tend towards mid fuselage propulsion system installation to meet pitch balance constraints. Studies

have indicated that two-dimensional exhaust systems generally have superior cruise installation characteristics relative to conventional axisymmetric exhaust systems in this type aircraft configuration.

Advanced V/STOL fighter aircraft normally include multi-mission objectives for transonic/supersonic cruise and combat and subsonic loiter. The nozzle/deflector exhaust system internal flowpath design is critically important to a multi-mission V/STOL fighter because of dual requirements for both low speed and high Mach capabilities with high installed performance. As supersonic and supersonic combat specific power (excess thrust) levels increase, variable geometry exhaust systems are required to provide nozzle throat area modulation and expansion area control to provide high nozzle thrust coefficients for a wide range of cruise/acceleration and maneuverability points. It is therefore a critical requirement that the thrust vectoring device does not compromise the exhaust system aerodynamic flowpath during forward mode operation.

AUGMENTED DEFLECTOR EXHAUST NOZZLE (ADEN)

Exhaust systems capable of deflecting or turning the exhaust gas of jet engines, to achieve vertical and short take-off and landing, have been considered for many years. A wide variety of thrust vectoring nozzles has evolved. In general these nozzles have one or more of the following limitations.

- o Low internal performance due to internal flowpath compromises required to accomodate the deflector system.

- o Limited to nonaugmented temperatures in the vectored mode of operation.
- o Excessive downward projection of nozzle/deflector hardware in the lift mode resulting in ground clearance problems.
- o Slow vector angle and nozzle area rate of variation.
- o Discontinuous vectoring performance between cruise mode and lift mode.
- o Airframe doors required to accomodate the nozzle in the vectored mode.
- o Installed performance problems due to excessive base area or nozzle boattail angles.
- o Low lift thrust available when compared to the required weight addition to the basic cruise engine.
- o Excessive complexity with consequent reliability limitations.

The Augmented Deflector Exhaust Nozzle (ADEN) is a simple, reliable, compact, high performance V/STOL nozzle which resolves all of the above listed limitations.

The ADEN (Figure 1) is a two-dimensional, variable area external expansion exhaust system. Basic components consist of (1) a transition casing from a round cross section at the tail pipe connect flange to the two-dimensional cross section at the nozzle throat station. (2) a two-dimensional variable geometry convergent divergent flap assembly, (3) a two-dimensional variable ventral flap (4) a two-dimensional external expansion ramp which can be fixed or variable depending on specific installation requirements and

(5) a rotating deflector for thrust vectoring. In the stowed (cruise mode) position the deflector is located outside the casing so that it does not compromise the required internal flowpath contours.

As depicted in figure 2, nozzle area control is achieved by the variable convergent/divergent flap assembly. The variable ventral flap located downstream of the throat controls the nozzle expansion area ratio as required over the range of operating pressure ratios. Note that the throat is forward of the ventral flap such that nozzle area is independent of the ventral flap position.

For V/STOL operation, the rotating deflector diverts the jet downward (Figure 3). The nozzle flap assembly is rotated to the maximum open position to substantially reduce the flow Mach number approaching the turn. The throat is established between the tip of the ventral flap and the deflector bonnet and rotates with the deflector such that flow turning is accomplished subsonically at all deflector settings.

An additional feature of the ADEN design is the capability to provide inflight thrust vector control by utilizing a variable aft expansion ramp. Less than $\pm 10^\circ$ rotation of the expansion ramp will provide an upward or downward thrust component as desired. Considerable higher rotation of the ramp can be achieved without imposing any additional mechanical or structural design constraints on the exhaust system.

The impact of the ADEN inflight thrust vectoring capability on aircraft system performance is strongly configuration dependent. For example in

aft fuselage installations, small variations in the ADEN resultant thrust vector can significantly contribute to the aircraft pitch control authority possibly resulting in downsizing the horizontal control surfaces and minimizing trim drag. On twin wing pod mounted installations, the aircraft can be designed such that the nozzle exit coincides with the wing trailing edge. In this type installation the nozzle expansion ramp can be integrated with the wing flap system and the ADEN inflight thrust vectoring capability can be utilized to produce wing lift enhancement/supercirculation effects. A schematic of the ADEN installation in both cruise and lift mode is shown in Figure 4. It can be noted that the ADEN aspect ratio (dry cruise throat width/height ratio), and the arrangement of the nozzle flaps, deflector, expansion flap, actuators and structural elements have been carefully selected to allow high performance afterbody contours. The two-dimensional nozzle shape blends well with airframe contours without drag producing base regions. The aspect ratio of 4 design allows the exhaust system to be installed on the GE YF101 engine without increasing frontal projected area.

PERFORMANCE

The cruise and vectored mode performance characteristics of the ADEN were verified by a series of cold flow static internal performance tests. A multi-component flow through force balance arrangement was used to measure axial and vertical thrust components and pitch moment and to determine the resultant thrust vector point of application. Flow coefficient and external static pressure data were also recorded. Tests simulated forward and vectored mode operation over the range of power setting and nozzle

deflection angles. To provide assurance that a stable internal flowfield was maintained as the nozzle throat plane rotated with the deflector, dynamic pressure instrumentation was installed along the nozzle flaps and deflector. Data was recorded as the deflector was continuously rotated from fully stowed to the maximum deflected position. Test results indicated a positive stable transition of the throat from the nozzle flap to the deflector at the initiation of deflected mode operation and showed that throat stability was maintained over the full vectoring range.

The ADEN exhibits high levels of internal performance at reheat power settings. Although emphasis was placed in improved combat and supersonic performance, a marginal performance gain was also achieved at subsonic cruise. Only at dry throat area and low pressure ratio settings (loiter) was a slight performance deficiency of the ADEN apparent.

Exhaust system installed performance during forward mode operation is highly dependent on the particular aircraft/engine installation. Studies of both twin installations and wing pod mounted installations show that ADEN installation characteristics can provide a significant reduction of exhaust system base area, especially at dry power operation. A wind tunnel test program to investigate ADEN installed performance characteristics and inflight vectoring performance on an advanced multi-mission V/STOL aircraft will be conducted during Nov. - Dec. 1975 at the NASA Langley 16 ft. high speed tunnel.

The ADEN exhibited continuous, efficient performance characteristics over the full 0 to 110° vectoring range as shown by Figure 5. Deflected per-

formance at the nozzle pressure ratio range ($P_T/P_0 = 2.5$ to 3.0) typical of VTOL operation. As the deflector initially rotates into the gas stream, insufficient flow guidance in the turn results in a slight performance loss. Further deflector rotation, however, achieves the desired internal flowpath and maximum performance is attained at approximately 70° resultant thrust vector. Turning losses result in a slight performance decrease as the thrust vector angle is then increased to 110° .

In summary, studies and tests have shown that:

- (1) The internal performance of the ADEN approaches the performance levels of conventional axisymmetric exhaust systems over the range of flight conditions.
- (2) The ADEN has excellent vectored mode performance characteristics.
- (3) The ADEN integrates favorably with the airframe for minimum installation loss.

COOLING SCHEME ANALYSIS

Since cooling of the ADEN is a more complex problem than cooling of conventional exhaust systems, a one-quarter scale ADEN (relative to J101 size) component test was conducted to substantiate the cooling design and provide data in support of the design effort.

The cooling test set-up consisted of an existing jet fuel burner facility modified by adding cooling air lines and flow metering sections to simulate the quantity, temperature and pressure level of cooling air supplied by the J101 engine. The design also simulated the coolant distribution design of the ADEN.

Since the augmentor burning length could not be scaled down with diameter, the forward portion was water-cooled and only the geometrically scaled ADEN section was cooled by the metered air supply. Portions of the ADEN model not critical to the cooling system evaluation were of boiler plate design for ease and economy of hardware fabrication. However, all hot parts simulated the flight weight design relative to material, thickness, construction and cooling design. A sketch of the quarter-scale ADEN test set-up is presented in Figure (6).

The condition of the internal surfaces after testing revealed only minor distortion in the deflector corners. The cooling film tended to migrate from the corner toward the center of the deflector due to secondary flow effects in the turn. This was corrected by local redistribution of the cooling flow.

The quarter scale high temperature cooling flow system verification test program was highly successful.

FULL SCALE ADEN DEMONSTRATOR TEST

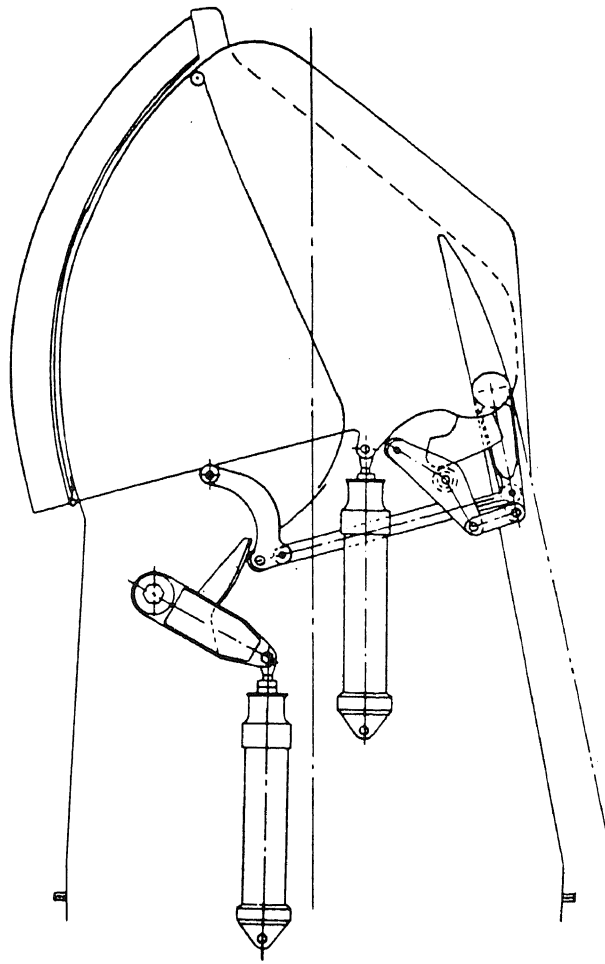
Currently, manufacturing of the demonstrator ADEN is progressing on schedule and testing will begin in mid 1976 at the General Electric Peebles test facility. The ADEN will be demonstrated statically on a YJ101 engine at both dry and reheat power. The engine will be suspended from an overhead structure and oriented to deflect the jet in the horizontal plane to eliminate ground and facility jet impingement and to allow visual observation of hot metal surfaces including the deflector liners and nozzle flaps.

A multi-component force balance arrangement will measure nozzle thrust and resultant thrust vector angle and point of application over the complete

vectoring range at reheat power settings. Exhaust gas temperature, metal temperatures and coolant flow temperatures and pressures will be measured. A total of 25 test hours are planned.

This ADEN Demonstrator program will provide a quantum jump in the experience/data base for two dimensional exhaust system technology and will have reached a prerequisite milestone towards a full scale ADEN demonstration program.

ADEN V/STOL NOZZLE ACTUATION



NONAUGMENTED
CRUISE MODE

FIGURE (2)

ADEN FLOW PATH

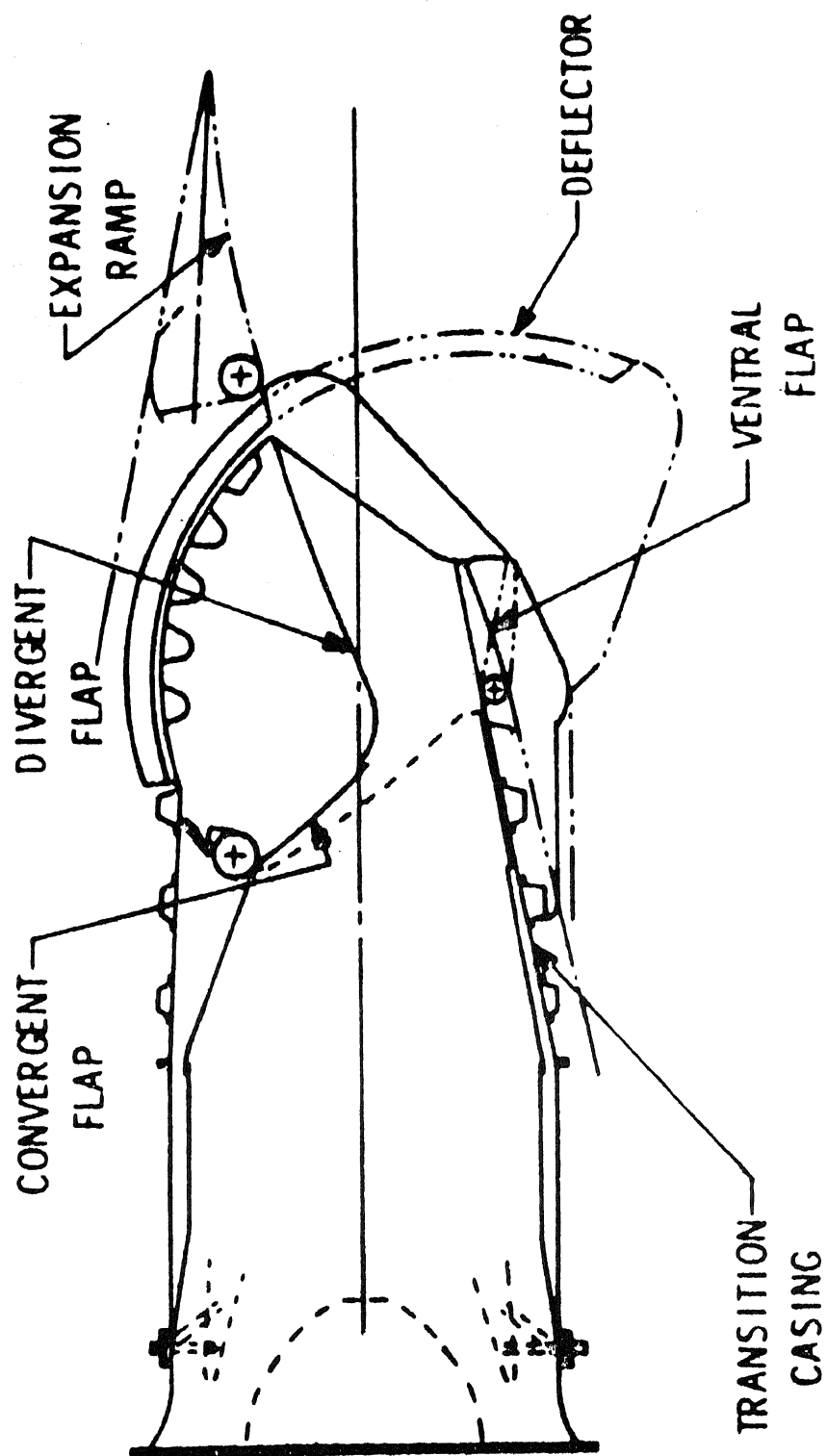
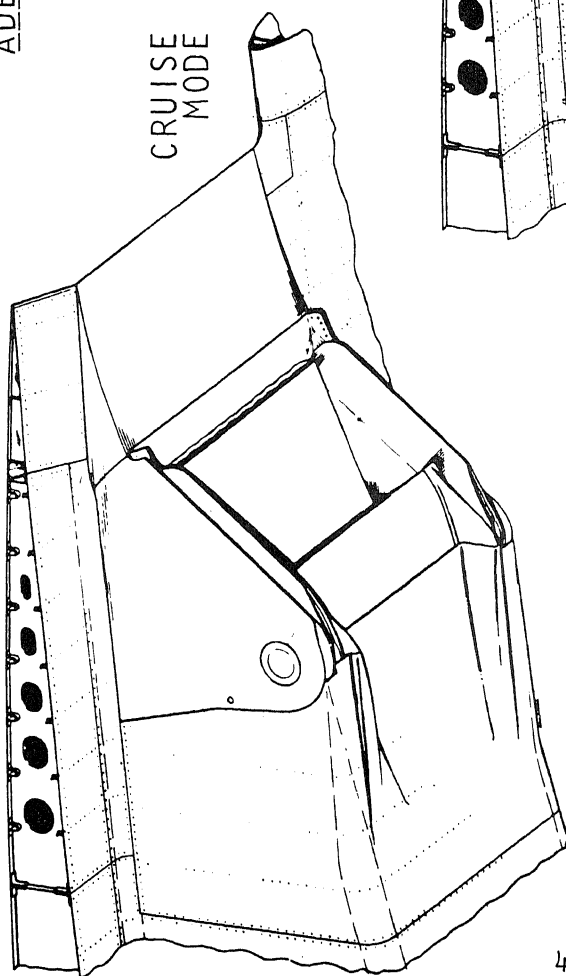
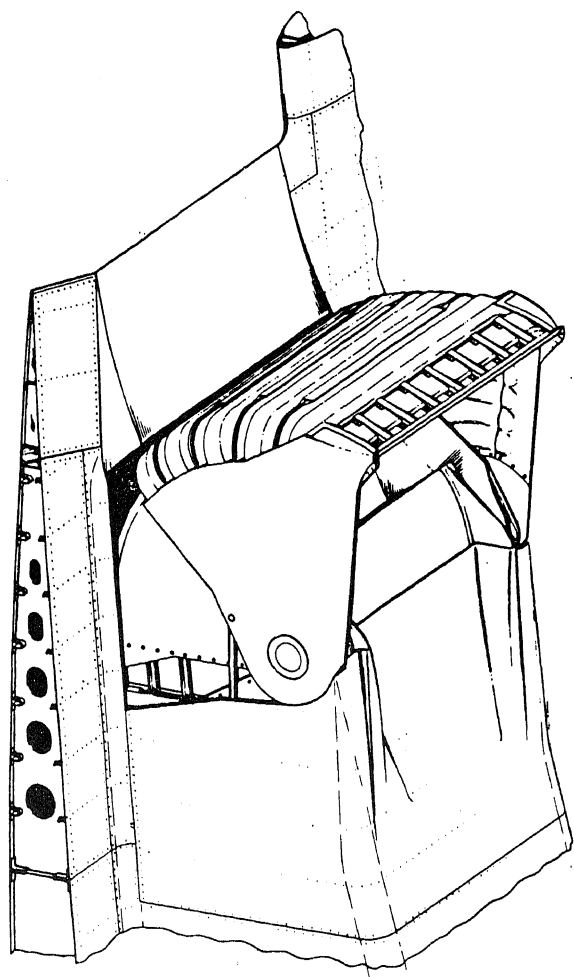


FIGURE (1)

ADEN INSTALLATION



CRUISE
MODE



LIFT
MODE

FIGURE (4)

ADEN V/STOL NOZZLE ACTUATION

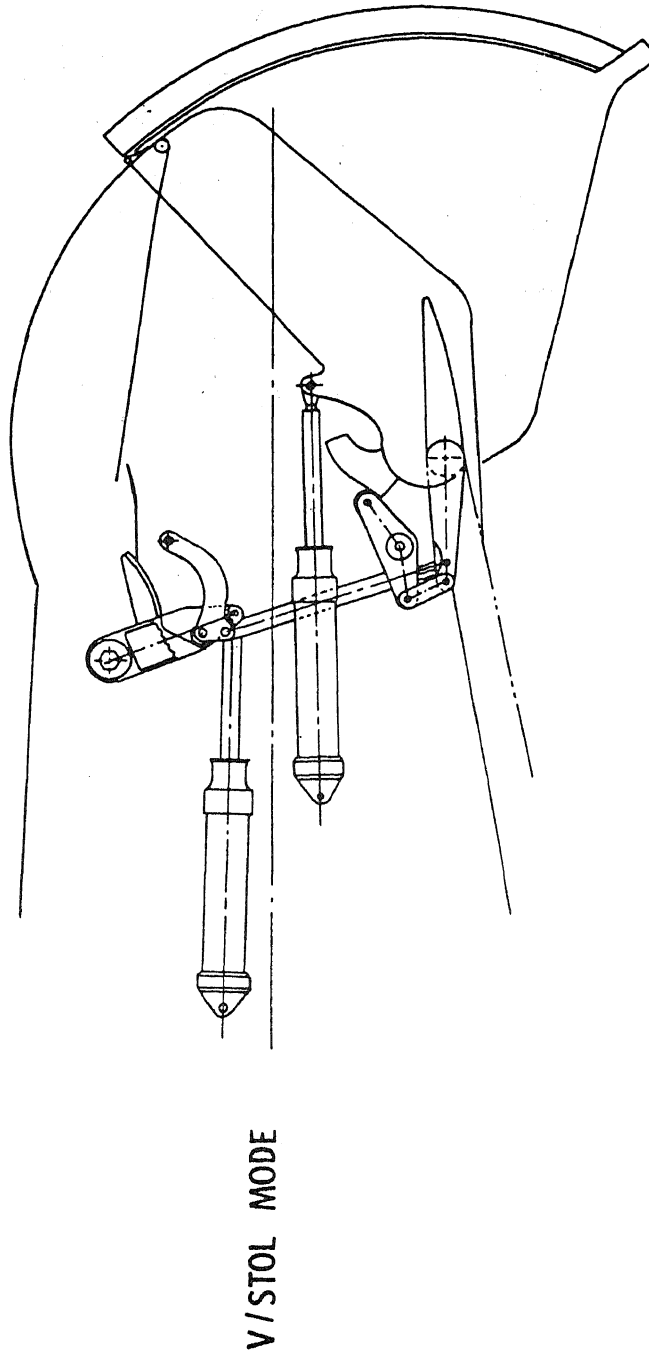


FIGURE (3)

ADEN DEMONSTRATOR

SCALE MODEL TEST

VECTORED MODE

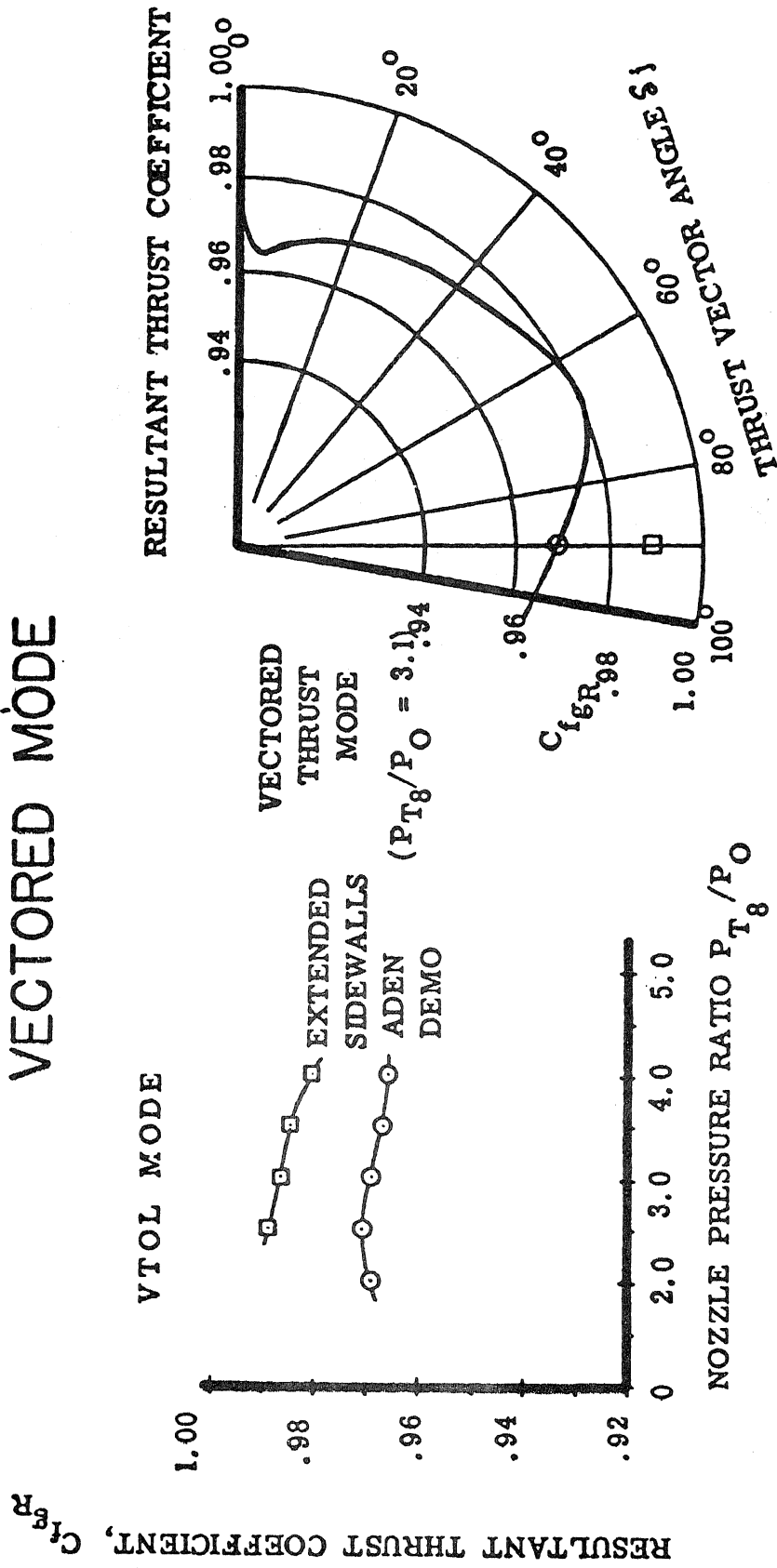


FIGURE (5)

V/STOL DEFLECT

BY T.A. WYNOSKI

JULY 30, 1975



ABSTRACT

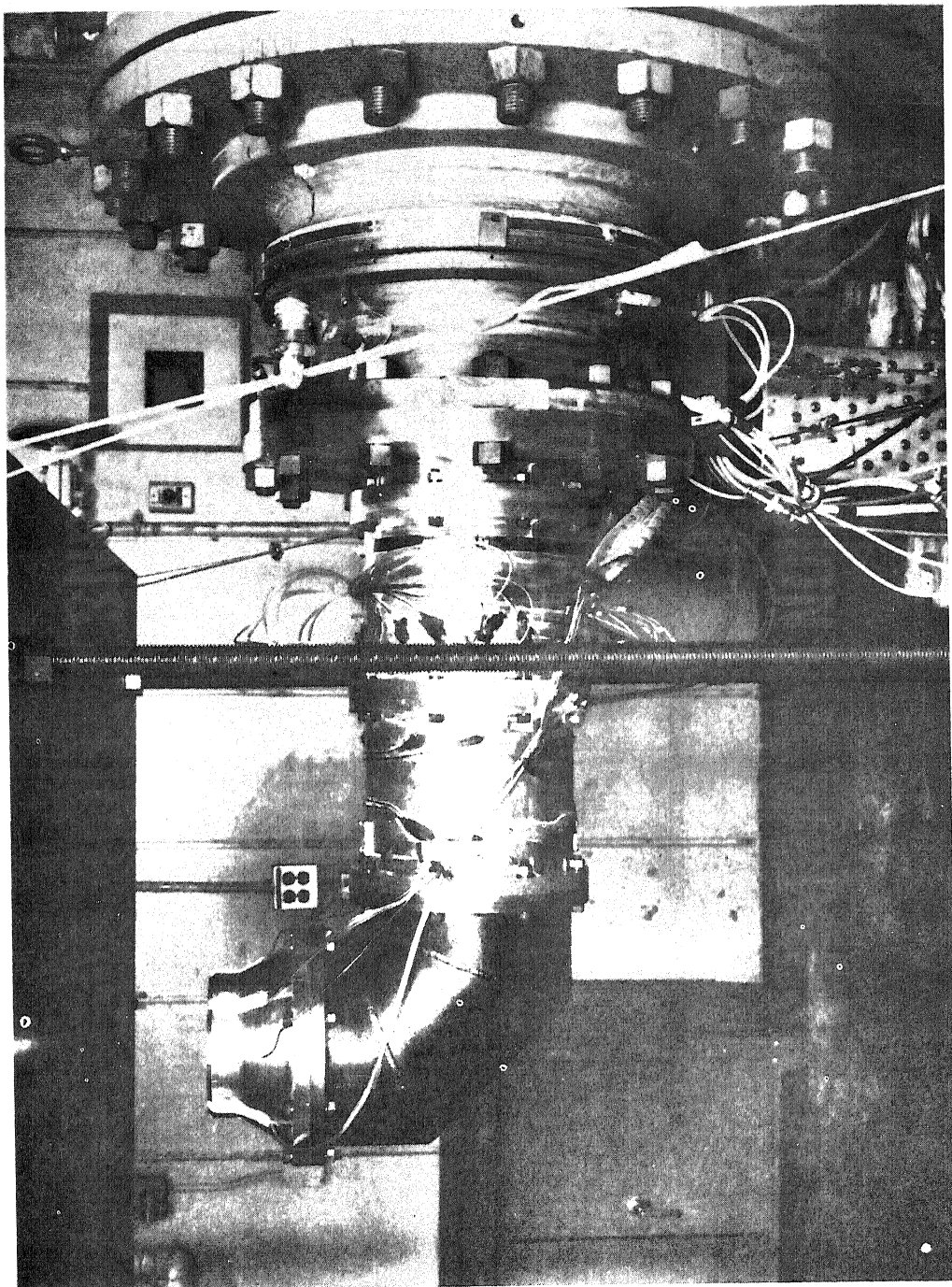
An 18 month Deflector/Nozzle Technology Contract was conducted by Pratt and Whitney Aircraft under the technical direction of the Naval Air Propulsion Test Center during the period 1 July 1972 through 31 December 1973. Under this program, basic propulsion system design information was developed to support future V/STOL systems studies which might incorporate jet or turbofan exhaust deflection. The study subjects included: ground suppression correlations, basic internal aerodynamic studies, and conceptual design studies. Because of the emphasis in locating the vertical thrust vector as far forward (as close to the airplane Cg) as possible, the internal aerodynamic and design studies concentrated on an evaluation of potential problems which might arise from locating the deflector close to the engine flow path. In particular, fan duct distortion, nozzle performance, and design feasibility were studied.

The various aspects of this contract work were reported in detail in the references. It was felt that the objectives of the "Workshop on Prediction Methods for Jet V/STOL Propulsion Aerodynamics" would best be met by extracting only the end result working correlations and conclusions from these various studies. These self explanatory view charts are attached. The background data, facility descriptions, etc. are well documented in the references, which should be readily available.

V/STOL DEFLEC

- **GROUND SUPP**
- **INTERNAL AERODYNAMICS**
 - **FAN DUCT DISTORTION**
 - **NOZZLE PERFORMANCE**
- **CONCEPTUAL DESIGNS**

TEST RIG USED IN GROUND SUPPRESSION STUDIES

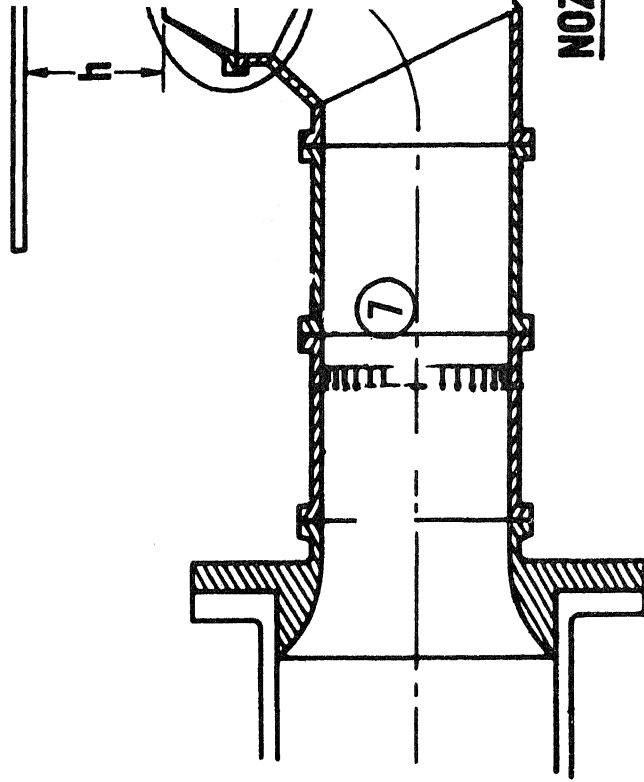


J8236-4
732010

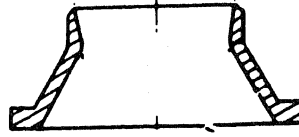
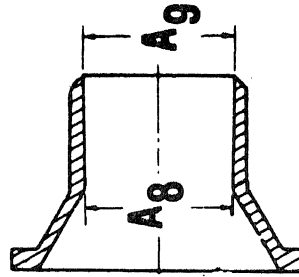
NOZZLE GEOMETRY VARIATIONS

SUPPRESSION STUDY

MOVABLE
(SOLID AND GRATED)



NOZZLE INSERTS



TEST VARIABLES

$h/D_8 = 0.2 \text{ TO } \infty$
 $P_{T7}/P_{S0} = 1.4 \text{ TO } 4.0$

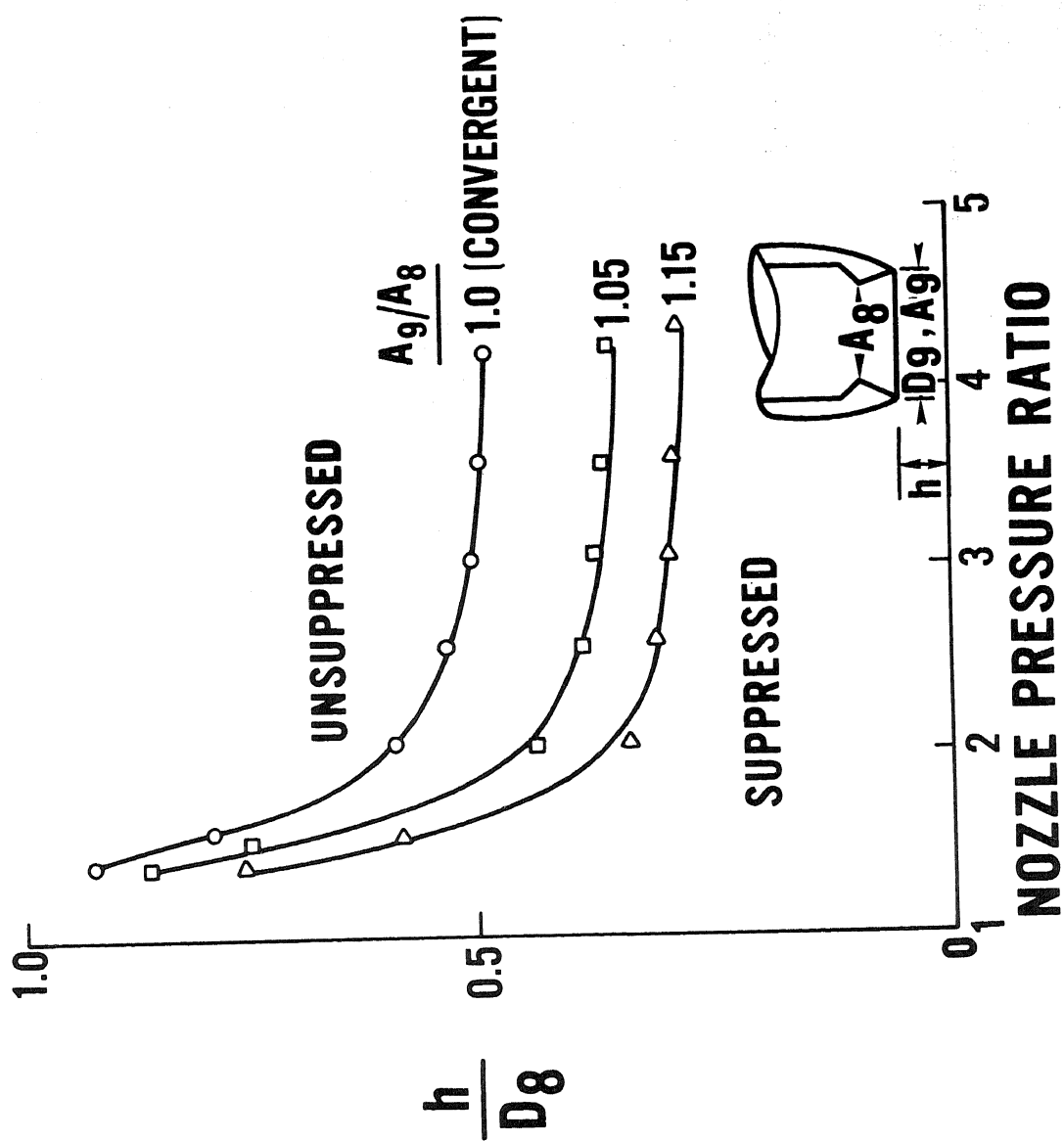
CONVERGENT

$A_9/A_8 = 1.05$

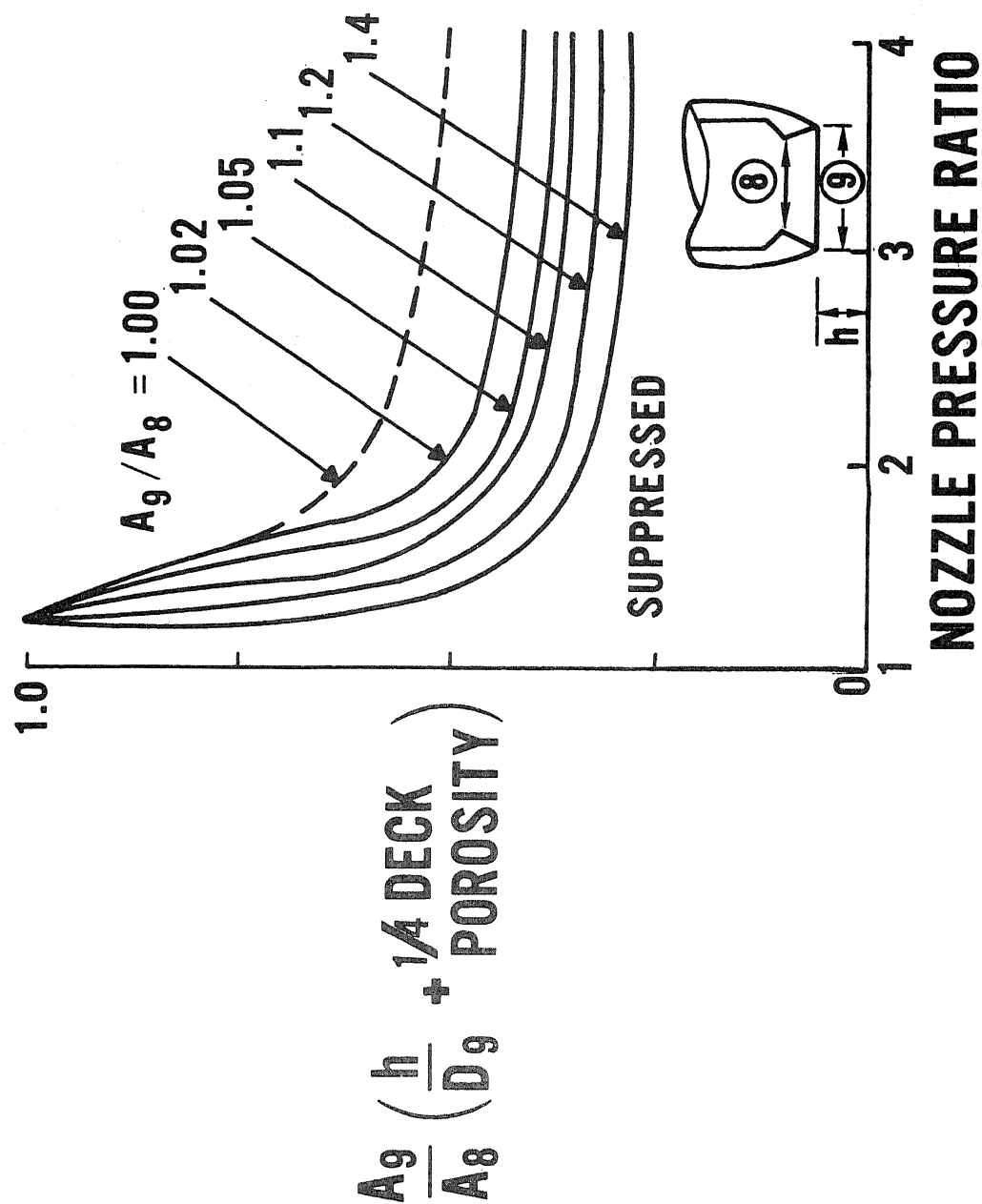
$A_9/A_8 = 1.15$

J8236-3
R751707

ONSET OF SUPPRESSION FOR THREE TEST NOZZLES



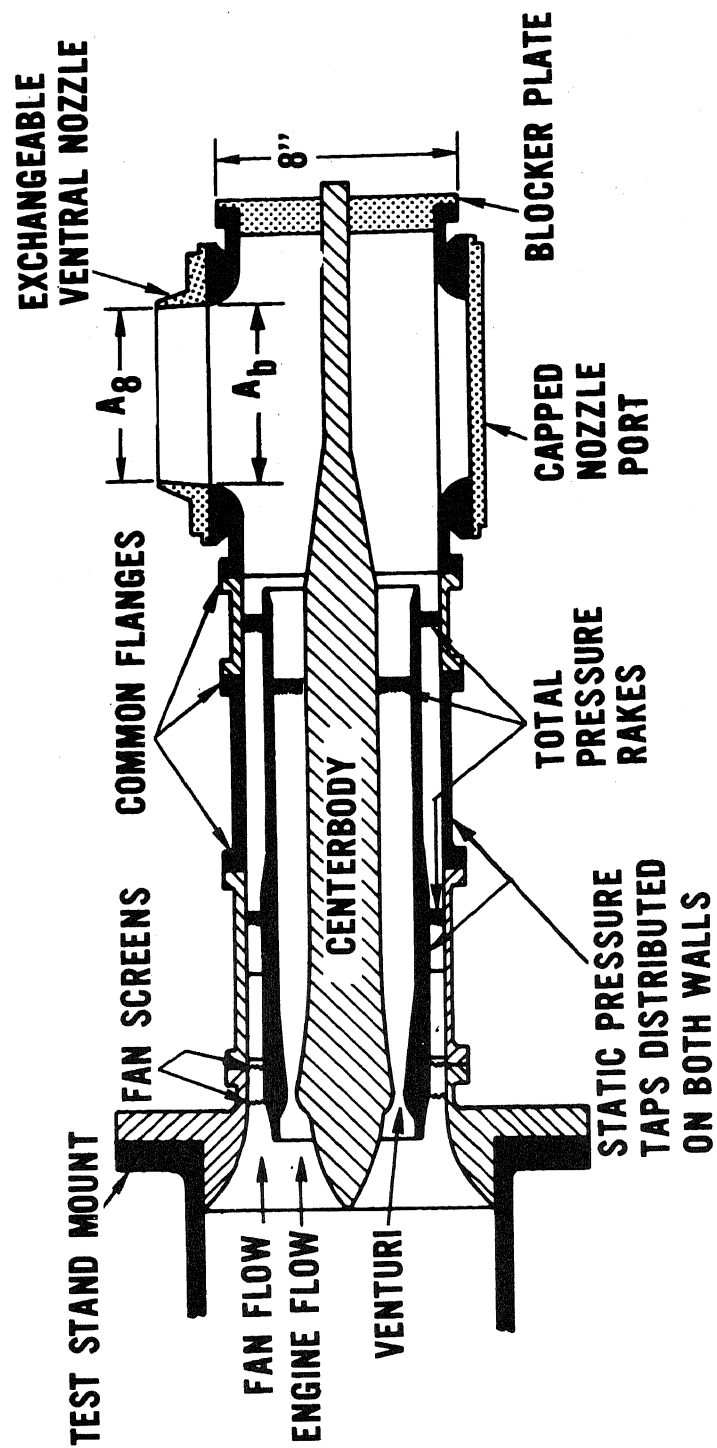
CORRELATION FOR ESTIMATING ONSET OF SUPPRESSION



DEFLECTOR DESIGN DATA

- **FAN DUCT PRESSURE PATTERNS**
- **NOZZLE PERFORMANCE**

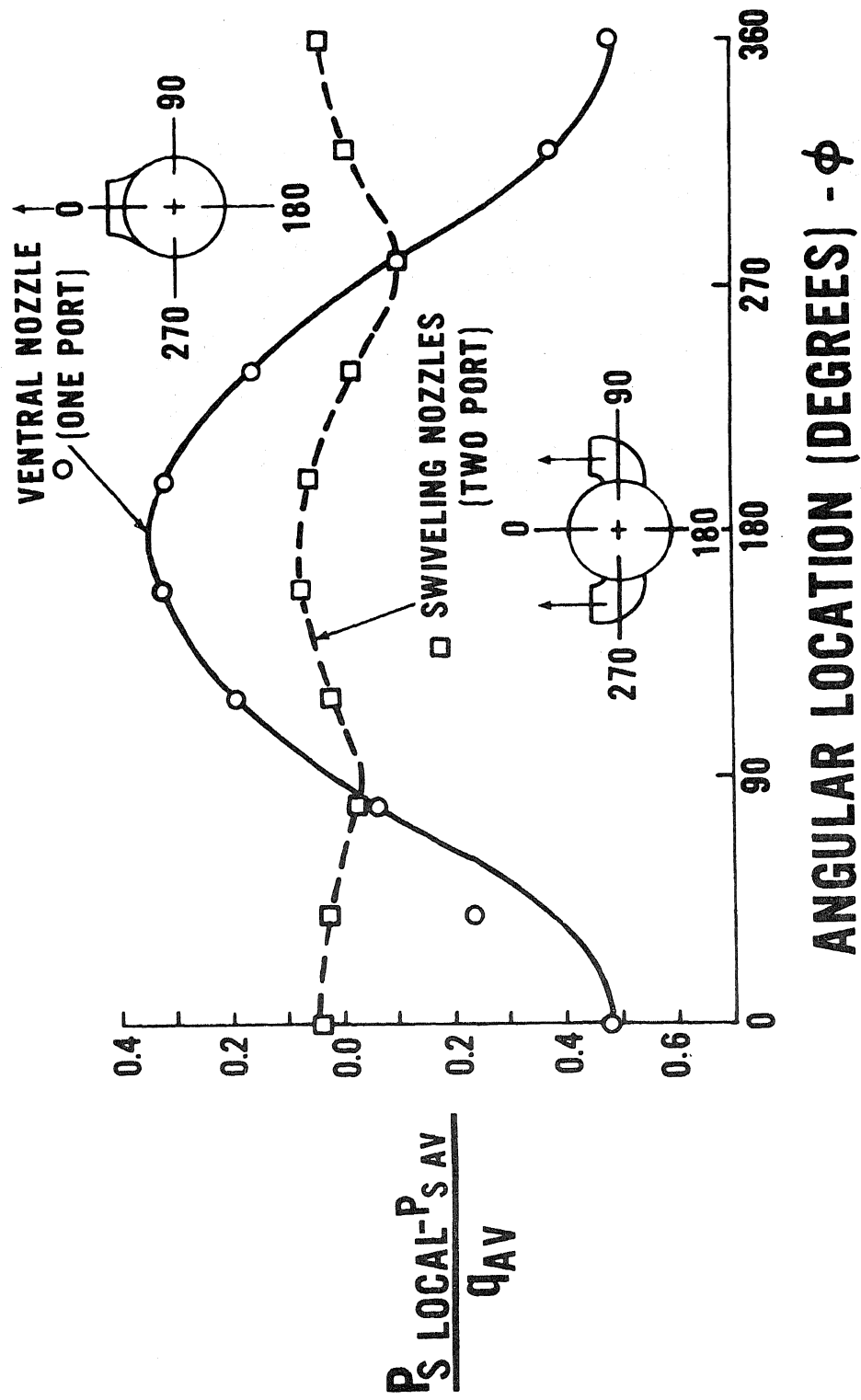
CLOSE COUPLED DEFLECTOR/ENGINE TEST MODEL



J8236-8
732010

DUCT STATIC PRESSURE PROFILE BEHIND FAN

DURING DEFLECTION



J8236-10
732210

STATISTICALLY FIT EQUATIONS TO APPROXIMATE DISTORTION PROFILES

SYMBOLS ~ DATA

— ~ EQUATION

ONE-PORT PROFILE

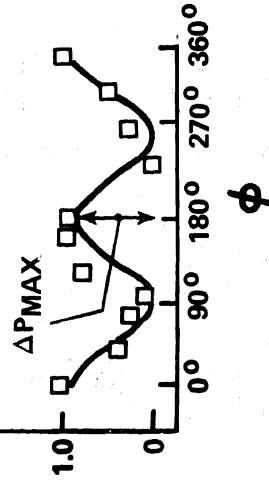
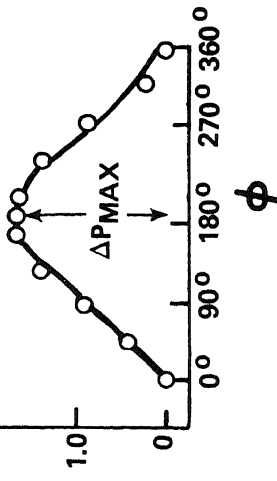
TWO-PORT PROFILE

$$\frac{\Delta P}{q_{AVG}} = .25 \left[\frac{\Delta P_{MAX}}{q_{AVG}} \right] \left[5e^{-.164 (\phi - \pi)^2} - 1.0 \right]$$

$$\frac{\Delta P}{q_{AVG}} = \frac{\Delta P_{MAX}}{q_{AVG}} \left[\frac{1.0 + \cos 2\phi}{2.0} \right]$$

$\frac{P_S, \text{LOCAL} - P_S, \text{MIN}}{q_{AVG}}$

$\sim \frac{\Delta P}{q_{AVG}}$

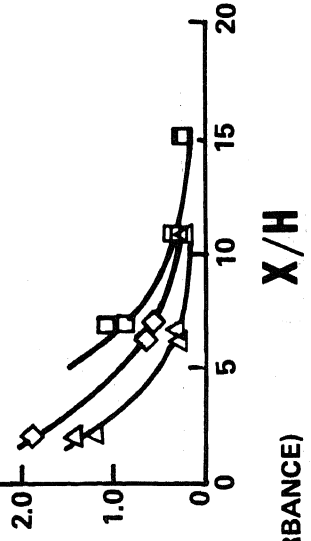
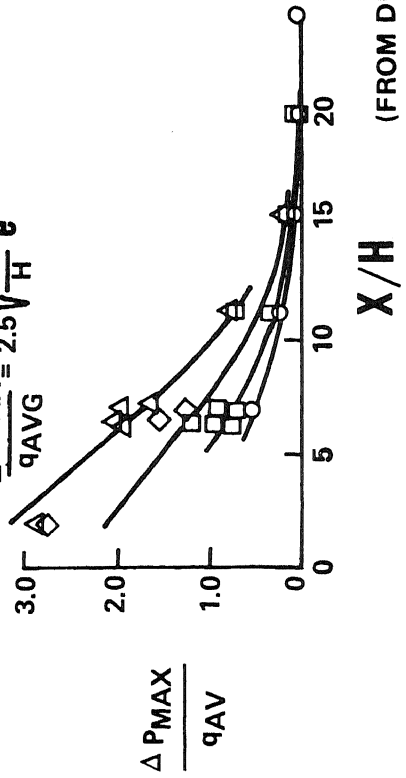


ONE-PORT AMPLITUDE DECAY

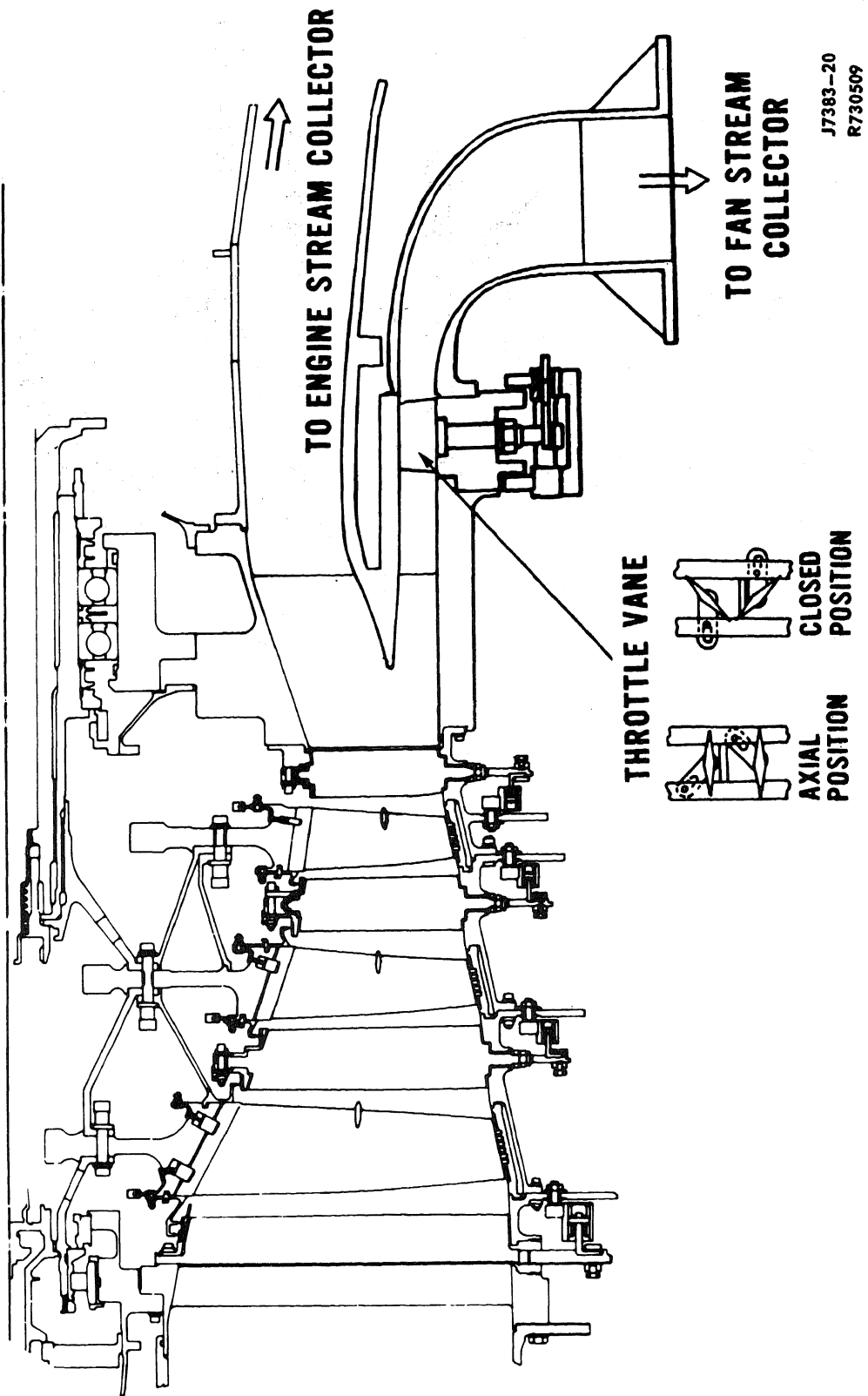
TWO-PORT AMPLITUDE DECAY

$$\frac{\Delta P_{MAX}}{q_{AVG}} = 2.5 \sqrt{\frac{X}{H}} e^{.1 (S/H - 3 X/H)}$$

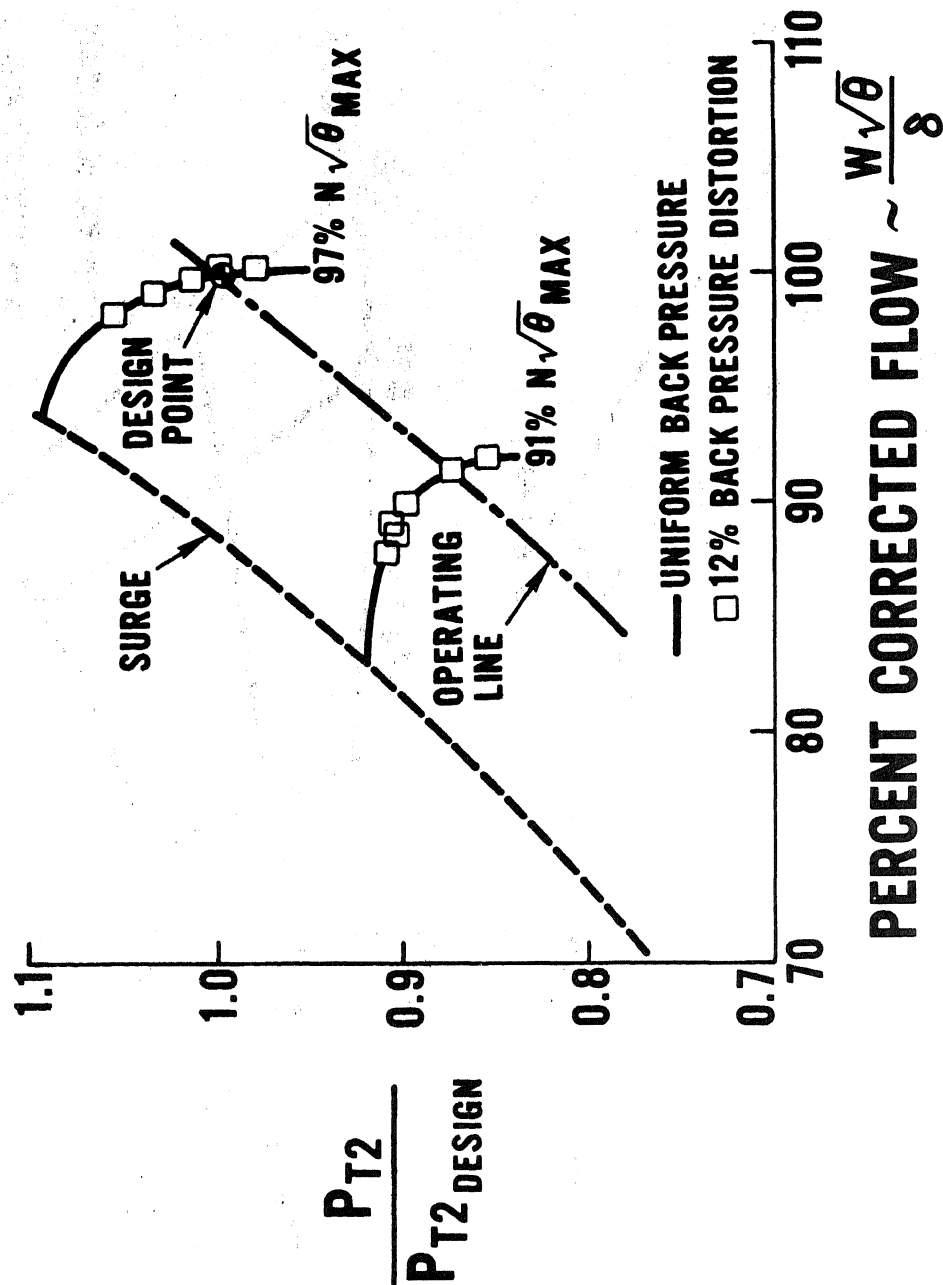
$$\frac{\Delta P_{MAX}}{q_{AVG}} = \frac{2.2}{3 \sqrt{X/H}} e^{-1 (S/H + 1.2 X/H)}$$



FAN RIG DISTORTION SIMULATION

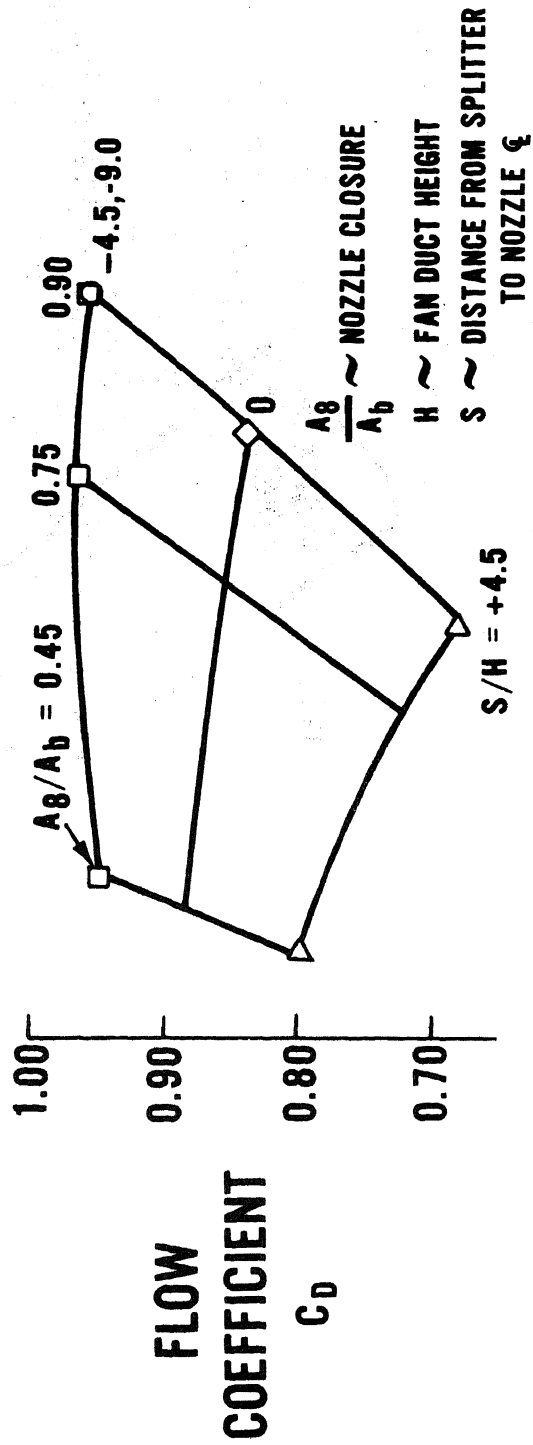
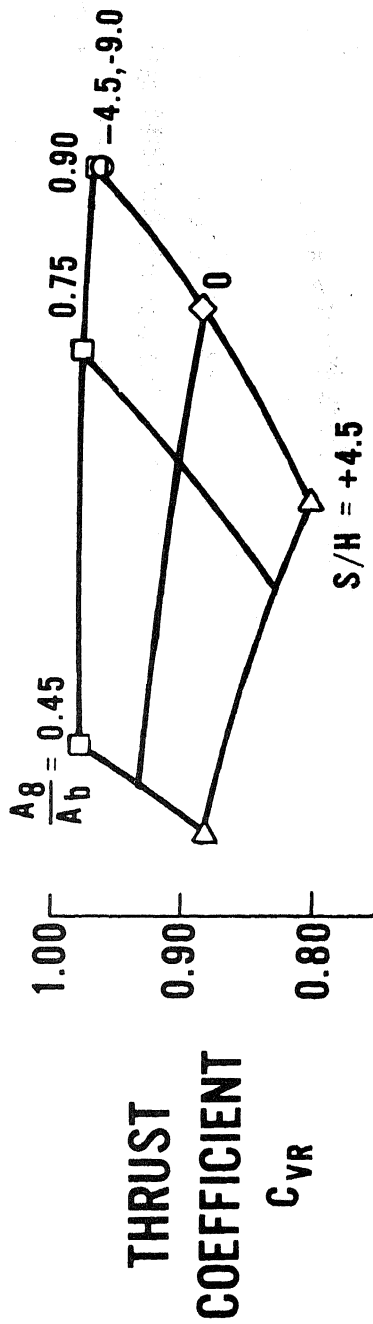


COMPARISON OF FAN PERFORMANCE WITH AND WITHOUT DISTORTION

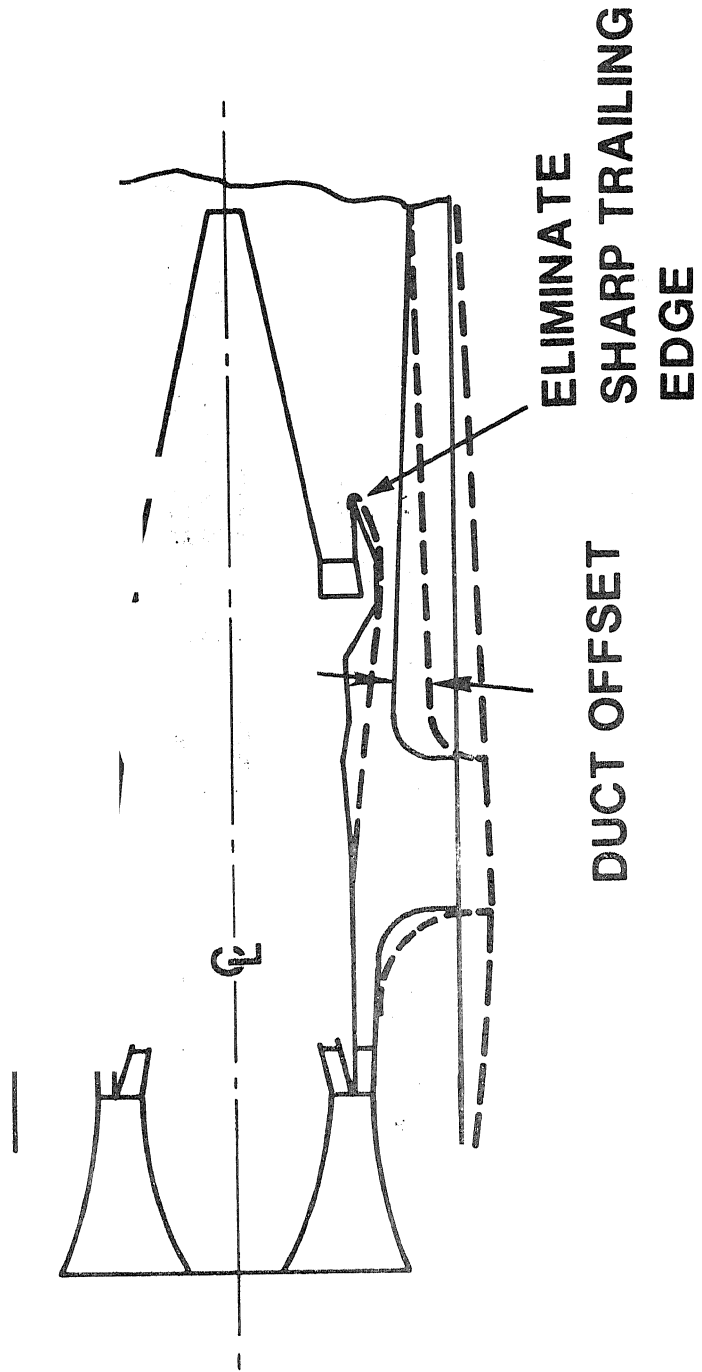


J7828-12
730409

IMPACT OF DEFLECTOR AXIAL POSITIONING ON NOZZLE PERFORMANCE

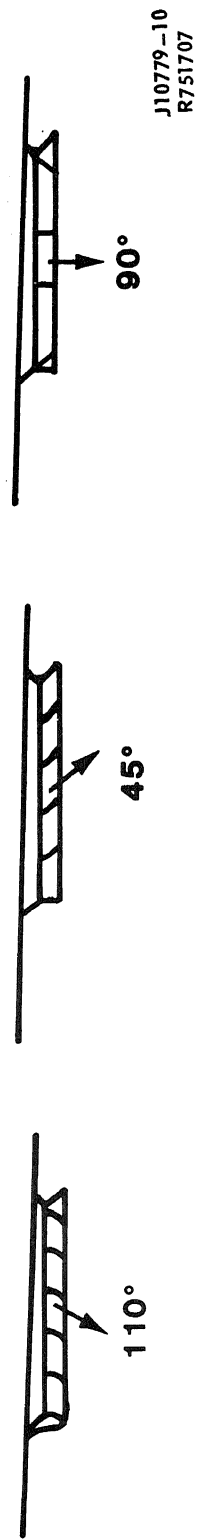
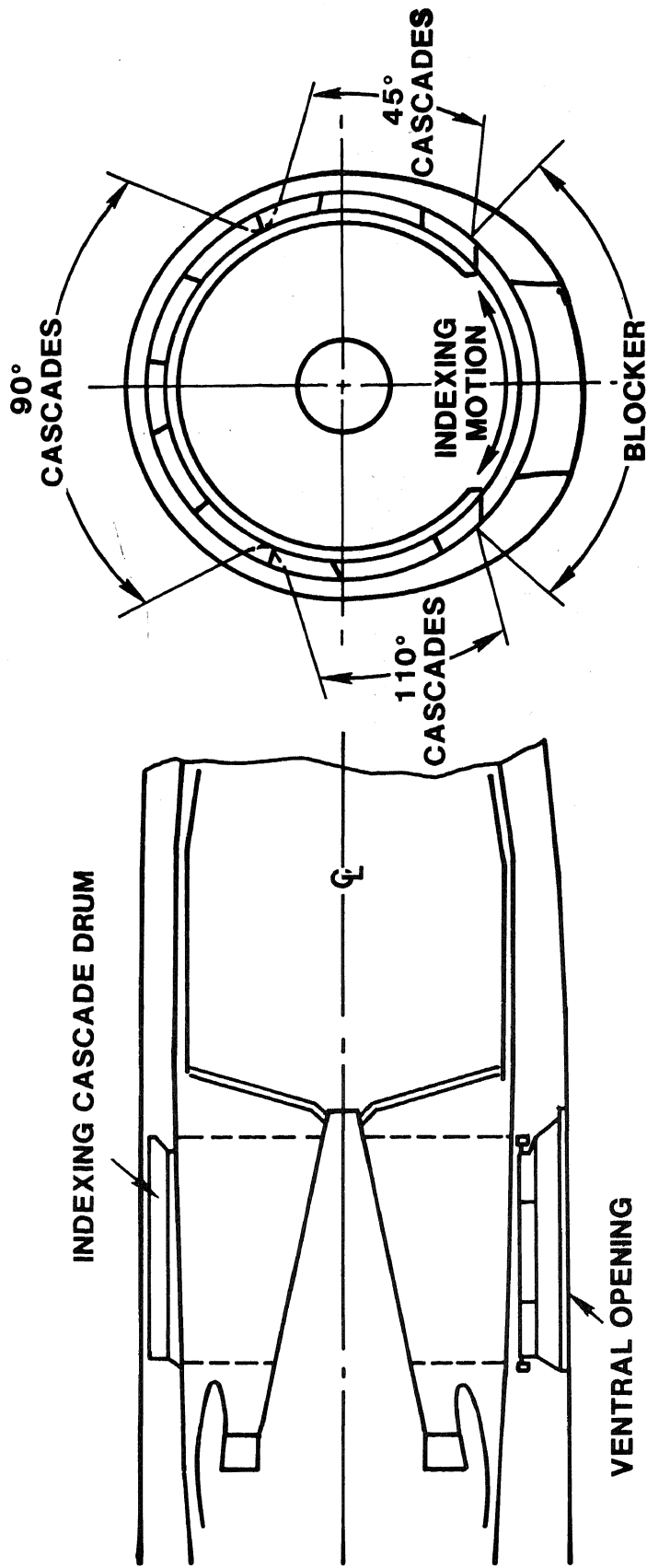


FLOW TO REDUCE



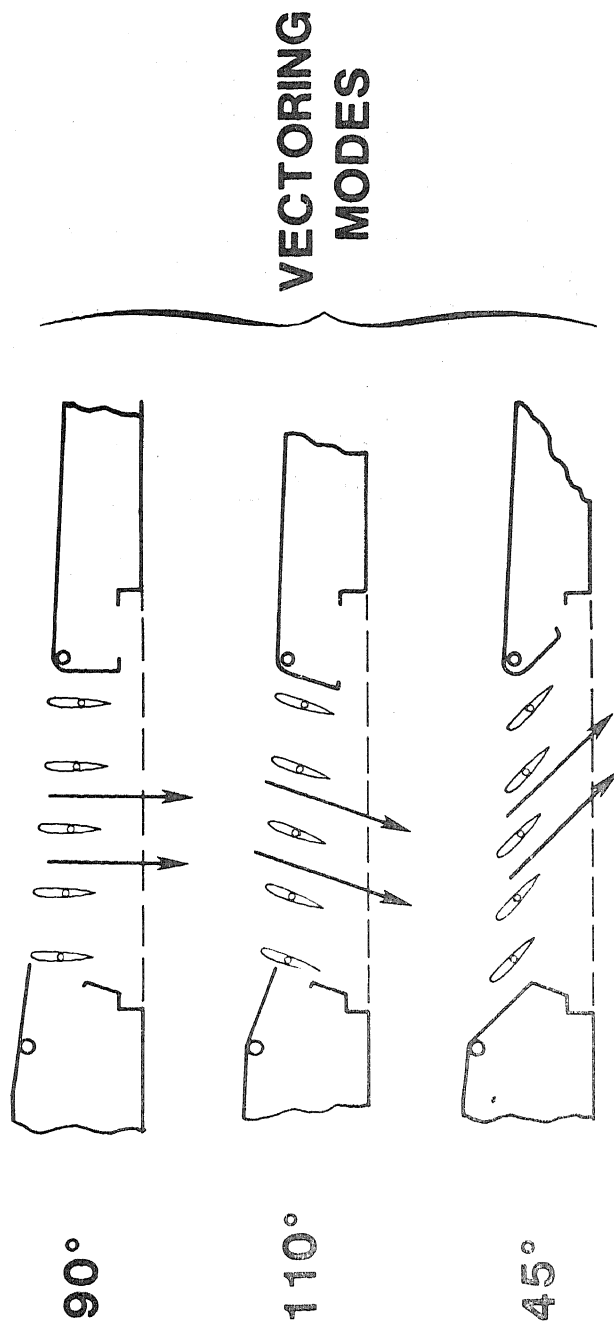
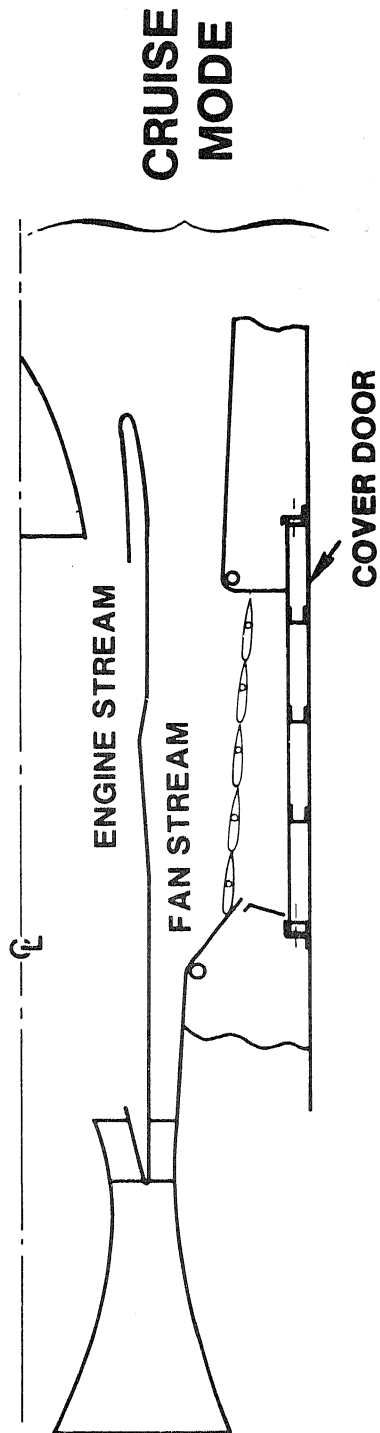
CONCEPTUAL DESIGN STUDIES

INDEXING CASCADE/DRUM VENTRAL



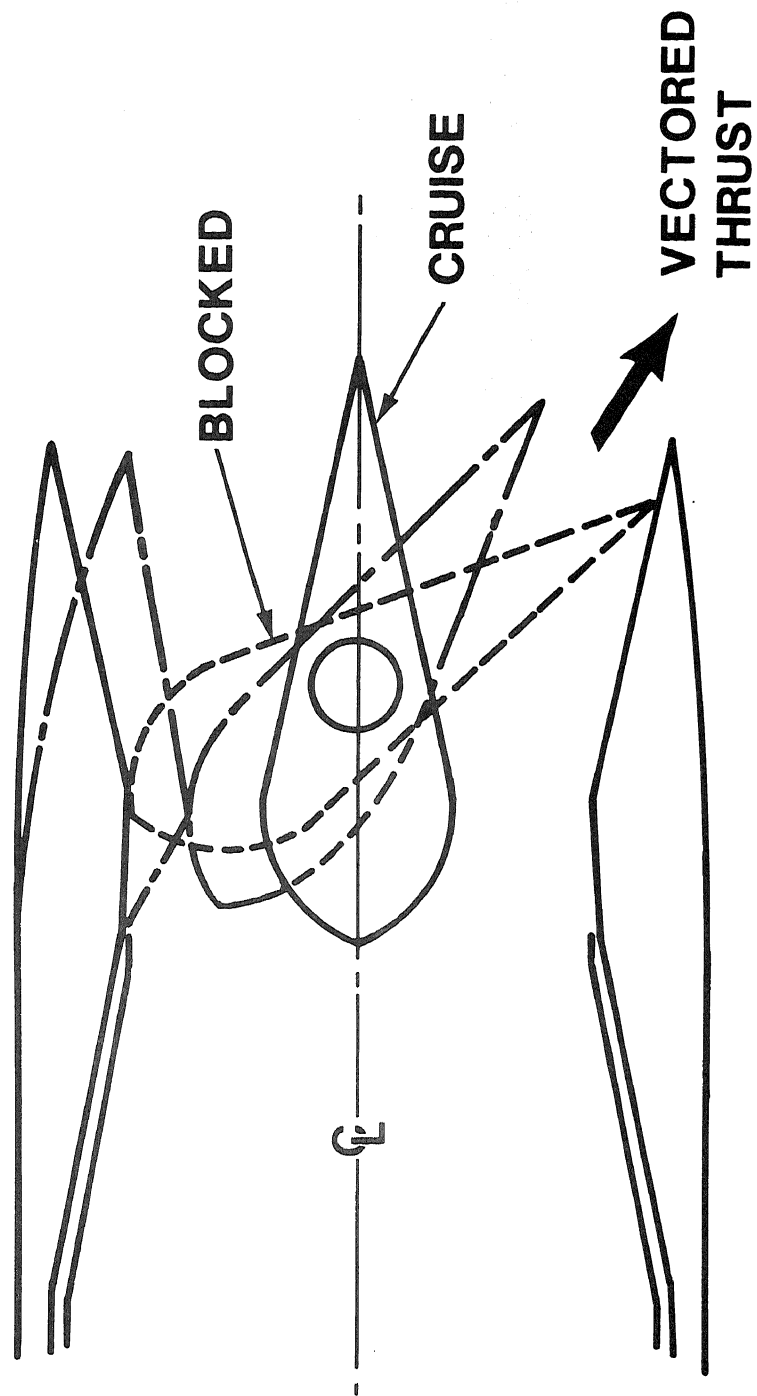
J10779-10
R751707

VENETIAN BLIND VENTRAL



J10779-12
740910

TWO-DIMENSIONAL MULTIPLE EXPANSION ROTATING PLUG



SUMMARY

- **GROUND SUPPRESSION CORRELATIONS DEVELOPED**
- **FAN DUCT PRESSURE PATTERNS CORRELATED**
- **NOZZLE PERFORMANCE DEFINED**
- **CONCEPTUAL DESIGNS PRESENTED**

CONCLUSIONS AND REC FOR FUTURE ST

- **GROUND SUPPRESSION NOT AS SEVER
AS PREVIOUSLY THOUGHT**
- **DEFLECTOR INDUCED DISTORTIONS DID NC
FAN PERFORMANCE**
**SHOULD BE STUDIED IN COMBINATION
WITH INLET DISTORTION**
- **AERO FLOWPATH MODIFICATIONS TO ALLOW CLOSE COUPLING
NEEDS TEST CONFIRMATION**
- **CONCEPTUAL DESIGNS ALLOWED UPSTREAM VENTRAL
POSITIONING WITH COMPETITIVE PERFORMANCE**
**NEEDS MUTUAL AIRFRAME/ENGINE
COMPANY DEVELOPMENT**

REFERENCES

- “V/STOL Deflector Duct Profile Study” by Dr. R. Strough and T. A. Wynosky, AGARD Propulsion and Energetics Panel Meeting on V/STOL Propulsion Systems. Schliersee, Germany, September 17-21, 1973.
- “V/STOL Deflector Aerodynamic Design Criteria” by T. A. Wynosky and C. J. Szyszko, AIAA/SAE 9th Propulsion Conference, Las Vegas, Nevada, November 5-7, 1973.
- “V/STOL Deflector Concepts” by T. A. Wynosky, R. A. Streib and W. J. Usab, AIAA/SAE 10th Propulsion Conference, San Diego, California, October 21-23, 1974.
- Deflector/Nozzle Program Phase I Final Report Contract No. N00019-72-C-0612 for Naval Air Propulsion Test Center, February 15, 1974.
- Deflector/Nozzle Program Conceptual Design Phase II Final Report Contract No. N00019-72-C-0612 for Naval Air Propulsion Test Center, March 1975.

SECURITY CLASSIFICATION OF THIS PAGE (When Data Entered)

REPORT DOCUMENTATION PAGE		READ INSTRUCTIONS BEFORE COMPLETING FORM
1. REPORT NUMBER	2. GOVT ACCESSION NO.	3. RECIPIENT'S CATALOG NUMBER
4. TITLE (and Subtitle) PREDICTION METHODS FOR JET V/STOL PROPULSION AERODYNAMICS, PROCEEDINGS OF A WORKSHOP Volume I		5. TYPE OF REPORT & PERIOD COVERED Workshop Proceedings
7. AUTHOR(s) Max F. Platzer		6. PERFORMING ORG. REPORT NUMBER
9. PERFORMING ORGANIZATION NAME AND ADDRESS Naval Air Systems Command		8. CONTRACT OR GRANT NUMBER(s)
11. CONTROLLING OFFICE NAME AND ADDRESS Naval Air Systems Command (AIR-310) Washington, D. C. 20361		10. PROGRAM ELEMENT, PROJECT, TASK AREA & WORK UNIT NUMBERS
14. MONITORING AGENCY NAME & ADDRESS (if different from Controlling Office)		12. REPORT DATE July 28-31, 1975
		13. NUMBER OF PAGES
		15. SECURITY CLASS. (of this report) Unclassified
16. DISTRIBUTION STATEMENT (of this Report) Unlimited		15a. DECLASSIFICATION/DOWNGRADING SCHEDULE
17. DISTRIBUTION STATEMENT (of the abstract entered in Block 20, if different from Report)		
18. SUPPLEMENTARY NOTES		
19. KEY WORDS (Continue on reverse side if necessary and identify by block number) V/STOL Aircraft, Low Speed Aerodynamics, V/STOL Propulsion, Duct Flows, V/STOL Testing, Lift Fan Propulsion, Transition Aerodynamics, Thrust Augmenting Ejectors, Flow Vectoring Devices, Ground Interference Effects		
20. ABSTRACT (Continue on reverse side if necessary and identify by block number) This report contains the proceedings of the Workshop on Prediction Methods for Jet V/STOL Propulsion Aerodynamics held on July 28-31, 1975, at the Institute for Defense Analyses, Arlington, VA. This workshop was sponsored by the Naval Air Systems Command. The workshop participants in- cluded representatives from industry, government, universities and abroad.		

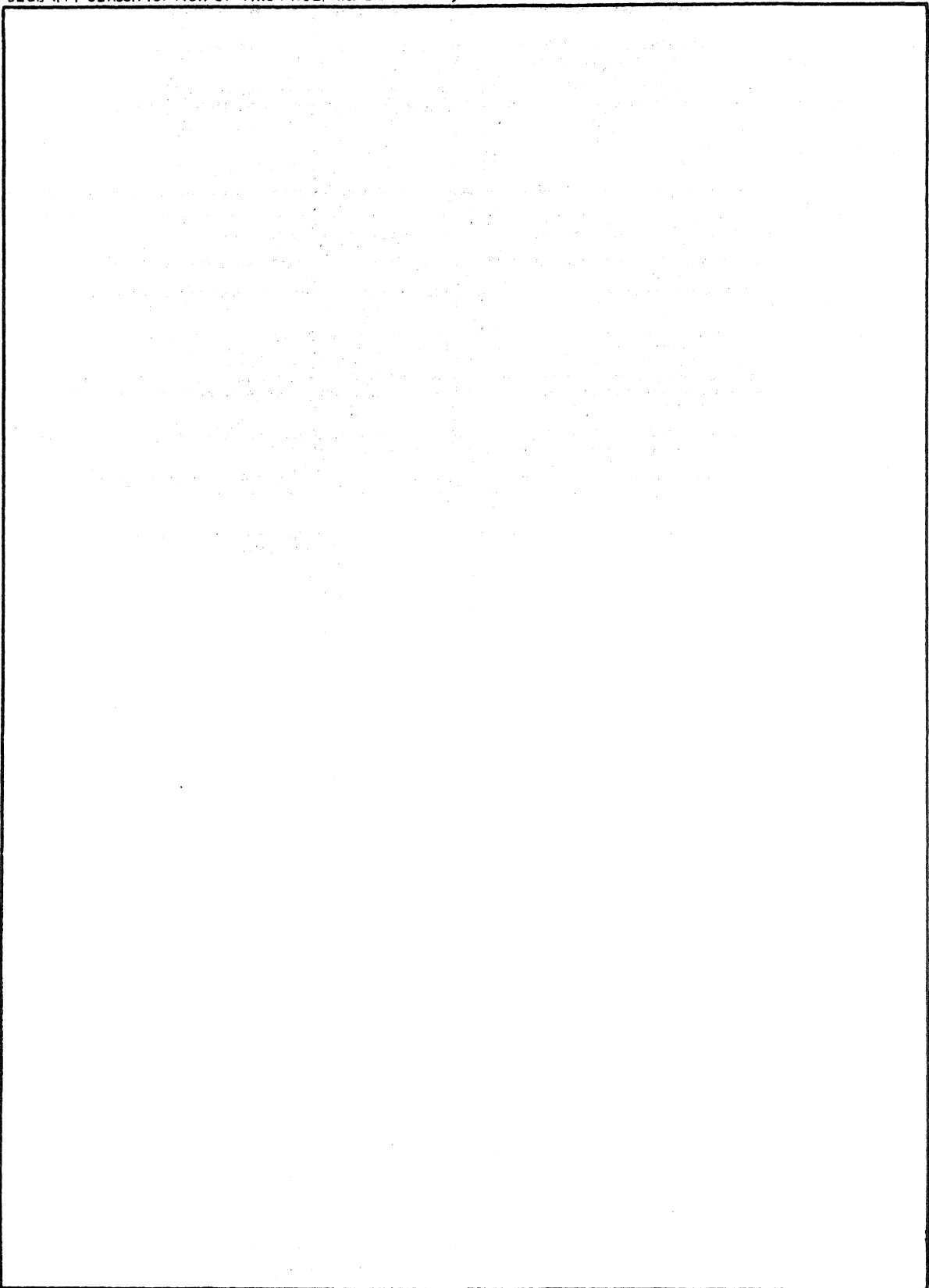
DD FORM 1 JAN 73 1473

EDITION OF 1 NOV 65 IS OBSOLETE
S/N 0102-014-6601

UNCLASSIFIED

SECURITY CLASSIFICATION OF THIS PAGE (When Data Entered)

SECURITY CLASSIFICATION OF THIS PAGE(When Data Entered)



SECURITY CLASSIFICATION OF THIS PAGE(When Data Entered)

INSTRUCTIONS FOR PREPARATION OF REPORT DOCUMENTATION PAGE

RESPONSIBILITY. The controlling DoD office will be responsible for completion of the Report Documentation Page, DD Form 1473, in all technical reports prepared by or for DoD organizations.

CLASSIFICATION. Since this Report Documentation Page, DD Form 1473, is used in preparing announcements, bibliographies, and data banks, it should be unclassified if possible. If a classification is required, identify the classified items on the page by the appropriate symbol.

COMPLETION GUIDE

General. Make Blocks 1, 4, 5, 6, 7, 11, 13, 15, and 16 agree with the corresponding information on the report cover. Leave Blocks 2 and 3 blank.

Block 1. Report Number. Enter the unique alphanumeric report number shown on the cover.

Block 2. Government Accession No. Leave Blank. This space is for use by the Defense Documentation Center.

Block 3. Recipient's Catalog Number. Leave blank. This space is for the use of the report recipient to assist in future retrieval of the document.

Block 4. Title and Subtitle. Enter the title in all capital letters exactly as it appears on the publication. Titles should be unclassified whenever possible. Write out the English equivalent for Greek letters and mathematical symbols in the title (see "Abstracting Scientific and Technical Reports of Defense-sponsored RDT/E," AD-667 000). If the report has a subtitle, this subtitle should follow the main title, be separated by a comma or semicolon if appropriate, and be initially capitalized. If a publication has a title in a foreign language, translate the title into English and follow the English translation with the title in the original language. Make every effort to simplify the title before publication.

Block 5. Type of Report and Period Covered. Indicate here whether report is interim, final, etc., and, if applicable, inclusive dates of period covered, such as the life of a contract covered in a final contractor report.

Block 6. Performing Organization Report Number. Only numbers other than the official report number shown in Block 1, such as series numbers for in-house reports or a contractor/grantee number assigned by him, will be placed in this space. If no such numbers are used, leave this space blank.

Block 7. Author(s). Include corresponding information from the report cover. Give the name(s) of the author(s) in conventional order (for example, John R. Doe or, if author prefers, J. Robert Doe). In addition, list the affiliation of an author if it differs from that of the performing organization.

Block 8. Contract or Grant Number(s). For a contractor or grantee report, enter the complete contract or grant number(s) under which the work reported was accomplished. Leave blank in in-house reports.

Block 9. Performing Organization Name and Address. For in-house reports enter the name and address, including office symbol, of the performing activity. For contractor or grantee reports enter the name and address of the contractor or grantee who prepared the report and identify the appropriate corporate division, school, laboratory, etc., of the author. List city, state, and ZIP Code.

Block 10. Program Element, Project, Task Area, and Work Unit Numbers. Enter here the number code from the applicable Department of Defense form, such as the DD Form 1498, "Research and Technology Work Unit Summary" or the DD Form 1634, "Research and Development Planning Summary," which identifies the program element, project, task area, and work unit or equivalent under which the work was authorized.

Block 11. Controlling Office Name and Address. Enter the full, official name and address, including office symbol, of the controlling office. (Equates to funding/sponsoring agency. For definition see DoD Directive 5200.20, "Distribution Statements on Technical Documents.")

Block 12. Report Date. Enter here the day, month, and year or month and year as shown on the cover.

Block 13. Number of Pages. Enter the total number of pages.

Block 14. Monitoring Agency Name and Address (if different from Controlling Office). For use when the controlling or funding office does not directly administer a project, contract, or grant, but delegates the administrative responsibility to another organization.

Blocks 15 & 15a. Security Classification of the Report: Declassification/Downgrading Schedule of the Report. Enter in 15 the highest classification of the report. If appropriate, enter in 15a the declassification/downgrading schedule of the report, using the abbreviations for declassification/downgrading schedules listed in paragraph 4-207 of DoD 5200.1-R.

Block 16. Distribution Statement of the Report. Insert here the applicable distribution statement of the report from DoD Directive 5200.20, "Distribution Statements on Technical Documents."

Block 17. Distribution Statement (of the abstract entered in Block 20, if different from the distribution statement of the report). Insert here the applicable distribution statement of the abstract from DoD Directive 5200.20, "Distribution Statements on Technical Documents."

Block 18. Supplementary Notes. Enter information not included elsewhere but useful, such as: Prepared in cooperation with . . . Translation of (or by) . . . Presented at conference of . . . To be published in . . .

Block 19. Key Words. Select terms or short phrases that identify the principal subjects covered in the report, and are sufficiently specific and precise to be used as index entries for cataloging, conforming to standard terminology. The DoD "Thesaurus of Engineering and Scientific Terms" (TEST), AD-672 000, can be helpful.

Block 20. Abstract. The abstract should be a brief (not to exceed 200 words) factual summary of the most significant information contained in the report. If possible, the abstract of a classified report should be unclassified and the abstract to an unclassified report should consist of publicly-releasable information. If the report contains a significant bibliography or literature survey, mention it here. For information on preparing abstracts see "Abstracting Scientific and Technical Reports of Defense-Sponsored RDT&E," AD-667 000.

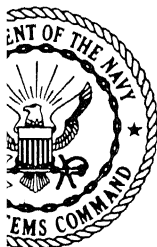


**PREDICTION METHODS
FOR
JET V/STOL PROPULSION
AERODYNAMICS**

ITEM # 0374

JULY 1975

VOLUME I



**NAVAL AIR SYSTEMS COMMAND
RESEARCH & TECHNOLOGY GROUP**

